

# Lawrence Berkeley National Laboratory

## Lawrence Berkeley National Laboratory

### **Title**

Conference on Physics with Large Gamma-Ray Detector Arrays, Volume II Proceedings

### **Permalink**

<https://escholarship.org/uc/item/5t082124>

### **Author**

Lawler (editor), G.

### **Publication Date**

1994-12-01

Peer reviewed

# CONFERENCE ON PHYSICS FROM LARGE $\gamma$ -RAY DETECTOR ARRAYS

Clark Kerr Campus  
Berkeley, California

August 2-6, 1994

## Volume II Proceedings

### The Organizing Committee

J.A. Becker  
B. Cederwall  
R. M. Clark  
M.A. Deleplanque  
R.M. Diamond  
P. Fallon  
E.A. Henry  
I.Y. Lee  
A.O. Macchiavelli  
F.S. Stephens

### The International Advisory Committee

G. Dracoulis  
D. Fossan  
S. Frauendorf  
J. Garrett  
B. Haas  
B. Herskind  
H. Hubel  
R. Janssens  
A. Johnson  
S. Lunardi  
B. Mottelson  
W. Nazarewicz  
P. Twin  
D. Ward

**Conference Chairperson:** M.A. Deleplanque

**Conference Coordinator:** Mollie Field

**Conference Secretary:** Barbara Phillips

LBL35687

CONF-940888

Nuclear Science Division, Lawrence Berkeley Laboratory  
University of California, Berkeley, CA 94720

This work was supported by the Director, Office of Energy Research, Office of Basic Energy Sciences,  
of the U.S. Department of Energy under Contract No. DE-AC03-76SF00098.

# MASTER

DISTRIBUTION OF THIS DOCUMENT IS UNLIMITED.

## **DISCLAIMER**

**This report was prepared as an account of work sponsored by an agency of the United States Government. Neither the United States Government nor any agency thereof, nor any of their employees, make any warranty, express or implied, or assumes any legal liability or responsibility for the accuracy, completeness, or usefulness of any information, apparatus, product, or process disclosed, or represents that its use would not infringe privately owned rights. Reference herein to any specific commercial product, process, or service by trade name, trademark, manufacturer, or otherwise does not necessarily constitute or imply its endorsement, recommendation, or favoring by the United States Government or any agency thereof. The views and opinions of authors expressed herein do not necessarily state or reflect those of the United States Government or any agency thereof.**

## **DISCLAIMER**

**Portions of this document may be illegible in electronic image products. Images are produced from the best available original document.**

## **Foreword**

The Conference on "Physics from Large  $\gamma$ -ray Detector Arrays" is a continuation of the series of conferences that have been organized every two years by the North American Heavy-ion Laboratories. The aim of the conference this year was to encourage discussion of the physics that can be studied with such large arrays. We were very pleased by the strong interest in this conference, the high quality of the talks, and the lively discussions. This volume contains contributions from the speakers. They are in the same order as the talks given at the meeting. We hope you will enjoy reading the exciting science that was presented at the conference.

The Organizing Committee

# TABLE OF CONTENTS

## C<sub>4</sub> SYMMETRY

<b>Rotation of superdeformed nuclei in the presence of Y<sub>44</sub> deformation.</b>	<b>1</b>
<i>Mottelson, B.</i>	

<b>C<sub>4</sub> symmetry and bifurcation in superdeformed bands.</b>	<b>14</b>
<i>Pavlichenkov, I.M.</i>	

<b>Evidence for <math>\Delta I = 2</math> staggering in superdeformed bands.</b>	<b>19</b>
<i>Cederwall, B., Ahmad, I., Becker, J.A., Brinkman, M.J., Carpenter, M.P., Crowell, B., Deleplanque, M.A., Diamond, R.J., Draper, J.E., Duyar, C., Fallon, P., Farris, L.P., Galido-Uribarri, A., Hackman, G., Henry, E.A., Henry, R.G., Hughes, J.R., Janssens, R.V.F., Khoo, T.L., Lauritsen, T., Lee, I.Y., Macchiavelli, A.O., Mullins, S.M., Radford, D.C., Rubel, E., Stephens, F.S., Stoyer, M.A., Satula, W., Waddington, J.C., Wiedenhoever, I., and Wyss, R.</i>	

## NEW REGIONS OF SUPERDEFORMATION, HYPERDEFORMATION

<b>Studies of superdeformation near N=80.</b>	<b>24</b>
<i>Mullins, S. M., Hackman, G., Haslip, D., Schmeing, N.C., Andrews, H. R., Clark, R. M., Cromaz, M., DeGraaf, J., Drake, T.E., Flibotte, S., Galindo-Uribarri, A., Hauschild, K., Hibbert, I. M., Janzen, V. P., Kuehner, J. A., Paul, E. S., Pilotte, S., Radford, D. C., Semple, A. T., Tiniar, J., Thorslund, I., Vaska, P., Waddington, J. C., Wadworth, R., Walker, L., Ward, D., and Yao, L.</i>	

<b>Hyperdeformation in <sup>152</sup>Dy from proton-gamma coincidence experiments.</b>	<b>29</b>
<i>Lunardon, M., Bazzacco, D., Burch, R., de Angelis, G., De Poli, M., Fabris, D., Fioretto, E., Lunardi, S., Medina, N., Nebbia, G., Prete, G., Rico, J., Rossi-Alvarez, C., Vedovato, G., Viesti, G.</i>	

## NEW EFFECTS IN ROTATION

<b>Intrinsic vorticity in rapidly rotating nuclei.</b>	<b>34</b>
<i>Quentin, P., and Mikhailov, I.N.</i>	

<b>Microscopic study of wobbling motions.</b>	<b>40</b>
<i>Shimizu, Y.R., Matsuzaki, M.</i>	

<b>The structure of <math>\pi^{1/2} [660]_{1/2+}</math> bands in Lu-isotopes.</b>	<b>45</b>
<i>Schnack-Peterson, H., Bark, R.A., Bengtsson, R., Bosetti, P., Brockstedt, A., Carlsson, H., Ekström, L.P., Hagemann, G.B., Herskind, B., Ingebretsen, F., Jensen, H.J., Leoni, S., Nordlund, A., Ryde, H., and Tjøm, P.O.</i>	

## TILTED AXIS CRANKING

<b>Tilted cranking.</b>	<b>52</b>
<i>Frauendorf, S., Meng, J., and Reif, J.</i>	

<b>High-K structures at the yrast line.</b>	63
<i>Walker, P.M.</i>	
<b>Lifetimes of shears bands in <math>^{199}\text{Pb}</math>.</b>	68
<i>Hübel, H., Neffgen, M., Baldsiefen, G., Korten, W., Mehta, D., Nenoff, N., van Severen, U. J., Grawe, H., Kluge, H., Maier, K. H., Korichi, A., Piiparinen, M. J., Meng, J., Frauendorf, S.</i>	
<b>Lifetimes of states in the M1-bands of <math>^{197, 198}\text{Pb}</math>.</b>	73
<i>Clark, R. M., Wadsworth, R., Andrews, H. R., Beausang, C. W., Bergstrom, M., Clarke, S., Dragulescu, E., Drake, T., Dagnall, P. J., Galindo-Uribari, A., Hackman, G., Hauschild, K., Hibbert, I. M., Janzen, V. P., Jones, P. M., MacLeod, R. W., Mullins, S. M., Paul, E. S., Radford, D. C., Semple, A., Sharpey-Schafer, J. F., Simpson, J., Ward, D., Zwartz, G.</i>	
<b>On I4 and I6-staggering in superdeformed bands and in the ground bands of even-even actinide nuclei.</b>	78
<i>Peker, L. K., Hamilton, J. H., and Rasmussen, J. O.</i>	
<b>IDENTICAL BANDS</b>	
<b>Relativistic description of superdeformed bands.</b>	83
<i>Ring, P.</i>	
<b>A comparison of superdeformed band transition energies.</b>	89
<i>Fallon, P., Stephens, F.S., Clark, R.M., Asztalos, S., Cederwall, B., Deleplanque, M.A., Diamond, R.M., Lee, I.Y., Macchiavelli, A.O.</i>	
<b>Configuration dependence of inertial parameters in identical and non-identical bands at normal deformation.</b>	94
<i>Zhang, Jing-ye, Ragnarsson, I., and Riedinger, L.L.</i>	
<b>Identical degenerate bands in the second minimum in <math>^{131}\text{Ce}</math>.</b>	99
<i>Nolan, P. J., Beausang, C. W., Forbes, S. A., Paul, E. S., Semple, A. T., Wilson, J. N., Clark, R. M., Hauschild, K., Wadsworth, R., Gizon, A., Santos, D. Gizon, A., Foin, C., Genevey, J., Pinston, J. A., Nyakó, B. M., and Zolnai, L.</i>	
<b>SYMMETRIES, SUPERDEFORMATION</b>	
<b>Pseudo-spin in doubly decoupled structures and identical bands.</b>	104
<i>Kreiner, A. J., Cardona, M. A., Somacal, H., Debray, M. E., Hojman, D., Davidson, J., Davidson, M., DeAcuna, D., Napoli, D. R., Rico, J., Bazzacco, D., Burch, R., Lenzi, S. M., Rossi Alvarez, C., Blasi, N., LoBianco, G.</i>	
<b>"Identical" SD Band in <math>^{151}\text{Dy}</math> and the pseudospin coupling scheme.</b>	109
<i>Nisius, D., Janssens, R. V. F., Fallon, P., Crowell, B., Ahmad, I., Beausang, C. W., Carpenter, M. P., Cederwall, B., Daly, P. J., Deleplanque, M. A., Diamond, R. M., Gassmann, D., Grabowski, Z. W., Henry, R. G., Khoo, T. L., Lauritsen, T., Lee, I. Y., Macchiavelli, A. O., Mayer, R. H., Stephens, F. S., Twin, P. J.</i>	

<b>Excited bands in the doubly-magic superdeformed <math>^{152}\text{Dy}</math> nucleus: band talk, band interaction and evidence for the first <math>N=7</math> proton hyper-intruder orbital.</b>	<b>114</b>
<i>Beausang, C. W., Dagnall, P. J., Twin, P. J., Bentley, M. A., Beck, F. A., Byrski, Th., Clarke, S., Curien, D., Duchêne, G., de France, G., Forsyth, P. D., Haas, B., Paul, E. S., Simpson, J., Styczen, J., Vivien, J. P., Zuber, K.</i>	
<b>M1 transitions between superdeformed states in <math>^{194,195}\text{Tl}</math>: the fingerprint of the <math>i_{13/2}</math> proton intruder orbital.</b>	<b>119</b>
<i>Duprat, J., Azaiez, F., Sharpey-Schafer, J. F., Aïche, Bastin, G., Beausang, C.W., Bourgeois, C., Clark, R. M., Cullen, D.M., Dagnall, P.J., Deloncle, I., Fallon, P., Forsyth, P.D., Fotiades, N., Gale, S.J., Gall, B., Hannachi, F., Harissopoulos, Hauschild, K., Hibbert, I., Jones, P.M., Joyce, M.J., Kaci, A., Kalfas, C.A., Kelly, W. H., Korichi, A., Le Coz, Y., Meyer, M., Paul, E. S., Perrin, N., Poffé, N., Porquet, M. G., Redon, N., Riley, M. A., Sergolle, H., Schuck, C., Simpson, J., Twin, P.J., Vlastou, R., Wadworth, R.</i>	
<b>OTHER DETECTOR SYSTEMS</b>	
<b>Recent results from APEX.</b>	<b>125</b>
<i>Ahmad, I., Austin, S.M., Back, B.B., Bazin, D., Betts, R.R., Calaprice, F.P., Chan, K.C., Chishti, A., Chowdhury, P., Dunford, R.W., Fox, J.D., Freedman, S.J., Freer, M., Hallin, A.L., Happ, T., Last, J., Kaloskamis, N., Kashy, E., Kutschera, W., Lister, C.J., Liu, M., Maier, M.R., Mercer, D., Perera, A., Rhein, M.D., Roa, D.E., Schiffer, J.P., Trainor, T., Wilt, P., Winfield, J.S., Wolanski, M., Wolfs, F.L.H., Wuosmaa, A.H., Xu, G., Young, A., and Yurkon, J.E.</i>	
<b>First results with the microball and Gammasphere.</b>	<b>130</b>
<i>Sarantites, D.G., Hua, P.-F., LaFosse, D., Kororija, M., Elson, J., Hood, J.T., Baktash, C., Gross, C., Jin, H.-Q., Stracener, D.W., Lee, I.Y., Macchiavelli, A., Cederwall, B., Fallon, P., Rathbun, W., Christando, F., Landulfo, E., Saladin, J.X., Döring, J., and Tabor, S.L.</i>	
<b>Collective high spin states in <math>^{45}\text{Sc}</math>.</b>	<b>135</b>
<i>Bednarczyk, P., Styczen, Broda, R., Lach, M., Meczynski, W., Bazzacco, D., Brandolini, F., de Angelis, G., Lunardi, S., Müller, L., Medina, N., Petrache, C., Rossi-Alvarez, C., Scarlassara, F., Segato, G. F., Signorini, C., Soramel, F.</i>	
<b>Gamma spectroscopy with the recoil filter detector--recent results and perspectives.</b>	<b>140</b>
<i>Spohr, K., Meczynski, W., Fitzgerald, J. B., Fossan, D. B., Gorska, M., Grawe, H., Heese, J., Lach, M., Maier, K. H., Maj, A., Merdinger, J. C., Rejmund, M., Schubart, R., Styczen, J.</i>	
<b>Reaction mechanism of multinucleon transfer in the system <math>^{110}\text{Pd} + ^{52}\text{Cr}</math>.</b>	<b>145</b>
<i>Vetter, K., Bazzacco, D., Elze, Th. W., Gerl, J., Happ, T., Härtlein, T., Korten, W., Kröll, T., Napoli, D., Rossi Alvarez, C., Schubert, R., Wollersheim, H. J., Xie, H.</i>	
<b>DETECTOR DEVELOPMENTS</b>	
<b>Performance of Gammasphere split detectors.</b>	<b>149</b>
<i>Macchiavelli, A.O., Lee, I.Y., Cederwall, B., Clark, R.M., Deleplanque, M.A., Diamond, R.M., Fallon, P., and Stephens, F.S.</i>	



<b>Performances of a new type of Ge detector: the clover detector.</b>	<b>154</b>
<i>Beck, F.A.</i>	
<b>The segmented clover detector for EUROBALL.</b>	<b>159</b>
<i>Gerl, J., Vetter, K., Elze, Th.W., Kröll, Th., and Xie, H.</i>	
<b>Performance of CLUSTER detectors.</b>	<b>160</b>
<i>Eberth, J.</i>	
<b>HARTREE-FOCK RESULTS, PAIRING</b>	
<b>Pairing correlations and superdeformation.</b>	<b>165</b>
<i>Flocard, H., Bonche, P., Heenen, P. H., Mehrem, R., Weiss, M. S.</i>	
<b>Moments of inertia and identical bands: a sensitive probe to pairing correlations at super-deformed shape.</b>	<b>171</b>
<i>Satula, W., and Wyss, R.</i>	
<b>Alignments of multi-quasiparticle bands and seniority-dependent reduced pairing.</b>	<b>178</b>
<i>Dracoulis, G.D.</i>	
<b>Superdeformation in odd-A Pb.</b>	<b>183</b>
<i>Farris, L. P., Henry, E.A., Becker, J.A., Brinkman, M.J., Cederwall, B., Cizewski, J.A., Deleplanque, M.A., Diamond, R.M., Draper, J.E., Duyar, C., Fallon, P., Hughes, J.R., Kelly, W.H., Lee, I.Y., Machiavelli, A.O., Rubel, E.C., Stephens, F.S., Stoyer, M.A., and Vo, D.T.</i>	
<b>BAND TERMINATION</b>	
<b>Terminating bands.</b>	<b>188</b>
<i>Ragnarsson, I.</i>	
<b>Intruder bands to very high frequencies in <sup>109</sup>Sb and <sup>114</sup>Te: smooth termination.</b>	<b>194</b>
<i>Fossan, D. B., LaFosse, D. R., Schnare, H., Beausang, C. W., Hauschild, K., Hibbert, I. M., Hughes, J. R., Janzen, V. P., Mullins, S. M., Paul, E. S., Radford, D. C., Ragnarsson, I., Thorslund, I., Vaska, P., Wadsworth, R., Waring, M. P.</i>	
<b>Multiple band termination spectroscopy in <sup>157,158</sup>Er with Eurogram.</b>	<b>199</b>
<i>Simpson, J.</i>	
<b>Unpaired spectroscopy around and beyond spin 50<math>\hbar</math> in <sup>155,156</sup>Dy.</b>	<b>206</b>
<i>Riley, M. A., Simpson, J., Brown, T.B., Sharpey-Schafer, J. F., Archer, D.E., Döring, J., Fallon, P., Kalfas, C. A., and Tabor, S. L.</i>	
<b>CONTINUUM, CHAOS</b>	
<b>Warm rotating nuclei.</b>	<b>212</b>
<i>Døssing, T.</i>	

<b>Study of the rotational transition strength in the warm nuclei <math>^{163}\text{Tm}</math> and <math>^{168}\text{Yb}</math>.</b>	225
<i>Leoni, S.</i>	
<b>Chaos in nuclear physics: statistical aspects of excited nuclear states.</b>	231
<i>Åberg, S.</i>	
<b>DECAY OF SUPERDEFORMED BANDS</b>	
<b>Decay from superdeformed to normal states: measured and calculated spectra of the connecting <math>\gamma</math> rays.</b>	238
<i>Khoo, T.L.</i>	
<b>Decay of the <math>^{194}\text{Pb}</math> superdeformed band.</b>	242
<i>Brinkman, M.J.</i>	
<b>Decay of the highly deformed band in the nucleus <math>^{137}\text{Nd}</math>.</b>	247
<i>Lunardi, S., Venturelli, R., Bazzacco, D., Rossi-Alvarez, C., Petrache, C. M., de Angelis, G., Bucurescu, D., Ur, C.</i>	
<b>COULOMB EXCITATION, GIANT RESONANCES</b>	
<b>Collective motion in superheavy elements.</b>	252
<i>Gaardhøje, J. J., Tveter, Trine, Atac, A., Herskind, B., Korten, W., Ramsoy, T., Sletten, G., Camera, F., Bracco, A., Million, B., Pignanelli, M., Nifenecker, H., Menthe, A., Pinston, J. A., Schussler, F., Krolas, W., Maj, A., Bacelar, J., Buda, A., Ploeg, H. v. d.</i>	
<b>Fission and internal pair studies of hot giant resonances.</b>	263
<i>Paul, P., Hofman, D.J., Schadmand, S., Varma, R., and Banerjee, S.R.</i>	
<b>OCTUPOLE DEFORMATIONS</b>	
<b>Periodic orbits and new shell structure generated by a combination of quadrupole and octupole deformations.</b>	268
<i>Arita, K., and Matsuyanagi, K.</i>	
<b>A superdeformed band with a unique pattern of decay: possible evidence for octupole vibration in <math>^{190}\text{Hg}</math>.</b>	274
<i>Crowell, B., Janssens, R.V.F., Carpenter, M.P., Ahmad, I., Henry, R.G., Harfenist, S., Khoo, T.L., Lauritsen, T., Nisius, D., Wilson, A. N., Sharpey-Schafer, J. F., Skalski, J.</i>	
<b>Multi-phonon states in <math>^{232}\text{Th}</math>.</b>	279
<i>Korten, W., Bröcking, P., Kröll, Th., Bazzacco, D., Ender, Ch., Elze, Th. W., Gerl, J., Haertlein, T., Happ, Th., Hübel, H., Kaspar, M., Napoli, D. R., Peter, I., Pohler, W., Reiter, P., Rossi-Alvarez, C., Schaffner, H., Schubert, R., Schwalm, D., van Severen, U. J., Vetter, K., Willsau, P., Wollersheim, H. J.</i>	
<b>NUCLEI FAR FROM STABILITY</b>	
<b>Physics with radioactive beams.</b>	284
<i>Nazarewicz, W., Dobaczewski, J., and Werner, T.R.</i>	

<b>Near-yrast structures in neutron-rich nuclei.</b>	<b>298</b>
<i>Phillips, W. R.</i>	
<b>Separation and identification of <math>^{100}\text{Sn}</math> at the GSI projectile fragment separator FRs.</b>	<b>304</b>
<i>Schneider, R., Friese, J., Reinhold, J., Zeitelhack, K., Faestermann, T., Gernhäuser, R., Gilg, H., Heine, F., Homolka, J., Kienle, P., Körner, H. J., Geissel, H., Münzenberg, G., Sümmerer, K.</i>	
<b>The <math>N = 40</math> neutron subshell closure in the <math>^{68}\text{Ni}</math> nucleus.</b>	<b>309</b>
<i>Broda, R., Fornal, B., Krolas, W., Pawlat, T., Bazzacco, D., Lunardi, S., Rossi-Alvarez, C., Menegazzo, R., de Angelis, G., Bednarczyk, P., Rico, J., De Acuna, D., Daly, P. J., Mayer, R. H., Sferrazza, M., Grawe, H., Maier, K. H., Schubart, R.</i>	
<b>Gamma-ray spectroscopy using deep-inelastic reactions.</b>	<b>314</b>
<i>Lee, I.Y., Cederwall, B., Deleplanque, M.A., Diamond, R.M., Fallon, P., Macchiavelli, A.O., Phair, L., Stephens, F.S., Wozniak, G.J., Becker, J.A., Henry, E.A., Hua, P.F., Sarantites, D.G., Saladin, J.X., Yu, C.H.</i>	
<b>IMPRESSIONS</b>	
<b>Impressions I.</b>	<b>318</b>
<i>Sharpey-Schafer, J.F.</i>	
<b>Impressions, Perspectives.</b>	<b>324</b>
<i>Herskind, B.</i>	
<b>Impressions.</b>	<b>334</b>
<i>Hamamoto, I.</i>	
<b>PROGRAM</b>	<b>341</b>
<b>REGISTERED PARTICIPANTS</b>	<b>343</b>

## Rotation of Superdeformed Nuclei in the Presence of $Y_{44}$ Deformation.

B. Mottelson

*NORDITA and NBI, Blegdamsvej 17  
DK-2100 Copenhagen Ø, Denmark*

*and*

*ECT\*, Villa Tambosi, Strada delle Tabarelle 286  
I-38050 Villazzano (Trento), Italy*

The discovery last year by a EUROGAM collaboration (Flibotte et al (1993)) of  $\Delta I = 4$  structure in the superdeformed rotational band of  $^{149}\text{Gd}$ , has revealed yet another fascinating new facet in the dynamics of these remarkable nuclear systems. The observed structure corresponds to a small energy displacement of the states with  $\Delta I = 4$  with respect to the complementary sequence with spins lying halfway in between. In more recent months, several groups have found this phenomena in a number of other superdeformed sequences; since new examples are being found at a breathtaking rate and all the principle participants in this adventure will be reporting their latest results to this meeting I shall *not* attempt any summary of the present status of the experiments. However I would like already in this introduction to make one observation concerning the experimental situation with respect to these small energy shifts: the magnitude of the observed displacements are of the order of  $0.1\text{MeV}$  and thus close to the limit of a accuracy of the current state of the art with large  $\gamma$ -ray arrays. The observation of the effect is thus a beautiful vindication of the ingenuity and perseverance of the experimental community that has been able to push the accuracy and sensitivity to this limit. And at the same time it is a powerful inspiration to achieve accuracies just a little bit better in order to make possible a more systematic study of these effects and to look for the somewhat more complicated patterns of displacements that, as we shall see, are suggested by the theoretical analysis – but this is getting way ahead of myself, so lets now start at the beginning.

Everything I am reporting today is the result of a joint investigation that Ikuko Hamamoto and I started about 6 months ago. We began with the belief, that has been common for all investigators who have looked at this phenomena, that  $\Delta I = 4$  implies the existence of a 4-fold axis of symmetry,  $C_4$ , somewhere or other. Our first task is therefore to establish where this axis is located with respect to the other directions that are defined for these superdeformed rotating nuclei. We start from the classical superdeformed shape: an axially symmetric strongly prolate (2:1) deformation. If we wish to impose some additional deformation on this system and end with a shape that has a 4-fold axis, there is in fact only one direction that can support such a 4-fold axis and that is the prolate axis of the superdeformed shape. The argument here is a simple geometrical fact: if we wish to generate a 4-fold axis

by deformation, the direction of this axis must have had an even higher symmetry (ie  $C_{4n}$ , which includes, of course,  $C_\infty =$  axial sym) before the deformation. In the  $SD$  shape, only the prolate axis has symmetry higher than  $C_4$ . We must also, locate the axis of collective rotation with respect to these directions, but that is not difficult since it is a well established fact that the collective rotation takes place about an axis perpendicular to the prolate axis (the evidence for this comes, of course, from the observed very large moment of inertia for the  $SD$  bands as well as from the enormous intensity of the  $E2$  transitions between the neighboring members of  $SD$  bands.) So we have the collective angular momentum  $\vec{I}$  perpendicular to the  $C_4$  axis, which is a very interesting and unconventional geometry for this kind of problem. You may even wonder whether it is possible to obtain  $\Delta I = 4$  structures from this geometry since all our previous experience with this kind of problem has been built on the well known prototype of  $\Delta I = 2$  structure resulting from  $C_2$  symmetry with respect to the rotation axis (signature). We shall see that it is indeed possible to get  $\Delta I = 4$  structure from this geometry but before demonstrating the interesting issues involved, I would like to compare the above geometrical arguments with those of other workers who have considered this problem; this gives me the chance to review the above arguments and to begin the discussion with these other workers whom I am sure will want to take up the comparison of the different approaches. As I have already said there are three directions in the problem

1. the  $C_4$  axis
2. the prolate axis of the  $SD$  shape,  $\underline{S}$
3. the direction of the rotational angular momentum,  $\vec{I}$

and three different arguments have been used in order to relate these directions

- A.  $C_4 \parallel \underline{S}$  (only  $\underline{S}$  can support  $C_4$ )
- B.  $\vec{I} \perp \underline{S}$  (yrast state selects direction of max  $\mathfrak{S}$  for rotation axis)
- C.  $C_4 \parallel \vec{I}$  (analogy with  $\Delta I = 2$  structure resulting from  $C_2$  symmetry with respect to  $\vec{I}$ )

It is clear that these three relations are inconsistent with each other, and so it will be necessary to give up at least one of them. As far as I know three groups have looked at the  $\Delta I = 4$  questions and have selected three different possibilities for their approach.

Flibotte et al (Phys. Rev. Lett. 71(93)	ABC
Pavlichenkov and Flibotte (subm. to this Conf.)	A $\bar{B}$ C
Hamamoto and Mottelson (to be publ. in Phys. Lett.)	AB $\bar{C}$

The original paper reporting the observation of  $\Delta I = 4$  structure (Flibotte et al) contained a discussion suggesting that this structure could result from a  $Y_{44}$  type deformation about an axis coinciding with the direction of collective rotation. It was argued that the rotation  $\vec{I}$  which they also place perpendicular to  $\mathcal{S}$  could align hexadecapole quanta along its own direction and this might lead to a  $Y_{44}$  deformation with respect to this direction. It seems to me that this alignment of hexadecapole quanta is a very improbable mechanism for generating  $Y_{44}$ , but the important point is that even if it happened, it would not generate a system with  $C_4$  symmetry. In this picture the direction of  $\vec{I}$  even before the deformation has only  $C_2$  symmetry and further deformation of  $Y_{44}$  type cannot make it  $C_4$  – the system remains with its  $C_2$  symmetry.

The only other attempt that I know of to explain  $\Delta I = 4$  structure in terms of  $C_4$  deformations is the contribution by Pavlichenkov and Flibotte to this conference that will be presented in the talk immediately following. In this work, the  $C_4$  axis is indeed coincident with the prolate axis  $\mathcal{S}$ , but the collective rotation is about a direction that is approximately aligned in the same direction; thus it seems to me, for the reasons given before, that this analysis is inappropriate for describing the observed superdeformed yrast bands.

In any case I am now going to explore the yrast structures that result from insisting on  $A + B$  and therefore giving up the direct connection between  $C_4$  and  $\Delta I = 4$  structure that would be provided by  $C$ . The rotational energy to 4th order in  $\vec{I}$  for a system with the indicated geometry can be written

$$H_{rot} = A_o \vec{I}^2 + AI_3^2 + B_1(I_1^2 - I_2^2)^2 + B_2(I_2^2 + I_3^2)^2 + \dots \quad (1)$$

$A > 0$	and large
$B_1 > 0$	(by choice of coord syst); this is the leading order axial symmetry breaking effect of the $Y_{44}$ deformation
$B_2 < 2(A/I^2)$	to preserve the condition $\vec{I} \perp \mathcal{S}$ ; this is a 4th order axial; symmetric term

$A_0$  determines the main  $I$ -dependence of the yrast states but does not effect the orientation of  $|\vec{I}|\vec{I}$  with respect to this intrinsic frame and thus we ignore this term in the rest of the discussion. It is useful to consider the function (1) as defining an energy function on the surface of the sphere  $|\vec{I}| = \text{const.}$  This function describes the dependence of the rotational energy on the direction of  $\vec{I}$  with respect to the intrinsic coordinate system (see Fig. 1). The function (1) gives rise to 4 minima in the equator that are related to each other by  $90^\circ$  rotations about the  $\mathcal{S}$ -axis. For yrast states the angular momentum will get trapped in one of these minima, spend some time vibrating around that direction, and then tunnel to one of the two adjacent minima; subsequent tunneling will lead to a stationary state with equal amplitude in each of the 4-minima. However the amplitude in the different minima can have different sign combinations and thus there are generated 4 different almost degenerate quantal states. The linear combinations created by the tunneling are eigenstates of the  $C_{4v}$  symmetry group and thus carry the quantum numbers that label the irreducible representations of this group see Table I. Since the intrinsic Hamiltonian is also invariant under the  $C_{4v}$  symmetries, the intrinsic state determines the  $C_{4v}$  symmetry of all the states in the rotational band (just as the intrinsic state determines the  $K$  quantum number ( $K = \Omega$ ) for a rotational band of an axially symmetric nucleus). Thus for a given rotational band, only rotational states with the same  $C_{4v}$  quantum number as that of the intrinsic state will appear in the spectrum. Now at last we can begin to see how the underlying  $C_4$  symmetry in its present guise could possibly lead to  $\Delta I = 4$  structure: if the tunnelling matrix element,  $t$ , were to change sign regularly every time the rotational angular momentum increased by two units, we would indeed observe in the associated rotational band an alternating shift of the eigenvalue (if we are looking at an  $A1$  or  $B1$  band) being first pushed up and then pushed down by the tunnelling energy.

In just a moment we shall attempt a more systematic discussion of this tunnelling problem but before we do that I would like to show some examples obtained by direct diagonalization of the Hamiltonian (1); this can introduce us to the variety of things that could happen and at the same time whet our appetite for the attack on the tunnelling problem. We consider three examples of (1), all with the same second order ( $A$ ) and 4-fold ( $B_1$ ) term, but differing in the 4th order axially symmetric term ( $B_2$ ) (see Table II). We see (Fig. 2) that the Hamiltonian (1) can indeed produce  $\Delta I = 4$  structure that

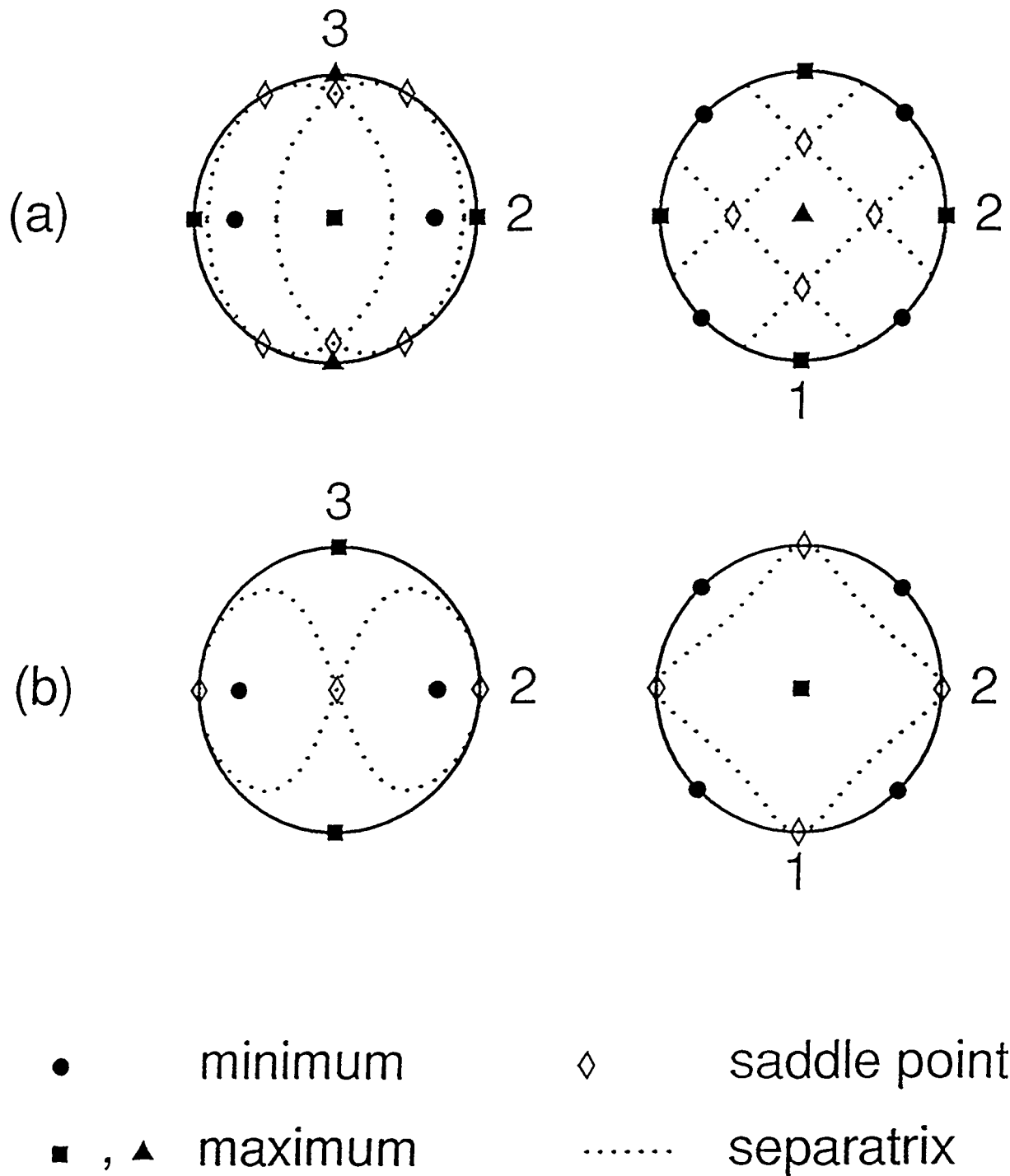


Fig.1



Table 1. Irreducible representation (IR) of  $C_{4v}$  point symmetry group (see, for example, ref [8]) and example of symmetry of wave functions. The component of angular momentum  $I$  along the symmetry axis is denoted by  $K$ .

IR of $C_{4v}$ group	Degeneracy	$^{ex}I = \text{even-integer case}$
$A1$	1	$ K\rangle +  \bar{K}\rangle$ where $K = 0, 4, 8, \dots$
$A2$	1	$ K\rangle -  \bar{K}\rangle$ where $K = 4, 8, \dots$
$B1$	1	$\left. \begin{array}{l} \\ \\ \end{array} \right\}  K\rangle \pm  \bar{K}\rangle$ where $K = 2, 6, 10, \dots$
$B2$	1	
$E$	2	$\left\{ \begin{array}{l} K = \dots, -3, 1, 5, \dots \\ K = \dots, -5, -1, 3, \dots \end{array} \right.$

Table II

Hamiltonian	A	$B_1$	$B_2$	$\Delta I = 4$ structure for yrast states
H1	100	1	- 1/2	irregular
H2	100	1	0	regular oscillation
H3	100	1	-1	no oscillation

$$H = AI_3^2 + B_1(I_1^2 - I_2^2)^2 + B_2(I_1^2 + I_2^2)^2$$

ENERGY-SPLITTING OF 4 LOWEST STATES

$\Delta$  B1 (1 degen.)  
 $+$  E (2 degen.)  
 $\bullet$  A1 (1 degen.)

$$H1 = 100I_3^2 + (I_1^2 - I_2^2)^2 - 0.5(I_1^2 + I_2^2)^2$$

5.4	4.6	1.3	1.4	3.0	1.5	2.0	2.3
(-1)	(-1)	(-1)	(-2)	(-3)	(-3)	(-4)	(-5)
$\bullet$	$\Delta$	$\bullet$	$\Delta$	$\Delta$	$\bullet$	$\Delta$	$\Delta$
$+$	$+$	$+$	$+$	$+$	$+$	$+$	$+$
$\Delta$	$\bullet$	$\Delta$	$\bullet$	$\bullet$	$\Delta$	$\bullet$	$\bullet$

$$H2 = 100I_3^2 + (I_1^2 - I_2^2)^2$$

6.5	4.0	2.7	1.9	1.4	1.1	8.6	6.9	5.7
(-1)	(-1)	(-1)	(-1)	(-1)	(-1)	(-2)	(-2)	(-2)
$\bullet$	$\Delta$	$\bullet$	$\Delta$	$\bullet$	$\Delta$	$\bullet$	$\Delta$	$\bullet$
$+$	$+$	$+$	$+$	$+$	$+$	$+$	$+$	$+$
$\Delta$	$\bullet$	$\Delta$	$\bullet$	$\Delta$	$\bullet$	$\Delta$	$\bullet$	$\Delta$

$$H3 = 100I_3^2 + (I_1^2 - I_2^2)^2 - (I_1^2 + I_2^2)^2$$

1.4	1.7	1.6	1.3	8.4	5.1	2.8
(1)	(0)	(-1)	(-2)	(-4)	(-5)	(-6)
$\Delta$	$\Delta$	$\Delta$	$\Delta$	$\Delta$	$\Delta$	$\Delta$
$+$	$+$	$+$	$+$	$+$	$+$	$+$
$\bullet$	$\bullet$	$\bullet$	$\bullet$	$\bullet$	$\bullet$	$\bullet$

Fig.2

10 12 14 16 18 20 22 24 26

SPIN (I)

resembles the regular oscillations of the experimental data, but with rather minor changes in the parameters this Hamiltonian can also generate a surprising variety of different patterns! In order to understand these matters we must look much more seriously into the structure of the tunnelling problem.

In order to obtain analytic (semiclassical) expressions for the tunnelling we must introduce canonically conjugate variables to describe the dynamics of  $\vec{I}$ ; this involves a transformation from the variables  $(I_1 I_2 I_3)$  to  $(I_3, \phi)$  where

$$\begin{aligned} I_1 &= \sqrt{I^2 - I_3^2} \cos \phi \\ I_2 &= \sqrt{I^2 - I_3^2} \sin \phi \end{aligned} \quad (2)$$

which gives

$$H(I_3, \phi) = AI_3^3 + (I^2 - I_3^2)^2(B_1 \cos^2 2\phi + B_2) \quad (3)$$

the minima of this function occur at

$$I_3^* = 0 \quad \phi^* = \pm \frac{\pi}{4}, \quad \pm \frac{3\pi}{4} \quad E^* \equiv H(I_3^* \phi^*) = B_2 I^4 \quad (4)$$

The tunnelling amplitude involves the action generated in going from one minimum to an adjacent minimum

$$S_{12} = \int_{\min 1}^{\min 2} I_3(\phi) d\phi. \quad (5)$$

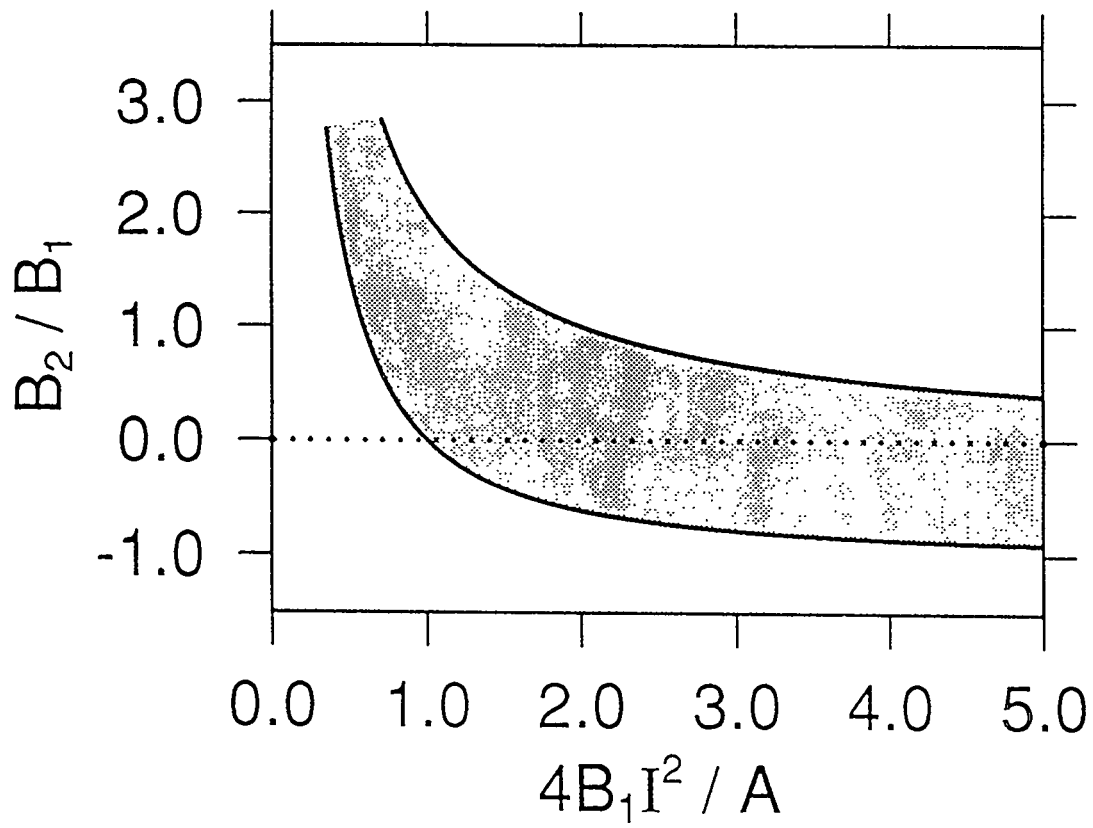


Fig.3

where the momentum  $I_3(\phi)$ , at  $\phi$ , is obtained solving  $H(I_3, \phi) = E^*$

In the usual tunnelling problems taught in the textbooks, the momentum ( $I_3$ ) in the barrier region is a pure imaginary and thus the tunnelling amplitude  $e^{iS}$  is a simple exponential function that does not ever change sign. However in the problem defined by (3),(4), and (5), it is possible for  $I_3(\phi)$  to become complex (acquire a real part) and then the tunnelling amplitude will involve  $\cos(\Re e S/\hbar)$  which could change sign as a function  $I$  in order to generate the observed  $\Delta I = 4$  structure. Thus our first task is to identify the regions of parameter space which leads to complex values of the momentum in the barrier region; a simple analysis of (3) yields the condition

$$1 + \sqrt{\frac{B_1}{B_1 + B_2}} < \frac{B_2 I^2}{A} < 1 - \sqrt{\frac{B_1}{B_1 + B_2}} \quad (6)$$

The condition ( $\frac{B_2 I^2}{A} < 1$ ), necessary in order to ensure  $I_3 \ll I$  is in fact more restrictive than the left hand inequality and so we are left with the shaded area in Fig. 3 as the region of parameter space that is of interest because it satisfies the necessary conditions for  $\Delta I = 4$  structure. Fig. 3 already explains for us the failure of the parameter  $H3$  to generate  $\Delta I = 4$  oscillation since this Hamiltonian defines a trajectory that lies entirely in the region below the shaded area in Fig. 3.

The real part of the tunnelling integral for  $H2$  yields also a simple expression; indeed quite generally for  $B_2 = 0$  we have

$$\Re e S_{12} = \begin{cases} \frac{\pi}{2}(I - \sqrt{\frac{A}{4B_1}}) & \text{if } I > \sqrt{\frac{A}{4B_1}} \\ 0 & \text{if } I < \sqrt{\frac{A}{4B_1}} \end{cases} \quad (7)$$

Thus we see that if  $I > \sqrt{\frac{A}{4B_1}}$  this Hamiltonian gives a tunnelling matrix element that changes sign regularly in order to generate  $\Delta I = 4$  structure. There are several features of this interpretation of  $\Delta I = 4$  structure that may be of interest for experimental testing:

- (a) in the same nucleus (even  $A$ ) and assuming the same deformations,  $A_1$  and  $B_1$  intrinsic states should oscillate with similar amplitude but in opposite phase, while  $E$  states will show no oscillation
- (b) in odd  $A$  nuclei the  $E1^1$  and  $E2^1$  configurations oscillation in opposite phase and with an amplitude that is  $\frac{1}{2}\sqrt{2}$  times as much as an even  $A$  nucleus with the same deformation
- (c) the  $I$  independent phase shift in (7) implies that the oscillations are proportional to  $\cos\left(\frac{\pi}{4}\sqrt{A/B_1}\right)$  and thus small changes in the parameters  $A$  or  $B_1$  can change the phase of the oscillations. Numerical evaluation of the oscillations obtained from the quantal diagonalizations of (1) show that the semi-classical phase shift should be corrected by  $\sqrt{\frac{A}{4B_1}} \rightarrow \sqrt{\frac{A}{4B_1} - \frac{3\hbar^2}{2}}$

The irregular oscillations of  $H1$  can be understood from the asymptotic evaluation of the real part of the action for this Hamiltonian

$$\Re S_{12} \approx \frac{\pi}{4} I \sqrt{2} \cos \frac{\pi}{8} \quad (8)$$

the irrational number  $\left(\frac{1}{2}\sqrt{2} \cos \frac{\pi}{8} = 0.653281 \dots\right)$  multiplying  $\frac{\pi}{2} I$  implies that the sign changes with  $\Delta I = 2$  have no regularly repeating periods and thus give rise to an erratic pattern of oscillations.

### Where do we stand?

As a final summing up I would like to attempt to bring together our view of the present status of this attempt to understand the  $\Delta I = 4$  structures:

1. The discussion we have presented provides a first step in identifying the qualitative mechanisms that may generate these structures but has not attempted any detailed fitting of the parameters of the theory to the experimental data. This is not because we expect any great difficulty in finding such a fit but rather because such fitting appears to be too easy! there are three parameters ( $A$ ,  $B_1$ , and  $B_2$ ) and each may change (smoothly) with  $I$ , and on top of that the staggering will be sensitive to small amounts of  $C_{4v}$  violating terms (such as a pinch of  $\gamma$ -deformation). Thus the problem at present is not to find a fit, but rather to find constraints that may help to delimit the parameter space and eventually to make the fitting unique. I imagine that such constraints may come partly from more systematic experimental data and partly from microscopic theory that may illuminate the connection between intrinsic structure and  $Y_{44}$  deformation and the connection between deformation parameters and the rotational parameters  $A$ ,  $B_1$  and  $B_2$ .

2. Even without any detailed fit to the data, there are a number of qualitative features of this description that can be tested:

(i) in even- $A$  nuclei: bands built on  $A1$  and  $B2$  intrinsic states can exhibit  $\Delta I = 4$  staggering but those built on intrinsic states of  $E$  type should not exhibit staggering.  $A1$  and  $B1$  oscillate out of phase with each other and phase changes can occur either because of changes in the ratio  $A/B_1$  or as a result of a small  $B_2 \neq 0$  term.

(ii) in odd- $A$  nuclei: in the appropriate region of parameter space all rotational bands exhibits oscillations, except for improbable singular choices of the parameters.

(iii) in both even and odd  $A$ : the regular  $\Delta I = 4$  oscillations occur only for rather special regions of parameter space. Thus, *a priori* we would expect the irregular oscillations to be *even more common* ! where are they ?

three possible answers:

( $\alpha$ ) some, (unknown) stability condition tends to lock in on the special parameter values

( $\beta$ ) the irregular oscillations are present but have not yet been found by the experimentalists because they look so much like experimental errors.

( $\gamma$ ) something important is missing in the mechanism discussed in this presentation

3. All the present discussion has involved the consequences that follow from the occurrence of a 4-fold axis of symmetry in the nuclear shape. In the superdeformed shell structure, one might expect the generation of a 3-fold axis to be at least as easy as that of a 4-fold axis. If the nucleus acquires such a shape ( $C_{3v}$ ), the rotational Hamiltonian would have  $C_{6v}$  symmetry and the yrast spectrum exhibits close doublets with splittings that are only generated by tunnelling between the six equivalent minima. A very interesting structure !



# $C_4$ SYMMETRY AND BIFURCATION IN SUPERDEFORMED BANDS

I. M. Pavlichenkov

*Russian Research Center "Kurchatov Institute", Moscow, 123182, Russia*

## 1 Introduction

The quantum rotation is a specific type of excitation of molecules and nuclei with a regular sequence of energy levels, which are grouped into rotational bands. Over the last decade the new methods for studying the rotational states with high- $I$  values have been developed in molecular and nuclear spectroscopy. The large  $\gamma$ -ray detector arrays have allowed experimentalists to find the long rotational bands built on superdeformed nuclear configurations. It has recently been discovered [1, 2] that superdeformed bands may exhibit weak  $\Delta I=2$  energy staggering where states differing by  $4\hbar$  of angular momentum are perturbed in the same direction. The experimental data exhibit an increase of the staggering amplitude with spin. This feature suggests that an alignment mechanism involves in the phenomenon. This allows us to apply the phenomenological theory of bifurcations in rotational spectra [3] in order to explain the experimental data.

A simplest system modeling a rotational dynamics is a rigid asymmetric top with the Hamiltonian

$$H_{rig} = AI_1^2 + BI_2^2 + CI_3^2, \quad (1)$$

where  $I_\alpha$  are the projections of the total angular momentum operator on the BFF (body-fixed frame) axes  $\alpha = 1, 2, 3$ . The rotational constants  $A$ ,  $B$  and  $C$  are inversely proportional to principal moments of inertia. The rotational band of an asymmetric top consists of rotational multiplets, i.e., of the levels with the same value of the quantum number  $I$ . Besides  $I$ , these levels are characterized by the irreducible representations of the  $D_2$  group, which are labeled  $A_1, A_2, B_1, B_2$ . Another important characteristic of a rotational motion is a phase space. It is two dimensional because of two integrals of motion  $\mathbf{I}^2$  and  $I_z$ . We map this space on the sphere of the  $I$  radius with a center in the origin of the BFF. The point on the sphere with coordinates  $\theta$  and  $\varphi$  determines the orientation of the vector  $\mathbf{I}$  in the BFF. Thus, the trajectories of the tip of  $\mathbf{I}$  on the sphere are classical trajectories of the system in its phase space. When the rotational energy is close to  $AI^2$  or  $CI^2$ , where  $A$  and  $C$  correspond to the maximal or minimal moment of inertia, the classical trajectories are small ellipses around axes 1 or 3. They represent precession motion around these stable axes.

## 2 Bifurcations in rotational spectra

The rotational dynamics of the real systems – molecules and nuclei – is more complicated than that of a rigid top because the centrifugal and the Coriolis forces. To

describe their spectra we have to use instead of (1) *an effective rotational Hamiltonian*, which is in general an infinite power series in operators  $\dot{I}_\alpha$ . In order to consider the alignment of  $\mathbf{I}$  along the 1-axis, which is perpendicular to the long 3-axis of the prolate (not necessary axial) nuclear shape, this Hamiltonian is most conveniently taken as

$$H_{eff} = \sum_{m=0}^{\infty} \left[ I_+^m f_m^* (\mathbf{I}^2, I_1) + f_m (\mathbf{I}^2, I_1) I_-^m \right], \quad (2)$$

where  $I_\pm = I_2 \pm iI_3$  are the ladder operators. The Hamiltonian (2) is invariant with respect to time reversal and inversion of the BFF. The invariance properties impose some restrictions on functions  $f_m$ .

Let us introduce the rotational energy surface [4] as an energy function (2) on the rotational phase space. By using the spherical coordinates in the BFF

$$I_1 = I \cos \theta, \quad I_2 = I \sin \theta \cos \varphi, \quad I_3 = I \sin \theta \sin \varphi. \quad (3)$$

we can express the surface

$$\varepsilon(\theta, \varphi) = 2f_0(I, \cos \theta) + \sum_{m=1}^{\infty} [f_m^*(I, \cos \theta) e^{im\varphi} + f_m(I, \cos \theta) e^{-im\varphi}] \sin^m \theta, \quad (4)$$

as a function of the angles  $(\theta, \varphi)$  and the angular momentum  $I$ . The lines at constant energy on this surface represent the classical trajectories of the tip of the vector  $\mathbf{I}$ . They coincide with the trajectories obtained from the equation of motion

$$\dot{I}_\alpha = \{H_{eff}, I_\alpha\}, \quad (5)$$

where  $\{\dots\}$  is the Poisson bracket.

We will consider the change of rotational motion with changing  $I$  in a small region of the phase space near the 1-axis, which coincides with the  $C_n$  symmetry axis. The rotation around such an axis is stationary because  $\{H_{eff}, \mathbf{I}\} = 0$ . The *aligned* stationary state  $\mathbf{I}(I, 0, 0)$  corresponds to the fixed point  $\theta = 0$  of the classical energy surface (4). Considering this surface near the fixed point, we can expand the function (4) in a power series of the small angle  $\theta$ . The first two terms of an expansion are obvious. They are the energy  $\varepsilon_0(I)$  of rotation around the 1-axis and  $-a_1(I)\theta^2$ . Assuming that the angular-momentum vector  $\mathbf{I}$  becomes parallel to the 1-axis at the critical value  $I = I_c$  and aligned state has minimal energy, then,  $a_1 > 0$  and  $a_1 < 0$  for  $I < I_c$  and  $I > I_c$ , respectively. Since it has different sign on either side of  $I_c$ , the coefficient  $a_1$  must vanish at  $I = I_c$ . Thus we can approximate  $a_1$  by  $\alpha(I - I_c)$  with  $\alpha < 0$ . The spin  $I_c$  corresponds to the critical point of the energy surface (4). To consider the surface near the critical point one needs to add next terms, which forms depend on the symmetry axis. For example we have

$$\varepsilon(\theta, \varphi) = \varepsilon_0(I) - \alpha(I - I_c)\theta^2 + 2b\theta^3 \cos 3\varphi, \quad \text{for axis } C_{3v}, \quad (6)$$

$$\varepsilon(\theta, \varphi) = \varepsilon_0(I) - \alpha(I - I_c)\theta^2 + (a_2 + 2c \cos 4\varphi)\theta^4, \quad \text{for axis } C_{4v}. \quad (7)$$

Eq. (6-7) is the canonical form of a catastrophe function for the Hamiltonian system with the  $C_{3v}$  and  $C_{4v}$  symmetry [5]. Our approach resembles the Landau theory of

second-order phase transitions [6]. The polar angle  $\theta$  plays the role of a symmetry parameter and aligned state corresponds to the "high symmetry state."

The catastrophe function (6) is a useful guide for the determination of the quantum Hamiltonian that describes the yrast states near the bifurcation point  $I_c$ . According to Eq. (7), we have the following four-parameter Hamiltonian for the  $C_{4v}$  bifurcation

$$H_{C_{4v}} = \alpha(I - I_c) \frac{I_1^2 - I^2}{I^2} + a_2 \left( \frac{I_1^2 - I^2}{I^2} \right)^2 + c \frac{I_+^4 + I_-^4}{I^4}. \quad (8)$$

The states of the catastrophe Hamiltonian (8) correspond to the motion of  $\mathbf{I}$  localized in the small region confined near the north pole ( $\theta = 0$ ) of the phase sphere if  $|a_2| > 2c > 0$ . The energy of these states is calculated relative to  $\epsilon_0(I)$ .

### 3 $\Delta I = 2$ staggering in superdeformed bands

The main idea consists in using the operator (8) as the effective Hamiltonian for reproducing *only* staggering phenomena in superdeformed bands [7]. If the parameter  $\alpha < 0$ , the bifurcation modifies the precessional motion as follows. As the spin increases, the delocalized precession around four equivalent axes located symmetrically near the north pole transforms itself into the localized precession around the 1-axis. Thus the bifurcation is accompanied by the alignment of  $\mathbf{I}$  along the  $C_{4v}$  symmetry axis. The yrast states for integer spins, belonging to the  $C_{4v}$  symmetry group with quantum numbers  $A_1$ ,  $A_2$ ,  $B_1$ ,  $B_2$ , and  $E$ , transform from the six-fold quasi-degenerate clusters  $A_1 + A_2 + B_1 + B_2 + E$  into a system of approximately equidistant quasi-degenerate doublets  $A_1 + A_2$ ,  $B_1 + B_2$  and degenerate doublets  $E$ . The six-fold quasi-degenerate clusters for  $I < I_c$  are the result of the delocalized quantum precession, which involves the tunneling of  $\mathbf{I}$  across the potential barriers that separate the four equivalent precessional axes. For even values of  $I$ , the lowest multiplet state is  $A_1$  for the sequence of spins  $I = (0 \text{ mod } 4)$  and  $B_1$  for  $I = (2 \text{ mod } 4)$ . Only the full symmetric  $A_1$  states exist in nuclear rotational bands. Thus, the alternating order of the lowest  $A$  and  $B$  states produces the  $\Delta I = 2$  staggering.

In other words, the yrast superdeformed band is split into two families shifted in energy. Let us call the sequence with lower energy the favored band and the other, unfavored. For fixed  $I$ , the distance between these bands  $\Delta E(I) = E_u(I) - E_f(I)$  is equal to the spacing between the  $A$  and  $B$  levels. It is possible to extract this value from the experimental  $\gamma$ -ray transition energies supposing the energy of the favored and unfavored bands are smooth functions of spin. One of the energies  $E_u(I)$  or  $E_f(I)$  belongs to the non-physical  $B$  state. To find it we have to continue the corresponding function from the neighboring physical  $A_1$  states. By using for example expansion of  $E_f$  in the states with spin  $I \pm 2$ ,  $I \pm 4$ , we find

$$E_f(I) = \frac{9}{16} [E_f(I + 2) + E_f(I - 2)] - \frac{1}{16} [E_f(I + 6) + E_f(I - 6)]. \quad (9)$$

Eq.(9) is accurate up to third derivative of  $E_f(I)$  that is a fairly good approximation because of the regularity of superdeformed bands. The formulae for  $\Delta E(I)$  can be

easy expressed in terms of the  $\gamma$ -ray energies ( $E_\gamma(I) = E(I+1) - E(I-1)$ ) as follows

$$\Delta E(I) = \frac{1}{16}[E_\gamma(I+5)+E_\gamma(I+3)-8E_\gamma(I+1)+8E_\gamma(I-1)-E_\gamma(I-3)-E_\gamma(I-5)]. \quad (10)$$

Let us consider for example the transition 1444.2 keV in the yrast superdeformed band of  $^{148}\text{Gd}$ . The staggering value calculated by means of Eq. (10), the methods of Ref. [1] and Ref. [2] are  $-0.19(7)$ ,  $-0.33(18)$  and  $0.16(7)$  respectively. Although the obtained values are different, all the methods reveal the important features of the staggering pattern: 1) there is a spin region where the staggering effect is small followed by 2) large  $\Delta I=2$  oscillations and 3) an inversion of the oscillating pattern at high spin. The fitting of the experimental data with using the lowest  $A_1$  eigenvalues of the Hamiltonian (8) reproduces these features [7].

The staggering mechanism is different before and after the critical spin  $I_c$ . In the region  $I < I_c$ , the staggering is due to the tunneling of  $\mathbf{I}$  between the four minima of the energy surface. A qualitative analysis of this mechanism has been performed in Ref. [8] by evaluating the tunneling matrix element between adjacent minima. The imaginary part of this matrix element gives the staggering amplitude. In our case, it is proportional to  $\exp\{-sI(I_c - I)\}$  where  $s$  is independent of  $I$ . The fact that the amplitude depends on  $I_c - I$  explains the increase of the oscillations when  $I$  approaches  $I_c$ . The real part of the matrix element produces the modulation of the amplitude and can generate inversions of the staggering pattern [8]. It should be noted that the inversion point close to critical spin  $I_c$  is always the last inversion point in a staggering pattern. The region  $I > I_c$  involves a precessional staggering mechanism because the spacing between the lowest levels with symmetry  $A_1$  and  $B_1$  is equal to the precessional frequency  $\omega = 2\alpha(I_c - I)/I$ .

The Hamiltonian (8) allows us to consider another rotational regime recently studied by Hamamoto and Mottelson [8]. The authors are using the Hamiltonian identical with (8). In this regime, the axis of rotation is perpendicular to the  $C_4$ -symmetry axis, i.e., the  $C_4$ -symmetry axis is parallel to the long 3-axis of the superdeformed prolate nuclear shape. Thus, after the permutation of the axis labels  $(1,2,3) \rightarrow (3,1,2)$  in Eq. (8), one can obtain the following relationships between the parameters of both Hamiltonians

$$A = a_1/I^2 + 2a_2/I^3 - 10c/I^4, \quad B_1 = 4c/I^4, \quad B_2 = (a_2 - 2c)/I^4, \quad (11)$$

and an additional term  $\varepsilon_0(I) = AI^2 + B_1I(2I - 1) + B_2I^2$ . The parameter  $a_1$  has been used in these expressions instead of  $\alpha(I - I_c)$  because there is no bifurcation in this regime and the angular-momentum vector is localized in the neighborhood of four energy minima in the plane perpendicular to the  $C_4$  axis. Therefore the tunneling mechanism results in a staggering amplitude proportional to  $\exp(-sI)$ . A fast damping of the  $\Delta I=2$  energy oscillations with increasing spin cannot explain the experimental staggering. It should be pointed out that the same mechanism is responsible for the formation of clusters in molecular rotational spectra [4].

The two different rotational regimes of the Hamiltonian (8) suggest different microscopic origins for the  $\Delta I=2$  staggering. On one hand, the Hamamoto and Mottelson

regime could be realized by the presence of a static hexadecapole deformation  $\varepsilon_{44}$  in the nuclear shape. The  $I_+^4 + I_-^4$  term in the  $C_{4v}$  invariant rotational Hamiltonian would be a direct consequence of this deformation. On the other hand, our regime suggests the alignment of an angular-momentum vector. This dynamical effect *excludes* the  $C_{4v}$  symmetry of the nuclear shape. The  $\Delta I=2$  staggering would originate because of a  $C_{4v}$  invariant part of the Hamiltonian. Let us consider for example the angular momentum  $\mathbf{J}$  (phonon or single-particle) coupled with a core by the  $C_{4v}$  invariant interaction. The corresponding rotational Hamiltonian would have the form

$$H = A_1(\mathbf{I} - \mathbf{J})^2 + (A_3 - A_1)(I_3 - J_3)^2 + a_1 J_1^2 + a_2 J_1^4 + c(J_+^4 + J_-^4), \quad (12)$$

where  $A_1$  and  $A_3$  are rotational constants. The term proportional to  $(I_3 - J_3)^2$  violates the  $C_{4v}$  symmetry and mixes the states  $A$  and  $B$ . This perturbation would be reduced when considering only the motion with small values of  $I_3 - J_3$ , i.e., with the rotational angular momentum  $\mathbf{R} = \mathbf{I} - \mathbf{J}$  close to the direction of the 1-axis. The corresponding classical trajectories in the phase space would be quasi-symmetrical. In the quantum case, these orbits produce the scars of the  $C_{4v}$  symmetry in the rotational bands of some superdeformed nuclei. The symmetry property is no longer associated with a particular state, but is reflected in the modulation of the whole spectrum. This phenomenon is typical of non-linear dynamics. As an example, the simplest system exhibiting the scars of the  $SO(2,2)$  symmetry is the hydrogen atom in a magnetic field [9]. The magnetic field plays an analogous role to the  $C_{4v}$ -symmetry breaking term  $(I_3 - J_3)^2$  in Eq. (12). If this scenario is responsible for the staggering effect in superdeformed bands, then one could expect to observe the scars of the  $C_{3v}$  symmetry in rotational band due to the alignment of an angular momentum in the field having such a symmetry.

## References

- [1] S. Flibotte *et al.*, Phys. Rev. Lett. **71**, 4299 (1993).
- [2] B. Cederwall *et al.*, Phys. Rev. Lett. **72**, 3150 (1994).
- [3] I. M. Pavlichenkov, Physics Reports **226**, 175 (1993).
- [4] W. G. Harter, Comp. Phys. Rep. **8**, 319 (1988).
- [5] M. Golubitsky and I. Stewart, Physica D **24**, 391 (1987).
- [6] L. D. Landau and E. M. Lifshitz, *Statistical Physics* (Pergamon, Oxford, 1965).
- [7] I. M. Pavlichenkov and S. Flibotte, in *Conference on Physics from Large  $\gamma$ -Ray Detector Arrays, Berkeley, August 1994*, Vol. I, Abstracts, p. 17 and to be published.
- [8] I. Hamamoto and B. Mottelson, Phys. Lett. **B333**, 294 (1994).
- [9] D. Delande and J. C. Gay, Phys. Rev. Lett. **59**, 1809 (1987).

# Evidence for $\Delta I = 2$ Staggering in Superdeformed Bands

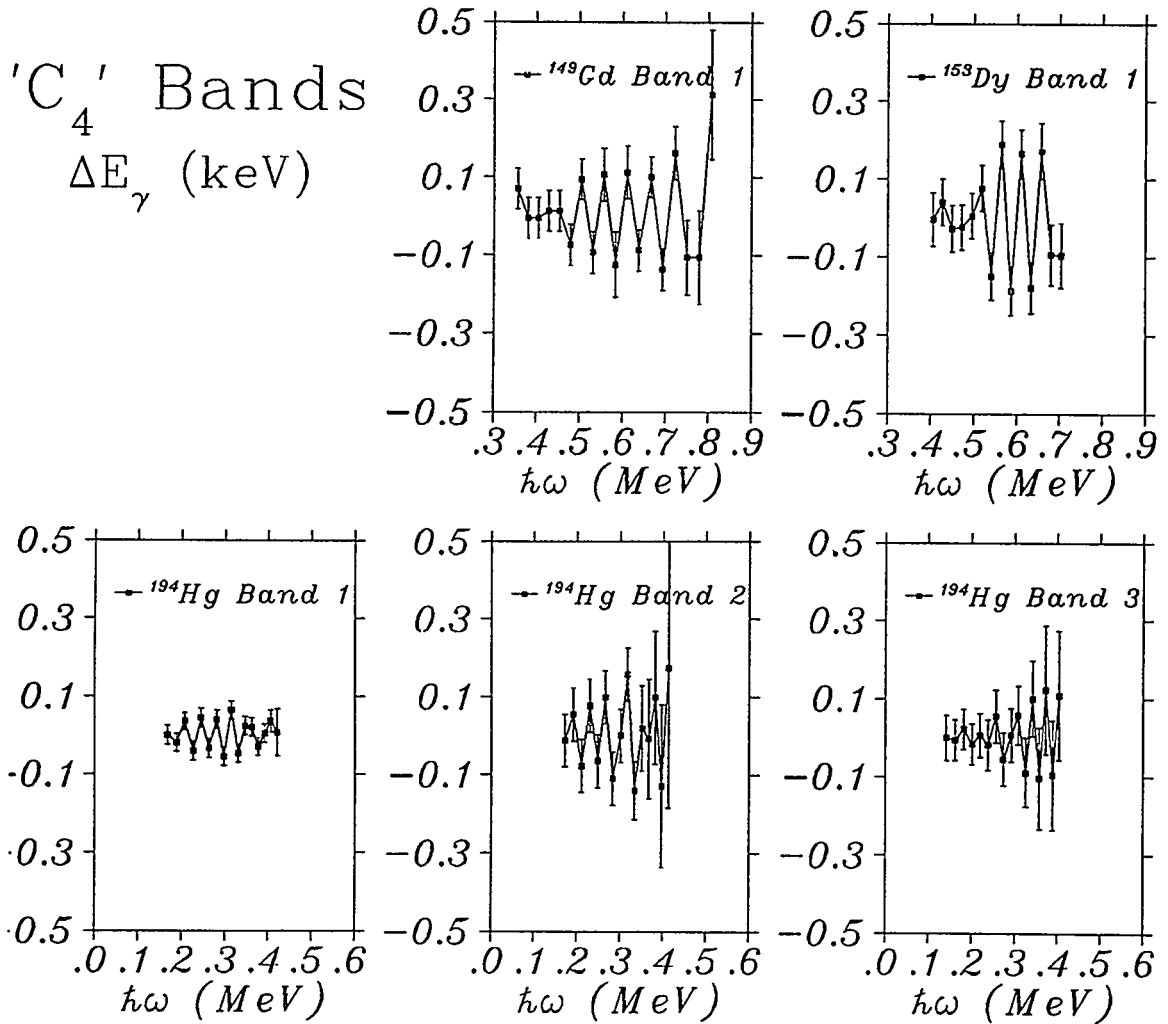
B. Cederwall,<sup>(1)</sup> I. Ahmad,<sup>(2)</sup> J. A. Becker,<sup>(3)</sup> M. J. Brinkman,<sup>(3)</sup> M. P. Carpenter,<sup>(2)</sup> B. Crowell,<sup>(2)</sup> M. A. Deleplanque,<sup>(1)</sup> R. M. Diamond,<sup>(1)</sup> J. E. Draper,<sup>(4)</sup> C. Duyar,<sup>(4)</sup> P. Fallon,<sup>(1)</sup> L. P. Farris,<sup>(3)</sup> A. Galindo-Uribarri,<sup>(5)</sup> G. Hackman,<sup>(6)</sup> E. A. Henry,<sup>(3)</sup> R. G. Henry,<sup>(2)</sup> J. R. Hughes,<sup>(3)</sup> R. V. F. Janssens,<sup>(2)</sup> T. L. Khoo,<sup>(2)</sup> T. Lauritsen,<sup>(2)</sup> I. Y. Lee,<sup>(1)</sup> A. O. Macchiavelli,<sup>(1)</sup> S. M. Mullins,<sup>(5)</sup> D. C. Radford,<sup>(5)</sup> E. Rubel,<sup>(4)</sup> F. S. Stephens,<sup>(1)</sup> M. A. Stoyer,<sup>(3)</sup> W. Satula,<sup>(7)</sup> J. C. Waddington,<sup>(6)</sup> I. Wiedenhoever,<sup>(8)</sup> and R. Wyss<sup>(9)</sup>

<sup>(1)</sup>Lawrence Berkeley Laboratory, Berkeley, California 94720, USA; <sup>(2)</sup>Argonne National Laboratory, Argonne, Illinois 60439, USA; <sup>(3)</sup>Lawrence Livermore National Laboratory, Livermore, California 94550, USA; <sup>(4)</sup>Physics Dept., University of California, Davis, California 95616, USA; <sup>(5)</sup>Chalk River Nuclear Laboratories, Canada; <sup>(6)</sup>Tandem Accelerator Laboratory, McMaster University, Canada; <sup>(7)</sup>Institute of Theoretical Physics, University of Warsaw. PL-00681 Warsaw, Poland; <sup>(8)</sup>Universität zu Köln, IKP, D-5000 Köln, Germany; <sup>(9)</sup>Royal Inst. of Technology, Physics Dept., S-100 44 Stockholm, Sweden

## 1 Introduction

Spectroscopy of superdeformed (SD) bands has revealed and continues to reveal new aspects of the physics of atomic nuclei under extreme conditions. The new generation of detector arrays for  $\gamma$ -ray spectroscopy has extended our means to study nuclei as quantum rotors to levels where possible new subtle symmetry effects are observed. Perhaps the most challenging features of superdeformation found to date are the appearance of so called “identical” bands and the very recent discovery of SD bands exhibiting a  $\Delta I = 2$  staggering. The possibilities of additional symmetries in the Hamiltonian revealed by these features are intriguing and may have important implications for the general understanding of finite many-body systems. The  $\Delta I = 2$  staggering phenomenon was first reported in normal-deformed bands in the actinide region[1], but has not been confirmed nor extended in these nuclei. At present there are two recently published cases of  $\Delta I = 2$  staggering in SD bands, one for each of the  $A \approx 150$  and  $A \approx 190$  SD mass regions. The first observation in a SD nucleus was in the yrast SD band of  $^{149}\text{Gd}$ [2] from an experiment at Eurogam and the possibility of a four-fold rotational ( $C_4$ ) symmetry term in the SD Hamiltonian was thereby inferred. Subsequently, similar staggering effects were also observed in the SD bands of  $^{194}\text{Hg}$ [3] in a Gammasphere experiment. Furthermore, from another experiment at Gammasphere we have tentative evidence for a  $\Delta I = 2$  staggering pattern in the yrast SD band of  $^{153}\text{Dy}$ . The evidence for  $\Delta I = 2$  staggering in SD bands is summarized in Fig. 1 where the  $\gamma$ -ray transition energies are plotted vs rotational frequency, with a quadratically interpolated smooth reference subtracted. For SD bands 1 in  $^{149}\text{Gd}$ [2],  $^{194}\text{Hg}$  and  $^{153}\text{Dy}$  the error bars include only statistical uncertainties.

**Fig. 1**



The staggering effect is experimentally observed at the limit of our present detecting capabilities, typically of the order of  $10^{-4}$  times the measured  $\gamma$ -ray energies themselves. Therefore its study poses a tremendous experimental challenge, justified however by the opportunity to further our understanding of nuclear excitations. Some phenomenological - macroscopic approaches[4, 5, 6] have provided some understanding on how a staggering may occur but microscopic models are still lacking.

We will here try to present an overview of the present experimental situation and address some of the problems encountered in the data analysis. From discussions at this Conference[7], it is apparent that the experimental situation encountered in analyzing the small staggering effect is by no means clear. We use data from two

Gammasphere experiments on SD states in  $^{153}\text{Dy}$  and  $^{194}\text{Hg}$  as illustrative examples of these analyses.

## 2 Data analysis - general

The data analysis proceeds in three basic steps.

- Extraction of accurate  $\gamma$ -ray energies and their uncertainties
- Choice of smooth reference  $E_{\gamma ref}$ , defining deviations  $\Delta E_\gamma$  from the regular rotation:

$$\Delta E_\gamma(I) = E_\gamma(I) - E_{\gamma ref}(I)$$

- Establish statistical significance of any proposed  $\Delta I = 2$  stagger

It is clear that the most important, and also most difficult step in the analysis is the extraction of the  $\gamma$ -ray energies and their uncertainties. In high-fold data sets the background is complex and the additional errors that occur if background subtraction is necessary are very difficult to estimate, primarily because these backgrounds are not smooth and the possibility of interference from even very small contaminating lines may be significant. Furthermore, a proper background spectrum contains not only background gates but, depending on the fold  $f$ , also various peak-background gate combinations ( $\sum a_i \cdot (\text{peak gate})^j \times (\text{background gate})^k$ ;  $(j + k = f; k \geq 1)$ ). Therefore it becomes richer in SD transitions with increasing fold and thus depletes the statistics in the final spectrum. Since the background subtraction complicates the error analysis, a simple practical approach is to check that the  $\gamma$ -ray energies are not sensitive to different “reasonable” background subtractions. Ideally, the high-fold data are sufficiently clean so that a background need not be subtracted at all.

Most SD bands in both the  $A \approx 150$  and  $A \approx 190$  regions (especially near  $A = 190$ ) have non-constant moments of inertia. Therefore, in order to analyze very small deviations from the regular rotation, the smooth behavior of a given band has to be subtracted out. There are many different ways to extract such a smooth reference, ranging from Harris type or higher order polynomial fits, to interpolations of various order through the data points. The advantage of using an interpolation is that the error analysis becomes more straightforward. We have generally adopted second-order interpolation of the  $\gamma$ -ray energies which can take into account also the large dynamic range of  $E_\gamma$  in the  $A \approx 190$  SD bands, yielding the following expression for the  $\gamma$ -ray energy staggering parameter:

$$\Delta E_\gamma(I) = \frac{3}{8} \left( E_\gamma(I) - \frac{1}{6} (4E_\gamma(I-2) + 4E_\gamma(I+2) - E_\gamma(I-4) - E_\gamma(I+4)) \right).$$

The final step in the data analysis involves evaluation of the statistical significance of a possible staggering pattern. There are also here many possible ways to go. We



present one simple method that we have developed. In this method, the signs of the deduced  $\Delta E_\gamma$  values in each band were changed for every other transition, and the new average  $\overline{\Delta E'_\gamma}$  and uncertainty  $\sigma'$  of the altered values were compared with the corresponding values  $\overline{\Delta E_\gamma}$  and  $\sigma$  of the original data. If the staggering is consistent with a random fluctuation, the distributions of the altered values and the original data will be very similar. On the other hand, a statistically significant difference indicates the existence of a staggering. A confidence level C.L. which measures the difference between the two distributions (assumed to be Gaussians) can be defined as:

$$C.L. = \int_{-\infty}^{+\infty} erf(\Delta E_\gamma, \overline{\Delta E_\gamma}, \sigma) \cdot g(\Delta E_\gamma, \overline{\Delta E'_\gamma}, \sigma') d\Delta E_\gamma,$$

where  $erf(\Delta E_\gamma, \overline{\Delta E_\gamma}, \sigma) = \int_{-\infty}^{\Delta E_\gamma} g(x, \overline{\Delta E_\gamma}, \sigma) dx$  and  $g(x, \overline{\Delta E_\gamma}, \sigma)$  is a Gaussian function centered at  $\overline{\Delta E_\gamma}$  with standard deviation  $\sigma$ . Two identical distributions give a confidence level of 0.5; whereas distributions separated by one, two or three standard deviations give confidence levels of 0.76, 0.92 or 0.98, respectively.

### 3 Experiments and data analysis results

High-spin states in the SD nuclei  $^{153}\text{Dy}$  and  $^{194}\text{Hg}$  have been studied with the Gamma-sphere Ge detector array located at the LBL 88-Inch Cyclotron facility. The counting statistics in the two experiments were of the order of  $1 \times 10^9$  and  $5 \times 10^8$  three- and higher-fold events, respectively. The high quality of the data yielded extended spectroscopic information on the known SD bands in both nuclei and in addition we observed two new SD bands which could be assigned to  $^{153}\text{Dy}$ . Furthermore, the accuracy in the determination of the transition energies is higher than that obtained in the previous work on these nuclei due to the greater resolving power achieved with high-statistics high-fold data. Similarly to the  $^{149}\text{Gd}$  case, when analyzing the transition energies carefully we observe evidence for a  $\Delta I = 2$  staggering in SD  $^{194}\text{Hg}$  as well as tentative (see below) evidence for staggering in the yrast SD band of  $^{153}\text{Dy}$ . As in  $^{149}\text{Gd}$ , the effect is very small, of the order of  $10^{-4}$  of the  $\gamma$ -ray transition energies, which is just barely within the limits of the present detector systems.

As mentioned above, the resolving power resulting from a high-fold data set is essential in the analysis of the small staggering effect. In our  $^{194}\text{Hg}$  data set, we obtained sufficiently high statistics and average fold for the yrast SD band in order to obtain accurate transition energies from up to five-fold data. In fact, down to the level of the small observed staggering effect, we obtained transition energies that were consistent between unsubtracted triple- and quadruple-gated spectra and background-subtracted double-gated spectra. This insensitivity to fold and background cuts makes us confident that the measured transition energies of this SD band are not significantly affected by accidental coincidences with contaminating lines. A somewhat similar situation seems to have been the case for the "original"  $^{149}\text{Gd}$  data set. However, for the two excited SD bands in  $^{194}\text{Hg}$ , only background-subtracted double-gated spectra could be used. Since the additional energy uncertainties from

the background subtraction are difficult to determine, it is hard to estimate the reliability of the measured transition energies of these excited SD bands. For the  $^{153}\text{Dy}$  data set the situation is intermediate. In the case of the yrast SD band in  $^{153}\text{Dy}$  a staggering pattern is present in background-subtracted three-fold and four-fold data; however, for the three-fold data the transition energies are somewhat sensitive to varying backgrounds and the statistics in the fourfold data did not allow a definitive study of the effect of varying backgrounds. We have therefore chosen to classify the evidence for  $\Delta I = 2$  staggering in  $^{153}\text{Dy}$  as tentative.

Given the measured  $\gamma$ -ray energies, we have obtained the following results from the simple statistical analysis outlined above. The yrast SD bands in  $^{149}\text{Gd}$  and  $^{194}\text{Hg}$  emerge as by far the most solid candidates for exhibiting a true  $\Delta I = 2$  stagger. If we take into account only statistical contributions to the uncertainties the staggering in these two bands is significant on a  $3\sigma$  level. For the two excited SD bands in  $^{194}\text{Hg}$  an apparent inversion is present in the staggering pattern at  $\hbar\omega = 0.30$  MeV. Since these bands are believed to be built on the same intrinsic configuration it may be justified to take this inversion into account. Only if this is done do we obtain a statistical significance on approximately a  $2\sigma$  level for a staggering in these bands. The observed staggering pattern in the yrast SD band of  $^{153}\text{Dy}$ , with the above reservations concerning the possible additional uncertainties from the background subtraction, has a statistical significance on the  $3\sigma$  level in this analysis. However, because of these potential uncertainties in the measured transition energies, we consider this case as tentative.

This work has been supported in part by U.S. Department of Energy under Contract Nos. DE-AC03-76SF00098, W-31-109-ENG-38 and W-7405-ENG-48.

## References

- [1] L. K. Peker *et al.*, Phys. Rev. Lett. **50**, 1749 (1983)
- [2] S. Flibotte *et al.*, Phys. Rev. Lett. **71**, 4299 (1993).
- [3] B. Cederwall *et al.*, Phys. Rev. Lett. **72**, 3150 (1994).
- [4] I. Hamamoto and B. Mottelson, Phys. Lett. **B333**, 294 (1994).
- [5] I. M. Pavlichenkov, these Proceedings, and to be published.
- [6] A.O. Macchiavelli *et al.*, submitted to Phys Rev. C.
- [7] J.H. Hamilton, these Proceedings.

# Studies of Superdeformation near $N = 80$

S.M. Mullins<sup>†</sup>, G. Hackman<sup>†</sup>, D. Haslip<sup>†</sup>, N.C. Schmeing<sup>†</sup>, H.R. Andrews<sup>†</sup>,  
R.M. Clark<sup>§</sup>, M. Cromaz<sup>¶</sup>, J. DeGraaf<sup>¶</sup>, T.E. Drake<sup>¶</sup>, S. Flibotte<sup>†,‡</sup>,  
A. Galindo-Uribarri<sup>†</sup>, K. Hauschild<sup>%</sup>, I.M. Hibbert<sup>%</sup>, V.P. Janzen<sup>†</sup>, J.A. Kuehner<sup>†</sup>,  
E.S. Paul<sup>#</sup>, S. Pilotte<sup>&</sup>, D.C. Radford<sup>†</sup>, A.T. Semple<sup>#</sup>, J. Tiniar<sup>#</sup>, I. Thorslund<sup>§</sup>,  
P. Vaska<sup>§</sup>, J.C. Waddington<sup>†</sup>, R. Wadsworth<sup>%</sup>, L. Walker<sup>#</sup>, D. Ward<sup>†</sup> and L. Yao<sup>†</sup>.  
<sup>†</sup>*Dept. of Physics and Astronomy, McMaster University, Hamilton, ON L8S 4M1, Canada*  
<sup>‡</sup>*AECL Research, Chalk River Laboratories, Chalk River, ON KOJ 1J0, Canada*  
<sup>§</sup>*Lawrence Berkeley Laboratory, 1, Cyclotron Road, Berkeley, CA 94550, USA*  
<sup>¶</sup>*Dept. of Physics, University of Toronto, Toronto, ON M5S 1A7, Canada*  
<sup>%</sup>*Dept. of Physics, University of York, Heslington, York, YO1 5DD, UK*  
<sup>#</sup>*Oliver Lodge Laboratory, University of Liverpool, P.O. Box 147, Liverpool, L69 3BX, UK*  
<sup>&</sup>*Dept. of Physics, University of Ottawa, Ottawa, ON K1N 6N5, Canada*  
<sup>§</sup>*Dept. of Physics, S.U.N.Y-Stony Brook, Stony Brook, NY 11794, USA*

## Abstract

A superdeformed band has been observed in the  $N = 80$  nucleus  $^{145}\text{Tb}$ . The  $\mathcal{J}^{(2)}$  dynamic moment of inertia shows no evidence for the  $N = 6$  quasiproton alignment that is observed in the isotone  $^{144}\text{Gd}$ . It is suggested that, as in the two lighter isotones  $^{142}\text{Sm}$  and  $^{143}\text{Eu}$ , the proton intruder configuration is  $\pi 6^1$ , so that the alignment that occurs in the  $\pi 6^2$  configuration in  $^{144}\text{Gd}$  is blocked. Evidence for an excited SD band in  $^{142}\text{Sm}$  is presented. The structure of SD bands in the odd-odd nuclei  $^{142}\text{Eu}$  and  $^{144}\text{Eu}$  is also discussed.

## 1 Introduction

The favourability of neutron number  $N = 80$  with respect to superdeformation has long been predicted by mean-field calculations based on either a Nilsson [1] or Woods-Saxon [2] single-particle potential. The calculations show a large energy gap at  $N = 80$  that corresponds to a prolate quadrupole deformation of  $\beta_2 \simeq 0.5$ . Experimental investigations of this prediction initially focussed on the  $Z = 64$   $N = 80$  isotone,  $^{144}\text{Gd}$ . All of these initial forays met without success, which seemed to cast doubt on the predictive power of the calculations. This uncertainty was removed when a superdeformed band was found in  $^{143}\text{Eu}$  ( $Z = 63$ ,  $N = 80$ ) [3]. Since this initial case, superdeformed bands have now been reported in two other  $N = 80$  nuclei, namely  $^{142}\text{Sm}$  [4] and the previously troublesome  $^{144}\text{Gd}$  [5]. We have recently found a superdeformed (SD) band in the next  $N = 80$  isotone,  $^{145}\text{Tb}$  ( $Z = 65$ ) [6]. The assignment of valence-proton configurations in the chain of  $N = 80$  isotones will be discussed below.

The “stability” of the  $N = 80$  gap to the addition or removal of a neutron has also been investigated. We have focussed on  $^{143}\text{Eu}$  as the optimum  $N = 80$  core, and have found SD bands in  $^{142}\text{Eu}$  and  $^{144}\text{Eu}$ . Possible configurations for these bands will be presented.

## 2 Superdeformation in $N = 80$ Nuclei

### 2.1 Yrast Valence-Proton Configurations in $N = 80$ SD Bands

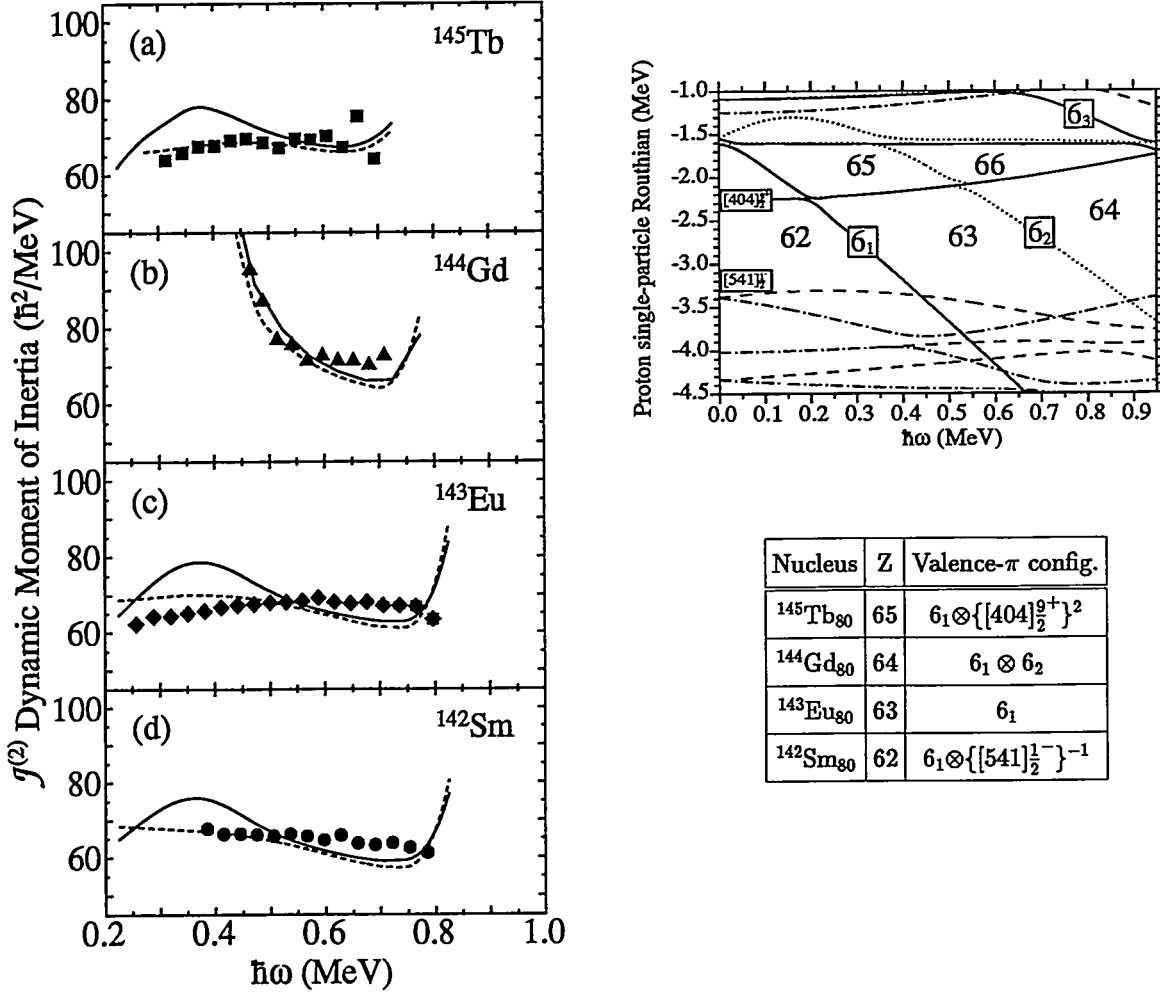


Figure 1: *left*:  $\mathcal{J}^{(2)}$  moments of inertia for the yrast  $N = 80$  SD bands; *right*: proton-routhians appropriate for the  $N = 80$  SD bands; *table*: suggested valence-proton configurations.

A superdeformed band has been observed in  $^{145}\text{Tb}$  with the  $8\pi$  spectrometer [6]. The  $\mathcal{J}^{(2)}$  dynamic moment of inertia derived from the band is shown in figure 1, together with those from the three other  $N = 80$  SD bands. Inspection suggests that the proton band-crossing that causes the rise in the  $\mathcal{J}^{(2)}$  of  $^{144}\text{Gd}$  is blocked in  $^{143}\text{Eu}$ ,  $^{142}\text{Sm}$  and now  $^{145}\text{Tb}$  as well. Cranked Woods-Saxon calculations [2] predict that the band-crossing in  $^{144}\text{Gd}$  is due to the first pair of  $N = 6$  quasiprotons, so that the band has a  $\pi 6^2$  intruder configuration. The occupancy of the first  $N = 6$  orbital in  $^{143}\text{Eu}$  and  $^{142}\text{Sm}$  blocks the crossing. The absence of the crossing in  $^{145}\text{Tb}$  suggests that the intruder configuration is either  $\pi 6^1$  or  $\pi 6^3$ . Single-proton routhians appropriate for the  $N = 80$  SD bands are also shown in figure 1. Important orbitals and particle numbers have been labelled. It is suggested that in  $^{145}\text{Tb}$  only the first proton-intruder is occupied, and that the sixty-fourth and sixty-fifth protons reside in the  $g_{9/2}[404]9/2^+$  orbital. This is indicated in the table in figure 1, together with the valence-proton configurations for the other  $N = 80$  SD bands.

## 2.2 Excited Superdeformed Band in $^{142}\text{Sm}$

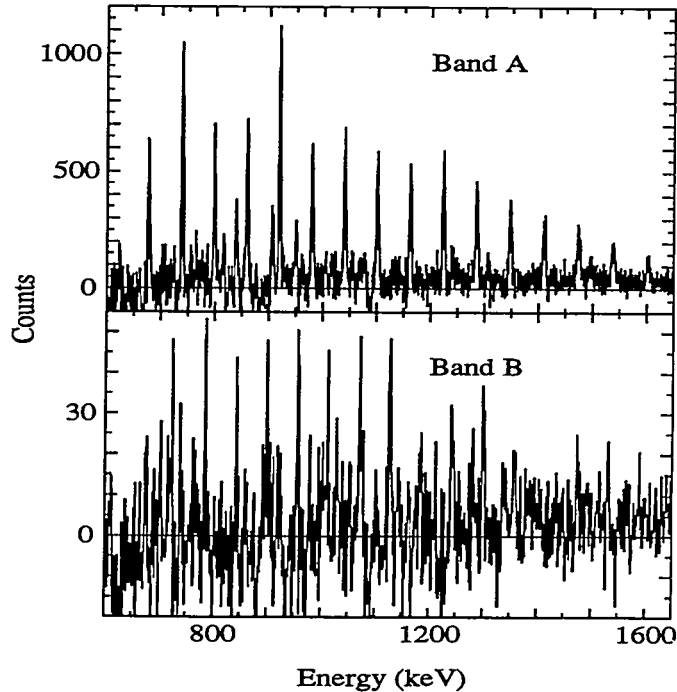


Figure 2: Superdeformed bands in  $^{142}\text{Sm}$ .

In a recent experiment led by the University of York, excited SD bands were searched for in  $^{142}\text{Sm}$ . States in  $^{142}\text{Sm}$  were populated with the  $^{124}\text{Sn}(^{24}\text{Mg},6n)^{142}\text{Sm}$  reaction at a beam energy of 145 MeV. Triple and higher-fold  $\gamma$ -ray coincidences were obtained with the GAMMASPHERE spectrometer. Analysis of the data enabled confirmation of two previously tentative transitions in the yrast band (A), and a two further transitions were added, as shown in figure 2. A search of the four-fold data indicated the existence of another superdeformed band (B) also shown in figure 2. We assign this as an excited SD band in  $^{142}\text{Sm}$ . Since the transition energies do not bear any simple relationship to those in a neighbouring SD band, we are unable to give a straightforward interpretation to the band.

## 2.3 Neutron Pairing at the $N = 80$ SD Shell Gap

In the three cases where the  $N = 6$  quasiproton is blocked, there is no evidence for the predicted  $N = 6$  quasineutron crossing [2]. This crossing is responsible for the hump in the calculated  $\mathcal{J}^{(2)}$  moments of inertia for  $^{142}\text{Sm}$ ,  $^{143}\text{Tb}$  and  $^{145}\text{Tb}$  delineated by the full lines in figure 1. Previously this was interpreted as evidence for a strong residual  $n$ - $p$  interaction between the proton-intruder and the aligning quasineutrons. An alternative explanation is that the neutron-pairing correlations are essentially quenched due to the large gap at  $N = 80$ . When the moments of inertia are recalculated with the neutron-pairing gap set to zero, the hump is removed and a better agreement with the data is achieved. This can be seen from the dashed lines in figure 1.

### 3 Superdeformation in $^{144}\text{Eu}$ and $^{142}\text{Eu}$

#### 3.1 Three Superdeformed Bands in $^{144}\text{Eu}$

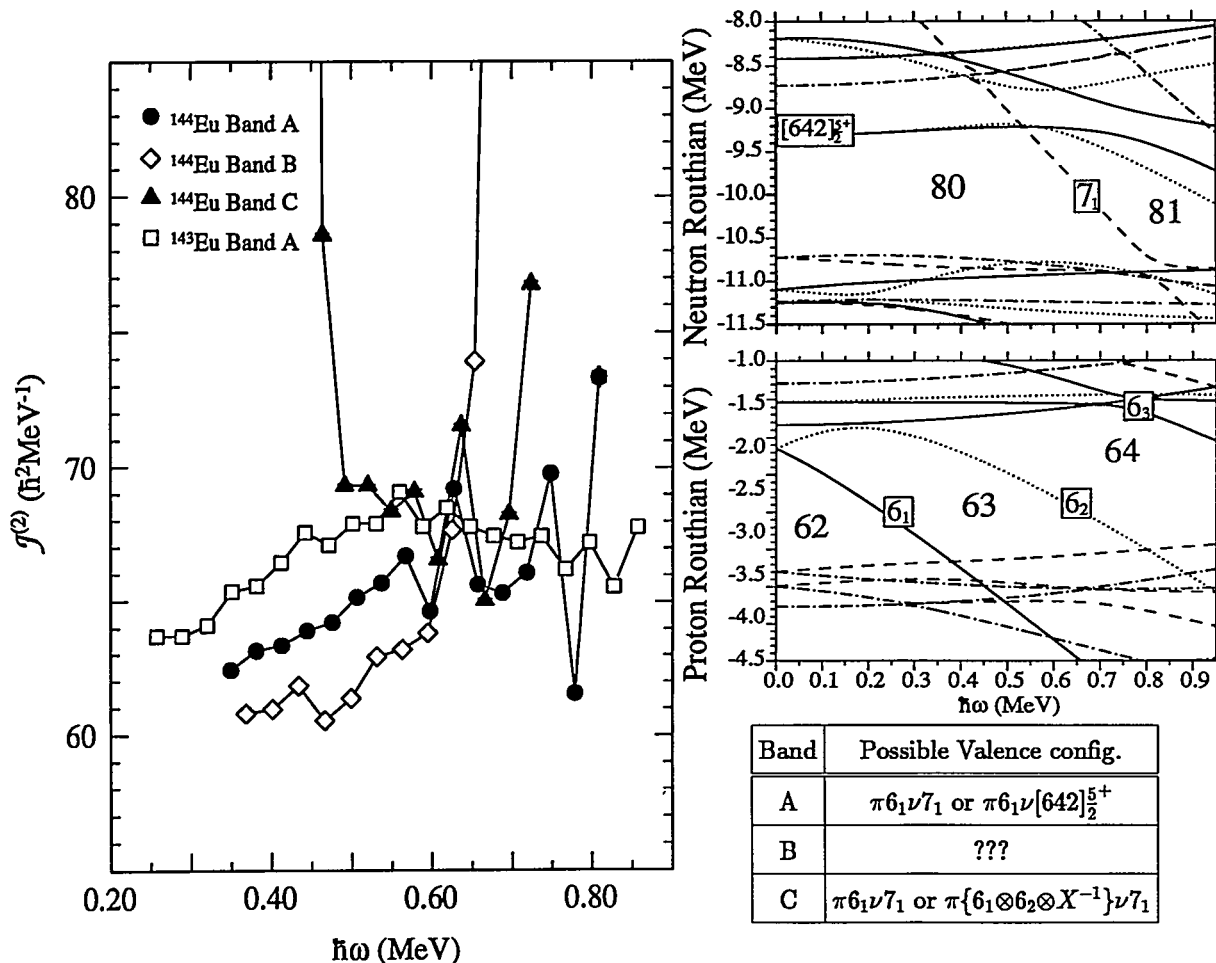


Figure 3: *left:*  $\mathcal{J}^{(2)}$  moments of inertia for the SD bands in  $^{144}\text{Eu}$ ; *right:* single-particle routhians for  $^{144}\text{Eu}$ ; *table:* possible valence configurations for bands A and C in  $^{144}\text{Eu}$ .

Three SD bands have been found in  $^{144}\text{Eu}$  from a recent experiment with the GAMMASPHERE spectrometer. One of the bands (C) is a confirmation of a candidate found with the  $8\pi$  spectrometer [7]. The same reaction was used as in [7], namely  $^{122}\text{Sn}(^{27}\text{Al}, 5n)^{144}\text{Eu}$  at a beam-energy of 142 MeV. The moments of inertia for the three bands are shown in figure 3, where they are compared with  $^{143}\text{Eu}$ . The single-particle routhians for both protons and neutrons, appropriate for  $^{144}\text{Eu}$ , shown in figure 3 suggest that the yrast intruder-configuration should be  $\pi 6_1 \nu 7_1$ . It is not clear at present whether band A or band C has this configuration. The rapid rise in the  $\mathcal{J}^{(2)}$  of band C is at  $\hbar\omega \simeq 0.45$  MeV is suggestive of the  $N = 6$  quasiproton crossing that is observed in  $^{144}\text{Gd}$ . If this is so, then band C must be a proton-excitation, with the  $\pi 6_2$  orbital occupied. Band A has a lower  $\mathcal{J}^{(2)}$  than the  $^{143}\text{Eu}$ -core, which is expected to have a smaller deformation than the  $\nu 7_1$  configuration. Band B has an even lower  $\mathcal{J}^{(2)}$  and appears to suffer a band-crossing at  $\hbar\omega \simeq 0.65$  MeV. Further calculations are in progress to aid with the interpretation of these bands.

### 3.2 Superdeformed Band in $^{142}\text{Eu}$ : Hole in the $N = 80$ Closed Shell

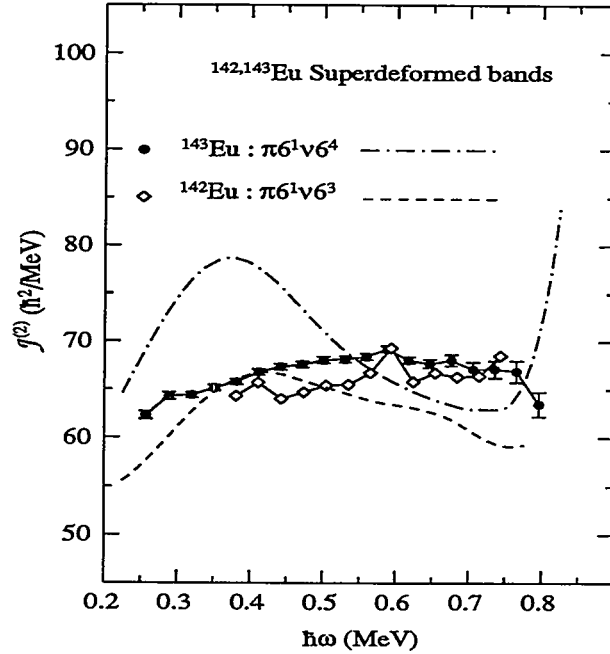


Figure 4:  $J^{(2)}$  moment of inertia for the SD band in  $^{142}\text{Eu}$ , compared with  $^{143}\text{Eu}$ .

An SD band has been found in  $^{142}\text{Eu}$  with the  $8\pi$ -spectrometer following the reaction  $^{120}\text{Sn}(^{27}\text{Al}, 5n)^{142}\text{Eu}$  at a beam-energy of 152 MeV. The lack of a signature-partner suggests that the hole in the  $N = 80$  closed-shell probably occurs in the the  $\nu 6_4$  orbital. The  $J^{(2)}$  moment of inertia is compared with  $^{143}\text{Eu}$  and theory in figure 4. Note that this band is different to the one recently published [8] by the GA.SP collaboration.

## 4 Summary

The valence-proton configurations in the  $N = 80$  chain of SD bands have been understood in a systematic way in terms of the Cranked Woods-Saxon model. An excited SD band has been assigned to  $^{142}\text{Sm}$ , the first such case in an  $N = 80$  nucleus. SD bands have also been found in the isotopes either side of  $^{143}\text{Eu}$ , one band in  $^{142}\text{Eu}$  and three bands in  $^{144}\text{Eu}$ .

We thank the staff at TASSC and the 88" Cyclotron. This work was supported by NSERC (Canada), AECL Research, the D.O.E., the N.S.F and N.A.T.O.

## References

- [1] Tord Bengtsson and Ingemar Ragnarsson *Nucl.Phys.* **A436**, 14 (1985)
- [2] W.Nazarewicz, R.Wyss and A.Johnson, *Nucl.Phys.* **A503**, 285 (1989)
- [3] S.M.Mullins *et al.*, *P.R.Lett.* **66** 1677 (1991); A.Ataç *et al.*, *P.R.Lett.* **70**, 1069 (1993)
- [4] G.Hackman *et al.*, *P.R.* **C47** R433 (1993)
- [5] S.Lunardi *et al.*, *P.R.Lett* **72** 1427 (1994)
- [6] S.M.Mullins, N.C.Schmeing *et al.*, *Phys.Rev.C* (1994) submitted
- [7] S.M.Mullins *et al.*, *Z. für Physik* **A346** 327 (1993)
- [8] A.Ataç *et al.*, *Z. für Physik* **A348** 251 (1994)

# HYPERDEFORMATION IN $^{152}\text{Dy}$

## FROM PROTON-GAMMA COINCIDENCE EXPERIMENTS

M. Lunardon, D. Bazzacco, F. Brandolini, R. Burch, D. Fabris, S. Lunardi,  
N.H. Medina, G. Nebbia, P. Pavan, C. Rossi-Alvarez, G. Viesti

*I.N.F.N. and Dipartimento di Fisica dell'Università di Padova  
I-35131 Padova, Italy*

G. de Angelis, M. Cinausero, M. De Poli, E. Fioretto, E. Farnea, D.R. Napoli,  
G. Prete, J. Rico, P. Spolaore, G. Vedovato

*I.N.F.N. Laboratori Nazionali di Legnaro  
I-35020 Legnaro ( Padova ), Italy*

### ABSTRACT

The hyperdeformed ridge structure with  $\Delta E_\gamma = \pm 30$  keV, recently observed in the reaction 187 MeV  $^{37}\text{Cl} + ^{120}\text{Sn}$ , has been confirmed in a new proton- $\gamma$  coincidence experiment and assigned to the  $^{152}\text{Dy}$  nucleus.

The first experimental evidence for hyperdeformed ( HD ) nuclear shape ( axis ratios 3:1 ) was the observation of a ridge structure in a  $\gamma$ - $\gamma$  coincidence matrix in the reaction 187 MeV  $^{37}\text{Cl} + ^{120}\text{Sn}$  [1]. In that experiment the separation of the ridges from the diagonal was measured to be  $\Delta E_\gamma = E_{\gamma 1} - E_{\gamma 2} = \pm 30 \pm 3$  keV which corresponds to a dynamical moment of inertia  $J^2 \approx 130 \hbar^2 \text{ MeV}^{-1}$ . The ridges at  $\pm 30$  keV have been observed only when a coincidence with a proton was required, as suggested in Ref. 2. A cascade of 10 discrete lines with an average energy spacing of 30 keV was also proposed in the same experiment which anyway could not be conclusive for the assignment of the HD structure to a specific Dy isotope (  $^{152}\text{Dy}$  or  $^{153}\text{Dy}$  ). We report here results of new proton-gamma coincidence experiments using the  $^{37}\text{Cl} + ^{120}\text{Sn}$  reaction which we have performed with the aim to confirm the earlier observation and to further study the HD ridge.

Two experiments have been performed at the XTU Tandem facility of Legnaro using the GASP spectrometer [3] in coincidence with different ancillary detectors. In the first experiment charged particles have been detected using a light particle hodoscope (LPH) consisting of 8 silicon detectors, 300  $\mu\text{m}$  thick, having an area of 6 cm  $\times$  4 cm each. The detectors were closely packed to form a 18 cm  $\times$  18 cm wall which was placed 8 cm from the target in the forward hemisphere. Particles emitted at  $\theta_{lab} \approx 10^\circ - 50^\circ$  were detected with a geometrical efficiency of  $\approx 90\%$ .



Approximately  $8 \times 10^8$  events, consisting of triples or higher fold Ge-coincidences with multiplicity  $k > 3$  on the BGO ball, were collected in a 8 days run at 187 MeV bombarding energy ( beam intensity 1-3 pA, targets of  $2 \times 500 \mu\text{g}/\text{cm}^2$  foils of  $^{120}\text{Sn}$ ). From those events only  $2.5 \times 10^7$  were in coincidence with protons, because of the limited solid angle covered by the LPH and of the low cross section of the *xpyn* channels ( $\approx 20\%$  of the total evaporation residue yield). A second experiment has been very recently performed using the ISIS  $4\pi$  charged particle detector ( 40  $\Delta E$ -E telescopes ) at 187 and 192 MeV bombarding energies. The data analysis of the ISIS experiment is in progress. We report here mainly results from the first experiment.

Using different gating conditions on the  $\gamma$ -ray sum energy  $H$  and fold  $k$  registered in the BGO ball, various  $\gamma$ - $\gamma$  matrices were produced from the proton-gated triples Ge-data. Cuts perpendicular to the main diagonal  $E_{\gamma 1} - E_{\gamma 2}$  were subsequently made on these  $\gamma$ - $\gamma$  matrices in order to observe the ridges corresponding to deexcitations of the final nuclei along particular rotational structures.

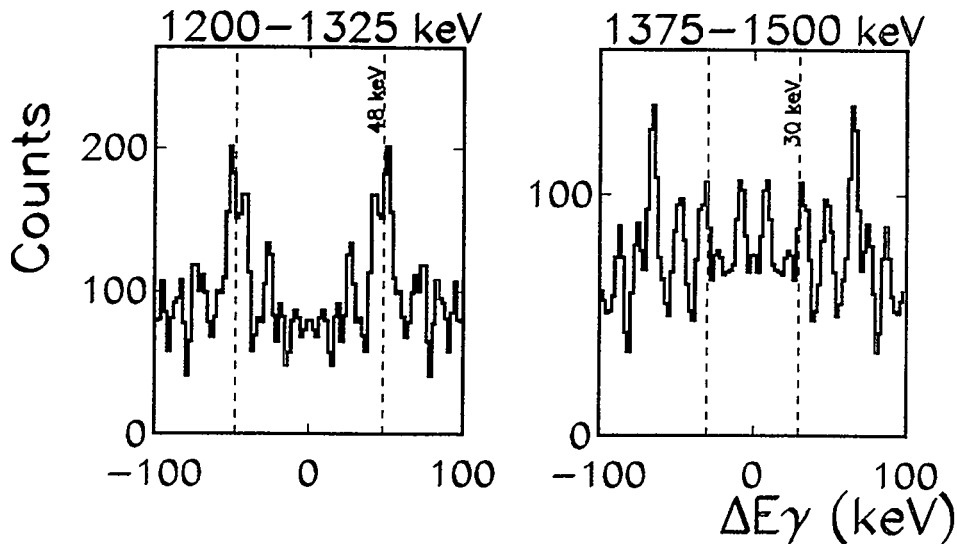


Fig.1 Diagonal cuts in the  $H > 14$  MeV,  $k > 10$  matrix

With a cut in the energy range  $1200 \leq (E_{\gamma 1} + E_{\gamma 2})/2 \leq 1325$  keV we clearly see the well known ridge located at 48 keV from the diagonal ( see Fig. 1a), resulting from transitions between rotational levels of SD bands. Known discrete transitions of the  $^{152}\text{Dy}$  [4],  $^{153}\text{Dy}$  [5] SD bands lie in the energy region considered. We could observe in our data only the discrete transitions of the yrast SD band of  $^{152}\text{Dy}$ . The transitions which are inside the cut limits account for  $\approx 40\%$  of the total  $\pm 48$  keV ridge intensity. As in Ref. 1, we made also a cut in the energy range  $1375 \leq (E_{\gamma 1} + E_{\gamma 2})/2 \leq 1500$  keV. In the resulting spectrum shown if Fig.

1b many ridges are observed, among them one at  $\Delta E_\gamma = \pm 32 \pm 3$  keV. A two dimensional correlation technique has been used in order to check if this ridge is due to a rotational cascade based on an hyperdeformed nuclear shape. Through this grid search we have found that the part of the 32 keV ridge at  $\Delta E_\gamma = 30$  keV is due to events correlated in a rotational sequence. Fig. 2 shows the results of this analysis. After summing six diagonal cuts, each 5 keV wide, separated by 30 keV in the  $E_\gamma \geq 1250$  keV region we observe an enhancement of the 30 keV ridge when the N cuts are at some definite energies. Fig. 2a reports the area of the 30 keV ridge as a function of the energy of the first cut  $(E_{\gamma 1} + E_{\gamma 2})/2$ . The maxima at cut energies  $\approx 1278 + (N \times 30)$  keV suggest the presence of a rotational cascade with  $\Delta E_\gamma = 30$  keV and with transition energies  $\approx 1263 + (N \times 30)$  keV. Such energies are compatible with those proposed for the members of the HD band [1].

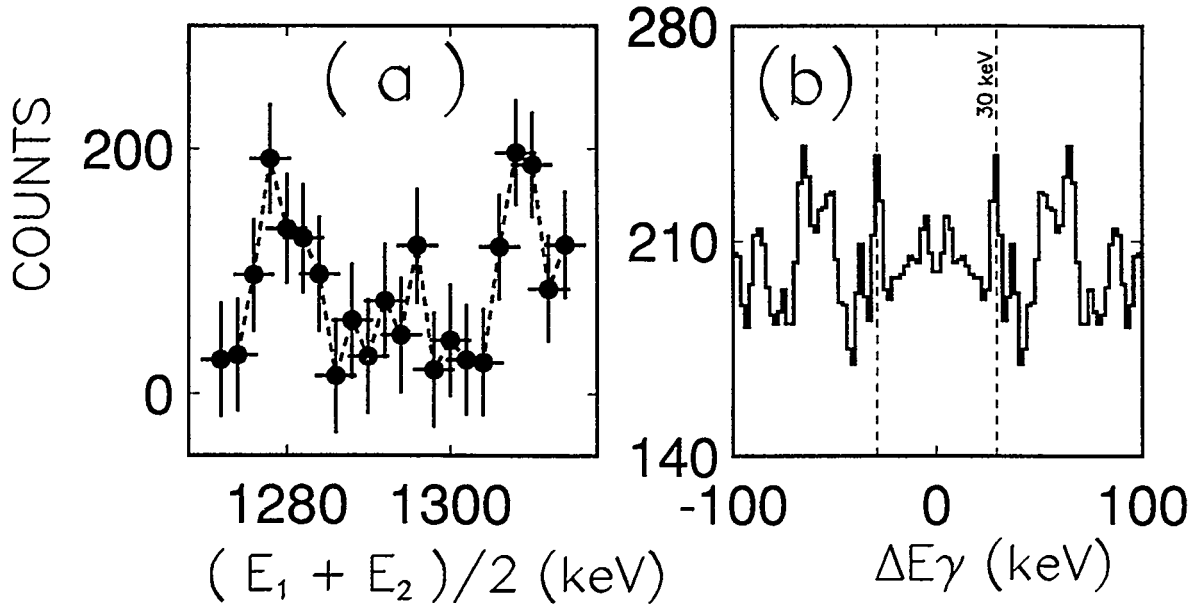


Fig.2 a) Area of the 30 keV ridge in the spectra obtained summing six diagonal cuts 5 keV wide and separated by 30 keV ( $H > 14$  MeV and  $k > 10$ ). b) The spectrum obtained when summing the six cuts described in a) at the positions of the maximum.

Of course the energy difference between consecutive cuts has been also varied, but the 30 keV ridge is clearly observed only when the just mentioned conditions ( $\Delta E_\gamma = 30$  keV and first cut at 1278 keV) are satisfied, as shown in Fig. 2b. We stress that the yield of the ridge with this condition is distributed rather uniformly over all the six cuts. With other conditions we find that the main part of the ridge intensity is due to the contribution of only a pair of cuts, suggesting the presence of strong discrete transitions which contribute to the  $\Delta E_\gamma = \pm 32$  keV ridge in the energy range  $1375 \leq (E_{\gamma 1} + E_{\gamma 2})/2 \leq 1500$  keV. With this procedure we have

spanned the  $24 \leq \Delta E_\gamma \leq 55$  keV region obtaining similar results also in the case of the superdeformed ridge at 48 keV ( i.e. maximum intensity when the energy difference between cuts is 48 keV and the position of the first cut correspond to one of the transition energies of the yrast SD band of  $^{152}\text{Dy}$ ). We could therefore compare the intensity of the HD ridge to that of the superdeformed one. A relative intensity of HD:SD of  $\approx 10\%$  has been extracted.

We have also analysed our data in order to assign the 30 keV ridge to one of the two Dy isotopes (  $^{152}\text{Dy}$  or  $^{153}\text{Dy}$  ). From the  $(2k)^3$  symmetrized cube in coincidence with protons we have produced  $\gamma - \gamma$  matrices setting gates on the prominent discrete lines of the different Dy isotopes. As shown in Fig. 3, the hyperdeformed ridge is clearly visible in the matrix with no conditions on the third gamma ( see Fig. 3a) which accounts for  $5.2 \times 10^7$  events. When gating on the prominent lines of  $^{152}\text{Dy}$  above the  $17^+$  isomer ( $\tau=60$  ns ), a matrix with only  $3.4 \times 10^6$  events is obtained. Despite the reduced statistics, the ridge stands clearly as shown in Fig. 3b. Only few counts are present at  $\Delta E_\gamma = \pm 30$  keV in the matrices obtained with gates on other Dy isotopes. This indicates that the proposed HD bands which originate the ridge at  $\Delta E_\gamma = \pm 30$  keV are in  $^{152}\text{Dy}$ . The cross section of those HD bands is estimated to be  $\sigma_{HD} \sim 50 \mu\text{b}$ , less than  $1 \times 10^{-4}$  of the total evaporation residue cross section.

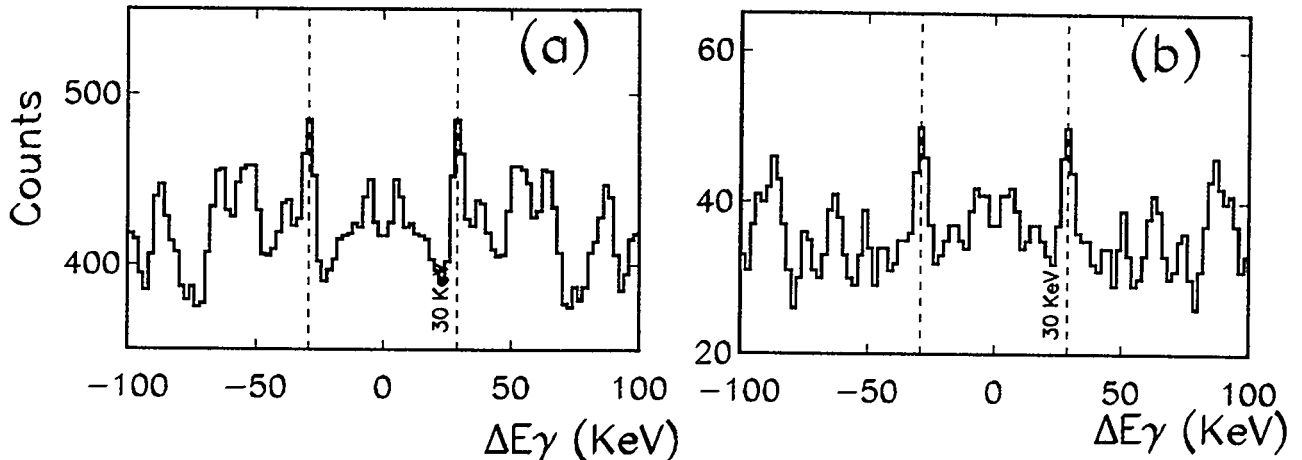


Fig.3 The 30 keV ridge in the spectra obtained a) without and b) with gates on the prominent gamma lines of  $^{152}\text{Dy}$  (  $k > 5$ ).

In recent calculations for  $^{152}\text{Dy}$  the HD minimum appears at spin  $60 \hbar$  and becomes yrast at spin  $\approx 80-90 \hbar$  [2]. It is therefore very interesting to study the conditions for which such extremely high spin values may be sustained by nuclei

in elongated shapes without fissioning. Octupole correlations have been found [6] to be very large at hyperdeformed shapes for nuclei of the  $A=150$  region. A stable minimum is predicted for  $^{152}\text{Dy}$  at  $\beta_2 = 0.93$  and  $\beta_4 = 0.13$ . Calculations of the moments of inertia give a  $J^{(2)}$  value of  $130 \hbar^2 \text{ MeV}^{-1}$ , very similar to the rigid-body moment of inertia and also in perfect agreement with the one extracted from the experimental data.

In the 187 MeV  $^{37}\text{Cl}+^{120}\text{Sn}$  reaction, the  $^{157}\text{Ho}$  compound nucleus is populated at  $E_x=84$  MeV excitation energy with a critical angular momentum  $J_{crit}=77\hbar$ . From systematics we derive that the boundary between evaporation and fission is around  $J\sim 70$ , being the fission channel centered around  $\langle J^{fiss} \rangle = 74\hbar$ . Therefore the proposed range  $62-82 \hbar$  for the observed HD ridge [1] strongly overlaps with the fission region and extends up to the highest partial waves populated in the fusion reaction. Preliminary results from the 192 MeV bombarding energy show that the yield of the SD yrast band in  $^{152}\text{Dy}$  slightly decreases respect to the lower bombarding energy. This effect is well known and demonstrates that the entry states populating those structure are defined by the fission-evaporation competition. We found that the observation of the HD ridge is also more difficult at the higher energy due to the increased background. Furthermore the inspection of the proton spectra in coincidence with the HD ridge at  $E_{beam}=187$  MeV strongly suggests that charged particles are emitted first in the  $p4n$  decay chain increasing the probability of surviving fission [7]. The importance of the proton emission in increasing the survival probability of deformed states as well as in tagging the Dy channels, is also demonstrated by recent unsuccessful searches of the HD ridge in  $xn$  decay channels [8].

With the high statistics obtained in the recently performed GASP-ISIS experiments we hope to obtain a deeper insight in the HD phenomena in the Dy region and to clarify the population mechanisms of evaporation residues at extreme angular momenta where fission dominates.

- 1) A. Galindo-Uribarri et al., Phys. Rev. Lett. **71** (1993) 231.
- 2) J. Dudek, T. Werner and L. L. Riedinger, Phys. Lett. **B211** (1988) 252.
- 3) D. Bazzacco, in Proc. Intern. Conf. on Nuclear Structure at high angular momentum ( Ottawa 1992 ), Vol. 2, Proceedings AECL 10613.
- 4) P. J. Twin et. al., Phys. Rev. Lett. **57** (1986) 811.
- 5) J. K. Johansson et. al., Phys. Rev. Lett. **63** (1989) 2200.
- 6) S. Aberg, Nucl. Phys. **A557** (1993) 17c.
- 7) M. Lunardon et al., in Proc. Fifth Intern. Conf. on Nucleus-Nucleus Collisions ( Taormina 1994 ), to be published in Nucl. Phys.
- 8) A. Galindo-Uribarri, private communication.

# INTRINSIC VORTICITY IN RAPIDLY ROTATING NUCLEI

P. QUENTIN /1,2/ and I.N. MIKHAILOV /3,4/

/1/ CENBG (IN2P3-CNRS and Université Bordeaux-1), Gradignan, France

/2/ Theory Group, Nucl. Sci. Div., LBL, Berkeley, California, USA

/3/ Bogolyubov Lab. Theor. Phys. (JINR), Dubna, Russia

/4/ CSNSM (IN2P3-CNRS), Orsay, France

**ABSTRACT:** *Using a formal analogy between canonical (local) point transformations in Classical Mechanics and specific unitary transformations in Quantum Mechanics, we have generalized the usual routhian or cranking approach for global rotations to allow the study of a variety of collective modes. It is applied here to the coupling of a global rotation with a uniform intrinsic vortical motion in the aligned case, analogous to the flow motion in classical S-type Riemann ellipsoids. The semiclassical approximation of the corresponding stationary solutions in the Hartree-Fock limit gives the classical Riemann results at the Thomas-Fermi level together with small corrections at order  $\hbar^2$ . In a simple quadratic energy limit, it is demonstrated that the quantal results may yield a staggering in rotational bands similar to what has been recently found experimentally in  $^{159}\text{Dy}$  and  $^{194}\text{Hg}$ .*

In the classical hamiltonian formalism, a local point transformation implies the adjunction to the hamiltonian of a generating function of the type  $\alpha \cdot \mathbf{p}$  where  $\mathbf{p}$  is the moment and  $\alpha$  a vector field depending only on the position. Upon associating a collective motion to such a transformation, the corresponding velocity field  $\mathbf{u}$  is exactly  $-\alpha$ , as it has been demonstrated in ref. 1. There, it has also been shown that the unitary Thouless transformations of one-body density matrices where the time-dependence is factorized out and which are linear in  $\mathbf{p}$ , can be considered as quantal analogs of the local point transformations. These unitary transformations yield an extra hamiltonian term in the TDHF equation of motion which is precisely of the above  $\alpha \cdot \mathbf{p}$  type. The corresponding stationary problem is therefore cast into a variational form :

$$\delta \langle h(\rho) + \alpha \cdot \mathbf{p} \rangle = 0 \quad (1)$$

where  $h(\rho)$  is the Hartree-Fock field depending on the density matrix  $\rho$  of its solution. Considering  $-\alpha$  as the quantal analog of the collective velocity associated to the considered motion is fostered by the fact that in the Thomas-Fermi limit the current associated with the solution of eq. (1) may be written as

$$\mathbf{j}(\mathbf{r}) = -\frac{\hbar}{m} \rho(\mathbf{r}) \alpha(\mathbf{r}) \quad (2).$$

Now, we assume that the collective flow is a combination of a global rotation of angular velocity  $\Omega$  with a uniform intrinsic vortical motion defined by a "vortical angular velocity"  $\omega$ , aligned with  $\Omega$ , e.g. along the z-axis. Namely, the components on the principal axis of the field  $\mathbf{u} = -\alpha$  in the inertial frame, are:

$$u_x = -(\Omega + \omega q)y, \quad u_y = \left(\Omega + \frac{\omega}{q}\right)x, \quad u_z = 0 \quad (3)$$

where  $q$  is the ratio of some characteristic lengths  $a_x, a_y$  in the  $x$  and  $y$  directions respectively. This field is a particular solution of the well known classical Dirichlet problem defined by the most general linear field bounded by an ellipsoidal surface as studied by Riemann and Chandrasekhar [2] and currently applied for the study of the equilibrium shapes of celestial objects [3]. Using such a linear velocity field in Nuclear Physics had been already proposed by Cusson [4] and extensively analysed by Rosensteel [5,6] in the limit where the shape parameters are fixed. Upon solving the generalized cranking problem of eq. (1), one gets the total laboratory energy  $E$  as a function of  $\Omega$  and  $\omega$ . Even though the study of the most general case is possible and has been sketched in ref. 1, we will here only illustrate the dynamical motion under study, in the particular case where  $E$  is a quadratic function of  $\Omega$  and  $\omega$  :

$$E(\Omega, \omega) = \frac{1}{2} A \omega^2 + B \omega \Omega + \frac{1}{2} C \Omega^2 \quad (4)$$

where  $A, B$  and  $C$  are inertia parameters resulting from the variational calculation of eq. (1). Defining two functions  $I$  and  $J$  of  $\Omega$  and  $\omega$ , and their inverses, such that

$$\frac{\partial E}{\partial I} = \Omega, \quad \frac{\partial E}{\partial J} = \omega \quad (5),$$

one then gets

$$I = B\omega + C\Omega, \quad J = A\omega + B\Omega \quad (6)$$

$$E(I, J) = \frac{1}{AC - B^2} \left( \frac{A}{2} I^2 - B IJ + \frac{C}{2} J^2 \right) \quad (7).$$

One may now define the yrast line by imposing

$$\left. \frac{\partial E}{\partial J} \right|_I = 0 \quad (8)$$

which leads readily to

$$J_{yrast} = \frac{B}{C} I, \quad E_{yrast} = \frac{I^2}{2C} \quad (9).$$

Thus,  $E_{yrast}$  assumes exactly the pure rotor value. Was it therefore necessary to introduce a new degree of freedom to describe the yrast line?. It is crucial at this point to introduce the quantification of this classical model, in particular the quantification of

J, suggested from intuitive arguments in ref. 7, and later substantiated by a group-theoretical analysis in ref. 8. Indeed, J is found to commute with H and to satisfy :

$$[J, \Theta] = 0, \quad [J, \theta] = \frac{\hbar}{i} \quad (10)$$

where  $\Theta$  and  $\theta$  are the angles associated with the rotations of which  $\Omega$  and  $\omega$  respectively, are the angular velocities. Equations (10) lead to the following form for the operator associated to J :

$$\hat{J} = \frac{\hbar}{i} \frac{\partial}{\partial \theta} \quad (11).$$

The quantization of J results, as in the case of the angular momentum I, from the matching of the corresponding wavefunction at the end points of the definition domain for the angle  $\theta$ . If a left-right reflection symmetry ( $C_2$ ) is present, then J will be quantified by two units of  $\hbar$ . As a consequence,  $J_{yrast}$  is now given by

$$J_{yrast} = 2\hbar \left[ \frac{B}{C} \frac{I}{2\hbar} \right] \quad (12)$$

where  $[x]$  stands for the integer part of x. The plot of the energy  $E(I)$  as a function of I, is a collection of points located on displaced identical parabolas, each corresponding to a given value of J :

$$E(I, J) = \frac{J^2}{2A} + \frac{1}{2} \frac{A}{AC - B^2} \left( I - \frac{B}{A} J \right)^2 \quad (13),$$

$$E(I, J) = \frac{I^2}{2C} + \frac{1}{2} \frac{C}{AC - B^2} \left( J - \frac{B}{C} I \right)^2 \quad (14).$$

The yrast energy parabola given by eq. (9) is the envelope of these parabolas. Now the true quantal yrast line is made of pieces of parabolas each corresponding to a given value of J. Neglecting the residual interactions beyond the model collective hamiltonian of eq. (7), it then appears that this yrast line presents kinks at each parabola crossing. These kinks will result in irregularities in the yrast line transition energies. The periodicity in I of the contact of each J-parabola with the envelope is given by  $\Delta I = (2C)/B$ . Now, if  $(B/C) = 1/2$ , one gets for the yrast line energy

$$E_{yrast} = \frac{I^2}{2C} + \frac{2}{4A - C} \left( 2 \left[ \frac{I}{4} \right] - \frac{I}{2} \right)^2 \quad (15)$$

which exhibits a  $\Delta I = 4$  structure, i.e. a staggering of the energies which has recently found experimentally for some rotational bands in super deformed nuclear states [9,10]

for which alternative explanations involving the  $Y_{44}$  collective degree of freedom have also been invoked [9,11,12]. A stringent test of these speculations merely based on energies, is clearly provided by the assessment of electromagnetic properties. In our case, does the fragmentation of the yrast line into several parabolic cusps prevent such a set of states to constitute a band whose members are linked by strong E2 transitions ? Let us answer this question in the idealized case of a  $\Delta I = 4$  energy structure as given by eq.(15). It is likely that the residual interaction will mix for a given value of I, the unperturbed yrast state and its closest neighbour, as for instance

$$|I\rangle_{yrast} = \alpha |I, J_0\rangle + \sqrt{1-\alpha^2} |I, J_0+2\rangle \quad (16)$$

$$|I-2\rangle_{yrast} = \beta |I-2, J_0\rangle + \sqrt{1-\beta^2} |I-2, J_0+2\rangle \quad (17)$$

with obvious notation. It may be proven [1] that the Poisson bracket of J with an E2 perturbative electromagnetic field is vanishing. Therefore in the quantal case, the J value is not affected by this supplementary field, so that between two yrast states with spins I and I-2, the E2 transition probability will write

$$\langle I|O(E2)|I-2\rangle = \left( \alpha\beta + \sqrt{(1-\alpha^2)(1-\beta^2)} \right) X \quad (18)$$

where X is some matrix element involving the intrinsic state common to both states. If one assumes I to be a spin where parabola crossing occurs and that the mixing is maximum there (i.e.  $\alpha^2 = 0.5$ ) and if one also estimates the mixing for the other spin to be reasonably weak (for instance  $\beta^2 = 0.9$ ), one gets a quenching factor for the relevant matrix element of  $\sim 0.9$ , which is within the experimental error bars from lifetime measurements in superdeformed states [13]. As a conclusion on this, our hypothesis for the staggering is not contradicted by the present status of electromagnetic properties measurements. Let us also mention that from eq. (6), one may find for a set of given J states, a collective alignment given by  $(B/A) J$ , since

$$I = \left( C - \frac{B^2}{A} \right) \Omega + \frac{B}{A} J \quad (19).$$

We will now provide some semiclassical estimates of the various inertia parameters A, B and C. For that purpose, we have used the theoretical method developed in ref. 1, corresponding to a semiclassical expansion of the solution of eq. (1) when using a full-fledged Skyrme effective interaction. This approach is a generalization of what has been done in ref. 14 only for the routhian case. The density will be schematically described as being constant and bounded by a sharp edged ellipsoid whose semi axes are given by

$$a_x = a_0 q^{2/3}, \quad a_y = a_z = a_0 q^{-1/3} \quad (20)$$



where  $a_0$  is given in terms of the total number of particles  $N$  and of the usual size parameter  $r_0$ , by  $a_0 = r_0 A^{1/3}$ , whereas  $q$  is the ratio of  $a_x$  and  $a_y$ . We will also use below the following unit of angular momentum

$$\gamma = \frac{2}{5} m r_0^2 N^{5/3} q^{1/3} \quad (21)$$

which is nothing but the rigid body moment of inertia for a sphere multiplied by the shape factor  $q^{1/3}$ . The various inertia parameters are given below to order  $\hbar^2$  (the first terms being the Thomas-Fermi estimates) :

$$A = \gamma R \left[ 1 - \left( \frac{D}{\gamma} \right) R \right], B = \gamma \left[ 1 - \left( \frac{D}{\gamma} \right) R \right], C = \gamma R \left[ 1 - \left( \frac{D}{\gamma R} \right) \right] \quad (22)$$

where  $R$  is a geometrical factor given by  $R = 1/2 (q + 1/q)$  and the dimensionless semiclassical expansion factor  $D/\gamma$  is approximated within a simplified model in terms of the effective mass in nuclear matter  $(m^*/m)_{NM}$  by

$$\frac{D}{\gamma} = 5 \left( \frac{8}{9\pi} \right)^{2/3} \left( m^*/m \right)_{NM}^{-1} N^{-2/3} \quad (23)$$

(note that its inverse surface dependence makes  $D/\gamma$  small with respect to 1 in heavy nuclei). The contact periodicity in  $I$  is given by

$$\frac{2C}{B} = 2R \left[ 1 + \left( \frac{D}{\gamma} \right) (R^2 - 1) \right] \quad (24).$$

From eq. (24), disregarding the small second order correction, one sees that one gets exactly the  $\Delta I = 4$  energy structure when  $q = 2 \pm \sqrt{3}$ , which is not the expected superdeformed value. Of course, this discussion shows merely that such a description of the observed structure by an intrinsic vortical motion is not completely out of range. However, one has to improve it in two directions : first release the ellipsoidal shape constraint and, most importantly, include shell effects. It is also worth noting that the collective alignment appearing in eq. (19) is found even at second order in  $\hbar$ , to be independent of the size since it is equal to  $J/R$ . As shown in the classical case in ref. 5, the kinematic moment of inertia of S-type Riemann ellipsoids is given, in terms of the Rigid Body and irrotational moments of inertia, with obvious notation, by

$$\frac{I}{\Omega} = I = r I_{RB} + (1-r) I_{irrot.} \quad (25)$$

$$r = 1 + \frac{\omega C}{\Omega B}, \quad I_{irrot} = C - \frac{B^2}{C}, \quad I_{RB} = C \quad (26).$$

Assuming for instance  $r = 0.75$ , as it has been fitted by Swiatecki [15] for the first discovered super deformed band in  $^{152}\text{Dy}$  and  $q$  to be equal to two, one gets a ratio  $\omega/\Omega$  of about -20%. The previous estimate of course rely on the assumption that the reduction of the moment of inertia from its rigid body value which is understood since a very long time as coming from residual interaction beyond the mean field [16], can indeed be all explained in terms of an intrinsic vortical motion.

We have provided here a rather natural extension of the routhian approach, in a direction which has been found classically important [2,5,8]. There are obvious limitations to the present approach. We have only studied the quadratic case, excluding all "Harris formula" effects due to contributions to the energy of the angular velocities at powers higher than two. Moreover, all estimates so far have only been semiclassical. The influence of shell effects on the parameters A, B and C remains thus to be assessed. Nevertheless, the intrinsic vortical motion seems to generate a potentially interesting new set of collective degrees of freedom whose quantification yields amusing consequences as an alternative description of the staggering in rapidly rotating nuclei or a quantified, not integer or half-integer necessarily though, collective alignment independent of size. For the staggering, it should be noted however that the validity of our conclusions requires only a quadratic form of the energy in terms of two quantized quantities. The first one (I) being obviously unescapable, our description of the second (J), relies only on some classical analogies as well as on a qualitative assessment of the range of the relevant hamiltonian parameters. Ultimately, as in all collective model modelisations, it would be crucial to check whether or not the intrinsic vorticity mode is rather pure, i.e. not strongly coupled with many other degrees of freedom.

*Acknowledgments: This work was performed partly in Berkeley through a collaboration agreement between LBL and IN2P3. In that respect, it was supported by the Director, Office of Energy Research, Office of High Energy and Nuclear Physics, Division of Nuclear Physics, of the U.S. Department of Energy under Contract DE-AC03-76SF00098. It has also benefitted from a collaboration agreement between the JINR Dubna and IN2P3. The authors wish to express their gratitude to the Theory Group and the High Spin group of the Nuclear Science Division in LBL, as well as to the CSNSM for the warm hospitality extended to them.*

#### References:

- [1] I.N. Mikhailov and P. Quentin, preprint CSNSM Orsay (1994), submitted for publication.
- [2] S. Chandrasekhar, "Ellipsoidal Figures of Equilibrium" (Yale Univ. Press, New Haven, 1969).
- [3] see e.g. N.R. Lebovitz, Annu. Rev. Astr. Astrophys. 5 (1967) 465.
- [4] R.Y. Cusson, Nucl. Phys. A114 (1968) 289.
- [5] G. Rosensteel, Ann. of Phys. 186 (1988) 230.
- [6] G. Rosensteel, Phys. Rev. C46 (1992) 1818.
- [7] E.B. Balbutsev, I.N. Mikhailov and Z. Vaishvila, Nucl. Phys. A457 (1986) 222.
- [8] M. Cerkaski and I.N. Mikhailov, Ann. of Phys. 223 (1993) 151.
- [9] S. Flibotte et al., Phys. Rev. Lett. 71 (1993) 4299.
- [10] B. Cederwall et al., Phys. Rev. Lett. 72 (1994) 3150.
- [11] I. Hamamoto and B. Mottelson, preprint Lund MPh-94/05 (May 1994); B. Mottelson, these Proc..
- [12] I.M. Pavlichenkov and S. Flibotte, these Proc.; I.M. Pavlichenkov, Phys. Rep. 226 (1993) 173.
- [13] see e.g. E.F. Moore et al., Phys. Rev. Lett. 64 (1990) 3127.
- [14] K. Bencheikh, P. Quentin and J. Bartel, Nucl. Phys. A571 (1994) 518.
- [15] W.J. Swiatecki, Phys. Rev. Lett. 58 (1987) 1184.
- [16] Å. Bohr and B. Mottelson, Dan. Mat. Fys. Medd. 30 n°1 (1955).

# Microscopic Study of Wobbling Motions

Yoshifumi R. Shimizu and Masayuki Matsuzaki<sup>\*)</sup>

*Department of Physics, Kyushu University, Fukuoka 812, Japan*

*\*) Department of Physics, Fukuoka University of Education,  
Munakata, Fukuoka 811-41, Japan*

## Abstract

The nuclear wobbling motion is investigated from a microscopic viewpoint. It is shown that the expressions of not only the excitation energy but also the  $E2$  transition rate in the microscopic RPA framework can be cast into the corresponding forms of the macroscopic rotor model. The condition that the microscopic RPA solution can be interpreted to be the wobbling motion is clarified.

## §1 Introduction

In this talk We would like to discuss the wobbling motion<sup>1)</sup>, which is a collective motion expected in nuclei by an analogy with the classical motion of the asymmetric top. It is a kind of the three dimensional motion in the sense that the rotation axis and the inertia axis of the body do not coincide. Quite recently the "tilted axis cranking" scheme has been proposed<sup>3)</sup>. It might be instructive to compare characteristic features of these two. They are similar since the rotation axis deviates from the inertia axis, but these two are conceptually different as in the following, although it might be difficult to distinguish in the experimental data. In the wobbling motion the angular momentum vector and the angular frequency vector are not parallel in the body-fixed frame of coordinate and then the motion is not stationary. Hence the two vectors draw some trajectories even in the body-fixed frame. In contrast the angular momentum and the angular frequency vectors are parallel and as a result the rotation is stationary and uniform in the tilted axis cranking. When quantized the tilted axis cranking gives a description for an isolated band just like the usual cranking does, but the wobbling motion generally corresponds to a multiple band structure in the quantal spectra.

There is a basic vacuum band, e.g. the yrast band, from which excited bands are generated just like the multi-phonon structure; one wobbling phonon excited band, two wobbling phonon excited band, and so on. In each bands (horizontal sequences) states are connected by the strong rotational  $E2$  transitions, while these phonon bands are also vertically connected by  $\Delta I = \pm 1$   $E2$  or  $M1$  transitions in general. Here the vacuum band is just described by the usual cranking, i.e. the uniformly rotating states around the inertia axis of the largest moment of inertia, but when the wobbling phonons are excited the rotation axis deviates from the inertia axis more and more. Since higher excited bands are difficult to access in experiments, we concentrated on the first wobbling band and discuss the characteristic feature of the  $\Delta I = \pm 1$   $E2$  transition to the vacuum band in the following.

## §2 Microscopic formulation

Now how to calculate such a excited band like the wobbling phonon band? We use the microscopic formalism<sup>2)</sup> based on the random phase approximation (RPA), which is generally known to be suitable for describing the vibrational motions. For the first excited wobbling band, the deviation of the angular momentum vector from the usual

cranking axis,  $x$ -axis, is expected to be small and the excitation mode transfer the angular momentum by  $\pm 1$  unit so that it has definite signature  $r = -1$ , or  $\alpha = 1$ .

The excitation energy is given by the well-known RPA eigen-value equation. Since the equation generally gives many solutions, most of which are of non-collective nature, we denote the  $n$ -th eigen-value,  $\hbar\omega_n$ :

$$[H - \hbar\omega_{\text{rot}}J_x, X_n^\dagger]_{\text{RPA}} = \hbar\omega_n X_n^\dagger, \quad (1)$$

where  $X_n^\dagger$  is the  $n$ -th phonon creation operator and as for the microscopic hamiltonian we use the cranked-Nilsson single-particle potential and the pairing plus  $QQ$  residual interactions. Another important observable is the  $\Delta I = \pm 1$   $E2$  transitions from the  $n$ -th RPA phonon excited state to the vacuum state, the transition energy of which is given by  $E_\gamma(n) = \hbar\omega_n \mp \hbar\omega_{\text{rot}}$ , and can be quite simply calculated in the high-spin limit:

$$B(E2)_{\Delta I=\pm 1}^{\text{inter}} \approx \frac{1}{2} |\langle f | (Q_{K=1}^{(-)} \pm Q_{K=2}^{(-)})^{(E)} | i \rangle|^2 \rightarrow \frac{1}{2} ((Q_y(n) \mp Q_z(n))^{(E)})^2, \quad (2)$$

where the transition operator is composed of the signature-coupled quadrupole operators with  $K$  (with respect to  $z$ -axis) = 1 and 2 and  $r = -1$ , and explicitly written as

$$Q_{K=1}^{(-)} = -\frac{1}{2} \sqrt{\frac{15}{4\pi}} \sum_{a=1}^A (xz)_a \equiv Q_y, \quad Q_{K=2}^{(-)} = i \frac{1}{2} \sqrt{\frac{15}{4\pi}} \sum_{a=1}^A (xy)_a \equiv Q_z. \quad (3)$$

The transition matrix elements are evaluated by a commutator with the phonon annihilation operator,  $Q_{y,z}(n) \equiv [X_n, Q_{y,z}]_{\text{RPA}}$ , and are denoted by script  $Q$ 's. Here we introduced the notation,  $Q_y$  and  $Q_z$  for these non-diagonal part of the quadrupole tensor. This is because these operators describe the shape fluctuations around  $y, z$ -axes. Actually, by taking the commutation relations with the corresponding angular momentum operator,  $J_{y,z}$ ,

$$[Q_y, iJ_y]_{\text{RPA}} = \sqrt{\frac{15}{4\pi}} \sum_{a=1}^A \langle (x^2 - z^2)_a \rangle \equiv 2R^2 \alpha_y, \quad (4)$$

$$[J_z, Q_z]_{\text{RPA}} = \sqrt{\frac{15}{4\pi}} \sum_{a=1}^A \langle (x^2 - y^2)_a \rangle \equiv 2R^2 \alpha_z, \quad (5)$$

we get the diagonal part of the quadrupole tensor, or the static deformations around  $y, z$ -axes. Here we denote the corresponding parameters,  $\alpha_y \approx \sqrt{\frac{5}{9\pi}} \epsilon_2 \sin(\gamma + \frac{4\pi}{3})$  and  $\alpha_z \approx -\sqrt{\frac{5}{9\pi}} \epsilon_2 \sin \gamma$ . As is well-known, the in-band  $\Delta I = \pm E2$  transitions can be calculated by these static deformations for both the vacuum and the wobbling bands within the RPA as

$$B(E2)_{\Delta I=\pm 2}^{\text{in-band}} \approx \left(e \frac{Z}{A}\right)^2 \frac{1}{2} R^4 (\alpha_y - \alpha_z)^2. \quad (6)$$

Note that in the ground state, where no rotation is imposed, either  $Q_y$  or  $Q_z$  amplitudes is zero. If the system is cranked  $\Delta K = \pm 1$   $K$ -mixing induced by the rotation makes both amplitude non-zero at the same time. Then the transition rates with  $\Delta I = +1$  and  $-1$  transitions can be different and show staggering just like the well-known staggering of  $B(M1)$  between the signature partner bands in odd nuclei<sup>5)</sup>.

From the calculational point of view the discussion until now is enough. But then how the wobbling picture comes out? One must make a (time-dependent) coordinate transformation in order to see this. Though not mentioned explicitly, we have worked out, up to now, in the so-called uniformly rotating (UR) frame. There the rotation is still around the  $x$ -axis. It is, however, not the appropriate coordinate system because the (time-dependent) shape-fluctuations are induced by the excitation of the wobbling phonon so that the quadrupole tensor of the system is non-diagonal. As in the description of the rigid-body, we naturally come to the so-called principal axis (PA) frame<sup>2)</sup> by diagonalizing the quadrupole tensor. Then the shape fluctuations disappear and, in place of it, the coordinate transformation makes the angular momentum and angular frequency vectors to wobble around the  $x$ -axis. Namely, in terms of the time-dependent mean-field theory, the single particle hamiltonian corresponding to the state with the wobbling phonons excited is

$$h_{\text{UR}}(t) = h_{\text{def}} - \hbar\omega_{\text{rot}}J_x - \kappa_y Q_y(t)Q_y - \kappa_z Q_z(t)Q_z, \quad (7)$$

in the UR frame, while

$$h_{\text{PA}}(t) = h_{\text{def}} - \hbar\omega_{\text{rot}}J_x - \hbar\omega_y(t)J_y - \hbar\omega_z(t)J_z, \quad (8)$$

in the PA frame, where  $\omega_{\text{rot}} \approx \omega_x$  in the small amplitude RPA approximation. Since the angular momentum vector is not parallel to the angular frequency vector, three moments of inertia can be defined in the PA frame, as is usual, by  $\mathcal{J}_{x,y,z}^{\text{eff}}(n) = (I_{x,y,z}(n))_{\text{PA}}/\hbar\omega_{x,y,z}(n)$  where the  $(n)$  denotes that  $\mathbf{I}$  and  $\boldsymbol{\omega}$  vectors are evaluated with respect to the  $n$ -th RPA solution. Note  $\mathcal{J}_x^{\text{eff}} \approx \mathcal{J}_x \equiv I/\hbar\omega_{\text{rot}}$ , where  $I$  is the spin of the vacuum cranked state, again within the small amplitude approximation.

Using the three moments of inertia thus introduced, it can be shown that the excitation energy is written as<sup>2)</sup>,

$$\hbar\omega_n = I\sqrt{W_y(n)W_z(n)} \quad \text{with} \quad W_{y,z}(n) \equiv 1/\mathcal{J}_{y,z}^{\text{eff}}(n) - 1/\mathcal{J}_x, \quad (9)$$

and the  $E2$  transition is as<sup>6)</sup>,

$$B(E2)_{\Delta I=\pm 1}^{\text{inter}} \approx \left( e \frac{Z}{A} \right)^2 \frac{1}{I} R^4 c_n^2 \left( \alpha_y \left( \frac{W_z(n)}{W_y(n)} \right)^{1/4} \mp \sigma_n \alpha_z \left( \frac{W_y(n)}{W_z(n)} \right)^{1/4} \right)^2, \quad (10)$$

where  $(Q_{y,z})^{(E)} = (eZ/A)Q_{y,z}$  is assumed. Notice that these expressions formally coincide with those given by the macroscopic rotor model, except the overall factor  $c_n^2$  and the sign  $\sigma_n$  for the  $E2$  transitions probability, namely, if  $c_n^2 = 1$  and  $\sigma_n = +$  then it exactly coincides. Let us call the microscopic RPA solution wobbling-like if it (approximately) satisfies these conditions. Generally,  $c_n^2$  is not exactly 1 microscopically even for the ideal case\* because there are many RPA solutions in

\*Actually, a kind of "some rule",  $\sum_{n \neq \text{NG}} c_n^2 \sigma_n = 1$ , can be proved<sup>6)</sup>.

contrast to the simple rotor model, but the presence of the definite sign factor  $\sigma_n = +$  gives us an important phase rule. Comparing with the original expression eq.(2), relative sign between the static and the dynamic deformation coincide if the sign factor  $\sigma_n = +$ ;

$$\text{sign of } (Q_y(n)/Q_z(n)) = \text{sign of } (\alpha_y/\alpha_z). \quad (11)$$

Thus, the zigzag behaviour of the  $\Delta I = \pm 1$   $E2$  transitions, in addition to the energy spectra, reflect the behaviours of both the triaxiality of the mean-field and the three moments of inertia. Especially, as a result, for the wobbling-like RPA solutions, which transition probability is larger, i.e. one with  $I \rightarrow I + 1$  or  $I \rightarrow I - 1$ , is determined solely by the triaxiality. The relations are schematically summarized in Fig.1.

It should be mentioned that the appreciable amount of deformation around  $y, z$ -axes are necessary,  $\alpha_y \neq 0$  and  $\alpha_z \neq 0$ , in order for the transformation to be perform from the UR to the PA frame: Namely, the small amplitude ansatz of the "wobbling" motion in the PA frame should be satisfied<sup>6)</sup>,

$$\begin{aligned} O(1/\sqrt{I}) &\sim i(I_y(n))_{\text{PA}}/I = Q_z(n)/2R^2\alpha_z, \\ O(1/\sqrt{I}) &\sim -(I_z(n))_{\text{PA}}/I = Q_y(n)/2R^2\alpha_y. \end{aligned} \quad (12)$$

This equation also shows that the amplitude of the "wobbling" of the angular momentum vector in the PA frame is related to the fluctuations of deformation around  $y, z$ -axes, i.e. the ratios of the dynamic and the static deformations, in the UR frame.

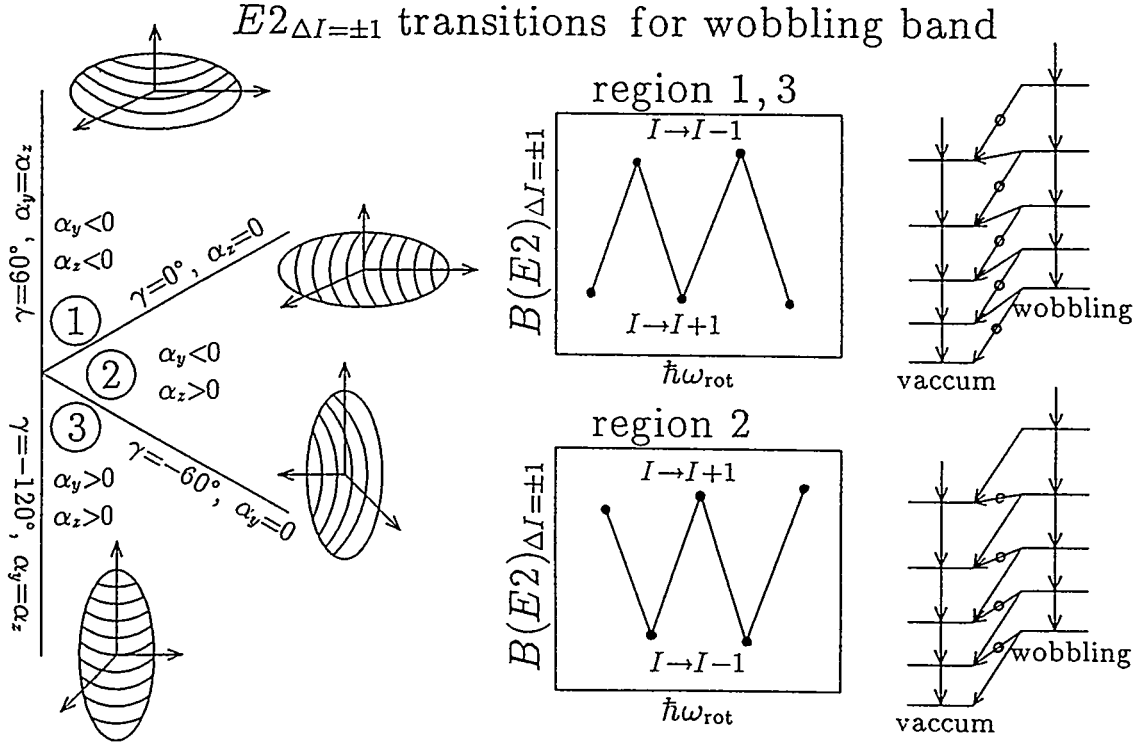


Figure 1: Schematic figure depicting the relation between the triaxiality of the mean-field and the  $\Delta I = \pm E2$  transitions from the wobbling band to the vacuum band. The transitions with stronger  $B(E2)$ 's are marked in the spectra (right panels).

### §3 Discussions

In contrast to the case of the  $M1$  transitions between the signature partner bands in odd nuclei, the zigzag behaviours of the  $\Delta I = \pm 1$  interband  $E2$  transitions in even-even nuclei are not observed so often. The only exceptions are the transitions between the well-known  $\gamma$  band and the ground-state band at low-spin. It has been shown<sup>6)</sup> that our basic formulation can be applicable also in such cases and gives satisfactory agreements with data.

Encouraged with these results, we have performed some realistic calculations<sup>6)</sup> at higher-spins, where the  $\Delta K = \pm 1$  mixing effects caused by the Coriolis interaction and the alignments of quasiparticles are expected to more favour the appearance of the wobbling-like collective motions. One of candidates of the wobbling band has been known<sup>4,5)</sup> in  $^{182}\text{Os}$ . We have found another possible candidate in  $^{124}\text{Xe}$ , whose yrast is the  $s$ -band (two neutron quasiparticles aligned) after  $I > 8\hbar$  and expected to have  $\gamma \approx -45^\circ$ . As in the case of  $^{182}\text{Os}$  this nucleus belongs to the region 2 in Fig.1 and, therefore, has stronger  $I \rightarrow I + 1$   $B(E2)$ 's. It should be mentioned, however, the  $M1$  transitions are non-negligible in this nuclei in contrast to the case of  $^{182}\text{Os}$ , see ref.6) for details.

Interestingly enough, as far as we have studied, when the collective RPA solution exists the lowest always satisfies the condition of the wobbling-like solution, eq.(11). However, it has been shown<sup>6)</sup> at the same time that the microscopically calculated  $\gamma$ -dependence of the three moments of inertia is neither irrotational nor rigid-body like. Therefore the microscopic properties of the nuclear wobbling motion is not so simple as is expected from the macroscopic rotor model. As an example, the  $M1$  transitions can be very strong depending on the quasiparticle configuration of the vacuum band, e.g. whether quasineutrons or quasiprotons are aligned. It should be noticed that important information of the triaxiality and the three moments of inertia can be extracted from the combined use of both the energy spectra, eq.(9), and the ratio between the in-band, eq.(6), and the interband, eq.(10),  $B(E2)$ 's.

The  $\Delta I = \pm 1$   $E2$  transitions under discussions are typically ten times the Weisskopf unit. Although largely enhanced, they are still an order of magnitude smaller compared to the in-band rotational  $E2$  transitions. We hope that new generations of the large array of the crystal ball will give us more detailed information of the electromagnetic transitions, which are necessary to confirm our predictions and to identify the nuclear wobbling motion if they exist.

### References

- 1) Å. Bohr and B. R. Mottelson, *Nuclear Structure*, Vol. II, (Benjamin, New York, 1975), Chap. 4, p.158ff.
- 2) E. R. Marshalek, Nucl. Phys. **A331** (1979), 429.
- 3) S. Frauendorf, Nucl. Phys. **A557** (1993), 257c; the talk in this conference.
- 4) M. Matsuzaki, Nucl. Phys. **A509** (1990), 269.
- 5) Y. R. Shimizu and M. Matsuzaki, in the Proceedings of the International Conference on *Nuclear Structure at High Angular Momentum*, May 18-21, 1992, Ottawa, AECL-10613, pp.278-282.
- 6) Y. R. Shimizu and M. Matsuzaki, to be published.

# The structure of $\pi i_{13/2}[660]1/2^+$ bands in Lu-isotopes

H. Schnack-Petersen<sup>1</sup>, R.A. Bark<sup>1</sup>, R. Bengtsson<sup>2</sup>, P. Bosetti<sup>3</sup>,  
 A. Brockstedt<sup>4</sup>, H. Carlsson<sup>4</sup>, L.P. Ekström<sup>4</sup>, G.B. Hagemann<sup>1</sup>, B. Herskind<sup>1</sup>,  
 F. Ingebretsen<sup>5</sup>, H.J. Jensen<sup>1</sup>, S. Leoni<sup>1,3</sup>, A. Nordlund<sup>4</sup>, H. Ryde<sup>4</sup> and  
 P.O. Tjøm<sup>5</sup>

## INTRODUCTION

Rotational bands built on the proton  $i_{13/2}[660]1/2^+$  intruder orbital are known in the heavier rare earths odd-Z nuclei. This orbital is predicted [1] to polarize the nucleus in the prolate direction c.f. the negative slope in the Nilsson diagram shown in fig. 1. A moderately increased deformation for this band has indeed been found in <sup>179</sup>Ir [2]. A theoretical investigation of the shape evolution of the intruder bands can be found in ref. [3], which also contains references for experimental  $i_{13/2}[660]1/2^+$  bands in Re and Ir isotopes. With decreasing Z the  $i_{13/2}[660]1/2^+$  orbital moves further away from the Fermi surface, unless a larger increase in deformation is encountered.

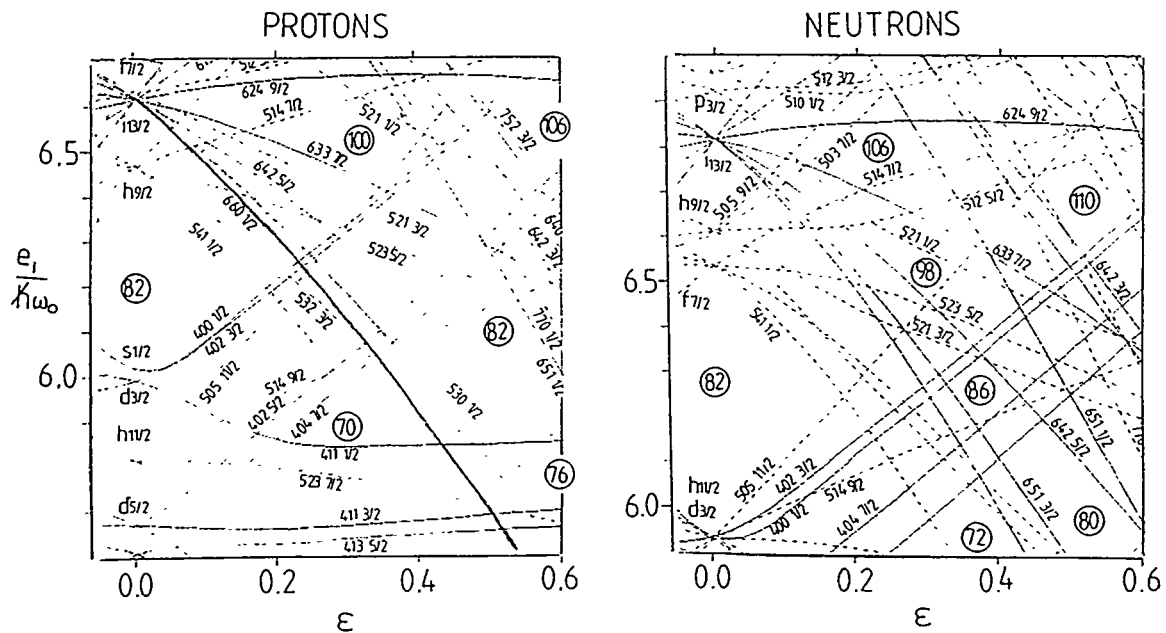


Fig. 1. Single-particle energies as functions of the quadrupole deformation parameter  $\epsilon$  for protons, left and neutrons, right. The calculations are from ref. [4] in which the parameters used in the Nilsson potential are given. The proton  $i_{13/2}[660]1/2^+$  orbital is emphasized by a thicker line.

- 1 The Niels Bohr Institute, University of Copenhagen, Roskilde, Denmark.
- 2 Dept. of Math. Physics, Lund Institute of Technology, Lund, Sweden
- 3 Department of Physics, University of Milano, Italy
- 4 Department of Physics, University of Lund, Sweden
- 5 Department of Physics, University of Oslo, Norway



Recently a strongly deformed rotational band has been discovered [5, 6] in  $^{163}\text{Lu}$  with  $\beta_2 \sim 0.42$ . Based on the large deformation, this band was interpreted as corresponding to the  $\pi i_{13/2}[660]1/2^+$  configuration which is expected to be deformation driving [5, 6].

### MEASUREMENTS in $^{165}\text{Lu}$

The nucleus  $^{165}\text{Lu}$  has been studied using the detector array, Nordball, at the NBI Tandem accelerator laboratory, applying the reactions,  $^{138}\text{Ba}(^{31}\text{P}, 4n)^{165}\text{Lu}$  and  $^{150}\text{Sm}(^{19}\text{F}, 4n)^{165}\text{Lu}$ , at bombarding energies of 155 and 86 MeV respectively. The previously known [7, 8] rotational bands in this nucleus have been considerably extended. Bands built on the normal positive parity configurations,  $[404]7/2^+$ ,  $[411]1/2^+$  and  $[402]5/2^+$  are strongly mixed at certain spin values, and the  $[404]7/2^+$  band is furthermore complicated by feeding from a new positive parity band, presumably of three-quasiparticle nature, over a broad spin range. In addition, a rotational band with transition energies identical (within 1-2 keV) to those in the strongly deformed band in  $^{163}\text{Lu}$  was found, see fig. 2. (The fact that the strongest populated band in  $^{163}\text{Lu}$  was not observed in the present experiments rules out the possibility of the bands being truly identical.) Based on the similarity, we interpret this new band in  $^{165}\text{Lu}$  as also associated with the  $[660]1/2^+$  intruder configuration.

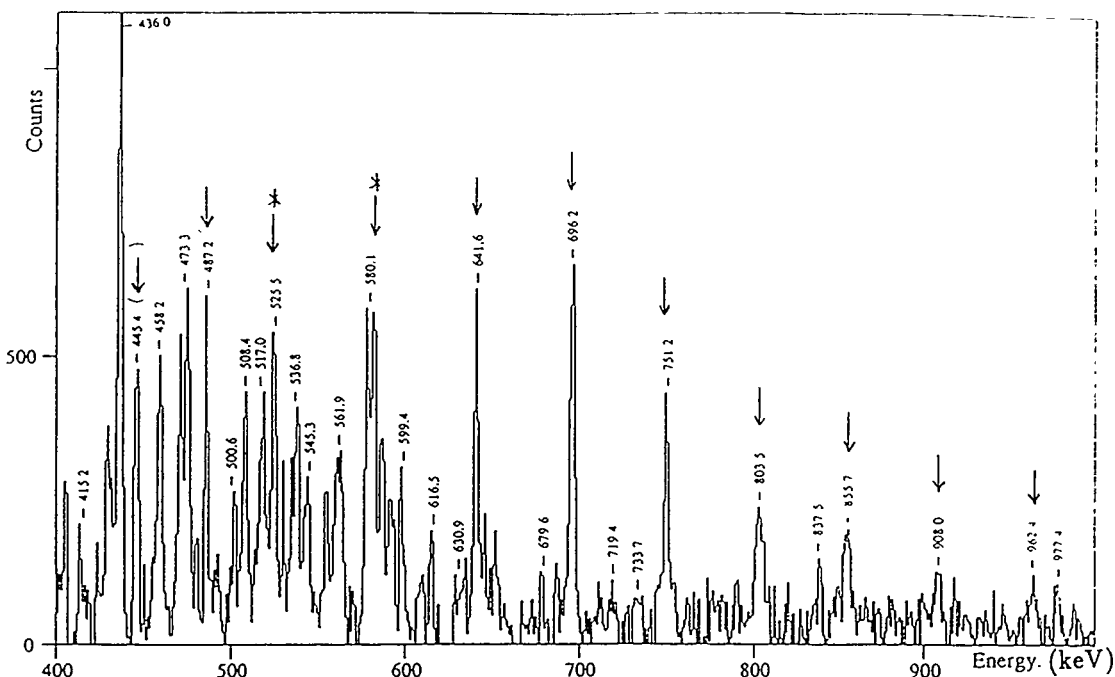


Fig. 2. Spectrum of  $\gamma$ -rays in the new  $[660]1/2^+$  band corresponding to the sum of gates on the transitions marked with an asterisk. Transitions in the band are marked with arrows, which are given in parenthesis for transitions feeding out of the band.

This new  $[660]1/2^+$  band decays into the  $[404]7/2^+$  as well as to the  $[402]5/2^+$  structures. The decay pattern is difficult to trace due to the presence of mixing and all the connecting transitions have not been firmly established. The relative alignment and excitation energy of the  $[660]1/2^+$  band together with some of the 'normal' bands are shown in fig. 3. The population strength of the  $[660]1/2^+$  band in  $^{165}\text{Lu}$  is  $\sim 16\%$  relative to the  $h_{11/2}[514]9/2^-$  band compared to a population of the  $[660]1/2^+$  band in  $^{163}\text{Lu}$  of  $\sim 29\%$

relative to the  $h_{11/2}[523]7/2^-$  band [5, 6] in the spin range  $37/2 - 53/2 \hbar$ . This population difference could be compatible with the larger excitation energy in  $^{165}\text{Lu}$ .

Both bands show gradual alignment gain in the entire spin range covered, relative to the reference used in fig. 3. This alignment behaviour is very different from the other bands in the region of the  $i_{13/2}$  AB neutron crossing.

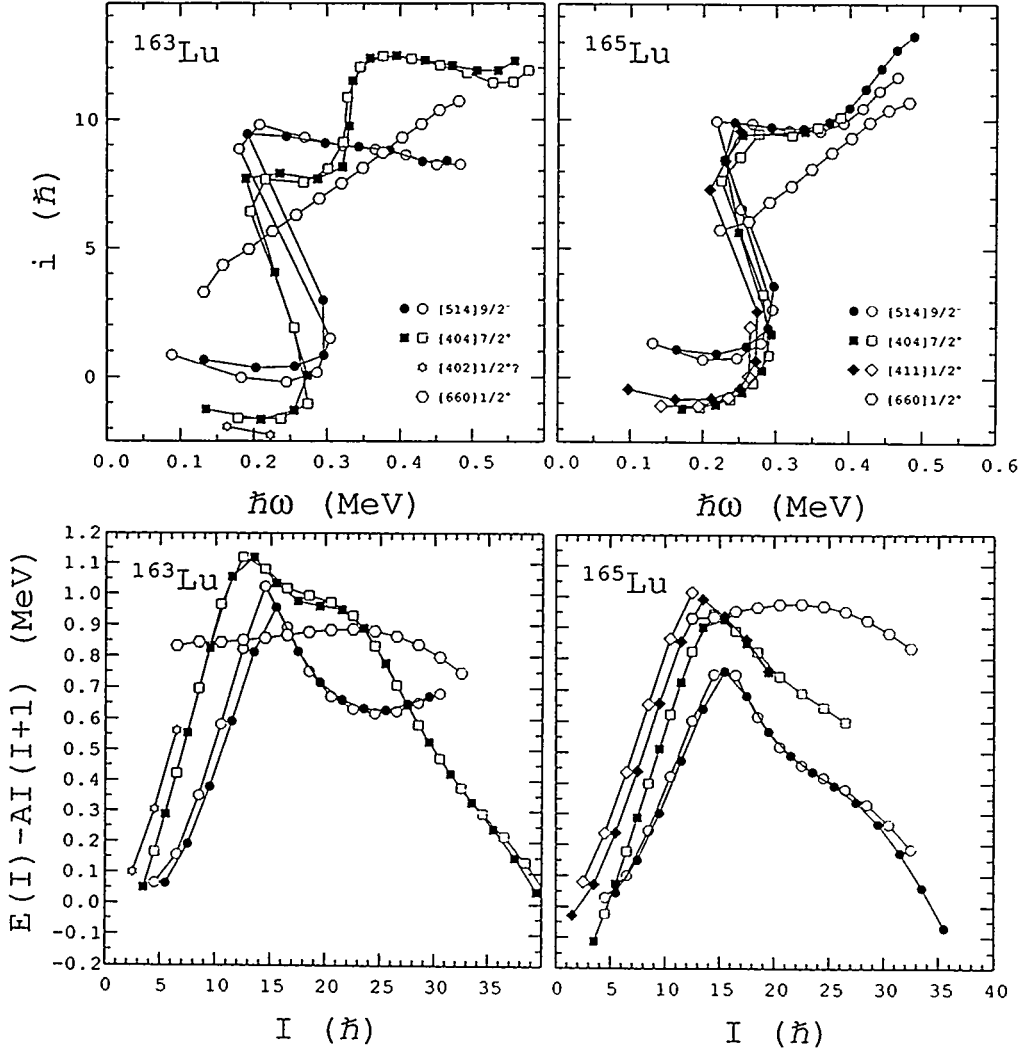


Fig. 3. Experimental properties for selected bands in  $^{163}\text{Lu}$  (left) and  $^{165}\text{Lu}$  (right). Top: Alignment,  $i$ , relative to a reference with Harris parameters  $\mathfrak{S}_0 = 35\hbar^2\text{MeV}^{-1}$  and  $\mathfrak{S}_1 = 40\hbar^4\text{MeV}^{-3}$ , versus rotational frequency. Bottom: Excitation energy relative to a rigid reference with  $\mathfrak{S} = 63.3\hbar^2\text{MeV}^{-1}$  versus spin.

## CALCULATIONS

A local minimum with large deformation was found in total routhian surface (TRS) calculations of the lowest surface with  $(\pi, \alpha) = (+, +1/2)$  for  $^{163}\text{Lu}$ , in qualitative agreement with the measured quadrupole moments [6, 9].

Calculations of potential energy surfaces using the "Ultimate Cranker" [10] have been performed for  $^{165}\text{Lu}$  and  $^{163}\text{Lu}$  at several spin values following the procedure described in ref. [11].

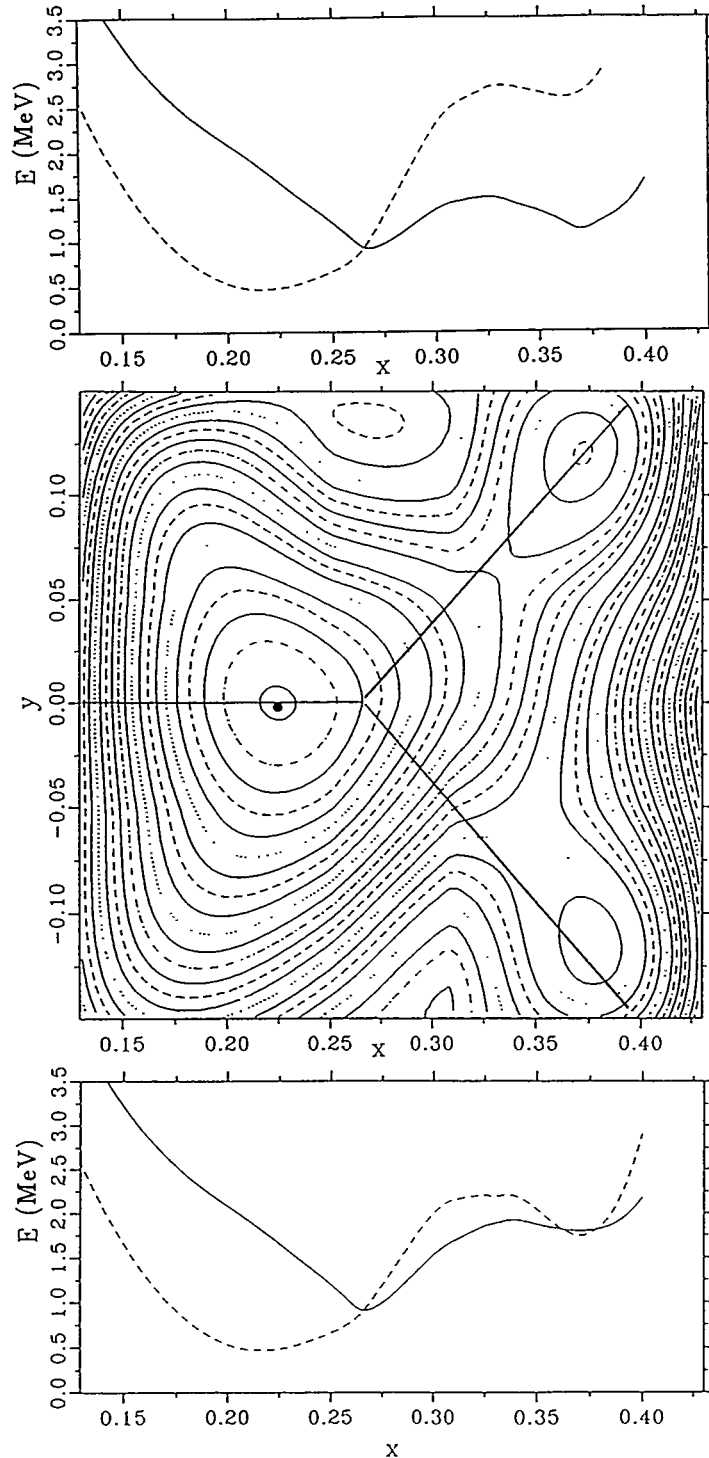


Fig. 4. Center: Lowest spin-adiabatic potential energy surface for  $(\pi, \alpha) = (+, +1/2)$  at  $I=14.5$  in  $^{165}\text{Lu}$ . The energy difference between contour lines is 0.1 MeV. At the top and bottom are shown the potential energy corresponding to the separated (spin-diabatic) surfaces shown in fig. 5, as a function of  $x = \varepsilon_2 \cos \gamma$  following the straight lines cutting through the relative minima with  $\gamma > 0$  and  $\gamma < 0$  respectively, symmetrically around  $\gamma = 0$ . The full and broken lines correspond to the  $[660]1/2^+$  and the lowest of the  $[404]7/2^+$  and  $[411]1/2^+$  configurations respectively.

For such calculations the energy is minimized with respect to  $\varepsilon_4$  in addition to  $\varepsilon_2$  and  $\gamma$ . As an example the spin-adiabatic potential energy surface for the lowest surface with parity and signature  $(\pi, \alpha) = (+, 1/2)$  is shown in the center part of fig. 4.

It should be noted, that in a spin-adiabatic surface as the one shown in fig. 4, the frequency will have large variations from the average, in particular at the nonaxial deformations. Spin-diabatic surfaces for specific configurations have been calculated. These are followed throughout the deformation space by a diabatic treatment of crossings, i.e. interactions of small and moderate strength are removed [11]. The intruder orbitals such as  $[660]1/2^+$ , have, for most deformations, a rather large slope in the routhian diagrams, and are therefore more easily followed. Two examples of separated spin-diabatic surfaces in  $^{165}\text{Lu}$  are shown in fig. 5.

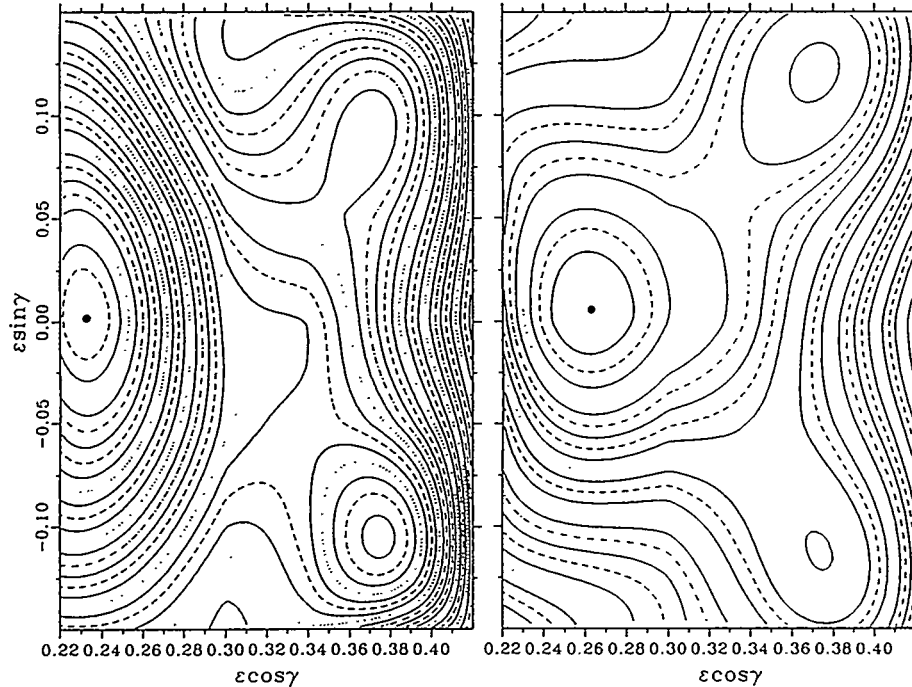
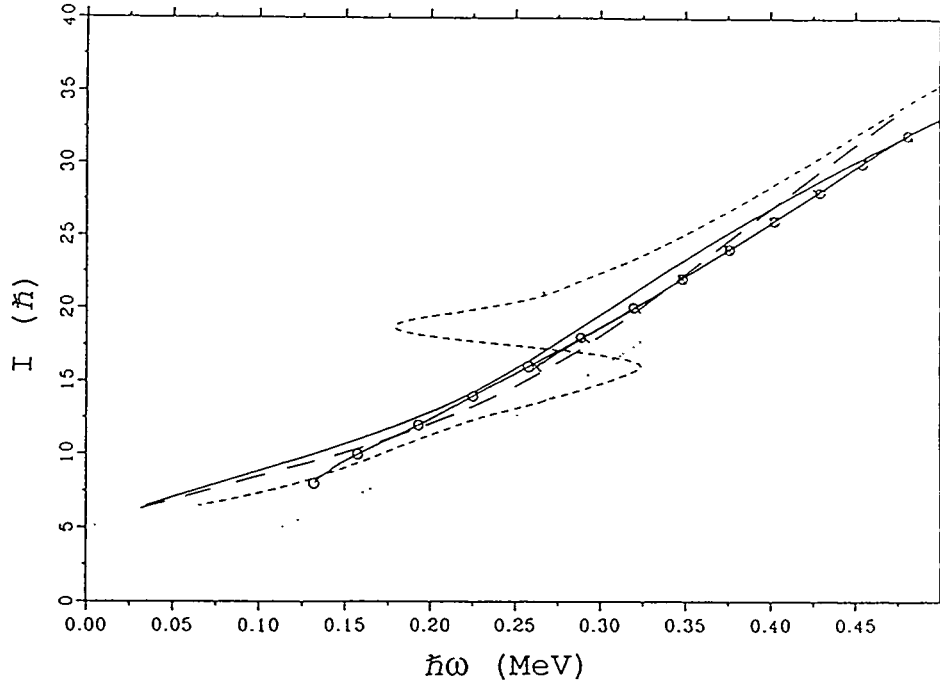


Fig. 5. Separated (spin-diabatic) potential energy surfaces corresponding to the  $[404]7/2^+$  (in part of the deformation space  $[411]1/2^+$ ) configuration (left) and the  $[660]1/2^+$  configuration (right). The energy difference between contour lines is 0.1 MeV

Both at moderate and higher spin the yrast positive parity configuration with signature  $\alpha = +1/2$  has minimum energy at  $\varepsilon_2 = 0.23$  (fig. 5, left hand side) whereas the configuration corresponding to  $[660]1/2^+$ , followed diabatically through band crossings, reveals a minimum at  $\varepsilon_2 = 0.26$  (fig. 5, right hand side) which is substantially smaller than the experimental value for  $^{163}\text{Lu}$  [6]. However, highly deformed ( $\varepsilon_2 = 0.39$ ) local minima at  $\gamma \sim \pm 18^\circ$  with excitation energies relative to the global minimum of  $\sim 0.2$  and  $0.8$  MeV for positive and negative  $\gamma$ , respectively, are found. Similar highly deformed local minima exist also for the yrast  $(\pi, \alpha) = (-, +1/2)$  configuration, as well as for the  $(\pi, \alpha) = (+, +1/2)$  configuration, shown in the left hand side of fig. 5. The latter corresponds throughout the deformation plane to the  $[404]7/2^+$  or  $[411]1/2^+$  Nilsson orbital. For the  $N=4 (+, +1/2)$  configuration, the local minimum with  $\gamma < 0$  is lower than that with  $\gamma > 0$ , with an excitation energy relative to the global minimum at  $\varepsilon = 0.23$  of  $\sim 1.4$  MeV. Note that the

energies plotted in the top and bottom part of fig. 4 do not correspond to the preferred route into the nonaxial local minima for both structures since these minima are slightly displaced, see fig. 5.

For the  $[660]1/2^+$  band in  $^{163}\text{Lu}$  very similar deformed structures are, as could be expected, found in the calculated potential energy surfaces. Furthermore, the relation between  $I$  and  $\omega$  obtained from pairing self consistent cranking calculations for the  $[660]1/2^+$  band at the well deformed minimum with  $\gamma > 0$  show for both of the two neighbouring even- $N$  Lu isotopes a very similar gradual increase with  $\omega$ , in qualitative agreement with the data. See fig. 6. In the calculations a pair of quasineutrons is aligned at the highest spin, i.e. the  $i_{13/2}$  neutron crossing occurs with a very large interaction in both Lu isotopes. The calculated results for the other minima found in  $^{165}\text{Lu}$  are also shown in the figure. For the normal deformed minimum with  $(\epsilon_2, \gamma) = (0.26, \sim 0)$  the  $i_{13/2}$  neutron crossing is clearly seen.



*Fig. 6. Calculated and experimental (open circles) spin versus rotational frequency for the three different relative minima for the  $[660]1/2^+$  band in  $^{165}\text{Lu}$ . The short-dashed line corresponds to the less deformed minimum, the full and dotted lines correspond to the well deformed minima with  $\gamma > 0$  and  $\gamma < 0$  respectively. For  $^{163}\text{Lu}$  the calculation for the well deformed relative minimum with  $\gamma > 0$  is shown with a long-dash symbol.*

## CONCLUSION

As demonstrated, nonaxial, highly deformed local minima seem to appear as a general phenomenon. An investigation of the wave functions of these potential energy surfaces indicate a more complex structure of the highly deformed bands involving changes in occupation for both neutrons and protons. In the proton system particles are transferred from the unblocked, less polarizing  $N=4,5$  orbitals as for example  $h_{11/2}$  into the unblocked down-sloping intruder orbitals, in particular  $h_{9/2}$ , in a rearrangement of the core. The

difference between the wave functions for the two well deformed local minima with opposite sign in  $\gamma$  is found in a difference in the occupation of the  $\Omega$  components on the rotation axis of the same  $N, j$ . To verify the predicted sizeable divergence from axial symmetry is a challenge for further experiments, as well as theoretical studies of possible measurable spectroscopic consequences.

The same low- $\Omega$  intruder orbitals which are occupied in the well-deformed minima in these Lu isotopes are also responsible for shape coexistence in the Pb-Hg-Pt region, and super-deformation in the  $A \sim 150$  region.

This work has been supported by the Danish Natural Science Foundation, the Nordball collaboration and the Swedish Natural Science Research Council. The availability of software written by D.C. Radford used in the data analysis is highly appreciated.

## References

- [1] W. Nazarewicz, M.A. Riley and J.D. Garrett, Nucl. Phys. **A512**(1990)61
- [2] D. Müller, A. Virtanen, R. Julin, S. Juutinen, A. Lampinen, S. Törmänen, F. Christancho, A.P. Byrne, G.D. Dracoulis, B. Fabricius, C. Fahlander, A. Johnson, K.P. Lieb, J. Nyberg, I. Thorslund and R. Wyss, Phys. Lett. **B332**(1994)265
- [3] R.A. Bark, R. Bengtsson and H. Carlsson, Phys. Lett. in press.
- [4] T. Bengtsson and I. Ragnarsson, Nucl. Phys. **A436**(1985)14
- [5] W. Schmitz, C.X. Yang, H. Hubel, A.P. Byrne, R. Musseler, N. Singh, K.H. Maier, A. Kuhnert and R. Wyss, Nucl. Phys. **A539**(1992)112
- [6] W. Schmitz, H. Hubel, C.X. Yang, G. Baldsiefen, G. Frölingsdorf, D. Metha, R. Musseler, M. Neffgen, P. Willsau, J. Gascon, G.B. Hagemann, A. Maj, D. Müller, J. Nyberg, M. Piiparinen, A. Virtanen and R. Wyss, Phys. Lett. **B303**(1993)230
- [7] S. Jónsson, J. Lyttkens, L. Carlen, N. Roy, H. Ryde, W. Walus, J. Kownacki, G.B. Hagemann, B. Herskind and J.D. Garrett, Nucl. Phys. **A422**(1984)397
- [8] P. Frandsen, R. Chapman, J.D. Garrett, G.B. Hagemann, B. Herskind, C.-H. Yu, K. Schiffer, D. Clarke, F. Khazaie, J.C. Lisle, J.N. Mo, L. Carlen, P. Ekström and H. Ryde, Nucl. Phys. **A489**(1988)508
- [9] R. Wyss, private communication 1993.
- [10] T. Bengtsson, Nucl. Phys. **A496**(1989)56 and **A512**(1990)124
- [11] R. Bengtsson, T. Bengtsson, M. Bergström, H. Ryde and G.B. Hagemann, Nucl. Phys. **A569**(1994)469

# Tilted Cranking

S. Frauendorf, J. Meng and J. Reif

Institut für Kern- und Hadronenphysik, Forschungszentrum Rossendorf e.V.  
PF 510119, 01314 Dresden, Germany

October 8, 1994

**Abstract:** The Tilted Axis Cranking theory is used to describe the coexistence of high and low K bands in yrast spectra of well deformed nuclei, magnetic rotation of transitional nuclei and to calculate the parameters of a rotational hamiltonian with a fourfold symmetry axis that generates  $\Delta I = 4$  staggering in the yrast band

The orientation of the deformed density distribution relative to the (space fixed) angular momentum vector becomes a useful concept at high spin. Tilted Axis Cranking (TAC) [1] is the version of the meanfield theory that permits to calculate the the orientation of the deformed field together with the parameters that define its shape. Since its introduction [2] it has turned out to be a reliable approximation to calculate both energies and intra band transition probabilities. The possibility to construct classical vector diagrams showing the angular momentum composition is of great help to understand the structure of the rotational bands. In this talk I shall discuss three applications of TAC: i) multiband spektra containing high and low K bands, ii) shears bands and magnetic rotation and iii) an attempt to find the microscopic origin of  $\Delta I = 4$  staggering.

## 1 Multiband spectra

In TAC one seeks HF solutions that rotate uniformly about the angular momentum axis  $\vec{J}$  that has a tilt with the symmetry axis of the deformed field. In order to find the angle  $\vartheta$  one diagonalizes the single particle routhian

$$h' = h_{def} - \omega(\sin \vartheta j_1 + \cos \vartheta j_3) \quad (1)$$

where  $h_{def}$  is the hamiltonian of the non rotating deformed field, containing pairing if necessary. Each configuration constructed from the single particle or quasiparticle levels corresponds to a rotational band. Each band has its individual tilt that is determined by minimizing the total routhian  $E'(\omega, \vartheta)$  at fixed  $\omega$ . At the minimum the angular momentum vector and the angular velocity

$$\vec{J} = \langle \vec{j} \rangle \quad \vec{\omega} = (\omega \sin \vartheta, \omega \cos \vartheta) \quad (2)$$

are parallel [1]. As in the traditional cranking theory, which assumes that that axis of rotation coincides with one of the principal axes of the deformed field (Principal Axis Cranking - PAC), there exist several possibilities to calculate  $E'$  from the single particle

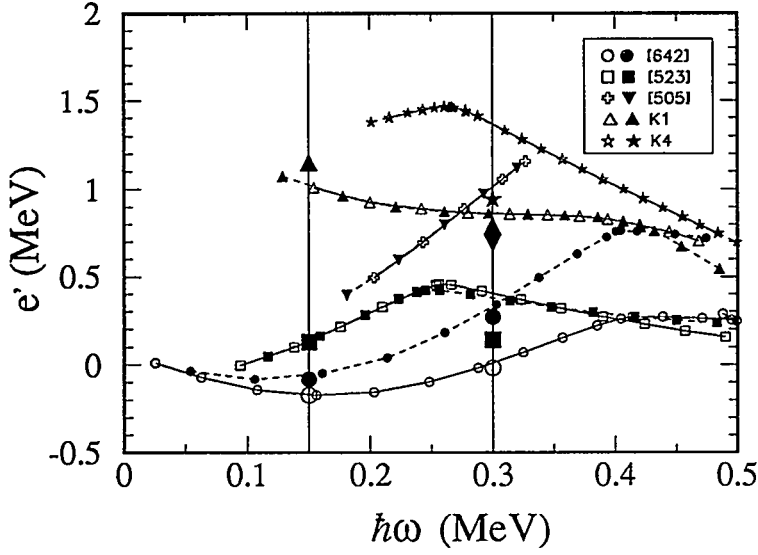


Figure 1: Experimental routhians of  $^{163}\text{Er}$  compared to TAC calculations. The TAC routhians  $E'(\omega)$  are shown as the large symbols on the two vertical lines located at the frequencies for which calculations have been carried out. The data is from [3]

wavefunctions generated by (1), as e. g. Strutinsky renormalization or Skyrme HF. So far, most calculations have been carried out in the HFB frame defined by the Pairing + QQ Interaction [1, 4]. If one is not interested in deformation changes it is sufficient to minimize  $E' = \langle h' \rangle$ .

The results of the TAC calculations are interpreted in the following way:

If  $E'(\omega, \vartheta)$  has its minimum at  $\vartheta = 0$  the band has not started yet. These solutions are disregarded. For each band there is a band head frequency (and spin as well) where the curvature of  $E'(\omega, \vartheta)$  changes sign and the minimum begins to move towards  $90^\circ$ . The band head frequency and spin are characteristic for each band and experimentally well known.

Each TAC configuration represents a  $\Delta I = 1$  band (i. e. two degenerate signatures) as long as  $\vartheta < 90^\circ$ . When  $\vartheta = 90^\circ$  one has the ordinary PAC solution that is interpreted as a  $\Delta I = 2$  band of the calculated signature. This change of interpretation leads to a discontinuous description (what is a well known consequence of symmetry breaking). However, there are no missing or extra states among the lowest bands. The only unphysical feature is a jump of the unfavored signature branch instead of a continuous onset of signature splitting.

Using the constraint  $J = |\vec{J}| = I + 1/2$  one can fix the frequency  $\omega$  and calculate the energy  $E = E' + \omega J$ . Often it is more convenient to introduce experimental routhians by means of the relations

$$\omega(I - \frac{1}{2}) = \frac{1}{2} (E(I) - E(I - 2)) \quad (3)$$

$$E'(I - \frac{1}{2}) = \frac{1}{2} (E(I) + E(I - 2)) - \omega(I - \frac{1}{2})(I - \frac{1}{2}) \quad (4)$$

The functions  $I(\omega) - \frac{1}{2}$  and  $E'(\omega)$ , obtained in this way, can directly be compared with the calculated quantities  $J(\omega)$  and  $E'(\omega)$ . This has the advantage that one can choose how accurately one wants to study the  $\omega$  - dependence. Fig. 1 gives an example. TAC calculations only are carried out for  $\omega = 0.15$  and  $0.30 \text{ MeV}$ . Ideally the calculated routhians



should lie at the intersections of the vertical lines with the experimental routhians. As seen, there is reasonable correspondence. In particular, the relative position of the high and low  $K$  bands is well accounted for. For the two bands denoted by K1 and K4 no TAC solution is found at  $\omega = 0.15 MeV$ . Accordingly they start above this frequency in experiment. Note, eq.(3) differs from the definition of the frequency, usually used in CSM (which corresponds to  $\omega_1$ ). Since no assumption about  $J_3$  ( $=K$  at the band head in CSM) is involved, it is free of any ambiguity.

The intraband transition probabilities are calculated by means of the semiclassical expressions

$$BM1 = \frac{3}{8\pi} [\sin \vartheta (J_{3\pi} + 2.91S_{3\pi} - 2.61S_{3\nu}) - \cos \vartheta (J_{1\pi} + 2.91S_{1\pi} - 2.61S_{1\nu})]^2 \quad (5)$$

$$BE2 = \frac{15}{32\pi} [(\sin \vartheta)^2 eQ_0]^2 \quad (6)$$

where the vectors of angular momentum,  $\vec{J}$ , and of spin,  $\vec{S} = \langle \vec{s} \rangle$  and the proton quadrupole moment,  $Q_0 = \langle q_0 \rangle$  are calculated from the TAC conf.  $|\rangle$ . The free spin magnetic moments are attenuated by a factor of 0.7. Examples of calculations of transition probabilities can be found in refs. [1, 3, 4, 5].

In order to test the reliability of the TAC approximation we have carried out extensive comparisons of Two Particle + Rotor calculations with the TAC approximation to this model. Typically it is found that TAC describes rather well both the energies and the intra band transition probabilities of at least the lowest 5 bands. The agreement deteriorates with the excitation energy. It turns out that for high  $K$  bands only TAC gives a reliable description, whereas the procedures based PAC become problematic. The version that keeps  $J_3$  constant equal to the  $K$  value at the band head becomes inaccurate for high spin, since even small changes of  $J_3$  lead to substantial changes of the energies and transition probabilities. The other procedure that uses  $J_3 = \sqrt{\langle j_3^2 \rangle}$  fails if more than one quasiparticle contribute to the total value of  $J_3$ . For example, if the proton and the neutron both have the same  $k$  then one has a  $K = 0$  and a  $K = 2k$  band, whereas the PAC prescription results in two bands with  $K = \sqrt{2}k$ .

## 2 Magnetic Rotation

The recently discovered shears bands in the nuclei around  $^{200}Pb$  (c. f. e. g. [4] and the lecture by H. Hübel) represent a new kind of rotation, whose nature was first understood in the framework of the TAC [1]. The experimental evidence is the observation of regular sequences of magnetic dipole transitions in the irregular spectra that are characteristic for spherical nuclei. The BM1 values are very large (several  $\mu_N^2$ ). If seen at all, the crossover transitions have very small BE2 values ( $Q_t < 1(eb)^2$ ). *Thus, one observes very regular bands with a substantial dynamic moment of inertia ( $\mathcal{J}^{(2)} \sim 15...25 MeV^{-1}$ ) in nuclei that are almost spherical.*

The explanation of this apparent paradox is the shears mechanism that is illustrated in fig. 2. The active high  $j$  orbitals are  $i_{13/2}$  and  $h_{9/2}$  protons and  $i_{13/2}$  neutron holes. The nucleus has a slight oblate deformation ( $\epsilon_2 \sim -0.1$ ). This deformed field tends to align the protons with the symmetry axis 3 and the neutron holes with the 1 - axis, since the former have toroidal the latter dumbbell like density distributions. The bands start with  $\vec{j}_\nu$  perpendicular to  $\vec{j}_\pi$ . Along the band angular momentum and energy increase by

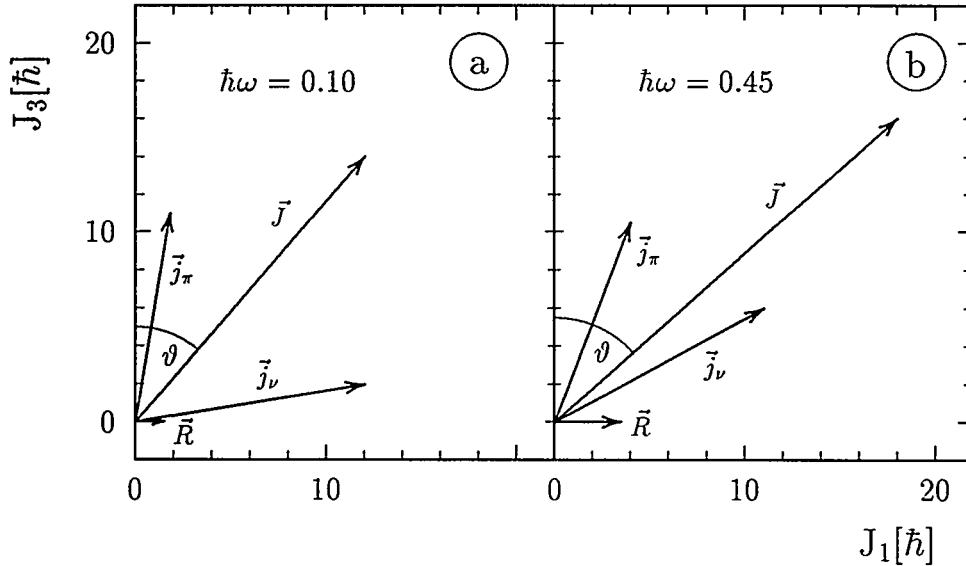


Figure 2: Angular momentum composition of the shears band  $\pi h_{9/2}, \pi i_{13/2}, \pi [s_{1/2}]^{-2}, [\nu i_{13/2}]^{-2}$  in  $^{198,200}\text{Pb}$  (from [4])

simultaneous alignment of both vectors with the total angular momentum  $\vec{J}$ , which keeps an angle of about  $45^\circ$  with the symmetry axis. The name "shears bands" alludes to the similarity with closing a pair of shears for sheep (which has a spring to keep it open).

Calculations based on the Pairing + QQ version of TAC account well for the energies and spins of the shears bands observed in  $^{197-201}\text{Pb}$  [1, 4]. It turns out that most of the dynamic moment of inertia results from the shears mechanism, the part due to the deformation is about  $7MeV^{-1}$ . The very small BE2 values are also well reproduced. TAC predicts BM1 values in the order of  $5\mu_N^2$ , which decrease with angular momentum. The decrease is a direct consequence of the shears mechanism, since closing the blades reduces the length of the component of the magnetic dipole moment perpendicular to  $\vec{J}$ . The M1 lifetime measurements are discussed in the lectures by H. Hübel [6] and R. Clark [7]. Some of the experimental BM1 values show the decrease with spin but some not. It seems to be important to clarify whether there exists a systematic discrepancy between theory and experiment.

States that are related to each other by recoupling of high j orbitals are quite common in nuclei with small deformation. They are also connected by fast M1 transitions. However, they do not show the regular level spacings over many spin values that justify the name band. In order to find the relation between these "multiplets" and the shears bands, we have studied the origin of the regular spacing by means of the spherical shell model. In order to keep to computational effort within reasonable limits we study the following model: The configuration space for neutrons is  $[i_{13/2}]^{-n}$ ,  $n = 1, 2$  and  $[p_{1/2}, p_{3/2}, f_{5/2}]^n$ ,  $n = 0, \dots, 12$ . For the protons we assume the stretched configuration  $[h_{9/2}i_{13/2}]_{J=11}$  combined with  $[s_{1/2}]^{-2}$ . We use experimental spherical single particle levels and a surface  $\delta$ -interaction, whose strength is adjusted to the spherical spectra of the region. Effective charges and g-factors typical for the region are used. The physics of this model amounts to freeze the proton blade of the shears but to let the neutrons do what they like.

The calculations reproduce fairly well the energies and transition probabilities of the

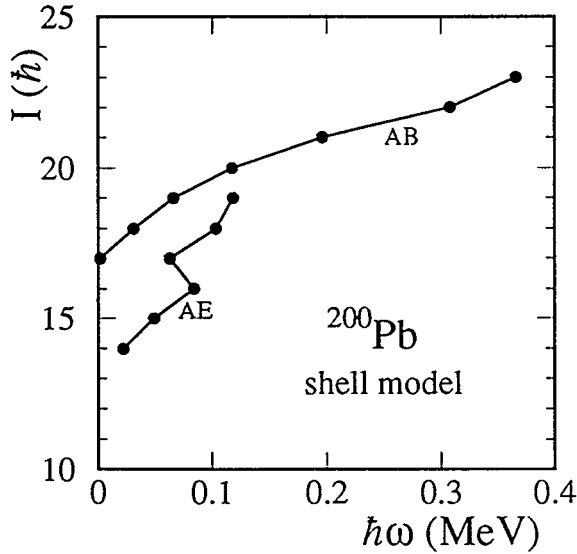


Figure 3: Angular momentum as function of the frequency (transition energy) calculated by means of the shell model. The bands AB and AE have the configurations  $\pi[h_{9/2}, i_{13/2}]_{11}, \pi[s_{1/2}]^{-2}$  and  $[\nu i_{13/2}]^{-2}, \nu[fp]^6$  and  $\nu[i_{13/2}]^{-1}, \nu[fp]^7$ , respectively.

observed shears bands. The BM1 values show the characteristic decrease with spin. Fig. 3 shows as an example the function  $I(\omega)$  for two configurations in  $^{200}\text{Pb}$ , where AB contains two and AE only one  $\nu i_{13/2}$  holes. It illustrates the general tendency that the more high  $j$ -orbitals are forming the blade the more regular the band becomes. This holds also for the different proton configurations, which we have studied as well.

A second feature is illustrated by fig. 4 that summarizes the results for two  $i_{13/2}$  neutron holes and different even numbers of neutrons in the  $fp$  states. There is a general increase of the energy with the angular momentum. This is a consequence of the short range interaction, which prefers a perpendicular orientation of the angular momentum vectors of the protons and neutron holes, because their spatial density distributions are tori or dumbbells, respectively. The level spacings are irregular if the  $fp$  shell is empty or full. The wavefunctions show that this irregularity is accompanied by changes of the orientation of the two  $i_{13/2}$  neutron holes relative to each other. Regular bands appear only in the middle of the  $fp$  shell, where the wavefunctions show that the two  $i_{13/2}$  neutron holes are predominantly coupled to  $J = 12$ . There is a gradual transition from the multiplets to the shears bands. Hence, the  $fp$  neutrons act as a kind of glue that keeps the two neutron holes in stretched coupling. Such a long stiff neutron blade can take on many different orientations with respect to the proton blade, resulting in a regular shears band.

How does the glue act? The wave function of the  $fp$  neutrons is mainly composed of states with  $J = 0, 2, 4$ , which may combine to a slightly deformed density distribution. The following feedback mechanism seems to be active:

*On the one hand, the slightly deformed  $fp$  density aligns the orbitals forming a blade, on the other hand, the spatial density distributions of these orbitals induce the deformation of the  $fp$  density.*

Regular shears bands appear only if this feedback is strong enough. If fewer high  $j$  orbitals are involved or the low  $j$  orbitals are less polarizable, the sequence of the M1 transitions becomes less regular. Also experimentally, the regular shears bands and the irregular

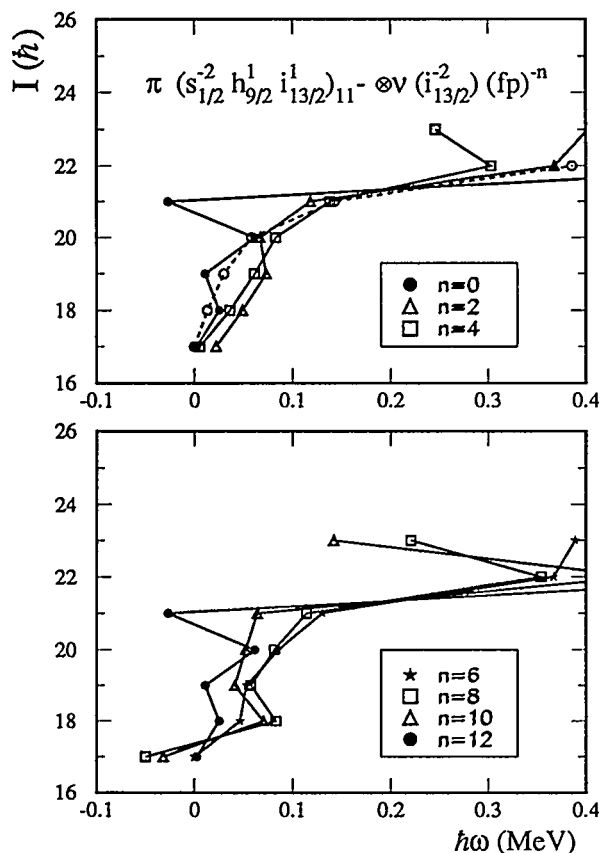


Figure 4: Angular momentum as function of the frequency (transition energy) calculated by means of the shell model. The bands have the configuration  $\pi[h_{9/2}, i_{13/2}]_{11}, \pi[s_{1/2}]^{-2}$  and  $[\nu i_{13/2}]^{-2}, \nu[fp]^{-n}$ .

multiplets are just the two limits of a variety of more or less regular M1 sequences.

The regular M1 sequences with the very weak crossover E2 transitions suggest the concept of *magnetic rotation*. The name accounts for the fact that it is the *magnetic dipole* vector what rotates about the angular momentum vector. In the case of the familiar rotation of well deformed nuclei this role is played by the deformed electrical charge distribution. Thus in this context, the name *electrical rotation* seems to be appropriate for it. The analogies and differences of the two types of rotation are listed in the table. Magnetic rotation extends our concept of collective rotation, emphasizing the fact that it is not always the spatial density distribution that defines the orientation.

Magnetic and electric rotation appear often combined, like e. g. in many high  $K$  bands of well deformed nuclei. The new aspect is that there are cases when the electrical part is strongly suppressed or almost absent. Fig. 5 gives an overview where such situations may be expected. The shears bands in the light Pb isotopes and their neighbors are examples of rather pure magnetic rotation. Many regular  $\Delta I = 1$  sequences with high BM1 values are also found around  $Z = 60$  and  $N = 70$ . There, the electric part is stronger, since one is further in the open shell where the deformation is larger. It would be interesting to study the nuclei closer to  $Z = 50$  and  $N = 82$ , where a smaller electrical component is expected.

## Electric and Magnetic Rotation

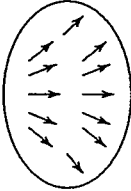
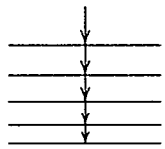
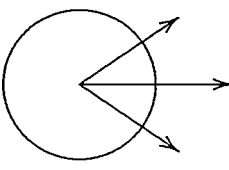
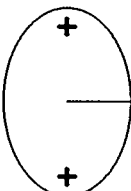
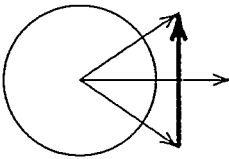
$\Delta I = 2$ ordinary bands	Characteristic of rotational bands	$\Delta I = 1$ shears bands
 <p style="text-align: center;">gradual alignment of many short vectors</p>	<p style="text-align: center;">regular <math>E_\gamma \propto I</math></p>  <p style="text-align: center;">enhanced transitions</p>	 <p style="text-align: center;">gradual alignment of few long vectors</p>
<p style="font-size: 1.2em; font-weight: bold;">E2</p>  <p style="text-align: center;">electric quadrupole mass distribution</p> <p style="text-align: center;">classic and quantal</p>	<p style="text-align: center;">possibly to define the orientation (with respect to the a. m. vector)</p> <p style="text-align: center;">large, collective isotropy broken "inertia" <math>\mathcal{J}^{(2)} = \Delta I / \Delta E_\gamma</math></p>	<p style="font-size: 1.2em; font-weight: bold;">M1</p>  <p style="text-align: center;">magnetic dipole current distribution</p> <p style="text-align: center;">quantal</p>
<b>electric</b>	<b>rotation</b>	<b>magnetic</b>

Table 1: The relation between electric and magnetic rotation

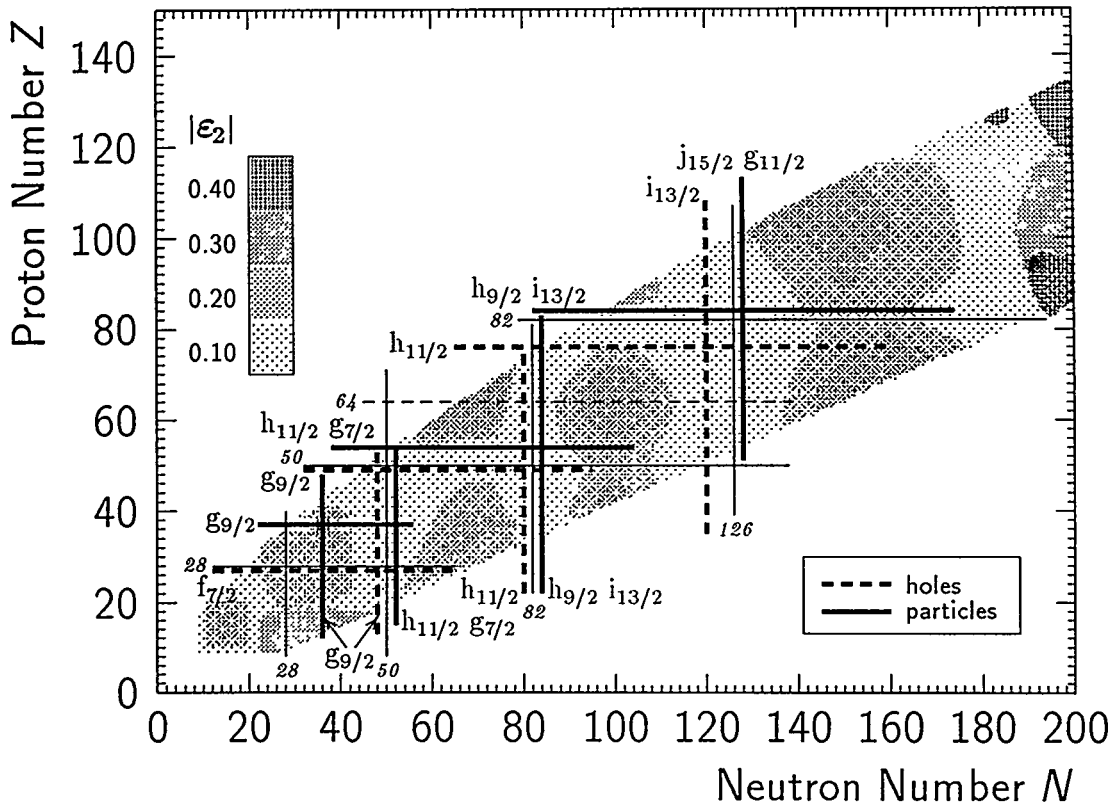


Figure 5: Appearance of magnetic rotation. Full drawn lines indicate the location of the high  $j$  particles and dashed ones of the high  $j$  holes. The grey scale gives the deformation. The corners where full and dashed lines intersect are particularly favorable for magnetic rotation.

Weakly deformed nuclei may show regular rotational sequences. These are not related to deformed configurations coexisting with the spherical ones. They are a manifestation of the rotation of a long magnetic dipole vector, which breaks the spatial isotropy. The fingerprint of this magnetic rotation are bands with strong M1 and very weak E2 crossover transitions.

### 3 $\Delta I = 4$ staggering

It has recently been found that some superdeformed  $\Delta I = 2$  bands in the mass 150 and 190 regions [8, 9] but also normally deformed nuclei [10, 11] show a slight  $\Delta I = 4$  staggering, i. e. the curve found by interpolating the sequence  $I = I_0 + 4n$  is by a few  $keV$  displaced from the curve obtained by interpolating the sequence  $I = I_0 + 2 + 4n$ . This energy displacement has been interpreted as a consequence of an inherent fourfold symmetry. The subject is discussed in the lectures by I. Hamamoto, B. Mottelson and I. Pavlichenko [12, 13]. Hamamoto and Mottelson ascribe the staggering to a nonaxial deformation that makes the *long* axis of the nucleus to a fourfold ( $C_4$ ) symmetry axis. In their approach the bands are described by the rotational hamiltonian

$$H = A_1 I_1^2 + A I_3^2 + B_1 (I_1^2 - I_2^2)^2, \quad A = A_3 - A_1 = \frac{1}{2} \left( \frac{1}{\mathcal{J}_3} - \frac{1}{\mathcal{J}_1} \right) \quad (7)$$

(We have added the first term that is unimportant for the staggering.) It is found that a sizable staggering appears only if  $B_1/A > 10^{-2}$ .

As an alternative to Hamamoto's and Mottelson's explanation of the origin of the staggering we trace it back to the restriction of the basis in a bandmixing picture (c. f. also the poster by A. Macciavelli et al. at this conference [14]). Using the conjugate variables  $I_3$  and  $\phi$ , where  $\phi$  is the angle appearing for  $\vec{I}$  in polar coordinates, the hamiltonian (7) is given by (c. f. [12])

$$H = A_1 I^2 + A I_3^2 + B_1 I^4 (\cos 2\phi)^2 \quad (8)$$

In the basis  $|K\rangle$  of the eigenfunctions of  $I_3$  one has

$$\langle K | (\cos 2\phi)^2 | K' \rangle = -\frac{1}{4} \delta_{KK' \pm 4} + \frac{1}{2} \delta_{KK'} \approx -\frac{d^2}{dK^2} \quad (9)$$

As a consequence of the  $C_4$  symmetry, the hamiltonian couples  $K$  only in steps of 4. The eigenvalue problem corresponds to a harmonic oscillator with the spring constant  $C = 2A$  and the mass parameter  $M = (2I^4 B_1)^{-1}$ . The ground state probability distribution has the width  $\Delta K = I(B_1/A)^{1/4}$ . There is the additional constraint that  $K \leq I$ . The fact that all components with  $K > I$  must be equal to zero makes the yrast energy somewhat larger than the one of the oscillator without the constraint. The constraint is relaxed with increasing  $I$  but only in steps of 4, since the  $K$  values differ by 4. The  $\Delta I = 4$  staggering reflects the fact that every 4 units in  $I$  there is a relaxation giving rise to an extra energy gain. However, sizable staggering appears only, if the wavefunction is large enough for  $K = I$  to experience the constraint. The numerical calculations indicate that this is the case for  $\Psi(K = I)^2 > 5 \times 10^{-5}$  or  $B_1/A > 10^{-2}$ . From the uncertainty principle it follows that the distribution in  $\phi$  must be sufficiently narrow ( $\Delta\phi \sim 1/\Delta K$ ). This localization requires a sufficiently strong  $\phi$ -dependence of  $H$ .

We have used TAC to investigate whether a deformation of the  $C_4$  type is able to generate staggering. Our approach is the following: As any Cranking theory, TAC only permits to calculate the classical energy. This function  $E(I, \vartheta, \phi)$  is compared with the energy obtained from the rotational hamiltonian (7) by substituting for the angular momentum operator  $\vec{I}$  the classical vector  $\vec{J}$ . In other words, the rotational hamiltonian is constructed by quantizing the classical one calculated by means of TAC.

We find the single particle states generated by the TAC routhian

$$h' = h_{mho}(\varepsilon_2) - \hbar\omega_o\varepsilon_{44}\rho^2(Y_{44} + Y_{4-4}) - \vec{\omega} \cdot \vec{j} \quad (10)$$

$$\vec{\omega} = \omega(\sin \vartheta \cos \phi, \sin \vartheta \sin \phi, \cos \vartheta) \quad (11)$$

as functions of the orientation of the angular velocity, where  $h_{mho}(\varepsilon_2)$  is the standard Nilsson hamiltonian. The classical energy is calculated as

$$E(I, \vartheta, \phi) = \langle h' \rangle + \vec{\omega} \cdot \vec{J} \quad (12)$$

where  $\vec{J} = \langle \vec{j} \rangle$  and  $\omega$  is chosen such that  $J = I + 1/2$ .

As an example, we study  $Z = 80$  and  $N = 114$  with the deformations  $\varepsilon_2 = 0.42$  and  $\varepsilon_4 = 0.1$  at the angular momentum  $J = 39$  corresponding to  $\omega \approx 0.3 \text{ MeV}$ . The deformed potential substantially deviates from axial symmetry. Its shape looks like of a double pyramid with rounded edges.

As seen from eq. (8), the fourth order term disappears for  $\phi = 45^\circ$  and the angular momentum components should be given by the relation

$$J_1 = \mathcal{J}_1 \omega \sin \vartheta \quad J_3 = \mathcal{J}_3 \omega \cos \vartheta \quad (13)$$

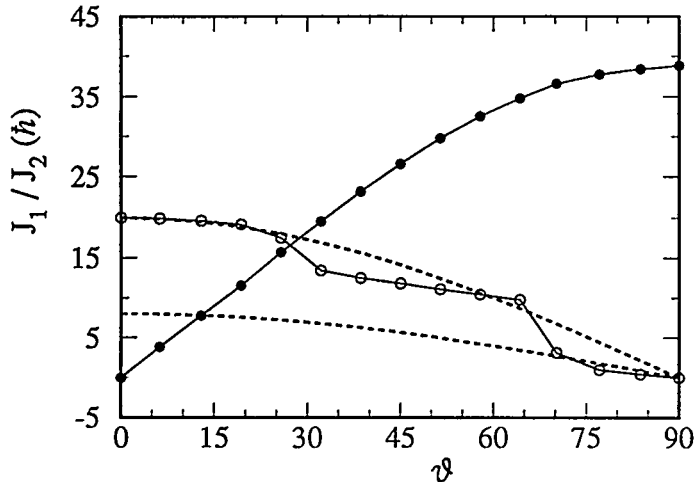


Figure 6: Angular momentum expectation values as functions of the orientation angle  $\vartheta$ . The filled circles give  $J_1$  and the open circles  $J_3$ .

fixing the two moments of inertia. Fig. 6 shows the calculated angular momenta. The component along the short axis shows the expected dependence, where  $\mathcal{J}_1 = 0.13keV^{-1}$ . The function  $J_3(\vartheta)$  shows steps, indicating rearrangements of particles. Hence, even with the assumed large  $\varepsilon_{44}$  value the long axis is not very collective and the application of a pure rotor hamiltonian at such high angular momentum is problematic. Accordingly, the determination of  $\mathcal{J}_3$  becomes to certain extent ambiguous. We find  $\mathcal{J}_3 = 0.07keV^{-1}$  if we decide to follow the steps adiabatically or  $\mathcal{J}_3 = 0.02keV^{-1}$  if the configuration at  $\vartheta = 90^\circ$  is kept fixed ( c. f. the dashed lines in fig. 6). Hence, our calculations place  $A$  in the interval  $4keV < A < 21keV$ .

The function  $E(J, \vartheta = 90^\circ, \phi)$  follows the expected  $(\cos(2\phi))^2$  dependence to a good approximation. For the coefficient we find  $B_1 J^4 = 50keV$  and  $370keV$  for the yrast and the lowest neutron p - h excitation, which correspond to  $B_1 = 2 \times 10^{-5}keV$  and  $1 \times 10^{-4}keV$ , respectively. Even if the lower limit  $A = 7keV$  is assumed the ratio  $B_1/A \sim 10^{-4} \dots 10^{-5}$ . This is much too small to generate any sizable staggering. In order to localize  $\phi$  sufficiently one needs  $B_1 > 10^{-2} \times A$ , corresponding to the coefficient  $B_1 J^4 > 180MeV$  for  $J = 40$ . It seems hard to imagine how a deformed potential could be capable of producing such a high barrier between the four minima of  $E(\phi)$ .

Assuming a substantial  $C_4$  distortion for superdeformed  $^{194}Hg$  we are able to construct a classical hamiltonian that has the form of the rotational hamiltonian used by Hamamoto and Mottelson to describe the  $\Delta I = 4$  staggering. However, the calculated variation of the energy when turning the angular momentum vector around the  $C_4$  axis is by far too small to allow the quantized version of this hamiltonian to generate a staggering of the observed order of magnitude.

## References

- [1] S. Frauendorf, Nucl. Phys. **A557** (1993) 259c
- [2] S. Frauendorf, T. Bengtsson, AIP Conference Proceedings **259** (1992) 223



- [3] A. Brokstedt et al. Nucl. Phys. **A571** (1994) 337 and G. Hagemann, lecture at this conference
- [4] G. Baldsiefen et al. Nucl. Phys. **A574** (1994) 521
- [5] J. B. Oliviera et al. Phys. Rev. **D** in print
- [6] H. Hübel, lecture at this conference
- [7] R. M. Clark, lecture at this conference
- [8] S. Flibotte et al., Phys. Rev. Lett. **71** (1993) 4299
- [9] B. Cederwall et al., Phys. Rev. Lett. **72** (1994) 3150
- [10] J. Hamilton, lecture at this conference
- [11] L. Peker et al., Phys. Rev. Lett. **50** (1983) 1749
- [12] I. Hamamoto and B. Mottelson, lectures at this conference
- [13] I. Pavlichenko, lecture at this conference
- [14] A. Macchiavelli et al., contribution to this conference and to be pub.

# High- $K$ structures at the yrast line

P.M. Walker

*Department of Physics, University of Surrey, Guildford GU2 5XH, UK*

*Multi-quasiparticle  $K$  isomers provide unique nuclear-structure information, but they are found only in the  $A \approx 180$  mass region of deformed nuclei. Good evidence for quenching of the monopole pair gaps and for the importance of residual interactions comes from isomer excitation energies, and decay rates show a remarkable sensitivity to the isomer's proximity to the yrast line. "Anomalous" decays appear to be related to the existence of large  $t$ -band components in the populated states.*

The first multi-quasiparticle  $K$  isomer, with two or more broken nucleon pairs, was discovered in  $^{178}\text{Hf}$  following neutron capture [1]. This 4-quasiparticle state was subsequently found to have  $K^\pi = 16^+$  and a mean-life of  $\tau = 45$  years. Nowadays, a far more potent method of producing  $K$  isomers is through fusion-evaporation reactions. The highest-spin yrast trap thus found in a well deformed nucleus is a 7-quasiparticle isomer in  $^{177}\text{Ta}$ , with  $K^\pi = 49/2^-$  and  $\tau = 200 \mu\text{s}$  [2]. Its decay path is shown in fig.1, where the coexistence of collective and intrinsic excitations is well illustrated. A 9-quasiparticle isomer with  $K^\pi = (57/2^-)$  and  $\tau > 10$  ns has been proposed [3] in  $^{175}\text{Hf}$ . Despite these successes, many other predicted  $K$  isomers are inaccessible, due to the present lack of appropriate beam/target combinations to generate sufficient angular momentum. Keeping in mind this restriction, which could lead to some bias in the interpretation, the present data are reviewed with regard to isomer excitation energies and decay rates.

Jain *et al.* [4] have recently found a successful prescription for calculating multi-quasiparticle excitation energies. There are three principal ingredients: the BCS approximation, blocking and residual interactions. The BCS method uses a monopole pair force to calculate the pair gap, with neutrons and protons treated separately; the correct average particle number is obtained by adjustment of the Fermi level. Blocking is accounted for by removing the Nilsson states with single occupancy from the BCS summations. Orbital-dependent residual interactions are estimated from the empirical  $n$ - $n$ ,  $p$ - $p$  and  $n$ - $p$  splittings for 2-quasiparticle states in even-mass nuclei, and then summed over all 2-nucleon combinations within a multi-quasiparticle configuration. Each of these three features is important for a realistic description of high- $K$  states, and excitation energies up to at least 5 MeV can be calculated to within a few percent. The ability of the calculations to reproduce the observed excitation energies is illustrated in fig.1 for  $^{177}\text{Ta}$ . The calculations also show a collapse of the pairing gap when three (or more) quasiparticles of a given nucleon type form a configuration close to the yrast line. Many new high- $K$  states have been predicted, and further experimental data are eagerly awaited. An interesting prediction that has just been confirmed [5] is the existence of an 8-quasiparticle yrast trap in  $^{178}\text{W}$ . In this case, the rotational band above the isomer provides additional information, as is discussed in another talk [6] at this conference.

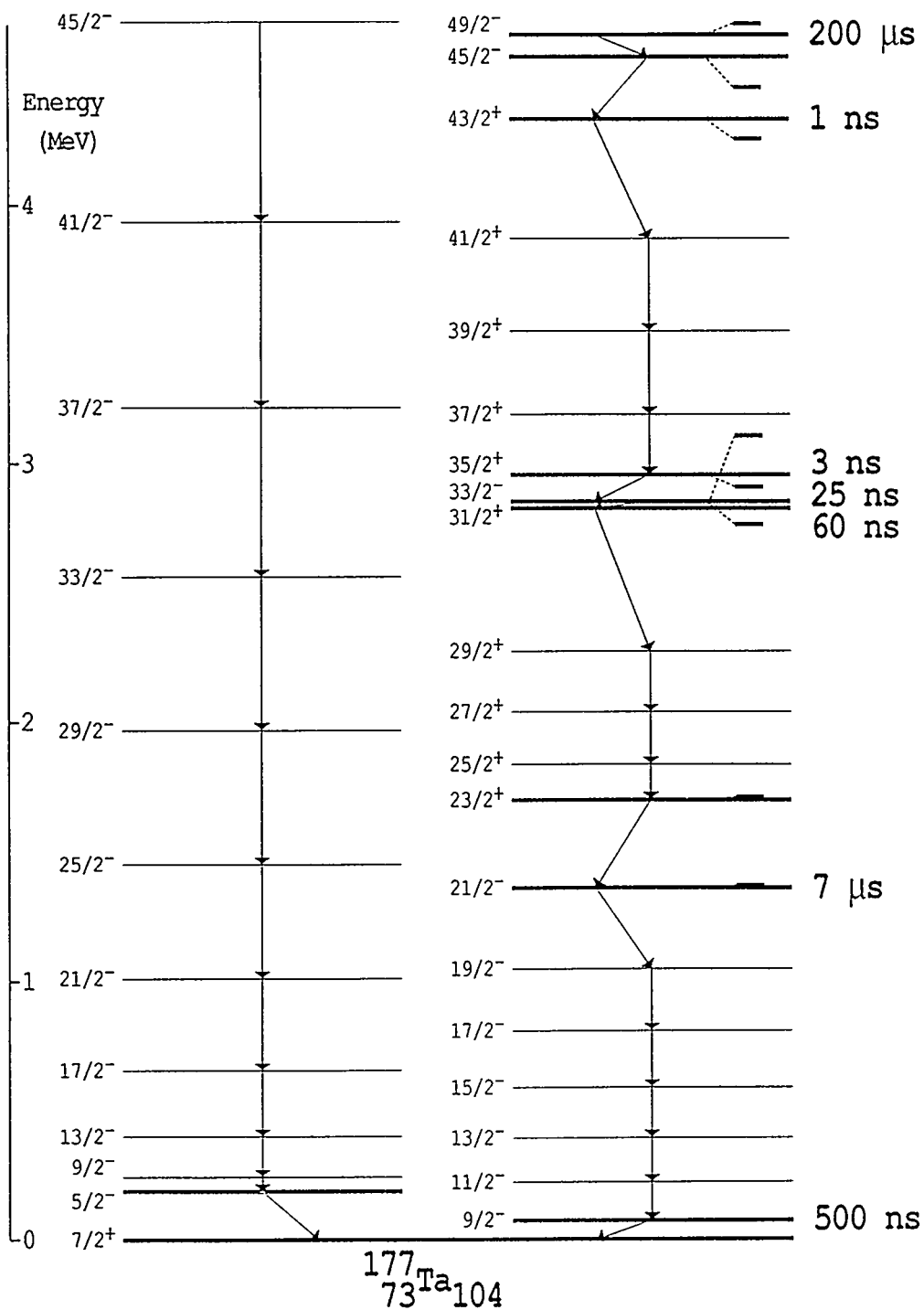


Figure 1. Schematic representation of the decay path of the 7-quasiparticle isomer in  $^{177}\text{Ta}$ , compared with the lowest-energy low- $K$  rotational band. The narrow levels on the right-hand side are those calculated (see text).

The transitions associated with  $K$ -isomer decays are frequently “forbidden” (*i.e.* when  $\Delta K > \lambda$ , the transition multipolarity) or at least they are highly retarded. The transition rates are therefore dependent on small wave-function admixtures, making them sensitive probes of the nuclear structure. The  $N=106$  isotones, for example, show a mean-life variation of 17 orders of magnitude in the decay of 4- and 5-quasiparticle isomers between  $^{178}\text{Hf}$  and  $^{182}\text{Os}$ , while the isomer excitation energies change by only a factor of two.  $^{178}\text{Hf}$  has the lowest 4-quasiparticle energy, with the longest mean-life, in the whole of the  $A \approx 180$  region. Of course, much of the mean-life variation comes from the trivial transition-energy factor, but even allowing for this, together with the multipolarity and the degree of  $K$  forbiddenness ( $\nu = \Delta K - \lambda$ ) the *reduced hindrance* still shows a strong excitation-energy dependence. (The reduced hindrance is defined by  $f_\nu = (\tau_\gamma/\tau_W)^{1/\nu}$ , where  $\tau_\gamma$  is the partial  $\gamma$ -ray mean-life and  $\tau_W$  is the Weisskopf single-particle estimate.) Indeed, the trend persists for all 4-or-more-quasiparticle isomers decays, illustrated in fig.2 for E2 transitions with  $\nu > 2$ .

One way to view the excitation-energy dependence is in terms of the density of states. The further above the yrast line that an intrinsic state of a given spin and parity is located, the more will be the admixtures of other lower- $K$  wave-functions, simply on account of their being more closely spaced. At least, the average effect of this should be in accordance with the observed trend of decreasing hindrance with increasing excitation energy, though large fluctuations might be expected. The lower reduced-hindrance values for the 5-quasiparticle isomer decays could possibly be related to a higher density of states in odd- $A$  nuclei.

It is striking that  $^{174}\text{Hf}$  [7],  $^{176}\text{W}$  [8] and  $^{182}\text{Os}$  [9], which have the highest energies relative to yrast, also have “anomalous” isomer decays, apparently bypassing intermediate- $K$  structures. (Note that it is the  $K^\pi = 16^{(+)}$  4-quasiparticle isomer that is represented for  $^{182}\text{Os}$ , not the  $K^\pi = 25^{(+)}$  6-quasiparticle isomer. The latter decays to the yrast band by a  $\Delta I = 1$ , presumably M1 transition.) There may be no need to invoke a tunneling description for their decay, since there is no clear deviation from the overall trend that would suggest the involvement of barrier *heights*. (The barrier height would be expected to drop significantly, on account of greater softness to axially asymmetric distortions, in going from  $^{174}\text{Hf}$  to  $^{182}\text{Os}$ .) However, there is other evidence to support a role for tunneling [8,9]. At the other extreme, the *yrast*-isomer decays are strongly retarded and do not show a decline in hindrance with increasing angular momentum, providing evidence for the stability of axial symmetry.

The above discussion is concerned primarily with  $K$  admixtures in the isomers themselves. It is important also to consider possible  $K$  admixtures in the *populated* states. In the  $A \approx 180$  region,  $t$  bands [10,11,12], that is  $(i_{13/2})^2$  bands with  $\langle K \rangle \approx \Omega_1 + \Omega_2$ , provide a mechanism for the introduction of high- $K$  components into *apparently* low- $K$  rotational bands, and there is evidence [13,14] for strong mixing between  $t$  bands and the usual  $s$  bands (with  $\langle K \rangle \approx |\Omega_1 - \Omega_2|$ ).

At least four data points in fig.2 are (or may be) significantly affected by  $t$ -band mixing, but the only clear case is  $^{179}\text{W}$ , where the  $t$  band is relatively well defined

[10]. A value of  $f_\nu = 2$  was previously deduced for the strongest 5-quasiparticle isomer decay path (a 610 keV, E2 transition) whereas  $f_\nu = 8$  is found after quantitative allowance for  $t$ -band mixing, and consistency with the systematics of fig.2 is then obtained (as illustrated). The other prime candidates for significant  $t$ -band influence are  $^{174}\text{Hf}$ ,  $^{176}\text{W}$  and  $^{182}\text{Os}$ , all with very low reduced-hindrance values. The corresponding data points in fig.2 have no allowance for  $t$ -band mixing. The  $^{182}\text{Os}$  value, for example, could increase from  $f_\nu = 2$  to  $f_\nu = 6$ , with comparable changes for  $^{174}\text{Hf}$  and  $^{176}\text{W}$ . Although there is insufficient experimental information to make quantitative corrections, it is clear that the intermediate- $K$  structures that appear to be bypassed by “anomalous” isomer decays, are not so much *bypassed* as *hidden* in the form of  $t$  bands. The influence of  $t$  bands on the tunneling interpretation remains to be explored.

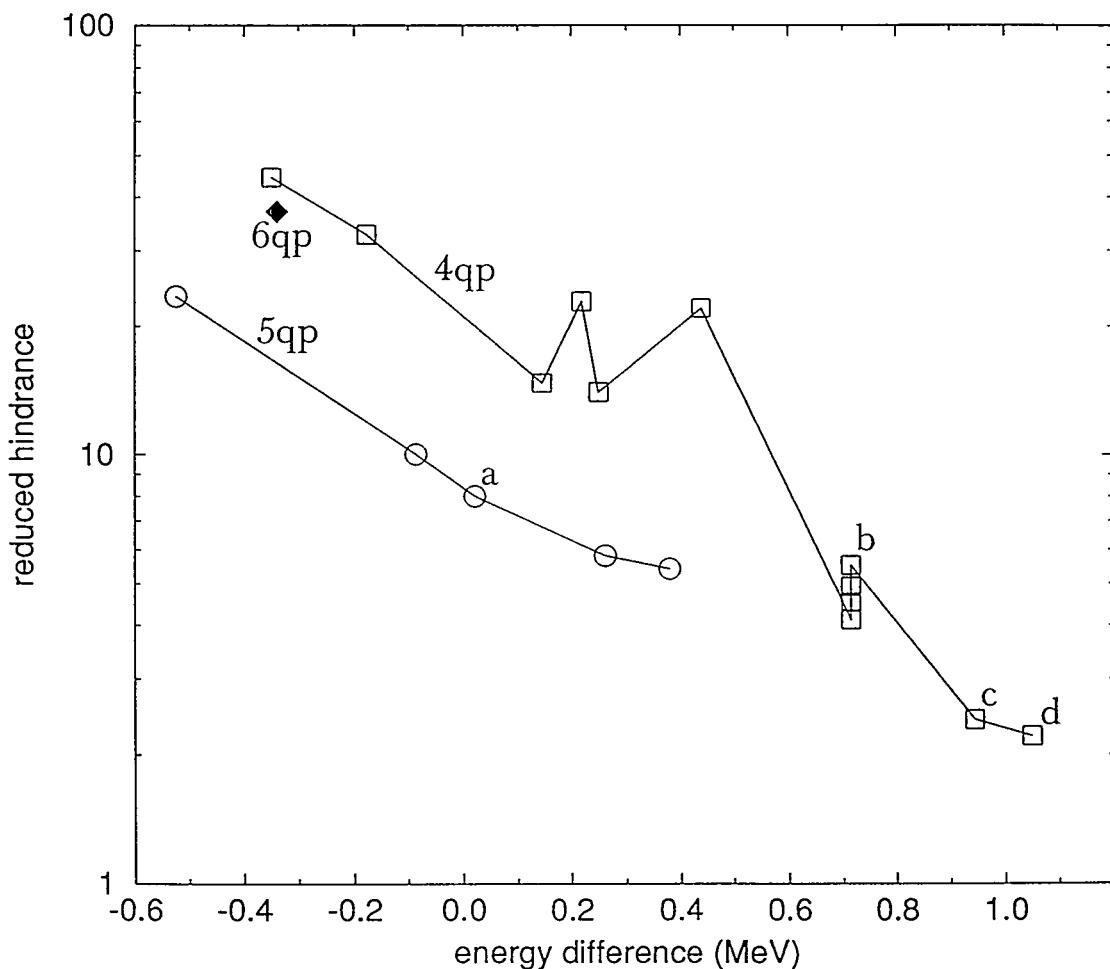


Figure 2. Reduced hindrance values for E2 transitions from 4-, 5- and 6-quasiparticle isomers, as a function of the isomer's energy relative to yrast (or yrare, if the isomer is itself yrast). There are no corresponding data for higher quasiparticle numbers. The data points labelled by letters correspond to isomer decays in  $^{179}\text{W}$  (a),  $^{174}\text{Hf}$  (b),  $^{176}\text{W}$  (c) and  $^{182}\text{Os}$  (d), discussed in the text.

Given the systematic nature of the reduced hindrance factors shown in fig.2, it is pertinent to consider whether this is a representative selection of nuclei, even within the confines of the  $A \approx 180$  region. Apparently it is not. Isomers surely exist with  $I > 16$  in  $^{178}\text{Hf}$  [15], but there is not the means to populate them. Higher-spin  $K$  isomers have been found, but not in the most favourable nuclei. Assuming that in some sense  $^{178}\text{Hf}$  is at the centre of a "diamond" of nuclei extending in the  $N, Z$  plane from  $^{174}\text{Hf}$  to  $^{182}\text{Hf}$ , and from  $^{174}\text{Er}$  to  $^{182}\text{Os}$ , each with, potentially, 6-or-more-quasiparticle isomers, only twelve of the 41 candidate nuclei are currently accessible at sufficiently high angular momentum. Of these twelve, six are now known to contain 6- or 7-quasiparticle isomers with  $\tau > 5$  ns, three have 6- or 7-quasiparticle states with shorter lifetimes, and three remain to be adequately studied. The other 29 candidates are inaccessible with stable beams and targets. At present, only *one part of one facet* of the isomer diamond is available for study.

In summary, considerable advances have been made with the study of multi-quasiparticle isomers, both theoretically and experimentally, but many issues remain to be clarified. Among these are the roles of higher-order pairing correlations,  $t$  bands and tunneling. From an experimental point of view, the availability of appropriate radioactive beams would enormously expand the range, in  $N$ ,  $Z$  and angular momentum, of accessible isomers.

## References

- [1] R.G. Helmer and C.W. Reich, Nucl. Phys. **A114** (1968) 649
- [2] M. Dasgupta et al., Phys. Lett. **B328** (1994) 16
- [3] N.L. Gjørup et al., Z. Phys. **A337** (1990) 353
- [4] K. Jain et al., Phys. Lett. **B322** (1994) 27,  
and SCNP preprint 94/6
- [5] P.M. Walker et al., to be published
- [6] G.D. Dracoulis et al., contribution to this conf.
- [7] P.M. Walker et al., Phys. Rev. Lett. **65** (1990) 416
- [8] B. Crowell et al., Phys. Rev. Lett. **72** (1994) 1164
- [9] P. Chowdhury et al., Nucl. Phys. **A485** (1988) 136
- [10] P.M. Walker et al., Nucl. Phys. **A568** (1994) 397
- [11] P.M. Walker et al., Phys. Lett. **B309** (1993) 17
- [12] S. Frauendorf, Nucl. Phys. **A557** (1993) 259c
- [13] P.M. Walker, Int. Conf. on the Future of Nuclear Spectroscopy, Crete (1993)
- [14] S. Frauendorf et al., contribution to this conf.
- [15] S. Åberg, Nucl. Phys. **A306** (1978) 89

## Lifetimes of Shears Bands in $^{199}\text{Pb}$

H. Hübel, M. Neffgen, G. Baldsiefen, W. Korten, D. Mehta, N. Nenoff, U.J. van Severen (Institut für Strahlen- und Kernphysik, Universität Bonn), H. Grawe, H. Kluge, K.H. Maier, (HMI Berlin), A. Korichi (IPN Orsay), M. Piiparinen (NBI Risø), Jie Meng and S.Fraundorf (Forschungszentrum Rossendorf)

In nuclei in the mass region around  $A=190-200$  a large number of regular sequences of strong M1 with weak E2 crossover transitions have recently been found [1-16]. An example of the  $\gamma$ -ray coincidence spectra obtained in-beam with the OSIRIS spectrometer array is shown in figure 1. It is the spectrum of band 2 in  $^{199}\text{Pb}$ , populated in the reaction  $^{186}\text{W} (^{18}\text{O},5n)$ . A partial level scheme of  $^{199}\text{Pb}$  is shown in figure 2. The regular sequences in the Pb region, like the one shown in figure 1, look like normal rotational bands built on excited quasiparticle states of high spin. Indeed, they follow very nicely the  $I(I+1)$  energy dependence. However, there exist several important differences which show that these bands are not of collective nature.

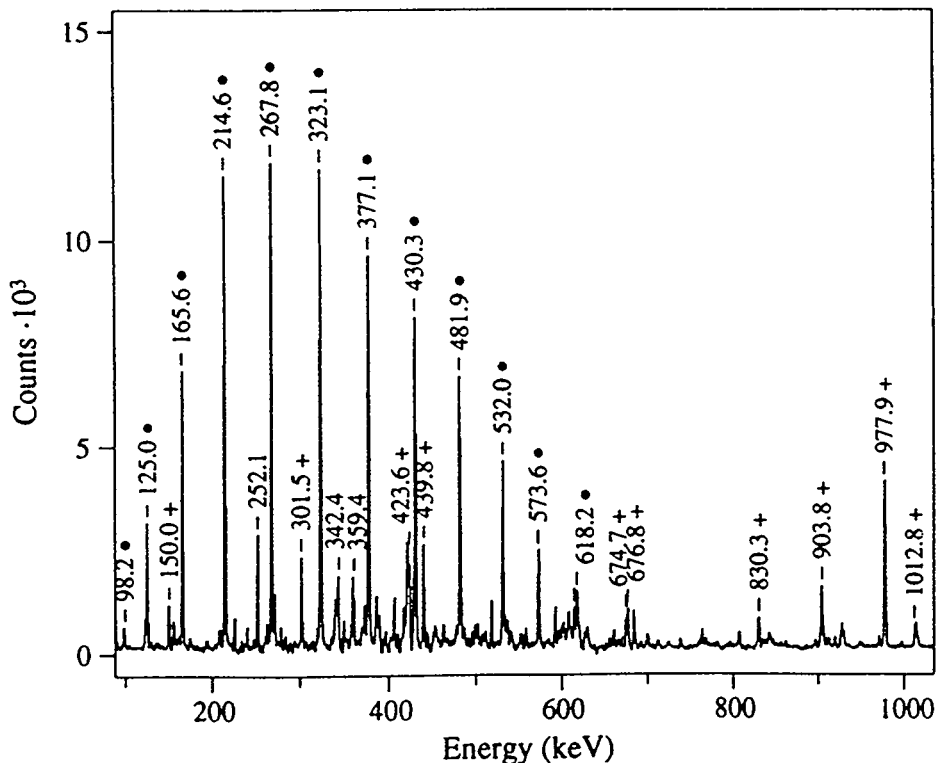


Fig. 1: Coincidence spectrum for dipole band 2 in  $^{199}\text{Pb}$  (see partial level scheme of fig. 2). Spectra with gates on several transitions have been added. Transitions marked by dots belong to the band, those marked by '+' signs to the spherical states in  $^{199}\text{Pb}$  [16].





In several light Pb isotopes there exist high-spin proton two-particle two-hole (2p2h) excitations with small oblate deformation, e.g. the  $8^+$  and  $11^-$  states with  $\pi\{h_{9/2}^2 s_{1/2}^{-2}\}8^+$  and  $\pi\{h_{9/2} i_{13/2} s_{1/2}^{-2}\}11^-$  structures, respectively. However, no rotational bands have been observed that are built directly on these states. Obviously their deformation and moment of inertia are so small that the collective rotational states lie too high in energy to compete with the other yrast or near-yrast states. The band heads of the dipole bands observed here

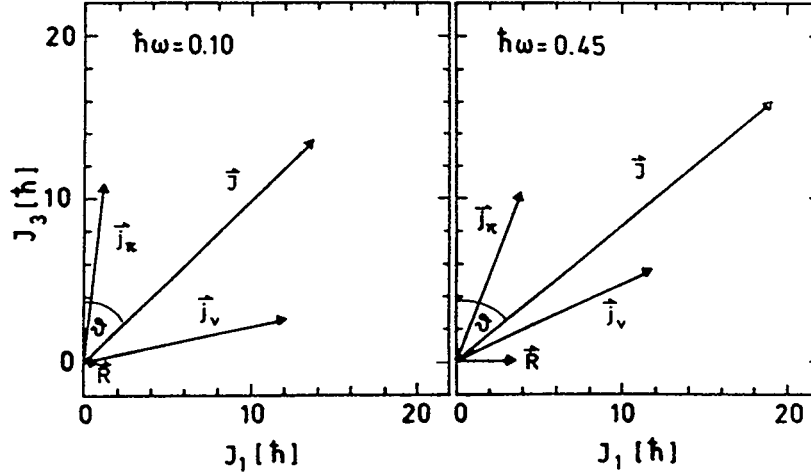


Fig. 3: Angular momentum coupling scheme at low and high rotational frequencies for the oblate  $\Delta I=1$  bands in the Pb region.

have higher spins. It has been suggested [1-5] that, in addition to the deformation-aligned high-K proton 2p2h excitations, rotation-aligned low-K neutron  $i_{13/2}$  hole states contribute to the configurations. Near the band head the proton-particle and neutron-hole spins are approximately perpendicular and the resulting total nuclear spin, therefore, points in-between these two directions. The coupling scheme is shown schematically on the left-hand side of figure 3. But the bands built on these excitations cannot be normal high-K rotational bands. Normal high-K bands develop a signature splitting at high spins due to the symmetry for rotation of  $180^\circ$  around an axis perpendicular to the deformation axis of the nucleus which is generally not observed here (see e.g. figs. 1 and 2).

We have performed calculations within the tilted-axis cranking (TAC) model [17] to describe the outlined situation theoretically. Within this model uniform rotation about an axis that is not one of the principal nuclear axes is considered. The tilting angle  $\vartheta$  (see figure 3) for which the energy in the rotating frame becomes minimal was calculated for various proton-neutron configurations. As expected, the tilting angle increases with an increasing number of neutron-hole excitations. However, within each configuration the angle depends only weakly on the rotational frequency or spin along the bands. This result is in striking contrast to normal high-K bands as they are known in many deformed nuclei. In those cases  $\cos\vartheta = K/I$  depends strongly on the spin  $I$  within the bands. Near the band head, where the total spin is dominated by the quasiparticle angular momenta ( $I \approx K$ ),  $\vartheta$  is close to zero (deformation alignment), but with increasing frequency the rotational angular momentum, which is perpendicular to the symmetry axis, gains more and more influence ( $I > K$ ), causing the total angular momentum to tilt into the direction

of the rotational angular momentum. Consequently the tilting angle increases from  $0^\circ$  towards  $90^\circ$  in the normal high-K bands. Because the tilting angle depends so little on the rotational frequency for the dipole bands, the collective angular momentum cannot play a dominant role in generating the total angular momentum. The major part of the angular momentum is gained by a gradual alignment of the individual proton and neutron spins into the direction of the total spin (see figure 3).

The continuous alignment of the proton and neutron spins into the direction of the total angular momentum may be viewed as the closing of the blades of a pair of shears, we therefore suggest to call these sequences "shears bands" [16]. The shears effect is an efficient way to gain angular momentum in cases where there are large particle and hole spins at right angles near the band head and the deformation is so small that the collective rotation takes more energy than the reorientation of the single-particle spins.

The measurement of lifetimes is a crucial test of the collectivity of nuclear states. Lifetimes of shears bands have been measured previously in  $^{197,198}\text{Pb}$  [18-20]. Although the experimental uncertainties are large, the results show that, indeed, the quadrupole collectivity is very low ( $B(E2) \approx 10$  Wu) and the deformation is small ( $\beta_2 < 0.1$ ). We have performed lifetime measurements of bands 1 and 2 in  $^{199}\text{Pb}$  (see fig. 2) using the Doppler-shift attenuation method (DSAM). The bands were populated in the reaction  $^{186}\text{W}(^{18}\text{O},5n)^{199}\text{Pb}$ . Two backings, Al and W, were used. Gamma-ray coincidences were measured with the OSIRIS and NORDBALL arrays at Berlin and Risø, respectively. Coincidence spectra with gates set on transitions below and above the states of interest were analysed. Lifetimes were obtained by fits of calculated line-shape curves to the Doppler-broadened lines [21] in the high-spin regions of the two bands. In the overlap region, the results for the two different backings are in agreement.

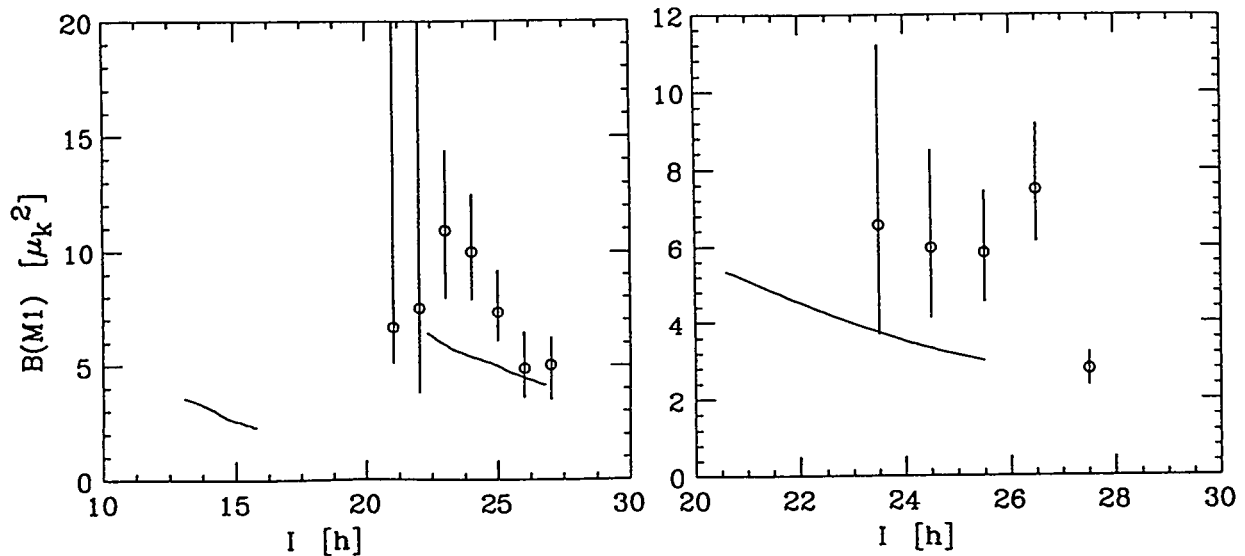


Fig. 4:  $B(M1)$  values for transitions in bands 1 (right) and 2 (left) of  $^{199}\text{Pb}$ . The curves have been calculated within the TAC model [16,17].

The  $B(M1)$  values that are deduced from the lifetimes are shown in fig. 4 where they are compared to the predictions of the TAC calculations. The agreement is reasonable. The large  $B(M1)$  rates support the proton configurations assumed for the bands. Using the lifetimes and the  $\Delta I=1/\Delta I=2$  intensity branching ratios, the  $B(E2)$  values can also be obtained. Here, the uncertainties are larger because of the small  $\Delta I=2$  E2 crossover intensities, but the resulting  $B(E2)$  rates are of the order of a few Weisskopf units confirming the previous conclusion of low quadrupole collectivity.

For most of the normal rotational bands the ratio of the moment of inertia to the square of the quadrupole moment,  $J/Q^2$ , is around unity. For the shears bands, however, this ratio is more than an order of magnitude larger. This shows that another effect than the rotation of the deformed density distribution - i.e. the shears effect described above - is mainly responsible for the moment of inertia. Since the apparent moment of inertia originates from the reorientation of the proton and neutron spins whose absolute values are frozen by the quantization of the single-particle motion, it has been called "quantal inertia" [16,17].

#### References

- 1) G. Baldsiefen et al., Proc. of the X. Intern. School on Nucl. Phys., Neutron Phys. and Nucl. Energy, Varna, 1991, eds. W. Andreitscheff and D. Elenkov (Inst. of Nucl. Research and Energy, Sofia) and Phys. Lett. B275 (1992) 252
- 2) R.M. Clark et al., Phys. Lett. B275 (1992) 247
- 3) A. Kuhnert et al., Phys. Rev. C46 (1992) 133 and Nucl. Phys. A553 (1993) 567c
- 4) R.M. Clark et al., Z. Phys. A342 (1992) 371
- 5) G. Baldsiefen et al., Z. Phys. A343 (1992) 245
- 6) J.R. Hughes et al., Phys. Rev. C48 (1993) R1337
- 7) P. Dagnall et al., J. Phys. G19 (1993) 465
- 8) D. Mehta et al., Z. Phys. A346 (1993) 169
- 9) R.M. Clark et al., Nucl. Phys. A562 (1993) 121
- 10) A.J.M. Plompen et al., Nucl. Phys. A562 (1993) 61
- 11) R.M. Clark et al., J. Phys. G19 (1993) L57
- 12) P. Dagnall et al., to be published
- 13) N. Roy et al., Phys. Rev. C47 (1993) R930
- 14) B. Cederwall et al., Phys. Rev. C47 (1993) 2443
- 15) Y. LeCoz et al., Z. Phys. A348 (1994) 87
- 16) G. Baldsiefen et al., Nucl. Phys. A574 (1994) 521
- 17) S. Frauendorf, Nucl. Phys. A557 (1993) 259c
- 18) T.F. Wang et al., Phys. Rev. Lett. 69 (1992) 1737
- 19) J.R. Hughes et al., Phys. Rev. C48 (1993) 2135
- 20) R.M. Clark et al., Phys. Rev. C, in press
- 21) W. Schmitz et al., Nucl. Phys. A539 (1992) 112

# Lifetimes of States in the M1-Bands of $^{197,198}\text{Pb}$

R.M.Clark<sup>1,8</sup>, R.Wadsworth<sup>1</sup>, H.R.Andrews<sup>2</sup>, C.W.Beausang<sup>3</sup>, M.Bergstrom<sup>3</sup>, S.Clarke<sup>3</sup>,  
E.Dragulescu<sup>1,7</sup>, T.Drake<sup>4</sup>, P.J.Dagnall<sup>3</sup>, A.Galindo-Uribarri<sup>2</sup>, G.Hackman<sup>5</sup>, K.Hauschild<sup>1</sup>,  
I.M.Hibbert<sup>1</sup>, V.P.Janzen<sup>2</sup>, P.M.Jones<sup>3</sup>, R.W.MacLeod<sup>2</sup>, S.M.Mullins<sup>5</sup>, E.S.Paul<sup>3</sup>, D.C.Radford<sup>2</sup>,  
A.Semple<sup>3</sup>, J.F.Sharpey-Schafer<sup>3</sup>, J.Simpson<sup>6</sup>, D.Ward<sup>2</sup>, G.Zwartz<sup>4</sup>

<sup>1</sup> Department of Physics, University of York, Heslington, York, YO1 5DD, UK.

<sup>2</sup> AECL Research, Chalk River Laboratories, Chalk River, ON KOJ 1J0, Canada.

<sup>3</sup> Oliver Lodge Laboratory, University of Liverpool, Liverpool, L69 3BX, UK.

<sup>4</sup> Department of Physics, University of Toronto, Toronto, ON M5S 1A7, Canada.

<sup>5</sup> Department of Physics and Astronomy, McMaster University, Hamilton, ON L8S 4M1, Canada.

<sup>6</sup> Nuclear Structure Facility, Daresbury Laboratory, Daresbury, Warrington, WA4 4AD, UK.

<sup>7</sup> Institute for Atomic Physics, Tandem Laboratory, Bucharest-Magurele R-79600, Romania.

<sup>8</sup> Nuclear Science Division, Lawrence Berkeley Laboratory, Berkeley, CA 94702, USA.

## Abstract

Lifetimes of states in four of the M1-bands in  $^{197,198}\text{Pb}$  have been measured with the recoil-distance technique. Using all the available data on lifetimes and branching ratios, and assuming pure magnetic dipole transitions, we deduce reduced transition probabilities. The results are consistent with weakly oblate structures involving high-K proton configurations coupled to rotationally aligned neutrons. Comparisons are made to the theoretical estimates of the Dönau and Frauendorf semi-classical model and the Tilted Axis Cranking (TAC) model.

## 1 Introduction

The recent observation of cascading sequences of magnetic dipole transitions in the neutron-deficient Pb [1,2] and Bi [3,4] nuclei has prompted a great deal of interest. These structures have generally been interpreted as weakly oblate ( $\beta_2 \sim -0.05$  to  $-0.15$ ) high-K proton configurations coupled to rotationally aligned neutrons. The assignment of configurations to each band has so far been based on considerations, such as:

- Regularity of energy spacing,  $\Delta E_\gamma$ , between successive transitions.
- Lower limits to the  $B(M1)/B(E2)$  ratios.
- Behaviour of the dynamic moments of inertia,  $\mathfrak{J}^{(2)}$ , as functions of rotational frequency,  $\omega$ .
- Identical transition energies (to within  $\sim 3$  keV) of different bands in different nuclei.

In order to provide further evidence for configuration assignments accurate lifetime measurements for states within the bands have to be made. These can then be related to theoretical predictions of the magnetic dipole (M1) transition rates for the various possible configurations. If accurate branching ratios are known for the crossover decays, the E2 transition rate can be used to deduce the quadrupole moments of the structures. The first Doppler Shift Attenuation Method (DSAM) lifetime measurements have recently been reported for two of the bands in  $^{198}\text{Pb}$  [5] and for the strong regular band in  $^{197}\text{Pb}$  [6]. These support the oblate interpretation but do not uniquely specify a configuration for each band.

Here, we present lifetime measurements of several states in each of four different dipole sequences, two in  $^{197}\text{Pb}$  and two in  $^{198}\text{Pb}$ . The results were obtained from a recoil distance (RDM) experiment with the 8pi spectrometer at the Chalk River Laboratory, which was specifically aimed at measuring the lifetimes of states near to the bandheads of each structure, complementing the previous DSAM measurements. Accurate branching ratios, required to deduce B(M1) and B(E2) transition rates,

Table 1: Measured lifetimes,  $\tau$  (ps), branching ratios,  $B_\gamma$ , and reduced transition strengths,  $B(M1)$  (Wu) and  $B(E2)$  ( $e^2b^2$ ), of states in  $^{197}\text{Pb}$  and  $^{198}\text{Pb}$ . The third column indicates the lifetime experiment. DSAM results came from [5,6], whilst RDM results are from the present study. All the branching ratios, used to calculate  $B(M1)$ -values, are from the EUROGAM data. A dash in that column indicates that no associated E2-crossover transition could be identified. The 207 keV transition of band 1 in  $^{198}\text{Pb}$  is marked with an asterisk since it is a doublet and the lifetime extracted will have a contribution from both  $\gamma$ -ray components.

	M1 (keV)	Expt	$\tau$ (ps)	$B_\gamma$	$B(M1)$ (Wu)	E2 (keV)	$B(E2)$ ( $eb$ ) <sup>2</sup>
Band 3 $^{198}\text{Pb}$	476	DSAM	0.27(7)	0.77(2)	$0.74^{+0.34}_{-0.14}$	948	$0.091^{+0.032}_{-0.019}$
	472	DSAM	0.22(6)	0.84(2)	$0.99^{+0.49}_{-0.19}$	917	$0.092^{+0.035}_{-0.020}$
	445	DSAM	0.24(4)	0.87(2)	$1.07^{+0.38}_{-0.17}$	868	$0.090^{+0.018}_{-0.013}$
	423	DSAM	0.46(10)	0.88(2)	$0.69^{+0.26}_{-0.12}$	813	$0.060^{+0.017}_{-0.011}$
	390	DSAM	0.72(10)	0.91(2)	$0.55^{+0.11}_{-0.08}$	733	$0.051^{+0.008}_{-0.006}$
	343	DSAM	1.14(23)	0.89(2)	$0.48^{+0.11}_{-0.08}$	622	$0.085^{+0.021}_{-0.015}$
	279	RDM	2.1(5)	-	$0.45^{+0.12}_{-0.09}$	-	-
	216	RDM	1.8(5)	-	$0.83^{+0.32}_{-0.18}$	-	-
	156	RDM	2.7(9)	-	$0.67^{+0.34}_{-0.17}$	-	-
B $^{198}\text{Pb}$	322	RDM	>8	-	-	-	-
	264	RDM	>4	-	-	-	-
	532	RDM	>4	-	-	-	-
Band 1 $^{198}\text{Pb}$	506	DSAM	0.052(11)	0.86(2)	$3.7^{+1.1}_{-0.9}$	970	$0.24^{+0.06}_{-0.04}$
	464	DSAM	0.099(25)	0.91(2)	$2.6^{+0.9}_{-0.5}$	886	$0.14^{+0.05}_{-0.03}$
	422	DSAM	0.20(4)	0.90(2)	$1.6^{+0.5}_{-0.3}$	797	$0.11^{+0.03}_{-0.02}$
	375	DSAM	0.36(10)	0.91(2)	$1.2^{+0.5}_{-0.3}$	701	$0.12^{+0.05}_{-0.03}$
	326	DSAM	0.58(15)	0.95(2)	$1.1^{+0.5}_{-0.3}$	607	$0.10^{+0.03}_{-0.02}$
	280	RDM	1.1(6)	-	$0.8^{+1.0}_{-0.3}$	-	-
	238	RDM	0.85(30)	-	$1.5^{+0.8}_{-0.4}$	-	-
	207*	RDM	2.1(4)*	-	$0.75^{+0.18*}_{-0.12}$	-	-
A $^{198}\text{Pb}$	429	RDM	3.5(15)	-	-	-	-
	228	RDM	4.6(14)	-	-	-	-
Regular $^{197}\text{Pb}$	371	DSAM	0.36(13)	-	$1.3^{+0.4}_{-0.4}$	-	-
	467	DSAM	0.20(5)	0.88(2)	$1.4^{+0.4}_{-0.4}$	913	$0.08^{+0.03}_{-0.03}$
	446	DSAM	0.12(6)	0.83(2)	$2.2^{+1.2}_{-1.2}$	850	$0.26^{+0.09}_{-0.06}$
	404	DSAM	0.21(5)	0.91(2)	$2.0^{+0.5}_{-0.5}$	741	$0.16^{+0.09}_{-0.06}$
	337	DSAM	0.42(12)	-	$1.6^{+0.5}_{-0.5}$	-	-
	267	RDM	1.2(3)	-	$1.01^{+0.67}_{-0.29}$	-	-
	201	RDM	0.9(4)	-	$2.08^{+1.25}_{-0.57}$	-	-
	151	RDM	1.8(8)	-	$1.32^{+1.32}_{-0.44}$	-	-
Irregular $^{197}\text{Pb}$	294	RDM	1.3(3)	0.90(2)	$0.59^{+0.17}_{-0.12}$	659	$0.050^{+0.015}_{-0.010}$
	365	RDM	1.3(3)	0.85(2)	$0.34^{+0.11}_{-0.08}$	750	$0.040^{+0.012}_{-0.007}$
	385	RDM	1.1(3)	0.87(2)	$0.35^{+0.14}_{-0.08}$	755	$0.039^{+0.015}_{-0.008}$
	370	RDM	1.3(3)	0.89(2)	$0.34^{+0.11}_{-0.07}$	729	$0.034^{+0.010}_{-0.006}$
	359	RDM	1.3(3)	0.92(2)	$0.38^{+0.11}_{-0.08}$	629	$0.051^{+0.015}_{-0.010}$
	270	RDM	2.8(4)	-	$0.31^{+0.06}_{-0.05}$	-	-
	152	RDM	3.1(7)	-	$0.76^{+0.22}_{-0.14}$	-	-

were found by the analysis of high-fold, high-statistics data taken with the EUROGAM spectrometer at the Daresbury Laboratory. Details of both of these experiments can be found in [7]. The deduced M1 transition rates are compared with theoretical estimates of the Dönau and Frauendorf semi-classical model [8] and the Tilted Axis Cranking (TAC) model [9].

## 2 Results

The lifetimes of sixteen levels from four bands (two in  $^{197}\text{Pb}$  and two in  $^{198}\text{Pb}$ ) have been measured. In addition, estimates of the lifetimes of several states beneath both the bands in  $^{198}\text{Pb}$  have been made. In order to aid the discussion, the labelling scheme given in [1] will be used for the structures in  $^{198}\text{Pb}$ . The two bands in  $^{197}\text{Pb}$  for which lifetime measurements were possible are those described in [10,11].

Table 1 summarizes the results obtained in the present work together with the results of the previous DSAM measurements for the bands in  $^{198}\text{Pb}$  [5] and the regular band in  $^{197}\text{Pb}$  [6]. Table 1 also contains the corresponding B(M1) and B(E2) values which have been deduced from the formulae:

$$B(M1) = \frac{0.03183B_\gamma}{E_\gamma^3\tau(1 + \alpha_{TOT})} \quad [Wu] \quad (1)$$

$$B(E2) = \frac{0.08156B_\gamma}{E_\gamma^5\tau(1 + \alpha_{TOT})} \quad [e^2b^2] \quad (2)$$

$E_\gamma$  is the transition energy in MeV and  $\tau$  is the mean intrinsic lifetime of the state in ps. The in-band transitions were assumed to be of pure M1 character. This assumption is based on the results of previous studies which generally found very small negative mixing ratios. The branching ratios,  $B_\gamma$ , measured from the EUROGAM data are also given in Table 1. This is the first time that several associated E2-quadrupole transitions have been firmly identified in this type of structure.

## 3 Discussion

In the following discussion it is convenient to use the labelling convention developed in [1] whereby the (unpaired) neutron occupations are given relative to the oblate N=120 subshell closure. The configurations that have been previously proposed for the four structures [1] are presented in Table 2. Different configurations will generally have different B(M1) values associated with them. By comparing the values in Table 1 it is clear that the B(M1) rates for band 1 in  $^{198}\text{Pb}$  and the regular band of  $^{197}\text{Pb}$  are similar. They are greater on average than the values for band 3 in  $^{198}\text{Pb}$  which in turn are greater than the B(M1) values for the irregular sequence in  $^{197}\text{Pb}$ . The situation is illustrated in Fig. 1. It may be concluded from these observations that at least three different configurations must be involved in these structures. This is in accordance with the configuration assignments show in Table 2.

Table 2: The proposed configurations from [1] for the bands in  $^{197,198}\text{Pb}$ .

Structure	Nucleus	Configuration
Band 1	$^{198}\text{Pb}$	$\pi(h_{9/2} \otimes i_{13/2}) \otimes \nu 6^{-4}$
Band 3	$^{198}\text{Pb}$	$\pi(h_{9/2})^2 \otimes \nu 6^{-3} 5^{-1}$
Regular	$^{197}\text{Pb}$	$\pi(h_{9/2} \otimes i_{13/2}) \otimes \nu 6^{-3} 5^{-2}$
Irregular	$^{197}\text{Pb}$	$\pi(h_{9/2} \otimes s_{1/2}) \otimes \nu X$

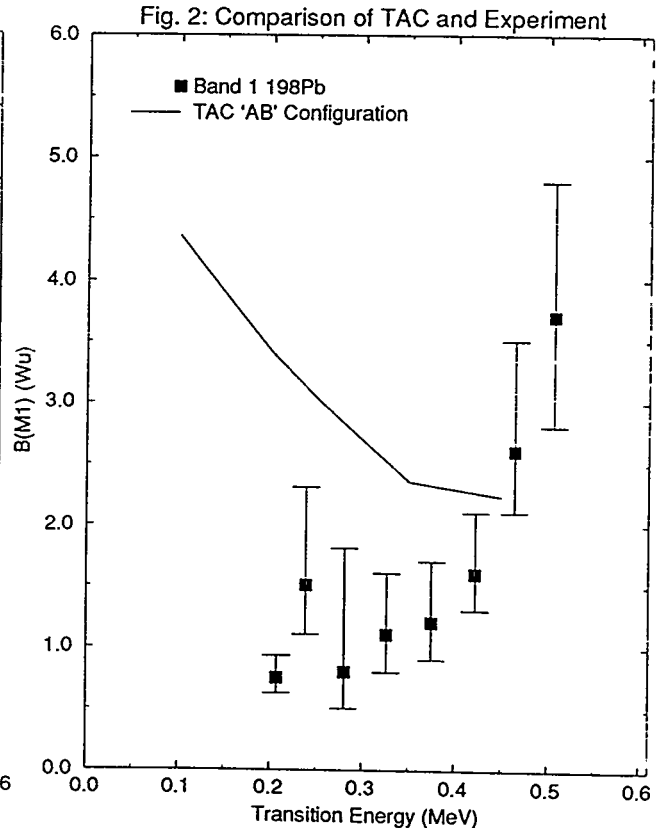
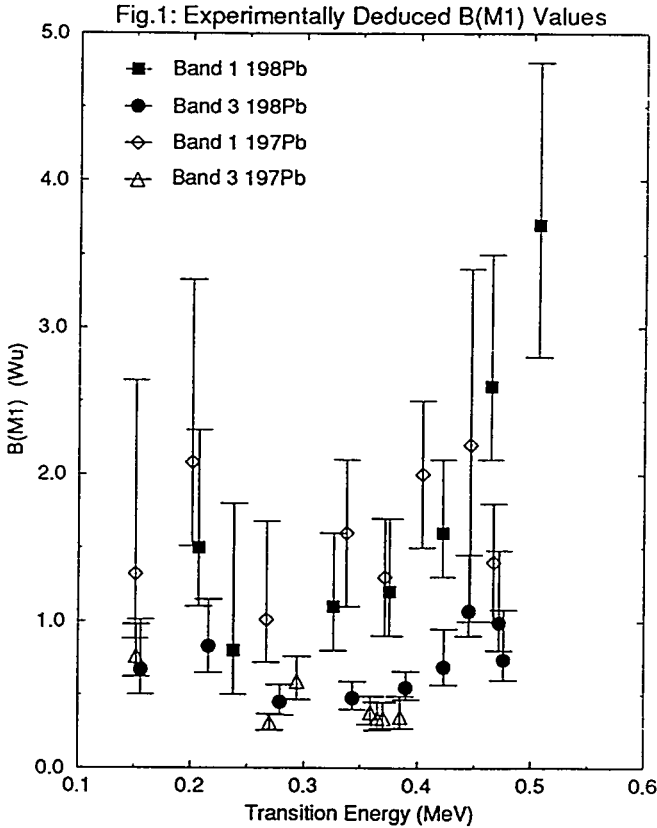
The  $(h_{9/2} \otimes i_{13/2})_{K=11}$  proton configuration is predicted to be the most deformed of the structures and it is expected to have larger B(M1) and B(E2) transition rates than either the  $(h_{9/2})^2_{K=8}$ , or  $(h_{9/2} \otimes s_{1/2})_{K=5}^{-1}$  configurations (assuming similar numbers of  $i_{13/2}$  (N=6) neutrons). Indeed, the

highest measured B(M1) and B(E2) values are found for the two structures that are associated with this proton configuration. Using the B(E2) values it is possible to obtain estimates of the intrinsic quadrupole moment since, in a rigid rotor model:

$$B(E2) = \frac{5}{16\pi} Q_0^2 \langle I + 2K \mid 20 \mid IK \rangle^2 \quad (3)$$

Note, to estimate the  $Q_0$  values a model dependent approach is necessary. The accuracy of eqn. (3) can therefore be questioned. This is especially true since  $K$  is not a good quantum number, and the validity of using a rigid rotor approximation is unclear. The intrinsic quadrupole moment of the irregular band in  $^{197}\text{Pb}$  was found to be  $Q_0=1.0(1)$  eb while that of band 1 in  $^{198}\text{Pb}$  was  $Q_0=2.0(2)$  eb. The intrinsic quadrupole moment for band 3 in  $^{198}\text{Pb}$  was found to lie at an intermediate value. These are very weakly oblate deformed structures. There is consistency with the configuration assignments presented in Table 2 since the TRS calculations predict that the  $(h_{9/2} \otimes s_{1/2})_{K=5}$  proton configuration should have the lowest deformation ( $\beta_2 \sim 0.07$ ) while the  $(h_{9/2} \otimes i_{13/2})_{K=11}$  structure should have the largest deformation ( $\beta_2 \sim -0.15$ ). The deformation of the  $(h_{9/2})_{K=8}^2$  configuration is between these two ( $\beta_2 \sim -0.10$ ).

Evidently there is good qualitative agreement between the results and the proposed configuration assignments presented in Table 2. For a more quantitative comparison absolute B(M1) transition probabilities need to be calculated within an appropriate theoretical framework. A simple approach is to apply the semi-classical Dönau and Frauendorf formula [8] which computes contributions to the B(M1) from both the deformation-aligned protons and rotationally aligned neutrons. The theoretical values overestimate the measured B(M1)'s by at least a factor of two, especially when one or more  $i_{13/2}$  neutrons are involved. For instance, the average value of the experimentally deduced B(M1)'s for band 1 of  $^{198}\text{Pb}$  is  $1.66^{+0.26}_{-0.16}$  Wu while the Dönau and Frauendorf theoretical estimate for the  $\pi(h_{9/2} \otimes i_{13/2})_{K=11} \otimes \nu i_{13/2}^2$  configuration is  $\simeq 5.0$  Wu. The contribution of other alignable neutrons ( $N=5$ ), occupying orbitals close to the Fermi surface (e.g.  $p_{3/2}$ ,  $p_{1/2}$ ,  $f_{5/2}$ ), will raise the calculated B(M1) estimates by  $\sim 10\%$ .



The combination of high-spin protons and high-spin neutrons associated with these oblate dipole bands presents an unusual circumstance, possibly not described by the familiar coupling schemes of angular momentum. A new approach has been provided by Tilted Axis Cranking (TAC) [9]. This provides a semi-classical description of many-quasiparticle  $\Delta I=1$  bands at high-spin. Enhanced M1 transitions arise naturally as a consequence of the breaking of signature symmetry.

A calculation of the B(M1) transition rates for the  $\pi(h_{9/2} \otimes i_{13/2}) \otimes \nu(6^{-x} 5^y)$  configurations in  $^{198}\text{Pb}$  has recently been reported [9]. The neutron configurations were generated by excitations of the  $i_{13/2}$  ABC quasineutron states and the negative parity state E (in Cranked Shell Model notation). The deformation was fixed at  $\beta_2=0.12$  and  $\gamma=-60^\circ$  (i.e. weakly oblate). A simple geometric picture arises whereby combinations of the protons with the  $i_{13/2}$  neutrons gives rise to an equilibrium with the rotation axis (which is parallel to the total angular momentum vector,  $\mathbf{I}$ ) lying at  $\sim 45^\circ$  relative to the symmetry axis. The total angular momentum vector is increased when the individual proton,  $i_\pi$ , and neutron,  $i_\nu$ , spins gradually tilt towards  $\mathbf{I}$  (the so-called 'shears mechanism'). Fig. 2 shows the result of such a calculation for the  $(h_{9/2} \otimes i_{13/2})$  proton configuration coupled to the AB neutron configuration (i.e. two  $i_{13/2}$  neutrons). For comparison the experimentally deduced B(M1) values of band 1 in  $^{198}\text{Pb}$  are also shown in the figure. Clearly, the calculations predict large B(M1) values. However, the calculations again overestimate the experimental values by approximately a factor of two. In addition, the gradual alignment of the proton and neutron spins along the tilted rotation axis should push the B(M1) values down as the angular momentum increases [9]. This feature is not observed.

A number of important experimental imperatives remain. Firstly, lifetime measurements of states in these bands need to be extended to a wider variety of structures in several different nuclei. Some preliminary results of a DSAM measurement for M1-bands in  $^{199}\text{Pb}$  have been reported at this conference [12]. Secondly, measurement of the g-factors for states in these M1-bands would provide information on the component of the magnetic moment in the direction parallel to the total angular momentum vector,  $\mathbf{I}$ . The g-factors, combined with the deduced B(M1) values from lifetime measurements (which give the component of the magnetic moment perpendicular to  $\mathbf{I}$ ), could indicate how accurately the generation of angular momentum follows the TAC 'shears' mechanism. Finally, it would be very interesting to compare the predictions of TAC against measured B(M1) transition rates of  $\Delta I=1$  bands in the  $A \sim 130$  region [13]. These bands have similar properties to the M1-bands in the  $A \sim 190$  region, including: (1) large B(M1)/B(E2) ratios [ $\geq 10 \mu_N / (\text{eb})^2$ ], (2) small, negative  $\delta_{E2/M1}$  mixing ratios ( $Q_0 < 0$ ) for the  $\Delta I=1$  transitions, and (3) Low dynamic moments of inertia ( $\mathcal{S}^{(2)} \sim 15-25 \hbar^2 \text{MeV}^{-1}$ ) These sequences are generated in an analogous manner to the  $A \sim 190$  oblate dipole bands, but in this lighter mass region high-K  $h_{11/2}$  protons couple to alignable  $h_{11/2}$  neutrons.

## References

1. R.M.Clark et al., Nucl. Phys. A 562 (1993) 121
2. G.Baldsiefen et al., Nucl. Phys. A 574 (1994) 521
3. R.M.Clark et al., J. Phys. G 19 (1993) L57
4. P.J.Dagnall et al., to be published
5. T.F.Wang et al., Phys. Rev. Lett. 69 (1992) 1737
6. J.R.Hughes et al., Phys. Rev. C 48 (1993) R2135
7. R.M.Clark et al., Phys. Rev. C 50 (1994) 84
8. F.Dönau and S.Frauentorf, Proc. Int. Conf. on High Angular Momentum Properties of Nuclei, Oak Ridge (1982), Nucl. Sci. Res. Conf. Series vol. 4 (Harwood, New York) p. 143
9. S.Frauentorf, Nucl Phys A 557 (1993) 259c
10. R.M.Clark et al., Z. Phys. A 342 (1992) 371
11. A.Kuhnert et al., Phys. Rev. C 46 (1992) 133
12. H.Hubel et al., contribution to this conference
13. D.B.Fossan et al., Nucl. Phys. A 520 (1990) 214c



# On I4 and I6-Staggering in Superdeformed Bands and in the Ground Bands of Even-Even Actinide Nuclei

L.K. Peker<sup>a</sup>, J.H. Hamilton<sup>b</sup>, and J.O. Rasmussen<sup>c</sup>

In 1983 we reported the first observation of the possible hexadecapole  $\Delta I = 4$  splitting in the octupole vibrational bands,  $K = 0^-$ , in  ${}^{236}_{90}\text{U}_{144}$  and probably in  ${}^{238}\text{U}$  ref. [1]. We observed significant oscillation of

$$\Delta E_\gamma = E_\gamma(I + 2 \rightarrow I) - E_\gamma(I \rightarrow I - 2) = 4\hbar^2/\mathfrak{S}^{(2)}$$

along the octupole  $K^\pi = 0^-$  band ( $\mathfrak{S}^{(2)}$  -dynamical moment of inertia). We suggested that this effect is associated with hexadecapole deformation ( $C_4$ -symmetry) in octupole vibrational bands. Hamamoto and Mottelson ref. [2] are now making the case that the effect is due to  $Y_{44}$  deformation in the body frame of the prolate nuclear spheroid. Their work was prompted by similar spectral features observed in some superdeformed nuclear bands. Such oscillations of  $\mathfrak{S}^{(2)}$  were recently noted in superdeformed bands in  ${}^{149}\text{Gd}$  ref. [3] and  ${}^{194}\text{Hg}$  ref. [4]. It is important to establish if these are isolated cases or if such I4 staggering is a more general phenomenon. To investigate this question we use a simple, but sensitive, method of analysis, plotting the second difference of gamma transition energies vs. initial spin of the central transition. (This is nearly the same as first differences of the dynamic moment-of-inertia.)

$$\Delta^2 E_\gamma(I) = E_\gamma(I - 2) - 2E_\gamma(I) + E_\gamma(I + 2),$$

along the rotational band of interest.

The question arises, does such  $\Delta I = 4$  splitting occur in ground bands? If there is such a split, we may look for oscillation of  $E_\gamma$  along the ground rotational band. Because we already know from data on octupole and superdeformed bands that the  $\Delta I = 4$  splitting and oscillation effects are very weak ( $\Delta E_\gamma/E_\gamma \leq 0.5$ )<sup>[1,3]</sup>, it is important to use methods of analysis that are sufficiently sensitive to detect such small effects.

In Fig. 1(a-d) we present the second-difference plots for several reported superdeformed bands. The presence of an odd neutron or proton seems generally to enhance the staggering compared to even-even neighbors in the superdeformed cases. In the actinide ground bands Fig. 1 (e) there is I4-oscillation in  ${}^{238}_{94}\text{Pu}$  and in  ${}^{238}_{92}\text{U}$ . The lighter nuclei  ${}^{232,234}\text{U}$  do not show (Fig. 1f) any oscillations. We are fairly confident in the case of  ${}^{238}_{94}\text{Pu}$ , since the independent experiments of Stoyer and of Devlin, as tabulated in ref. [6], agree on the size and phase of the staggering. Another interesting

case is the main superdeformed band (designated SD-1 in ref. [7]) in  $^{153}\text{Dy}$ , not plotted here. The second difference plot clearly shows I6 oscillations for the highest-spin members.

The fact that the staggering only sets in above spin 10 suggests to us that the effect has to do with admixture of spin-aligned configurations. In the spin-aligned system one or more nucleons in one of the highest- $j$  orbitals tend to align their spins along the spin axis, which is perpendicular to the ordinary prolate-spheroidal long axis. If there are one or two aligned nucleons from an orbital without  $j$ -mixing, their wave functions will form a pancake density distribution perpendicular to the spin axis and possessing a cylindrical symmetry. If there are low- $j$  orbitals of the same parity near the highest- $j$  orbitals and both are near the Fermi energy, there could arise a Jahn-Teller distortion breaking the cylindrical symmetry of the aligned-orbital system to a lower rotational symmetry of even order equal to the vector difference in  $j$  (or  $L$ ) values. Indeed, for both protons and neutrons in the vicinity of  $^{238}_{94}\text{Pu}$  a Nilsson diagram of levels in the spheroidal potential well show such possible crossings. In the proton case the downgoing  $i_{13/2}$  orbitals cross the upcoming orbitals from  $s_{1/2}$  and  $d_{3/2}$ , giving a driving force for a 6-fold or 4-fold distortion. For neutrons the same arguments apply for the downgoing  $j_{15/2}$  and upgoing  $p_{1/2}$ ,  $p_{3/2}$ , and  $f_{5/2}$  orbitals.

Let us outline a model approach to quantitative study of such distortion. Though it could be studied in either body or aligned (lab) frame, the latter is easier to visualize. We consider microscopically the families of neutrons and protons in the aligning-orbital system. The rapidly rotating prolate core of all other nucleons provides an average oblate spheroidal field in the aligned frame. The Hamiltonian is as follows:

$$H_{\text{aligned}} = H_{\text{sp}} - V_{\text{SDI}} + H_{\text{rot}} + \sum_{jmj'm'} \left[ C_{20} D_{00}^2 Y_{20} + C_{22} D_{22}^2 Y_{22} - \omega m \delta_{mm'} \right] a_{jm}^{\dagger} a_{j'm'},$$

where the  $D_{\mu\nu}^{\lambda}$  functions are the usual symmetric top rotor functions and  $Y_{\lambda\nu}$  spherical harmonics of the nuclear angular coordinate,  $V_{\text{SDI}}$  is a nucleon-nucleon (like and unlike) surface delta interaction or other short-range interaction.  $H_{\text{rot}}$  is the usual rotor Hamiltonian.

$$V_{\text{SDI}} = V_0 \sum_{j_i m_i} \left[ \int \chi_{j_1 m_1} \chi_{j_2 m_2} \chi_{j_3 m_3} \chi_{j_4 m_4} d\tau \right] a_{j_1 m_1}^{\dagger} a_{j_2 m_2}^{\dagger} a_{j_3 m_3} a_{j_4 m_4}.$$

The  $H_{\text{sp}}$  is the spherical single-particle Hamiltonian,  $C_{20}(\beta)$  and  $C_{22}(\beta, \gamma)$  are coefficients of the quadrupole interaction terms between the single nucleons and the prolate rotor field. The  $a_{jm}^{\dagger}$  and  $a_{jm}$  are the usual nucleon creation and annihilation operators, respectively. The  $\chi_{jm}$  are the spinor functions of the single nucleons. The integration over  $d\tau$  is an integration over angles  $\theta$  and  $\phi$  and summation over spin projections. The  $m_i$  values are constrained such that their sum is the aligned angular momentum.

The largest  $|m_j|$  orbitals lie lowest in the average oblate field. The Routhian term splits the Nilsson degeneracy proportional to the angular velocity  $\omega$ . In the level-crossing regions we have singled out, there will be near the Fermi energy a number

of energy levels from the upcoming low- $j$  orbitals with  $m$  averaging zero. There will also be from the downgoing high- $j$  orbitals  $m$  values averaging around 4 (or 6) in situations favorable to staggering effects. In such cases there will be many ways to construct configurations with a given aligned angular momentum  $i_\alpha$  and aligned values differing by 4 (or 6) units. The short-range nucleon-nucleon interaction will connect many of these configurations with one another. Hence, there is a quantal system quite analogous to that giving rise to ground-state pairing, where many rearrangements of pair occupations of orbitals near the Fermi surface have similar energies and are connected by the pairing force. Analogous treatment to BCS may give a fuzzy phase transition to  $n$ -fold distortion of the aligned system.

With  $n$ -fold distortion the system of aligned nucleons would show a rotor spectrum with only multiples of  $n$  as  $J$  values. In the complete nuclear system the aligned rotor  $J$  and the normal prolate rotor angular momentum  $R$  would generally be in a stretched configuration with total angular momentum  $I$  the sum of  $J$  and  $R$ . The prolate rotor rod would be rotating in the plane of the pancake distribution of the aligned system. To the extent that 6-fold or 4-fold distortion set in there could be some coupling of the two rotor systems. Even without coupling, if the moment-of-inertia of the aligned system exceeds that of the prolate rotor, the resulting band will show  $n$ -fold staggering in energies. A more familiar way of viewing the systems in the staggering region is in terms of band crossings by aligned bands. In a staggering regime there are crossings by aligned bands differing in aligned angular momentum by 4 (or 6) units.

This division of the nucleons into separate systems of orbitals of a given parity, each constituting a rotor (one oblate aligned and one prolate, with axis perpendicular to spin) could also apply to the superdeformed region. An examination of the Nilsson diagram for the rare-earth region of superdeformation suggests that the orbital crossings giving rise to cylindrical symmetry breaking in the pancake are at considerably larger deformation than in the actinides. This can be understood in that the lighter nuclei experience potential wells closer to the harmonic oscillator limit, where the  $N$  and  $N+2$  shells cross at deformations with axis ratios near 2:1. The heavier nuclei have more nearly square well potentials, where the oscillator degeneracy of high and low  $L$  orbitals is broken the most and crossings occur at smaller deformations. If the present pattern holds that actinide ground bands and superdeformed bands in the Hg and Dy regions show the most staggering, then our hypothesis about the need for  $N$  and  $N+2$  band crossings near the Fermi energy is sustained. It follows that we believe that  $Y_{44}$  or  $Y_{66}$  distortion in the spin-aligned frame, considered also by Pavlichenkov ref. [8], is a more likely source of the energy staggering effect than is the corresponding distortion in the body-frame, as proposed in ref. [2].

#### Acknowledgements

Work at Vanderbilt University is supported in part by the U.S. Department of Energy under grant No. DE-FG05-88ER40407. This work at Lawrence Berkeley Laboratory is supported by the Director of Energy Research, Division of Nuclear Physics of the

Office of High Energy and Nuclear Physics of the U.S. Department of Energy under contracts Nos. DE-FG03-87ER40323, W-7405-ENG48, and DE-AC03-76SF00098.

- a. Brookhaven National Laboratory, Upton (LI), NY 11973
- b. Physics Department, Vanderbilt University, Nashville, TN 37235
- c. Lawrence Berkeley Laboratory, Berkeley, CA 94720

#### References

1. L. Peker, et al., Phys. Rev. Lett. 50 (1983) 1749.
2. I. Hamamoto and B. R. Mottelson (1994), preprint/Lund-MPh-94/05.
3. S. Flibotte, et al., Phys. Rev. Lett. 71 (1993) 4299.
4. B. Cederwall, et al., Phys. Rev. Lett. 72 (1994) 3150.
5. L. K. Peker, J. H. Hamilton, and J. O. Rasmussen, submitted to Phys. Lett., 1994.
6. M. A. Stoyer, Ph.D. thesis, U.C. Berkeley, 1991 (unpublished), and M. Devlin, et al., Phys. Rev. 47C (1993) 2178.
7. R. B. Firestone and B. Singh, "Table of Superdeformed Nuclear Bands and Fission Isomers," LBL Report 35916 (June, 1994)
8. I.M. Pavlichenkov, "C4 Symmetry and Bifurcation in Superdeformed Bands.", invited talk, "Conference on Physics from Large Gamma-ray Detector Arrays," Berkeley August, 1994.

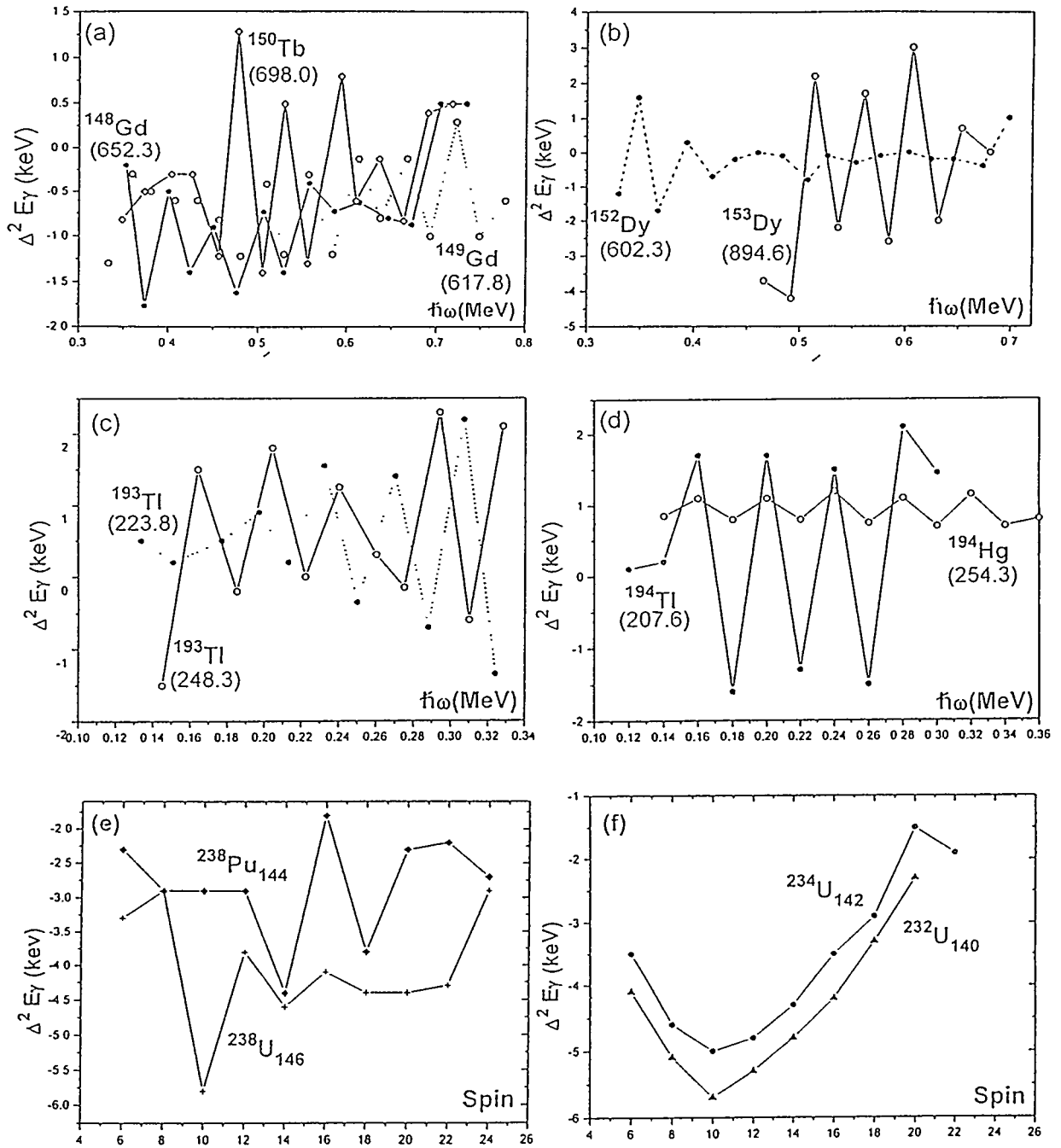


Fig. 1. The  $\Delta^2 E_\gamma$  data as a function of spin are given (a-d) for several superdeformed nuclei and (e,f) for the ground bands in  $^{232,234,238}\text{U}$  and  $^{238}\text{Pu}$ .

# Relativistic Description of Superdeformed Bands \*

P. Ring

Technische Universität München, D-85747 Garching, Germany

## Abstract:

Relativistic Mean Field theory in the Rotating Frame presents a fully self-consistent description of rotating superdeformed bands in the Dy- and the Hg-region. We find excellent agreement with the observed quadrupole moments as well as the dynamical moments of inertia  $\mathcal{J}^{(2)}$  in the Dy-region, where – because of the relatively high angular momenta – pairing correlations can be neglected. In particular we are able to reproduce the moments of inertia of identical bands in even-even and odd-even nuclei in this region without any further parameters up to an accuracy of  $\pm 2$  keV in the transitional  $\gamma$ -energies. The importance of nuclear magnetism is discussed.

## 1 Introduction

Since the early days of nuclear physics one has known, that the spin plays an important role in our understanding of nuclear spectra, and that, in principle, one should use a relativistic theory for a complete description of the nuclear system even in the low energy domain. Early attempts in this direction of Teller et al, however, have been neglected and it was much later Walecka who pointed out in the seventies the power, the simplicity and the elegance of a phenomenological relativistic description of the nuclear system. In recent years these methods have been extended so far, that they can be applied nowadays not only to nuclear matter and to the ground state of doubly closed shell spherical nuclei, where the very few phenomenological parameters are adjusted to experimental data, but also to the entire region of the periodic table, to exotic nuclei with large neutron excess as well as to deformed and superdeformed nuclei and even to rotating nuclei.

This theory is conceptually similar to density dependent Hartree Fock Theory with Skyrme forces, which is nowadays standard for the microscopic description of nuclear properties over the entire periodic table. It shares with this theory, that so far pairing is taken into account in a very primitive way in the so-called constant gap approximation, which used experimental gap parameters works and works rather well for the ground states of even-even nuclei, where experimental gaps are available. Its predictive power, however, is limited in exotic nuclei far from the stability line, where no experimental gap parameters are known and in the high spin region, where pairing is quenched and where the finite range of the pairing interaction should be taken into account.

We therefore concentrate in this talk on investigations without pairing in superdeformed nuclei of the Dy-region at relatively high angular momentum, where pairing is expected to play a smaller role and on the description of several identical bands in the Hg-region, where – because of the lack of pairing – we cannot expect to find good agreement for the absolute inertia parameters, but where we still find identical bands, which only small differences in the dynamical moments of inertia.

In section 2 a short overview of the basic facts of relativistic mean field theory is given and in section 3 and 4 we discuss results for superdeformed bands in the Dy- and in the Hg-region.

---

\*Invited talk at the *Conference of Physics with Large  $\gamma$ -Ray Detector Arrays*, Berkeley, August 2-6, 1994, supported by the BMFT under the project 06 TM 733.

## 2 Relativistic Mean Field Theory

Relativistic Mean Field (RMF) theory is a classical relativistic field theory similar to classical electrodynamics. Only the nucleons are treated as quantum mechanical Dirac-particles with the four component wave functions  $\psi_i$  moving with relativistic dynamics in a number of classical meson fields. As in any mean field theory, these fields describe in an average way the interaction produced by the exchange of the corresponding mesons. The theory is phenomenological similar as the density dependent Hartree-Fock theories of Skyrme or Gogny type. Therefore the number of mesons entering this theory is limited and the corresponding parameters, the meson masses  $m_{meson}$  and the coupling constants  $g_{meson}$  between mesons and nucleons are neither derived from a more fundamental theory, nor taken from the properties of these mesons in the vacuum, but are adjusted to a data of the correlated nuclear many-body system. The mean field of single pions which breaks parity – a fact which is not observed in the nuclear mean field – is neglected. Pions are, however, taken into account by the mean field of the so-called  $\sigma$ -meson. This particle so far not been observed in the vacuum but it has been interpreted as a complicated bound state of two pions in the medium. On the phenomenological level we cannot decide whether this interpretation is the proper one. Many experimental observations, however indicate the importance of a large scalar field in the nucleus. This scalar field is taken into account by the phenomenological  $\sigma$ -meson in RMF-theory. Since relativistic covariance leads to an attractive fields for scalar particles and to repulsive fields for vector particles, we need in addition a vector meson, the  $\omega$ -meson, which has been observed in nature as a resonance at  $m_\omega = 783$  MeV.  $\sigma$ - and  $\omega$ -meson carry both isospin 0. For nuclei with large neutron excess we need in addition a meson carrying isospin 1, the  $\rho$ -meson, which is also observed in nature as a resonance at  $m_\rho = 763$  MeV. Finally we need the Coulomb-force, i.e. the photon.

Apart from the Dirac wavefunctions  $\psi_i(x)$  ( $i = 1 \dots A$ ) for the nucleons we therefore have one field for the scalar  $\sigma$ -meson  $\sigma(x)$  and 4 fields for each Lorentz-vector particle, i.e. for the  $\omega$ -meson:  $\omega^\mu(x)$ , for the three iso-vector  $\rho$ -mesons  $\vec{\rho}^\mu(x)$  and for the photon  $A^\mu(x)$ .

In order to keep the number of adjustable parameters small, we use the experimental values for the masses of the nucleon  $m_N$  and the masses of the  $\omega$ - and the  $\rho$ -meson. In this most primitive version of the theory we therefore have only four parameters, the mass of the  $\sigma$ -meson  $m_\sigma$  and the three coupling constants  $g_\sigma$ ,  $g_\omega$  and  $g_\rho$ . The rest is more or less given by Lorentz invariance and the principle of simplicity (minimal coupling). It leads to the Lagrangian density:

$$\begin{aligned} \mathcal{L} = & \bar{\psi} (\not{p} - g_\omega \not{\omega} - g_\sigma \sigma - m_N) \psi \\ & + \frac{1}{2} \partial_\mu \sigma \partial^\mu \sigma - \frac{1}{2} m_\sigma^2 \sigma^2 - \frac{1}{4} \Omega_{\mu\nu} \Omega^{\mu\nu} + \frac{1}{2} m_\omega^2 \omega_\mu \omega^\mu \end{aligned} \quad (1)$$

where  $\Omega_{\mu\nu} = \partial_\mu \omega_\nu - \partial_\nu \omega_\mu$  is the field tensor for the vector mesons. For simplicity we neglect here the  $\rho$ -meson and the photon, which are, however, taken into fully account in the calculations.

Also this simple version of the Walecka-model is able to give a qualitative description of saturation and many nuclear properties, it fails to describe the proper experimental surface properties. Boguta and Bodmer[4] therefore extended the model by including a nonlinear self-coupling of the scalar mesons, i.e. the mass term  $\frac{1}{2} m_\sigma^2 \sigma^2$  is replaced by a polynomial of forth order  $U(\sigma) = 1/2 m_\sigma^2 \sigma^2 + 1/3 g_2 \sigma^3 + 1/4 g_3 \sigma^4$  containing additional 2 parameters. Conceptually this is equivalent to the modification of the original Skyrme force with its linear density dependence by modified density dependencies of the type  $\rho^\alpha$ . All the great quantitative achievements of RMF-theory

are only possible in this nonlinear version of the theory. It is nowadays standard and rather uniform parameter sets NL1 and NL-SH have been adjusted in the literature.

Hamiltons variational principle allows to derive Euler-equations as equations of motion, the Dirac equation for the nucleon spinors and Klein-Gordon equations for the meson fields. In the stationary case they have the form:

$$\{\alpha(\mathbf{p} + g_\omega \boldsymbol{\omega}) + g_\omega \omega_0 + \beta(M + g_\sigma \sigma)\} \psi_\alpha = \epsilon_\alpha \psi_\alpha \quad (2)$$

$$-\Delta \sigma + U'(\sigma) = -g_\sigma \rho_s \quad (3)$$

$$\{-\Delta + m_\omega^2\} \omega^0 = g_\omega \rho_v \quad (4)$$

$$\{-\Delta + m_\omega^2\} \boldsymbol{\omega} = g_\omega \mathbf{j} \quad (5)$$

The scalar density  $\rho_s = \langle \bar{\psi} \psi \rangle$ , the vector density  $\rho_v = \langle \psi^\dagger \psi \rangle$  and the currents  $\mathbf{j} = \langle \psi^\dagger \boldsymbol{\alpha} \psi \rangle$  are calculated from the solution of the Dirac equations. They serve as sources, which determine the mesons fields via the Klein-Gordon equations. These meson fields enter finally again the Dirac equation and determine the motion of the nucleons in a self-consistent way. The whole system of equations is solved by iteration.

In the ground state of even-even nuclei we have time-reversal invariance and therefore the currents  $\mathbf{j}$  and the spatial parts of the vector meson fields as for instance  $\boldsymbol{\omega}$  vanish. In order to describe rotating nuclei we use – completely in the mean field spirit – the Cranking idea and transform the Lagrangian to a frame rotating with constant angular velocity  $\Omega$  around the  $x$ -axis. This is an accelerated frame and using the techniques of general relativity one can derive the corresponding Lagrangian in the rotating frame. In the equation of motions this leads to the well know cranking term  $\Omega J_x$  in the Dirac equation and corresponding terms in the Klein-Gordon equations. Because of the bosonic nature of the mesons, however, these latter terms can be neglected. The cranking term in the Dirac equations violates time-reversal invariance in the intrinsic frame and induces currents. They are the source for spatial contributions  $\boldsymbol{\omega}$  of the vector mesons, which lead to field of a similar structure as the magnetic field in the Dirac equation. We call these fields *Nuclear Magnetism*. They lead to a time-reversal breaking mean field, an effect which is for instance never taken into account in phenomenological Nilsson-Strutinskii calculations of superdeformed bands. As we will see they play an important role in our understanding of identical bands.

### 3 Superdeformed Bands in the Dy-Region

In order to investigate the applicability of Relativistic Mean Field theory for the description of rotating superdeformed nuclei, we chose as an example the well know superdeformed band in the nucleus  $^{152}\text{Dy}$ . It was the first superdeformed band in rotating Rare Earth nuclei discovered experimentally by the Daresbury group[5].

We use the parameter set NL1, which has been adjusted to nuclear matter and a few spherical nuclei. This parameter set has turned out to be very successful for the description of many ground-state properties over the entire periodic table[1]. In particular one has found excellent agreement with ground state deformations in open shell nuclei.

In Fig.1 we show the static and the dynamic moment of inertia for the lowest superdeformed band in the nucleus  $^{152}\text{Dy}$  as a function of the angular momentum. It is clearly seen that a calculation without nuclear magnetism, i.e. without the spatial contributions of the vector meson-fields, which is in good agreement with the experimental quadrupole moments [3] produces much too small moments of inertia. A semiclassical correction where these contributions, derived in Thomas Fermi approximation using a rigid rotor current, are taken into account in first order perturbation



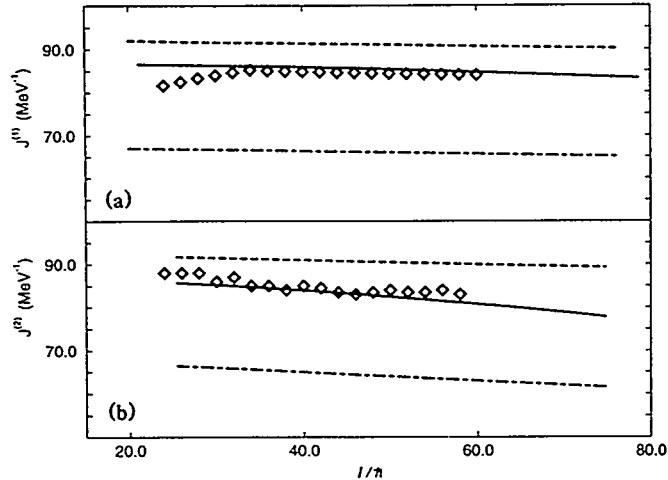


Figure 1: (a) Static ( $\mathcal{J}^{(1)}$ ) and (b) dynamic ( $\mathcal{J}^{(2)}$ ) moment of inertia for the lowest superdeformed band in the nucleus  $^{152}\text{Dy}$ . The dashed line corresponds to the calculation without the spatial contributions of the vector mesons. In the dotted line such contributions are taken into account in a semiclassical way and the full line represents the self-consistent solution including these contributions fully.

theory, overemphasized the moments of inertia by roughly 10 %. only if one takes these contributions into account in a fully self-consistent way, is perfect agreement with experimental data achieved. In the region of small angular momenta one still observes very small deviations, which could possibly be understood as the influence of remaining pairing correlations in this region of intermediate spins.

The average charge quadrupole moment is found to be 18.6 eb, which is in good agreement with a value of 18 eb obtained in a non-relativistic calculation by the Lund group, and the experimental value of 19 eb

Let us now investigate the problem of identical bands[6]. For this purpose we calculate, in a self-consistent way, bands in the neighboring nucleus  $^{151}\text{Tb}$  by removing one proton from the  $^{152}\text{Dy}$  core. The proton hole induces a polarization of the  $^{152}\text{Dy}$ -core, which has two effects: it leads to changes of deformation and in addition to changes in the current distribution.

We show in Fig. 2 the differences  $\Delta E_\gamma = E_\gamma(\text{Tb}) - E_\gamma(\text{Dy})$  between the transition energies in an excited band of  $^{151}\text{Tb}$  and in the lowest superdeformed band in  $^{152}\text{Dy}$ . The agreement with the experimental value is excellent. The energy differences are of order of 1 keV. This band correspond to a hole in the orbit with the approximate Nilsson quantum numbers  $[301]_{\frac{1}{2}}^-$ . This orbit has a very small number of oscillator quanta along the  $z$ -axis (the symmetry axis), which yields nearly vanishing contributions to the moment of inertia.

In order to investigate the very good quantitative agreement, we have carried out two additional calculations in Fig. 2 for the *identical bands*. First we neglected the polarization induced by the proton hole, i.e we calculated the energy differences for wave functions for the nucleus  $^{151}\text{Tb}$  obtained from the  $^{152}\text{Dy}$  core by just removing one proton, without requiring self-consistency for the odd mass configuration. In this case we find the dashed dotted line in Fig. 2, which is in sharp disagreement with the experimental data. Next we took into account the polarization, but we neglected nuclear magnetism, i.e. the contributions of the spatial components of the vector meson fields and find the dashed line in Fig. 2, which is also in disagreement with

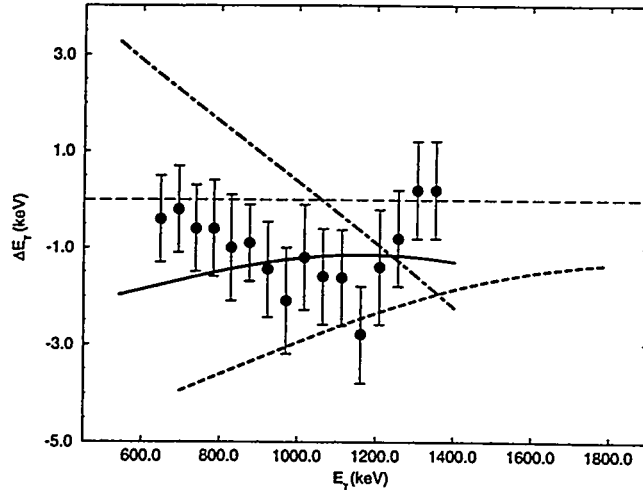


Figure 2: Differences  $\Delta E_\gamma$  for the identical bands in  $^{151}\text{Tb}$  and  $^{152}\text{Dy}$ . The fully self-consistent solution (full line) and solutions neglecting nuclear magnetism (dashed line) or polarization induced by the proton hole (dashed dotted line) are compared with the experiment (empty diamonds).

experiment.

## 4 Identical Bands in the Hg-Region

In the Hg-region the situation is more complicated. The identical bands are observed at much lower angular momenta and pairing plays an essential role. Nonetheless we show in Fig. 3 results of a calculation without pairing[7]. It turns out, that the energy differences for two of the bands are nonetheless in good agreement with the very small experimental limits indicated by the dashed lines.

## 5 Conclusions and Outlook

We therefore conclude, that a very delicate cancellation process occurs in identical bands in superdeformed nuclei. Polarization of the quadrupole moments and of the density alone would induce changes of the order of 5 – 10 per Mille. Neglecting nuclear magnetism would also lead to changes of this order of magnitude. Obviously both act in opposite direction, such that the final differences are only in the order of 1 per Mille. So far the precise mechanism for this cancellation is not fully understood. It requires definitely much more systematic investigations. Nonetheless it seems to us a very satisfying and surprising result, that without any free parameter, and simply using the set NL1 adjusted to nuclear matter and a few spherical nuclei, long before identical bands had been identified, we can obtain this degree of accuracy in the relatively simple minded relativistic mean field approach. We have to emphasize, however, that full self-consistency as well as the inclusion of the nuclear currents are very important in this context. A further problem, which is so not fully solved it the

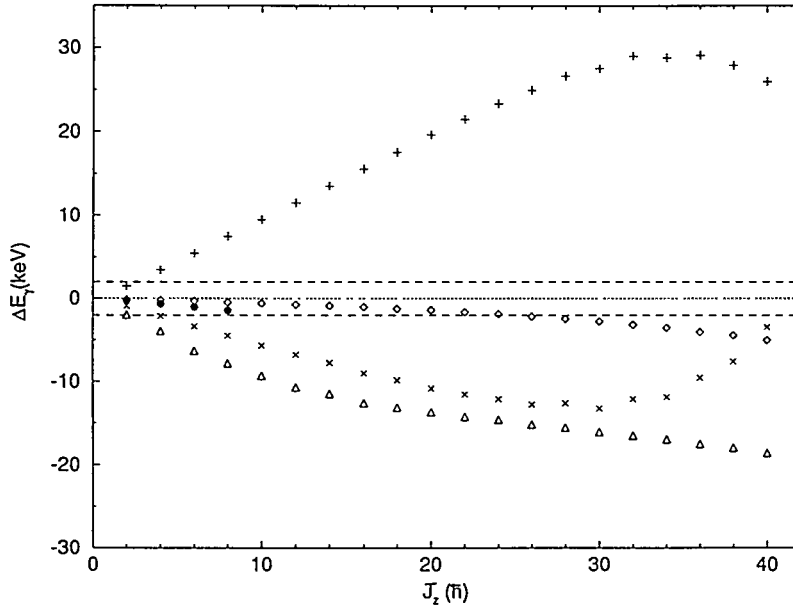


Figure 3: Differences  $\Delta E_\gamma$  between the yrast band in  $^{192}\text{Hg}$  and various other bands in this region:  $\triangle\triangle\triangle$   $^{194}\text{Hg}$  (two neutrons in [512]5/2),  $\diamond\diamond\diamond$   $^{194}\text{Hg}^*$  (two neutrons in [624]9/2),  $++++$   $^{194}\text{Pb}$  (two protons in [613]5/2),  $\times\times\times$   $^{194}\text{Pb}^*$  (two protons in [604]9/2, [613]7/2),  $\bullet\bullet\bullet$   $^{194}\text{Pb}^*$  (two protons in [512]3/2).

inclusion of proper pairing correlations. In particular in the Hg-region we are not able to describe the absolute values of the moments of inertia properly without pairing. Further investigations in this direction are in progress.

I would like to express my gratitude to all my collaborators, in particular to W. Koepf, J. König, and Z.Y. Zhu, without whom these investigations would not have been possible.

## References

- [1] Y.K. Gambhir, P. Ring, and A. Thimet, Ann. Phys. (N.Y.) **511**, 129 (1990)
- [2] W. Koepf and P. Ring, Nucl. Phys. **A493**, 61 (1989)
- [3] W. Koepf and P. Ring, Nucl. Phys. **A511**, 279 (1990)
- [4] J. Boguta and A.R. Bodmer, Nucl. Phys. **A292**, 413 (1977)
- [5] P.J. Twin et al., Phys. Rev. Lett. **57**, 811 (1986)
- [6] J. König and P. Ring, Phys. Rev. Lett **71** (1993) 3079
- [7] Z.Y. Zhu, J. König, and P. Ring, to be published

# A Comparison of Superdeformed Band Transition Energies

P.Fallon, F.S.Stephens, R.M.Clark, S.Asztalos, B.Cederwall, M.A.Deleplanque, R.M.Diamond,  
I.Y.Lee, A.O.Macchiavelli.

*Lawrence Berkeley Laboratory, Berkeley, Ca 94720.*

J.A.Becker, L.Farris, J.R.Hughes, E.A.Henry.

*Lawrence Livermore National Laboratory, Livermore, California 94550.*

## 1 Introduction

The first observations [1,2] of superdeformed (SD) bands in different nuclei, with long sequences of near identical transition energies, came at a time when the total number of SD bands was  $\sim 10$  in the  $A=150$  or  $A=190$  regions. Today  $\sim 50$  SD bands have been observed in both these regions and as a consequence it is now possible to use statistical techniques to study identical (ID) bands. Indeed, it has been suggested that the occurrence of ID bands may not be so surprising given, (i) the relatively small transition energy spacing (40-50 keV) within a SD band and (ii) the many SD bands known. Therefore, it is important to study the distribution of ID bands to determine whether or not this phenomenon simply results from choosing bands which just happen to be identical. We present here the first results from such an analysis of SD bands in the  $A=190$  and  $150$  regions and furthermore try to address the question; "how identical is 'identical'?"

## 2 Method

There is more than one way to compare properties between rotational bands. In this study we adopt a procedure which compares the transition energies for experimental data, or equivalently the relative alignments for calculated cases, in neighboring SD bands. Other studies (see contributions to these proceedings from C.Baktash and J.Zhang) compare the moments of inertia. Since we do not know the absolute spins, the relative alignments are only determined over a  $1\hbar$  range. For our purpose we found it useful to define ID bands as those which yield an incremental alignment (i) of zero or  $1/2$ , as given by the following expression [2];

$$i_{a,b} = 2 \left( \frac{\Delta E_{\gamma}^{a,b}}{\Delta E_{\gamma}^b} \right) + 0.5\delta_{(a-b,odd)} \quad (1)$$

where  $\Delta E_{\gamma}^{a,b}$  is the difference in the nearest transition energies between band 'A' and band 'B',  $\Delta E_{\gamma}^b$  is the in-band transition energy separation for band 'B' (the so called reference band), and the term  $0.5\delta_{(a-b,odd)}$  takes into account the fact that states in odd and even mass nuclei have a spin difference of  $0.5\hbar$ .

The method involves, for each  $E_{\gamma}$  in band A, finding the closest  $E_{\gamma}$  in band B. The band comparison is performed for all combinations of SD band-pairs, i.e., we do not choose a fixed reference band (however, the conclusions of the following analysis are the same whether one chooses a fixed reference or not). For each pair of SD bands compared, the transition energy range is from 0.2-0.8 MeV ( $A=190$ ) and 0.4-2.0 MeV ( $A=150$ ), therefore each band-pair gives 10 or more transition-pair points. The total number of transition pairs is plotted as a function of the transition energy difference. In all cases

discussed below we do not compare bands in the same nucleus or bands which occur in nuclei differing by more than two mass units.

### 3 Results

This section is split into two parts, devoted to the  $A=190$  and  $A=150$  regions respectively, and illustrates the results of our SD band comparison. We also include in this section a series of figures showing what one may expect from "theoretical-SD-bands", generated from cranked shell model (CSM) calculations (with and without pairing).

#### 3.1 $A \approx 190$

The results of the  $A=190$  SD band comparison for various groups of SD bands are illustrated in Fig. 1. For all plots the full range shown is  $-20$  to  $18$  keV ( $\approx 2\hbar$ ) however, since we compare closest neighbor transitions, the plots are cyclic over a  $1\hbar$  ( $\pm 10$  keV) range, which is indicated by filled symbols. Figure 1a shows how the transition energies compare for (i) the seven 'known' (good) identical bands (circles) and (ii) all ( $\sim 50$ ) SD bands in the  $A=190$  region (squares).

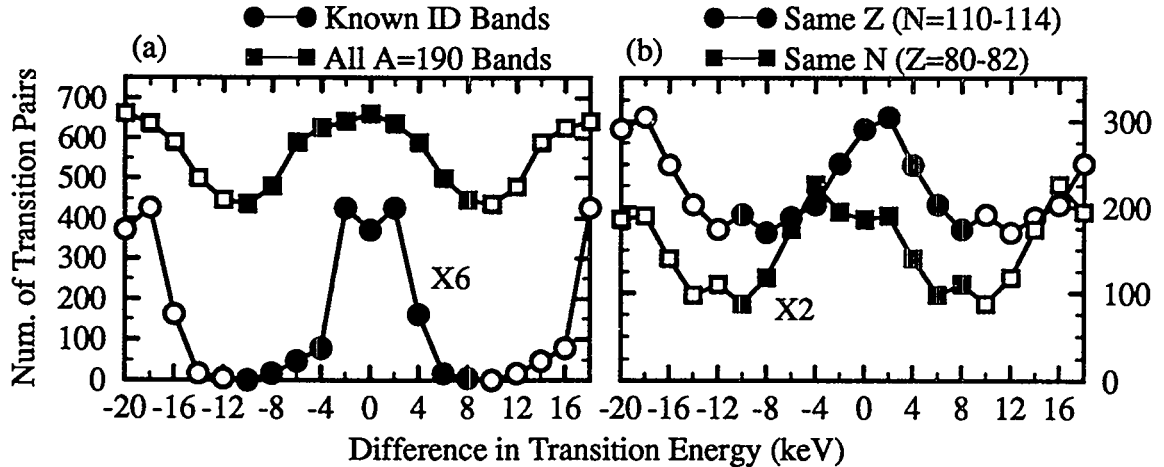


Figure 1. SD band  $E_\gamma$  comparisons for band-pairs in the following nuclei: (a) Circles : 'known' ID bands,  $^{191}\text{Hg}$  (1,2),  $^{192}\text{Hg}$  (1),  $^{193}\text{Hg}$  (2,3) and  $^{194}\text{Hg}$  (2,3). (a) Squares : All SD bands in nuclei from  $^{189}\text{Hg}$  to  $^{195}\text{Pb}$ . (b) Circles : Isotope chains (ie compare Hg with Hg, Tl with Tl and Pb with Pb). (b) Squares : Isotone chains (ie compare Hg with Tl, Hg with Pb and Tl with Pb).

As expected the known ID bands (Fig. 1a circles) produce a peak in the  $\Delta E_\gamma$  distribution, centered around zero. However, the peak width (FWHM) is larger than one may have expected ( $\sim 6-7$  keV) and covers  $\sim 1/3\hbar$  ( $\pm 10$  keV). The 'all-SD-band' comparison also shows a peak which is  $\sim 12-13$  keV wide but which sits on a high background. These results suggest that the number of near-identical  $A=190$  SD band-pairs is significant compared with the total number of bands. The effects on the SD band  $E_\gamma$ 's, due to varying either the neutron (circles) or proton (squares) number, is shown in Fig. 1b. Changing the neutron occupation produces a smaller spread in  $\Delta E_\gamma$ , compared with varying  $Z$ .

We now ask ourselves the question, what do we expect? As a first attempt to answer this we used a standard CSM calculation (Woods-Saxon potential) to derive the

alignments of the routhians near to the  $N=112$  and  $Z=80$  SD shell gaps. The individual routhian alignments are ‘projected’ over a frequency range applicable to the experimental data (i.e.,  $\hbar\omega=0.1-0.4$  MeV). Since we know the calculated alignments there is no restriction on the range.

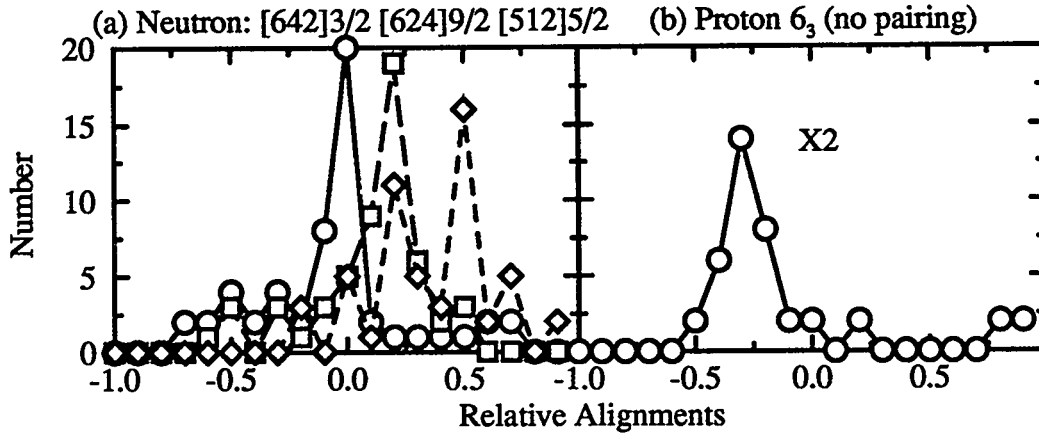


Figure 2. Routhian alignments summed over  $\hbar\omega=0.1-0.4$  MeV for (a) neutron ( $[642]3/2$ ,  $[512]5/2$ ,  $[624]9/2$ ) and (b) proton ( $[642]5/2$ ) orbitals close to the  $N=112$  and  $Z=80$  SD shell gaps. For neutrons the effect of increasing the pairing strength is also shown.

Figure 2 shows that the neutron orbitals ( $[642]3/2$ ,  $[512]5/2$ ,  $[624]9/2$ ) contribute little or no alignment (i.e., centered at  $\sim 0$ ) while the  $N=6$  proton levels contribute some alignment, equivalent to  $\sim 6$  keV in transition energy. These results compare qualitatively with those in Fig. 1, and imply that bands based on these neutron orbitals may well show near identical  $E_\gamma$ 's - if the core properties are not affected by the addition of the odd particle or hole. Indeed the unpaired routhians show a greater similarity in their relative alignments than required by experiment. Adding pairing increases the spread in the alignments (due to mixing). We also note that including the neutron  $N=7$  intruders causes a tail in the alignment distribution (not in Fig. 2), and that small (10%) changes in the deformation do not have a significant effect on the alignments of the non-intruder orbitals.

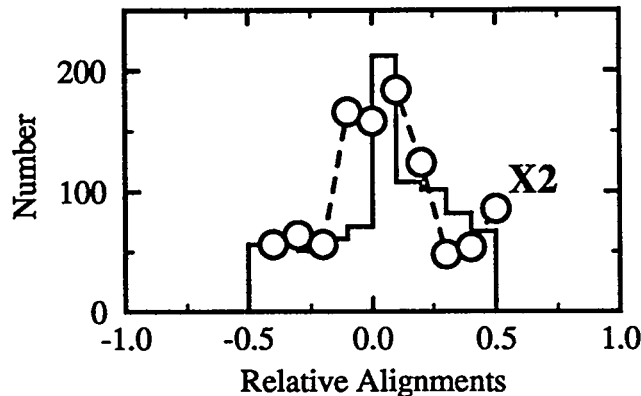


Figure 3. Comparison of relative alignments of ‘theoretical-bands’ generated from unpaired CSM routhians (solid-line) around  $N=112$  and for  $Z=80$  with experimental data (circles).

By assuming configurations for the observed SD bands, it is possible to generate

‘theoretical-band’ comparison plots. This is illustrated in Fig. 3 for unpaired routhians. The result is an ‘ID-band-peak’ superimposed on a background. We include various neutron configurations containing the [642]3/2, [512]5/2, [624]9/2 and  $N=7$  intruder orbitals and a common proton configuration (Hg,  $Z=80$  core). The difference between the experiment (circles) and calculation is most likely due the effects of pairing.

### 3.2 $A \approx 150$

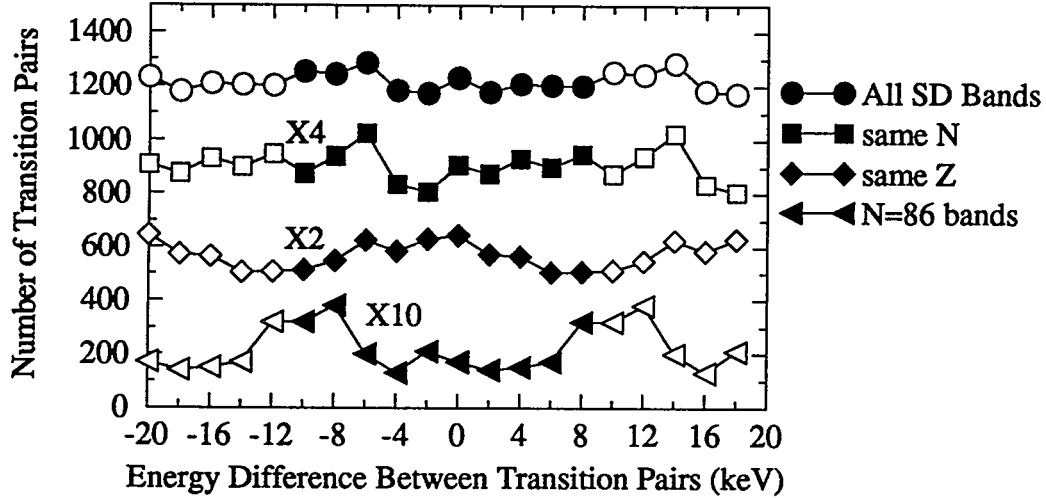


Figure 4. Comparison of  $A=150$  SD band transition energies for band-pairs in the following nuclei: Circles - All  $A=150$  SD bands, Squares - bands with the same  $N$ , Diamonds - bands with the same  $Z$ , Triangles -  $N=86$  bands ( $^{150}\text{Gd}$ ,  $^{151}\text{Tb}$ ,  $^{152}\text{Dy}$ ).

The results of a study of the  $A=150$  region are shown in Fig. 4. In contrast to the  $A=190$  region it is difficult to see any significant peak in the SD band transition energies, except when one restricts the number of SD bands to those with  $N=86$ . In this case the 2 pairs of known ID bands in  $^{150}\text{Gd}$ ,  $^{151}\text{Tb}$  and  $^{152}\text{Dy}$  (based on the [301]1/2 orbital) cause the peaks at  $\Delta E_\gamma \pm 10$  keV (since  $10 \text{ keV} \approx 0.5\hbar$ ). In the  $A=150$  region, SD bands with near identical  $E_\gamma$ 's appear to constitute a smaller fraction of the total number of bands.

## 4 Discussion

The difference between the  $A=190$  and  $A=150$  regions is striking and is most likely related to differences in the number of high- $N$  intruder orbitals occupied – intruders have a large contribution to the alignments and changes in alignment ( $\mathfrak{S}^{(2)}$ ). The  $A=150$  region is believed to be characterized by many changes in the number of intruder orbitals occupied, while the  $A=190$  SD bands are believed to differ mainly in the number of non-intruder orbitals, such as those studied in Fig. 1a. These orbitals may be labeled as ‘spectators’.

The occurrence of bands which only differ in ‘spectator’ orbitals is a necessary but not sufficient condition for near identical transition energies. Other effects (core properties) such as pairing must also be considered. Since pairing is generally accepted to be important in the  $A=190$  region (to explain the rise in the  $\mathfrak{S}^{(2)}$  moment of inertia), the large number of similar bands suggests that pair correlations are relatively insensitive to the blocking of non-intruder levels. This may be due to the pair correlations being of a

dynamic rather than static character (see contributions from Flocard and Wyss for more details on pairing at superdeformations). In the presence of weak pairing small changes in the configuration may not have such large effects on the pair gaps and hence one may indeed arrive a situation where neighboring SD bands have similar pairing (e.g., similar moments of inertia).

In light of our discussion on the moments of inertia it is useful to compare the  $\mathfrak{S}^{(2)}$ 's. In Fig. 5 we show the moments of inertia for all bands in the A=190 and A=150 region relative to  $^{192}\text{Hg}$  and  $^{152}\text{Dy}$  respectively. The A=190 bands exhibit a very small spread in their  $\mathfrak{S}^{(2)}$ 's while that of the A=150 region is somewhat larger.

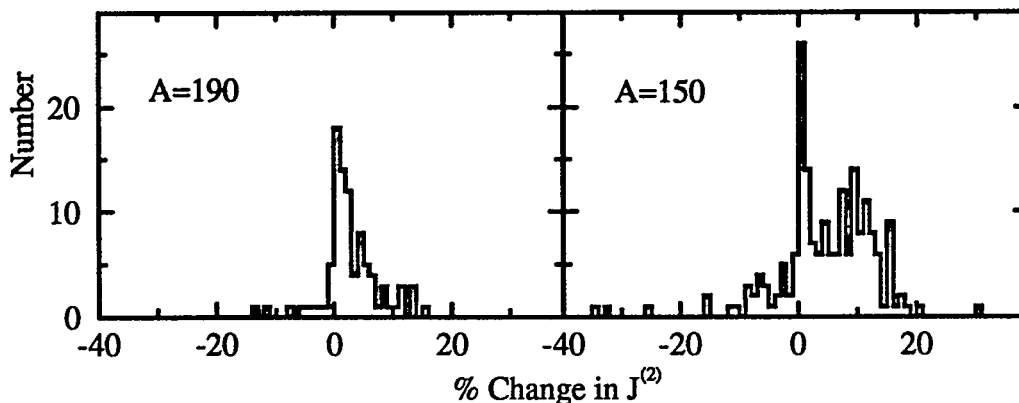


Figure 5. Distribution of deviations in the moments of inertia,  $\mathfrak{S}^{(2)}$ , for the A=190 and A =150 SD bands relative to  $^{192}\text{Hg}$  and  $^{152}\text{Dy}$  respectively

## 5 Summary

We began this talk with the question, how identical is 'identical'? From Figs. 1 and 3, we find that at best the similarity in the  $E_\gamma$ 's is not as close as one may have expected. Indeed the FWHM of the distribution associated with the so-called 'good' ID bands is  $\sim 1/3\hbar$ . Important differences are seen between the A=190 and A=150 regions, which together with comparisons with CSM calculations suggest that the large number of near identical bands in the A=190 region is related to the occurrence of spectator (non-intruder) orbitals which have near zero alignments over the SD band frequency range. In the A=190 region more SD bands (compared with the A=150 region) appear to be based on configurations involving changes in spectator rather than intruder orbitals. However, in the A=190 region, it is not so well understood why (i) the moments of inertia are so similar, and (ii) whether the proposed  $1\hbar$  spin difference [2] between some ID band pairs is due to either an alignment [2] of valence particles or to changes in the 'core' properties (e.g., small changes in pairing at low spins [3]).

## References

- [1] T.Byrski *et al.*, Phys. Rev. Lett. **64**, (1990) 1650.
- [2] F.Stephens *et al.*, Phys. Rev. Lett. **64**, (1990) 2623; Phys. Rev. Lett. **65**, (1990) 301.
- [3] P.Fallon *et al.*, Phys. Lett. **B276** (1992) 427-431.

Work supported in part by U.S. DOE under contract number DE-AC03-76SF0098.



# Configuration Dependence of Inertial Parameters in Identical and Non-Identical Bands at Normal Deformation

Jing-ye Zhang<sup>1,2,3</sup>, I. Ragnarsson<sup>4</sup> and L.L. Riedinger<sup>1</sup>

<sup>1</sup> Department of Physics, University of Tennessee, Knoxville, TN 37996-1200

<sup>2</sup> Physics Department, Brookhaven National Laboratory, Upton, NY 11973

<sup>3</sup> Institute of Modern Physics, Lanzhou, 730000, P.R. China

<sup>4</sup> Dept. of Math. Physics, Lund Inst. of Techn., P.O. Box 118, S-221 00 Lund, Sweden

## Abstract

A statistical analysis has been performed for the difference of moments of inertia in pairs of bands between odd- $A$  and adjacent  $A - 1$  even-even nuclei. The distribution of upsloping, flat, and downsloping configurations in the odd- $A$  partners is presented, and the underlying physics is discussed.

It is the purpose of this note to present the results of a statistical study [1] for identical and non-identical bands (IBs and non-IBs) in odd- $A$  and adjacent even-even nuclei. It is found that, in fact a very simple conclusion forcefully emerges and links the appearance of IBs (to be exact, bands with very similar moments of inertia) to the occupation of upsloping Nilsson orbitals.

To carry out this study a sample of 161 pairs of bands in odd- $Z$  nuclei and their  $A - 1$  even-even neighbors in mass region  $A = 150 - 190$  with  $Z = 66 - 79$  (data taken from [2]) was analyzed. The bands in odd- $Z$  nuclei, corresponding to the occupation of the odd proton in upsloping [402]5/2, [404]7/2, [514]9/2 and [505]11/2; approximately flat, [411]3/2, [411]1/2 and [523]7/2; and downsloping, [541]1/2, orbitals, are labeled below by phrases of upsloping, flat and downsloping configurations respectively.

As mentioned in ref. [3], one can construct the normalised average difference of the kinetic or the dynamic moment of inertia [4] between two bands as follows:

$$\delta\mathcal{J}^{(1)}(A_1) = \frac{1}{N} \sum_{n=1}^N \frac{|i_n|}{I_n(A_1)} \quad (1)$$

where  $i$  is the spin difference between bands in odd- $A$  and its  $A-1$  even-even neighbor at the same frequency and the index  $n$  is the label of the state. In this note only states before the first band crossing are included. We now introduce  $R(\mathcal{J}^{(1)})$  as a measure for the difference in  $\mathcal{J}^{(1)}$ :

$$R(\mathcal{J}^{(1)}) = \frac{\delta\mathcal{J}^{(1)}(A_1)}{\delta\mathcal{J}_m(A_1)} \quad (2)$$

where

$$\delta\mathcal{J}_m(A_1) = \frac{|A_1^{5/3} - A_2^{5/3}|}{A_1^{5/3}} \quad (3)$$

is the normalization factor. It is the relative difference in the moment of inertia between the nuclei with mass  $A_1$  and  $A_2$ , respectively, when all the other parameters except mass are the same for two bands. With  $A_1$  and  $A_2$  differing by 1, it is around 1% in the mass region discussed.

For the dynamic moment of inertia we define:

$$\delta\mathcal{J}^{(2)}(A_1) = \frac{1}{N-1} \sum_{n=1}^{N-1} \frac{|i_{n+1} - i_n|}{2}. \quad (4)$$

A measure of the difference in  $\mathcal{J}^{(2)}$  is then:

$$R(\mathcal{J}^{(2)}) = \frac{\delta\mathcal{J}^{(2)}(A_1)}{\delta\mathcal{J}_m(A_1)}. \quad (5)$$

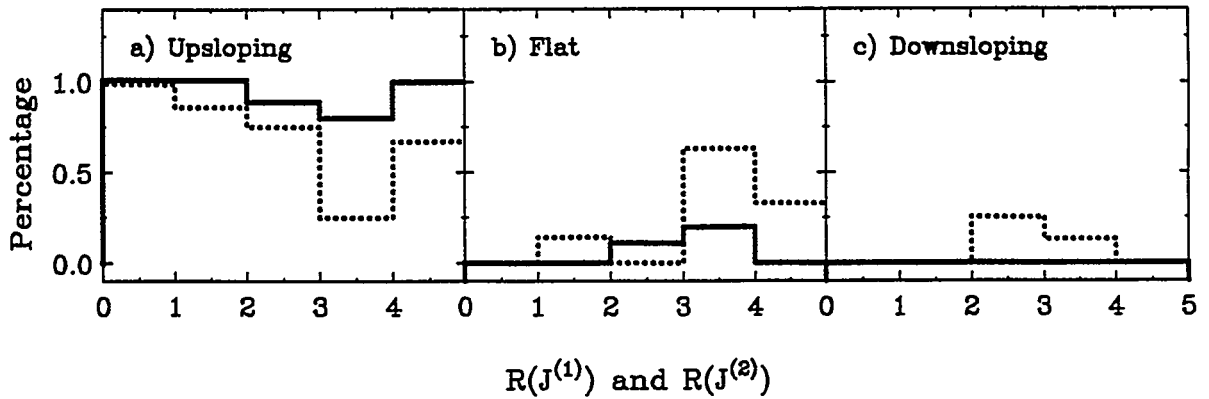


Fig. 1. The percentages of different configurations involved in the corresponding  $R(\mathcal{J}^{(1)})$  (solid) and  $R(\mathcal{J}^{(2)})$  ranges with step size equals to 1 : (a) upsloping, (b) flat and (c) downsloping configurations.

Figure 1 gives the detailed distribution of different types of configurations involved in the lowest range of  $R(\mathcal{J}^{(1)})$  and  $R(\mathcal{J}^{(2)})$ . Values from 0 to 5 are considered with the step size equal to 1. From panel (a) one can see that for  $R$  in the range of 0 – 1 ("identical bands" according to the criterion used in ref. [3]) upsloping configurations contribute 100% whichever criterion is used,  $R(\mathcal{J}^{(1)})$  (solid) or  $R(\mathcal{J}^{(2)})$  (dashed). Once  $R(\mathcal{J}^{(1)})$  and  $R(\mathcal{J}^{(2)})$  increase, flat configurations (panel (b)) and downsloping ones (panel (c)) start to contribute.

It is interesting to see if these features survive for a wider distribution of  $R(\mathcal{J}^{(1)})$  and  $R(\mathcal{J}^{(2)})$  values. Figure 2 gives the statistics of the  $R(\mathcal{J}^{(1)})$  (solid) and  $R(\mathcal{J}^{(2)})$  (dashed) distributions with step size equal to 5, for the upsloping (panel (a)), flat (panel (b)) and downsloping (panel (c)) configurations. The upsloping components have by far the largest contributions for low  $R(\mathcal{J}^{(1)})$  and  $R(\mathcal{J}^{(2)})$  values, and drop slightly faster for the  $R(\mathcal{J}^{(1)})$  distribution than for  $R(\mathcal{J}^{(2)})$ , as one can see from panel (a). As for both flat and downsloping configurations, they appear a little earlier for the  $R(\mathcal{J}^{(2)})$  distribution than for  $R(\mathcal{J}^{(1)})$ , as shown in panel (b) and (c) respectively.

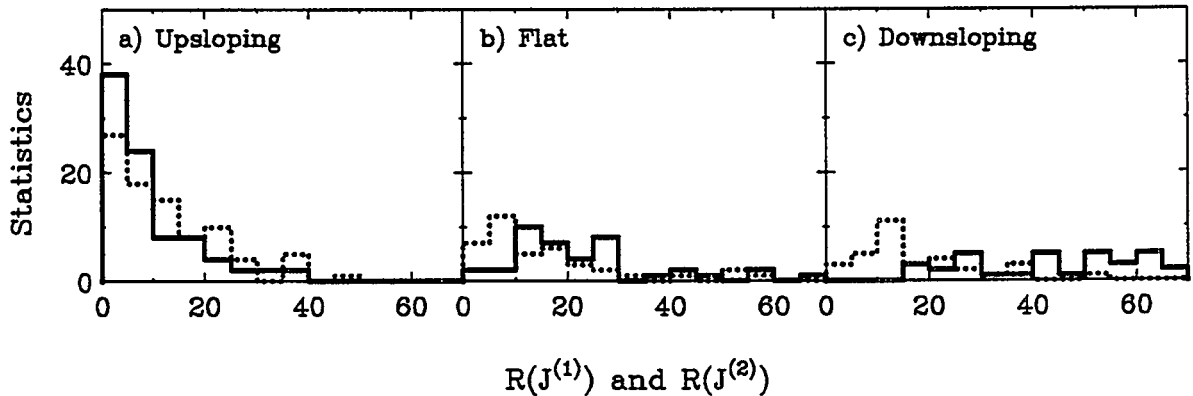


Fig. 2. The number of pairs for different configurations involved in the corresponding  $R(\mathcal{J}^{(1)})$  (solid) and  $R(\mathcal{J}^{(2)})$  ranges with step size equal to 5: (a) upsloping, (b) flat and (c) downsloping configurations.

Figures 1 and 2 demonstrate that the low  $R$ -values in this sample predominantly involve upsloping configurations. However, it is possible that this result merely reflects the greater number of upsloping configurations in this mass region. To study this point, we construct an alternate probability measure in figure 3. This figure gives the

probability that an upsloping, flat or downsloping configuration leads to the near-IBs ( $R \leq 5$ ). Such a probability therefore, in effect, normalizes out the different number of these three classes of configurations, and suggests their relative importance for near-IBs. Panel (a) tells that 43% of all upsloping configurations have  $R(\mathcal{J}^{(1)}) \leq 5$ , while only 5% of flat and none of the downsloping configurations lead to  $R(\mathcal{J}^{(1)}) \leq 5$ . For the larger  $\mathcal{J}^{(1)}$  difference, the probability that an upsloping, flat or downsloping configuration gives  $20 \leq R(\mathcal{J}^{(1)}) \leq 25$  is 5%, 10% and 6%, respectively (panel (b)). Thus, whether one looks at percentages of near-IBs that involve upsloping, flat or downsloping configurations (figs. 1, 2), or asks conversely what is the probability that an upsloping, flat or downsloping configuration gives the near-IBs (fig.3), the conclusion is the same: upsloping configurations are almost exclusively favored. The configuration dependence of  $R(\mathcal{J}^{(2)})$  values is similar.

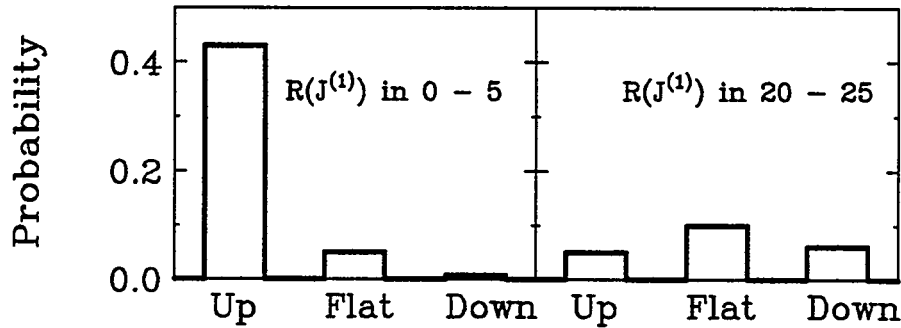


Fig. 3. The probability of given configurations leading to the corresponding  $R(\mathcal{J}^{(1)})$  values. (a)  $R(\mathcal{J}^{(1)})$  in 0 - 5, (b)  $R(\mathcal{J}^{(1)})$  in 20 - 25.

In conclusion, whatever criterion is used, the upsloping configuration is the key component to form bands with similar moments of inertia (small  $R$ -values), while the flat and downsloping configurations contribute more to higher  $R$  values. It is well known that the occupation of upsloping orbitals results in a decrease of the quadrupole deformation, which to certain extent compensates the effect on the moment of inertia from the odd particle blocking, which reduces the pairing correlation and then increases the moment of inertia [3, 5]. Such a cancellation picture is consistent with

the distributions presented in this note.

JYZ thanks Drs. R. Casten and V. Zamfir for valuable discussions. The project has been supported by the U.S. Department of Energy under contract No. DE-FG05-87ER40461 with the University of Tennessee and by the Swedish Natural Science Research Council.

## References

- [1] I. Ragnarsson, talk at ECT\* Workshop on High Spin and Novel Deformation, Nov 29 – Dec. 18, 1993, Trento, Italy.
- [2] The ORNL-University of Tennessee High Spin Data Base, as described by J.D. Garrett *et al.*, in Report No. ORNL-6508, 1988, p.70.
- [3] Jing-ye Zhang and Lee L. Riedinger, Phys. Rev. Lett. **69** (1992) 3448.
- [4] A. Bohr and B.R. Mottelson, Phys. Scripta **24**, (1981) 71.
- [5] I. Hamamoto and S. Mizutori, Phys. Lett. **B324**(1994)273.

## Identical degenerate bands in the second minimum in $^{131}\text{Ce}$

P. J. Nolan, C. W. Beausang, S. A. Forbes, E. S. Paul, A. T. Semple and J. N. Wilson  
*Oliver Lodge Laboratory, University of Liverpool, Liverpool, L69 3BX, U.K.*

R. M. Clark, K. Hauschild and R. Wadsworth  
*Department of Physics, University of York, York, YO1 5DD, U.K.*

J. Gizon, D. Santos, A. Gizon, C. Foin, J. Genevey and J. A. Pinston  
*Institut des Sciences Nucleaires, Grenoble, France.*

B. M. Nyakó and L. Zolnai  
*Institute of Nuclear Research, Debrecen, Hungary.*

In the region near  $A = 130$  superdeformed bands have been found in many nuclei. These bands correspond to structures within the second minimum in the potential well. The first band found was in  $^{132}\text{Ce}$  [1]. This band has a measured deformation of  $\beta_2 \sim 0.43$  [2] and it

is thought to have a high  $N$  particle configuration of  $\pi 5^4 \nu 6^2$ . In the neighbouring nucleus  $^{131}\text{Ce}$  a similar band was found [3] with a measured deformation [4] of  $\beta_2 \sim 0.35$ . Based on the properties of the band it has been assigned the configuration  $\pi 5^4 \nu 6^1$ . The difference in deformation is due to the different occupation of the  $N = 6$  orbital.

Several new bands have been found in these nuclei in an experiment carried out using the EUROGAM I spectrometer at Daresbury. The

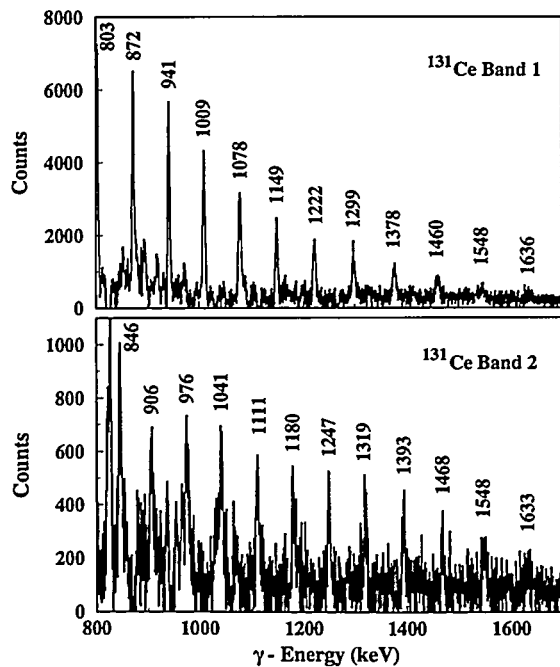


**Figure 1** Spectra from double gated coincidence events.

reaction used to populate the states was  $^{100}\text{Mo} + ^{36}\text{S}$  at a beam energy of 155 MeV. A single thin ( $\sim 600 \mu\text{g cm}^{-2}$ )  $^{100}\text{Mo}$  target was used. A high statistics data set was obtained containing in excess of  $2 \times 10^9$  for each of  $\gamma\text{-}\gamma$ ,  $\gamma\text{-}\gamma\text{-}\gamma$  and  $\gamma\text{-}\gamma\text{-}\gamma$  suppressed coincidence events. Analysis of the data has revealed two new excited superdeformed bands in  $^{132}\text{Ce}$  [5]. The data for  $^{131}\text{Ce}$  is shown in figure 1. These spectra are derived from double gated triple coincidences. The top

spectrum (band 1) is the previously known band. Band 2 is new and is the first example of an excited superdeformed second minimum band in  $^{131}\text{Ce}$ . Further detailed analysis of the data has revealed that the  $\gamma$ -ray peaks in the band 2 spectrum are multiplets. The first evidence for this can be seen in figure 2. This shows the Full Width at Half Maximum (FWHM) of the peaks for several bands in  $^{131,132}\text{Ce}$ . All the measurements are made on the same data set. Three sets of data ( $^{132}\text{Ce}$  bands 1 and 2,  $^{131}\text{Ce}$  band 1) follow the expected behaviour given the geometry of EUROGAM I and the reaction kinematics, band 2 in  $^{131}\text{Ce}$  is clearly different. The multiplet has been decomposed by fitting peaks with a fixed FWHM

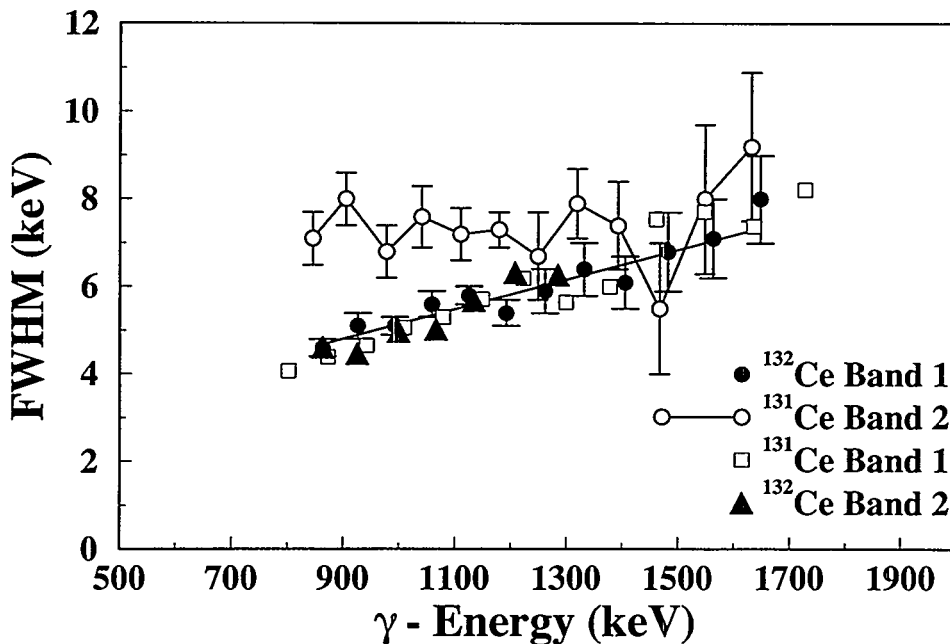


**Figure 2** FWHM of several bands in  $^{131,132}\text{Ce}$ . Representative errors are given. The line is a fit to the data (not  $^{131}\text{Ce}$  band 2).

that is gamma-ray energy dependent. The value for the FWHM is determined by the fitted line shown in figure 2. The procedure used was to increase the number of peaks until an acceptable chi-squared was obtained. The conclusion is that band 2 is in fact 2 bands. These bands can be thought of as identical in that the differences in the gamma-ray energies are less than the experimental resolution.

Prior to this work, identical bands had not been seen in the mass 130 region. A group of bands has now been identified in the nuclei  $^{131-133}\text{Ce}$  which are identical. This can be seen from the incremental alignment plot shown in figure 3. The configurations for these bands can be determined with the aid of cranking calculations (figure 4). All the excited bands are assumed to have a  $\nu 6^2$  configuration as they depopulate near  $\hbar\omega = 0.4$  MeV similar to the previously known band in  $^{132}\text{Ce}$ . The suggested configurations are given in the table.

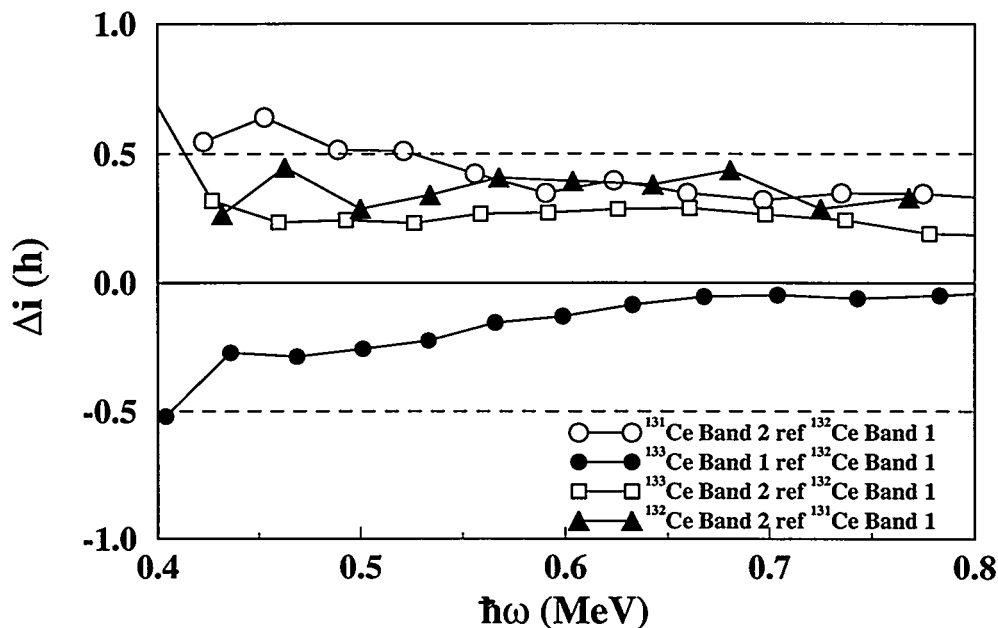


**Figure 3** Incremental alignment as a function of rotational frequency ( $\hbar\omega$ ).

**Table 1**

Suggested high N neutron configurations for the excited superdeformed bands in  $^{131-133}\text{Ce}$ . All bands have a  $\pi 5^4$  occupation.

$^{131}\text{Ce}$ band 1	$6^1$	$^{132}\text{Ce}$ band 1	$6^2$	$^{133}\text{Ce}$ band 1	$6^2[530]^1$
band 2	$6^2[411]^{-1}$	band 2	$6^2[523]^{-1}[530]^1$	band 2	$6^2[530]^1$
	and/or	band 3	$6^2[523]^{-1}[530]^1$		
	$6^2[523]^{-1}$				



The deformation used in figure 4 is  $\beta = 0.43$  consistent with the measured value for band 1 in  $^{132}\text{Ce}$ . At this deformation three neutron orbitals are near degenerate close to the Fermi surface, i.e. [411] positive signature and [523] both signatures, but only two excited bands have been found in both  $^{131,132}\text{Ce}$ . It is important, however, that the deformations of these bands are measured as they can change from nucleus to nucleus and band to band.

These configurations are consistent with some pairs of bands being identical. For example  $6^2$  and  $6^2[411]^{-1}$  configurations lead to identical bands with a predicted difference in incremental alignment of about  $-0.2\hbar$ , compared to the experimental value of  $0.3\hbar$  for  $^{131}\text{Ce}$  band 2. It is not clear from the calculations why some other pairs (e.g.  $6^1$  and  $6^2 [523]^{-1} [530]^1$ ) have a constant incremental alignment difference. In general there is little agreement between the experimental values and those expected for a fixed deformation.

### **Acknowledgement**

EUROGAM is funded jointly by EPSRC (UK) and IN2P3 (France).

### **References**

- [1] P J Nolan et al, J Phys G11 L17 (1985)
- [2] A J Kirwan et al, Phys Rev Lett 58 467 (1987)
- [3] Y X Luo et al, Z Phys A329 125 (1988)
- [4] Y J He et al, J Phys G16 657 (1990)
- [5] D Santos et al, to be published

Neutron single particle levels : Universal Woods-Saxon potential  
 $N= 74$ ,  $BETA2= 0.430$ ,  $BETA4= 0.000$ ,  $GAMMA= 0.0^\circ$ ,  
 $(\pi,\alpha)$  : solid= $(+,+1/2)$ , dotted= $(+,-1/2)$ , dot-dash= $(-,+1/2)$ , dashed= $(-,-1/2)$

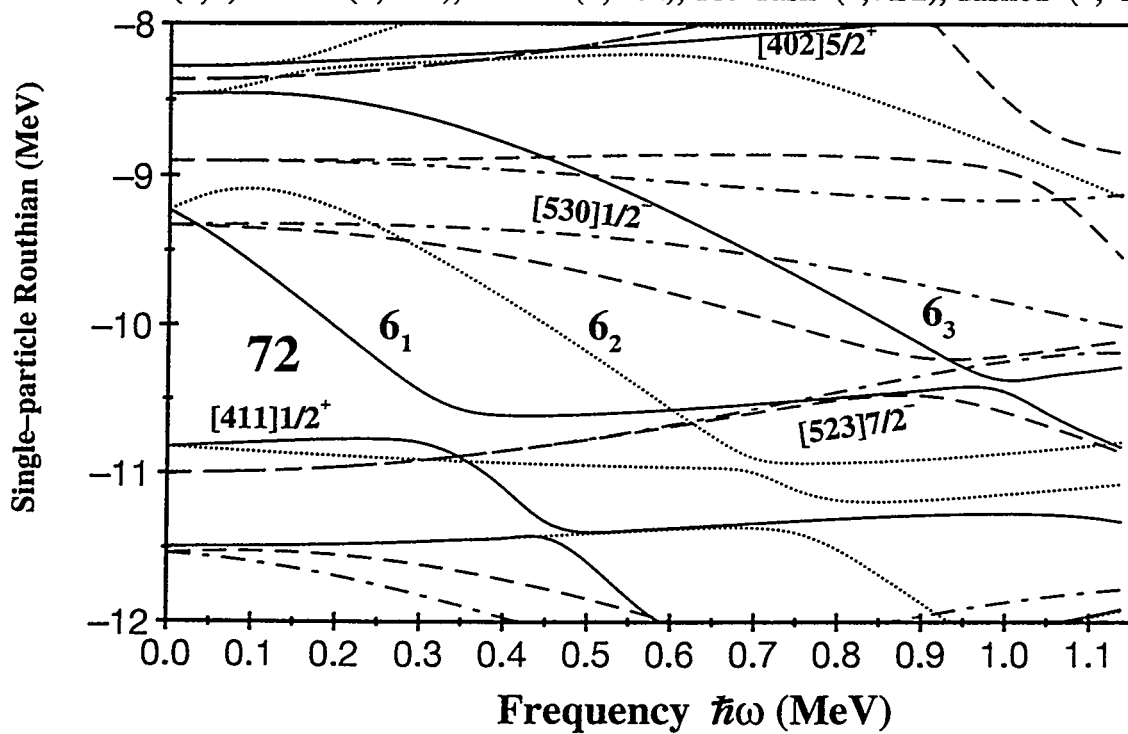


Figure 4. Single particle levels showing first three  $N=6$  intruder orbitals for region applicable to  $^{131,132}\text{Ce}$

# Pseudo-Spin Flip in Doubly Decoupled Structures and Identical Bands

A.J. Kreiner,<sup>a,b,c</sup> M.A. Cardona,<sup>a</sup> H. Somacal,<sup>a</sup> M.E. Debray,<sup>a,b</sup> D. Hojman,<sup>a,c</sup> J. Davidson,<sup>b,c</sup> M. Davidson,<sup>b,c</sup> D. De Acuña,<sup>d</sup> D.R. Napoli,<sup>d</sup> J. Rico,<sup>d</sup> D. Bazzacco,<sup>e</sup> R. Burch,<sup>e</sup> S.M. Lenzi,<sup>e</sup> C. Rossi Alvarez,<sup>e</sup> N. Blasi,<sup>f</sup> G. Lo Bianco<sup>f</sup>

<sup>a</sup> Departamento de Física, Comisión Nacional de Energía Atómica, 1429 Buenos Aires, Argentina. <sup>b</sup> Departamento de Física, Facultad de Ciencias Exactas y Naturales, UBA, Buenos Aires, Argentina. <sup>c</sup> CONICET, 1033 Buenos Aires, Argentina. <sup>d</sup> INFN, Laboratori Nazionali di Legnaro, Legnaro, Italy. <sup>e</sup> Dipartimento di Fisica, Sezione di Padova, Padova, Italy. <sup>f</sup> Dipartimento di Fisica and INFN, Sezione di Milano, Milano, Italy.

Unfavored components of doubly decoupled bands are reported for the first time. They can be interpreted as having the pseudo-spin flipped relative to the orientation in the favored components, i.e. antialigned with respect to the rotation axis. In addition, the differences in consecutive transition energies along the favored and unfavored sequences are strikingly similar among them up to  $I^\pi = 15^+$  and  $14^+$  respectively. This feature arises from a cancellation of differences in alignments and moments of inertia. It is shown that identical bands imply transitions whose energies differ by a constant amount only for the special case of constant moments of inertia.

Deformed nuclei can build up angular momentum by two different mechanisms, namely by rotating collectively and by aligning particle angular momenta along the rotation axis ( $I + 1/2 = R + 1/2 + i$ , where  $I$ ,  $R$  and  $i$  are the total, collective and aligned angular momenta respectively). This opens up the possibility of having bands in neighboring even-even and odd-mass nuclei, or odd-mass and doubly-odd nuclei, with identical transition energies if the alignment of the odd particle is quantized<sup>1</sup> (e.g., assumes the value  $1/2$ ). In this case the  $R$  values for the odd-mass nucleus, i.e.  $R = I - 1/2$  for the  $I = 1/2, 5/2, 9/2, \dots$  sequence, would be identical to the  $R$  values of the neighboring even-mass nucleus (the transition energies would only be equal if in addition the presence of the odd particle does not influence the kinematic moment of inertia associated with the collective rotation, denoted here as  $J_C^{(1)}$ ). Hence identical transition energies in two different bands require both identical collective angular momenta and identical collective moments of inertia which can be seen from the following expression<sup>2</sup>:

$$\frac{E_\gamma}{2} \simeq \omega = \left( I + \frac{1}{2} - i \right) / J_C^{(1)} \quad (1)$$

In the case of identical transition energies one speaks of twin bands (TB's). Identical bands in a more general sense (other than TB's) are only required to have identical dynamic moments of inertia.

Examples for this behavior were found both in the normal and superdeformed regimes<sup>3,4</sup>. In fact a particle with  $\Omega = 1/2$  ( $\Omega$  is the projection of the particle angular

momentum on the symmetry axis) and decoupling parameter +1 has a quantized value of its alignment of 1/2 behaving effectively<sup>5</sup> as a spin 1/2 excitation. This effective angular momentum is indeed the pseudo-spin<sup>6-8</sup>.

In view of the interest awakened by the identical band problem it is relevant to further investigate the coupling of aligned pseudo-spins to other excitations. Examples of these structures are doubly decoupled bands<sup>9,10</sup> in which an aligned neutron pseudo-spin (of the singlet type<sup>10</sup> in most cases) is coupled to an aligned proton ( $i_{np} = i_p + 1/2$ ). They appear systematically in the upper rare-earth region but so far only the favored components (namely those where neutron pseudo-spin and proton alignment are parallel) were found, consisting in odd-spin ( $I_f = 3, 5, 7, 9, \dots$ ) sequences connected by stretched  $E2$  transitions. The unfavored components ( $I_u = 4, 6, 8, \dots$ ) were predicted<sup>9,10</sup> to be rather degenerate with the favored ones, the degenerate partners being characterized by  $I_f = R + i_p + 1/2$ ,  $I_u = R + i_p - 1/2$  ( $(I_u, I_f) = (4, 5), (6, 7), \dots$ ). In other words the neutron spin is flipped from being aligned with the rotation axis to the opposite direction. These unfavored components, being shifted up in energy away from the yrast line, receive considerable less feeding and most likely for this reason were never detected so far. In view of this, a powerful last-generation  $\gamma$ -ray spectrometer like GASP<sup>12</sup> was utilized to explore these details.

The doubly odd nucleus<sup>11</sup>  $^{176}\text{Re}$  has been reexamined<sup>13</sup> here utilizing the 40 Compton Suppressed Ge, 80 BGO-element filter, GASP spectrometer, at the Legnaro Tandem Facility, through the  $^{165}\text{Ho}(^{16}\text{O}, 5n)$  reaction at 101 MeV bombarding energy. Only triple and higher fold Ge coincidences were stored on video tapes, recording  $\approx 10^9$  events in a two-day run on a 2 mg/cm<sup>2</sup> Ho target backed with 1.5 mg/cm<sup>2</sup> of Bi. From these events both  $E_{\gamma_1} - E_{\gamma_2} - E_{\gamma_3}$  cubes and (projected) double coincidence matrices were produced and extensively gated. The unfavored components alluded to above are reported here for the first time (see fig.1). One observes the  $f$  part of the  $\pi h_{9/2} \otimes \nu 1/2 [420]$  doubly decoupled band, being composed of stretched  $E2$  lines up to  $I^\pi = 27^+$  (first few transitions are, 76, 171, 268, 359, 441, 510 keV, etc.) and their  $u$  companions (162, 258, 349, 431, 500 keV, etc.). The  $u$  part is intensity wise of the order 30 % of the  $f$  part which is only  $\simeq 1/4$  of the total cross section for  $^{176}\text{Re}$ . The transitions linking the  $f$  and  $u$  parts are less than 18 % of the  $u$  transitions which means that we are studying details which are between 0.3 and 1.3 % of the total cross section.

A striking feature is that the differences in transition energies ( $\simeq 10$  keV) for corresponding transitions (e.g.  $7^+ \rightarrow 5^+$  and  $6^+ \rightarrow 4^+$ ) in the  $f$  and  $u$  sequences are almost identical for the first five pairs meaning automatically that the differences in consecutive transition energies along each sequence,  $\Delta E_\gamma$ , are also identical in both sequences (but decreasing here within each sequence). Remembering that the dynamic moment of inertia is defined as  $dI/d\omega$  and usually approximated by the finite differences  $\Delta I/\Delta\omega = 2/(\Delta E_\gamma/2) = 4/\Delta E_\gamma$  one would be tempted to conclude that these moments of inertia are identical for both sequences. However the equality holds for (slightly) different values of the rotational frequency. This remarkable feature is lost when the backbending region is reached. As it will become clear from the discussion below, the collective kinematic moments of inertia are also very similar

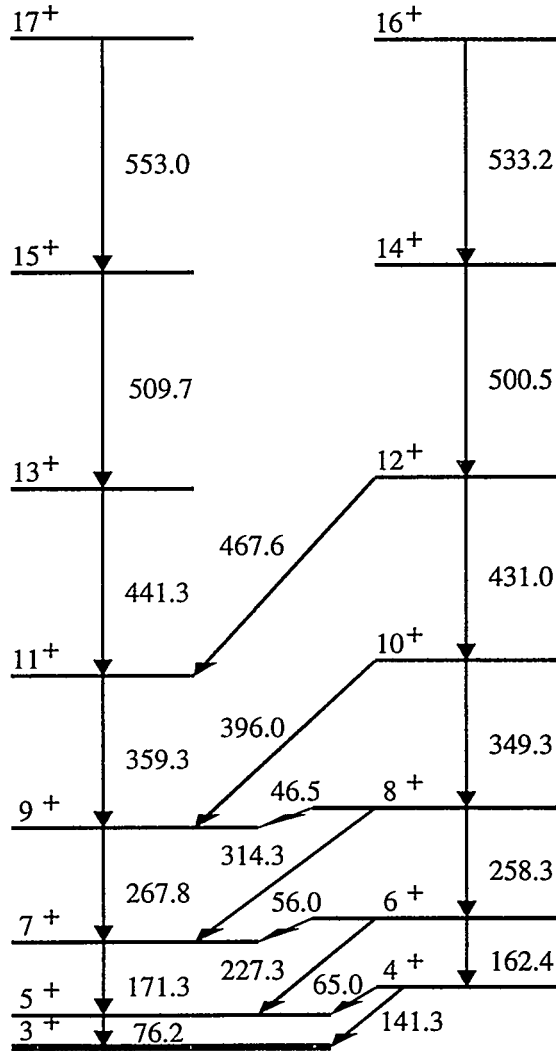


Figure 1: Level scheme of  $^{176}\text{Re}$  showing partially the favored ( $I=\text{odd}$ ) and favored ( $I=\text{even}$ ) portions of the doubly decoupled band.

while the transition energies themselves are not, because the pseudo-spin asymptotic limit is not fully reached. The parameters are extracted by fitting the level energies through a fourth order cranking formula:

$$E = \frac{1}{2}(J_0 + 3/2J_1 \omega^2) \omega^2 \quad (2)$$

where the rotational frequencies  $\omega$  are obtained from the third order equation

$$\sqrt{R(R+1)} \simeq R + 1/2 = (J_0 + J_1 \omega^2) \omega \equiv J_C^{(1)} \omega \quad (3)$$

with  $R = I - i$ . The difference in alignment between the  $f$  and  $u$  components of the DD band in  $^{176}\text{Re}$  is  $i_f - i_u \equiv \Delta_{fu}i = 0.86$  (vs. 0.77 and 0.84 in the  $\nu 1/2 [420]$  bands in, respectively<sup>14,15</sup>, the odd-N isotones  $^{175}\text{W}$  and  $^{177}\text{Os}$ ). The  $\simeq 10$  keV difference between corresponding  $f$  and  $u$  transitions can be understood by subtracting eq.(3) applied for a pair of them:

$$I - i_f + 1/2 - (I - 1 - i_u + 1/2) = 1 - \Delta_{fu}i \simeq J^{(2)}(\omega_u)\Delta_{fu}\omega \quad (4)$$

This expression is obtained by (a) considering equal  $J_C^{(1)}$  values (here equal  $J_0$ 's and  $J_1$ 's) for both bands and (b) expanding to first order in  $\Delta_{fu}\omega = \omega_f - \omega_u$  around  $\omega_u$ .  $J^{(2)}$  is the dynamic moment of inertia which turns out to be  $J_0 + 3 J_1 \omega^2$  for the fourth order cranking. We see clearly from eq.(4) that if  $\Delta_{fu}i$  is equal to 1 (asymptotic pseudo-spin limit) the transition energies are identical. However only the main part of the transition energy difference in  $^{176}\text{Re}$  can be explained by eq.(4). By refining the treatment and allowing for the difference in  $J_C^{(1)}$  for both bands ( $J_{Cf}^{(1)} - J_{Cu}^{(1)} \equiv \Delta_{fu}J_C^{(1)}$ ) one can show that:

$$\Delta_{fu}\omega = (1 - \Delta_{fu}i - \Delta_{fu}J_C^{(1)}\omega_u)/J_f^{(2)}(\omega_u) \quad (5)$$

so that TB's would demand both  $\Delta_{fu}i = 1$  and  $\Delta_{fu}J_C^{(1)} = 0$ .

Hence, in this context the remarkable constancy of 10 keV in the transition energy differences can be discussed as follows: (a) Since the  $J_1$  values for  $^{176}\text{Re}$  are much smaller than for  $^{175}\text{W}$  and  $^{177}\text{Os}$ , the frequency dependence of  $J_f^{(2)}$  is also much less pronounced implying that the contribution  $(1 - \Delta_{fu}i)/J_f^{(2)}$  in eq.(5) decreases only slowly. (b) Since both  $J_0$  and  $J_1$  are slightly smaller for the  $f$  than for the  $u$  part in  $^{176}\text{Re}$  this means that  $\Delta_{fu}J_C^{(1)} < 0$  implying that the second contribution  $-\Delta_{fu}J_C^{(1)}\omega_u/J_f^{(2)}$  in eq.(5) is positive compensating for the decrease in the first contribution. It is very interesting to observe<sup>14,15</sup> that both in  $^{175}\text{W}$  and  $^{177}\text{Os}$  the first transition energy difference is also of  $\simeq 10$  keV. In fact, the first few transition energies for  $^{175}\text{W}$ ( $^{177}\text{Os}$ ) are for the  $f$  part (in keV and starting with the  $9/2 \rightarrow 5/2$  transition): 194.9 (194.5); 289.4 (282.4); 370.7 (357.4); 439.8 (423.6) and for the  $u$  part: 184.6 (183.6); 280.7 (274.8); 364.9 (351.5); 437.9 (419.8). However, here the energy differences decrease very fast: 10.3 (10.9); 8.7 (7.6); 5.8 (5.9); 1.9 (3.8) keV. This is consistent with: (a) The much larger values of  $J_1$  which imply much larger values of  $J_f^{(2)}$  and hence a much faster decrease of the first contribution of eq. (5). (b) Contrary to the case of  $^{176}\text{Re}$  here  $\Delta_{fu}J_C^{(1)} > 0$  implying an even faster decrease in  $\Delta_{fu}\omega$ .

Hence, a constant difference in transition energies (i.e. in  $\omega$ ) is only possible if the inertia parameters of the two bands are (slightly) different so that the compensation mechanism implied by eq.(5) can occur. The difference in inertia parameters originates in the fact that the equality of  $\Delta E\gamma$  (and hence of  $J^{(2)}$ ) occurs in the two bands at slightly different values of  $\omega$  as already mentioned. There is an obvious exception to the above statement, namely the case where  $J^{(2)}$  is constant which is however rather unusual. In that case a constant value of  $\Delta_{fu}\omega$  in eq.(5) can still be obtained even if there is a finite difference in alignment provided  $\Delta_{fu}J_C^{(1)} = 0$ , corresponding to a special case of identical bands.

The powerful last generation GASP array has allowed a reexamination of the high-spin structure of  $^{176}\text{Re}$  and has led to the following results: (a) Unfavored components of a doubly decoupled band are reported for the first time. (b) All the

available evidence both from the energy spectrum and from the transition rates can be quantitatively accounted for by a model where the neutron pseudo-spin is flipped from being parallel to the rotation axis in the favored states to antiparallel in the unfavored ones. Residual interactions seem to play a minor role reinforcing the validity of the aligned pseudo-spin picture in more complex structures. (c) The remarkable equality in transition energy differences along the two sequences arrives mainly from a small deviation from the pseudo-spin asymptotic limit ( $\Delta_{f_u} i \leq 1$ ) and very similar dynamic moments of inertia, but on a more quantitative level from a subtle cancellation of differences in alignments and moments of inertia. The analysis of this example reveals that identical bands imply transitions whose energies differ by a constant amount only for the special case of constant dynamic moments of inertia.

Financial support from the Fundación Antorchas is gratefully acknowledged.

1. F.S.Stephens et al., Phys.Rev.Lett.64, 2623 (1990); Phys.Rev.Lett.65, 301 (1990).
2. A.J.Kreiner in *Future Directions in Nuclear 4 $\pi$  Gamma Detection Systems of the New Generation*, A.I.P.259 (1992) 131 (Eds. J.Dudek and B.Haas).
3. A.J.Kreiner, Phys.Rev. C38, R2486 (1988).
4. T.Byrski et al., Phys.Rev.Lett.64, 1650 (1990); W.Nazarewicz et al., Phys.Rev.Lett.64, 1654 (1990).
5. A.J.Kreiner et al., Nucl.Phys.489, 525 (1988).
6. K.T.Hecht and A.Adler, Nucl.Phys.A137, 129 (1969); R.D.Ratna Raju, J.P.Draayer, and K.T.Hecht, Nucl.Phys.A202, 433 (1973).
7. A.Arima, M.Harvey, and K.Shimizu, Phys.Lett.30B, 517 (1969).
8. A.Bohr, I.Hamamoto, and B.R.Mottelson, Phys.Scr.26, 267 (1982).
9. A.J.Kreiner et al., Phys.Rev.C29, R1572 (1984); Nucl. Phys.A432, 451 (1985).
10. A.J.Kreiner, Phys.Lett.B279, 233 (1992) and references therein.
11. J.Davidson et al., Z.Physik A324, 363 (1986); D.Santos et al., Phys.Rev.C39, 902 (1989).
12. GA.SP. Experiment: Project Report of a Gamma Spectrometer, Internal Report INFN/BE-90/11, (1990).
13. A.J. Kreiner, M.A.Cardona, H.Somacal, M.E.Debray, D.Hojman, J.Davidson, M.Davidson, D.De Acuña, D.R.Napoli, J.Rico, D.Bazzacco, R.Burch, S.M.Lenzi, C.Rossi Alvarez, N.Blasi, and G.Lo Bianco, Phys.Rev.C50(1994)R(in press).
14. P.M.Walker et al., J.Phys.G: Nucl.Phys.4, 1655 (1978).
15. G.D.Dracoulis et al., Nucl.Phys.A401, 490 (1983).

## “Identical” SD Band in $^{151}\text{Dy}$ and the Pseudospin Coupling Scheme

D. Nisius,<sup>(1,3)</sup> R. V. F. Janssens,<sup>(1)</sup> P. Fallon,<sup>(2)</sup> B. Crowell,<sup>(1)</sup> I. Ahmad,<sup>(1)</sup>  
C. W. Beusang,<sup>(4)</sup> M. P. Carpenter,<sup>(1)</sup> B. Cederwall,<sup>(2)</sup> P. J. Daly,<sup>(3)</sup>  
M. A. Deleplanque,<sup>(2)</sup> R. M. Diamond,<sup>(2)</sup> D. Gassmann,<sup>(1)</sup> Z. W. Grabowski,<sup>(3)</sup>  
R. G. Henry,<sup>(1)</sup> T. L. Khoo,<sup>(1)</sup> T. Lauritsen,<sup>(1)</sup> I. Y. Lee,<sup>(2)</sup> A. O. Macchiavelli,<sup>(2)</sup>  
R. H. Mayer,<sup>(3)</sup> F. S. Stephens,<sup>(2)</sup> P.J. Twin<sup>(4)</sup>

<sup>(1)</sup> Argonne National Laboratory, Argonne, Illinois 60439, USA

<sup>(2)</sup> Lawrence Berkeley Laboratory, Berkeley, California 94720, USA

<sup>(3)</sup> Purdue University, West Lafayette, Indiana 47907, USA

<sup>(4)</sup> Oliver Lodge Laboratory, U. of Liverpool, Liverpool L693BX, United Kingdom

### Abstract

Four new excited bands in  $^{151}\text{Dy}$  have been identified. One of these bands possesses transition energies that lie midway between the  $\gamma$ -ray energies of the superdeformed band in  $^{152}\text{Dy}$ . This is a significant result in terms of the “identical” band issue, as it confirms predictions based on the strong coupling model and the pseudospin coupling scheme.

The discovery of the first pairs of SD bands, ( $^{150}\text{Gd}^*$ ,  $^{151}\text{Tb}$ ) and ( $^{151}\text{Tb}^*$ ,  $^{152}\text{Dy}$ ), whose transition energies are identical [1] has brought about a flurry of theoretical activity attempting to describe the phenomenon. One such attempt [2] has received a lot of attention. It was shown in ref. [2] that within the strong coupling limit of the particle-rotor model, the bands in the two pairs of SD nuclei mentioned above can be understood as cases where the moments of inertia are identical and the decoupling parameter  $a = +1$  for the specific proton excitation involved (the measured  $\gamma$ -ray energies require  $a = 1.0 \pm 0.1$ [2]). This value of the decoupling parameter is achieved if it is determined within the framework of the pseudospin coupling scheme. This value is to be contrasted with the values  $a = 0$  deduced from the Nilsson asymptotic quantum numbers, and  $a = 0.85$  obtained in realistic calculations [2]. Thus, in ref. [2] these identical bands are interpreted as results of a pseudo-SU(3) symmetry at very large deformations. The observation of a pair of excited SD bands with no signature splitting in  $^{153}\text{Dy}$  [3] could also be explained within the strong coupling model as a case where the decoupling parameter  $a$  is exactly zero and, as a result, the averages of consecutive transitions in the signature partner bands equal the  $\gamma$ -ray energies of the  $^{152}\text{Dy}$  SD core.

It was pointed out in ref. [2] that important additional confirmation of the validity of the pseudospin interpretation within the strong coupling limit would be provided by finding an excited SD band in  $^{151}\text{Dy}$  corresponding to an excitation involving



the  $[\bar{3}\bar{1}\bar{0}]1/2$  pseudospin orbital (the orbital  $[\bar{3}\bar{1}\bar{0}]1/2$  is labelled  $[411]1/2$  with Nilsson asymptotic quantum numbers). The decoupling parameter is  $a = -1$  within the pseudospin coupling scheme and the transition energies in the SD band are predicted to lie half way between the  $\gamma$ -ray energies of the SD band in  $^{152}\text{Dy}$ . The experiments that followed searching for excited bands in  $^{151}\text{Dy}$  were unsuccessful [4]. The new generation of  $\gamma$ -ray spectrometers has now made it possible to revisit this important issue.

The experiment was carried out using the early implementation phase of the GAMMASPHERE spectrometer [5] which consisted at that time of 32 Compton-suppressed Ge detectors. The 175 MeV  $^{34}\text{S}$  beam, provided by the 88-Inch Cyclotron, bombarded a stack of three self-supporting  $350 \mu\text{g}/\text{cm}^2$   $^{122}\text{Sn}$  foils. The 5n evaporation channel from this reaction produced excited states in  $^{151}\text{Dy}$ . These are the same reaction conditions under which the yrast SD band in  $^{151}\text{Dy}$  was first discovered by Rathke et al [6]. An event was selected by requiring that three or more detectors register in prompt coincidence within a time window of 50 ns. A total of  $1.3 \times 10^9$  triple and higher-fold coincidence events was recorded. The data were analyzed by sorting all events into a three-dimensional histogram [7]. Double-gated one-dimensional histograms were created using full background-subtraction and proper propagation of errors [8].

A total of seven SD bands were found in the data. In addition to the yrast SD band (band 1) [6] and the strongest SD bands of  $^{152}\text{Dy}$  and  $^{151}\text{Tb}$  produced in the competing  $(^{34}\text{S},4\text{n})$  and  $(^{34}\text{S},\text{p}4\text{n})$  channels, four new bands in  $^{151}\text{Dy}$  with dynamic moments of inertia  $\mathcal{S}^{(2)}$  similar in magnitude to that seen in band 1 were found in this experiment. These four SD bands (which have been labelled 2-5) have respective intensities of 39(7), 30(5), 20(7) and 13(4)% relative to the intensity of band 1, which carries about 1% of the total  $\gamma$ -ray flux reaching the  $^{151}\text{Dy}$  ground state.

Band 4 in  $^{151}\text{Dy}$  is characterized by a dynamic moment of inertia  $\mathcal{S}^{(2)}$  which is essentially the same as the yrast  $^{152}\text{Dy}$  SD band and strongly suggests that band 4 has the same high-N intruder configuration as the  $^{152}\text{Dy}$  SD band. As can be seen from the spectrum of fig. 1, band 4 consists of 15 transitions ranging in energy from 712 to 1375 keV. The transition energies in the new  $^{151}\text{Dy}$  SD band are very close to the mid-point transition energies of the  $^{152}\text{Dy}$  SD band. In fact, the r.m.s. energy (fig. 2) difference between the two bands is 1.58 keV, a number which compares well with the r.m.s. differences of 1.37 and 1.57 keV observed in the  $(^{153}\text{Dy}^*, ^{152}\text{Dy})$  and  $(^{151}\text{Tb}^*, ^{152}\text{Dy})$  pairs discussed above. It is then proposed that band 4 in  $^{151}\text{Dy}$  can be associated with the identical SD band calculated in ref. [2], thus it is the first identical SD band corresponding to a decoupling parameter of  $a = -1$ .

While band 4 seems to find a natural explanation within the coupling scheme outlined above, there are a few differences which need to be addressed. First, as illustrated in fig. 2, the energy differences in the  $(^{153}\text{Dy}^*, ^{152}\text{Dy})$  pair and  $(^{151}\text{Tb}^*, ^{152}\text{Dy})$  pair have nearly a constant value, while these differences in the  $(^{151}\text{Dy}^*, ^{152}\text{Dy})$  pair become more constant at the higher energies ( $E_\gamma > 900$  keV). A possible factor con-

tributing to the gradual rise of the energy differences might be found in the interaction at the lowest frequencies of the orbital of interest ( $[\bar{3}\bar{1}\bar{0}]1/2$ ) with other natural parity orbitals which lie relatively close in excitation energy [9].

Second, it was shown by Curien et al [10] that for the identical bands near  $A=150$ , the decay-out mechanism is strongly affected by neutron pairing correlations and by the occupancy of high- $N$  neutron intruder orbitals. In the case of band 4 in  $^{151}\text{Dy}$ , the decay out of the band occurs at higher frequency than in the  $^{152}\text{Dy}$  SD band (fig. 1 inset), an unexpected result since the configurations of the two identical bands are characterized by the same high- $N$  intruders (i.e.  $\pi 6^4\nu 7^2$  in terms of high- $N$  intruder orbital labelling [9, 11]). The decay out of a SD band is a complex process depending on an number of factors, and it appears that the generalization proposed in ref. [10] does not always apply.

Third, the issue of the presence of the signature partner to band 4 needs to be addressed. In the strong coupling limit, when the decoupling parameter has the value  $a = -1$ , the two signature partner bands ( $r = \pm i$ ) should have the same transition energies. We have tried to determine whether band 4 corresponds to a single band or a superposition of two signature partners by comparing the widths of the  $\gamma$ -ray peaks of all the SD bands in our data. It was found that peaks of band 4 had the same widths within the experimental resolution as all the other SD peaks. Thus it is proposed that band 4 corresponds to only the favoured ( $r = -i$ ) signature partner. This is not so suprising considering that the unfavoured ( $r = +i$ ) band is calculated to lie  $\sim 700$  keV in excitation energy above the favoured partner in the region of spin and frequency where it is fed by the reaction. As a result, it is likely that this  $r = +i$  band is fed with substantially lower intensity than its partner and it is possible that it would escape detection in the present experiment.

To summarize, four new SD band has been identified in  $^{151}\text{Dy}$ . One (band 4) having transition energies mid-way between the transition energies of the  $^{152}\text{Dy}$  SD band, in agreement with longstanding expectations based on the strong coupling model and the pseudospin coupling scheme [2]. This result can be regarded as further evidence for the presence of the pseudospin symmetry at extreme conditions of large elongation and high spins. Whether an interpretation in terms of this symmetry provides a general explanation for all identical bands or applies only to a selected class of nuclei in the vicinity of  $^{152}\text{Dy}$  remains to be established.

The work was supported in part by the Department of Energy, Nuclear Physics Division, under contract no. W-31-109-ENG-38 (ANL), DE-AC03-76SF00098 (LBL) and DE-FG02-87ER40346.

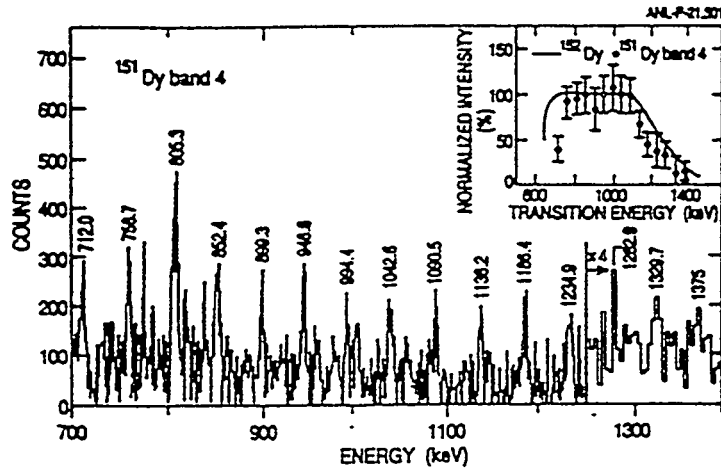


Figure 1: Spectrum obtained for band 4 in  $^{151}\text{Dy}$ . Note that the highest energy part of the spectrum has been compressed by a factor of 4. The inset compares the intensity patterns of band 4 (data points) and of the SD band in  $^{152}\text{Dy}$  (curve).

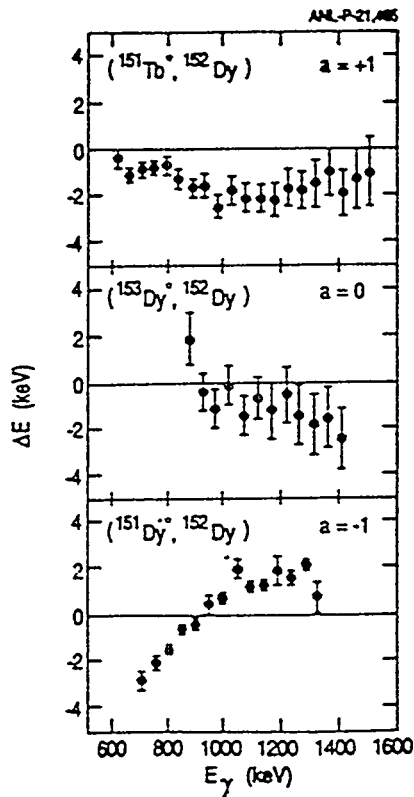


Figure 2: Comparison between the pairs of identical SD bands corresponding to the three limiting values  $a = +1, 0, -1$  of the decoupling parameter. For the  $(^{151}\text{Tb}, ^{152}\text{Dy})$  pair (top), the points in the figure represent the differences between transition energies in the two SD bands. For the  $(^{153}\text{Dy}, ^{152}\text{Dy})$  pair (middle), the differences are calculated from the average energies of consecutive transitions in the two signature partner bands of  $^{153}\text{Dy}$  and the  $\gamma$ -ray energies in  $^{152}\text{Dy}$ . In the  $(^{151}\text{Dy}, ^{152}\text{Dy})$  comparison (bottom), the differences were obtained by subtracting the average energies of consecutive transitions in  $^{152}\text{Dy}$  from the  $\gamma$ -ray energies of band 4 in  $^{151}\text{Dy}$ .

## References

- [1] T. Byrski et al., Phys. Rev. Lett. **64**, 1650 (1990).
- [2] W. Nazarewicz et al., Phys. Rev. Lett. **64**, 1654 (1990).
- [3] J.K. Johansson et al., Phys. Rev. Lett. **63**, 2200 (1989).
- [4] T. Lauritsen et al., ANL Report No 92-16, (1992).
- [5] I.Y. Lee, Nucl. Phys. **A520**, 641c (1990).
- [6] G.-E Rathke et al., Phys. Lett. **B209**, 177 (1988).
- [7] J.A. Kuehner, J.C. Waddington and D. Prevost, Proc. Int. Conf. on Nuclear Structure at High Angular Momentum, Ottawa, May 1992, AECL-10613, p. 413.
- [8] B. Crowell et al., Nucl. Instr. Meth. in press.
- [9] W. Nazarewicz, R. Wyss and A. Johnson, Nucl. Phys. **A503**, 285 (1989).
- [10] D. Curien et al., Phys. Rev. Lett. **71**, 2559 (1993).
- [11] T. Bengtsson, I. Ragnarsson and S. Åberg, Phys. Lett. **B208**, 39 (1988).

**Excited Bands in the Doubly-Magic Superdeformed  $^{152}\text{Dy}$  Nucleus: Band Talk, Band Interaction and Evidence for the First  $N=7$  Proton Hyper-Intruder Orbital**

C.W. Beausang<sup>1</sup>, P.J. Dagnall<sup>1</sup>, P.J. Twin<sup>1</sup>, M.A. Bentley<sup>2</sup>, F.A. Beck<sup>3</sup>, Th. Byrski<sup>3</sup>, S. Clarke<sup>1</sup>, D. Curien<sup>3</sup>, G. Duchene<sup>3</sup>, G. deFrance<sup>3</sup>, P.D. Forsyth<sup>1</sup>, B. Haas<sup>3</sup>, E.S. Paul<sup>1</sup>, J. Simpson<sup>4</sup>, J. Styczen<sup>5</sup>, J.P. Vivien<sup>3</sup>, and K. Zuber<sup>5</sup>

<sup>1</sup> Oliver Lodge Laboratory, University of Liverpool, L69 3BX, United Kingdom.

<sup>2</sup> School of Sciences, Staffordshire University, Stoke-on-Trent, United Kingdom.

<sup>3</sup> Centre de Recherches Nucleaires, IN2P3-CNRS/Universite Louis Pasteur, F-67037 Strasbourg, Cedex, France.

<sup>4</sup> SERC Daresbury Laboratory, Daresbury, Warrington, WA4 4AD, Cheshire, United Kingdom.

<sup>7</sup> Institute of Nuclear Physics, PL-31-42, Krakow, Poland.

Five excited superdeformed (SD) bands have been observed [1] in the doubly closed-shell SD nucleus  $^{152}\text{Dy}$ . Three of the new bands are interpreted in terms of single neutron excitations across the  $N = 86$  shell gap. The other two excited SD bands are believed to involve single proton excitations across the  $Z = 66$  shell gap. In particular, a proton excitation into the  $N = 7$  [770]1/2 intruder orbital has been identified. This is the first evidence of the influence of this deformation driving 'hyper-intruder' orbital in the SD minimum.

The  $^{152}\text{Dy}$  nucleus was populated via the  $^{108}\text{Pd}(^{48}\text{Ca},4n)^{152}\text{Dy}$  reaction at 200 MeV. Two stacked  $^{108}\text{Pd}$  targets, each  $500 \mu\text{g}/\text{cm}^2$  thick, were used and arranged so that the product nuclei recoiled into vacuum. Prompt  $\gamma$ -rays were measured using the Eurogam array [2, 3, 4] located at the Nuclear Structure Facility at Daresbury Laboratory. An isomer detector positioned 25 cm down stream of the target was used to select, with an efficiency of  $\sim 70\%$ , transitions preceding the 60ns isomeric state in  $^{152}\text{Dy}$ . Gamma-ray coincidence events were recorded only when the number of unsuppressed Ge detectors was at least 5. A total of  $1.7 \times 10^9$  suppressed coincidence events were recorded with a mean suppressed fold of 3. After unpacking higher Ge-fold coincidences these events yielded a total of  $8.5 \times 10^9$  double and  $4.3 \times 10^9$  triple coincidence events.

Analysis of this data set resulted in the observation of five new SD bands which have been assigned to  $^{152}\text{Dy}$  based on their coincidence relationships with the known decay scheme and with the 60 ns isomer. Coincidence spectra for these new bands (labeled bands 2-6), and for the yrast SD band (band 1), are presented in Fig. 1 while their  $\mathcal{J}^{(2)}$  moments of inertia are compared with other SD bands in Fig. 2. The measured intensities of the new bands, relative to the yrast SD band (band 1) are  $7.5 \pm 1.5\%$ ,  $8.4 \pm 1.2\%$ ,  $4 \pm 1\%$ ,  $4 \pm 1\%$  and  $5 \pm 1\%$ , respectively. The low intensities of the excited bands are in contrast to that observed in other nuclei in this mass region and are compelling evidence that a large energy gap exists for both protons and neutrons between the yrast and excited SD configurations in  $^{152}\text{Dy}$  at the very high spins ( $> 50\hbar$ ) where SD states are populated.

The microscopic structure of the bands can be interpreted in terms of single particle excitations across the proton and neutron shell gaps. Three of the bands (bands 4-6) are based on neutron excitations.

- Bands 4 and 5 are signature partners and their  $\mathcal{J}^{(2)}$  are similar to that of the yrast SD band in  $^{151}\text{Dy}$ , see fig. 2. They are assigned a structure based on the  $[770]1/2 \rightarrow [402]5/2$  neutron excitation giving the same  $\pi 6^4\nu 7^1$  high- $N$  configuration as  $^{151}\text{Dy}$ .
- The  $\mathcal{J}^{(2)}$  of band 6 is similar to that of the yrast SD band in  $^{153}\text{Dy}$  and this band is assigned the  $\pi 6^4\nu 7^3$  high- $N$  configuration with the  $86^{\text{th}}$  neutron being excited from one of the  $[642]5/2$ ,  $[651]1/2$ , or  $[411]1/2$  positive parity low- $N$  orbitals.

The other two excited SD bands are believed to involve single proton excitations across the  $Z = 66$  shell gap. The most likely proton excitations originate from either the  $\pi[301]1/2$  or the  $\pi[651]3/2$  orbitals, see Fig 3. At a deformation ( $\beta_2 \sim 0.62$ ) appropriate for  $^{152}\text{Dy}$ , the  $\pi[770]1/2$  high- $N$  ‘hyper-intruder’ orbital is calculated to be the lowest excited orbital. Indeed at high rotational frequencies this orbital bridges the proton  $Z = 66$  shell gap. The  $\pi[770]1/2$  orbital is a strongly deformation driving orbital and its occupation is expected to lead to an enhanced quadrupole deformation, particularly if the proton originates from the  $\pi[301]1/2$  orbital.

Indeed, we believe that the most likely interpretation for band 2 is that it is a positive parity band associated with the  $\pi 6^4 7^1 [301]1/2^{-1} \nu 7^2$  configuration for the following reasons. Firstly, at high rotational frequencies its  $\mathcal{J}^{(2)}$  is similar to that of  $^{152}\text{Dy}$  band 1. This would be expected as the contributions from both the  $\pi[301]1/2$  and  $\pi[770]1/2$  orbitals to the dynamic moment of inertia are expected to be small. Secondly, at  $\hbar\omega \sim 0.5$  MeV, the  $\mathcal{J}^{(2)}$  of band 2 shows a large deviation. This behaviour is characteristic of a band interaction and can be qualitatively understood by the crossing between the  $\pi[770]1/2$  and  $\pi[530]1/2$  orbitals visible in Fig. 3 at  $\hbar\omega \sim 0.6$  MeV. The change in alignment of band 2 at the crossing, about  $3 \hbar$ , is roughly consistent with that expected from the  $\pi 7^1 \rightarrow \pi[530]1/2$  crossing.

A second possibility for the structure of band 2 involves an excitation from the  $\pi[651]3/2$  orbital into the  $\pi[770]1/2$  orbital giving a  $\pi 6^3 7^1 \nu 7^2$  intruder configuration and a negative parity band. It is expected that this configuration should have a  $\mathcal{J}^{(2)}$  similar to the yrast SD band in  $^{151}\text{Tb}$  ( $\pi 6^3 \nu 7^2$  configuration). However, the  $\mathcal{J}^{(2)}$  for band 2 is consistently  $\sim 5\%$  larger than  $^{151}\text{Tb}$  at high-frequencies. This difference can possibly be explained by the deformation driving forces of the  $\pi[770]1/2$  and  $\pi[651]3/2$  orbitals. In addition, if band 2 has a negative parity then octupole effects could also play a role.

Theoretically, strong octupole effects for SD shapes are expected [5, 6]. Recently RPA calculations [7] have been performed to test the effects of octupole correlations on the excitation spectrum of SD  $^{152}\text{Dy}$ . The calculations reproduce the increase in the  $\mathcal{J}^{(2)}$  of band 2 at  $\hbar\omega \approx 0.5$  MeV and further suggest that the structure of the crossing band has an octupole vibrational character rather than a pure single particle  $\pi[530]1/2$  configuration.

Band 3 may also be based on a proton excitation from the  $[651]3/2$  orbital, since its  $\mathcal{J}^{(2)}$  is similar (deviation  $\sim -5\%$ ) to that of  $^{151}\text{Tb}$  at high frequencies. In addition, the increase in  $\mathcal{J}^{(2)}$  of band 2 at  $\hbar\omega \sim 0.5$  MeV due to the crossing of the  $\pi[770]1/2$  and  $\pi[530]1/2$  orbitals appears to be mirrored by a decrease in the  $\mathcal{J}^{(2)}$  of band 3, see Fig. 1. Thus a possible configuration for band 3 at high rotational frequencies is

$\pi 6^3[530]1/2\nu 7^2$ .

Close examination of the spectrum for band 6 reveals a further effect of interest. Figure 1b shows part of the spectrum generated when gates are set on members of band 6. In addition to the expected transitions in band 6 there is also evidence for the lower spin members of the  $^{152}\text{Dy}$  yrast SD band. This suggests that band 6 decays, at least in part, to the yrast SD band as well as directly to states in the first minimum, which is the normal decay mode for SD bands. If our configuration assignments for these SD bands are correct the parity of the yrast band is positive ( $\pi 6^4\nu 7^2$ ) while that of band 6 is negative. In this case the transitions between the bands are predicted to be E1 in character. Using reasonable values for the excitation energy of band 6 relative to band 1 at high spins, we expect that the ‘linking’ transitions should lie in the energy range 1.5 to 2 MeV. An experiment is planned to search for these ‘linking’ transitions using Eurogam Phase II in Strasbourg. The transitions almost certainly link a single level in band 6 to a single level in band 1 with no intermediate states (unlike the situation in the decay from the second well to the normal deformed states). Therefore, identifying the individual transitions should be well within the capabilities of the Eurogam Phase II array. Identification of these linking transitions will fix the relative excitation energy of band 6 and hence give a quantitative measure of the SD shell gap at high rotational frequencies.

## References

- [1] P.J. Dagnall, et al, accepted for publication in Phys. Lett. **B**.
- [2] C.W. Beausang *et al*, Nucl. Instrum. and Meth. **A313** (1992) 37.
- [3] P.J. Nolan, Nucl. Phys. **A520** (1990) 657c.
- [4] F.A. Beck, Prog. Part. Nucl. Phys. **28** (1992) 443.
- [5] T. Bengtsson, M.E. Faber, G. Leander, P. Möller, M. Płoszajczak, I. Ragnarsson and S. Åberg, Phys. Scr. **24** (1981) 200.
- [6] S. Mizutori *et al*, Nucl. Phys. **A557** (1993) 125c. Lett.**65** (1990) 1547.
- [7] T. Matsuyanagi, S. Mizutori, T. Nakatsukasa, and W. Nazarewicz, private communication and to be published.

**Fig. 1:** (a) Double gated spectra showing the yrast (band 1) and new excited SD (band 2–6) bands in  $^{152}\text{Dy}$ . (b) Part of the spectrum generated when double gates are placed on members of band 6. As well as the expected transitions of band 6 (indicated by stars), transitions belonging to band 1 also appear and are indicated by their energies in keV.

**Fig 2:** The  $\mathcal{J}^{(2)}$  dynamic moments of inertia of the excited SD bands in  $^{152}\text{Dy}$  compared with those of the yrast SD bands in neighbouring nuclei.

**Fig 3:** Woods-Saxon single particle routhians versus rotational frequency for protons. The orbitals are labeled by their asymptotic Nilsson quantum numbers.

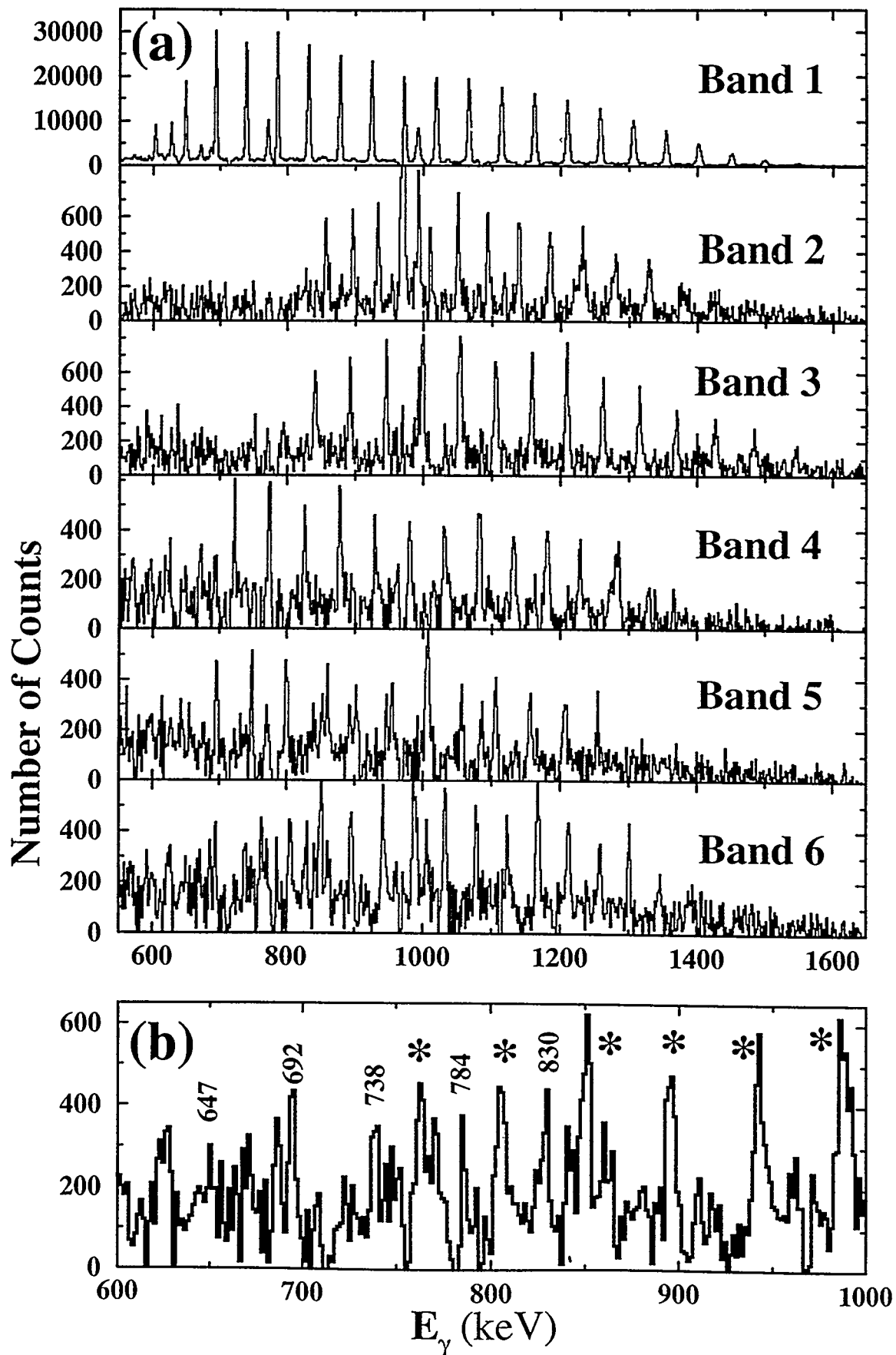


Fig. 1



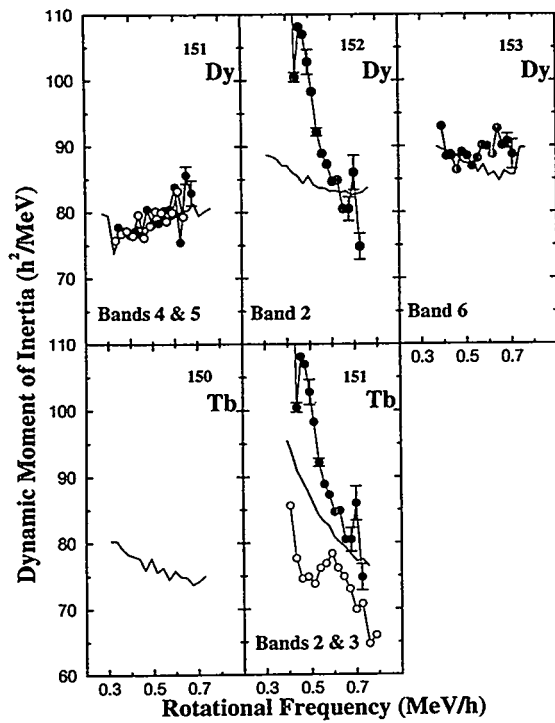


Fig. 2

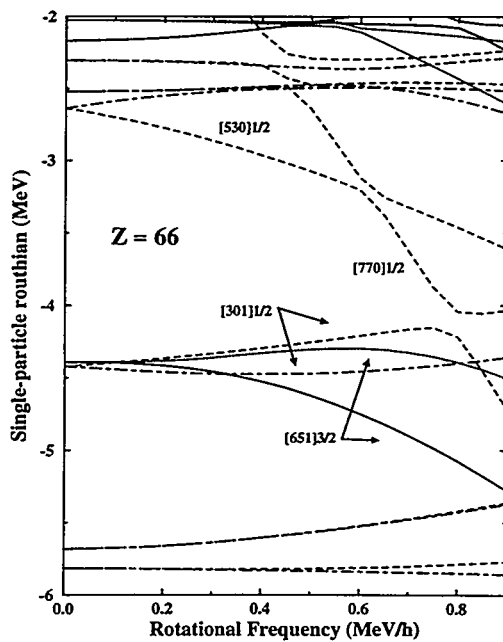


Fig. 3

# M1 transitions between superdeformed states in $^{194,195}\text{Tl}$ : the fingerprint of the $i_{13/2}$ proton intruder orbital

J. Duprat<sup>1)</sup>, F. Azaiez<sup>1)</sup>, J. F. Sharpey-Schafer<sup>2)</sup>, M. Aïche<sup>3)</sup>, G. Bastin<sup>3)</sup>, C.W. Beausang<sup>2)</sup>,  
C. Bourgeois<sup>1)</sup>, R.M. Clark<sup>6)</sup>, D.M. Cullen<sup>11)</sup>, P.J. Dagnall<sup>2)</sup>, I. Deloncle<sup>3)</sup>, P. Fallon<sup>10)</sup>, P.D. Forsyth<sup>2)</sup>,  
N. Fotiadis<sup>9)</sup>, S.J. Gale<sup>2)</sup>, B. Gall<sup>3)</sup>, F. Hannachi<sup>3)</sup>, S. Harissopoulos<sup>9)</sup>, K. Hauschild<sup>6)</sup>, I. Hibbert<sup>6)</sup>,  
P.M. Jones<sup>2)</sup>, M.J. Joyce<sup>2)</sup>, A. Kaci<sup>3)</sup>, C.A. Kalfas<sup>9)</sup>, W.H. Kelly<sup>7)</sup>, A. Korichi<sup>1)</sup>, Y. Le Coz<sup>5)</sup>, M. Meyer<sup>5)</sup>,  
E.S. Paul<sup>2)</sup>, N. Perrin<sup>1)</sup>, N. Poffé<sup>1,8)</sup>, M.G. Porquet<sup>3)</sup>, N. Redon<sup>5)</sup>, M.A. Riley<sup>12)</sup>, H. Sergolle<sup>1)</sup>,  
C. Schuck<sup>3)</sup>, J. Simpson<sup>4)</sup>, P.J. Twin<sup>2)</sup>, R. Vlastou<sup>9)</sup>, R. Wadworth<sup>6)</sup>

1) Institut de Physique Nucléaire, 91406 Orsay Cedex, France

2) Oliver Lodge Laboratory, University of Liverpool, L69 3BX, UK

3) C.S.N.S.M., IN2P3-CNRS, 91405 Orsay Cedex, France

4) Nuclear Structure Facility, Daresbury Laboratory, Daresbury, Warrington, WA4 4AD, UK

5) Institut de Physique Nucléaire de Lyon, IN2P3-CNRS, Université Claude Bernard,  
69622 Villeurbanne Cedex, France

6) Department of Physics, University of York, Heslington, York, YO1 5DD, UK

7) Iowa State University, Ames, IA 50011

8) University of Oxford, Department of Physics, Keble Road, Oxford, UK

9) Nuclear Research Center Demokritos, Aghia Paraskevi, Attiki, Greece

10) Lawrence Berkeley Laboratory, 1 Cyclotron Road, Berkeley, CA 94720, USA

11) Oak Ridge National Laboratory, Oak Ridge, Tennessee 37831, USA

12) Dept. of Physics, Florida State University, Tallahassee, Florida, FL 32306, USA

**Abstract:** Recent data from the EUROGAM array have revealed dipole transitions linking signature partner superdeformed bands in  $^{194}\text{Tl}$  and  $^{195}\text{Tl}$  nuclei. Measurements of the decay branching ratios, taken together with the average quadrupole moment of the neighboring superdeformed nuclei, enable the absolute M1 strengths to be determined. From these data and using the strong coupling model, we find that two SD bands in  $^{195}\text{Tl}$  are due to the  $81^{st}$  proton being in the  $[642]5/2^+$  orbital and four from the six SD bands in  $^{194}\text{Tl}$  correspond to a configuration where the intrinsic spins of the single proton and neutron are aligned.

## Introduction :

One of the currently most interesting research areas in nuclear physics is the study of superdeformed (SD) nuclei. Because of their large quadrupole deformation, typically  $\beta_2 = 0.6$  in the mass 150 region [1] and  $\beta_2 = 0.47$  in the mass 190 region [2-3], the decay sequences in the SD bands were found to be completely dominated by stretched E2 transitions. However, in the heavier mass-region of observed SD nuclei, around  $^{192}\text{Hg}$ , the decay extends to considerably lower spins,  $I_0 = 8\hbar$ , compared to  $I_0 = 24\hbar$  in the  $A=150$  region, and to correspondingly smaller transition energies. Thus several M1 transitions have been found to compete strongly with E2 transitions in several SD bands in the  $^{193}\text{Hg}$ ,  $^{195}\text{Tl}$  and  $^{194}\text{Tl}$  nuclei. Recently, M.J. Joyce et al.[4] have measured the photon decay branching ratio between two signature partner bands in  $^{193}\text{Hg}$ . Assuming the deformation to be the same as the one measured for the core nucleus  $^{192}\text{Hg}$  [3, 5], i.e.  $Q_0 = 19 \pm 2$  eb, a least square fit was made to the experimental  $I_\gamma(\text{M1})/I_\gamma(\text{E2})$  ratios giving  $(g_K - g_R)K/Q_0 = -0.14 \pm 0.01$  (eb)<sup>-1</sup> so that  $g_K = -0.65 \pm 0.14$  ( $g_R$  is taken equal to  $Z/A$ ). The measured g-factor was in good agreement with  $g_K = -0.61$  given by the strong coupling model for the proposed  $[512]5/2^-$  neutron orbital [6]. In

this contribution, the magnetic properties extracted from the M1 and E2  $\gamma$  competition in the superdeformed  $^{194}\text{Tl}$  and  $^{195}\text{Tl}$  nuclei will be discussed.

### Experiments and results :

Two different experiments were carried out at the Tandem accelerator at the Nuclear Structure Facility, Daresbury Laboratory, using the EUROGAM array with 45 large-volume Compton suppressed germanium detectors [7]. The two following reactions  $^{186}\text{W}(^{15}\text{N},6n)^{195}\text{Tl}$  ,  $^{184}\text{W}(^{15}\text{N},5n)^{194}\text{Tl}$ , at beam energies of 105 and 96 MeV respectively, were used. A total of  $300 \times 10^6$  events for each reaction were recorded with an unsuppressed fold  $\geq 5$ . An event is defined as a coincidence between any number of suppressed  $\gamma$ -rays. In all experiments, targets consisting of thin self-supporting foils were used, in order to have the residual nuclei emitting their  $\gamma$ -rays with the full recoil velocity. The results will be discussed separately for  $^{195}\text{Tl}$  and  $^{194}\text{Tl}$  nuclei.

### $^{195}\text{Tl}$ :

Two SD bands have been reported in  $^{195}\text{Tl}$  [8]. They have been interpreted as signature partners, with the single proton occupying the  $i_{13/2}$  ( $\Omega=5/2$ ) intruder orbital.

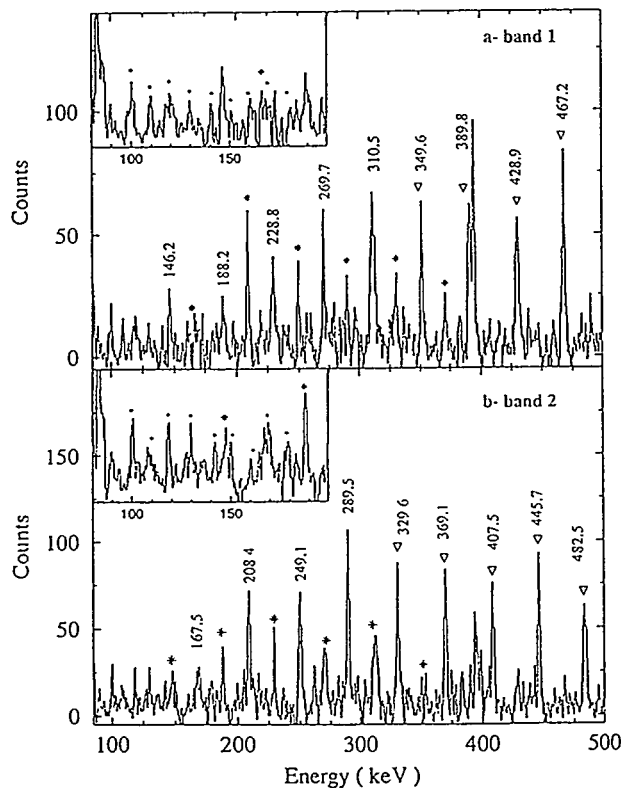
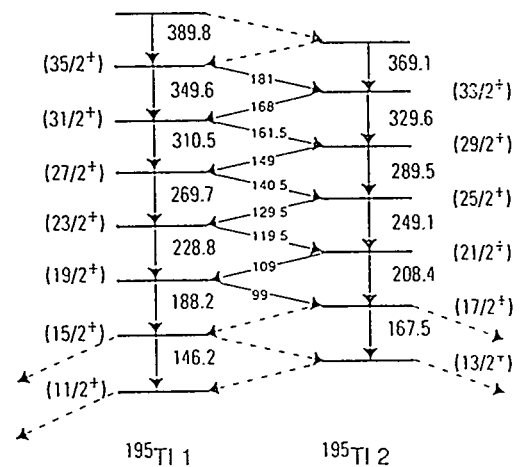


Fig. 1 - Spectra of SD bands 1 and 2 in  $^{195}\text{Tl}$ . The spectra are from quadruple coincidences showing  $\gamma$  rays in coincidence with three  $\gamma$  rays that are in the band of interest.

(a) Band 1 with members of band 2 denoted \* and candidates of interband dipoles (inset).

(b) Band 2 with members of band 1 denoted \* and candidates of interband dipoles (inset)

Fig. 2 - Level scheme for the pair of signature partner bands in  $^{195}\text{Tl}$ . The energies of the dipoles are assigned with 0.5 keV errors.



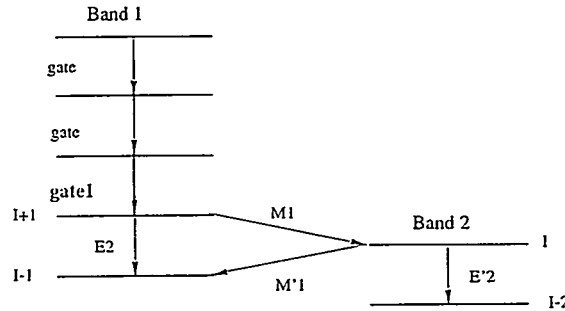
This orbital exhibit some signature splitting for rotational frequencies above 0.2 MeV. The triple-gated spectra of the two SD bands in  $^{195}\text{Tl}$ , obtained from the EUROGAM experiment, are displayed in fig.1. The higher selectivity of EUROGAM enables us to extend the bands to higher and lower transition energies [9]. The cross-talk transitions between the two bands (see insets) are very weakly seen at energies ranging from 100 keV to 180 keV. The interband transitions together with the transitions in band 1 and band 2 can be organised in a unique way as shown in figure 2. This suggests that the cross-talk transitions are probably dipoles. Having in mind the fact that band 1 and band 2 are the expected signature partner of the  $i_{13/2}$  ( $\Omega=5/2$ ) proton configuration, it is therefore suggested that in this case, the two-way cross talk would most likely indicate the presence of M1 decays. Because of the lack of statistics, and the weakness of the SD bands in  $^{195}\text{Tl}$ , we were not able to measure directly the intensities of the M1 transitions. Therefore an alternative method has been used in order to extract the branching ratios, and subsequently the M1 strengths. If we consider the decay sequence illustrated in figure 3, where double gates above the transition : I+1  $\rightarrow$  I-1 of band 1, including each time **gate1**, were required, the branching ratios of the decays of levels I+1 and I, can be respectively expressed as :

$$i) \frac{I_{\gamma}(M1)}{I_{\gamma}(E2)} = 14556.0 \times \frac{E_{\gamma}^3(M1)}{E_{\gamma}^5(E2)} \times \frac{B(M1)}{B(E2)} \quad \text{and} \quad ii) \frac{I_{\gamma}(M'1)}{I_{\gamma}(E'2)} = 14556.0 \times \frac{E_{\gamma}^3(M'1)}{E_{\gamma}^5(E'2)} \times \frac{B(M'1)}{B(E'2)}$$

where at the strong coupling limit :

$$iii) B(E2; \Delta I=2) = \frac{5}{16\pi} \langle IK20 | I-2K \rangle^2 Q_0^2 \quad \text{and} \quad iv) B(M1; \Delta I=1) = \frac{3}{4\pi} (g_K - g_R)^2 K^2 \langle IK10 | I-1K \rangle^2$$

Fig. 3 - Scenario where transitions above the level I+1 are used as gates, and where the intensities  $I_{\gamma}(E2)$  and  $I_{\gamma}(E'2)$  are used to extract the  $\frac{B(M1)}{B(E2)}$  value.



[  $B(E2)$  and  $B(M1)$  are measured in units of  $e^2\text{fm}^4$  and  $\mu_N^2$  ( $\mu_N$  denotes the nuclear magneton), respectively, and  $E_{\gamma}$  in MeV]. In addition, if we assume no decay out from the levels I+1 and I to normally deformed states, the total intensity conservation gives an additional equation (where the  $\alpha$ 's are the total internal conversion coefficients, taken from ref. 10):

$$v) [1+\alpha(M1)] I_{\gamma}(M1) = [1+\alpha(M'1)] I_{\gamma}(M'1) + [1+\alpha(E'2)] I_{\gamma}(E'2)$$

Using the equations i), ii), iii), iv) and v) one obtains the following expression of  $(g_K - g_R)^2 K^2 / Q_0^2$  which involves only the intensities of the observed E2 transitions :

$$\frac{(g_K - g_R)^2 K^2}{Q_0^2} = 2.86 \cdot 10^{-5} \frac{[1+\alpha(E'2)] I_{\gamma}(E'2)}{[1+\alpha(M1)] I_{\gamma}(E2) \frac{E_{\gamma}^3(M1)}{E_{\gamma}^5(E2)} f(I+1, K) - [1+\alpha(M'1)] I_{\gamma}(E'2) \frac{E_{\gamma}^3(M'1)}{E_{\gamma}^5(E'2)} f(I, K)}$$

where  $f(I,K)$  takes account of the dependence on Clebsch-Gordan coefficients of the branching ratio of the state with a spin  $I$ :  $f(I,K) = \langle IK10 | I-1K \rangle^2 / \langle IK20 | I-2K \rangle^2$ . This procedure has been applied, and  $(g_K - g_R)^2 K^2 / Q_0^2$  values have been extracted for several SD states in both bands. Figure 4 shows the deduced  $(g_K - g_R)K / Q_0$  values for different levels as function of the evaluated spins. The spins of the SD states are suggested using the methods of Draper et al. [11] and Becker et al. [12]. Assuming the quadrupole moment  $Q_0 = 19 \pm 2$  eb, which is the average of the measured quadrupole moments in the neighboring  $^{194}\text{Hg}$  [13] and  $^{194}\text{Pb}$  [3] nuclei and  $g_R = Z/A$ , we have indicated by full and dashed lines the theoretical limits [14,7] for the configurations where the single proton is occupying the orbitals [642]5/2 and [514]9/2 respectively (the limits come from the uncertainty on the adopted experimental  $Q_0$ ). These are presumably the two lowest available configurations for the single proton in the thallium-isotopes [15]. The data are in agreement with the assignment of the intruder configuration [642]5/2 (with both signatures) to the two SD bands in  $^{195}\text{Tl}$ . Subsequently, the corresponding experimental  $g_K$  value would be  $1.4 \pm 0.4$ , which is close to  $g_K = 1.45$  given by the strong coupling model for the proposed proton orbital [14 - 7]. Theoretical values of  $g_K$  are obtained using  $g_S^{\text{eff}} = 0.7 g_S^{\text{free}}$ .

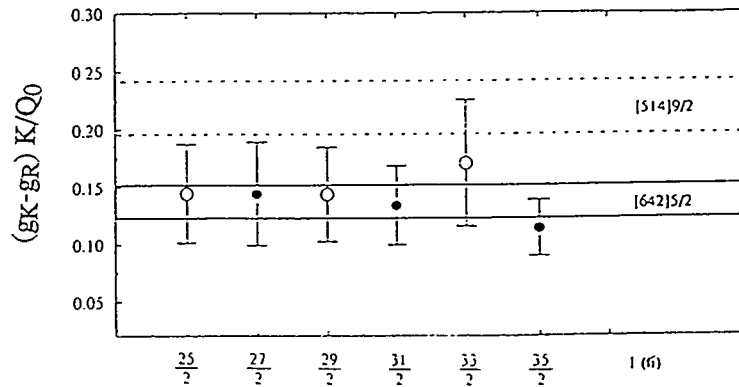


Fig. 4 - The extracted  $(g_K - g_R)K / Q_0$  values (in units of  $\text{eb}^{-1}$ ) for the pair of signature partner bands in  $^{195}\text{Tl}$ . The indicated spins are those of the considered states in band 1 (•) and in band 2 (o). The theoretical values for the [514]9/2 and [642]5/2 proton configuration are from ref. 10.

### $^{194}\text{Tl}$

Three pairs of bands have been reported in this isotope [17]. From the Eurogam data it has been possible to extend all these bands to lower (see figure 5), and higher transitions energies [18]. For both pairs of bands (2a-2b) and (3a-3b) the triple gated spectra in one band exhibits at low energy  $\gamma$ -transitions belonging to its signature partner. Whereas no clear evidence of any coincidence between band 1a and 1b has been observed. One should expect SD bands in  $^{194}\text{Tl}$  to involve the same neutron excitations as in the SD bands of its  $^{193}\text{Hg}$  isotone and the same proton configuration as in the SD bands of its  $^{193}\text{Tl}$  isotope [19]. The pair of bands (3a-3b) can be interpreted, from the behaviour of their dynamical moment of inertia, as the favored configuration resulting from the coupling of the proton  $i_{13/2}$  to the neutron  $j_{15/2}$  when both neutron and proton pairing are blocked [18]. The weak experimental  $B(M1)$  strength of these bands is in agreement with the one calculated by P.B. Semmes

et al.[6] (see Table 1). By coupling the proton [642]5/2 to the two neutrons [512]5/2, [624]9/2 one can obtain four pairs of signature partners: two pairs with  $K_{>} = \Omega_p + \Omega_n$  and two others with  $K_{<} = |\Omega_p - \Omega_n|$ . The  $K_{>}$  configurations are expected to lie at lower excitation energy according to  $E_{rot} = \frac{\hbar^2}{2J}$

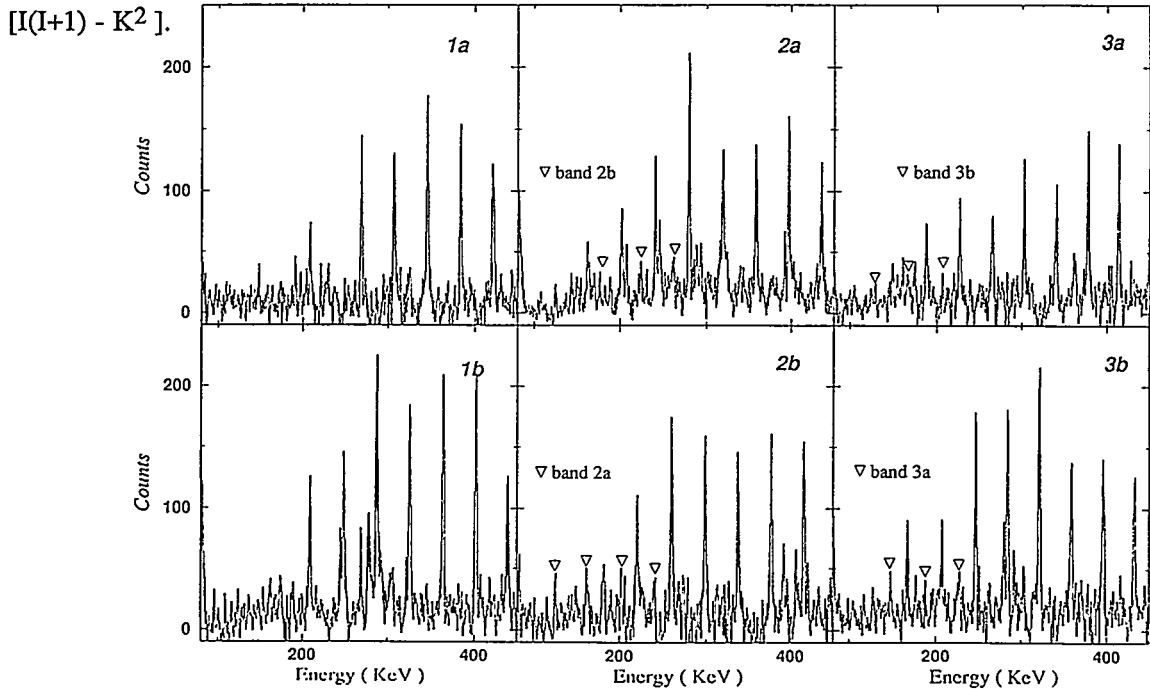


Fig. 5 - Spectra of the 6 SD bands in  $^{194}\text{Tl}$ . The spectra are from quadruple coincidences showing  $\gamma$  rays in coincidence with three  $\gamma$  rays that are in the band of interest.

On the other hand, there is no clear evidence of cross-talk between bands 1a-1b and the observed cross-talk intensity in bands 2a-2b is very weak. This is in agreement with the expected  $B(M1)$  strength [6] for the  $K_{>}$  configuration, see table1. In figure 6, the experimental intensities within band 2b are compared to the one calculated using theoretical branching ratios [6], for both the  $K_{<}$  and  $K_{>}$  configurations. Eventhough the experimental error bars are big, the  $K_{>}$  configuration fits better the data than the  $K_{<}$  configuration. The same comparison for the other three bands (1a,1b and 2a) also clearly indicates that the corresponding configurations are the one where the spin of the single proton and the spin of the single neutron are parallel. It is worth pointing out that these results are in agreement with the Gallagher-Moszkowski rule [20], well known from data on deformed odd-odd nuclei.

$\pi$ -orbital	$\nu$ -orbital	$K^\pi$	spin	$B(M1), I \gg K$
[642]5/2 <sup>+</sup>	[624]9/2 <sup>+</sup>	7 <sup>+</sup>	p	0.03
[642]5/2 <sup>+</sup>	[624]9/2 <sup>+</sup>	2 <sup>+</sup>	ap	3.9
[642]5/2 <sup>+</sup>	[512]5/2 <sup>-</sup>	5 <sup>-</sup>	p	0.01
[642]5/2 <sup>+</sup>	[512]5/2 <sup>-</sup>	0 <sup>-</sup>	ap	2.8

Table 1 - Two quasiparticle configurations in  $^{194}\text{Tl}$  (taken from ref.[6].)  
The abbreviations "p" and "ap" denote parallel and antiparallel intrinsic spin vectors

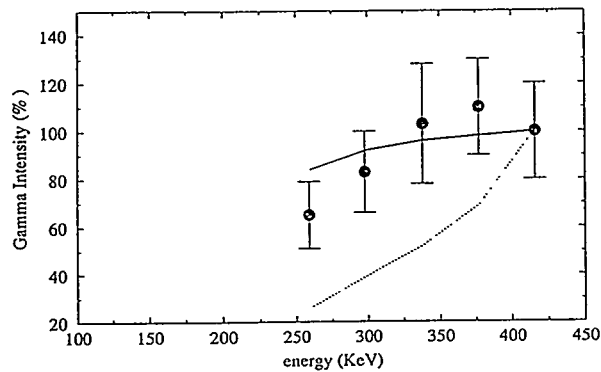


Fig. 6 -  $\gamma$ -intensity within band 2b measured relative to the 416 keV  $\gamma$ -transition ( $\bullet$ ). The configuration is assumed to be  $[642]5/2$  for the proton and  $[512]5/2$  for the neutron. The full and dotted lines indicate the calculated intensity for both  $K_>$  and  $K_<$  respectively.

### Conclusion :

We have observed dipole transitions between SD signature partner bands in  $^{195}\text{Tl}$  and  $^{194}\text{Tl}$  nuclei. This enable us to measure M1 strengths and to extract g-factors for the two SD bands in  $^{195}\text{Tl}$ . A fairly good agreement is found with the g-factors predicted by the strong coupling model for the proposed single-particle configurations. In the case of the  $^{194}\text{Tl}$  odd-odd nucleus, the observed cross-talk intensities between signatures partners indicate that the favored configurations have aligned intrinsic spins as expected (from both enregetical considerations and neutron-proton interaction). This represents an evidence that spectroscopic informations could be obtained on SD nuclei in the mass-190 region, despite the lack of informations on spins and excitation energies of the bands.

### References :

- 1 - P.J. Twin et al., Phys. Rev. Lett. 57, 811 (1986)
- M. A. Bentley et al., Phys. Rev. Lett. 59, 2141 (1987)
- 2 - E. F. Moore et al., Phys. Rev. Lett. 63, 360 (1989).
- 3 - M. P. Carpenter et al., Phys. Lett. B 240, 44 (1990).
- 4 - M. J. Joyce et al., Phys. Rev. Lett. 71, 2176 (1993).
- 5 - E. F. Moore et al., Phys. Rev. Lett. 64, 3127 (1990).
- 6 - P. B. Semmes et al. to be published.
- 7 - F. A. Beck, Workshop on Nucl. Phys., Megève, FR (unpublished), p.365 (1992).
- C. W. Beausang et al., Nucl. Instrum. Methods Phys. Res., Sect. A 313, 37 (1992).
- 8 - F. Azaiez et al., Z. Phys. A 338, 471 (1991).
- 9 - J. Duprat et al., to be published in Phys. Lett. B.
- 10 - F. Rosel et al., At. Data Nucl. Data Tables 21, 91 (1978).
- 11 - J. E. Draper et al., Phys. Rev. C 42, R1791 (1990).
- 12 - J. A. Becker et al., Phys. Rev. C 46, 889 (1992).
- 13 - J. R. Hughes et al., Phys. Rev. Lett. 72, 824 (1994).
- 14 - P. Willsau et al., Z. Phys. A344, 351 (1993)
- 15 - M. Meyer et al. to be published.
- 16 - B. Gall et al., Z. für Phys. in press.
- 17 - F. Azaiez et al., Phys. Rev. Lett. 66, 1030 (1991)
- 18 - J. Duprat et al., Int. Conf. on the future of nuclear spectroscopy, Crete (1993), to be published.
- 19 - F. B. Fernandez et al., Nucl. Phys. A517, 386 (1990).
- 20 - C.J. Gallagher and S.A. Moszkowski, Phys. Rev. 111, 1282 (1958)

## Recent Results from APEX

I. Ahmad<sup>a</sup>, S. M. Austin<sup>b</sup>, B. B. Back<sup>a</sup>, D. Bazin<sup>b</sup>, R. R. Betts<sup>a</sup>, F. P. Calaprice<sup>c</sup>,  
K. C. Chan<sup>d</sup>, A. Chishti<sup>d</sup>, P. Chowdhury<sup>d</sup>, R. W. Dunford<sup>a</sup>, J. D. Fox<sup>e</sup>, S. J. Freedman<sup>f</sup>,  
M. Freer<sup>g</sup>, J. S. Greenberg<sup>d</sup>, A. L. Hallin<sup>i</sup>, T. Happ<sup>j</sup>, J. Last<sup>a</sup>, N. Kaloskamis<sup>d</sup>,  
E. Kashy<sup>b</sup>, W. Kutschera<sup>a</sup>, C. J. Lister<sup>a</sup>, M. Liu<sup>i</sup>, M. R. Maier<sup>f</sup>, D. Mercer<sup>b</sup>, A. Perera<sup>k</sup>,  
M. D. Rhein<sup>a</sup>, D. E. Roa<sup>e</sup>, J. P. Schiffer<sup>a</sup>, T. Trainor<sup>l</sup>, P. Wilt<sup>a</sup>, J. S. Winfield<sup>b</sup>,  
M. Wolanski<sup>a,h</sup>, F. L. H. Wolfs<sup>k</sup>, A. H. Wuosmaa<sup>a</sup>, G. Xu<sup>d</sup>, A. Young<sup>c</sup>, and  
J. E. Yurkon<sup>b</sup>

<sup>a</sup>Physics Division, Argonne National Laboratory, Argonne, IL 60439

<sup>b</sup>Department of Physics & Astronomy, Michigan State Univ., East Lansing, MI 48824

<sup>c</sup>Physics Department, Princeton University, Princeton, NJ 08544

<sup>d</sup>Wright Nuclear Structure Laboratory, Yale University, New Haven, CT 06511

<sup>e</sup>Physics Department, Florida State University, Tallahassee, FL 32306

<sup>f</sup>Lawrence Berkeley Laboratory, Berkeley, CA 94720

<sup>g</sup>Department of Physics, University of Birmingham, Birmingham, B15 2TT, UK

<sup>h</sup>Department of Physics, University of Chicago, Chicago, IL 60637

<sup>i</sup>Physics Department, Queen's University, Kingston, Ontario, K7L 3N6, Canada

<sup>j</sup>GSI, Planckstrasse 1, 64291 Darmstadt, Germany

<sup>k</sup>Nuclear Structure Research Laboratory, University of Rochester, Rochester, NY 14627

<sup>l</sup>Nuclear Physics Laboratory, University of Washington, Seattle, WA 98195

Presented by C. J. Lister

### 1. INTRODUCTION

The physics I am going to discuss is somewhat different from the main themes of this conference. The focus of the APEX project is the study of the emission of electrons and positrons from collisions of heavy ions. However, scattering of this type involves intense Coulomb excitation of nuclear states so nuclear spectroscopy can never be far from our minds. We also have close connections with the conference title; the detector which I am going to describe does contain two large gamma arrays, each subtending 58% of  $4\pi$  and containing 24 position sensitive detectors. Finally, we will see our research may have uncovered some interesting new spectroscopy in the actinides, so the connections between APEX and this conference may be closer than is first apparent.

Before proceeding, I should point out that entire conferences have been dedicated to the field of research I am going to describe [1,2]. In order to have space to discuss our detector and first results I am going to have to be very brief about what has gone before. This is not intended to depreciate the many years of effort which have gone into understanding positron and electron emission from heavy ion collisions. So let's start with a quick review of what are the interesting mechanisms, what is understood, and what are the key unresolved questions.

For more than 50 years it has been realized that a point nucleus with  $Z > 1/\alpha = 137$  would have interesting atomic quantum mechanics, as the 1s atomic orbit would be bound by



>1022 keV, so the Coulomb field would have enough energy for spontaneous electron-positron production. A K-shell vacancy could be filled by a produced electron and a monochromatic positron emitted. This concept was an intellectual curiosity for many years as nuclei with  $Z > 100$  were not available for study. However, in the 1970's it was realized that during close collisions of heavy nuclei the electrons would rapidly be rearranged around the di-nuclear system and critical situations could be experimentally approached. The construction of the GSI facility allowed collisions of the heaviest nuclei at the Coulomb barrier and so experiments aimed at observing spontaneous positron production could be seriously contemplated. A flurry of theoretical interest ensued, centered on the Frankfurt school [3,4]. Realistic calculations indicated that finite size and relativistic corrections would move the critical  $Z$  up to about 176, and that the timescale of the collision dictated the positron spectrum shape: a passing collision with a timescale of about  $10^{-21}$  seconds would have a broad spectrum hundreds of keV wide, whereas formation of a true, long-lived nuclear molecule for more than  $10^{-19}$  seconds would result in the emission of monochromatic positrons with a linewidth less than detector resolution (about 10 keV).

Those are the ideas. Many experiments have been tried to search for these effects. However, there are immense technical difficulties arising from background processes. The collision of two high- $Z$  nuclei result in intense, time varying Coulomb fields which lead to copious delta electron production, dynamic positron production, X-rays and nuclear excitation. The excited nuclei can decay through gamma rays, by internal conversion or by internal pair production. Thus, the target environment has a huge flux of gammas, electrons and positrons. To devise experiments which are sensitive to the spontaneous positron mechanism is a real challenge. The experiments have produced a series of sensational results. Firstly, sharp peaks were observed in the positron energy spectra for a variety of colliding heavy systems [5,6]. However, the peaks were all located at approximately the same energy apparently contradicting a "nuclear molecule" explanation. Further, the positrons appeared in some cases correlated with monochromatic electrons [7,8] which led to the idea of a new neutral particle which was formed in the intense Coulomb field, but decayed in isolation by equal energy, back-to-back positron-electron emission. To confirm these observations and understand the production and decay mechanisms, improved experiments were needed. The GSI spectrometers were upgraded and a new experiment, APEX at Argonne National Laboratory was conceived.

## 2. THE APEX EXPERIMENT

Several design concepts were investigated before the operating principle of APEX was chosen [9]. In the end, a transverse low field solenoid was selected to transport electrons and positrons of greater than 120 keV to a counting environment shielded from the target. This design offered a promising technique for measuring lepton angles through an energy and time-of-flight method. The spectrometer was chosen to be left-right symmetric, allowing two simultaneous electron-positron spectra to be accumulated, reducing the possibility of statistical and systematic difficulties. The characteristics of the heavy ion scattering were determined by measuring ions in a large umbrella-shaped array of low pressure proportional counters [10] which subtend 20-70 degrees in scattering angle with 85% azimuthal coverage. Fig. 1 shows a schematic layout of the detector. By nuclear physics standards it is large, standing 4 meters high and 7 meters from side to side. The heart of the spectrometer are two pagoda shaped arrays of electron (or positron) detectors. Each array has 198, 3.0 cm x 0.5 cm, 1 mm thick PIN diodes with individual readouts [11,12]. They are located on the solenoid axis 120 cm from the target, and the energy, time of flight and position of hit detectors uniquely determine the energy and momentum vectors of the leptons emitted from the target. Positrons are differentiated from electrons

by detecting and reconstructing their annihilation radiation. This is done by surrounding the silicon arrays with barrels of NaI(Tl) bars[13]. These barrels, each of 24, 55 cm x 7 cm bars which are position sensitive, allow the location of the annihilation to be measured to 3 cm FWHM and this can be correlated with energy deposited in individual silicon detectors. This arrangement gives excellent positron identification. The NaI(Tl) array is also coupled to a fast front end processor which provides a master trigger for the experiment when opposite or near opposite bars fire in one of the barrels [14].

ANL-P-21,478

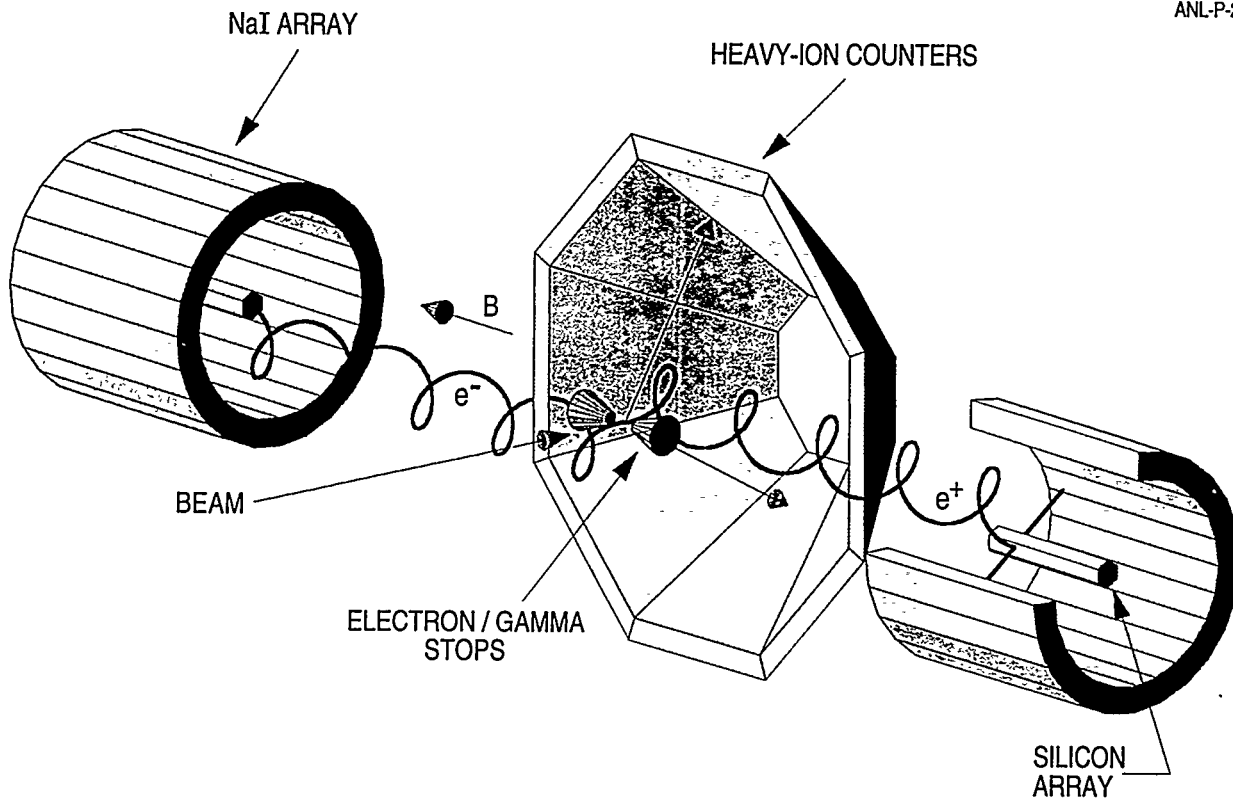


Fig. 1 A schematic layout of the APEX detector

Considerable effort has been invested in a target arrangement which allows beams of several particle nano-amps to be used in a stable and reproducible way. A rotating target wheel is used and the beamspot and target profile carefully monitored by high resolution ion chambers and CsI counters. The ability to utilize beams of several particle nano-amps, the high duty cycle of the ATLAS accelerator, and the good acceptance of the spectrometer allow us to collect data sets much larger than previous experiments.

### 3. THE FIRST EXPERIMENTS

During 1993 a series of commissioning experiments were performed culminating in November 1993 and March 1994 when the full system was operated. All the first studies were on the U + Ta system, as this is the technically easiest system to study for which positron peaks have been reported. Targets of 1 mg/cm<sup>2</sup> rolled material were used which were robust to degradation. Data were collected at 5.95, 6.1 and 6.3 MeV/A spanning the region where peaks have been seen [15,16]. Large data sets were collected, consisting of 13,000, 32,000 and 18,000 electron-positron coincidences with two detected heavy ions respectively. Based on published cross sections and decay scenarios these sets should be large enough to progress beyond previous studies. Despite intensive analysis similar to

those previously reported, we have not been able to observe peaks in any of our spectra. Whether this is due to an instrumental effect, to targetry, or to mismatched beam energies between GSI and Argonne has yet to be determined. These issues are being thoroughly explored in both laboratories.

As this is a conference mainly about gamma ray spectroscopy, I would like to turn to some gamma ray observations which may or may not be relevant to this puzzle. In the original APEX setup a 25% HpGe detector was installed intended to sample the gamma ray flux in order to monitor the performance of the heavy ion counters and to allow an estimate of the positrons from nuclear IPC to be made. The data were heavily downscaled in order to avoid excessive computer deadtime. However, these data indicated structure in the gamma ray spectra in a region of interest around 1760 keV, so more recent runs have used at least two 70% detectors without downscaling for events of higher energy than 1 MeV. Fig. 2 shows such a gamma ray spectrum which has been Doppler corrected for emission from U-like fragments. A clear peak near 1780 keV can be seen. The fact that an individual peak is so prominent at high excitation in  $^{238}\text{U}$  is surprising, as this is more than twice the energy of the collective octupole states and lies in a region of high level density. Its production cross section is 15 mb measured in coincidence with at least one detected heavy ion. This considerable strength is hard to reconcile with non-collective structure such as a state reported at 1780 keV in alpha scattering [17] which was anticipated with a cross-section of 2 mb. However, the peak we see is broad, about 16 keV FWHM, twice that expected from Doppler reconstruction, so it may arise from a superposition of several transitions. Whatever the origin of the state, or states, the structure seems to be both collective and unusual, so merits further investigation.

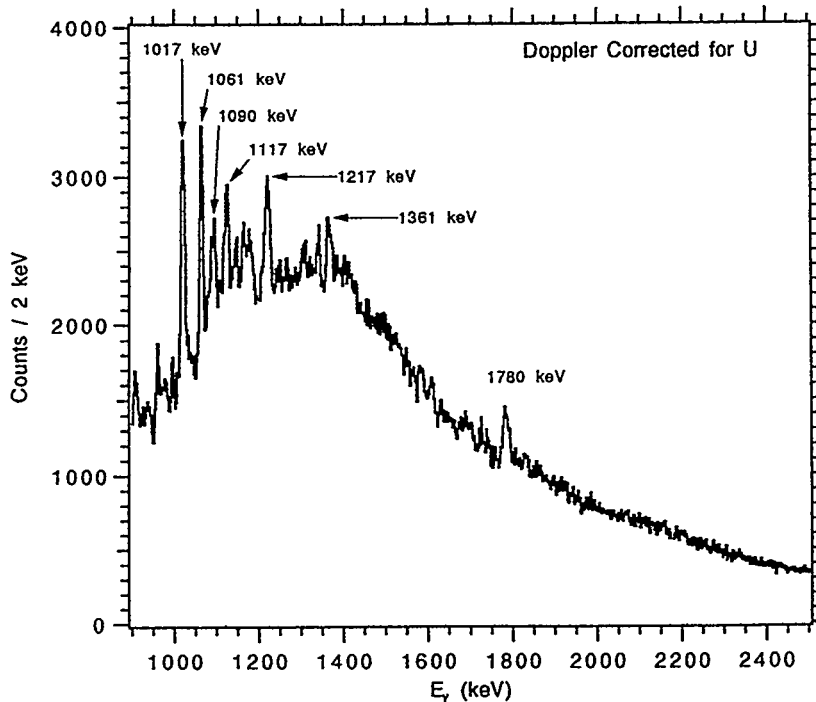


Fig. 2 The high energy part of the Doppler reconstructed spectrum for  $^{238}\text{U}$  fragments observed in the  $^{238}\text{U} + ^{181}\text{Ta}$  experiment at 5.95 MeV/A.

As a source of sharp electron-positron peaks it is hard to reconcile the photopeak with the lepton data for a variety of reasons. In absolute strength it is too weak -- even if the decay were E1 the IPC branch is only  $5.7 \times 10^{-4}$ . If the electron-positron peaks were due to IPC

from a moving uranium nucleus then the laboratory sum electron-positron spectrum would not have sharp lines but be in the form of a Doppler broadened bump of width  $\sim 140$  keV which could only be sharpened by lepton kinematic correction. Finally, the angular distribution and energy sharing of IPC is very different to the equal-energy, back-to-back scenario. Even so, a nuclear origin to the sharp lines remains a distinct possibility.

#### 4. CONCLUSIONS

So far, APEX has just reached the start of its research program and a whole array of questions emerge. Already there have been surprises which we do not understand. In particular, the lack of sharp peaks in all our spectra is a puzzle. With the published decay scenarios, yield curves and cross sections it is difficult to understand the discrepancy. It must be pointed out that the spectrometers in use all have different characteristics and acceptances, and that truly identical experiments to the GSI studies have not been performed by the APEX collaboration. We are naturally curious to see if our observation of no sharp line structures in U + Ta is ubiquitous; can we find peaks in any of the previously studied systems U + U, U + Th, U + Cm, etc.? Does this point to instrumental effects which either prevents us from observing peaks or creates peaks in the GSI experiments? Can we successfully perform experiments where strong nuclear IPC transitions are known to be populated? A study of the  $^{206}\text{Pb}$  1844 keV  $J^\pi = 3^- \rightarrow 2^+$  decay which has a  $4.2 \times 10^{-4}$  IPC branch is planned and appears feasible. Only time will tell us the answer to these questions. However, I am confident that after more than a decade of research in this field we will have conclusive answers by the next conference in this series in two years time. I look forward to explaining all these puzzles to you then.

#### REFERENCES

- [1] NATO Advanced Study Institute on the Physics of Strong Fields, Lahnstein, Germany, (1981).
- [2] Conf. of Physics of Strong Fields, Maratea, Italy, Ed. W. Greiner (Plenum Press, New York 1987).
- [3] J. Rafelski, B. Müller and W. Greiner, *Z. Phys.* **A285**, 49 (1978).
- [4] J. Reinhardt, U. Müller, B. Müller, and W. Greiner, *Z. Phys.* **A303**, 173 (1981).
- [5] J. Schweppe et al., *Phys. Rev. Letts.* **51**, 2261 (1983).
- [6] M. Clemente et al., *Phys. Lett.* **B137**, 41 (1984).
- [7] T. Cowan et al., *Phys. Rev. Letts.* **54**, 1761 (1985).
- [8] H. Tsertos et al., *Phys. Lett* **B162**, 273 (1985).
- [9] APEX Proposal, Argonne National Laboratory, 1989 (unpublished).
- [10] D. Mercer et al., *Nucl. Instrum. Methods* (1994) In Press.
- [11] I. Ahmad et al., *Nucl. Instrum. Methods* **A229**, 201 (1990).
- [12] S. Gazes, P. A. A. Perera, and F. L. H. Wolfs, *Nucl. Instrum. Methods* **A337**, 174 (1991).
- [13] N. I. Kaloskamis et al., *Nucl. Instrum. Methods* **A330**, 447 (1993).
- [14] M. Wolanski et al., submitted to *Nucl. Instrum Methods* (1994).
- [15] P. Salabura et al., *Phys. Lett* **A245**, 153 (1990).
- [16] I. Koenig et al., *Z. Phys.* **A346**, 153 (1993).
- [17] F. K. McGowan and W. T. Milner, *Nucl. Phys.* **A571**, 569 (1994).

## First Results with the Microball and Gammasphere

D.G. Sarantites<sup>(1)</sup>, P.-F. Hua<sup>(1)</sup>, D. LaFosse<sup>(1)</sup>, M. Kororija<sup>(1)</sup>, J. Elson<sup>(1)</sup>, J.T. Hood<sup>(1)</sup>, C. Baktash<sup>(2)</sup>, C. Gross<sup>(2)</sup>, H.-Q. Jin<sup>(2)</sup>, D.W. Stracener<sup>(2)</sup>, I.Y. Lee<sup>(3)</sup>, A. Macchiavelli<sup>(3)</sup>, B. Cederwall<sup>(3)</sup>, P. Fallon<sup>(3)</sup>, W. Rathbun<sup>(3)</sup>, F. Christando<sup>(4)</sup>, E. Landulfo<sup>(4)</sup>, J.X. Saladin<sup>(4)</sup>, J. Döring<sup>(5)</sup>, and S.L. Tabor<sup>(5)</sup>

<sup>(1)</sup>Department of Chemistry, Washington University, St. Louis, Missouri 63130

<sup>(2)</sup>Physics Division, Oak Ridge National Laboratory, Oak Ridge, Tennessee 37831

<sup>(3)</sup>Lawrence Berkeley Laboratory, Berkeley, California 94720

<sup>(4)</sup>Physics Department, University of Pittsburgh, Pittsburgh, Pennsylvania 15260

<sup>(5)</sup>Physics Department, Florida State University, Tallahassee, Florida 32306

The Microball, an improved  $4\pi$  multi-detector array, was used recently in conjunction with Gammasphere in three experiments. Highlights of the first results are presented here. The Microball consists of 95 CsI(Tl) scintillation detectors with individual Si photodiode readout, arranged in 9 rings. In these first experiments the Microball performed as designed, but the results in new physics exceeded our expectations. We can say with certainty that by its powerful channel selection the Microball enhanced the performance of Gammasphere by *one full coincidence fold*. This was possible for all exit channels involving charged particle emission, with increasing performance benefit as one progressed to lighter reaction systems.

Below we summarize the essential characteristics of the Microball and give some performance benchmarks. A detailed description of the Microball will be given in Ref. [1]. The essential features of the signal processing has been presented in a IEEE meeting [2].

The Microball has the following design and performance characteristics :

- (1) Excellent ( $p$ ,  $d$ ,  $t$ ,  ${}^3\text{He}$ , and  ${}^4\text{He}$ ) particle identification (PID) resolution down to low energies.
- (2) Large solid angle coverage (geometric coverage  $\simeq 98\%$  of  $4\pi$ ).
- (3) Low mass (540 g) that degrades the peak-to-total ratio of the Ge detectors from 54% to 49% for  ${}^{60}\text{Co}$ .
- (4) Good charged particle energy resolution (2.7% for 8.78 MeV  $\alpha$ 's).
- (5) Sufficient segmentation that increases at the forward angles. This allows angular distribution measurements to be made and helps equalize the counting rate with angle.
- (6) Good counting rate stability (much better compared to the Dwarf Ball system [3] with PMT's). No gain shift corrections were necessary for PID between protons and alphas.
- (7) It keeps up with the high rates of Gammasphere and suffers *smaller* pile-up losses than Gammasphere.
- (8) The signals are processed by 6 16-channel modules that include: pole zero correction, base line restoration, constant fraction discriminators, multiplicity counters, pile-up rejection, time-to-FERA converters, computer controlled output inspection signals, and computer controlled threshold and gain setting.
- (9) For digitization 18 FERA ADC modules are used. The entire electronics setup is very compact. It provides processing for 288 parameters and fits into 2 CAMAC crates with an additional NIM bin for the trigger gates.
- (10) For data acquisition in the experiments with the early implementation of Gammasphere we adopted the approach of the MSU  $4\pi$  group. The Microball signals were

processed by reading the 18 FERA modules (6 for energy, 6 for PID and 6 for timing). The Gammasphere and Microball information was read via the ECL bus of the ADC's of both systems. A transputer system controlled the FERA-Faucet-Maier module and the Memory unit where the event data were buffered. Blocks of 4 kB were transferred to a Sun Spark station, which wrote the events on tape and placed them on the ethernet for two other VMS Vax stations to histogram and monitor during the run.

Beam tuning was done with an optical fiber periscope that permitted rapid focussing without removing any element from the Microball. All but one of the Microball channels performed reliably during the 2 weeks running. One detector channel was intermittent. Setting up the detector gains was possible with computer control via a PC computer. Matching of the gains was done in less than 15 minutes. The gains were set to specified  $\alpha$  particle energies at the full ADC range for each ring by using previously determined calibration files and non-linear algorithms.

The acquisition system was reasonably robust, and the loss of data due to down time was insignificant. A software PID parameter defined as the ratio of the fast to the slow component in the CsI(Tl) was used for crude on-line channel gating and monitoring of the experiment.

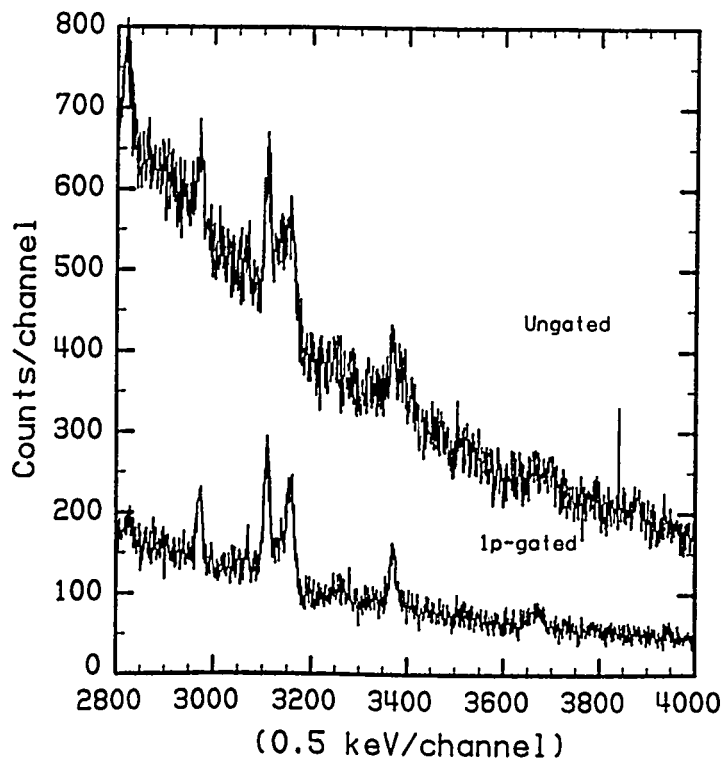


Figure 1. One proton gated and ungated spectra of  $\gamma$ -rays from the 230 MeV  $^{51}\text{V} + ^{100}\text{Mo}$  reaction. A peak to background improvement by a factor of 3.9 is clearly seen.

The systems studied were:  $^{51}\text{V} + ^{100}\text{Mo} \rightarrow ^{151}\text{Tb}^*$  at 230 MeV,  $^{29}\text{Si} + ^{58}\text{Ni} \rightarrow ^{87}\text{Mo}^*$  at 128 MeV, and  $^{32}\text{S} + ^{58}\text{Ni} \rightarrow ^{90}\text{Ru}^*$  at 135 MeV. The event rates for the mass 150 and 90 regions were somewhat different. In the mass 150 run the total charged particle multiplicity was 0.5 per event. The Microball was operated at  $\approx 1500$  c/s per detector, with all detectors counting approximately at the same singles rate, while in the Gammasphere we had the maximum rate of  $\approx 10,000$  c/s per detector. For the mass 90 region experiments the average charged-particle multiplicity was 3.0 and the Microball detectors were operated at a rate of 2500-3000 c/s, again with similar rates in each detector. Under these

conditions the Ge detectors were counting between 6000-7000 c/s close to the maximum. It is possible to run the Microball in this lighter system with rates commensurate with the maximum rates in the Gammasphere without compromising the particle identification. However, this reaches the rate limit for CsI(Tl) scintillation. At counting rates above 4000 c/s some loss in PID resolution occurs only for protons and deuterons. The proton to alpha separation is maintained in all the detectors, except for the most backward angles where the proton and alpha energies come down to a few MeV. For heavier systems and for normal kinematics reactions the proton alpha separation is good at all energies.

It is important to protect the particle detectors from elastic scattering at the forward angles and from target electrons for the remaining angles. In the present experiments we had 25 to 15 mg/cm<sup>2</sup> Sn-Pb absorbers in the forward 4 rings, and 5 mg/cm<sup>2</sup> Sn-Pb for the remaining rings. We found that for the mass 90 reactions with <sup>28,29</sup>Si and <sup>32</sup>S beams these absorbers were satisfactory. However, for the 230 MeV <sup>51</sup>V + <sup>100</sup>Mo → <sup>151</sup>Tb\* reaction we observed a sudden loss of PID resolution from ring 4 to ring 5 (5mg/cm<sup>2</sup> absorber). This indicates that for the heavier beams at least 10 mg/cm<sup>2</sup> of Sn-Pb may be necessary.

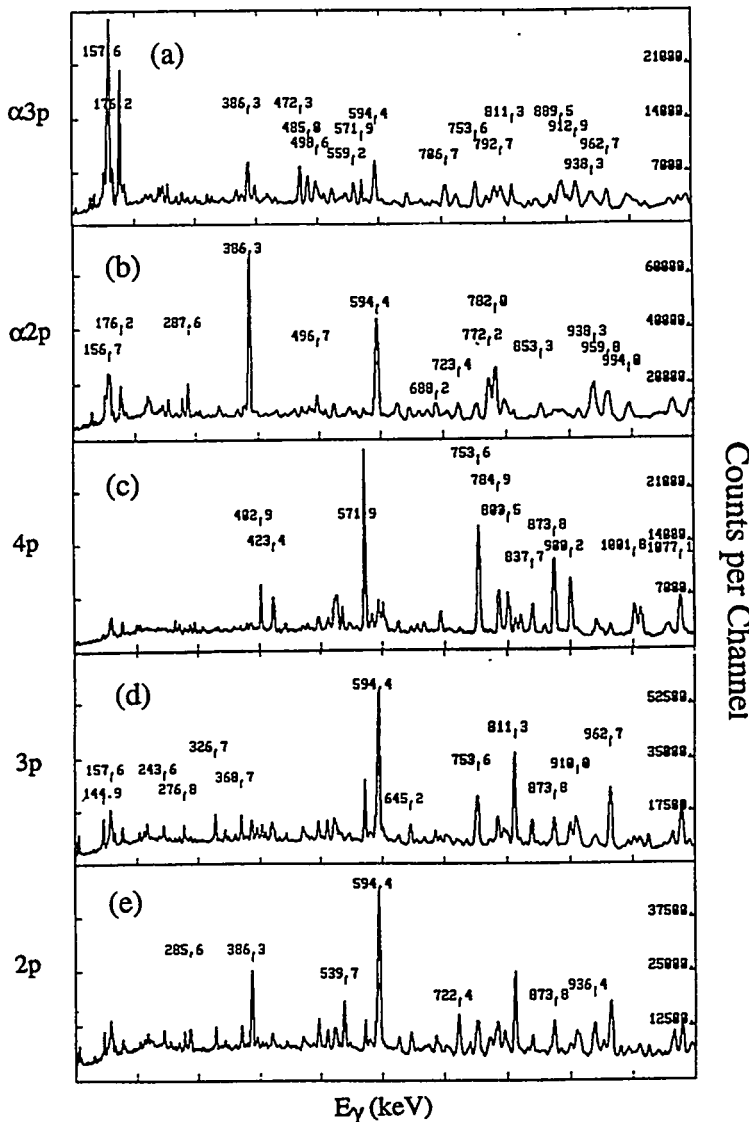


Figure 2. Spectra of  $\gamma$ -rays from the  $\alpha 3p$ ,  $\alpha 2p$ ,  $4p$ ,  $3p$ , and  $2p$  gates from the reactions of 128 MeV <sup>29</sup>Si + <sup>58</sup>Ni, as indicated for the panels (a) - (e), respectively. The prominent peaks are labelled in keV. Each spectrum shows  $\gamma$ -rays mainly from two nuclei. The scales for the counts shown on the right of the spectra reflect the relative cross sections for the gates. Five additional gates, not shown, namely  $\alpha$ ,  $2\alpha p$ ,  $2\alpha 2p$ ,  $3\alpha p$ ,  $3\alpha 2p$  carry about 20% of the total yield.

The channel selection performance of the Microball is determined by the overall efficiency for detection of each particle that enters with the power of its multiplicity. Thus

for the  $^{100}\text{Mo}(^{51}\text{V},\text{pxn})$  reaction with a measured a 90% proton efficiency, the peak to background improvement, or the Resolving Power (RP) of the Microball is given by the  $0.90/f_{\text{pxn}}$ , where  $f_{\text{pxn}}$  is the fraction of the  $\text{pxn}$  channels to the total. In the  $^{151}\text{Tb}^*$  system we found a Microball RP of  $0.90/0.23 = 3.9$  as seen in Fig. 1. For the  $^{58}\text{Ni}(^{29}\text{Si}, 4\text{p})$  channel the selection efficiency was  $0.87^4 = 0.57$ , while the Microball RP was  $0.87^4/f_{4\text{p}} = 0.87^4/0.08 = 7.2$ . This RP is close to the Resolving Power of Gammasphere, which is given by  $\frac{P}{T} \times \frac{\Delta E_\gamma}{FWHM} \approx 0.5 \times \frac{60}{4} = 7.5$ , where  $\frac{P}{T}$  is the peak to total ratio of the Ge detectors. While the RP of Gammasphere may be independent of the reaction used, the Microball RP depends on the channel cross section fraction  $f_{\text{chan}}$ . Therefore the Microball RP can exceed that of Gammasphere if  $\epsilon^{M_{\text{part}}}/f_{\text{chan}} > \frac{P}{T} \times \frac{\Delta E_\gamma}{FWHM}$ , where  $\epsilon$  is the particle detection efficiency and  $M_{\text{part}}$  is the particle multiplicity. We conclude that for charged particle channels the Microball can enhance Gammasphere by a full coincidence fold or more, without significant loss of efficiency. This benefit is true for all mass regions and it becomes more pronounced for the lighter systems and for low cross section channels.

In all cases studied in the mass 90 reactions we found that in each particle gate mainly 2 exit channels were present in the spectra (see Fig. 2 for five indicated particle gates). This means that the low spin background radiation originates from the channel with the larger number of emitted particles in each gate.

The high selectivity of the Microball allowed us to assign a recently reported superdeformed band in the mass 80 region to  $^{83}\text{Sr}$  (4p channel), and to observe new SD bands in  $^{81}\text{Sr}$  ( $\alpha 2\text{p}$  channel) and  $^{84}\text{Zr}$  (2pn channel). In the  $^{87}\text{Mo}^*$  system had  $\sim 3$  times less total statistics compared to a similar Eurogam I experiment in which the reaction  $128 \text{ MeV } ^{30}\text{Si} + ^{56}\text{Fe}$  was employed without particle selection. Here we obtained a 4p-gated cube containing only  $4 \cdot 10^7$  events compared to  $1.5 \cdot 10^9$  from the Eurogam I experiment. Despite the low statistics from a  $\approx 25 \text{ mb}$  channel we easily identified a SD band with 1.7% yield of the 4p channel. Without the Microball one has to look for an  $\approx 0.05\%$  population of the SD band in the presence of all the reaction channels. Not only we were able to see the SD bands, but we could easily identify the nuclei where these SD bands are, a totally impossible task from the same data without the channel selection. As an illustration, we note that the most intense  $\gamma$ -ray of the  $^{83}\text{Sr}$  SD band has an intensity of 1.7% of the 874 keV transition in Fig. 2(c).

We should mention that because the detection efficiency for charged particles is less than 100% , some of the yield of each channel is transferred to gates containing a subset of detected particles (e.g. part of the 4p channel yield appears in the 3p gate, etc.). Since the efficiency can be measured quantitatively, it is possible, for example, to subtract the appropriate fraction of the 4p matrix or spectra from the 3p-gated matrix or spectra. This procedure has been employed extensively in our data analysis. This made it possible to study a weak 2pn channel in the presence of large 3pxn or 4p cross sections. In fact we identified the properties of the SD band in  $^{84}\text{Zr}$  in this way.

Finally, we have found that charged particle emission widens the ER recoil angle and thus decreases the energy resolution compared to the channels emitting only neutrons. Since in the lighter reaction systems there is very little neutron emission, most of the channels of interest emit only protons or  $\alpha$  particles. The contribution to broadening of a proton and an  $\alpha$  particle are in the ratio of 1.7 and 3.0 compared to neutrons. Since we



measured nearly all the particles we can reconstruct on an event by event basis the recoil correction and completely remove the loss of resolution due to the recoil angle. In fact we should obtain better resolution than that for the xn exit channels. Preliminary analysis indicates that this is feasible and in fact it is absolutely essential for channels involving  $\alpha$  particles, where before correction the FWHM is about 2 times larger than in the xn channels at the same  $\gamma$ -ray energy.

In the  $^{151}\text{Tb}^*$  system we searched for evidence of hyperdeformation (HD) in  $^{147}\text{Gd}$  produced by the ( $^{51}\text{V}$ ,  $p3n$ ) reaction. In this data set we identified clearly known SD bands in  $^{146}\text{Gd}$  ( $p4n$  channel),  $^{147}\text{Gd}$  ( $p3n$  channel) and  $^{143}\text{Eu}$  ( $\alpha3n$  channel). A search for a HD ridge structure was made. From the proton gated 4+higher fold Ge data, a background subtracted  $E_\gamma$ - $E_\gamma$  matrix was constructed that exhibited a ridge with a  $32\pm 1$  keV spacing in the energy interval 1.0–1.35 MeV. In addition, from the  $p$ -gated 3+higher fold Ge data a cube was constructed. Background subtracted [4] cuts perpendicular to the cube diagonal (“snow flakes”) were constructed and carefully examined. Evidence for a weak hexagonal snow flake was found primarily in the 1.05–1.10 MeV cut. Its spacing is  $35\pm 1$  keV. In this way the probability of accidentally obtaining a cascade of three extraneous  $\gamma$ -rays with the 35 keV spacing is reduced substantially. Unfortunately this is achieved by substantial loss of statistics. However, if this is indeed a ridge from HD then assuming  $\mathfrak{S}^{(1)} = \mathfrak{S}^{(2)}$  and an upper energy of 1.3 MeV we estimate the maximum spin to be  $2\cdot E_\gamma/\Delta E_\gamma \approx 74 \hbar$ . This is a much more comfortable estimate than  $\approx 95 \hbar$  from Ref. [5].

## References

- [1] P.-F. Hua, D.G. Sarantites, J. Elson, J.T. Hood, M.R. Maier, and A. Vander Mollen, to be published.
- [2] J. Elson, P.-F. Hua, J.T. Hood, D.G. Sarantites, L.G. Sobotka, and M.R. Maier, IEEE (in press).
- [3] D.W. Stracener, *et al.* Nucl. Instr. Meth. **A294**, 485 (1990).
- [4] G. Hackman and J.C. Waddington, *This conference* LBL-35687 Rep. p. 141.
- [5] A. Galindo-Uribarri *et al.*, Phys. Rev. Lett., **71**, 231 (1993).

# Collective high spin states in $^{45}\text{Sc}$ \*

P. Bednarczyk<sup>a,b</sup>, J. Styczeń<sup>a</sup>, R. Broda<sup>a</sup>, M. Lach<sup>a</sup>, W. Męczyński<sup>a</sup>, D. Bazzacco<sup>c</sup>, F. Brandolini<sup>c</sup>, G. de Angelis<sup>b</sup>, S. Lunardi<sup>c</sup>, L. Müller<sup>c</sup>, N. Medina<sup>c</sup>, C. Petrache<sup>b</sup>, C. Rossi-Alvarez<sup>c</sup>, F. Scarlassara<sup>c</sup>, G.F. Segato<sup>c</sup>, C. Signorini<sup>c</sup>, F. Soramel<sup>d</sup>

<sup>a</sup> Institute of Nuclear Physics, Kraków, Poland

<sup>b</sup> INFN, Laboratori Nazionali di Legnaro, Legnaro, Italy

<sup>c</sup> Dipartimento di Fisica dell'Università and INFN, Padova, Italy

<sup>d</sup> Dipartimento di Fisica dell'Università and INFN, Udine, Italy

The high-spin states in  $^{45}\text{Sc}$  were studied with the GASP multidetector array. The nuclei were excited by the  $^{30}\text{Si}(^{18}\text{O}, p2n)^{45}\text{Sc}$  reaction at  $E_{LAB}=60$  MeV and separated with the Recoil Mass Spectrometer. Lifetimes were extracted from the analysis of the Doppler shift attenuation of gammas observed in the  $^{12}\text{C}(^{35}\text{Cl}, 2p)^{45}\text{Sc}$  reaction. Several new high-spin levels extending the known single-particle and collective structures were observed. Energies of the negative-parity states agree with the shell model predictions whereas the positive-parity-intruder rotational band extends up to very high rotational frequencies and continues beyond the maximum angular momentum available from the single-particle  $f_{7/2}$  configuration. The lifetimes measurement suggests a deformation with  $\beta \approx 0.25$  for the positive-parity band.

## 1. Introduction

The nuclei of the  $f_{7/2}$  shell which lie between the doubly magic  $^{40}\text{Ca}$  and  $^{56}\text{Ni}$  are good candidates to observe the competition between collective and single particle modes of nuclear excitation. In this region, the spherical shell model predicts well the properties of low-lying states [1]. On the other hand, collective features may also appear as the energy of some Nilsson model  $f_{7/2}$  subshells falls down with the increasing nuclear deformation. Of a special interest are positive parity intruder states in odd-A  $f_{7/2}$ -shell nuclei. They arise due to  $d_{3/2}$ - or  $s_{1/2}$ -hole excitations and constitute rotational-like bands with a deformation parameter  $\beta \approx 0.25$  at low spins [2]. The experimental data for high spin states in  $f_{7/2}$  nuclei, however, are still scarce because of the unsatisfactory efficiency and limited selectivity of the techniques used so far. The new generation of high efficiency  $\gamma$ -ray spectrometers combined with recoil mass separators or filters opened new perspectives in the study of high spin phenomena in such light nuclei.

## 2. Experimental results

Our investigation of high-spin excitations in the  $^{45}\text{Sc}$  nucleus was performed with

---

\*This work was partially supported by the polish state committee for scientific research under grant no. 204519101

the GASP multidetector array and the Recoil Mass Spectrometer at Legnaro. We applied the  $^{30}\text{Si}(^{18}\text{O}, p2n)^{45}\text{Sc}$  reaction with a beam energy of 60 MeV provided by the XTU Tandem of Laboratori Nazionali di Legnaro. A thin target consisting of 3 layers of  $120 \mu\text{g}/\text{cm}^2$   $\text{SiO}_2$  each on a  $15 \mu\text{g}/\text{cm}^2$  carbon backing was used. The signals from 36 Compton suppressed HP Ge detectors and of the BGO multiplicity filter of the GASP array were accumulated as well as the positions at the RMS focal plane and the time of flight of the recoils separated by the RMS. Events were accepted when at least two Ge detectors and two scintillators of the BGO ball fired in coincidence.

Double and triple  $\gamma$ -coincidence data were analyzed. The  $\gamma$ -recoils coincidences reduced significantly the huge Doppler broadening of the high-energy  $\gamma$ -transitions observed in the experiment, which is caused by the high recoil velocity ( $v/c \approx 0.03$ ). They were also useful to establish the proper positions of the peaks in the  $\gamma$ -spectrum.

The level scheme of  $^{45}\text{Sc}$  which resulted mainly from analysis of the triple  $\gamma$ -coincidences is shown in fig.1.

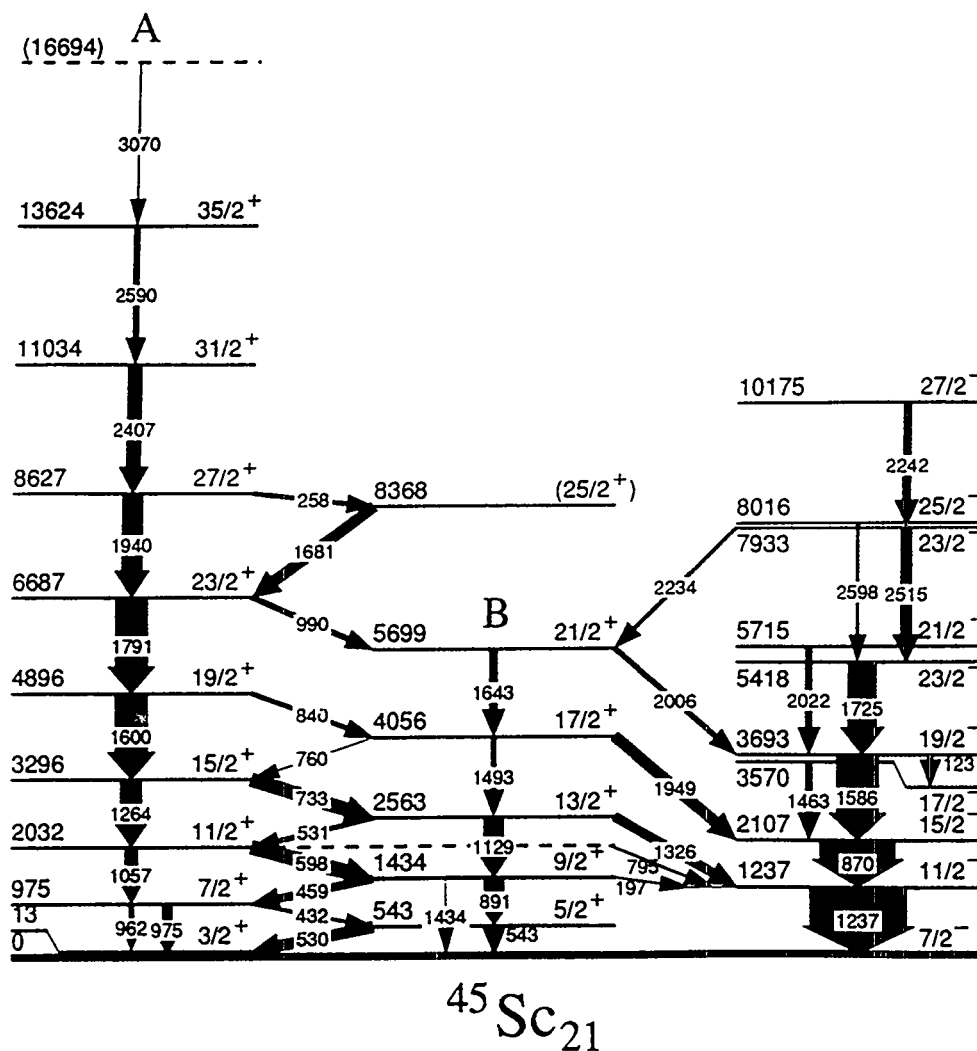


Figure 1. The level scheme of  $^{45}\text{Sc}$

Several new high spin levels lying above the previously known  $15/2^+$  and  $23/2^-$  states [3] were identified. The transitions connecting the positive and negative parity states in the level scheme were also observed. The measured DCO ratios and angular anisotropies of gammas registered in coincidence with the recoils provided arguments for spin assignments of the most populated levels.

Recently, lifetime measurements were performed at LNL using the Doppler Shift Attenuation Method in a reversed reaction of a thick  $^{12}\text{C}$  target bombarded with  $^{35}\text{Cl}$  projectile at 120 MeV. The previously identified transitions up to the spin  $J^\pi = 35/2^+$  were measured. The line-shapes of gammas from the decay of the positive parity states in  $^{45}\text{Sc}$  seen in the forward ( $36^\circ$ ) and backward ( $144^\circ$ ) angle spectra were fitted using the stopping power of Ziegler [4]. In fig.2 the example of the best fit for the 1791 keV and 1940 keV lines at  $36^\circ$  is shown. The experimental spectrum was extracted by putting the gates on the  $\gamma$ -transitions from the lowest positive-parity levels. The data evaluation is still in progress.

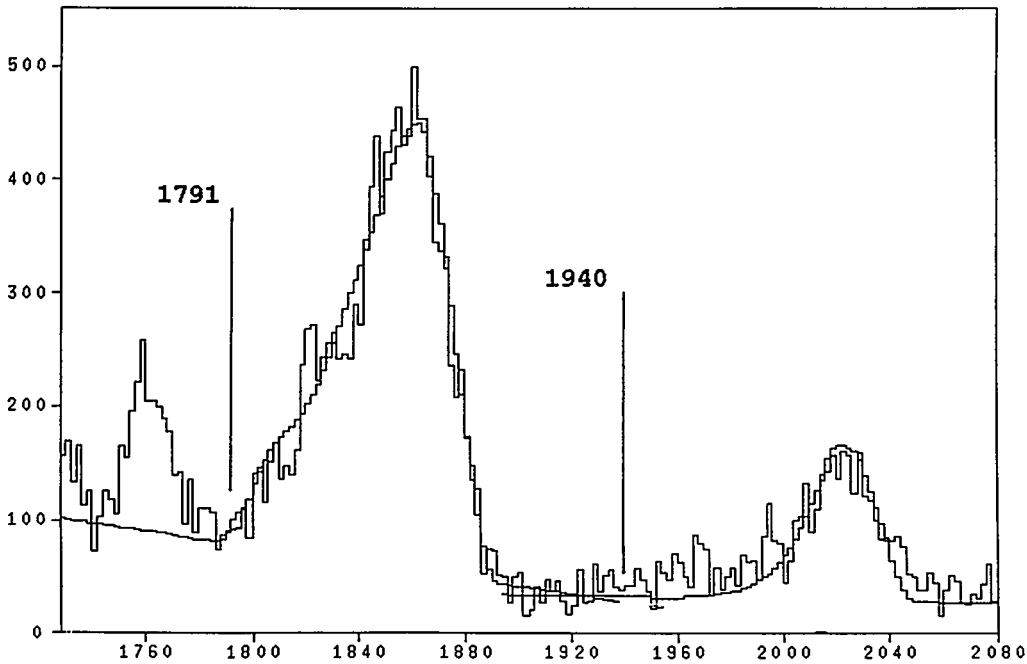


Figure 2. Example of line-shape fits to the 1791 keV ( $23/2^+ \rightarrow 19/2^+$ ) and the 1940 keV ( $19/2^+ \rightarrow 15/2^+$ ) transitions observed at  $36^\circ$ . The obtained lifetimes are  $\tau_{1791} = 0.25(5)$  ps and  $\tau_{1940} = 0.15(5)$  ps they correspond to the deformation  $\beta = 0.24$  and  $\beta = 0.25$  respectively.

### 3. Discussion

The sequence and energies for the negative parity states in  $^{45}\text{Sc}$  are well reproduced by a shell model calculation (see fig. 3) based on the  $f_{7/2}$  configuration with only one particle excited to the higher  $p_{3/2}$ ,  $p_{1/2}$ ,  $f_{5/2}$  levels [5].

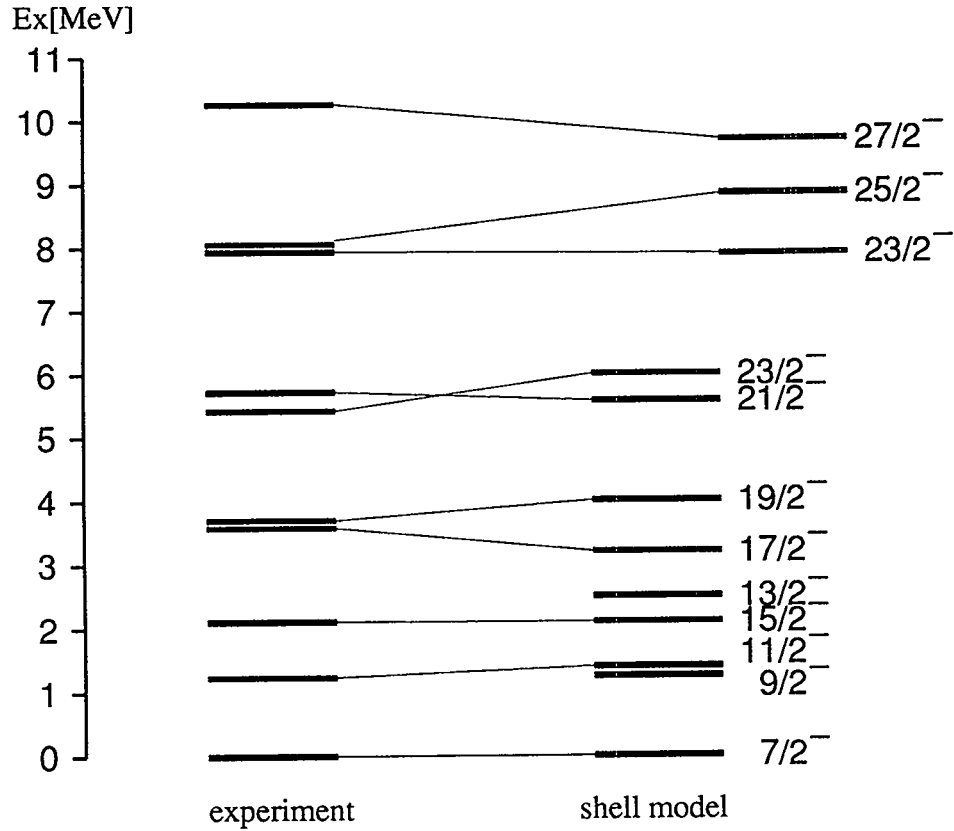


Figure 3. A comparison between the observed negative-parity states and shell model calculations in  $^{45}\text{Sc}$ .

The presence of positive-parity states is a result of hole excitation in the proton  $d_{3/2}$  shell. In the present experiment, two levels have been observed above the state with the maximum angular momentum  $J^\pi = 31/2^+$  obtained when all the active nucleons from  $d_{3/2}$  and  $f_{7/2}$  orbitals are aligned. This feature could be explained by assuming rotational degrees of freedom and/or complicated multi hole-particle excitation in  $^{45}\text{Sc}$ .

The angular momentum for the positive-parity **A** and **B** intruder bands follows the rotational behaviour  $J \sim \hbar\omega$ , as shown in fig.4 and points to the collective origin of these states.

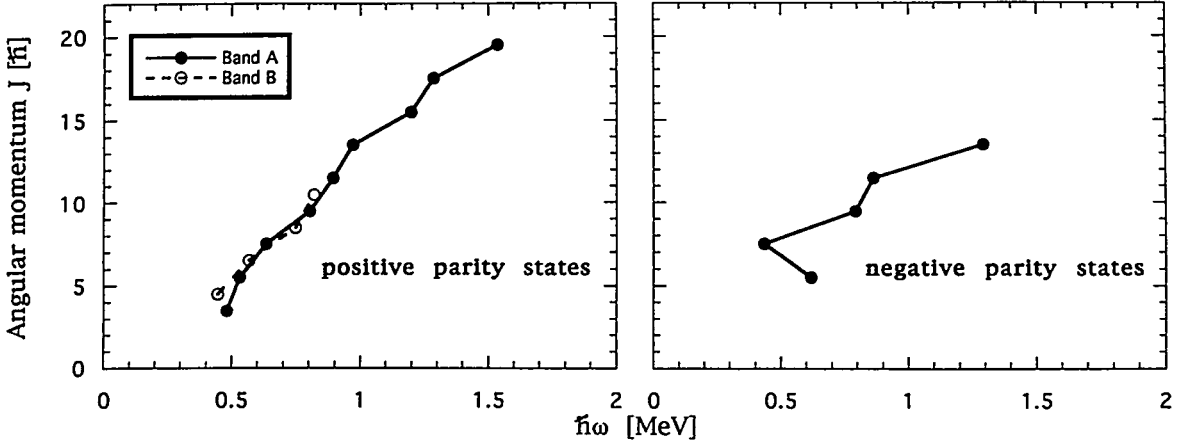


Figure 4. The angular momentum versus rotational frequency for bands observed in the  $^{45}\text{Sc}$  nucleus. For the negative-parity levels, irregularities typical for states of single particle character are observed

Preliminary estimates of the band A lifetimes measured for the levels up to to the spin  $J^\pi = 35/2^+$  suggest quite high and stable deformation  $\beta \approx 0.25$ . This result is consistent with the conclusion of [2] where the prolate deformation for the positive-parity band is predicted.

#### 4. Summary

The experiment confirms the expected competition between the dominant single-particle motion and the collective degrees of freedom which become significant for the nuclei in the middle of the  $f_{7/2}$  shell. The presently observed positive parity rotational band extends up to very high rotational frequencies and continues beyond the maximum angular momentum available from the single-particle  $f_{7/2}$  configuration. This feature of  $^{45}\text{Sc}$  points to the coexistence of spherical and deformed shapes in this nucleus and suggests a weak influence of the single particle motion on the collective degrees of freedom in this case.

#### References

- [1] E.K.Warburton, C.W.Beausang, D.B.Fossan, L.Hildingsson, W.F.Piel, Phys. Rev. **C34** (1986) 136
- [2] J.Styczeń, J.Chevallier, B.Haas, N.Schulz, P.Taras, N.Toulemonde, Nucl. Phys. **A262** (1976) 317
- [3] P.G.Bizzeti, A.M.Bizzeti-Sona, M.Bucciolini, R.Huber, W.Kutschera, H.Morinaga, R.A.Ricci, C.Signorini, Nuovo Cimento **26A** (1975) 25
- [4] J.F.Ziegler, The Stopping and Range of Ions in Matter (Pergamon, New York, 1985)
- [5] A.Yokoyama, H.Horie, Phys. Rev. **C31** (1985) 1012

# Gamma Spectroscopy with the Recoil Filter Detector

## Recent Results and Perspectives

K. Spohr<sup>1</sup>, W. Meczynski<sup>2</sup>, J. B. Fitzgerald<sup>1</sup>, D. B. Fossan<sup>5</sup>,  
M. Gorska<sup>3</sup>, H. Grawe<sup>1</sup>, J. Heese<sup>1</sup>, M. Lach<sup>2</sup>, K. H. Maier<sup>1</sup>,  
A. Maj<sup>2</sup>, J. C. Merdinger<sup>4</sup>, M. Rejmund<sup>3</sup>, R. Schubart<sup>1</sup>,  
J. Styczen<sup>2</sup>

<sup>1</sup> HMI Berlin, <sup>2</sup> IFJ Krakow, <sup>3</sup> Warsaw University, <sup>4</sup> CRNS Stras-  
bourg, <sup>5</sup> SUNY Stony Brook

### Abstract

A detector (RFD) has been developed that measures evaporation residues in coincidence with  $\gamma$ -rays detected in a Ge-array. The RFD brings two advantages to fusion-evaporation  $\gamma$ -ray experiments: (1) The recoil time of flight discriminates against other types of reactions, in particular inelastic scattering including Coulomb excitation, fission and reactions with light target impurities (C, O); (2) The velocity vector of the  $\gamma$ -decaying recoil nucleus is determined by the location of the firing RFD module, which allows for event-by-event Doppler-shift correction. Recent experiments with OSIRIS at VICKSI studying <sup>199</sup>At and nuclei around <sup>56</sup>Ni are presented to show the properties of the RFD, and a short outlook for an RFD with the new arrays is given.

### Introduction

A detector for evaporation residues (recoil filter detector, RFD) has been built primarily to select  $\gamma$ -rays from fusion-evaporation reactions, when other reaction mechanisms dominate. As the RFD also measures the velocity vector of the recoils,  $\gamma$ -energies can be Doppler corrected event by event. The RFD has been designed and built jointly by IFJ Krakow and HMI Berlin, and has been used with the OSIRIS array at VICKSI [1]. It has been described in ref. [2]. Evaporation residues are detected 74 cm behind a thin target by 18 cylindrical detector elements arranged in two concentric circles around the beam and covering the range of angles between 2.8° and 12.5° with 65% geometrical efficiency. Each element consists of an aluminized Mylar foil, 0.5 to 2.0  $\mu\text{m}$  thick and 60 mm diam. The ions knock around 100 electrons out of the foil. These electrons are accelerated by 20kV and focussed on a 10  $\mu\text{m}$  thick and

20mm diam. plastic scintillator producing a 2 MeV signal. This detection scheme gives acceptable pulseheights for slow heavy nuclei, such as 10 MeV Pb, and is fast. Recoils can be detected 50 ns after a hit by a scattered beam particle. The beam is pulsed with typically 300 ns repetition time and a fast linear gate cuts out the time interval when scattered beam arrives. Evaporation residues are separated by time of flight from other reaction products. The measured time of flight and the granularity of the RFD determine the velocity vector of the nucleus and facilitate a corresponding event by event Doppler correction. The experience with the RFD and its major features are presented for some recent experiments and the perspectives for similar detectors together with the new balls are discussed.

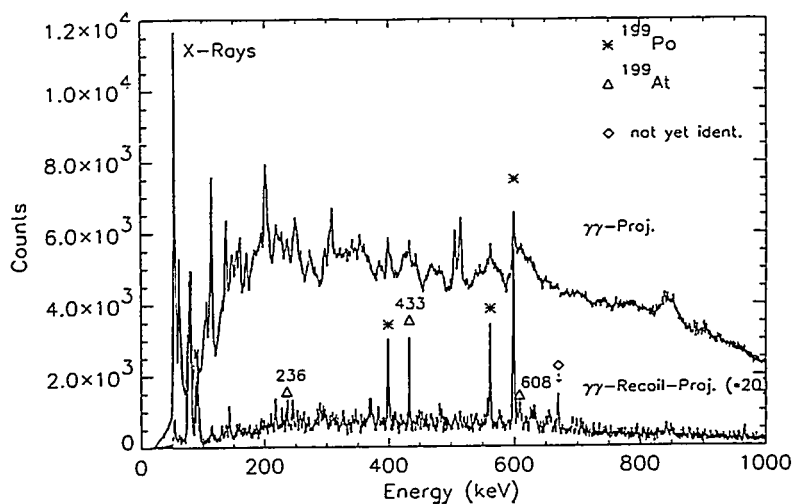


Fig.1 Total projection of  $\gamma - \gamma$ -coincidences for the reactions of 141 MeV  $^{28}\text{Si}$  with  $^{175}\text{Lu}$  ( $1\text{mg}/\text{cm}^2$ ). The lower spectrum is in coincidence with the RFD, lines in  $^{199}\text{At}$  are marked by their energy. In the upper spectrum the otherwise dominant Coulomb excitation is suppressed by a window on the sum energy of the ball and requiring ball multiplicity between 1 and 11.

### Spectroscopy of $^{199}\text{At}$

Intruder states have been found in  $^{198,196}\text{Po}$  and the  $2^+$ -state in  $^{196}\text{Po}$  is significantly lowered [3, 4, 5]. The occurrence of such collective features should be more pronounced in Astatine with three instead of two active protons. Coincidences between two Ge-detectors, the 48 element BGO-ball and the RFD have been



measured with the  $^{175}\text{Lu}(^{28}\text{Si}, 4n)^{199}\text{At}$  reaction at 141 MeV with a  $1\text{ mg/cm}^2$  Lu-target. Fig. 1 shows that RFD-coincidences give clean spectra; a PACE calculation gives the total fusion cross section ( $\approx$ fission) as 100 mb and 1 mb for  $^{199}\text{At}$ , while an estimate from beam current, measuring time and OSIRIS-efficiency gives  $100\ \mu\text{b}$  for  $^{199}\text{At}$ . The RFD-efficiency was 16% in this experiment, with a large variation between individual elements; the efficiency of the best modules, if matched by all elements, would correspond to a total efficiency of 25%.  $\gamma$ -rays at 433 keV in coincidence with the parallel 608, 236 and 372 keV lines are assigned to  $^{199}\text{At}$  from coincident X-rays. In the heavier isotopes the first excited  $13/2^-$ -level lies above 600 keV. The present data reveal a significant drop of the energy of the first excited state to most likely 433 keV, which is similar to the change from  $^{198}\text{Po}$  to  $^{196}\text{Po}$ .

#### Nuclei around $^{56}\text{Ni}$

An experiment with a 68 MeV  $^{20}\text{Ne}$  beam on a  $1\text{ mg/cm}^2$   $^{40}\text{Ca}$ -target has been performed to study nuclei around doubly magic  $^{56}\text{Ni}$ . In this case the RFD primarily improves the resolution. Table 1 gives estimates of the major contributions to the Doppler broadening of the 2290keV line in  $^{57}\text{Co}$ . Its width is reduced from 20keV to 7keV with the event by event correction. With a thinner target a part of the broadening could have been avoided, but this rolled target was remarkably clean and free of oxygen. Fig. 2 shows the improvement of the measured spectrum, and the irregular, as yet incomplete, scheme of  $^{57}\text{Co}$  (fig. 3) with its high energy transitions demonstrates that improvement is needed.

The measured total efficiencies and ratio of outer to inner ring countrate (in parantheses) of the RFD for different final nuclei in this experiment were:

$^{58}\text{Ni}$  (2p) 31% (0.41),  $^{57}\text{Ni}$  (2pn) 42% (0.49),  $^{57}\text{Co}$  (3p) 30% (0.50),  $^{56}\text{Fe}$  (4p) 38% (0.53),  $^{54}\text{Fe}$  ( $\alpha$ 2p) 28% (1.02)

About 3 scattered beam particles per beam pulse hit each inner RFD- element according to TRIM-calculations, and fourfold direct hits of the scintillator with its ten times smaller area could be clearly seen. Detection of evaporation residues started 50 ns after the scattered beam. The scintillators were discolored from radiation damage after the experiment.

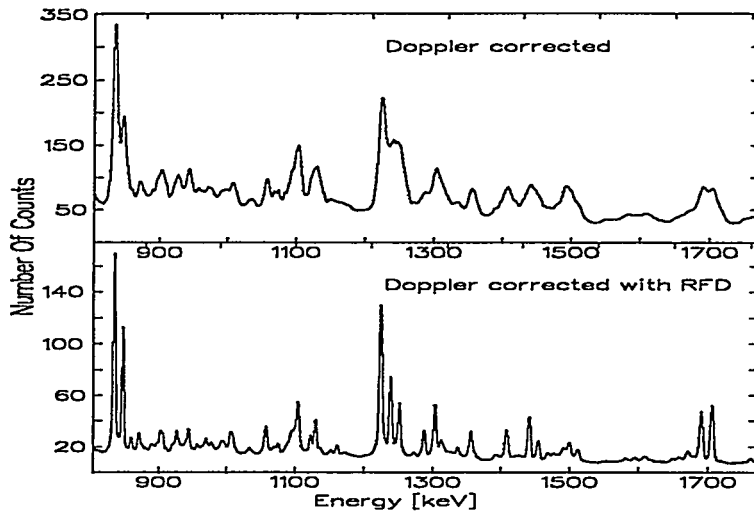


Fig.2 Total  $\gamma - \gamma$ -projection for  $^{20}\text{Ne} + ^{40}\text{Ca}$  Doppler corrected for the average and the individually measured recoil velocity.

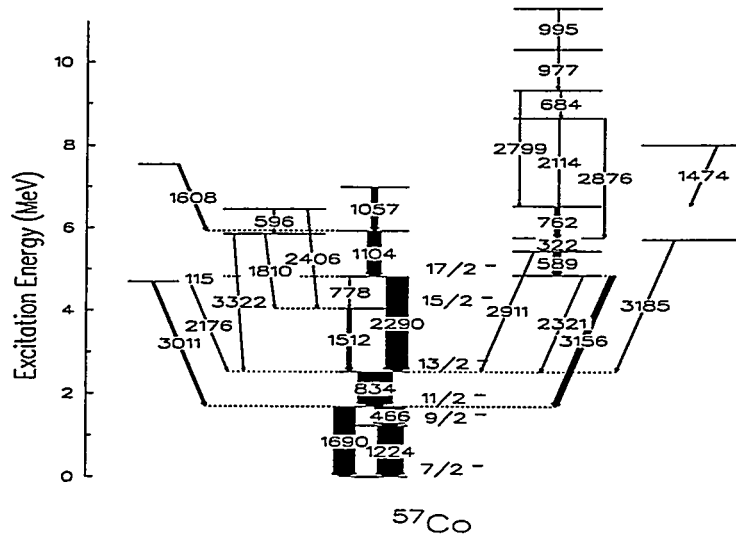


Fig. 3 Provisional, partial level scheme of  $^{57}\text{Co}$

Table 1 Contributions [keV] to Doppler broadening of 2290 keV line  
 $68 \text{ MeV } ^{20}\text{Ne} + 1 \text{ mg/cm}^2 \text{ } ^{40}\text{Ca} \rightarrow ^{57}\text{Co} + 3 \text{ p}, v/c(^{57}\text{Co})=0.028$

cause	0°	90°	cause	0°	90°
Ge angle $\Delta\Theta = 10^\circ$	0	11	Recoil angle $\Delta\Theta = 11^\circ$	0	13
angle straggling target	0	7			
$\Delta v$ proton emission	9	0	energy loss target	23	0

Measured: 20 keV with average corr., 7 keV with individual corr.

#### Perspectives for an RFD with the new $\gamma$ -Arrays

The RFD has been proven as a reliable instrument in the experiments with OSIRIS, that of course were selected for maximum benefit from the RFD and therefore show huge improvements in background and/or line width. The main shortcoming that is left, is that the efficiency is 30% to 50% less than expected, because signals are lost in the noise.

The new arrays with 100 times higher efficiency than OSIRIS for  $\gamma - \gamma$ -coincidences will enable the study of heavy nuclei produced with  $\sigma \leq 10 \mu\text{b}$  against an overwhelming fission background. Doppler broadening due to the velocity distribution of the nuclei becomes more important with the higher granularity of the balls and the use of higher folds. Judging from the gained experience the RFD should improve a majority of experiments with thin targets. RFD- $\gamma^f$ -coincidences are expected to be cleaner and have better statistics than  $\gamma^{f+1}$ -coincidences. An RFD obstructs the  $\gamma$ -measurement little, the present RFD uses  $\leq 2\%$  of the solid angle. It can therefore be used in addition to any normal measurement of only  $\gamma$ -rays, if the beam is pulsed and some restrictions of the target thickness are accepted. The price of the RFD is comparable to that of one Compton suppressed Ge-detector channel. A second RFD has been built for EUROBALL at Strasbourg; it covers the angles from  $1.4^\circ$  to  $6.7^\circ$ , again with 18 similar elements at 128 cm flightpath. Work on a proposal of an RFD for GAMMASPHERE is under way.

#### References

1. J. Heese et al. Phys. Lett. B 302 (1993) 390
2. J. Heese et al. Acta Physica Polonica B24(1993) 61
3. D. Alber et al. Z. Phys. A339 (1991) 225
4. J. Wauters et al. Z. Phys. A344 (1992) 29
5. M. Lach et al. submitted to Z. Phys. A

## Reaction mechanism of multinucleon transfer in the system $^{110}\text{Pd} + ^{52}\text{Cr}$

K.Vetter<sup>1</sup>, D. Bazzacco<sup>2</sup>, Th.W. Elze<sup>1</sup>, J. Gerl<sup>3</sup>, T. Happ<sup>3</sup>, T. Härtlein<sup>4</sup>, W. Korten<sup>5</sup>,  
T. Kröll<sup>1</sup>, D. Napoli<sup>2</sup>, C. Rossi Alvarez<sup>2</sup>, R. Schubert<sup>3</sup>, H.J. Wollersheim<sup>3</sup>, H. Xie<sup>3</sup>

<sup>1</sup>Univ. Frankfurt, <sup>2</sup>INFN, Padova, <sup>3</sup>GSI, Darmstadt, <sup>4</sup>Univ. Heidelberg, <sup>5</sup>Univ. Bonn

The system  $^{110}\text{Pd} + ^{52}\text{Cr}$  characterized by well adjusted Q-values for neutron and proton transfer and large nucleon pairing energies was chosen to study the mechanism of multinucleon transfer. In an experiment at the accelerator laboratory of the INFN in Legnaro (Italy) a  $^{110}\text{Pd}$  target of  $855\mu\text{g}/\text{cm}^2$  was bombarded by  $^{52}\text{Cr}$  ions at energies in the vicinity of the Coulomb barrier (170MeV, 185MeV, 200MeV and 215MeV). The set-up consisted of the  $4\pi$ - $\gamma$  spectrometer GASP and the PYRAMID [1] array of position sensitive parallel plate avalanche counters covering the scattering angle region  $80^\circ \leq 160^\circ$ . Particle- $\gamma$  coincidence data were recorded, demanding a hit in at least one of the Ge-detectors of GASP, while the sum-energy and  $\gamma$ -multiplicity information of the inner BGO ball was taken whenever it responded.

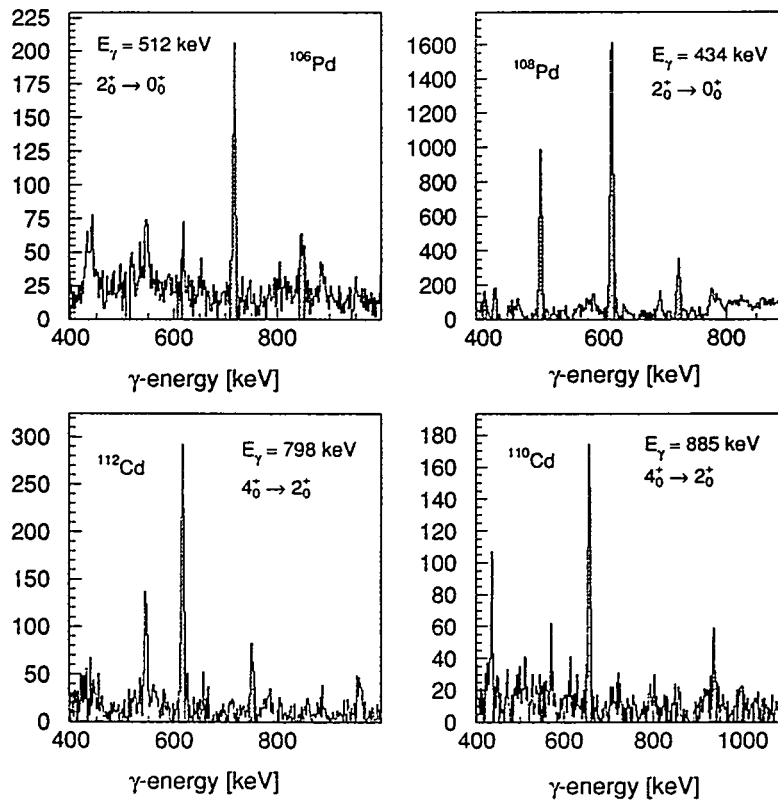


Fig. 1:  $p\gamma\gamma$  coincidence spectra of selected reaction channels.

The high efficiency of GASP enabled the identification of 10 different transfer channels by their characteristic  $\gamma$ -decay. Fig. 1 shows examples of corresponding  $\gamma$ -spectra. The relative intensity of all the identified transfer channels is shown in fig. 2. The most exotic  $4p6n$  transfer leading to  $^{100}\text{Mo}$  has a cross section of only  $\sigma_{tr} \approx 40\mu\text{b}$ . Considering the similarity of the effective Q-values the observed population pattern for exotic channels seems to be in favour of correlated multinucleon transfer.

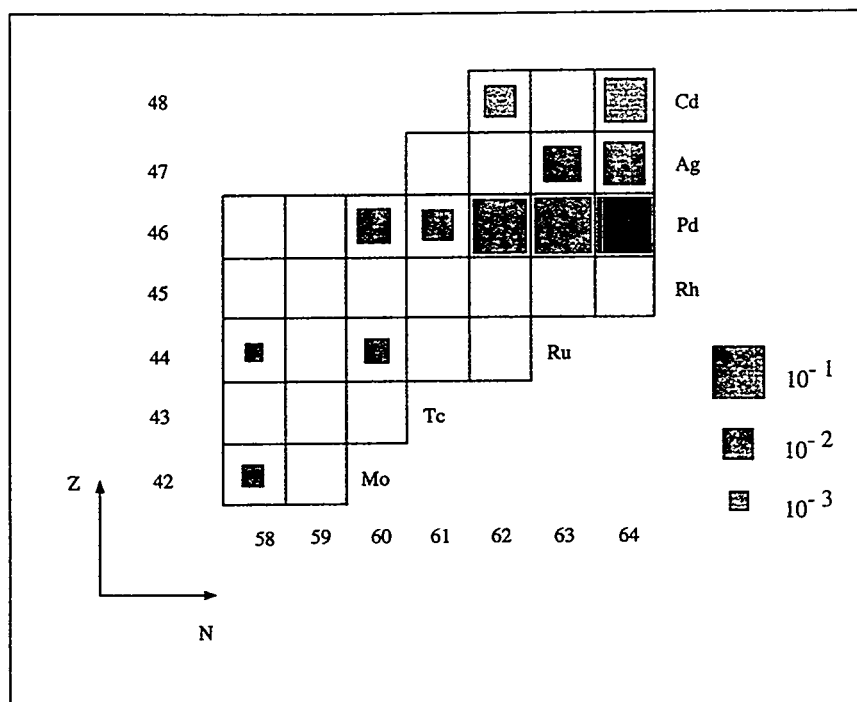


Fig. 2: Relative intensities of transfer products ( $E_b=200\text{MeV}$ ).

With the inner BGO ball of GASP it was possible to measure total excitation energies as a function of the  $\gamma$ -multiplicity. The correlation for pure Coulomb excitation ( $E_b=170\text{MeV}$ ) and for the most prominent transfer channels ( $E_b=200\text{MeV}$ ) is depicted in fig. 3. The Coulex channel is leading mainly to collective excitations along the yrast line. The transfer channels show also such a 'cold' component, which can be interpreted as an indication for correlated pair transfer, but are dominated by higher sum energies, interpreted as quasi-particle excitations.

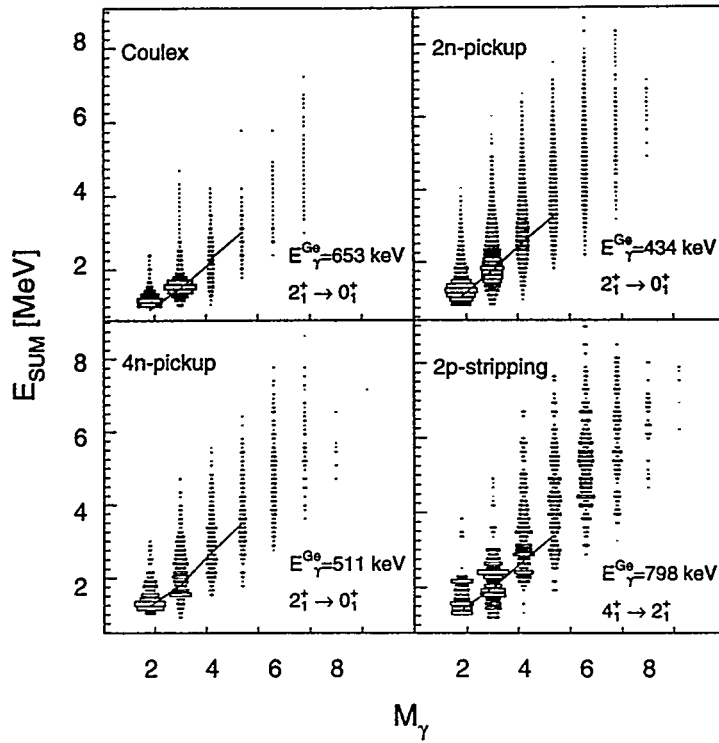


Fig. 3: Sum energy  $\gamma$ -multiplicity correlations for selected channels.

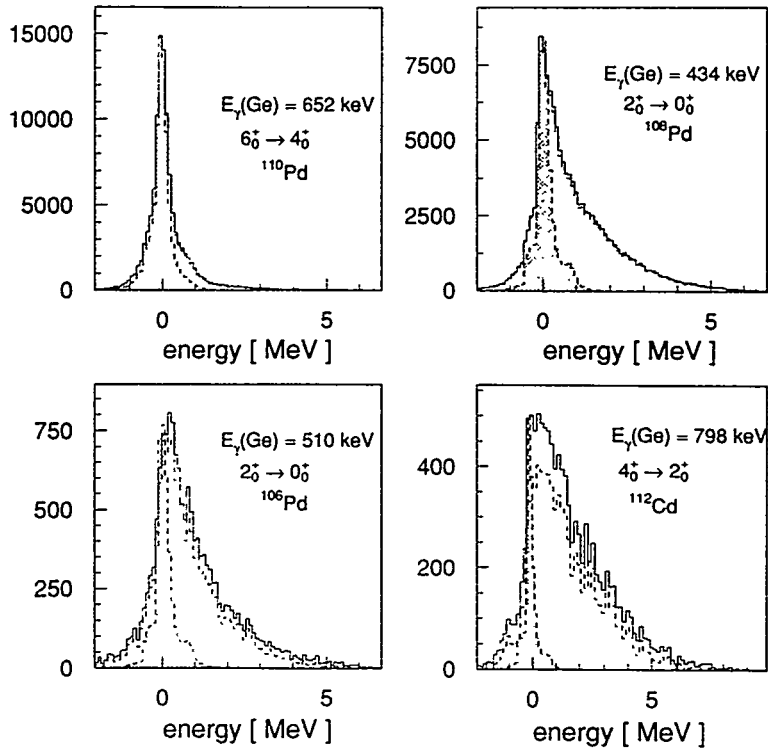


Fig. 4: Projection of the excitation energies above the yrast line for the reaction channels shown in fig. 3.

The projection of the excitation energies above the yrast line shown in fig. 4 enables a quantitative determination of the 'cold' part, being defined as lying at the yrast line within the resolution (FWHM) of the  $\gamma$ -spectrometer. For the 2n and 2p channel this fraction is compared in table 1 with values obtained for other transfer systems [2]. From the  $Q_{eff}$ -values and the pairing energies  $\delta_d$  and  $\delta_a$  of the corresponding donor and acceptor nuclei it may be concluded that 'cold' (correlated pair) transfer is strong if the pairing energies are larger than the Q-value. However, such a simple explanation for the occurrence of 'cold' transfer needs further experimental proof.

Table 1.

	channel	$P_{cold}$ [%]	$Q_{eff}$ [MeV]	$\delta_d$ [MeV]	$\delta_a$ [MeV]
$^{52}\text{Cr} \rightarrow ^{110}\text{Pd}$	+2n	30(3)	2.7	2.7	1.8
	-2p	18(9)	3.0	2.3	3.9
$^{18}\text{O} \rightarrow ^{232}\text{Th}$	+2n	14(4)	0.01	1.3	3.6
$^{90}\text{Zr} \rightarrow ^{232}\text{Th}$	+2n	<1	4.3	1.3	1.4
$^{130}\text{Te} \rightarrow ^{232}\text{Th}$	+2n	<3	2.5	1.3	1.7

[1] K. Vetter, Th.W. Elze, M. Kaspar, T. Kröll and J. Gerl, Nucl. Instr. Meth. A344 (1994) 607.

[2] J. Gerl, W. Korten, D. Habs, D. Schwalm and H.J. Wollersheim, Z. Phys. A334 (1989) 195.

# Performance of Gammasphere Split Detectors<sup>†</sup>

A.O.Macchiavelli, I.Y.Lee, B.Cederwall, R.M.Clark,  
M.A.Deleplanque, R.M.Diamond, P.Fallon and F.S.Stephens  
Nuclear Science Division, Lawrence Berkeley Laboratory, Berkeley, CA 94720

## I. Introduction

An important property of large HPGe detector arrays is the energy resolution ( $\delta E$ ) of the individual counters. The sensitivity or figure of merit of such an array for F-fold coincidence events depends on  $1/\delta E^F$ . While intrinsic resolutions are usually 2 keV at 1 MeV, in a typical (Heavy-Ion,xn) reaction the effective resolutions are affected by Doppler broadening. These are most severe for those detectors positioned around  $90^\circ$  with respect to the beam direction. This is qualitatively seen from the expression  $\delta E_{Doppler}/E_0 \approx \delta\beta\cos\theta + \delta\theta\beta\sin\theta$ , that relates the broadening to changes in the velocity  $\delta\beta$  and opening angle  $\delta\theta$ . A quantitative example is shown in Fig. 1 where the different effects contributing to the effective resolution are shown.

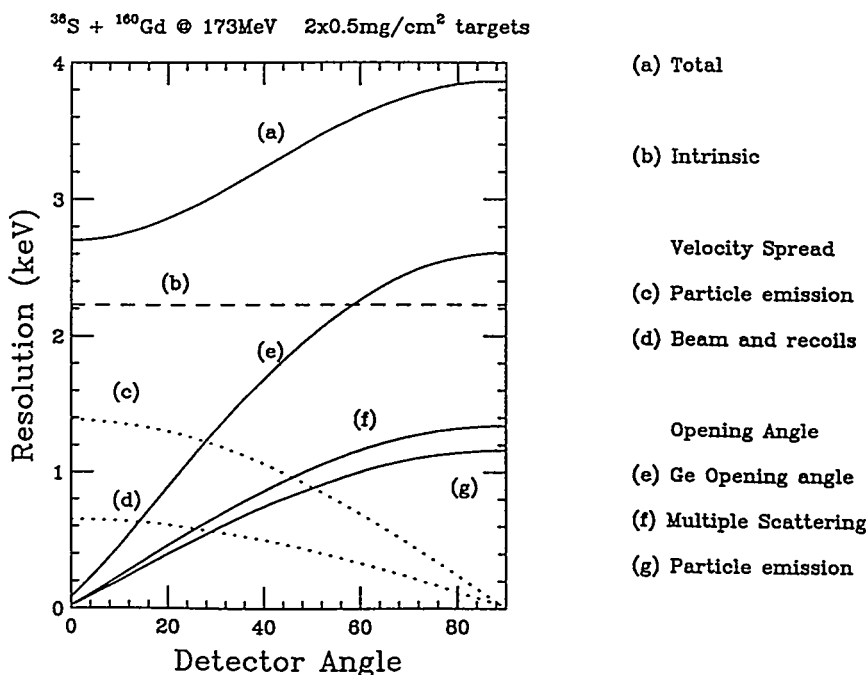


Fig. 1 Effective resolution as a function of the angle between a Ge detector and the beam.

Using a detector split in two halves, it is possible to reduce the degradation in the resolution by correcting the  $\gamma$ -ray energy in software using information on the energy deposited in each half of the detector. In this work we present results obtained with prototype detectors developed for Gammasphere.



## II. Configurations

Shown in Fig. 2 are two possible solutions that have been considered for Gammasphere:

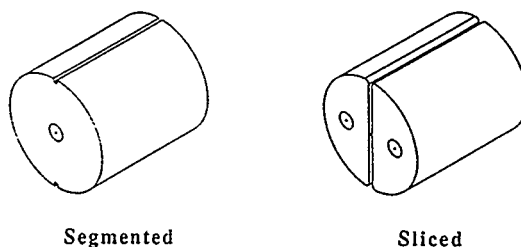


Fig. 2 Schematic drawing of the split detectors for Gammasphere.

1) A physically split detector consisting of two D-shaped HPGe crystals housed in a single cryostat, usually referred to as "sliced" and 2) A single crystal with a segmented outer electrode referred to as "segmented".

In the *sliced* configuration the two halves are treated as different detectors requiring two high-resolution electronic channels. In the *segmented* configuration there is only one high-resolution signal common to both sectors, obtained from the inner electrode; signals from the outer contact provide low resolution position information.

## III. Results

Detectors of each design have been tested with radioactive sources and in beam. Some characteristics of these prototypes are shown in table 1.

Configuration	Vendor	FWHM <sup>a)</sup> (keV)	Efficiency(%)	Volume(cc)
Sliced	EGG ORTEC	2.2 <sup>b)</sup>	25 <sup>b)</sup>	306 <sup>c)</sup>
		2.3 <sup>b)</sup>	25 <sup>b)</sup>	
			65 <sup>c)</sup>	
Segmented	EGG ORTEC	2.2 (14) <sup>d)</sup>	82	330
	EURISYS	2.4 (14) <sup>d)</sup>	82	302

a) at 1.33 MeV, b)individual crystal, c) total, d) side-channel resolution

Table. 1 Some properties of the prototype detectors tested in this work.

### III.1 Sliced

As mentioned earlier, for this type of detector we used two high-resolution channels. In Fig. 3 we present the relative efficiency of such a detector decomposed into the contributions from confined events in either crystal A or B and the shared events A+B.

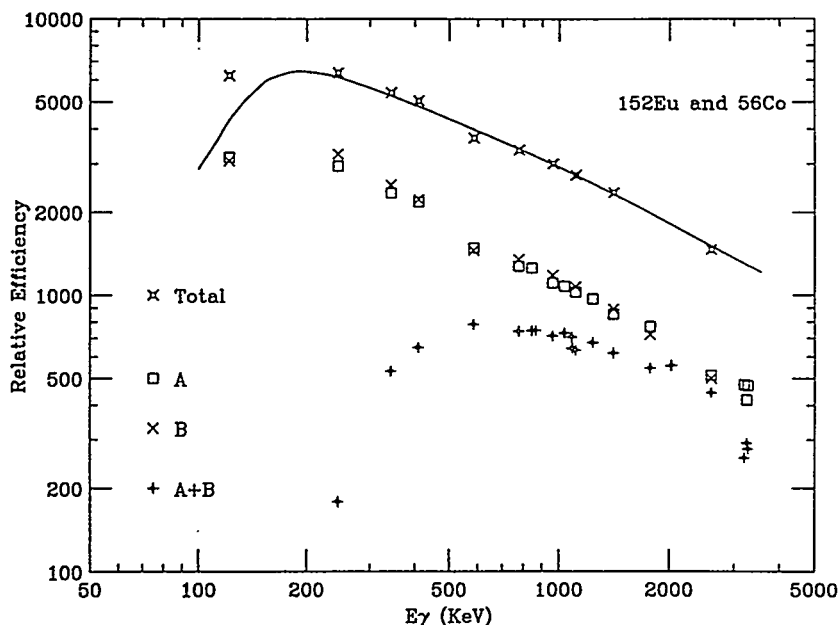


Fig. 3 Relative efficiency of a sliced detector showing the contributions from confined and shared events.

As expected, the contribution from shared events is more important at high gamma ray energies. After an absolute normalization, we determined that at 1.33MeV  $^{60}\text{Co}$  the total efficiency is  $\epsilon_{total} = \epsilon_A + \epsilon_B + \epsilon_{AB} \approx 25\% + 25\% + 15\% = 65\%$ . This loss in efficiency as compared with a normal detector with similar volume of Ge is a drawback of this configuration. This together with the fact that two high-resolution channels of electronics are required made us question the use of such a device for Gammasphere, since the gain in energy resolution was not enough to offset the loss in efficiency and the extra cost in the electronics.

### III.2 Segmented

Computer simulations performed with the code GEANT<sup>1)</sup> showed that the energy deposition in the crystal allowed the determination of the side where the initial  $\gamma$ -ray hit the detector. The segmentation of the outer electrode did not present a major problem, but the crucial question was the design of a preamplifier for the side-channels that will provide the position information with sufficient resolution and do so without affecting the resolution of the main energy signal<sup>2)</sup>. We studied the energy distribution with radioactive sources by illuminating only a slice of the detector using a Pb collimator, as sketched in Fig. 4. By requiring  $E_{total} = 1.33\text{MeV}$  we look at how the difference  $E_{\gamma A} - E_{\gamma B}$  is distributed when a

slice in side A of the detector was illuminated by the  $^{60}\text{Co}$  source. The spectrum obtained is shown in Fig. 4. For this energy, there is a 5% chance that the energy seen in the other side of the detector is larger than that of the side where the  $\gamma$ -ray hit, in very good agreement with simulations.

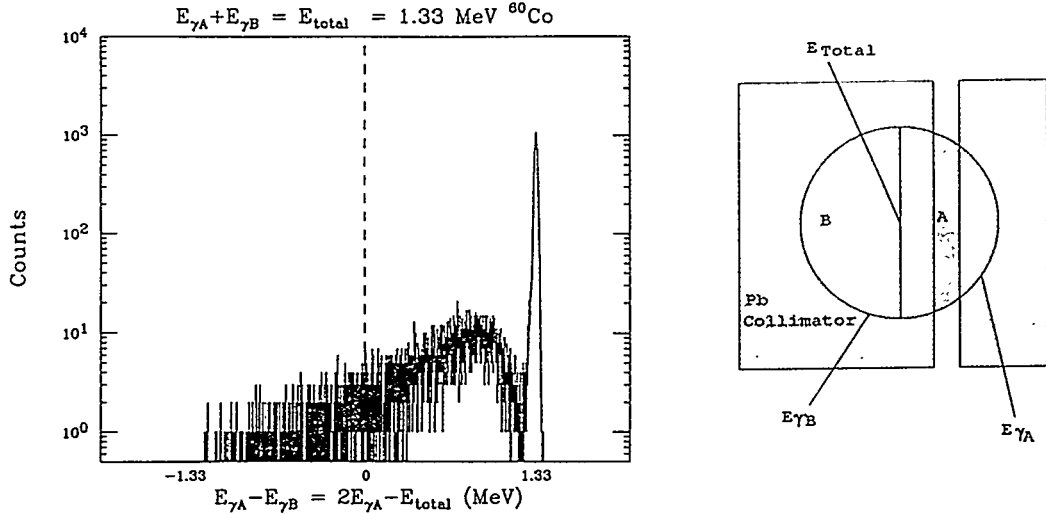


Fig. 4 Energy distribution for  $\overline{E}_{\gamma A} - \overline{E}_{\gamma B}$  with the condition that  $\overline{E}_{total} = 1.33\text{MeV}$

We have tested these detectors in several in-beam experiments. As an example, we show in Fig. 5 a portion of a spectrum obtained in the reaction<sup>3)</sup>  $^{56}\text{Fe} + ^{64}\text{Ni}$ . Two peaks of around 660 keV are decomposed into the contributions from the two sides of the segmented detector using the simple algorithm of assigning the total energy to one side when its side-channel energy was larger than 50% of the total. By aligning the peaks in software before adding them we obtain an improvement of a factor of 1.3 in resolution. Both the energy difference and the width of the components in Fig. 4 are in agreement with calculations.

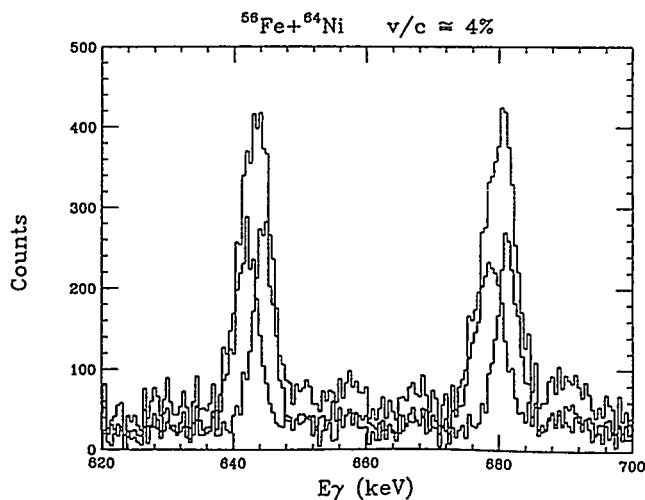


Fig. 5 Portion of a spectrum showing the contributions from the two sides of the detector and their sum before applying the Doppler correction.

## IV Conclusions

We have tested prototype split detectors for Gammasphere. Our results indicate that the segmented configuration works as expected and therefore it will be implemented for the remaining Gammasphere detectors. This will provide an increase of a factor of about two in the resolving power of the array. These detectors can also be used as polarimeters to obtain information on the electric or magnetic character of the  $\gamma$ -rays. Other configurations to achieve higher granularity are being used at Eurogam and being considered for Euroball<sup>4)</sup>.

## References

- † Work supported in part by U.S. DOE under contract number DE-AC03-76SF0098.
- 1) J. R. Beene and I. Y. Lee, private communication.
  - 2) F. Goulding, private communication.
  - 3) Gammasphere experiment EI44, D. Fossan et al.
  - 4) See contributions by F. Beck, J. Eberth, J. Gerl et al. in these Proceedings.

## Acknowledgments

We would like to thank Prof. David Fossan and collaborators for allowing us to use part of their EI44 data for some of the tests carried out in this work.

# Performances of a new type of Ge detector : the clover detector

F.A. BECK

CRN Strasbourg - IN2P3/CNRS and Université L.Pasteur de Strasbourg  
B.P. 28 - F 67037 STRASBOURG Cedex 2

*Abstract : A composite Ge detector has been developed for phase 2 of the France-UK multidetector EUROGAM with the purpose to achieve an increase of both the resolving power and the total peak efficiency of the array. It is constituted of 4 single Ge which are closely packed in the same cryostat. Twenty nine of those clovers have now been delivered by EURYSIS Mesures. The main characteristics of these detectors measured with EUROGAM in a fusion evaporation reaction, are reported here.*

## 1. Why composite Ge detectors?

Eurogam phase 1 was used at the NSF facility at Daresbury from October 1992 to end of March 1993 in a geometry based on a 72 detector Ge ball, each single detector being surrounded by a BGO Compton suppressor<sup>1</sup>). As the forward quadrant (for the use of the recoil mass spectrometer) and the 12 pentagonal holes were left empty, the array was only equipped with 45 tapered Ge detectors. Each of them has an intrinsic peak efficiency around 70% compared to a 7.6 cm x 7.6 cm NaI counter placed at a distance of 25 cm from a <sup>60</sup>Co source.

At the origin it was intended to complete the ball to 70 Ge counters of the same type for phase 2 at the VIVITRON at Strasbourg. Several reasons have led to the necessity to search for a new type of detector :

- the Doppler broadening observed in phase 1 at angles near 90° showed clearly that the granularity of the array had to be increased at these angles for phase 2 to reduce this effect which lowers strongly the resolving power

- the peak efficiency, especially for high energy gamma rays, depends on the size of the detectors. Unfortunately it is difficult to increase the diameter of the single Ge crystals above 70-75 mm, because of the electric field constraints

- in the future it will be of great interest to have the possibility to determine the multipolarity of the weak transitions such as those deexciting the superdeformed nuclei.

The response to these questions has been the development of the clover detector in collaboration with the company EURYSIS Mesures, following simulation calculations done at CRN Strasbourg<sup>2</sup>).

## 2. The clover detector

The clover design includes four closely packed single Ge. Each of them has a length of 70 mm and an initial diameter of 50 mm. The front of them is squared to 42 mm and they are tapered on a distance of 20 mm. The adjacent faces are cut in the same manner as the edges of the front face to allow the close packing of the detectors.

### *Energy resolution*

The mean individual energy resolution deduced from the

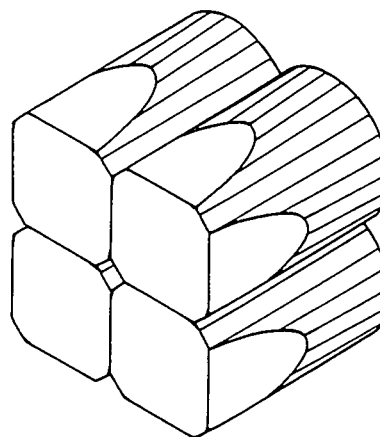


Figure 1 : Design of the clover

measurements of the 116 detectors of the 29 clovers are  $2.0 \text{ keV} \pm 0.2 \text{ keV}$  at 1332 keV and  $1.0 \pm 0.1 \text{ keV}$  at 122 keV respectively. Most of the crystals give values very near of the mean value. The mean energy resolution for the totality of the clover, after add-back of all the detectors; is 2.25 keV at 1332 keV

### Photopeak efficiency

The measured individual intrinsic photopeak efficiency is 21.5%. Again all the values measured for the 116 different detectors are very similar ( $\pm 5\%$ ). The total photopeak efficiency of the clover is very close to the predictions of the simulations calculations<sup>2)</sup> (135%) with a very narrow distribution for the values of the 29 clovers.

### Timing

The timing has been measured in coincidence with a small BaF<sub>2</sub> counter for the gamma-rays of a <sup>60</sup>Co source with a "real" threshold at 50 keV on the clover side. The mean value observed was 5.5 ns with very symmetric peaks.

## 3. Doppler shift corrections

### Simulations

One of the most important problem met in EUROGAM phase 1 was the large Doppler broadening effect observed near 90°. This effect increases of course with the energy of the gamma-rays and with the use of heavier beams (the velocity  $v/c$  varies from  $\sim 2\%$  for mass 30 to  $\sim 4.5\%$  for mass 80). Simulations had first been performed<sup>2)</sup> with the code GEANT III to calculate the gain which could be expected from detectors having a geometry like the clover detector (figure 2). These simulations have also permitted to found an easy method of correction : if one of the four crystals is single hit the mean angle of this detector is the reference, and if two detectors are fired their interface can be taken as the angle of reference. This method gives results comparable to those obtained with the general simulation method : the loss is only of the order of 0.1 keV, but the method makes easy the correction of the experimental data.

### Experimental results

The first tests of this clovers in nuclear reactions with heavy ions beams have been done very recently, in the second half of July, during the commissioning runs of both the new accelerator the VIVITRON and EUROGAM phase 2. Gamma-rays were detected in the reaction <sup>124</sup>Sn + <sup>30</sup>Si at a bombarding energy of 160 MeV leading mainly to the final nuclei <sup>149</sup>Gd and <sup>148</sup>Gd in the 5n and 6n channels respectively. The three upper spectra of figure 3 (lef part, center and right part of the clover) show clearly the energy shift due to the Doppler effect

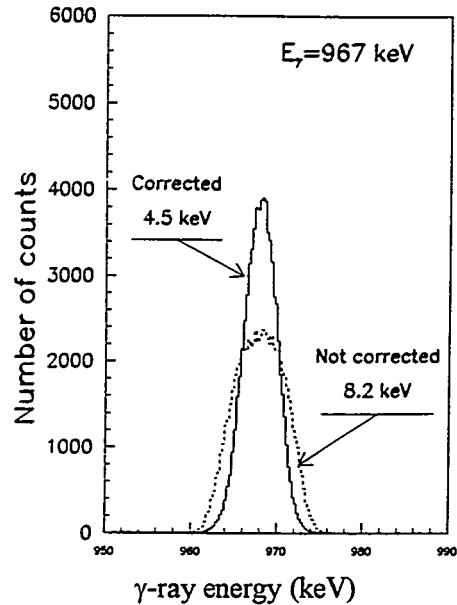


Figure 2 : Simulation spectra calculated with code GEANT III for a recoil velocity of 3%

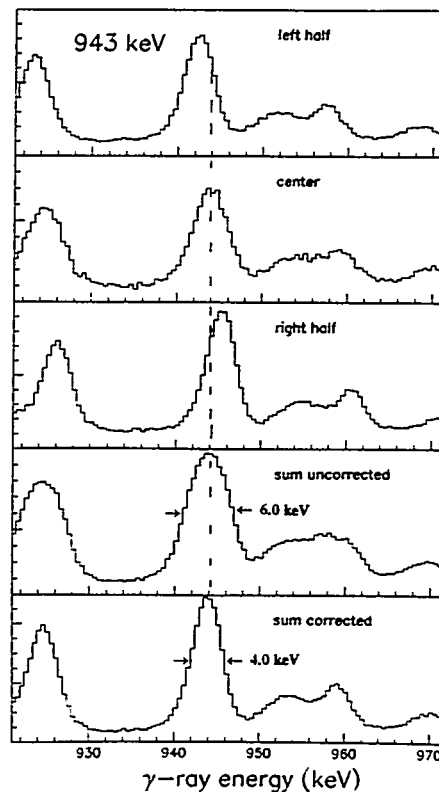


Figure 3 : Experimental spectra observed with a clover

even if the recoil velocity is quite small ( $v/c \sim 1.8\%$ ). The difference of width of the lines between the uncorrected add-back spectrum (6 keV) and the corrected one (4 keV) is exactly what was expected from the simulations.

An other illustration of the increase of resolving power with the clover detector is demonstrated in figure 4. The 1350-1550 keV region of the gamma spectra observed for the yrast superdeformed band in  $^{149}\text{Gd}$  is illustrated in the case of phase 1 and in the case of phase 2. The energy resolution gain (6.1 keV to 4.8 keV) observed in this sum spectra of all the detectors of the array is due to the clover detectors Doppler shift correction.

#### 4. Linear polarisations measurements

The feasibility, with a clover, of linear polarisations measurements has first been demonstrated by simulation calculations and later by a calibration run performed in beam by the use of E2 transitions fed in (p,p') reactions<sup>2)</sup>. These measurements show that the linear polarisation sensitivity stays reasonably high for a so closed geometry, in agreement with the simulation calculations. Correlated with the high efficiency of this polarimeters and their number (24 clovers  $\rightarrow$  48 polarimeters) this means a very great factor of merit and certainly the possibility to measure the linear polarisation of weak transitions as soon as the gamma lines can be isolated (high fold coincidences).

In figure 5 is shown a comparison of the "Vertical" and "Horizontal" counting rates observed in the 1 MeV gamma ray energy region. The E2 lines are characterized by a higher counting rate in the "Vertical" while the magnetic transitions are generally characterized by a higher counting rate in the "Horizontal", but mixing ratio values in the case of M1 + E2 transitions can change this general assessment. These spectra have been obtained in the same reaction  $^{124}\text{Sn} + ^{30}\text{Si}$  described above. The magnetic transitions, designed with arrows in figure 5, have effectively a very different behaviour as compared to the other transitions which are E2. The gamma ray line of 1002 keV is a M2 transition in  $^{148}\text{Gd}$ : the polarisation effect is large even if it is certainly reduced because of the long lifetime of the initial state.

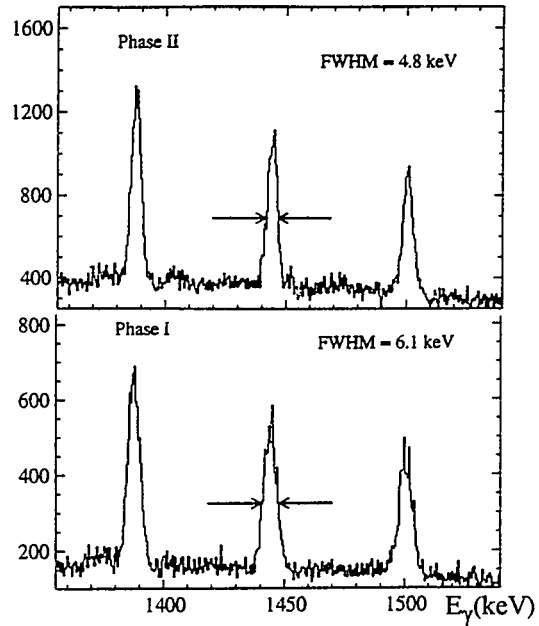


Figure 4 : Gamma lines widths of the  $^{149}\text{Gd}$  yrast SD band observed with EUROGAM phase 1 and phase 2

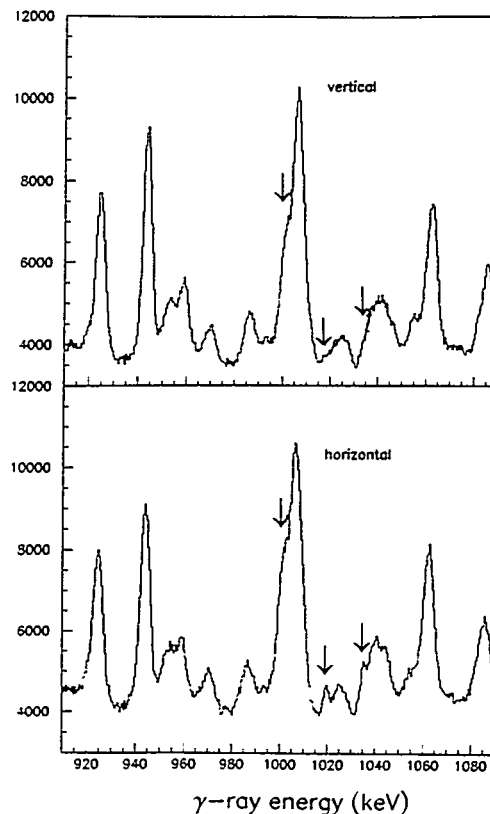


Figure 5 : "Vertical" and "Horizontal" linear polarisations spectra observed with the clovers

## 5. Clovers use in EUROGAM phase 2

EUROGAM phase 2 is based on the use of 30 tapered Ge detectors (efficiency 70%) and of 24 Ge clovers (efficiency 135%). The tapered detectors are at a distance of 20.5 cm from the target, half of them being in the backward quadrant and the other half in the forward quadrant. The clovers, which are at a distance of 23 cm from the target, are disposed in two rings of 12 detectors around  $90^\circ$ . With this arrangement the total photopeak efficiency of EUROGAM was increased from 5.6% in phase 1 to 8.2% in phase 2, the real values are in fact lower since the previous values do not take into account the efficiency reduction correlated to multiple hits due to gamma-rays and neutrons. Especially it would be interesting to reduce the large solid angle supported by the clover detectors.

The comparison of the spectra observed versus the coincidence fold in phase 1 and phase 2 for the  $^{149}\text{Gd}$  yrast superdeformed band is shown in figure 6. This spectra were obtained without any background subtraction. The phase 2 spectra were obtained in a much shorter time and as expected the counting rate of fold 5 is enhanced by a factor  $\sim 6.5$  in comparison to phase 1. One can also observe the very good peak to background ratio obtained for fold 6.

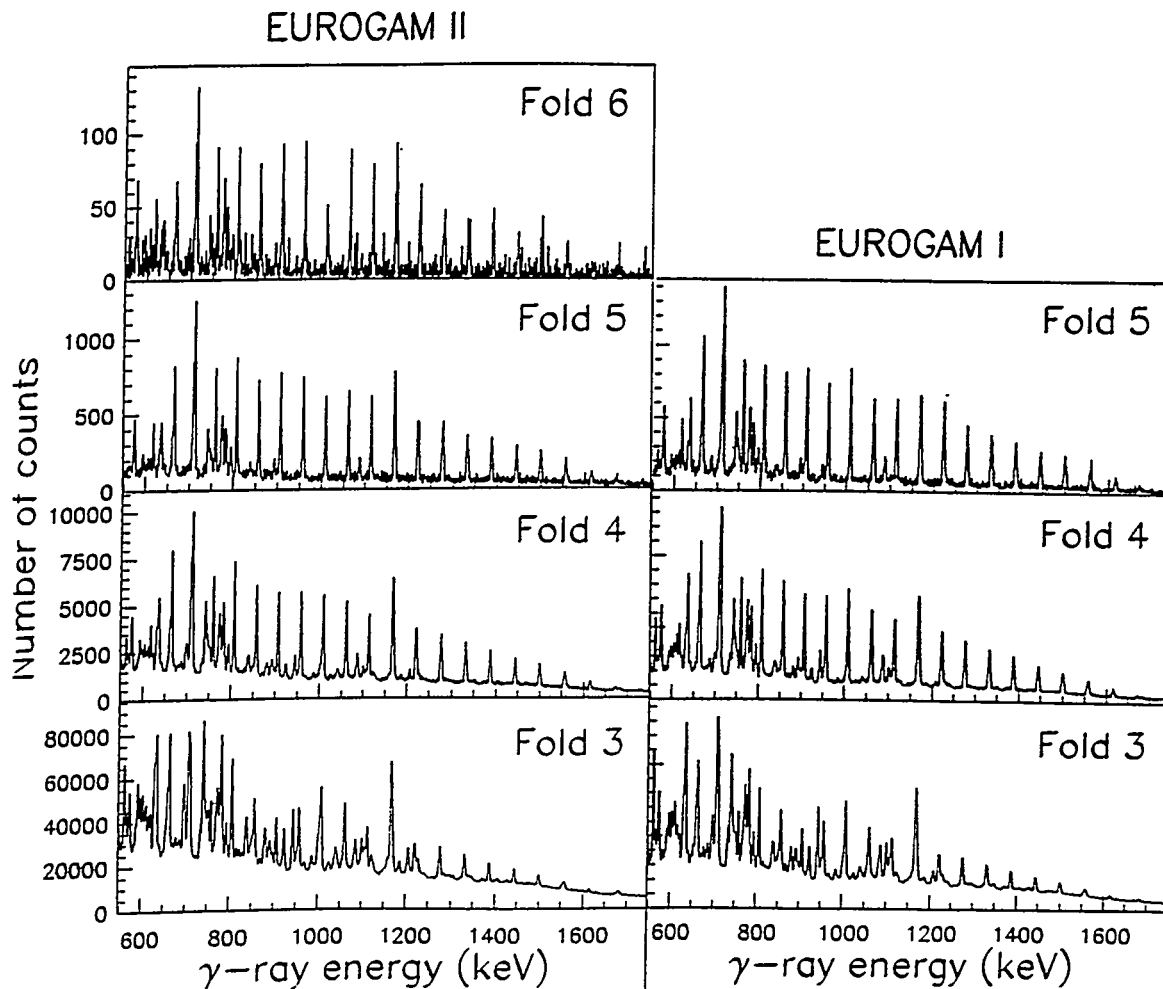
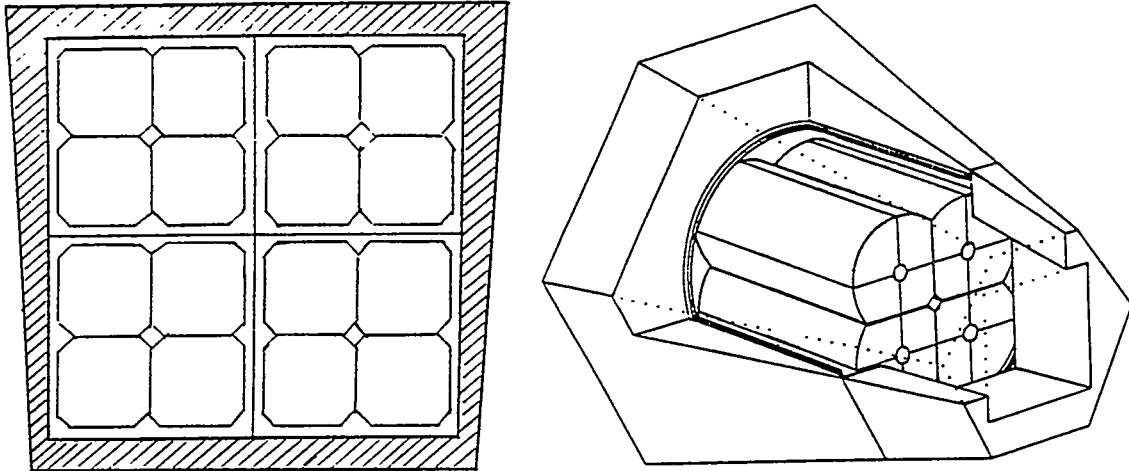


Figure 6 : Comparison of the  $^{149}\text{Gd}$  yrast superdeformed band spectra, versus the coincidence fold, observed with EUROGAM phase 1 and phase 2



## 6. Future developments on the clover design basis

As it has been demonstrated by the present results that the clover design works in a reliable manner it can be used now as a basis for future developments. The increase of both the granularity and the peak efficiency remaining the main goals for this new designs.



*Figure 7 : Two possible future developments of clover type detectors: schematic designs of a quad-clover viewed by the front and of a segmented clover*

The first idea (figure 7, left side) is to pack in a same cryostat four clovers of the type described earlier : the granularity is increased consequently and the efficiency is nearly doubled, due to the increase of the photopeak efficiency but also to a better coverage ratio Ge/BGO. This "quad clover" would use 16 individual Ge crystals.

Recently it becomes possible to segment electrically n-type Ge detectors. This technique brings an alternative solution to the quad-clover : the use Ge of larger diameter (70-75 mm) in a conventional clover geometry with an electrical segmentation of each of them. One ends with again 16 detectors. J.Gerl will give more information on preliminary tests and simulations of this type of detector in a later talk.

*This work would not have been possible without the large contributions of many members of the FRANCE - UK EUROGAM collaboration. The clover "adventure" thanks to all of them.*

### References

- 1) F.A. Beck, Prog. Part. Nucl. Phys. 28 (1992) 443
- 1) F.A. Beck, T. Byrski, D. Curien, G. Duchêne, G. de France et al, Proceedings on Large Gamma-Ray Detectors Arrays, Chalk River, Canada AECL - 10613 : p359-63 and p.364-8

## The SEGMENTED CLOVER detector for EUROBALL

J. Gerl<sup>1</sup>, K. Vetter<sup>2</sup>, Th. W. Elze<sup>2</sup>, Th. Kröll<sup>2</sup> and H. Xie<sup>1</sup>

<sup>1</sup> GSI, Darmstadt, <sup>2</sup> Universität Frankfurt

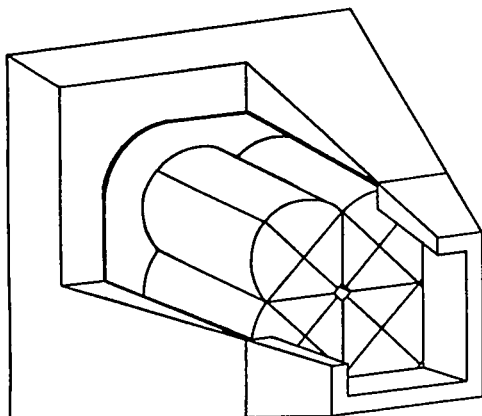


Fig. 1 Sketch of the SEGMENTED CLOVER detector.

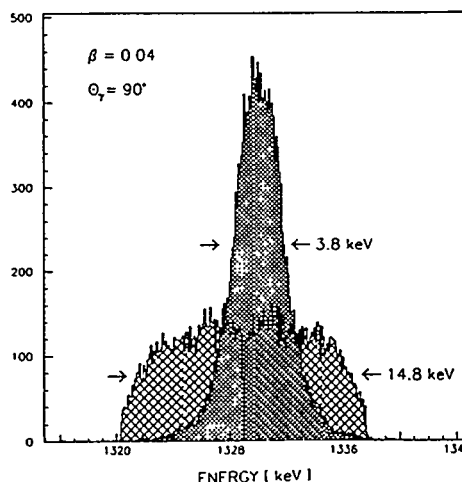


Fig. 2 Simulated photopeak with and without correction of the Doppler broadening.

The aim of the EUROBALL project is the development of  $\gamma$ -ray detectors with substantially improved qualities, to be employable in different kinds of arrays ranging from one detector up to the  $4\pi$  spectrometer EUROBALL III [1]. To achieve a total photopeak efficiency substantially larger than 10% for the  $4\pi$  array and to preserve the necessary energy resolution deteriorated by Doppler effects it is necessary to build composite detectors consisting of several Ge crystals. The most advanced designs which have been realized so far are the CLOVER and the CLUSTER detector with four and seven crystals.

The most ambitious composite detector is the SEGMENTED CLOVER detector which is currently being developed in a collaboration with the company Urisys, Strasbourg. It will consist of 4 closely packed coaxial Ge detectors of 14cm (!) length and 7cm diameter each. To further improve the Doppler correction capability the detector elements are segmented radially in quarters. The peak efficiency of the collimated SEGMENTED CLOVER detector has been calculated at 1.33MeV (11.7MeV) to be  $\epsilon_{ph}=0.42$  ( $\epsilon_{ph}=0.11$ ) with a P/T ratio of  $P/T=0.8$  ( $P/T=0.6$ ).

The first prototype element of the SEGMENTED CLOVER detector with a segmented n-type Ge crystal of 67mm diameter and 72mm length has been delivered in spring 1994 by the company Urisys. It has an efficiency at 1.33MeV of  $\epsilon_{ph}=0.169\pm 0.009$  for the full detector and  $\epsilon_{ph}=0.021 \dots 0.030$  for the segments. The peak/total ratio is  $P/T=0.25$  for the sum and  $P/T\approx 0.1$  for the segments. All measured values agree within the experimental errors with corresponding Monte Carlo calculations, which shows the reliability of detector simulations. The energy resolution of the ac-coupled sum signal has been measured to be 2.35keV and ranges from 2.2keV to 2.6keV for the segments. The time resolution of all five signals is better than 6ns.

After solving the main technical obstacle, the segmentation of a n-type Ge detector, the completion of the SEGMENTED CLOVER detector is expected for 1995.

[1] EUROBALL III, ed. J. Gerl and R.M. Lieder, GSI, Darmstadt (1992).

# Performance of CLUSTER Detectors

J. Eberth

Institut für Kernphysik, University of Köln,  
Zùlpicherstraße 77, D-50937 Köln, Germany

and the EUROBALL Collaboration

## Abstract

The performance of a first Germanium CLUSTER detector for EUROBALL III is presented. The detector consists of seven coaxial Ge detectors which are closely packed in a common cryostat and surrounded by a common BGO suppression shield. The individual Ge detectors are hermetically encapsulated in an Aluminum can to achieve reliable operation and easy maintenance of the large detector containing 10 kg of Germanium. A total-absorption efficiency of  $\epsilon_{\text{ph}} = 0.292$ , an energy resolution of  $\Delta E = 2.36$  keV (at 1.3 MeV) and a peak-to-total ratio of  $P/T = 0.61$  has been measured. 15 CLUSTER detectors with  $1\pi$  solid angle and a total-absorption efficiency of  $\geq 4\%$  are being built for EUROBALL III.

## 1. Introduction

The design criteria of the EUROBALL  $4\pi$  Germanium  $\gamma$ -ray detector array has been discussed in detail in previous publications [1,2,]. The most relevant quantities to achieve a low observational limit for the detection of weak  $\gamma$ -rays are the total-absorption efficiency  $\epsilon_{\text{ph}}$  of the Ge detectors and their granularity. The total-absorption efficiency determines the number of gates which can be set on the transitions in a  $\gamma$ -cascade. Each additional gate improves the peak-to-background ratio of the cascade considered by diluting the background in a matrix of a higher dimension and thus improves the observational limit. A high granularity of the detector array is needed to reduce the deterioration of the good intrinsic energy resolution of the Ge detectors by Doppler effects as in most experiments the  $\gamma$ -rays are emitted from fast recoiling nuclei.

Another quantity that has to be considered is the peak-to-total ratio  $P/T$  of the detectors which improves with increasing volume of the detectors. However, as in Ge the Compton effect dominates over the photoeffect for  $E_\gamma > 200$  keV a BGO suppression shield is commonly used to veto the  $\gamma$ -rays scattered out of the Ge detector.

In summary, a large total-absorption efficiency, a high granularity and a good peak-to-total ratio of the detector array is needed to observe a specific weak  $\gamma$ -branch among the many competing decay paths.

The lower curve in Fig. 1 shows the total-absorption efficiency  $P_{\text{ph}}$  as function of the number  $N$  of Ge detectors for the largest n-type detectors available surrounded by individual BGO suppression shields. The curve saturates for  $N > 110$  as the solid angle of

the Ge detectors becomes constant due to the space needed for the BGO shields. Thus, the total-absorption efficiency of a  $4\pi$  array with individually shielded Ge detectors is limited to  $P_{ph} \leq 10\%$ .

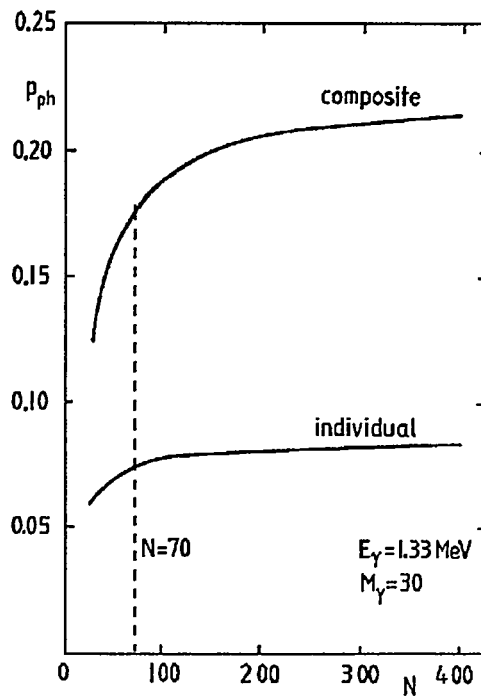


Fig. 1: Total-absorption efficiency  $P_{ph}$  as function of the number  $N$  of detectors

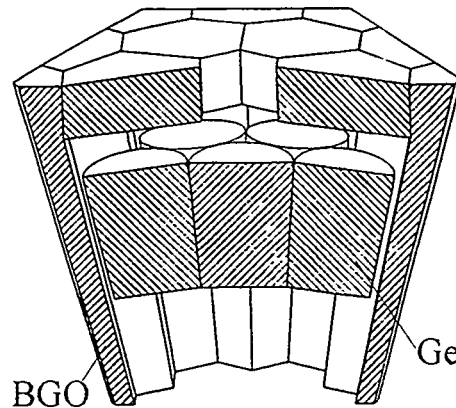


Fig. 2: The principle of the CLUSTER detector

For a further reduction of the observational limit much larger Ge detectors of high granularity are needed. To fulfil these demands with the present Ge technology a very large Ge detector has to be composed of several large coaxial Ge detectors which are closely packed in a common cryostat. This is the basic concept of the CLUSTER detector. An example of the total-absorption efficiency that can be achieved with composite detectors is given by the upper curve of Fig. 1.

## 2 The CLUSTER detector

The basic design of the CLUSTER detector is shown in Fig. 2. It consists of seven hexagonal tapered Ge detectors which are mounted in a common cryostat and surrounded by a BGO suppression shield. By adding all signals of the individual detectors the total-absorption efficiency and the peak-to-total ratio of a very large detector is achieved. The number of detectors in the CLUSTER, their shape and the shape of the BGO shield were optimized by Monte Carlo calculations performed by the Jülich group [1].

The main technical problems in the realization of the CLUSTER detector were expected to arise from the sensitive intrinsic surface of the Ge detectors operated in a common vacuum cryostat. To overcome these problems and to improve the reliability of Ge detectors in general a vacuum-tight encapsulation of the individual Ge detectors has been

developed by a collaboration of the University of Köln, the KFA Jülich and the company Eurisys [3].

## 2.1 The encapsulated Ge detector

A sketch of the encapsulated Ge detector is given in Fig. 3 together with a photograph of the final detector. The capsule is made from Aluminum with a wall thickness of 0.7 mm. It is hermetically sealed by electron welding of all feedthroughs and of the capsule lid. The pocket in the lid of the capsule contains a getter material which keeps the vacuum inside the capsule below  $10^{-6}$  mbar even at annealing temperatures of  $110^{\circ}$  C. A lifetime of 10 years and more including 40 annealings for neutron damage has been estimated for the capsule from quantitative outgassing measurements.

The cold part of the preamplifier is mounted on the capsule lid. Therefore it can be easily exchanged in case of damage or modified for different experimental applications. At the moment we use A.C. coupled preamplifiers to operate the capsule on ground potential. For cooling the capsule is attached by four screws to the cold frame of a cryostat.

The Ge detector shown in Fig. 3 has a length of 78 mm and a diameter of 70 mm at the cylindrical end. The distance of the Ge surface to the inner wall of the capsule is only 0.5 mm which gives a distance of  $\sim 2.5$  mm between the Ge surfaces of two neighboring detectors in the CLUSTER.

39 encapsulated detectors have been delivered since October 1992. The energy resolution varies between 1.88 and 2.3 keV at  $E_{\gamma} = 1.3$  MeV with an average resolution of 2.1 keV. The average resolution at  $E_{\gamma} = 122$  keV is 1.05 keV. The measured total-absorption efficiency varies between 55 and 64 % (relative to a  $3'' \times 3''$  NaJ detector) with an average value of 59%. The detectors are stored at room temperature and cooled down in a test cryostat time by time to control their performance. So far, we could not measure any change of the properties of the detectors.

The new technique of encapsulating Ge detectors seems to be a big step to more reliability and availability which is very important especially for their application in big arrays. The encapsulated detectors can be annealed for neutron damage in a standard furnace. As shown for the prototype detector, 2 hours at  $105^{\circ}$  C is sufficient to restore their original properties [1].

In summary, the encapsulated Ge detectors have excellent properties. They can be handled by the user for all maintenance purposes and exchanged in case of a failure.

## 2.2 Performance of the first CLUSTER detector

The first CLUSTER detector became operational in early 1994. The cryostat was designed and built at the University of Köln. The BGO suppression shield was designed at the KFA Jülich and built by Cyberstar/Crismatec. Fig. 4 shows the technical details. The whole cryostat can be assembled and disassembled by the user. The dewar has an active volume of 11.7 ltr  $\text{LN}_2$  which gives a holding time of 48 hours. The operational temperature of the Ge detectors is 95 - 97 K which from our previous studies [4] we believe is the optimum temperature to account as well for possible shallow electron trapping levels in large n-type crystals as for the influence of hole trapping levels induced by neutrons.

The BGO shield consists of 18 optically separated elements: 12 for the side part and 6 for the back part behind the Ge detectors. The energy resolution measured at 661 keV is

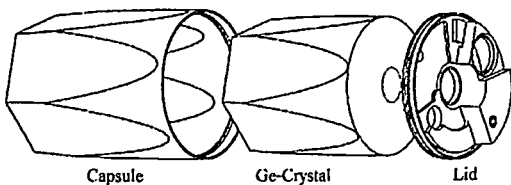
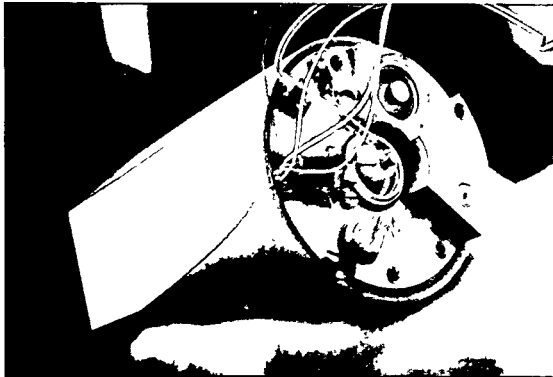


Fig. 3: The encapsulated Ge detector

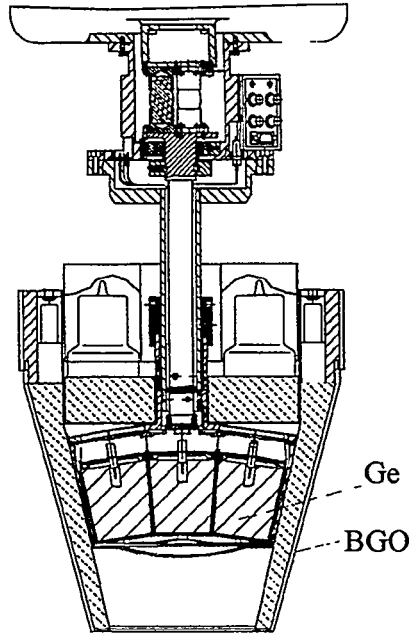


Fig. 4: The CLUSTER detector

< 23 % for the corner crystals, < 20 % for the middle crystals and < 14 % for the back crystals, respectively. All elements show a very low noise of < 6 keV.

The following performance of the first CLUSTER detector was measured with a  $^{60}\text{Co}$  source placed at 43 cm distance to the surface of the Ge detectors (which will be the distance target - detector in EUROBALL):

Energy resolution (in add-back mode)	$\Delta E_\gamma = 2.36 \text{ keV}$	
Total-absorption efficiency	$\epsilon_{\text{ph}} = 0.292$	(0.31 - 0.35)
Add-back factor	1.44	(1.45 - 1.47)
Peak-to-total ratio (threshold 200 keV),		
Ge unsuppressed	P/T = 0.39	(0.40 - 0.44)
suppressed	P/T = 0.61	(0.72 - 0.79)

The numbers given in brackets refer to the various Monte Carlo simulations performed by G. Hebbinghaus, D. Kutchin (KFA Jülich), J. Gerl (GSI) and J. Tain (University of Valencia). While the efficiency, the add-back factor and the peak-to-total ratio of the Ge array agree very well with the prediction of the simulation, the P/T after suppression with the BGO shield seems rather low as compared to the simulation. The energy threshold of the BGO detectors was  $\approx 25 \text{ keV}$ . By better electronics and a lower threshold we hope to improve the suppression by the BGO shield to a P/T value closer to the simulations.

15 Cluster detectors with  $1 \pi$  solid angle will be built in Europe to replace the 15 individually suppressed Ge detectors of EUROGAM II at backward angles and to upgrade EUROGAM II to EUROBALL III. From the results given above it can be estimated that the 15 CLUSTER detectors will have a total-absorption efficiency of  $P_{\text{ph}} \geq$

4 %. A full  $4\pi$  array of 70 CLUSTER detectors would have a total-absorption efficiency of  $P_{ph} \geq 18\%$ . Although it is unlikely to realize such an array in near future, it shows the potentiality of the composite detectors built with encapsulated Ge detectors.

The first in-beam experiments with 1 - 2 CLUSTER detectors will take advantage of the excellent properties of these detectors to study high energy  $\gamma$ -rays. Monte Carlo simulations predict a total-absorption efficiency of  $\epsilon_{ph} = 0.06$  and  $P/T = 0.4$  at  $E_\gamma = 11.7$  MeV which means that the quality of the spectra at 10 MeV should be comparable with the spectra measured at  $E_\gamma = 1$  MeV with conventional Ge detectors. Experiments will include the investigation of highly excited low spin states at the 11 MV - FN-Tandem of the University of Köln and  $(\gamma, \gamma')$  reactions to excite dipole modes in the energy range of 3 - 8 MeV at S-DALINAC in Darmstadt.

Experiments with six CLUSTER detectors will start in summer 1995 at the accelerator of the MPI Heidelberg. The geometry will be optimized to measure nuclear lifetimes and to study proton rich nuclei by neutron- $\gamma\gamma$  coincidences.

All 15 CLUSTER detectors should be available in late 1996. They are contributed by 4 European countries: Germany 8, Italy 4, Sweden 2, U.K. 1. EUROBALL III will commence operation in 1996/97 at Legnaro for a duration of 14 - 16 months before moving to its second site Strasbourg.

### 3 Conclusion

The Ge CLUSTER detector allows to build  $4\pi$   $\gamma$ -ray arrays of high granularity and a total-absorption efficiency of more than 10 %. The results presented for the prototype detector are close to the predictions of the Monte Carlo simulations and fulfil all our expectations. The central point of the CLUSTER development is the encapsulated Ge detector. This new technology improves the reliability of the Ge detectors and reduces the maintenance costs of the EUROBALL array.

As encapsulated Ge detectors can be handled by the user, the same set of detectors can be used for very different experiments in optimized geometry. An example given is the Ge Miniball as proposed by D. Schwalm which will be set up in spring 1995. The Miniball uses the first 42 encapsulated Ge detectors in a tight geometry without BGO suppression shields. In this way, a total-absorption efficiency of  $P_{ph} \approx 20\%$  can be achieved. The Miniball is expected to be an excellent instrument to study exotic decay modes in experiments with low  $\gamma$ -multiplicity and low recoil velocity.

The development of the CLUSTER detector was funded by the German Ministry of Research and Technology under contract No. 06 OK 143 and 06 OK 272I.

#### References:

1. EUROBALL, A European  $\gamma$ -ray facility, Eds. J. Gerl and R.M. Lieder, GSI 1992
2. Development of a composite Ge detector for EUROBALL, J. Eberth et al., Prog.Part. Nucl.Phys., Vol. 28 (1992) 495, Pergamon Press, Oxford
3. The encapsulated Ge detector: A new device for multipurpose application in  $\gamma$ -spectroscopy, J. Eberth, Nuclear Physics News, Vol. 3, No. 3 (1993) 8
4. Neutron induced radiation damage of a n-type Ge detector, Influence of the operating temperature, H.G. Thomas et al., NIM A332 (1993) 215

## PAIRING CORRELATIONS AND SUPERDEFORMATION

H. Flocard<sup>a)</sup>, P. Bonche<sup>b)</sup>, P.H. Heenen<sup>c)</sup>, R. Mehrem<sup>d)</sup> M.S. Weiss<sup>d)</sup>

a) *Division de Physique Théorique<sup>1</sup>, I.P.N., F91406 Orsay Cedex, France*

b) *DSM-SPhT, CEN Saclay, 91191 Gif sur Yvette Cedex, France*

c) *Physique Nucléaire Théorique, U.L.B., CP229, 1050 Brussels, Belgium*

d) *Physics Division, LLNL, Livermore 91450CA, USA*

The notion of effective force is central to microscopic studies of nuclear structure. Although the results of Brueckner-Hartree-Fock calculations have helped infer some characteristics of these forces, it is the comparison of results of HF, HF+BCS and HFB calculations with data which has provided the most useful criteria for a definition of the effective interactions that we are now using. It turns out that the most important advances have concerned the interaction in the particle-hole (p-h) channel. They have led to the construction of forces of various analytic structures which allow an accurate reproduction of a large body of data from the p-shell to the actinides. Most microscopic calculations are still performed with these well established forces, such as the Skyrme force in its SIII or SkM\*<sup>1)</sup> (or other) parametrizations or the D1S<sup>2)</sup> version of the Gogny force. For a study of the superdeformation properties of moderately neutron deficient nuclei, these old p-h interactions should be adequate at least at the first stage of the analysis.

The situation is not as favorable as far as the interaction in the particle-particle channel (p-p) is concerned. Before the availability of arrays of gamma detectors, and the blooming of high-spin physics, data related to this component of the force was limited. It concerned only global properties and indicated that the p-p force was especially important in the  $S=0$ ,  $T=1$  spin-isospin channel and was short ranged. Data also gave information on the magnitude of pairing matrix elements averaged over a major shell. In fact, for ground state properties, rather satisfactory results can be obtained with an interaction as schematic as the seniority force which assumes orbital-independent strengths. On the other hand, presently available data on high-spin behavior of a large number of rotational bands is very sensitive to orbital occupation. It therefore provides a deeper insight on the multipole structure of the p-p force. Moreover, because the surface-to-volume ratio is very much increased in superdeformed states compared to ground state configurations, one should be able to investigate the density dependence of the interaction whether in its p-h or its p-p channel. Nuclear matter calculations suggest that the effective force in the pairing channel is strongest when the density is about half the saturation density<sup>3,4,5)</sup>. This and other experimental evidences concerning the odd-even staggering of the radius isotope shifts justify that one look in more detail at the yet poorly known density dependence of the p-p force. In this communication, I will present some related results from our programme of investigation of the high-spin properties of SD nuclei.

The Hamiltonian  $H$  used in this work includes a kinetic energy term and an effective interaction. The p-h component of this interaction is provided by the SkM\* parametrization of the Skyrme force. Its p-p component is either generated by a seniority force or by a zero-range density dependent force. We then look for mean-field solutions in a frame rotating with constant angular velocity  $\omega$  around a fixed axis (for us the  $z$  axis). The problem reduces to the minimization of the total routhian:

$$\mathcal{H}^\omega = \langle H - \hbar\omega J_z - \mu N \rangle \quad (1)$$

---

<sup>1</sup>Unité de Recherches des Universités Paris VI et Paris XI, associée au C.N.R.S.



Because we want to study the effect of pairing correlations, the expectation value which defines  $\mathcal{H}^\omega$  is minimized within the space of BCS states and we must impose a constraint  $\mu N$  insuring that the BCS state will on the average have the correct number of particles

The HFB approximation induces two sorts of symmetry breaking. For the first which concerns quadrupole deformation and the associated phenomenon of collective rotation, the mean-field approximation is well justified at the high-spins we are considering here. It is another matter for the symmetry breaking related with the non conservation of particle number. While at zero spin, the nucleon number dispersion is large enough to justify the use of HFB for nuclear ground states, at large angular momenta, the Coriolis field destroys pairs and generates a restoration of the broken symmetry at the mean-field level. In the HFB approximation, the wave-function degenerates into a Slater determinant so that all the correlations due to the p-p component of the force become neglected. To remedy this deficiency which can affect adversely the evaluation of fine properties related to rotation, we have used the Lipkin-Nogami prescription for approximating the variation after projection method<sup>(6,5)</sup>. In it, the total Routhian is redefined as

$$\mathcal{H}^\omega = \langle H - \hbar\omega J_z - \mu N \rangle - \lambda_2 \langle \Delta N^2 \rangle \quad (2)$$

where the added term contains the square of the particle number deviation  $\Delta N = N - \langle N \rangle$ . For a given pairing force, this correction increases the correlations compared to HFB. As a result the strength of the p-p interaction must be diminished by about 10-15% if one is to still achieve a correct description of ground states properties. Another physical consequence of the use of the LN method is the disappearance of the spurious phase transitions found by HFB calculations.

The region of  $^{152}\text{Dy}$  with its two  $N=86$  and  $Z=66$  SD shell effects was the first where superdeformation was observed. However, at low spins, even for  $^{152}\text{Dy}$ , the shell stabilization of SD shapes and the Coulomb repulsion are not sufficient to overcome the increase of the surface energy. This phenomenon is visible on our results (fig. 1). At  $\langle J_z \rangle = 0$ , the HFBCS deformation energy curve only displays a shoulder near a value of the quadrupole moment  $Q_0 = 40b$ . This curve and all the HFB results concerning nuclei of the  $A = 150$  region have been obtained with the SkM\* force for the p-h channel. For the p-p component of the effective interaction, we have used a seniority interaction adjusted to reproduce average qp energies at ground state as they can be deduced from the mass table. Not until spin  $\langle J_z \rangle = 24\hbar$  does the barrier between the first and SD wells reach 1MeV. Only at  $\langle J_z \rangle = 36\hbar$ , the barrier becomes larger than 2MeV. This result is in good agreement with data concerning the decay of the SD bands. For the angular momentum  $\langle J_z \rangle = 36\hbar$ , our energy curve extends to deformations for which a hyperdeformed (HD) well is expected. A shoulder is indeed observed in the deformation energy curve around 65b. Calculations (not shown on fig. 1) at  $\langle J_z \rangle = 60\hbar$  do not find a deeper HD well. However, before drawing definite conclusions concerning the existence of HD bands as predicted by the SkM\* interaction, two effects must be investigated. First as we will discuss below, the pairing associated with the seniority force as we have defined it is probably too large at high spins. In order to evaluate how this could affect the HD well depth, we are presently performing cranked HF calculations at  $\langle J_z \rangle = 60\hbar$ . Another effect worth considering is that of static octupole deformations not taken into account in the present calculation and which, for such large elongations, may also play an important role.

On fig.2, we have plotted the evolution of the dynamical moment of inertia versus  $\hbar\omega$  for the two nuclei  $^{152}\text{Dy}$  and  $^{150}\text{Gd}$ . Although both  $\mathcal{J}_2$  are decreasing, the slope is much larger for  $^{150}\text{Gd}$ . This result is in agreement with data. The decomposition between neutron

and proton shows that is due to contributions from both species. It is a self-consistency effect : the decrease of  $Z$  induces a diminution of the deformation which in turn modifies the neutron Fermi sea. This can be understood from the proton HFB-Nilsson spectrum in which the proton SD shell effect appears at a smaller deformation for  $Z = 64$  than for  $Z = 66$ . As a result, in  $^{150}\text{Gd}$  at small angular momenta, the intruder level  $7_2\nu$  lies above the Fermi surface. As  $\hbar\omega$  increases it drops under it. Its occupation varies therefore much more than in  $^{152}\text{Dy}$  where it is always within the Fermi sea.

From the consideration of the routhian spectrum of  $^{150}\text{Gd}$  it appears favorable to define bands in  $^{151}\text{Tb}$  by the creation of qp's based on the  $6_3$  and  $6_4$  proton orbitals. On the other hand, the qp routhian spectrum of  $^{150}\text{Gd}$  suggests that at high spins, one considers also the qp associated with the orbital  $[301]s=-$ . Finally a fourth band can be built on the  $[301]s=+$  qp. In fact nine bands have been observed, the first four of which fit rather well this assignment pattern. Fig. 3 presents our results for the first three bands calculated with and without pairing correlations. Because of the high spin value, a decrease of the pairing strength leads to a *lower* moment of inertia. This is a direct consequence of the definition of the second moment of inertia (it would not be so for the first moment). Whether pairing is present or not, we find that  $\mathcal{J}_2$  decreases faster for the ground SD band than for the excited bands. In the HFB case we have checked this behavior down to  $\hbar\omega = .35\text{MeV}$ . The HF results are in even better agreement with data. This is evidence that a seniority force adjusted at ground state and used with the Lipkin-Nogami prescription gives too large pairing correlations. At  $\hbar\omega = .645\text{MeV}$  the HF calculation predicts that the band built by emptying the  $[301]s=-$  routhian (and therefore filling both  $6_3$  and  $6_4$  orbitals) is excited by about  $0.6\text{MeV}$  while the band obtained by a transfer of a particle from the  $6_3$  to the  $6_4$  has an excitation energy near  $0.9\text{MeV}$ . We have also found that the band with the  $[301]s=-$  orbital empty calculated without pairing correlations has the same dynamical moment of inertia as the ground state band of  $^{152}\text{Dy}$ . All these results fit well with experimental findings.

Let us now come to our investigation of the effect of the analytic structure of the pairing interaction on moment of inertia. In order to have a better sensitivity and to connect with zero spin pairing properties, we have chosen  $^{194}\text{Pb}$  because pairing is believed to play a more important role in the SD properties of nuclei of the  $A = 190$  region. We recall that the calculations for rare-earth nuclei have been done with a seniority force adjusted on properties at zero spin. This involves some arbitrariness in the choice of the relative neutron and proton intensities since the  $T_z$  behaviour of the p-p force is poorly known. Using a force eliminates this problem as one can make use of the isospin symmetry (as done for instance with the Gogny force). It also suppresses the need for an explicit  $N, Z$  parametrization of the strengths. Finally it allows an investigation of the multipole structure of pairing matrix elements.

We have first studied a zero-range force, because despite its simplicity, it possesses those odd-multipole components believed to be important when time-reversal is broken. We have chosen a parametrization which includes a density dependence.

$$V_P = \frac{V_0}{2}(1 - P_\sigma)\delta(\vec{r}_1 - \vec{r}_2)(1 - \alpha\rho(\frac{\vec{r}_1 + \vec{r}_2}{2})) \quad (3)$$

The spin exchange operator is denoted  $P_\sigma$ ;  $V_0$  and  $\alpha$  are two parameters. A quantity not shown in (3) is the active space cutoff playing the role of the finite range in the Gogny force. This cutoff is in fact tied to the intensity  $V_0$ . Here, it was chosen  $5\text{ MeV}$  above the Fermi surface. For  $\alpha = 0$ , (3) is a delta force acting over the entire volume of the nucleus. On the

other hand, when  $\alpha$  is taken equal to the inverse of the saturation density, one has a purely surface active force. In the calculation of  $^{194}\text{Pb}$  we have tested four forces ; All four were adjusted to reproduce the experimental second moment of inertia at small spins. One is the seniority force used in our general analysis of the even nuclei of the region<sup>8)</sup>. Another one is a simple delta force ( $V_0 = 250\text{MeV}\cdot\text{fm}^{-3}$ ,  $\alpha = 0$ ). In addition we have considered a purely surface active force ( $V_0 = 880\text{MeV}\cdot\text{fm}^{-3}$ ,  $\alpha = 1./16\text{fm}^3$ ) and a force repulsive inside the nucleus while attractive at the surface ( $V_0 = 1400\text{MeV}\cdot\text{fm}^{-3}$ ,  $\alpha = 1./14\text{fm}^3$ ).

The results are shown in figure 4. The volume-active delta force gives results very similar to those obtained with the seniority interaction. Therefore it does not seem that the odd multipole components it contains, modify significantly the average slope of the moment of inertia when the overall strength is such that the low spin value of  $\mathcal{J}_2$  is correctly reproduced. On the other hand, our results show that the density dependence of the p-p channel affects significantly the slope of the moment of inertia versus  $\omega$ . A peaking of the force at the surface gives a better agreement with data. Not apparent from this curve is an important variation of the proton versus neutron pairing as the action of the pairing force is shifted from volume to surface. In particular the proton pairing is significantly reduced for a surface active force. Of course, these calculations must be extended to other nuclei (odd and even) of this SD region. We also plan to test the same forces in other nuclei at SD deformations and near ground state.

#### Acknowledgements

This work was supported in part by the contract PAI-P3-043 of the Belgian Office for Scientific Policy. Work supported in part under the auspices of the US Department of Energy by Lawrence Livermore National Laboratory under Engineering Contract W-7405-ENG-48.

#### References

- 1) M. Beiner et al., Nucl. Phys. **A236** (1975) 29, J. Bartel et al. Nucl. Phys. **A386** (1982) 79
- 2) D. Cogne in Nuclear self-consistent fields, eds. G. Ripka and M. Porneuf (North-Holland, Amsterdam, 1975) p.333; JF. Berger et al. Nucl. Phys. **A428** (1984) 23c
- 3) H. Kucharek et al, Phys. Lett. **B216** (1989) 249.
- 4) G.F. Bertsch et al. Ann. Phys. (N.Y.) **209** (1991) 327
- 5) S. Takahara et al. peprint U. Tokyo-Komaba (1994)
- 6) P. Ring and P. Schuck, "The Nuclear Many-Body Problem" Springer-Verlag (1980)
- 7) H.J. Lipkin, Ann. Phys. (N.Y.) **9** (1960) 272; Y. Nogami, Phys. Rev. **134** (1964) B313; H.C. Pradhan et al. Nucl. Phys. **201** (1973) 357
- 8) B. Gall et al. Zeit. Phys. A (1994) in print.

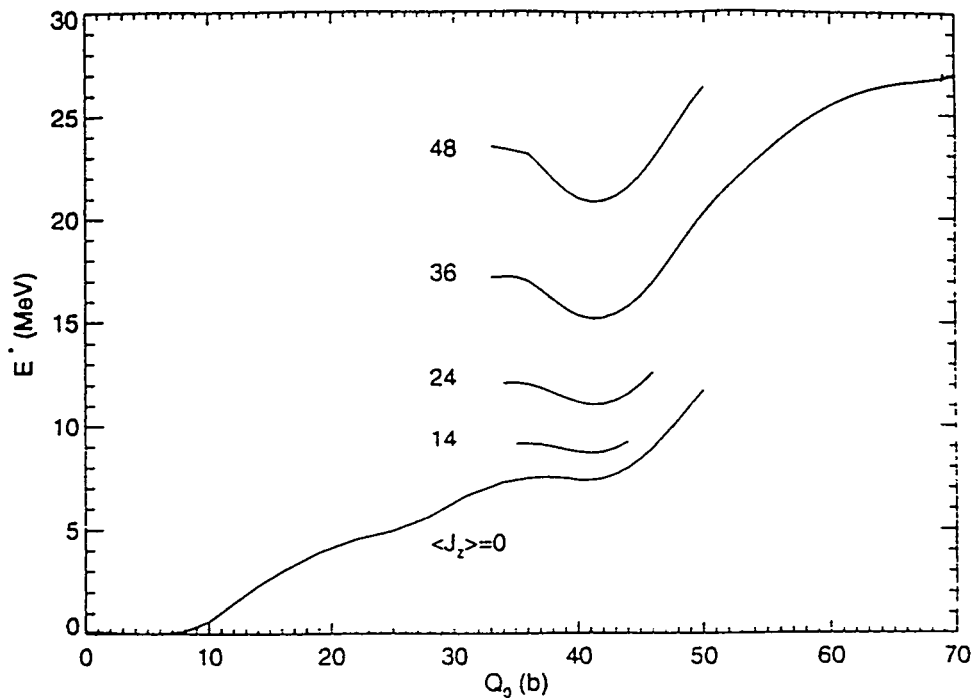


Figure 1 HFB deformation energy curves of  $^{152}\text{Dy}$  for different values of the average angular momentum  $\langle J_z \rangle$  as a function of the total quadrupole moment  $Q_0$  in barn.

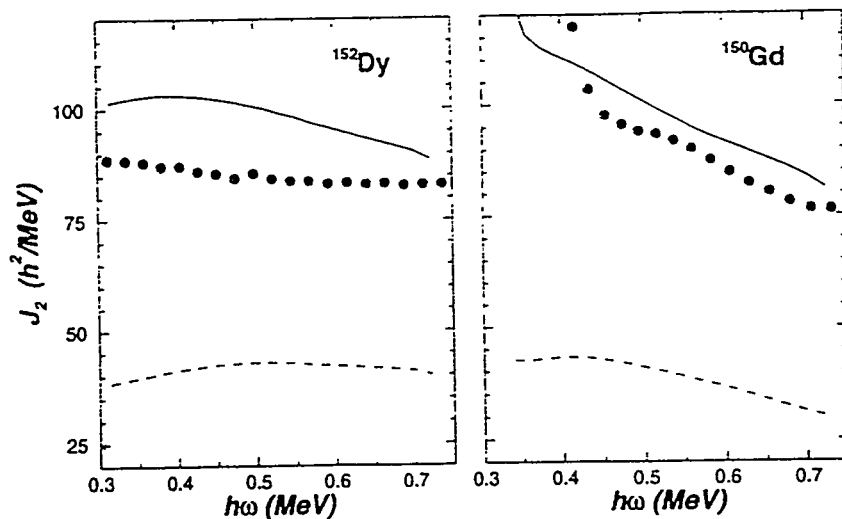
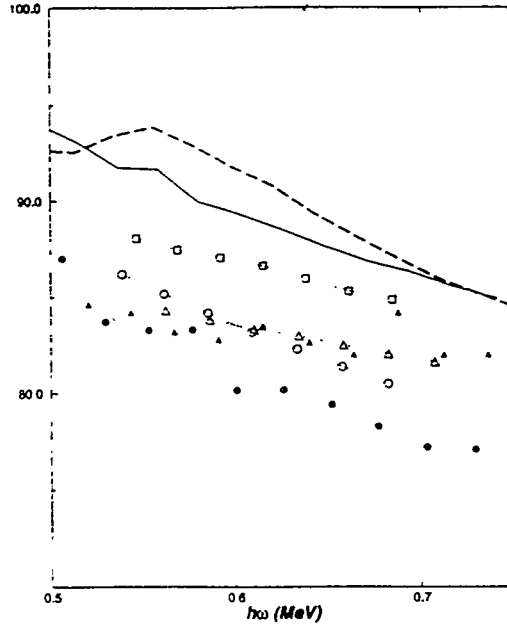
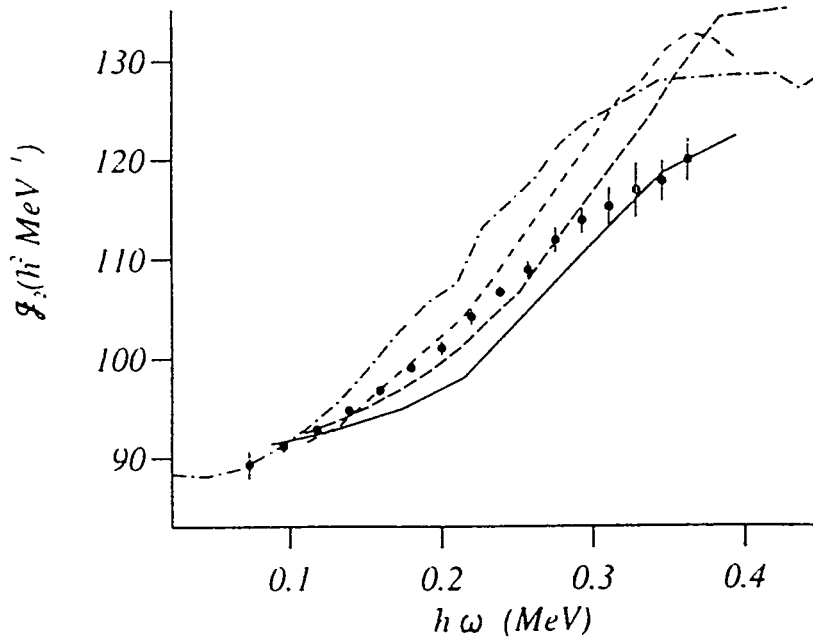


Figure 2 Evolution of the HFB calculated dynamical moment of inertia of the ground SD bands of the nuclei  $^{152}\text{Dy}$  (left) and  $^{150}\text{Gd}$  (right) (calculation: solid lines ; data: solid dots). The dashed and dotted curves give respectively the neutron and proton contribution to the moment of inertia.



**Figure 3** Evolution of the HFB calculated moment of inertia of the three lowest bands of  $^{151}\text{Tb}$ . The solid dots and triangles give the data for the first two bands. The empty dots, triangles and squares give the HF results (The markers correspond to values of  $\langle J_z \rangle$  spaced by  $2\hbar$  with an arbitrary choice for the  $\langle J_z \rangle$  origin.). The solid and dashed lines show the HFB results of the bands with orbitals  $6_4$  and  $6_3$  emptied respectively. For the ordering of the calculated bands, see text.



**Figure 4** Dynamical moment of inertia of  $^{194}\text{Pb}$ . The solid dots show the data. The dot-dashed, dashed and solid lines give our results obtained with the seniority, the volume-active and the two surface-active interactions respectively.

# MOMENTS OF INERTIA AND IDENTICAL BANDS: A SENSITIVE PROBE TO PAIRING CORRELATIONS AT SUPER-DEFORMED SHAPE \*

W. Satuła<sup>(a),(b)</sup> and R. Wyss<sup>(a)</sup>

<sup>(a)</sup>*The Royal Institute of Technology, Physics Department Frescati,  
Frescativägen 24, S-104 05 Stockholm, Sweden*

<sup>(b)</sup>*Institute of Theoretical Physics, University of Warsaw,  
ul. Hoza 69, PL-00 681 Warsaw, Poland*

(October 30, 1994)

The moments of inertia of super-deformed odd and odd-odd nuclei in the Hg-Pb region are investigated. Special emphasis is put on the identical band problem. Deformation and pairing effects are treated self-consistently by means of the cranked Strutinsky Lipkin-Nogami approach, that has been extended to include a quadrupole pairing interaction. It is shown that the double stretched quadrupole pairing force is dominated by the time odd component. The blocking effect is considerably weakened due to the simultaneous decrease of the  $\Delta_{21}$  field.

PACS numbers : 21.10.Re, 21.60.Jz, 21.60.Ev, 27.80+w

The experimental study of super-deformation in the mass  $A=190$  region revealed several interesting features that challenged the theoretical understanding of the nuclear many body problem. A common feature of the dynamical moments of inertia ( $\mathcal{J}^{(2)} \equiv \frac{dI_x}{d\omega}$ ) is (i) a smooth increase with frequency<sup>1</sup> (ii) essentially no difference for neighbouring nuclei, i.e. a multitude of identical bands (iii) vanishing blocking effects.

These phenomena are linked in the sense that the moments of inertia are identical not for a given constant value but in their correlated increase with frequency. Hence, to address only one of the issues raised above is not satisfactory. In other words, a comprehensive understanding of the identical bands problem in this mass region requires a rather accurate quantitative understanding of the moments of inertia.

Qualitatively, the rise in  $\mathcal{J}^{(2)}$  is understood in terms of a gradual alignment of  $j_{15/2}$  neutrons and  $i_{13/2}$  protons in the presence of pairing correlations [1,2]. However, quantitatively, the agreement between calculations and experiment was not accurate enough to address the above mentioned problems. The variation of the calculated  $\mathcal{J}^{(2)}$  with neutron and proton number e.g., were much too large as compared to experiment.

Previous calculations either treated pairing selfconsistently but kept deformation fix, or were deformation self consistent but invoked an approximative pairing interaction [2]. Hence, our first attempt to more accurately describe the moments of inertia was to calculate both pairing and deformation selfconsistently on a lattice in deformation space. Our model hamiltonian is based on the deformed mean field, given by a Woods-Saxon potential [3] with the Chepurnov parameters. [4] The total routhian  $E^\omega$ , is obtained via the Strutinsky shell correction method.

$$E^\omega(Z, N, \hat{\beta}) = E^{\omega=0}(Z, N, \hat{\beta}) + \left[ \langle \hat{H}^\omega(Z, N, \hat{\beta}) \rangle - \langle \hat{H}^{\omega=0}(Z, N, \hat{\beta}) \rangle \right] \quad (1)$$

Here,  $E^{\omega=0}(Z, N, \hat{\beta})$  represents the liquid drop energy of ref. [5] or [6], the single-particle shell correction defined by the Strutinsky averaging procedure, [7] and the pairing energy at zero frequency. The term in the bracket of eq. (1) corresponds to the change in energy due to rotation (for details see [8]).

---

\*talk presented by R. Wyss

<sup>1</sup>A small number of bands exhibits irregularities or are flat. They will be discussed separately and merely confirm the above observations

We employed an approximative particle number projection before variation by means of the Lipkin-Nogami approach. This method reduces the particle number fluctuation  $\langle \Delta N^2 \rangle$  by minimizing an operator up to second order,  $\mathcal{H} = \hat{H}^\omega - \lambda_2(\hat{N}^2 - \langle \hat{N} \rangle^2)$ , with  $\lambda_2$  calculated using certain subsidiary conditions [9]. The resulting Lipkin-Nogami equations (LNC) in the intrinsic frame of reference (cranking model) can be cast into the standard form of the cranked Hartree-Fock-Bogolyubov equations (for details we refer the reader to [10-12]). In these calculations the total routhian surface (TRS) is minimized with respect to deformation parameters  $\beta_2$ ,  $\beta_1$  and  $\gamma$  at each frequency, the chemical potential  $\lambda$ , the pairing gap  $\Delta$  and  $\lambda_2$  being determined selfconsistently. The results of these pairing and deformation self consistent calculations improved the agreement with experiment, but deficiencies were still present, especially in the low frequency regim [11,13].

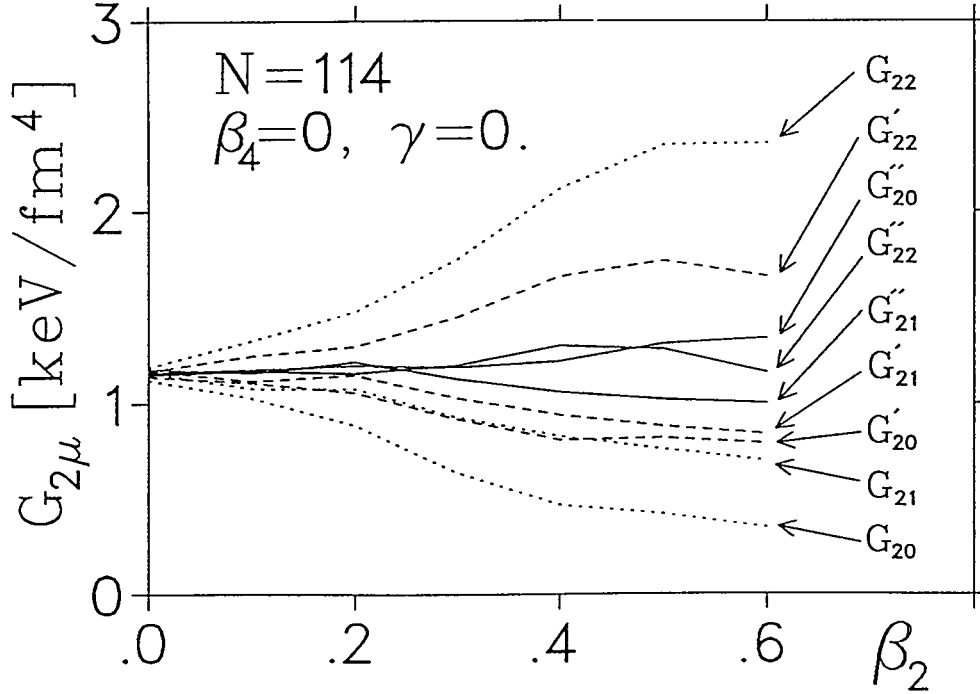


FIG. 1. The deformation dependence of the selfconsistent strength  $G_{2\mu}$  for three different kind of QQ-pairing interactions: non-stretched, stretched (') and the presently used version of double stretched('').

In the next step, we extended the pairing force to include all components of quadrupole type, which implies the presence of the time odd component,  $Q_{21}$ . Already early investigations by Migdal [14] showed the importance of the time odd part of the pairing interaction with respect to the moments of inertia (the Migdal term). These ideas were further developed by the work of Belyev. [15] Quite recently it was also suggested with in the frame work of a simple model, that the  $K = 1^+$  part of the pairing might be of importance for the moments of inertia in the SD Hg-Pb region. [16]

The two body part of our hamiltonian is then specified by antisymmetrized matrix elements of the monopole and quadrupole pairing interaction ( $\tilde{\beta} \equiv \hat{T}\beta$  denotes time-reversed state).

$$\bar{v}_{\alpha\beta\gamma\delta}^{(\lambda\mu)} = -G_{\lambda\mu} g_{\alpha\tilde{\beta}}^{(\lambda\mu)} g_{\gamma\tilde{\delta}}^{*(\lambda\mu)} \quad (2)$$

$$g_{\alpha\tilde{\beta}}^{(\lambda\mu)} = \begin{cases} \delta_{\alpha\tilde{\beta}} & \lambda = 0, \quad \mu = 0 \\ \langle \alpha | \tilde{Q}_\mu | \tilde{\beta} \rangle, & \lambda = 2, \quad \mu = 0, 1, 2 \end{cases} \quad (3)$$

In our model we use the double stretched quadrupole-quadrupole (QQ) pairing interaction. It has been demonstrated by Kishimoto and Sakamoto that effective interactions in the particle-hole channel can be realized in general by means of double-stretched operators [17]. Hence, the natural extension to the QQ-pairing force also invokes double-stretched operators ( $Q''_\mu = \tau''^2 Y''_{2\mu}$ ):

$$\begin{aligned}\tilde{Q}_0 &= Q''_{20}, \\ \tilde{Q}_\mu &= \frac{1}{\sqrt{2}}(Q''_\mu + Q''_{-\mu}), \quad \mu = 1, 2.\end{aligned}\quad (4)$$

The strength of the quadrupole pairing force stems from the requirement of restoring the local galilean invariance of the system under  $\lambda$ -pole collective shape oscillations [18]. The monopole pairing strength  $G_{00}$  is determined by the average gap method of Ref. [19]. Since the strength of the quadrupole pairing interaction  $G_{2\mu}$  corresponds to the self-consistent coupling constants of [18], our approach does not involve any adjustable strength parameters. Note also that all three strength parameters  $G_{2\mu}$  are calculated within the concept of self consistency.

The use of double-stretched quadrupole operators has pronounced advantages compared to previous calculations with a QQ-pairing force. In fig. 1, the selfconsistent strength parameters for three different versions of the quadrupole pairing force are depicted. In case of the double stretched interaction, the coupling constants of the pairing strength are essentially equal by analogy to the spherical case,  $G_{20} \approx G_{21} \approx G_{22}$ , and almost independent of deformation. This is not at all the case for the stretched or non stretched pairing interaction, which both show spurious deformation dependence. This is a sever problem when performing calculations on a lattice, where deformation is changing.

A further advantage lies in the fact that the modification of qp levels calculated at  $\hbar\omega = 0$  MeV is less than 100 keV, irrespectively of deformation. This effect is demonstrated in Table 1, where we show the relative shifts of the qp energies of high-j orbitals calculated for SD  $^{194}\text{Hg}$  using the different versions of QQ-pairing. In the cases of non-stretched and stretched QQ-pairing forces (these are the versions used so far in the literature<sup>2</sup> [20,21]) these shifts are large and contain pronounced, spurious deformation dependence. In order to incorporate these shifts, the single particle energies of the deformed field would have to be readjusted. In previous applications, all orbitals with positive quadrupole moment in a prolate deformed nucleus (especially those with low- $\Omega$  and high-j) were shifted up [20,21]. On the other hand, within the double-stretched pairing force, the average quadrupole moment is close to zero, and  $\Delta_{20}$  might be either positive or negative. For example  $\Delta_{20}$  of neutrons in SD  $^{194}\text{Hg}$  is negative implying that the  $\nu j_{15/2}$  orbital is pushed down in energy (cf table 1).

orbital	non stretched	stretched	double-stretched
$\nu j_{15/2}$	+1286 keV	+538 keV	-43 keV
$\pi i_{13/2}$	+1324 keV	+634 keV	+5 keV

Table1: The relative shift of the quasi-particle energies of the high-j orbitals  $j_{15/2}$  (neutrons),  $i_{13/2}$  (protons) in the presence of different kinds of quadrupole pairing interaction (non-stretched, stretched and double-stretched). The shift stems essentially from the  $Q_{20}$  component of the force. The calculations were done for the nucleus  $^{194}\text{Hg}$  at a representative deformation of the SD band ( $\beta_2 = 0.480$ ,  $\beta_4 = 0.072$ ;  $\gamma = 0^\circ$ ).

The type of residual interaction in the particle-particle channel is connected with the fundamental question of how to construct residual interactions on top of the deformed mean field. It seems that only the double stretched QQ-pairing interaction is in agreement with the mean field concept. It further solves the long standing problem of how to determine the strength and radial form factor. The time odd component of the force emerges as the most important quite naturally, since the commonly strong  $\Delta_{20}$  field now is rather weak.

In a survey of the super-deformed even-even nuclei in the mass  $A=190$  region within the concept of our extended TRS-model we presented results, which for the first time quantitatively agreed with the data over the entire frequency range. A new role of the time odd component was demonstrated, in that it smoothes out the previously present isotonic and isotopic difference in  $\mathcal{J}^{(2)}$ . [22]

A striking features of the rotational bands at super-deformed shape is the similarity of the moments of inertia, in that e.g. the bands of  $^{191,193}\text{Hg}$  are identical to those of  $^{192,194}\text{Hg}$ , the two quasi-particle

<sup>2</sup>In fact in [20] no radial form-factor at all was taken into account



(2qp) band of  $^{194}\text{Hg}$  identical to  $^{192}\text{Hg}$  etc. [23,24] According to common wisdom, one expects a substantial increase in the moment of inertia in odd nuclei because of the well known blocking effect, that reduces superfluidity and hence increases  $\mathcal{J}^{(2)}$ . [25] What is observed in super-deformed nuclei is nothing the like, since  $\mathcal{J}^{(2)}$  doesn't change when going from an even to an odd system. Even when going to an odd-odd nucleus, the change is almost negligible small. Hence, in the present work we extend our calculations to odd and odd-odd nuclei where the state of the odd particle is blocked self consistently, see e.g. [11,26]. Since the calculations are performed on a grid in deformation space, the blocked configuration may change adiabatically. Hence, we focused on cases where the configuration of the odd particle remains essentially unchanged. For the neutrons, it implies that we do not block the  $j_{15/2}$  orbital, which contributes in a major way to the angular momentum gain. This orbital crosses other orbitals of negative parity and then we are not able to construct a 'adiabatic' surface. In the subsequent calculations, we block only orbitals of positive parity, corresponding to a multitude of the observed bands.

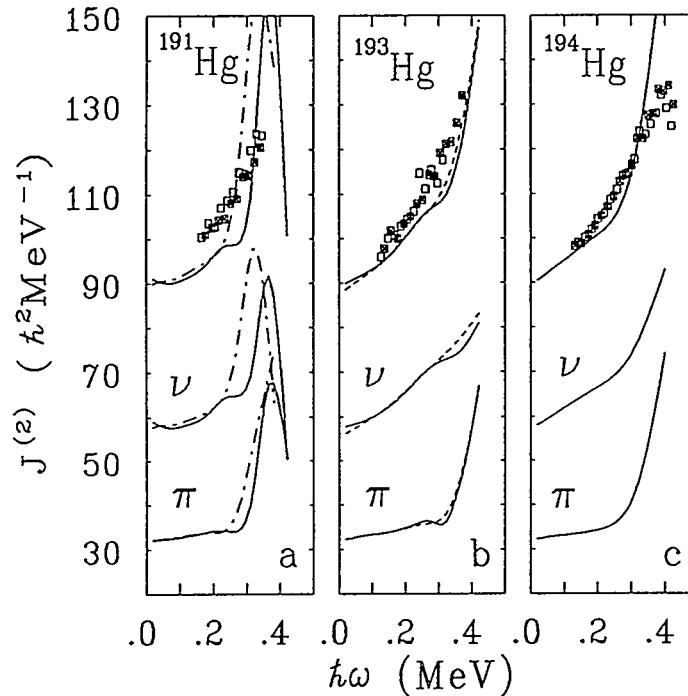


FIG. 2. Comparison of calculated (solid line:(+,+1/2), dashed (+,-1/2)) and experimental ( $\square$ ,  $\circ$ )  $\mathcal{J}^{(2)}$  moments of inertia of  $^{191}\text{Hg}$ ,  $^{193}\text{Hg}$  and the 2qp band of  $^{191}\text{Hg}$ . Proton and neutron contributions are depicted separately. In the case of  $^{194}\text{Hg}$ , the configurations (+,+1/2) and (+,-1/2) were blocked (solid line).

Starting with the Hg-isotones we find indeed that blocking has little effect for the evolution of the moments of inertia (Fig. 2). Our calculations nicely account for the behavior of  $^{191}\text{Hg}$  and  $^{193}\text{Hg}$ , as well as for the 2qp-band in  $^{194}\text{Hg}$ . Only in  $^{191}\text{Hg}$ , the onset of the neutron  $j_{15/2}$  alignment is somewhat too early related to a similar behavior for the N=110 core nuclei [22]. Note that the rather sharp rise for protons and neutrons is related to a sudden shrinking of the nucleus, yielding this enhanced alignment effect. Note also that in all cases the low frequency part of  $\mathcal{J}^{(2)}$  is very well reproduced. At very high frequencies, in the regime of vanishing pairing correlations, our method becomes less accurate. [10] We find mainly two causes for the weak blocking effect: (i) the monopole pairing gap is not very pronounced at super-deformed shape (ii) the influence of the time odd  $\Delta_{21}$  field. The first item has been discussed in connection with the observation of super-deformation in the Hg-nuclei [27], see also [1]. We find the monopole pairing gaps of the order of 0.7-0.8 MeV. For blocked configurations, these values are reduced by  $\approx 15\%$ . The second item emerges from our inclusion of QQ-pairing. Our calculations yield that a substantial part of the monotonous increase

of  $\mathcal{J}^{(2)}$  arises from the  $\Delta_{21}$  component of the pairing field. The  $\Delta_{21}$  field acts extremely coherently over the entire frequency range and contributes to  $\mathcal{J}^{(2)}$  in a collective manner. In the case of an odd nucleus, the reduced monopole pairing gap leads to a reduction of the  $\Delta_{21}$  component, thus counterbalancing the expected increase of  $\mathcal{J}^{(2)}$ . The two effects nearly cancel resulting in almost identical bands for odd and even nuclei. This effect is perhaps most pronounced in the 2qp band of  $^{194}\text{Hg}$  (Fig. 2c), where the calculated  $\mathcal{J}^{(2)}$  for neutrons still exhibit a smooth increase, although monopole pairing is substantially reduced (by  $\approx 35\%$ ).

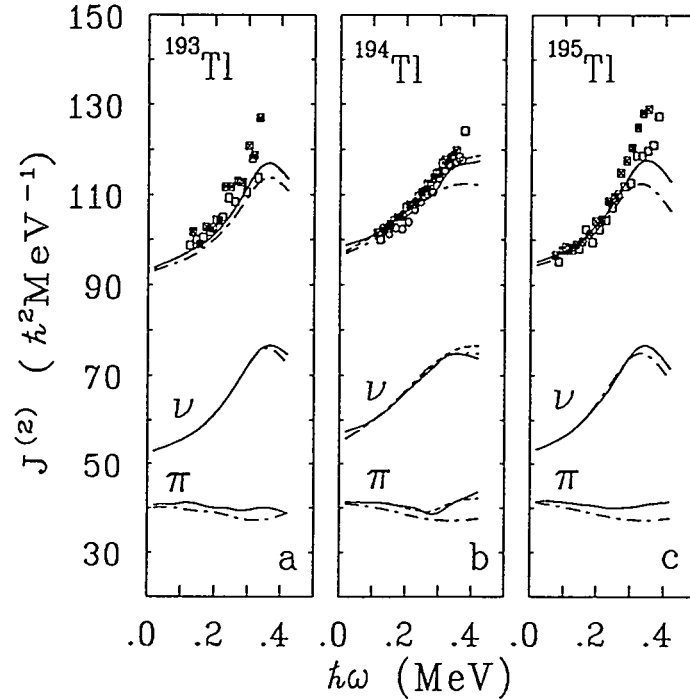


FIG. 3. Comparison of calculated (solid line:  $(+, +1/2)$ , dash-dotted:  $(+, -1/2)$ ) and experimental ( $\square$ ,  $\boxtimes$  and  $\circ$ )  $\mathcal{J}^{(2)}$  moments of inertia of  $^{193}\text{Tl}$ ,  $^{194}\text{Tl}$  and  $^{195}\text{Tl}$ . In the case of  $^{194}\text{Tl}$ , the neutron  $(+, +1/2)$  (solid and dash-dotted line) and  $(+, -1/2)$  configuration was blocked (dashed line).

To further pursue the effect of blocking we also investigate the odd proton nuclei,  $^{193-195}\text{Tl}$  (Fig. 3). Again, the agreement between experiment and theory is amazingly good. As visible, the odd proton does not contribute sizeable to the increase in  $\mathcal{J}^{(2)}$ , which is dominated by the neutron contribution, mainly coming from the  $j_{15/2}$  orbital. (Hence, it is not astonishing, that blocking the  $j_{15/2}$  neutron orbital might result in a flat moment of inertia). Note also the very weak effect of double blocking in the case of the odd-odd  $^{194}\text{Tl}$ . The differences in  $\mathcal{J}^{(2)}$  for the different signatures of the proton  $[651]3/2$  ( $i_{13/2}$ ) orbital reflects the slightly larger alignment gain of the favoured signature. On the other hand, no difference is found for the two signatures of the neutron high  $\Omega$   $[624]9/2$  orbitals (Fig. 2b,3b).

A direct comparison of the blocking effect is demonstrated for the pairs of  $^{193}\text{Hg}$ ,  $^{194}\text{Hg}$  and  $^{196}\text{Pb}$ ,  $^{195}\text{Tl}$ , i.e. the one neutron and proton hole, respectively (Fig. 4a,b). Blocking the odd neutron results in a slightly enhanced  $\mathcal{J}^{(2)}$  for neutrons. On the other hand, due to the reduced  $\Delta_{21}$  field, the neutron increase with frequency is smaller in the odd than in the even case and hence the moments of inertia converge. The effect is somewhat stronger in the calculations than in experiment, but a small difference in  $\mathcal{J}^{(2)}$  is visible at low frequency. The same effect is more pronounced in the case of the odd proton, where the agreement to experiment is even better. The blocked protons have an essentially flat moment of inertia, compared to the smoothly increasing part of the even proton system. The difference at the highest frequencies is a result of different shape evolution. Our obtained agreement in the present set of calculations allows us to address the questions of the spins.

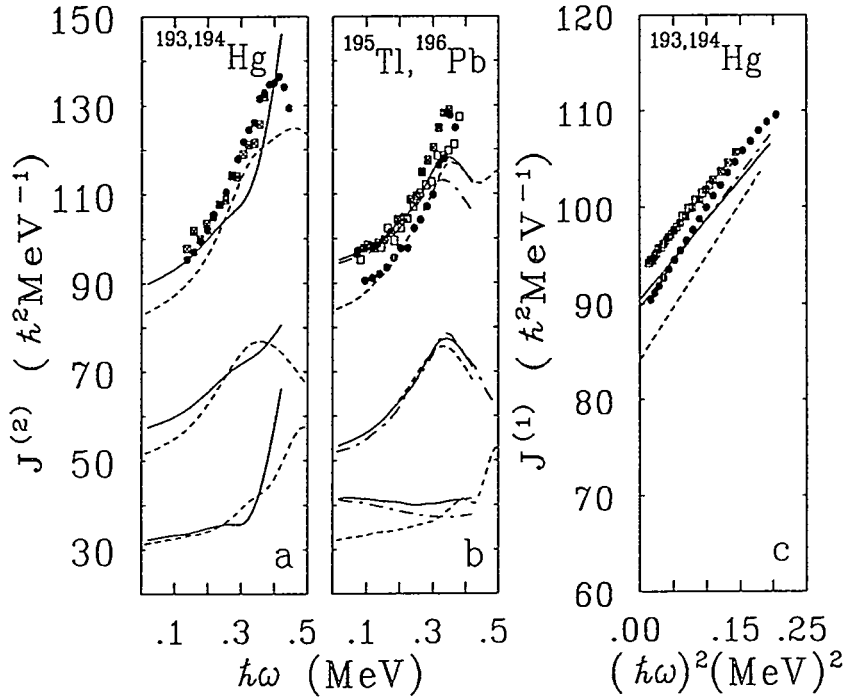


FIG. 4. Comparison of calculated and experimental dynamical  $J^{(2)}$  moments of inertia for even (stretched line -  $\bullet$ ) and odd nuclei (solid - dash-dotted -  $\square$ ,  $\boxtimes$ ). c) The  $J^{(1)}$  moment of inertia of  $^{193}\text{Hg}$  and  $^{194}\text{Hg}$ .

Since the decay out of the second well is unobserved, spins have not been measured. On the other hand, one can make a fit to the spins based on the Harris expansion. [28] Such a fit lead to the remarkable result that most of the odd nuclei exhibit an alignment of  $1\hbar$  (see the discussion in [23,24]). This is equivalent to having quantized rotational frequencies. In fig. 4c, we present calculated kinematical moments of inertia ( $\mathcal{J}^1 \equiv \frac{I_x}{\hbar\omega}$ ) versus  $(\hbar\omega)^2$ . The calculated  $\mathcal{J}^{(1)}$  is somewhat smaller than the experimental values, corresponding to roughly  $1/2\hbar$  in angular momentum. Both experiment and calculations, however, reveal the same trend: The odd nucleus has a larger initial moment of inertia (at  $\hbar\omega = 0\text{MeV}$ ). This effect results from blocking. (The value at frequency zero corresponds to  $J_0$  in the Harris expansion of  $I_x$ , the slope corresponding  $J_1$ .) On the other hand, the increase with frequency is smaller for odd nuclei, originating from the reduced  $\Delta_{21}$ . Integrating the low frequency difference in  $\mathcal{J}^{(2)}$  yields  $\approx 1 - 1.5\hbar$  difference in angular momentum between odd and even nuclei. Hence the presence of spin differences or alignment seem not to be surprising. A more detailed discussion is beyond the scope of the present work and will be done elsewhere.

We have extended our calculations to cover odd and odd-odd nuclei in the SD Hg-Pb region. We find only the double stretched QQ-pairing interaction to be in agreement with the concept of residual interactions and the deformed mean field. Within the double stretched QQ pairing interaction the time odd component emerges as the most important in a natural manner. Since the  $\Delta_{21}$  field acts extremely coherently, it smears out the isotonic and isotopic differences that are present in models without this force. The time odd component further reduces the blocking effect. Our extended TRS-model appears as a powerful tool in the analysis of the rotational bands in the second well. The physics of super-deformation indicate that the rotational energies in a restricted region of the nuclear chart are invariant with respect to change in particle number. In what respect this invariance is reflected by the symmetries of our residual interactions and the deformed field is under investigation.

This work is supported by the Göran Gustavson foundation, the Polish State Committee for Scientific Research (contract 20450 91 01) and the Swedish Natural Science Research Council (NFR).

- [1] M.A. Riley, et.al., Nucl. Phys. A512 (1990) 178.
- [2] R.V.F. Janssens and T.L. Khoo, Ann. Rev. Nucl. Part. Sci. 41 (1991) 321.
- [3] S. Cwiok, J. Dudek, W. Nazarewicz, J. Skalski and T. Werner, Comp. Phys. Comm. 46 (1987) 379.
- [4] V.A. Chepurinov, Yad. Fiz. 6 (1967) 955.
- [5] S. Cohen, F. Plasil and W.J. Swiatecki, Ann. Phys. (NY) 82 (1974) 557.
- [6] H.J. Krappe, J.R. Nix and A.J. Sierk, Phys. Rev. C20 (1979) 992.
- [7] V.M. Strutinsky, Yad. Fiz. 3 (1966) 614; Nucl. Phys. A95 (1967) 420.
- [8] W. Nazarewicz, R. Wyss and A. Johnsson, Nucl. Phys. A503 (1989) 285.
- [9] H.C. Pradhan, Y. Nogami and J. Law, Nucl. Phys. A201 (1973) 357.
- [10] P. Magierski, S. Cwiok, J. Dobaczewski and W. Nazarewicz, Phys. Rev. C47 (1993) 2418.
- [11] W. Satuła, R. Wyss and P. Magierski, Nucl. Phys. A578(1994)45 .
- [12] B. Gall, P. Bonche, J. Dobaczewski, H. Flocard and P.-H. Heenen, Z. Phys. A348 (1994) 183.
- [13] B. Cederwall, et.al. Phys. Rev. Lett. 72 (1994) 3150.
- [14] A.B. Migdal, Nucl. Phys. 13(1959) 655.
- [15] S.T. Beliaev, Nucl. Phys. A24 (1961) 322.
- [16] I. Hamamoto and W. Nazarewicz, Phys. Rev. C49 (1994) 2489.
- [17] H. Sakamoto and T. Kishimoto, Nucl. Phys. A501 (1989) 205.
- [18] H. Sakamoto and T. Kishimoto, Phys. Lett. 245B (1990) 321.
- [19] P. Möller and R. Nix, Nucl. Phys. A536 (1992) 20.
- [20] M. Wakai, A. Faessler, Nucl. Phys. A295 (1978) 86.
- [21] M. Diebel, Nucl. Phys. A419 (1984) 221.
- [22] W. Satuła and R. Wyss, Phys. Rev. C (1994), in press.
- [23] F.S. Stephens, et. al., Phys. Rev. Lett. 64, 2623 (1990).
- [24] F.S. Stephens, et. al., Phys. Rev. Lett. 65, 301 (1990).
- [25] A. Bohr and B.R. Mottelson, Nuclear Structure, vol. 2 (W.A. Benjamin, New York, 1975).
- [26] H.J. Mang, Phys. Rep. 18C (1975) 327.
- [27] D. Ye, et.al., Phys. Rev. C41 (1990) R13.
- [28] J.A. Becker, et.al. Phys. Rev. C41 (1990) R9.

# Alignments of Multi-quasiparticle Bands and Seniority-Dependent Reduced Pairing

G.D. Dracoulis

*Department of Nuclear Physics, Research School of Physical Sciences and Engineering, The Australian National University, Canberra ACT 0200, Australia*

*Pairing correlations in multi-quasiparticle states in deformed nuclei are expected to be reduced because of blocking. New intrinsic states and their associated rotational bands have been identified allowing comparisons to be made as a function of seniority and between nuclei. The possible effects of the reduced pairing on the collective rotation, and its manifestation in terms of alignment, are discussed*

Recent measurements [1–3] which exploit time-correlated  $\gamma$ – $\gamma$ - coincidence studies are producing a comprehensive map of the excitation energies and properties of states formed by combining individual nucleon orbits close to the Fermi surface. Proton subshell gaps near  $Z = 66$  and  $Z = 76$ , and neutron subshell gaps at  $N = 98$  and  $N = 108$  result in the effective isolation of the intervening groups of orbitals particularly in the case of the neutrons. High-K states obtained by the summation of the projections,  $\Omega_i$  of a number of nucleons, compete with collective rotation of low-seniority configurations as a means of carrying angular momentum. At the same time, however, blocking of the pairing correlations should affect the collective rotation in the high-seniority states themselves.

The dramatic effect on the pairing is illustrated in figure 1, for the case of  $^{177}\text{Ta}$ , recently reported by Dasgupta *et al* [2]. The lower panel shows their comparison of observed excitation energies of multi-quasiparticle states, many of them long-lived isomers, with the results of quasiparticle calculations, which treat the Fermi and pairing energies self-consistently [3, 4] and which include particle-number conservation [5]. (The small open symbols connected by lines show for comparison, how the excitation energies are *overestimated* if a simple summation of 1-quasiparticle energies is used, without due regard to the further reduction of pairing and the related change of Fermi level as the seniority increases.) The upper panel shows the calculated neutron and proton correlation energies  $\Delta_n$  and  $\Delta_p$  for each of the observed states. For most of the 5-quasiparticle states, which are assigned configurations of  $\pi^3\nu^2$  the proton pairing is close to zero while the neutron pairing is reduced to  $\sim 200$  keV. The two cases where the proton pairing persists are associated with  $\pi^1\nu^4$  configurations. For the 7-quasiparticle states ( $\pi^3\nu^4$ ) both neutron and proton pairing should have been quenched. While such calculations are known to produce a spuriously abrupt loss of pairing [6] significant effects might yet be expected.

The decay of high spin isomers such as the  $200\mu\text{s}$ ,  $49/2^-$  state in  $^{177}\text{Ta}$  is preferentially through other high-K states, and importantly through the rotational bands based on them. This information and the related "prompt" spectroscopic data in which these and other bands are extended to higher spins opens the prospect of examining the rotational behaviour as a function of both configuration, and of reduced pairing. The focus in high-spin studies, both theoretical and experimental, has

often been on the reduction of pairing induced by rotation [7], while configuration-dependent pairing reduction has been considered mainly to explain differences in band-crossing frequencies in certain 1-quasiparticle cases [8], essentially through the dependence of the *energies* of the excited bands on pairing.

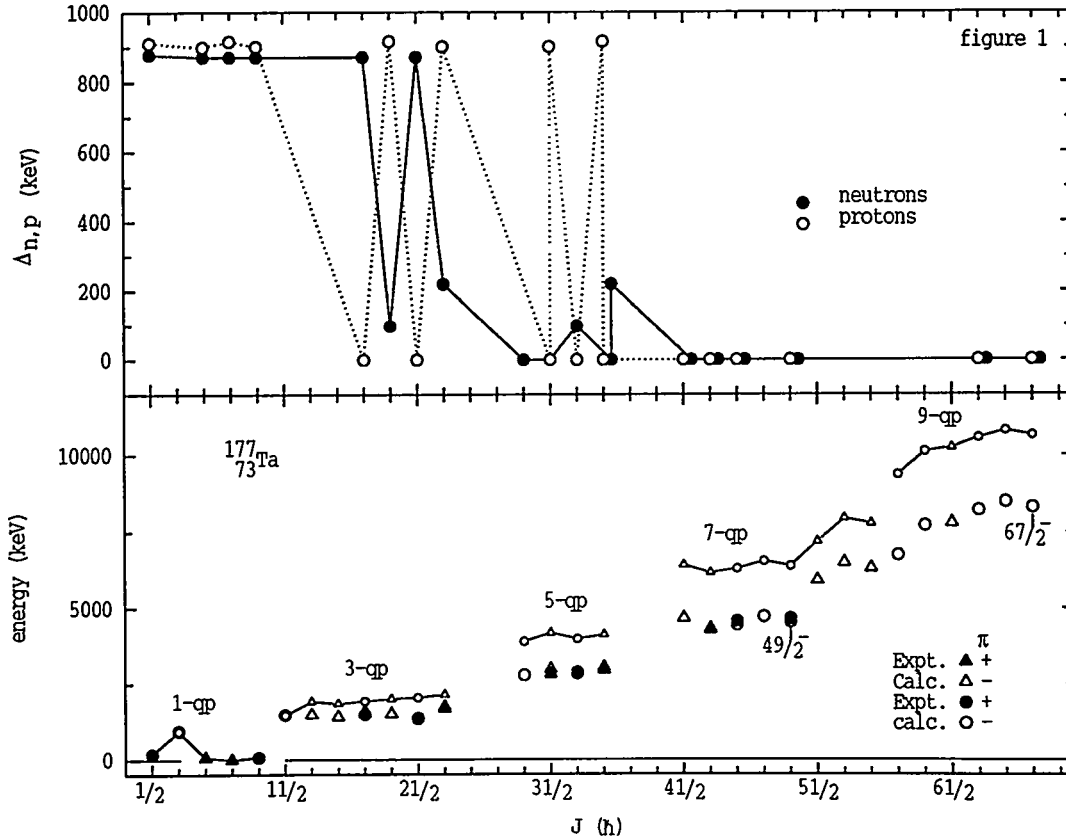


Figure 1: Comparison of observed and calculated multi-quasiparticle excitation energies in  $^{177}\text{Ta}$  ref [2] and the proton and neutron pairing in each state (upper panel).

As well as new results for  $^{177}\text{Ta}$ , the group at the ANU is engaged in a systematic study of other tantalum isotopes including  $^{175}\text{Ta}$ ,  $^{176}\text{Ta}$ ,  $^{178}\text{Ta}$  and  $^{179}\text{Ta}$  [9]. Complementary results are already known for multi-quasiparticle states in  $^{179}\text{W}$  [1], including rotational bands based on 5- and 7-quasiparticle states. Very recently new studies [10] of  $^{178}\text{W}$ , which were guided by predictions of calculations similar to those carried out for  $^{177}\text{Ta}$ , but with the inclusion of empirical residual,  $p-p$ ,  $n-n$  and  $p-n$  interactions [11] have found a number of multi-quasiparticle states, including an extensive rotational band based on an 8-quasiparticle yrast trap ( $\pi^4\nu^4$ ). Within each of these nuclei there are related multi-quasiparticle states whose configuration can be identified, or constrained, by the in-band properties, such as the  $M1/E2$  branching ratios which, These depend on the magnetic properties and to first order at least, allow one to count the proportion of participating protons and neutrons. As well, since many configurations involve one or two of the  $i_{13/2}$  neutrons ( $7/2^+[633]$  and  $9/2^+[624]$ ) and the  $h_{9/2}$  proton ( $1/2^-[541]$ ) which are strongly Coriolis-mixed,

examination of the alignments can be used as a signature of the component configurations. (See ref [1] for an evaluation of the  $^{179}\text{W}$  cases, where the presence of one or more  $i_{13/2}$  neutrons or the  $h_{9/2}$  proton is apparent, almost by inspection. ) The same rotational properties should also be a probe of the loss of pairing and its effect on the collective motion. Does the motion indeed tend towards "rigidity", through the loss of pairing correlations? How will that be manifested, and what effect is there on the high-j particles ?

Figure 2 shows the alignments calculated using particle-rotor band-mixing in a very simple model, which might be illustrative. Since in a realistic multi-particle case the subset of orbitals ( $\Omega = 1/2\dots 9/2$ ) from the  $h_{9/2}$  proton would be coupled to a high-K core (see ref[12]) for related calculations), there will be no decoupling parameter or diagonal contribution because the Coriolis operator cannot connect +K with -K components in the symmetrised wave function if K is large. The results have therefore been calculated with the decoupling parameter set to zero and with the Fermi level placed below the  $\Omega = 1/2^-$  orbital, in the  $h_{9/2}$  case and between the  $\Omega = 7/2^+$  and  $9/2^+$  orbitals for the  $i_{13/2}$  neutron, as expected for the nuclei in this region.

The results are shown in the form of the *apparent* alignment for the lowest sequence of states from diagonalisation of the Coriolis matrix, as a function of an arbitrary reduction of the proton pairing (with the neutron pairing fixed) and vice versa. The moments-of-inertia of the *unperturbed* bands built on each orbital have been increased as the pairing is reduced using the prescription of Migdal [13] with the proton and neutron contributions separated, so that

$$\mathfrak{S}_{tot} = \frac{N}{A}\mathfrak{S}_n(\Delta_n) + \frac{Z}{A}\mathfrak{S}_p(\Delta_p)$$

and

$$\mathfrak{S}_{p,n} = \mathfrak{S}_{rig}\left(1 - \frac{\ln(x\sqrt{1+x^2})}{x\sqrt{1+x^2}}\right)$$

with

$$x = \delta \frac{\hbar\omega_0}{2\Delta_{p,n}}$$

The reduction of pairing affects the mixing (which gives rise to the alignment) through (i) the change in quasiparticle energies of the orbitals, (ii) the occupation probabilities which are factors in the off-diagonal matrix elements (iii) the unperturbed moments-of-inertia, which as they increase towards the rigid body value, will reduce the off-diagonal matrix elements. The *apparent* alignments were deduced by subtracting from the final mixed states, a common reference;

$$i = I_x(\omega) - (\mathfrak{S}_0\omega + \mathfrak{S}_1\omega^3)_{ref.}$$

with  $\mathfrak{S}_0 = 30 \text{ MeV}^{-1}\hbar^2$ , the value that would be used for the "full" pairing ( $\Delta_n = 0.998 \text{ MeV}$  and  $\Delta_p = 0.915 \text{ MeV}$ ) as in the 1-quasiparticle alignments.

The implication of figure 2, therefore, is that if the pairing did fall, the *apparent* alignment could increase. If one were to use the *correct* reference, whose value in

general would not be known, but in the calculation at least, should be equal to the unperturbed moments-of-inertia that are the input to the band-mixing calculations, the real alignment would be revealed. That is shown for the proton case with  $\Delta_p = 0.092$  MeV, where the alignment is seen to be small at very low frequency, and rise with frequency to reach a value similar to that for the full pairing case. That the alignment persists despite the low pairing is consistent with the fact that the Coriolis effects are still large when the Fermi level is near the  $\Omega = 1/2$  orbital. For the  $i_{13/2}$  neutron case where the Fermi level is near mid-shell, the *apparent* alignment increases and has a more positive slope than the proton case, as the pairing is reduced, but the *real* alignment (as shown for  $\Delta_n = 0.053$  MeV) is very low, over the whole frequency range.

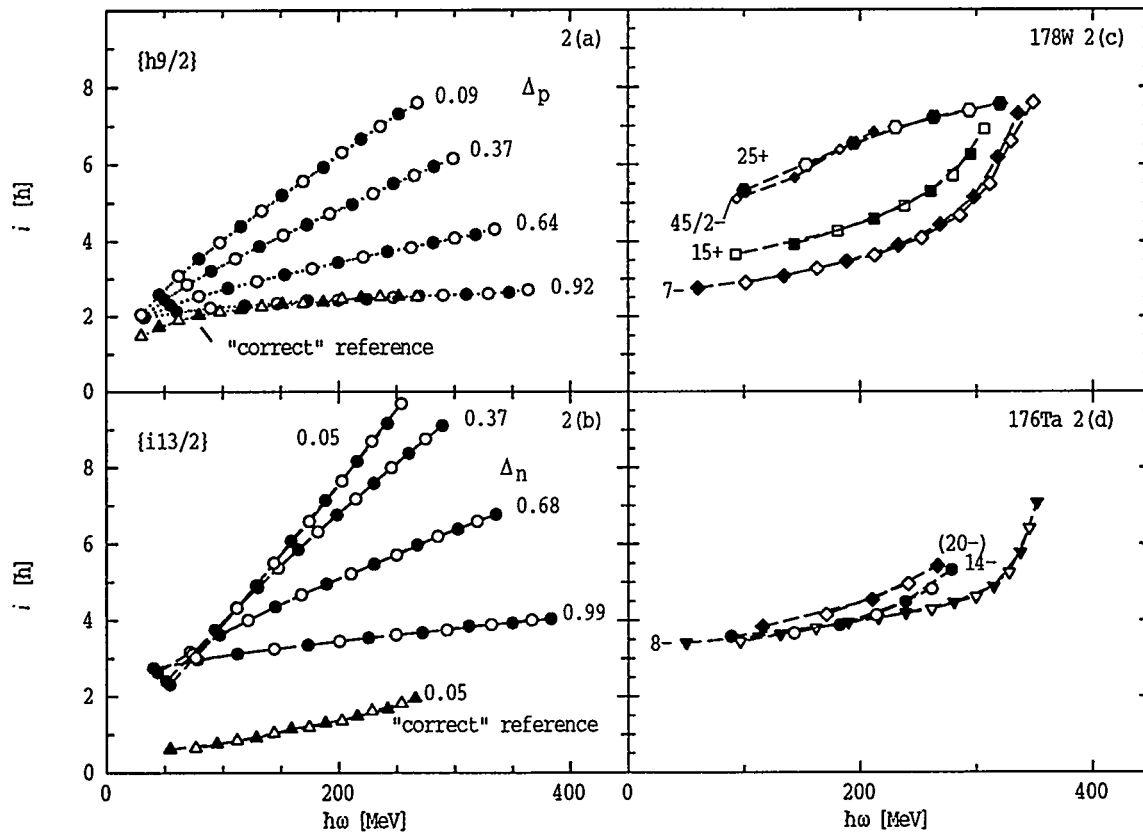


Figure 2: predicted alignments as a function of pairing for (a) the set of proton  $h_{9/2}$  orbitals (b) the set of neutron  $i_{13/2}$  orbitals, in an extreme model (see text); (c) observed alignments for bands in  $^{178}\text{W}$  and  $^{179}\text{W}$  [9,10,1]; (d) selected 2, 4 and 6 quasiparticle rotational bands in  $^{176}\text{Ta}$  [9]. All rotational frequencies have been determined taking  $K = \text{bandhead spin}$ .

In contrast to the expectation that the large changes in pairing with seniority would have severe effects, examination of states which have related configurations but in which the pairing is predicted to be very different, suggests that approximate additivity of alignment is obtained in some cases. For example, new bands found



[8] in  $^{176}\text{Ta}$  based on  $K^\pi = 8^-, 14^-$  and  $(20^-)$  intrinsic of seniority, 2, 4 and 6, have been assigned the configurations

$$\begin{aligned} \pi 9/2^- [514] \otimes \nu 7/2^+ [633] &= 8^-, \\ \pi 9/2^- [514], 5/2^+ [402], 7/2^+ [404] \otimes \nu 7/2^+ [633] &= 14^-, \\ \pi 9/2^- [514], 5/2^+ [402], 7/2^+ [404] \otimes \nu 7/2^+ [633] 7/2^- [514] 5/2^- [512] &= 20^-. \end{aligned}$$

The proton pairing should be much smaller in the  $14^-$  state than in the  $8^-$  band, and both proton and neutron pairing would have been quenched in the 6-quasiparticle  $20^-$  state. The alignments however are very similar (reflecting the presence of one  $i_{13/2}$  neutron), the small differences being largely attributable to the small contributions from the additional particles. Similar conclusions are reached in comparisons between nuclei, and for example in  $^{178}\text{W}$ , even for the new [10]  $25^+$  8-quasiparticle state, as shown in figure 2. As shown, its alignment is essentially identical to that for the  $^{179}\text{W}$   $45/2^-$  band [1] from which it can be formed by the addition of a  $5/2^-$  neutron.

Of course, there remain subtle differences between these and other cases, with respect to both absolute magnitude and frequency dependence, and further analyses are required before reaching conclusions regarding the quenching of pairing and its effect on the collective rotation. A consistent recipe for treating a number of particles outside a core in particle-rotor calculations is also required. Nevertheless, the growing suite of experimentally observed multi-quasiparticle states, with associated rotational bands holds promise for unravelling the single-particle and collective effects.

*The results presented here are drawn from work in progress, and I am grateful to my colleagues for making the results available, and for continuing discussions.*

## References

- [1] P.M. Walker *et al.*, Nucl. Phys. **A568**(1994) 397.
- [2] M. Dasgupta *et al.*, Phys. Lett. **B328**(1994)16 and to be published
- [3] M. Dasgupta *et al.*, contribution to this Conference
- [4] B. Fabricius *et al.*, Int. Conf. on Fut. of Nucl. Spectr., Crete (June 1993)
- [5] J.Y. Zeng and T.S. Cheng, Nucl. Phys. **A405** (1983) 1.
- [6] H.J. Mang, J.K. Poggenburg, J.O Rasmussen Nucl. Phys. **64** (1965) 353.
- [7] Y.R. Shimizu *et al* Rev. Mod. Phys. **61**(1989)131
- [8] J.Y. Zeng, T.S. Cheng, L. Cheng and C.S. Wu Nucl. Phys. **A411** (1983) 49.
- [9] F.G. Kondev *et al*, to be published
- [10] P.M. Walker *et al.*; C Purry *et al.* , to be published
- [11] K. Jain, G.D. Dracoulis, B. Fabricius, N. Rowley and P.M. Walker SCNP-94/6,
- [12] G.D. Dracoulis and P.M. Walker, Nucl. Phys. **A330** (1979) 186 ; Nucl. Phys. **A342** (1980) 335
- [13] A.B. Migdal , Nucl. Phys. **13** (1959) 655.

# Superdeformation in Odd-A Pb

L.P. Farris,<sup>1</sup> E.A. Henry,<sup>1</sup> J.A. Becker,<sup>1</sup> M.J. Brinkman,<sup>1\*</sup> B. Cederwall,<sup>2</sup>  
J.A. Cizewski,<sup>5</sup> M.A. Deleplanque,<sup>2</sup> R.M. Diamond,<sup>2</sup> J.E. Draper,<sup>3</sup> C. Duyar,<sup>3</sup>  
P. Fallon,<sup>2</sup> J.R. Hughes,<sup>1</sup> W.H. Kelly,<sup>4</sup> I.Y. Lee,<sup>2</sup> A.O. Macchiavelli,<sup>2</sup>  
E.C. Rubel,<sup>3</sup> F.S. Stephens,<sup>2</sup> M.A. Stoyer,<sup>1†</sup> and D.T. Vo<sup>4</sup>

<sup>1</sup>Lawrence Livermore National Laboratory, Livermore, CA 94551

<sup>2</sup>Lawrence Berkeley Laboratory, Berkeley, CA 94720

<sup>3</sup>University of California, Davis, CA 95616

<sup>4</sup>Iowa State University, Ames, IA 50010

<sup>5</sup>Rutgers University, New Brunswick, NJ 08901

## 1 Introduction

We report here the observation of four superdeformed (SD) bands in  $^{195}\text{Pb}$ , the first time superdeformation has been identified in an odd- $A$  Pb nucleus. It is also the first time that SD bands with constant dynamic moments of inertia ( $\mathcal{J}^{(2)}$ ) have been observed in an odd- $A$  nucleus in the  $A \approx 190$  region[1]. SD bands have been reported and extensively investigated in experimental studies of the even- $A$  Pb nuclei,  $^{192,194,196,198}\text{Pb}$  and in the isotones of  $^{195}\text{Pb}$ , namely  $^{193}\text{Hg}$  and  $^{194}\text{Tl}$ [2]. Despite previous extensive searches for SD states in odd- $A$  Pb nuclei, none had been identified. However, there appeared to be no theoretical reason why they should not support superdeformation. The observation of SD bands in odd- $A$  Pb would allow us to extend the systematics of SD in Pb and to observe the effects of Pauli blocking and of specific neutron quasiparticle orbitals on SD rotational properties.

Four new SD bands have been observed in  $^{195}\text{Pb}$  using GAMMASPHERE. Two of these bands have  $\mathcal{J}^{(2)}$  values that are approximately constant with  $\hbar\omega$ , and we propose that they are built upon the favored and unfavored signatures of the  $N = 7$  neutron intruder orbital. The other two bands have  $\mathcal{J}^{(2)}$  values that are similar to that of the yrast SD band in  $^{194}\text{Pb}$ , and are proposed to be signature partners built upon the deformation aligned  $\nu[624]9/2$  orbital. In addition, two bands have been observed in  $^{193}\text{Pb}$  that also have approximately constant  $\mathcal{J}^{(2)}$ 's. The details of that study will be provided in another report[3].

## 2 Experiment

Both the  $^{195}\text{Pb}$  and  $^{193}\text{Pb}$  experimental studies were performed at the Lawrence Berkeley Laboratory 88-Inch Cyclotron, with the early implementation configuration of GAMMASPHERE (29 Compton-suppressed,  $\sim 75\%$  efficient Germanium detectors for  $^{195}\text{Pb}$ , and 36 detectors for  $^{193}\text{Pb}$ ). The  $^{195}\text{Pb}$  nuclei were produced with the reaction  $^{174}\text{Yb}(^{26}\text{Mg}, 5n)$  at a beam energy of 130 MeV. The  $^{193}\text{Pb}$  data set was obtained using the  $^{174}\text{Yb}(^{24}\text{Mg}, 5n)$  reaction at a beam energy of 131 MeV. For both experiments, the target was a stack of three  $500 \mu\text{g}/\text{cm}^2$  thick foils. The data sets comprised  $4 \times 10^8$  events for  $^{195}\text{Pb}$  and  $5 \times 10^8$  for  $^{193}\text{Pb}$ , with a coincidence requirement of three or more "clean"  $\gamma$  rays. Doppler shift corrections were made on-line during the data accumulation.  $^{152}\text{Eu}$  and  $^{56}\text{Co}$  sources were counted to obtain information on the ADC non-linearity and the detector singles efficiency in the energy region of interest. The energies of previously known low-lying transitions in  $^{195}\text{Pb}$  [4, 5] were obtained to within 0.1 keV with the resulting energy calibration.

## 3 Data and Results

Four new SD bands have been identified in  $^{195}\text{Pb}$  (Fig. 1). The spectra display the typical behavior of SD bands in the  $A \approx 190$  region. The  $\gamma$ -ray transitions are regularly spaced in energy, with  $\Delta E_\gamma \approx 40$  keV at the bottom of the bands. As can be seen in Fig. 1, the 162-, 203- and 244-keV

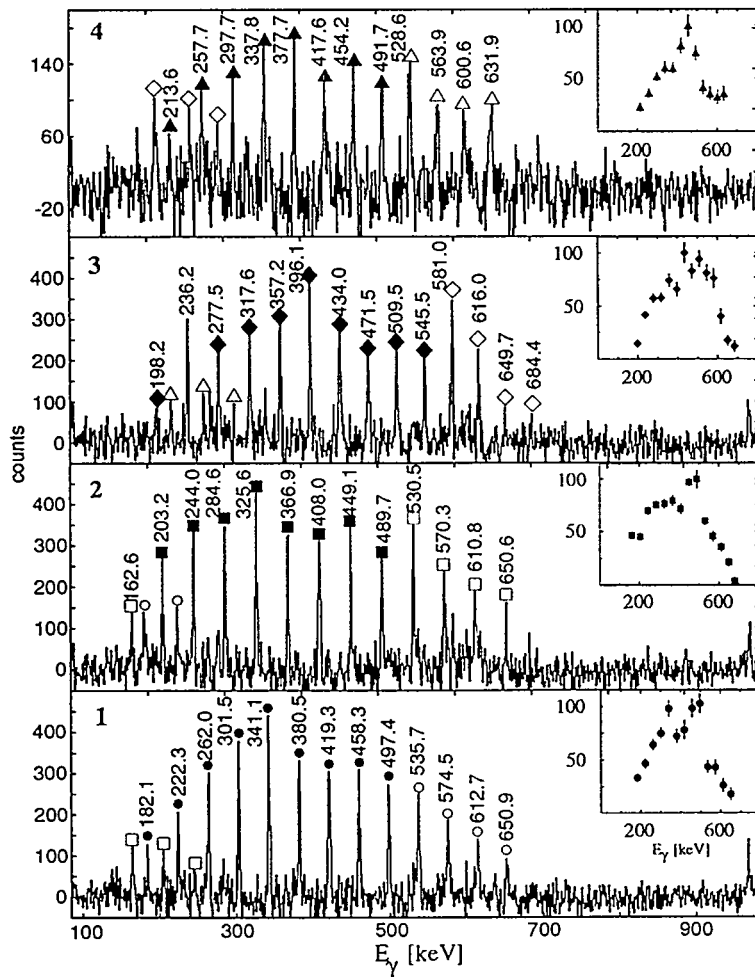


Fig. 1 Double-gated triples spectra of superdeformed bands in  $^{195}\text{Pb}$ . SD band  $\gamma$  rays are labeled by  $\circ$  — band 1,  $\square$  — band 2,  $\diamond$  — band 3, and  $\triangle$  — band 4. Filled symbols indicate gate transitions. Insets give the relative intensities of transitions, corrected for gating, singles efficiency, and internal conversion, as a percentage of the highest intensity in the band.

in the present experiment with those data obtained from our other experiments on neighboring nuclei. The known yrast SD band of  $^{196}\text{Pb}$  is observed at approximately the same intensity as  $^{195}\text{Pb}$  band 4 in the data from this experiment, while the  $^{194}\text{Pb}$  yrast SD band is not observed. In a large data set optimized for  $^{194}\text{Pb}$  ( $8.1 \times 10^8$  three- and higher-fold events), the bands assigned to  $^{195}\text{Pb}$  are observed, but not the  $^{196}\text{Pb}$  band. Similarly, we have searched in the present data for known SD bands in  $^{194,195}\text{Tl}$  and  $^{192,193}\text{Hg}$ , which are the most intense charged-particle channels, and have not found them. Thus we assign these four bands to  $^{195}\text{Pb}$ . Low-lying  $^{195}\text{Pb}$  transitions are observed in coincidence with the bands. However, their intensities vary greatly with the manner in which the background is subtracted. The only consistent coincidence is with the Pb X-rays.

The  $\mathcal{J}^{(2)}$ 's for the four bands in  $^{195}\text{Pb}$ , and the preliminary results for  $\mathcal{J}^{(2)}$ 's for two SD bands in  $^{193}\text{Pb}$ , are plotted in Fig. 2 as a function of frequency. Also shown in Fig. 2 for comparison is the  $\mathcal{J}^{(2)}$  for the SD band in  $^{194}\text{Pb}$ .  $^{195}\text{Pb}$  bands 3 and 4 have  $\mathcal{J}^{(2)}$ 's that are similar to those of  $^{194}\text{Pb}$  and most of the other SD bands in the  $A \approx 190$  region. The  $\mathcal{J}^{(2)}$ 's for  $^{195}\text{Pb}$  bands 1 and 2, and for the  $^{193}\text{Pb}$  bands, are quite constant as a function of frequency. The angular momenta

transitions of band 2 appear in coincidence with band 1, while the 182- and 222-keV gamma rays of band 1 appear in coincidence with band 2. Similarly, the 214-, 256- and 297-keV transitions of band 4 are in coincidence with band 3, and the 214 and 235-keV transitions of band 3 are in coincidence with band 4. We take this crosstalk as evidence that bands 1 and 2, and bands 3 and 4, share the same basic structures and form two sets of signature partner pairs. The relative intensities of the transitions in the four bands, corrected for efficiency and gating, are plotted in the insets in Fig. 1. It is difficult to determine the intensity of the bands as a fraction of the total  $^{195}\text{Pb}$   $\gamma$ -ray flux, as they are weakly populated, and several known long-lived isomers in  $^{195}\text{Pb}$  complicate the normalization to the total production in the 5n channel. We base our estimate of the relative yields of the  $^{195}\text{Pb}$  SD bands on data rates observed in our  $^{194}\text{Pb}$  experiment[6]. Thus, we estimate that the most intense band, band 1, comprises about 0.25% of the  $^{195}\text{Pb}$  channel. The weakest band, band 4, comprises about 0.1%.

The assignment of these four bands to  $^{195}\text{Pb}$  is based on a comparison of the data obtained

of the lowest observed levels in each  $^{195}\text{Pb}$  SD band were determined using the rotational model by extrapolating from the two lowest energy transitions in each band. The angular momenta were determined to be  $15/2$ ,  $13/2$ ,  $15/2$ , and  $17/2$  for bands 1 to 4, respectively.

## 4 Discussion

In order to understand the results of this experiment, we compare them to a Cranked Woods-Saxon calculation (CWS)[8] for  $^{195}\text{Pb}$ . The quasineutron Routhians are plotted in Fig. 3(a). The experimental Routhians for the bands are plotted in Fig. 3(b). We note that bands 1 and 2 are sharply downsloping, relative to bands 3 and 4 and to the yrast band in  $^{194}\text{Pb}$ , with signature splitting that increases with frequency. At low  $\hbar\omega$ , the transitions of band 2 are at the midpoints between the transitions of band 1, but diverge from this relationship at higher frequencies. Under the assumption that at  $\hbar\omega \approx 0$  these bands have the same energy, we observe a signature splitting in the Routhians of approximately 100 keV at  $\hbar\omega \approx 300$  keV. This is consistent with bands 1 and 2 being built upon the  $N = 7$  intruder orbital. The relative energies of the Routhians at higher frequency are consistent with the assignment of band 1 to the favored  $\alpha = -1/2$  signature, and band 2 to the unfavored signature. Since the  $N = 7$ ,  $\alpha = -1/2$  orbital is calculated to be the lowest quasiparticle excitation in the region of  $\hbar\omega$  in which the bands are populated, we expect the band built upon it to be the most intensely fed band, which is consistent with the above assignments. The assigned spins for the bands are consistent with these configurations. The intensity of the crosstalk is consistent with that expected for a  $j_{15/2}$ ,  $\Omega = 5/2$  orbital.

Bands 3 and 4 have no signature splitting in their  $\gamma$ -ray energies. In the CWS calculation, both the  $\nu[624]9/2$  and the  $[512]5/2$  orbitals match this property, but the  $[624]9/2$  orbital lies 200 keV lower in energy in the population region. Therefore, we propose that these bands are built upon the  $\nu[624]9/2$  orbital. However, bands built on the  $[512]5/2$  and the  $[624]9/2$  orbitals might have nearly identical transition energies, which would require a more sensitive experiment to resolve. Bands 3 and 4 are fed with less intensity than bands 1 and 2, consistent with the corresponding orbitals having higher excitation energies in the population region.

Let us now consider  $\mathcal{J}^{(2)}$ .  $\mathcal{J}^{(2)}$  of the  $^{194}\text{Pb}$  SD yrast band (Fig. 2) increases as a function of  $\hbar\omega$ , a property which is characteristic of most SD bands in the  $A \approx 190$  region. This rise in  $\mathcal{J}^{(2)}$  results from the alignment of paired particles in high- $j$ , low- $\Omega$  intruder orbitals, and from the gradual disappearance of pairing correlations with increasing frequency[10, 11]. An odd particle reduces the slope of  $\mathcal{J}^{(2)}$  by reducing the amount of pairing. An odd particle in the low- $\Omega$  intruder orbital further reduces the rise in  $\mathcal{J}^{(2)}$  by blocking the alignment of pairs in that orbital.

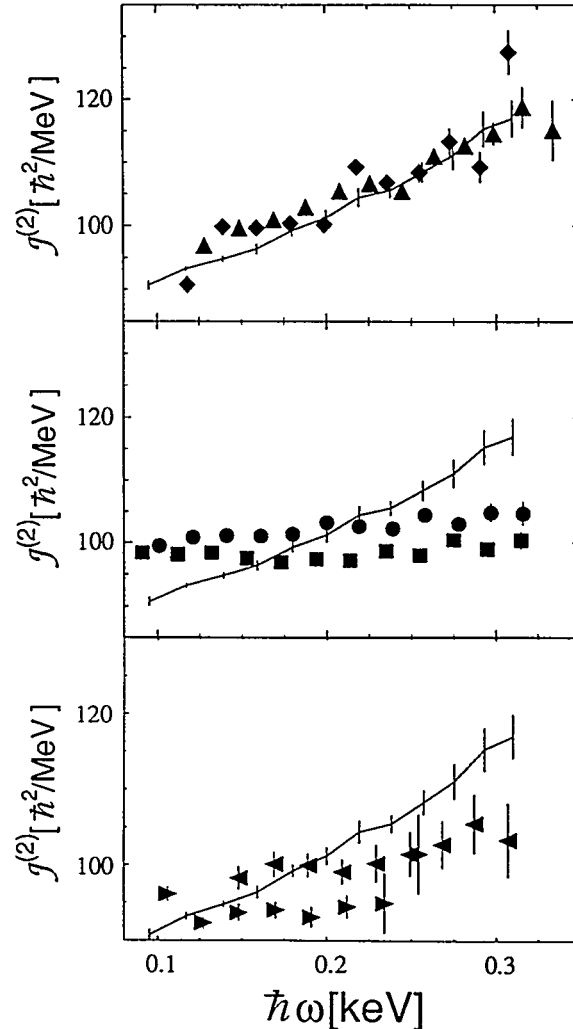


Fig. 2. The  $\mathcal{J}^{(2)}$  moments of inertia for the Pb SD bands.  $^{195}\text{Pb}$ : ● — band 1, ■ —  $^{195}\text{Pb}$  band 2, ◆ — band 3, ▲ — band 4.  $^{193}\text{Pb}$ : ◀ — band 1, ▶ — band 2.  $^{194}\text{Pb}$ —solid line.

This is consistent with the larger slope of the  $\mathcal{J}^{(2)}$  of bands 3 and 4 compared with bands 1 and 2 in  $^{195}\text{Pb}$ , given the configurations assigned to these bands. The relative values of the  $\mathcal{J}^{(2)}$  for bands 1 and 2 are consistent with the predicted curvatures in the CWS quasiparticle Routhians (Fig. 3(a)). The individual quasiparticle contributions to  $\mathcal{J}^{(2)}$  are given by  $-d^2 e_i/d\omega^2$ , where  $e_i$  are the quasiparticle Routhians. The  $N = 7$  unfavored signature, having a greater positive curvature than the favored signature at  $\hbar\omega > 200$  keV, is expected to support a band with lower  $\mathcal{J}^{(2)}$  than the favored signature.

The constant value of  $\mathcal{J}^{(2)}$  for bands 1 and 2 is quite surprising. The other cases of SD bands with constant  $\mathcal{J}^{(2)}$  in this mass region are  $^{192}\text{Tl}[7]$  and  $^{190}\text{Hg}[9]$ . In the case of  $^{192}\text{Tl}$  the constant  $\mathcal{J}^{(2)}$  was interpreted to be due to blocking of low- $\Omega$  intruder orbitals by both the odd proton and the odd neutron (double blocking). Clearly, double blocking is not likely for the lowest energy bands in  $^{193,195}\text{Pb}$ . The CWS calculations predict that proton pair alignment occurs at  $\hbar\omega \approx 450$  keV. This suggests that the constant  $\mathcal{J}^{(2)}$  of the  $^{193}\text{Pb}$  and  $^{195}\text{Pb}$  SD bands arises from blocking of the alignment of neutron pairs in the low- $\Omega$  intruder

orbital, combined with the absence of proton pair alignment in the measured frequency range. The similarity of the  $\mathcal{J}^{(2)}$ 's for  $^{194}\text{Pb}$  and  $^{192}\text{Hg}$  suggests that we should observe similar  $\mathcal{J}^{(2)}$ 's in the odd- $A$  Hg nuclei as in the odd- $A$  Pb nuclei. While the  $N = 7$  unfavored signature SD band in  $^{193}\text{Hg}$  [12] is consistent with this possibility, the bands built on the  $N = 7$  favored signature orbitals in  $^{189,191}\text{Hg}$ , and  $^{193}\text{Hg}$  band 1 after correction for its interaction with band 4, have slopes comparable with that of the yrast SD band in  $^{192}\text{Hg}$ . Another possible mechanism for the  $\mathcal{J}^{(2)}$  for bands 1 and 2 appearing to be approximately constant is an interaction between the favored  $\nu N = 7$  and the  $\nu[512]5/2$  orbitals, as was observed in  $^{193}\text{Hg}$  [13, 14]. However, no evidence for such an interaction was found.

## 5 Summary

Four new SD bands have been observed in  $^{195}\text{Pb}$ , and at least two new bands in  $^{193}\text{Pb}$ . The two bands built on the  $N = 7$  neutron intruder orbital in  $^{195}\text{Pb}$ , and the two bands observed in  $^{193}\text{Pb}$ ,

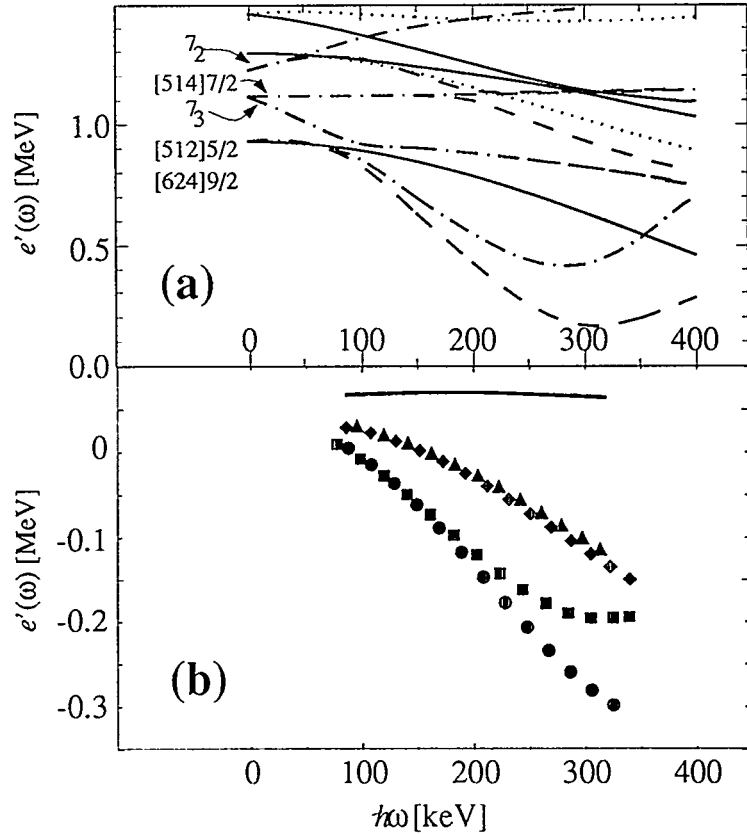


Fig. 3. (a) CWS quasineutron Routhians for  $^{195}\text{Pb}$  with deformation parameters  $\beta_2 = 0.47$ ,  $\beta_4 = 0.05$  and  $\gamma = 0$ . The orbitals are labeled by their asymptotic Nilsson quantum numbers, except for the  $N = 7$  orbitals, which are labeled  $7_1, 7_2, \dots$ , in order of increasing energy.  $(\pi, \alpha)$ : solid= $(+, +1/2)$ , dotted= $(+, -1/2)$ , dash-dotted= $(-, +1/2)$ , dashed= $(-, -1/2)$ . (b) Experimental Routhians for the  $^{195}\text{Pb}$  SD bands.  $\mathcal{J} = 88.5 + 100\omega^2 \hbar^2 \text{MeV}^{-1}$  is used for the reference. An arbitrary offset is applied to each Routhian, so that all bands extrapolate to  $e' = 0$  at  $\hbar\omega = 0$ .  $\bullet$  — band 1,  $\blacksquare$  — band 2,  $\blacklozenge$  — band 3,  $\blacktriangle$  — band 4, no symbol  $^{194}\text{Pb}$ .

have nearly constant  $\mathcal{J}^{(2)}$ 's as a function of rotational frequency. We attribute these constant  $\mathcal{J}^{(2)}$ 's to the blocking of the alignment of pairs in the neutron intruder orbital, and the absence of proton pair alignment in the measured frequency range. It does not seem possible to reconcile this absence both with the observed  $\mathcal{J}^{(2)}$ 's of the intruder bands in the odd- $A$  Hg nuclei and the similarity of the  $^{192}\text{Hg}$  and  $^{194}\text{Pb}$  yrast SD bands, at least within current models. This suggests that more work needs to be done before we come to a consistent understanding of superdeformation in the  $A \approx 190$  region.

We would like to thank P. Bonche, H. Flocard, P.-H. Heenan, and S.J. Krieger for stimulating and useful discussions, Jo Ann Heagney for making the targets, and the staff of the LBL 88-inch Cyclotron. This work was supported in part by U.S. Department of Energy, under Contract No.W-7405-ENG-48 (LLNL) and No.DE-AC03-76SF00098 (LBL), in part by the Research Corporation Grant No.R-152 and an IPA Independent Research Agreement with the Division of Undergraduate Education of the National Science Foundation, the U.S. Department of Energy Division of High energy and Nuclear Physics under Grants Nos. DE-FG02-92ER40692 and DE-FG02 87ER40371 (ISU), and in part by the National Science Foundation (Rutgers).

\* present address: Oak Ridge National Laboratory, Oak Ridge, TN 37831.

† present address: Lawrence Berkeley Laboratory, Berkeley, CA 94720.

## References

- [1] Preliminary report in E. A. Henry, et al., Bull. Am. Phys. Soc. 39, 1184 (1994).
- [2] R.B. Firestone and B. Singh, *Table of Superdeformed Nuclear Bands and Fission Isomers*, LBL-35916 UC-413, and references therein.
- [3] J.R. Hughes, et al., submitted to Phys. Rev. C.
- [4] M. Pautrat, et al., Phys. Scr. 34, 378 (1986).
- [5] H. Helppi, et al., Phys. Rev. C23, 1446 (1981).
- [6] M.J. Brinkman, et al., *Conference on Physics from Large  $\gamma$ -ray Detector Arrays*, Vol. 1, LBL-35697, 38 (1994).
- [7] Y. Liang, et al., Phys. Rev. C 46, R2136 (1992).
- [8] R. Wyss, W. Satula, W. Nazarewicz, A. Johnson, Nucl. Phys. A511, 324 (1990).
- [9] B. Crowell, et al., *Conference on Physics from Large  $\gamma$ -ray Detector Arrays*, Vol. 1, LBL-35697, 30 (1994).
- [10] M.A. Riley, et al., Nucl. Phys. A512, 178 (1990).
- [11] M.W. Drigert, et al., Nucl. Phys. A530, 452 (1991).
- [12] M. J. Joyce, et al., submitted to Phys. Lett. B.
- [13] D.M. Cullen, et al., Phys. Rev. Letters 65, 1547 (1990).
- [14] M.J. Joyce, et al., Phys. Rev. Letters, 71, 2176 (1993).

# Terminating bands

Ingemar Ragnarsson

Department of Mathematical Physics, Lund Institute of Technology,  
P.O. Box 118, S-221 00 Lund, Sweden

**Abstract:** It is pointed out that most nuclear configurations have a maximal spin and, with present experimental devices, this spin can be reached in many cases. Different ways to label configurations in order to follow them to their termination are discussed. Special attention is given to the smooth terminations recently observed in  $^{109}\text{Sb}$  and neighbouring nuclei.

Nuclear configurations can in general be labelled by the number of particles in different shells. Thus, the configurations of nuclei with a few particles outside closed shells are characterized by the  $j$ -shells in which the valence particles reside. Then, it is clear that the total spin of the configuration is limited. For example, if the 2 valence protons of  $^{210}\text{Po}$  are put in  $h_{9/2}$ , a maximal spin of  $I_{max} = 8^+$  is obtained; with one proton in  $h_{9/2}$  and the other in  $i_{13/2}$ ,  $I_{max} = 11^-$ . With more valence particles, a nice example is the  $27^-$  state in  $^{152}\text{Dy}$  [1] which is formed from 2  $h_{11/2}$  valence protons and 4 valence neutrons outside a  $^{146}\text{Gd}$  core. With 2 of the neutrons in  $f_{7/2}$  and one in each of the  $h_{9/2}$  and  $i_{13/2}$  subshells, it is easy to conclude that  $I_{max} = 27^-$ .

With more valence particles and thus larger tendencies for the nucleus to become deformed, it is questionable to treat the  $j$ -shells as pure. Still, however, the main quantum number of the different orbitals appears rather well-defined. This fact is explored in the formalism described in [2], where, in the diagonalisation of the cranked modified oscillator hamiltonian, the  $N$ -shells of the rotating oscillator are treated as pure resulting in well-defined terminations in most cases. For example, the superdeformed bands (e.g. [3]) around  $^{152}\text{Dy}$ , which are generally labelled by the number of particles in high- $N$  orbitals [4], are on the borderline between configurations which terminate and configurations for which the nucleus becomes more and more deformed with increasing spin [5]. When terminating, their maximal spin is in the range  $150 - 200\hbar$ , i.e. much higher than what can be observed experimentally. It is therefore natural that they behave as undisturbed rotational bands for all spins at which they can be studied experimentally.

Also for nuclei at normal deformation, the labelling of configurations in terms of occupation of  $N$ -shells is often useful but sometimes insufficient, however. Indeed, because the highest  $j$ -shell (the intruder shell [6]) within each  $N$ -shell separates from the other  $j$ -shells and does not couple strongly to them, it appears appropriate to treat the intruder shell separately whereas the other  $j$ -shells are considered as one entity. This has similarities with the pseudo-oscillator (pseudospin) coupling scheme and we will refer to these orbitals by  $\tilde{N}$ , for example the  $N = 4$  shell is divided into the  $g_{9/2}$  orbitals and the  $\tilde{N} = 3$  orbitals ( $g_{7/2}$ ,  $d_{5/2}$ ,  $d_{3/2}$  and  $s_{1/2}$ ). Then, for example, the ground band of a nucleus in the middle of the deformed rare earth region,  $^{166}\text{Er}$ , can be labelled as  $\pi(\tilde{N} = 3)^{10} (h_{11/2})^8 \nu(\tilde{N} = 4)^{10} (i_{13/2})^6$  outside a  $^{132}\text{Sn}$  core and  $I_{max}$  is easily obtained as  $82\hbar$ . Detailed calculations [2] suggest that configurations of this type stay in the yrast region up to  $I = 40$  but, for higher spins, configurations with particles excited to higher shells (protons in  $\tilde{N} = 4$  or in  $i_{13/2}$ ) become yrast. Therefore, also in this case, the maximal spin is of no direct significance.

In this contribution, we will concentrate on configurations which are collective in some spin range but where the termination in a non-collective state occurs at a spin value which can be studied experimentally. This could be the case closer to the borderlines of the deformed rare earth region. An interesting example is  $^{158}\text{Er}$ , which nucleus has been studied very carefully experimentally [7] and where terminating bands show up at high spin. The ground band proton configuration is the same as for  $^{166}\text{Er}$  ( $I_{max}^p = 33\hbar$ ) or possibly rather  $\pi(\tilde{N} = 3)^{12} (h_{11/2})^6$  with  $I_{max}^p = 32\hbar$ . To this we should add  $I_{max}^n = 30\hbar$  from the  $\nu(\tilde{N} = 4)^6 (i_{13/2})^2$  configuration. The total maximal spin is thus around  $60\hbar$  which is not so far from what can be studied experimentally.

A further important fact is then the rather large  $Z = 64$  gap. Because of this gap one might rather treat  $^{146}\text{Gd}$  instead of  $^{132}\text{Sn}$  as a closed core. The two proton configurations will then be referred to as  $\pi(d_{5/2}, g_{7/2})^{-4} (h_{11/2})^8$  and  $\pi(d_{5/2}, g_{7/2})^{-2} (h_{11/2})^6$  with  $I_{max}^p = 28\hbar$  and  $24\hbar$ , respectively<sup>1</sup>. The smaller maximal spins results because the  $\tilde{N} = 3$  orbitals are now divided in two groups,  $d_{5/2}$  and  $g_{7/2}$  below the  $Z = 64$  gap and the  $d_{3/2}$  and  $s_{1/2}$  orbitals above this gap. In the calculations, these two groups cannot be distinguished by any quantum numbers but at small deformations, the energy of occupied  $d_{5/2}$  and  $g_{7/2}$  orbitals is smaller than for the  $d_{3/2}$  and  $s_{1/2}$  orbitals so the yrast states before the terminations will correspond to configurations with no particles in  $d_{3/2}$  and  $s_{1/2}$  orbitals. The total spin of  $54\hbar$  in the  $\pi(h_{11/2})^6$  configuration is very close to what has been observed [7] today,  $50\hbar$ . The importance of terminations becomes even more explicit, however, because for high spin, the proton core tends to close corresponding to a  $\pi (h_{11/2})^4$  configuration with a maximal spin of  $16^+$ , i.e. a total spin of  $46^+$ . This terminating spin was predicted [8] and observed [9] long ago. As reported in another contribution to this conference [7], we have now a detailed knowledge of terminating bands and fully aligned states in  $^{158}\text{Er}$ . The observed spectrum is in close correspondence with theoretical expectations.

A region which has not been studied so much experimentally but where we predict terminating bands are the nuclei around  $^{100}\text{Ru}/^{102}\text{Pd}$ . Relative to a  $^{90}\text{Zr}$  closed core, these two nuclei have a neutron configuration of  $(\tilde{N} = 3)^4 (h_{11/2})^2$  and either 4 or 6  $g_{9/2}$  protons (6 or 4  $g_{9/2}$  holes relative to  $Z = 50$ ) with  $I_{max} = 32^+$ . According to our calculations [10], the corresponding rotational bands stay yrast or close to yrast all the way from the ground state to the termination.

Some nuclei of special interest are those with a few valence particles outside  $^{100}\text{Sn}$  [11, 12, 13]. In fig. 1, we show some low-energy configurations of  $^{109}\text{Sb}$ , obtained in cranking calculations with the modified oscillator potential[2]. The closed core configuration is essentially yrast up to its termination at  $I = 51/2$ . Within the valence space, somewhat higher spin can then be achieved by shifting more particles to  $h_{11/2}$  but this is expensive in terms of energy and of little practical interest. The obvious way to achieve higher spins is thus to excite protons across the  $Z = 50$  gap<sup>2</sup>; either one proton from  $g_{9/2}$  to  $g_{7/2}/d_{5/2}$  giving a spin contribution of  $7\hbar$  or making two holes in  $g_{9/2}$  putting one in  $g_{7/2}/d_{5/2}$  and the other in  $h_{11/2}$  giving a spin contribution

<sup>1</sup>From the point of view of getting maximal spins, holes or particles in some subshell(s) are equivalent.

<sup>2</sup>It should be noted that the full coupling between the  $g_{9/2}$  subshell and the other  $N = 4$  orbitals (the  $\tilde{N} = 3$  orbitals here referred to as  $g_{7/2}/d_{5/2}$ ) are included because the division into the two subsets is made first after the diagonalisation within the  $N = 4$  basis states of the rotating oscillator.



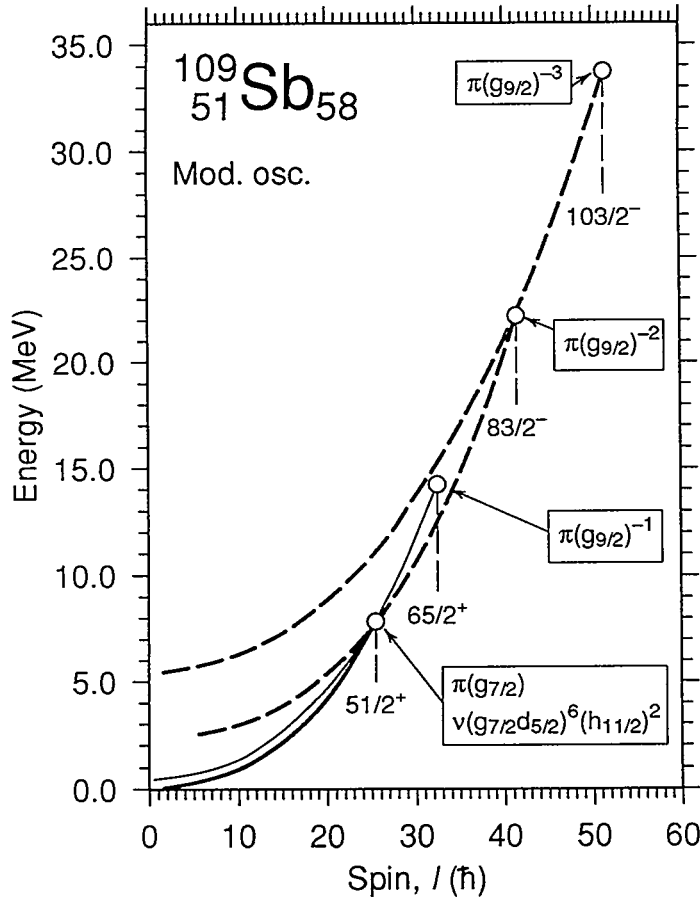


Fig. 1. Typical calculated low-energy configurations of  $^{109}\text{Sb}$  with 0, 1, 2 and 3 proton holes in  $g_{9/2}$  and thus 1, 2, 3 or 4 protons in the subshells above the  $Z = 50$  gap. Terminating aligned states are indicated by an open circle. As pairing is neglected, the results for low spins, e.g. with a regular rotational band for the zero hole configuration, are not realistic.

of  $16\hbar$ . This is illustrated in fig. 1. The interesting observation is now that already for the highest spin in the valence space,  $51/2^+$ , the 2 hole excitation (corresponding to a 3p-2h proton configuration) is energetically competitive with the 1 hole excitation. This is due to the energy gain from deformation. Indeed, the 2 hole excitation is calculated to stay yrast essentially from spin  $51/2$  to its termination at  $I = 83/2$ . Higher spins are then formed from 3 hole excitations but they do become competitive in energy first at the terminating spins for the 2 hole bands. In the 3 hole excitation illustrated in fig. 1, the four protons in orbitals "above the  $Z = 50$  gap" have the configuration  $(g_{7/2} d_{5/2})^2 (h_{11/2})^2$ . Furthermore, each p-h excitation tends to increase the deformation making it more favourable to put neutrons in  $h_{11/2}$ . Therefore, in the 4p-3h band shown in fig. 1, the neutron configuration is  $(g_{7/2} d_{5/2})^5 (h_{11/2})^3$ .

As mentioned above, a very important feature of fig. 1 is that the 3p-2h configuration stays yrast over such a large spin range. One reason for this is that each p-h excitation gives a large contribution to the spin because  $j$ -shells with high  $j$  are involved and the Pauli principle does not hinder the use of high  $j_x$  values. On the other hand, it is not clear to us why 3p-2h configurations are much more favoured than 2p-1h configurations. A more detailed view of the calculated bands in the yrast region is shown in fig. 2, where a smooth " $I(I + 1)$ " reference has been subtracted. From this figure, it is clear that more bands with one, two or three holes in  $g_{9/2}$  than those drawn in fig. 1 come close to yrast. Of special interest is that there are three very favoured 2 hole bands which however have different quantum numbers in terms of parity/signature. Consequently, in a large spin range, these bands are considerably

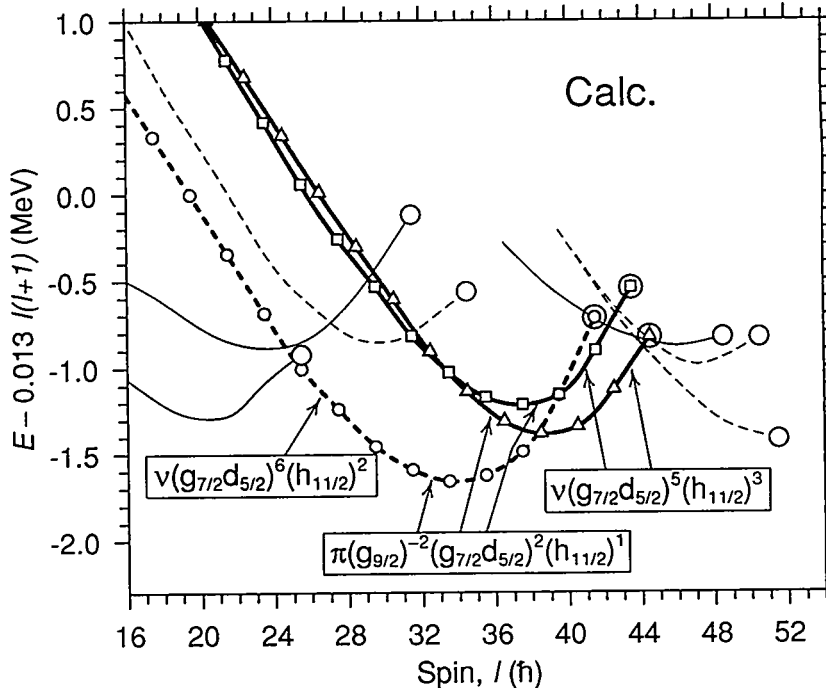


Fig. 2. A more detailed view of the calculated spectrum of  $^{109}\text{Sb}$  with an " $I(I+1)$ " reference subtracted. The dominant configurations are given for three bands drawn by thick lines. They are interpreted as corresponding to three experimental bands observed to their termination. The lower spin configurations have 1 hole in  $g_{9/2}$  and those at higher spin 3 holes in  $g_{9/2}$

lower than any other bands with which they could interact. One more important feature is that these bands have in total 11 particles and 2 holes outside the core which from the point of view of deformation is essentially equivalent to 13 particles. The configuration can thus be described as a number of subshells with rather high  $j$  and with either a few particles or a few holes. They will then all contribute to the deformation and collectivity forming nice essentially undisturbed rotational bands over a large spin range all the way to their termination.

In the experimental spectrum of  $^{109}\text{Sb}$ , three collective bands are observed [11, 12] to high spins and recently two additional bands which are less intense. It has not been possible to find the connections of these bands to the lower spin states so their spins are not known. With reasonable assumptions [12] about their spin values, however, we get a very good agreement [13] with the calculated bands and the comparison suggest that they have been observed to their termination at  $I^\pi = 41.5^-$ ,  $43.5^+$  and  $44.5^+$  respectively. If this interpretation is correct, it is the first time that it has been possible to follow one configuration which evolves in a smooth and continuous way over many spin states from a "normal collective" band at lower spins to a terminating state where all spin vectors are aligned along the same axis. This latter state is rotationally symmetric around the "rotation" axis. The calculated shape trajectory in the  $(\epsilon, \gamma)$ -plane for the three bands are shown in fig. 3.

An interesting feature of these rotational bands is that the transition energies become very large close to the termination, i.e. the curves in fig. 2 bend upwards. We refer to these kind of terminations as unfavoured. This behaviour is opposite to

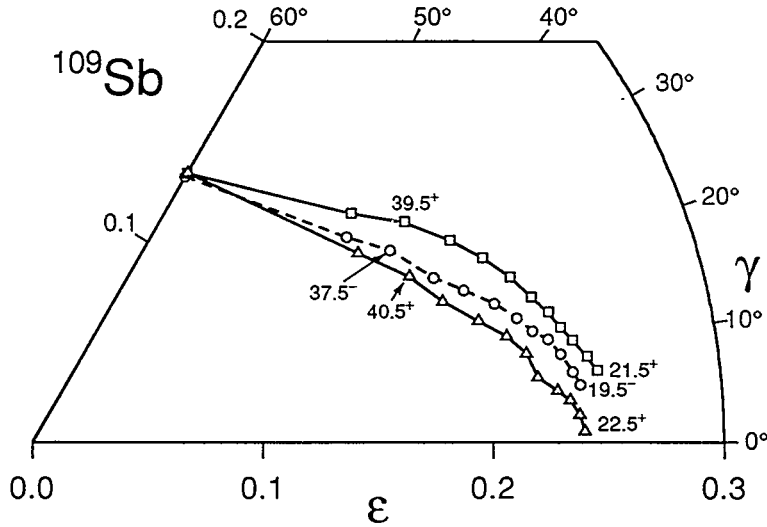


Fig. 3. Calculated shape trajectories in the  $(\epsilon, \gamma)$ -plane for the three configurations of  $^{109}\text{Sb}$  drawn by thick lines in fig. 2.

the properties of most other terminating bands observed at present, e.g. in the region of  $^{158}\text{Er}$ , where the last spin units are built very cheap in terms of energy; favoured terminations. The possibility of unfavoured terminations was anticipated long ago and discussed in sect. 9 of ref. [2] but has not been seen in experiment before. The reason why mainly favoured terminations have been considered previously is that bands of this type will more easily become yrast at their termination.

A drastic way to show the increasing transition energies in  $^{109}\text{Sb}$  is to plot the  $\mathcal{J}^{(2)}$  moment of inertia which, in both experiment and calculation, is only around 1/3 of the rigid body value at the termination. The fact that the last spin units are so difficult to achieve in  $^{109}\text{Sb}$  seems to be connected with the fact that it is difficult to fully align the spin vectors of the 2  $g_{9/2}$  holes in a surrounding of aligned particle states which latter lead to an oblate shape (fig. 3) at the termination.

If some more valence particles are added to the  $^{100}\text{Sn}$  core, the terminating spins in the valence space will become higher. Furthermore calculations on e.g.  $^{115}\text{I}$  [14] indicate that the high energy cost of the last spin units will make the rotational bands go away from yrast before they terminate. Consequently it will be difficult to observe the bands all the way to their termination but some of the typical features seen for the  $^{109}\text{Sb}$  bands will be present also in these cases, e.g.  $\mathcal{J}^{(2)}$  moments of inertia which are much smaller than the rigid body value. One could also note that bands with small  $\mathcal{J}^{(2)}$  values were calculated [2] long ago in  $^{118}\text{Te}$  although in that case, the formalism did not allow to distinguish between high- $j$  and low- $j$  orbitals and therefore, it was not possible to follow the rotational bands to their final termination.

In a somewhat similar way as for  $^{109}\text{Sb}$  the large deformation bands (e.g. [15]) in Ce/Nd nuclei have two proton holes in  $g_{9/2}$ . This suggests that we could see small  $\mathcal{J}^{(2)}$  values also in these bands in the  $I = 50 - 60$  region which seems to be about  $20\hbar$  lower than the terminating spin values. The low-deformation collective bands seen e.g. in  $^{152}\text{Dy}$  [16] is another example of rotational bands which could come close to termination. For example, one of the configurations suggested in ref. [17] is  $\pi(d_{5/2}g_{7/2})^{-4}(h_{11/2})^6 \nu(h_{11/2})^{-2}(f_{7/2} h_{9/2})^4 (i_{13/2})^2$  with a terminating spin of

$64\hbar$ . With the mixture of particles and holes, it would be interesting to calculate the behaviour of  $\mathcal{J}^{(2)}$  in the  $I = 50 - 60$  region and compare with experiment. This would hopefully also help to identify the configuration of this band.

In summary, we have pointed out that with present experimental devices, in several regions of nuclei, it becomes possible to come close to or even reach the maximal spin (the terminating spin) for rotational bands which are collective at low spin. Depending on the distribution of the valence particles over different shells or if the valence space is dominated by either particles or holes, very specific features will show up. We did especially discuss the terminating rotational bands in  $^{109}\text{Sb}$ . Some of the specific features in  $^{109}\text{Sb}$  and neighbouring nuclei are:

- The path to termination is very smooth both what concerns energy and shape change.
- The highest spin states are relatively high in energy so the termination can be referred to as unfavoured. This high energy is caused by the high energy cost to align the proton holes in  $g_{9/2}$  in an environment of particles in high- $j$  shells.
- The terminations are very definite in the way that the highest spin within the configuration has indeed been reached.

I am grateful to my coauthors on ref. [13] together with whom I have carried out the investigation of  $^{109}\text{Sb}$ . I want to thank Sigurd Madison for help in preparing the figures. This project has been supported by the Swedish Natural Science Research Council.

## References

- [1] D. Horn, O. Häusser, I.S. Towner, H.R. Andrews, M.A. Lone and P. Taras, *Phys. Rev. Lett.* **50** (1983) 1447.
- [2] T. Bengtsson and I. Ragnarsson, *Nucl. Phys.* **A436** (1985) 14.
- [3] P.J. Twin, *Nucl. Phys.* **A574** (1994) 51c.
- [4] T. Bengtsson, I. Ragnarsson and S. Åberg, *Phys. Lett.* **B208** (1988) 39.
- [5] I. Ragnarsson, *Phys. Lett.* **B199** (1987) 317.
- [6] F.S. Stephens, *Rev. Mod. Phys.* **47** (1975) 43.
- [7] J. Simpson *et al.*, *Phys. Lett.* **B327** (1994) 187, and references therein; J. Simpson *et al.*, these proceedings.
- [8] T. Bengtsson and I. Ragnarsson, *Physica Scripta* **T5** (1983) 165.
- [9] P.O. Tjøm, R.M. Diamond, J.C. Bacelar, E.M. Beck, M.A. Deleplanque, J.E. Draper and F.S. Stephens, *Phys. Rev. Lett.* **55** (1985) 2405.
- [10] A.V. Afanasjev and I. Ragnarsson, to be published.
- [11] V.P. Janzen *et al.*, *Phys. Rev. Lett.* **72** (1994) 1160.
- [12] D.B. Fossan *et al.*, these proceedings; H. Schnare *et al.*, to be subm. to *Phys. Rev. C*.
- [13] I. Ragnarsson, V.P. Janzen, D.B. Fossan, N.C. Schmeing and R. Wadsworth, subm. to *Phys. Rev. Lett.*
- [14] E.S. Paul *et al.*, *Phys. Rev.* **C50** (1994) 741.
- [15] P.J. Nolan, *Nucl. Phys.* **A553** (1993) 107c.
- [16] B.M. Nyako, J. Simpson, P.J. Twin, D. Howe, P.D. Forsyth and J.F. Sharpey-Schafer, *Phys. Rev. Lett.* **56** (1986) 2680.
- [17] I. Ragnarsson and S. Åberg, *Phys. Lett.* **B180** (1986) 191.

# Intruder bands to very high frequencies in $^{109}\text{Sb}$ and $^{114}\text{Te}$ : smooth termination

D B Fossan<sup>1</sup>, D R LaFosse<sup>1</sup>, H Schnare<sup>1</sup>, C W Beausang<sup>2</sup>, K Hauschild<sup>3</sup>, I M Hibbert<sup>3</sup>,  
J R Hughes<sup>1</sup>, V P Janzen<sup>4</sup>, S M Mullins<sup>5</sup>, E S Paul<sup>2</sup>, D C Radford<sup>4</sup>, I Ragnarsson<sup>6</sup>,  
I Thorslund<sup>1</sup>, P Vaska<sup>1</sup>, R Wadsworth<sup>3</sup>, M P Waring<sup>1</sup>

<sup>1</sup> *Department of Physics, State University of New York at Stony Brook, NY*

<sup>2</sup> *Oliver Lodge Laboratory, University of Liverpool, United Kingdom*

<sup>3</sup> *Department of Physics, University of York, Heslington, York, United Kingdom*

<sup>4</sup> *Chalk River Laboratories, AECL Research, Chalk River, Ontario, Canada*

<sup>5</sup> *Department of Physics, McMaster University, Hamilton, Ontario, Canada*

<sup>6</sup> *Department of Mathematical Physics, Lund Institute of Technology, Lund, Sweden*

Nuclei near the  $Z=50$  closed proton shell have revealed surprising collective structures, which coexist with the expected single-particle properties. Collective rotational bands result from particle-hole (ph) proton excitations across the  $Z=50$  shell gap via the  $\pi g_{7/2} - \pi g_{9/2}$  level crossing at prolate deformations, which appear to stabilize deformed core configurations. In  $Z=51$  odd-mass Sb nuclei, these rotational bands are associated with 2p1h and 3p2h proton excitations,  $\pi(g_{7/2})^2(g_{9/2})^{-1}$  and  $\pi[(g_{7/2})^2(g_{9/2})^{-2}] \otimes j$ , at low energies as recently shown in their entirety in the  $^{117}\text{Sb}$  nucleus [1], near the middle of the neutron shell. For lighter Sb nuclei as discovered in  $^{109}\text{Sb}$  [2], the nucleons outside of  $^{100}\text{Sn}$  align at higher rotational frequencies to contribute additional angular momentum to these intruder rotational bands, but in the process change the character of the nuclear structure. A similar effect was observed for the 2p2h deformed core excitation,  $\pi[(g_{7/2})^2(g_{9/2})^{-2}]$ , of the  $^{108}\text{Sn}$  nucleus [3]. For  $Z=52$  Te nuclei, the 4p2h proton excitation is expected to produce an yrast intruder band; such a band has been observed in  $^{112}\text{Te}$  [4]. Theoretical studies of intruder bands in this  $Z=50$  region suggest a gradual change from high collectivity to a non-collective structure, which results in a smooth termination of the bands [5].

The early implementation (EI) of GAMMASPHERE has been employed to investigate the properties of these intruder bands near the  $Z=50$  closed shell with improved resolving power. The high-spin properties of  $^{109}\text{Sb}$  have been studied via the  $^{54}\text{Fe}(^{58}\text{Ni},3p)$  reaction with a 243-MeV  $^{58}\text{Ni}$  beam together with the GAMMASPHERE (EI) array. Both thin- and backed-target experiments were performed. A forward-backward geometry with  $\theta \leq 37^\circ$  from the beam axis for  $\approx 30$  Ge detectors minimized the effects of Doppler broadening despite the large recoil velocity ( $v/c=4.7\%$ ).

The event data were unpacked into a doubles  $E_\gamma - E_\gamma$  coincidence matrix and into a triples  $E_\gamma - E_\gamma - E_\gamma$  coincidence cube. In addition, the events were unpacked into 4-folds and sorted into several double-gated matrices with different gating conditions. The combination of these double-gated matrices for the 4-fold data and the double-gated spectra extracted from the cube provided the sensitivity required in the search for high-spin intruder bands; this high sensitivity is also important in determining any terminating transitions and in locating the elusive linking transitions to the low-lying states of the nucleus. Detailed analyses of the data in the cube and in the different matrices were performed by using the analysis packages LEVIT8R (cube) and ESCL8R (matrix) [6].

Earlier results in  $Z=51$   $^{109}\text{Sb}$  [2] have been extended to higher frequencies ( $\hbar\omega \geq 1.4$  MeV) and to a total of five intruder bands. Sums of double-gated  $\gamma$ -ray coincidence spectra from the thin-target cube are shown for the three strongest intruder bands in Fig.1. Four of the five bands show smoothly decreasing dynamic moments of inertia with increasing spin to values as low as 1/3 the rigid-body value, as presented in Fig.2. This can be easily seen from the increasing  $\gamma$ -ray energy spacings of the spectra shown in Fig.1. The improved resolving power of the array is believed to have identified the terminating  $\gamma$ -ray transitions, which are near 2.8 MeV, reaching tentative termination spin values ranging from  $(83/2)\hbar$  to  $(89/2)\hbar$ . Although the band decay patterns are observed, definite links to the low-lying levels have not been identified. A partial level scheme of these five high-spin intruder bands in  $^{109}\text{Sb}$  is presented in Fig.3.

Theoretical calculations [5], showing a gradual alignment of the configuration valence particles outside  $Z=N=50$  with the nuclear shape moving across the  $\gamma$ -plane from a collective prolate shape ( $\gamma = 0^\circ$ ) to a noncollective oblate shape ( $\gamma = +60^\circ$ ) over many transitions, are remarkably consistent with these experimental results for all five intruder bands. These comparisons were presented by I. Ragnarsson earlier in this conference session. Band termination occurs when the valence particle spin of the specific band configuration has been exhausted. The configuration for band 1 is  $\pi[(g_{7/2})^2(g_{9/2})^{-2}]h_{11/2} \otimes \nu(g_{7/2}d_{5/2})^6(h_{11/2})^2$ , which terminates at  $83/2^-$ .

A second EI GAMMASPHERE experiment searched for intruder bands in  $Z=52$   $^{114}\text{Te}$  with the  $^{54}\text{Fe}(^{63}\text{Cu},3p)$  reaction at 245 MeV. Similar analyses of the event data as outlined above were made. Three intruder bands were found and observed to high frequencies; the linking transitions to the low-lying levels were established for one of the bands, and with less certainty for the other two. The bands reached spins ranging from  $(33)\hbar$  to  $(50)\hbar$  and transition energies up to 2.5 MeV. The dynamic moments of inertia decreased slowly with spin but not to the low values as in  $^{109}\text{Sb}$ . A double-gated  $\gamma$ -ray coincidence spectrum from the thin-target cube is shown for band 1, the strongest intruder band, in Fig.4. This band is followed up to a spin of  $(50)\hbar$ . The extracted  $^{114}\text{Te}$  level scheme is presented in Fig.5 in two parts with different energy scales.

The band-termination calculation [5] for the yrast configuration,  $\pi[(g_{7/2})^2(g_{9/2})^{-2}](h_{11/2})^2 \otimes \nu(g_{7/2}d_{5/2})^8(h_{11/2})^4$ , which terminates at  $52^+$ , agrees well with band 1 in  $^{114}\text{Te}$ . With the larger number of valence particles, the band calculations suggest that termination may not have been reached for the other  $^{114}\text{Te}$  intruder bands.

The 3pn channel of this experiment leading to  $^{113}\text{Te}$  also provided good statistics; however, no collective bands were found in this odd-N isotope. With sufficient strength in the  $\alpha 2p$  channel, three intruder bands were observed in  $^{111}\text{Sb}$  with similar properties.[7] The band analogous to band 1 in  $^{109}\text{Sb}$  was followed up to  $(83/2^-)$ .

- [1] D.R. LaFosse et al. Phys. Rev. Letters **69**, 1332 (1992)
- [2] V.P. Janzen et al., Phys. Rev. Letters **72**, 1160 (1994)
- [3] R. Wadsworth et al., Nucl. Phys. **A559**, 461 (1993)
- [4] E.S. Paul et al. Phys. Rev. C **50**, 698 (1994)
- [5] I. Ragnarsson et al., (to be published).
- [6] D.C. Radford, Proc. of Workshop on Large Gamma-Ray Detector Arrays, Chalk River 1992, AECL-10613, p.403
- [7] D.R. LaFosse et al. Phys Rev C **50**, Oct.(1994)

# $^{109}\text{Sb}$

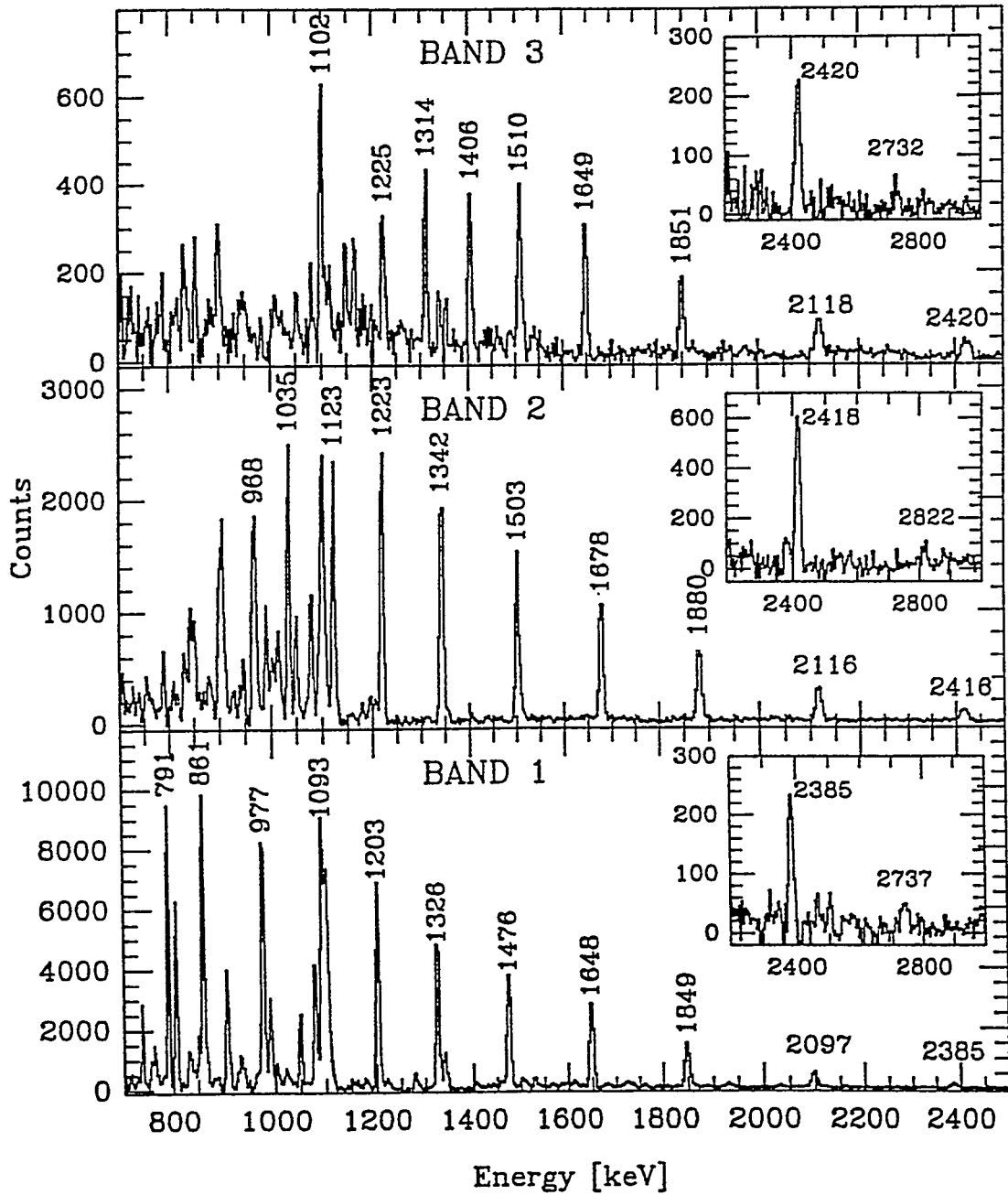


Fig.1

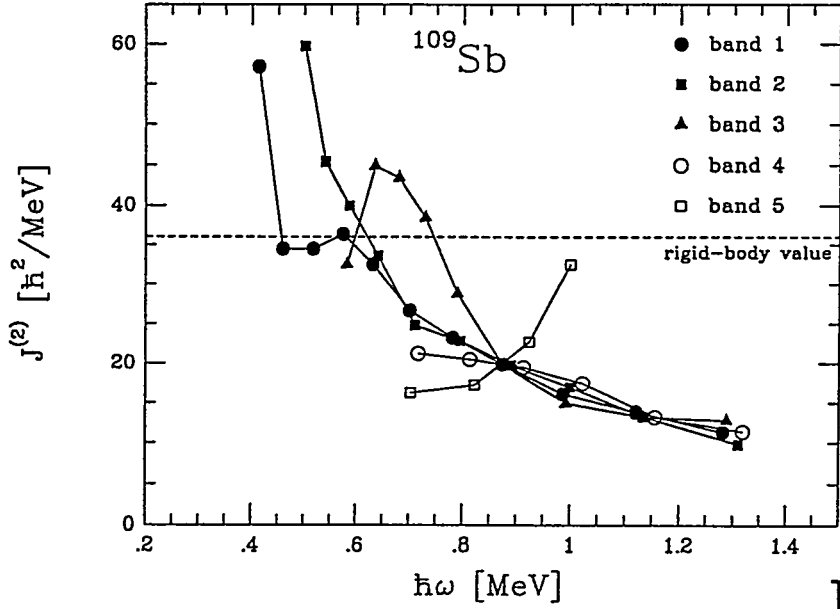


Fig.2

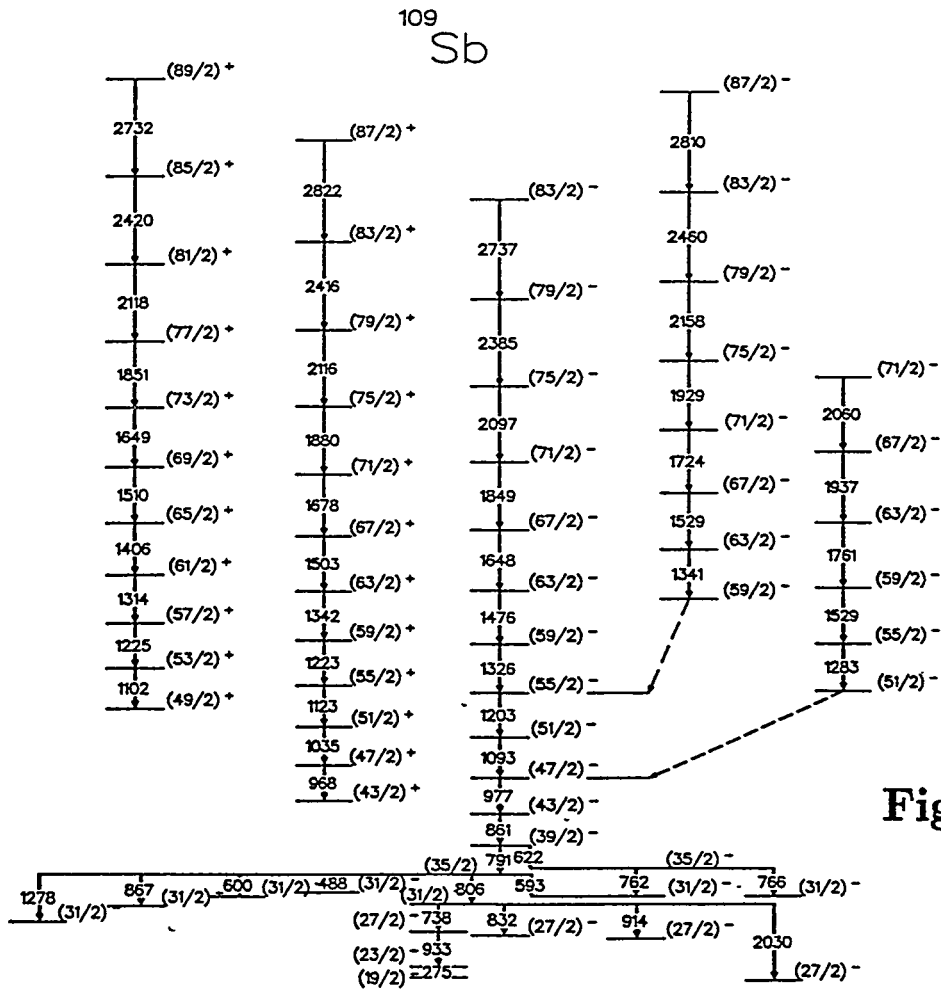


Fig.3





# Multiple Band Termination Spectroscopy in $^{157,158}\text{Er}$ with EUROGAM.

J.Simpson

*DRAL, Daresbury Laboratory, Daresbury, Warrington WA4 4AD, UK.*

## Abstract

The competition between collective rotation and single particle behaviour at high spin,  $40\hbar \leq I \leq 50\hbar$ , in  $^{157,158}\text{Er}$  has been investigated with the Eurogam spectrometer. Multiple band terminating and aligned states have been established and specific single particle configurations are assigned by comparison with cranked Nilsson-Strutinsky calculations. These special states are found to be related by simple single-particle excitations and indicate that a stable oblate mean field ( $\epsilon \sim -0.14$ ) is established.

### 1. Introduction

Spectroscopy near band termination enables a study of the balance and interplay between the two extreme facets of nuclear dynamics, collective rotation and single-particle alignment. The classic example of where this phenomenon occurs in heavy nuclei is in the transitional region around  $N = 90$  where band termination effects are observed near spin 40 [1–16]. This talk reports on the results from a Eurogam experiment on the nuclei  $^{157,158}\text{Er}$ . The transition from collective rotation to a regime of single-particle excitations is observed in several sequences in each nucleus and band termination states have been identified at  $I^\pi = \frac{81}{2}^+, \frac{87}{2}^-, \frac{89}{2}^-, 46^+, 48^-$  and  $49^-$  [17,18]. Specific single-particle configurations are assigned to these special states by comparison with cranked Nilsson-Strutinsky calculations.

### 2. Experimental method

High spin states in  $^{157}\text{Er}$  and  $^{158}\text{Er}$  were populated by the reaction  $^{114}\text{Cd}(^{48}\text{Ca}, 5n, 4n)$ . The 210 MeV beam of  $^{48}\text{Ca}$  was provided by the Nuclear Structure Facility at Daresbury Laboratory. The target consisted of two stacked thin foils of  $^{114}\text{Cd}$  each of thickness  $500 \mu\text{g cm}^{-2}$ . Gamma-rays were detected by the Eurogam spectrometer [19,20] with 44 escape suppressed spectrometers [21]. After unpacking the higher fold events the data yielded a total of  $5.2 \times 10^9$  triple ( $\gamma^3$ ) and  $4.1 \times 10^9$  quadruple ( $\gamma^4$ )  $\gamma$ -ray coincidence events.

### 3. Results

The level schemes of  $^{157}\text{Er}$  and  $^{158}\text{Er}$  were considerably extended with over 100 new  $\gamma$ -rays placed in  $^{158}\text{Er}$  alone. Figure 1 shows an example of the spectra obtained in this data. In  $^{158}\text{Er}$  above spin 38 the  $(+,0)$  decay path splits into two branches with the energetically favoured, irregular branch established to the known terminating state at  $46^+$ , see in figure 1(a). The data suggests that the terminating  $46^+$  state is fed by many weak high energy  $\gamma$ -rays; tentative candidates for these are at 939, 1380, 1454,

1539, 1602 and 1657 keV. The less favoured branch above spin  $38^+$ , interpreted as a continuation of the collective structure [4,23,25,26], has been extended from  $42^+$  to  $50^+$ . The  $(-,1)$  band is observed to split into two decay paths above the previously known state at  $41^-$  [3] in a very similar manner to the  $(+,0)$  band at  $38^+$ . This work has established the full decay path of the  $(-,0)$  states from their decay to the yrast band near spin 10 to  $48^-$ . This band interacts with a strongly coupled band between spins  $18^-$  and  $30^-$  which results in a very complicated decay path [22]. In  $^{157}\text{Er}$  the  $(+,+\frac{1}{2})$  band splits into three decay paths above  $\frac{69}{2}^+$ . The strongest path, of stretched E2 transitions is established up to  $\frac{85}{2}^+$ . A dipole transition also feeds the  $(\frac{69}{2}^+)$  state and a sequence of stretched E2 transitions which feed this state extends up to  $\frac{79}{2}^+$ . The negative parity sequences  $(-,+\frac{1}{2})$  and  $(-,-\frac{1}{2})$  are extended up to  $\frac{89}{2}^-$  and  $\frac{87}{2}^-$ , respectively.

#### 4. Band termination spectroscopy.

In figure 2 the excitation energy of the high spin states in  $^{157}\text{Er}$  and  $^{158}\text{Er}$  relative to a rigid rotor reference is plotted as a function of spin. Particularly favoured are observed in most of the sequences and in general downsloping behaviour compared with the rigid rotor energy is observed. This latter feature is a characteristic of weakly collective bands approaching termination [11]. In order to understand these features in detail these data are compared with the predictions of cranked Nilsson-Strutinsky calculations [11,23–25]. In these calculations different bands are formed by fixing a configuration and tracing the lowest energy states as a function of spin. The formalism for these calculations is described in detail in [11,23]. The configurations can be labeled by the occupation of particles outside the  $^{146}\text{Gd}$  core. Examples of the calculations for the lowest energy  $(+,0)$  states in  $^{158}\text{Er}$  and the  $(-,+1/2)$  states in  $^{157}\text{Er}$  are shown in figure 3.

The particularly favoured states at  $40^+$  and  $46^+$  in  $^{158}\text{Er}$  have been identified previously as oblate states with the configurations,  
 $40^+ \Rightarrow \pi(h_{11/2})^4]_{16+} \otimes [\nu(i_{13/2})^2(h_{9/2})^2(f_{7/2})^4]_{24+}$  and  
 $46^+ \Rightarrow [\pi(h_{11/2})^4]_{16+} \otimes [\nu(i_{13/2})^2(h_{9/2})^3(f_{7/2})^3]_{30+}$ . These states are clearly well reproduced in the calculations, see figure 3. The unfavoured  $(+,0)$  states between spin  $30^+$  and  $38^+$ , established in this work, appear, when a comparison is made with the calculations, to be the continuation of the terminating structure below spin  $40^+$ . This is the first observation of a non yrast terminating sequence over such a significant spin range. The experimental  $32^+$  state is observed to be slightly favoured in energy in this sequence. This is consistent with the prediction of a low lying oblate  $32^+$  state which has the same neutron configuration as the  $40^+$  state but with the four  $(h_{11/2})$  protons coupled to spin  $8^+$ .

The  $(-,1)$  states above  $41^-$  behave in a very similar manner to the  $(+,0)$  states above spin  $38^+$ . The favoured irregular branch is interpreted as a terminating structure and the particularly favoured states at  $43^-$  and  $49^-$  as oblate states. Again this interpretation is well reproduced in the calculations. The configuration of these favoured

states is

$$[\pi(h_{11/2})^4]_{16+} \otimes [\nu(i_{13/2})^3(h_{9/2})^2(f_{7/2})^3]_{27-} \text{ for the } 43^- \text{ state and} \\ [\pi(h_{11/2})^4]_{16+} \otimes [\nu(i_{13/2})^3(h_{9/2})^3(f_{7/2})^2]_{33-} \text{ for the } 49^-.$$

In the  $(-,0)$  states the favoured  $48^-$  state is identified as the band terminating state with the configuration  $[\pi(h_{11/2})^4]_{16+} \otimes [\nu(i_{13/2})^3(h_{9/2})^2(f_{7/2})^3]_{32-}$ . The crossing between the collective structure and the terminating, weakly collective structure, is predicted at  $\sim 44^-$  in this sequence.

In  $^{157}\text{Er}$  a similar analysis of the data is possible. For example, in the  $(-,+1/2)$  sequence the favoured states at  $\frac{77}{2}^-$  and  $\frac{89}{2}^-$  are interpreted as the single particle states

$$[\pi(h_{11/2})^4]_{16+} \otimes [\nu(i_{13/2})^2(h_{9/2}, f_{7/2})^5]_{45/2-} \text{ and} \\ [\pi(h_{11/2})^4]_{16+} \otimes [\nu(i_{13/2})^2(h_{9/2}, f_{7/2})^5]_{57/2-}, \text{ respectively.}$$

Table 1 summarises the oblate states established experimentally in  $^{157,158}\text{Er}$ . It is seen that the equivalent states in  $^{157}\text{Er}$  are related to those in  $^{158}\text{Er}$  by the removal of one  $i_{13/2}$  neutron in each case. Also given in table 1 are the predicted deformations for these states which are all at a very similar oblate deformation of  $\epsilon \sim -0.14$ . In total eleven single particle states have now been observed giving the full spectrum of states that can be formed by these favoured orbitals. The difference in energy of these, rather pure, single-particle states corresponds to a change in the occupation of specific neutron orbitals and therefore can be used to build up a detailed spectrum of states at this oblate deformation. The particle exchange  $\nu(h_{9/2, \Omega=5/2}) \rightarrow \nu(f_{7/2, \Omega=-7/2})$ , see table 2, is established in four sequences in  $^{157,158}\text{Er}$  and also in  $^{157}\text{Ho}$  [26]. The experimental energy differences are all very similar indicating a very stable oblate mean field.

Table 1. The lowest energy oblate states in  $^{157}\text{Er}$  and  $^{158}\text{Er}$ . The spin and parity of the state, the neutron configuration and the predicted deformation is given. The four valence protons have the configuration  $[\pi(h_{11/2})^4]_{16+}$  for all the states.

$I^\pi$	Configuration	$\epsilon$	$I^\pi$	Configuration	$\epsilon$
$\frac{69}{2}^+$	$[\nu(i_{13/2}), (h_{9/2}, f_{7/2})^6]_{37/2+}$	-0.131	$40^+$	$[\nu(i_{13/2})^2(h_{9/2}, f_{7/2})^6]_{24+}$	-0.146
$\frac{81}{2}^+$	$[\nu(i_{13/2}), (h_{9/2}, f_{7/2})^6]_{49/2+}$	-0.114	$46^+$	$[\nu(i_{13/2})^2(h_{9/2}, f_{7/2})^6]_{30+}$	-0.136
$\frac{77}{2}^-$	$[\nu(i_{13/2})^2, (h_{9/2}, f_{7/2})^5]_{45/2-}$	-0.144	$43^-$	$[\nu(i_{13/2})^3(h_{9/2}, f_{7/2})^5]_{27-}$	-0.151
$\frac{89}{2}^-$	$[\nu(i_{13/2})^2, (h_{9/2}, f_{7/2})^5]_{57/2-}$	-0.114	$49^-$	$[\nu(i_{13/2})^3(h_{9/2}, f_{7/2})^5]_{33-}$	-0.136
$\frac{87}{2}^-$	$[\nu(i_{13/2})^2, (h_{9/2}, f_{7/2})^5]_{55/2-}$	-0.130	$48^-$	$[\nu(i_{13/2})^3(h_{9/2}, f_{7/2})^5]_{32-}$	-0.137
$\frac{71}{2}^+$	$[\nu(i_{13/2}), (h_{9/2}, f_{7/2})^6]_{39/2+}$	-0.135	$41^+$	$[\nu(i_{13/2})^2(h_{9/2}, f_{7/2})^6]_{25+}$	-0.150

**Table 2.** Energy differences for the particle exchange  $\nu(h_{9/2, \Omega=5/2}) \rightarrow \nu(f_{7/2, \Omega=-7/2})$  observed in  $^{157}\text{Er}$ ,  $^{158}\text{Er}$  and  $^{157}\text{Ho}$  [26]. For  $^{157,158}\text{Er}$  comparison is made with the present calculations.

Particle Exchange	Experiment (keV)	Calcs (keV)
$^{157}\text{Er} - E_x(\frac{81}{2}^+) - E_x(\frac{69}{2}^+) \quad \nu(h_{9/2, \Omega=5/2}) \rightarrow \nu(f_{7/2, \Omega=-7/2})$	2831	2680
$^{157}\text{Er} - E_x(\frac{89}{2}^-) - E_x(\frac{77}{2}^-) \quad \dots \dots$	3051	2840
$^{158}\text{Er} - E_x(46^+) - E_x(40^+) \quad \dots \dots$	3284	2864
$^{158}\text{Er} - E_x(49^-) - E_x(43^-) \quad \dots \dots$	3127	2932
$^{157}\text{Ho} - E_x(\frac{87}{2}^-) - E_x(\frac{75}{2}^-) \quad \dots \dots$	3318	—

## References.

- [1] A. Bohr and B.R. Mottelson, Nuclear Structure, Vol 2 (Benjamin, New York, 1975) pp. 84.
- [2] T. Bengtsson and I. Ragnarsson Phys. Scr. **T5** (1983) 165.
- [3] J. Simpson et al., Phys. Rev. Lett., **53** (1984) 648.
- [4] P.O. Tjøm et al., Phys. Rev. Lett., **55** (1985) 2405.
- [5] E.M.Beck et al., Phys. Lett **B215** (1988) 624.
- [6] F.S.Stephens et al., Phys. Rev. Lett., **54** (1985) 2584.
- [7] H.W.Cranmer-Gordon et al., Nucl. Phys. **A465** (1987) 506.
- [8] W.C.Ma et al., Phys. Rev. Lett. **61** (1988) 46.
- [9] C.Baktash et al., Phys. Rev. Lett., **54** (1985) 978.
- [10] D.C.Radford et al., Nucl. Phys. **A545** (1992) 665.
- [11] I.Ragnarsson, Z.Xing, T.Bengtsson and M.A.Riley Phys. Scr. **34** (1986) 651.
- [12] T. Bengtsson and I. Ragnarsson Nucl. Phys. **A436** (1985) 14.
- [13] J. Dudek and W. Nazarewicz Phys. Rev. **C31** (1985) 298.
- [14] M.A. Riley et al., Phys. Lett. **B177** (1986)15.
- [15] I.Ragnarsson et al., Phys. Rev. Lett. **54** (1985) 982.
- [16] T. Bengtsson Nucl. Phys. **A512** (1990) 124.
- [17] J.Simpson et al., Phys. Lett. **B327** (1994) 187.
- [18] S.Gale et al., J.Phys.G submitted
- [19] F. Beck et al, Prog. Part. Nucl. Phys. **28**(1992) 443.
- [20] P.J.Nolan Nucl. Phys. **A520** (1990) 657c.
- [21] C.W.Beausang et al., Nucl. Instrum. and Meth., **A313** (1992) 285.
- [22] M.A.Riley et al., to be published.
- [23] T.Bengtsson and I.Ragnarsson Nucl. Phys. **A436** (1985) 14.
- [24] M.A.Riley et al., Phys. Lett. **B177** (1986)15.
- [25] T.Bengtsson Nucl. Phys. **A512** (1990) 124.
- [26] D.C.Radford et al., Nucl. Phys. **A545** (1992) 665.

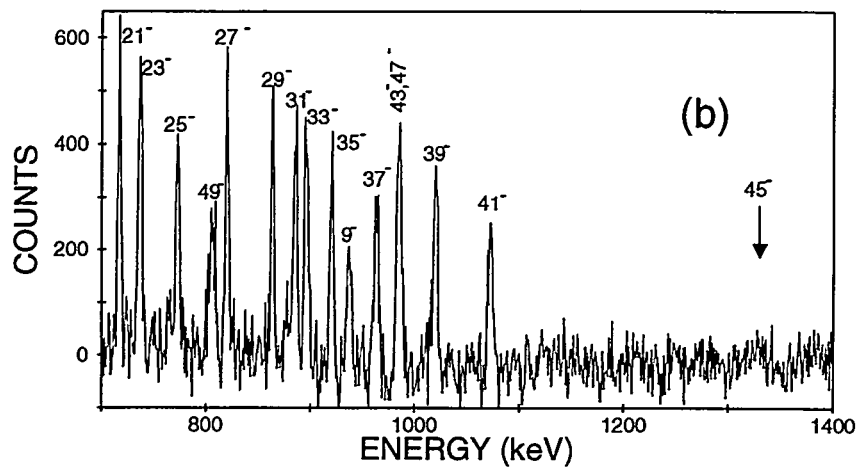
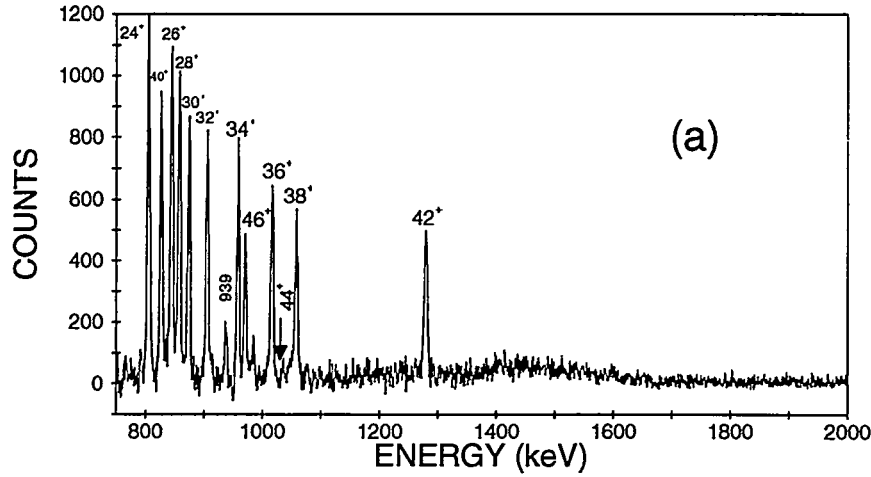


Figure 1: Transitions in coincidence with (a) the 1031 keV ( $44^+ \rightarrow 42^+$ )  $\gamma$ -ray from a matrix selected by pairs of  $\gamma$ -rays in the (+,0) sequence, (b) the 1330 keV ( $45^- \rightarrow 43^-$ )  $\gamma$ -ray from a matrix selected by single  $\gamma$ -rays in the (-,1) sequence.

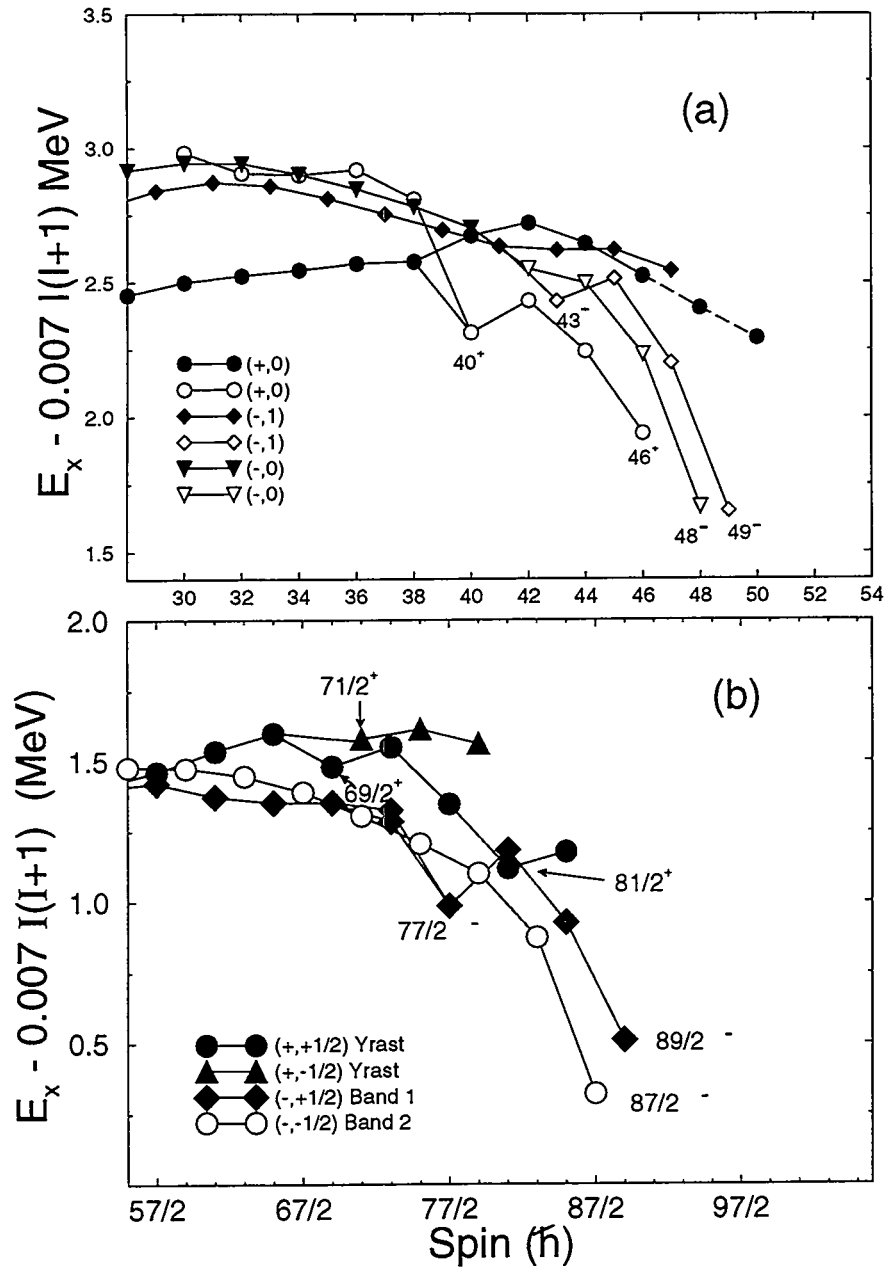


Figure 2: Excitation energy  $E_x$  minus a rigid rotor reference ( $0.007 I(I+1)$ ) as a function of spin for high spin states in (a)  $^{158}\text{Er}$  and (b)  $^{157}\text{Er}$ .

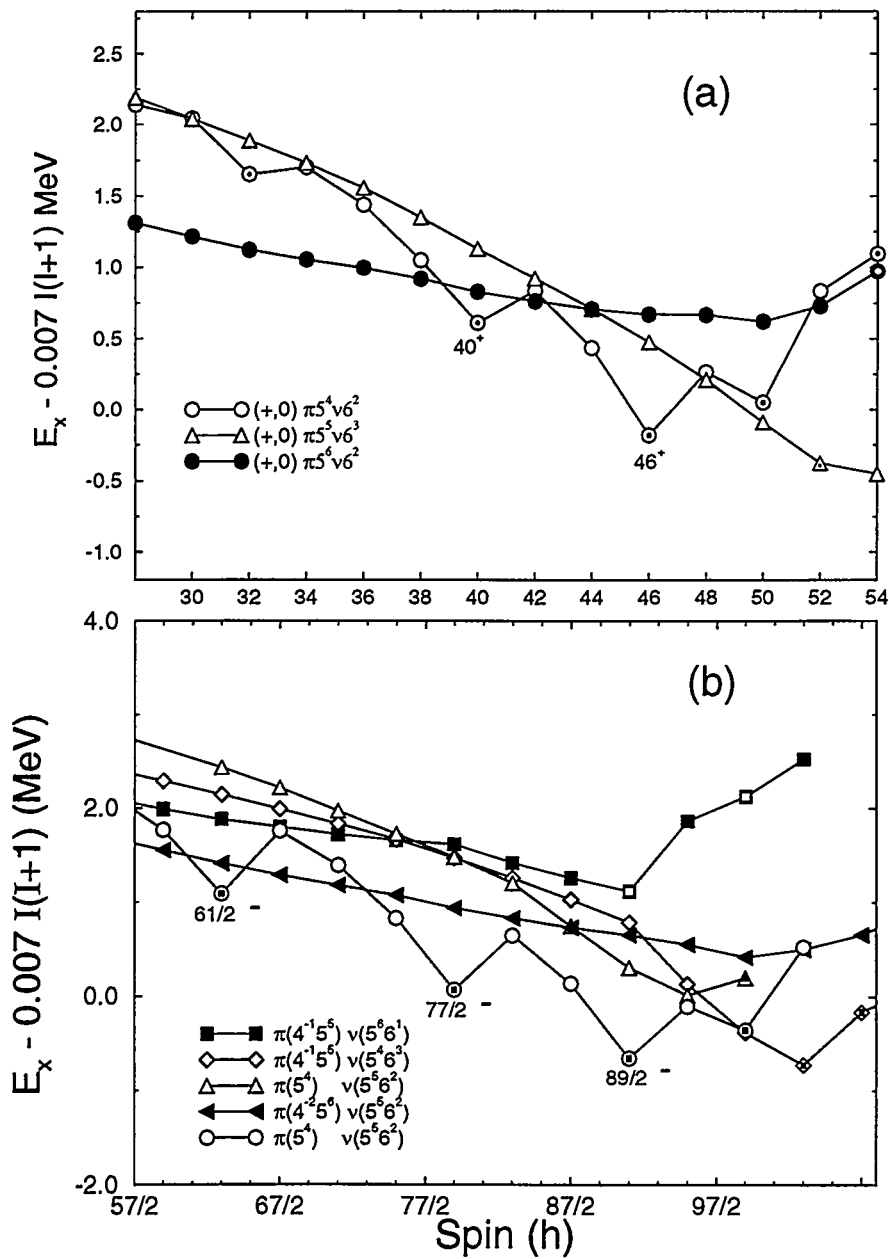


Figure 3: Excitation energy  $E_x$  minus a rigid rotor reference ( $0.007 I(I+1)$ ) as a function of spin for high spin states for (a) the  $(+,0)$  states in  $^{158}\text{Er}$  and (b) the  $(-,+1/2)$  states in  $^{157}\text{Er}$ . The oblate states are denoted by a dotted symbol.



# Unpaired Spectroscopy Around and Beyond Spin $50\hbar$ in $^{155,156}\text{Dy}$

M.A. Riley<sup>1</sup>, J. Simpson<sup>2</sup>, T.B. Brown<sup>1</sup>, J.F. Sharpey-Schafer<sup>3</sup>,  
D.E. Archer<sup>1</sup>, J. Döring<sup>1</sup>, P. Fallon<sup>4</sup>, C.A. Kalfas<sup>5</sup> and S.L. Tabor<sup>1</sup>

- 1) Department of Physics, Florida State University, Tallahassee, Florida 32306 USA
- 2) DRAL, Daresbury Laboratory, Daresbury, Warrington, WA4 4AD, U.K.
- 3) Oliver Lodge Laboratory, University of Liverpool, Liverpool L69 3BX, U.K.
- 4) Nuclear Science Division, Lawrence Berkeley Laboratory, Berkeley, CA 94720 USA
- 5) Institute of Nuclear Physics, NCSR Demokritos, 15310 Athens, Greece

**Abstract:** *Very high spin states in  $^{155,156}\text{Dy}$  have been observed using the early implementation of Gammasphere. In  $^{155,156}\text{Dy}$  the level schemes have been considerably extended up to and above spin  $50\hbar$ . The behavior of the  $(+,0)$  yrast band in  $^{156}\text{Dy}$  which splits into two branches above  $I = 40$  is interpreted in terms of an unpaired collective band crossing. In one sequence spin states up to  $I = 54^+$  were observed, the highest spin so far observed in a normal deformed nucleus. In  $^{155}\text{Dy}$  our results greatly enhance the picture of co-existing collective and terminating sequences in this nucleus. In addition, the level scheme of  $^{155}\text{Tb}$  is established up to spin  $30\hbar$  via the weak  $p4n$  channel extending the odd- $Z$   $N = 90$  systematics.*

**EXPERIMENTAL DETAILS:** Very high spin states in  $^{155,156}\text{Dy}$  were populated using the  $^{124}\text{Sn}(^{36}\text{S},5n,4n)$  reaction at a beam energy of 160 MeV. The beam was provided by the 88" Cyclotron at Lawrence Berkeley Laboratory. Both thin and backed target data were collected for nine and one shifts respectively. The thin target consisted of two stacked foils of  $^{124}\text{Sn}$  each of thickness  $500\mu\text{g}\cdot\text{cm}^{-2}$ . The backed target consisted of  $1.5\text{mg}\cdot\text{cm}^{-2}$  of  $^{124}\text{Sn}$  with a  $10\text{mg}\cdot\text{cm}^{-2}$  Au backing. Approximately  $1.5 \times 10^9$   $\gamma^3$  coincidence events were collected in the thin target experiment using the E.I. Gammasphere array with 34 Compton suppressed Ge detectors.

Initial analysis of the thin target data has been performed using RADWARE [1] in particular utilizing the cube inspection program LEVIT8R. Over 200 new transitions have been identified and placed in level schemes. Although the  $4n$ ,  $5n$ ,  $6n$  reaction channels to  $^{154,155,156}\text{Dy}$  account for about 95% of the observed reaction cross section, the wonderful ability of Gammasphere to resolve weak channels has enabled a great deal of new information to be extracted for the weak ( $< 1 - 2\%$ )  $p4n$  (Tb) and  $\alpha xn$  (Gd) channels.

**RESULTS FOR  $^{155}\text{Tb}$ :** The  $N = 90$  nuclei are the best studied normal deformed chain of isotones to very high spin. Fig. 1 shows a plot of proton number versus observed maximum spin observed in each of these nuclei. The sudden drop which occurs below  $Z=66$  (Dy) reflects the fact that only light ion beams ( $A \leq 11$ ) can be used to produce these  $Z \leq 65$  nuclei via the dominant  $(\text{HI},xn)$  reaction. In the case of  $^{155}\text{Tb}$  ( $Z=65$ ) the extremely low known maximum published spin value

( $I=11.5\hbar$ ) is also the result of the fact that it has not previously been studied using a modern Compton suppressed Ge array. Fig. 2 shows the preliminary level scheme to  $I \sim 30\hbar$  for the negative parity yrast band of  $^{155}\text{Tb}$  via the  $(^{36}\text{S},p4n)$  reaction. Fig. 3(a) shows the alignment plot for this band with the first (AB)  $i_{13/2}$  neutron backbend occurring in both signatures near  $\hbar\omega \sim 0.27$  MeV. These results are valuable since they complete the  $N=90$  high spin systematics from  $Z = 63$  to 71 allowing trends to be mapped out, such as the AB band crossing frequencies shown in Fig. 3(b).

**RESULTS FOR  $^{155}\text{Dy}$ :** The level scheme for  $^{155}\text{Dy}$  has been considerably extended in our initial analysis. For example, the lowest energy positive parity band has been extended from spin  $I = \frac{73}{2}^+$  to  $I = \frac{101}{2}^+$ . Fig. 4 shows a plot of excitation energy minus a rigid rotor reference for bands in  $^{155}\text{Dy}$  observed to very high spin. It is interesting to note the co-existence of both sharply downsloping bands as well as bands which continue in a regular smooth upward fashion. Part of the downsloping behavior had been observed previously and has been discussed as a signature of the approach to band termination [2,3,4,5]. Indeed lifetime measurements [5] had shown much smaller  $Q_t$  values for the downsloping negative parity bands as compared to the  $(+, +\frac{1}{2})$  band. Our results confirm and enhance these observations. Fig. 5 shows gated spectra from the thick target data for the continually upsloping  $(+, +\frac{1}{2})$  band 6 and the two strongly downsloping negative parity bands 5 and 7. Whereas all the high spin/energy transitions are sharp for the negative parity sequences indicating long feeding times, for the positive parity band (top) the peaks broaden out and quickly smear into the background indicating fast collective behavior. Thus these data beautifully illustrate the shape co-existence in this nucleus and verify the interpretation of strongly downsloping trajectories in plots such as Fig. 4 with terminating band structures undergoing drastic shape changes.

The unpaired cranking calculations of the Lund group [3,5] correspond rather well with the experimental observations for the negative parity bands above spin  $30\hbar$  correctly predicting the downsloping behavior ending in aligned band terminating oblate states just below  $50\hbar$ . However these calculations predict poorly the behavior of the  $(+, +\frac{1}{2})$  sequence where several band crossings and a sharp downsloping is expected between spins 30 to 50 but this is not observed in experiment. The underlying cause of this disagreement between theory and experiment is under investigation.

**RESULTS FOR  $^{156}\text{Dy}$ :** A large number of rotational bands had been observed previously in  $^{156}\text{Dy}$  [6,7] to high spin ( $I > 35\hbar$ ). Extensions to these previously known band structures up to and above spin 50 have been made. The present report concentrates on the yrast positive parity structures.

At  $I = 40^+$  the yrast  $(+, 0)$  band undergoes an irregularity for which two possible scenarios have been put forward [6,7,8]. The first possibility involved the perturbation of the yrast line by a low lying oblate state. Similar phenomenon had been observed in neighboring nuclei and indeed a favored configuration of  $\pi(h_{11/2})^2\nu[(f_{7/2})^3(h_{9/2})^3(i_{13/2})^2]$  was expected to occur at  $I = 40^+$  in keeping with these systematics. The second possibility which we proposed following a further experiment [7] interpreted the anomaly at  $I = 40^+$  as due to a crossing between two

collective bands. Indeed cranking calculations [9,10] without pairing correlations included predicted such a crossing near this spin. This latter picture seemed correct since Doppler shift attenuation data showed that the (+,0) structure which fragmented at spin 40 remained collective. More detailed lifetime measurements by Emling *et al.* [5] supported these suggestions but certain question marks remained.

In the present experiment the level structure around and above  $40^+$  has been clarified and extended up to  $I = 54^+$ , the highest spin state known in a normal deformed nucleus. Fig. 6 shows a plot of excitation energy minus a rigid rotor reference versus spin for the (+,0) structures in  $^{156}\text{Dy}$  compared with the unpaired cranking calculations of T. Bengtsson and I. Ragnarsson. The encircled theoretical data points correspond to oblate ( $\gamma = 60^\circ$ ) shape and are associated with band terminating states. The agreement between theory and experiment around and beyond spin 40 for the lowest energy sequences is remarkably good. Around spin 40 the calculated structures are predicted to be rather collective with quadrupole transition moments  $Q_t \sim 3-4$  eb. This fits in well with the earlier observations and measurements [5,7] as well as our present backed target results. This feature is in complete contrast to the neighboring  $N = 90$  nucleus  $^{158}\text{Er}$  where the high spin yrast transitions are sharp indicating much longer feeding times. From Fig. 6 it can be seen that the lowest energy bands in  $^{156}\text{Dy}$  are predicted to terminate at  $I = 50$  and slightly higher. Thus the question arises, "Is the yrast (+,0) band above  $I = 40$  really the  $\nu 6^2 \pi 5^4$  configuration and if so how exactly do the effects of band termination manifest themselves with regard to the  $Q_t$  values?" i.e. "Is there a gradual loss of collectivity with spin in this band as well as the second close lying (+,0) band, or is it a reasonably sharp effect which occurs quite close to the terminating spin value?" Further study and a dedicated lifetime experiment are required to answer these important questions.

The software support of D.C. Radford, R. McCleod and W.T. Milner is greatly appreciated. Support for this work was provided by the U.S. Department of Energy, the National Science Foundation, the State of Florida and the U.K. Science and Research Engineering Council. MAR and JS acknowledge the receipt of a NATO Collaborative Research Grant.

- [1] D.C. Radford, Conf. on Nucl. Str. at High Ang. Mom. and Workshop on Gamma-Ray Detector Arrays, Ottawa and Chalk River, May 1992, Vol.2,p403.
- [2] R. Vlastou *et al.*, Nucl. Phys. (in press).
- [3] Z. Xing, I. Ragnarsson and T. Bengtsson, Phys. Lett. **177B**, 265 (1986).
- [4] I. Ragnarsson *et al.*, Phys. Scr. **34**, 651 (1986).
- [5] H. Emling *et al.*, Phys. Lett. **217B**, 33 (1989).
- [6] M.A. Riley *et al.*, Nucl. Phys. **A486**, 4546 (1988).
- [7] J.D. Morrison *et al.*, Europhys. Lett. **6(6)**, 493 (1988).
- [8] M.A. Riley *et al.*, Phys. Lett. **135B**, 275 (1986).
- [9] J. Dudek and W. Nazarewicz, Phys. Rev. **C31**, 298 (1985).
- [10] T. Bengtsson and I. Ragnarsson, priv. comm.

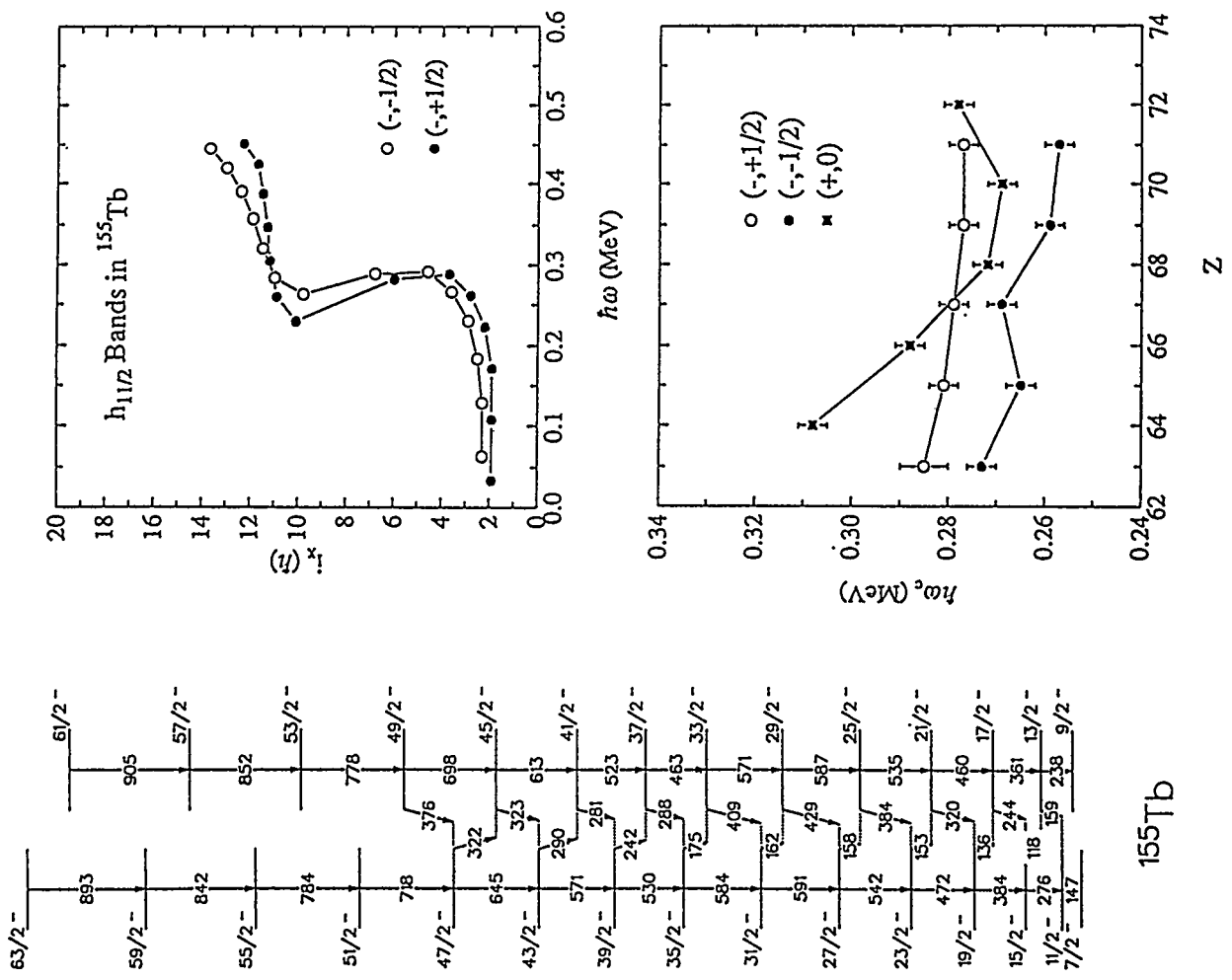


Fig. 1 (above) observed maximum spin versus Z for the N = 90 isotones.

Fig. 2 (middle)  $^{155}\text{Tb}$ , preliminary level scheme.

Fig. 3a (top right) alignment plot for  $^{155}\text{Tb}$  and 3b (bottom right) the systematics of the AB crossing frequencies for N = 90 nuclei.

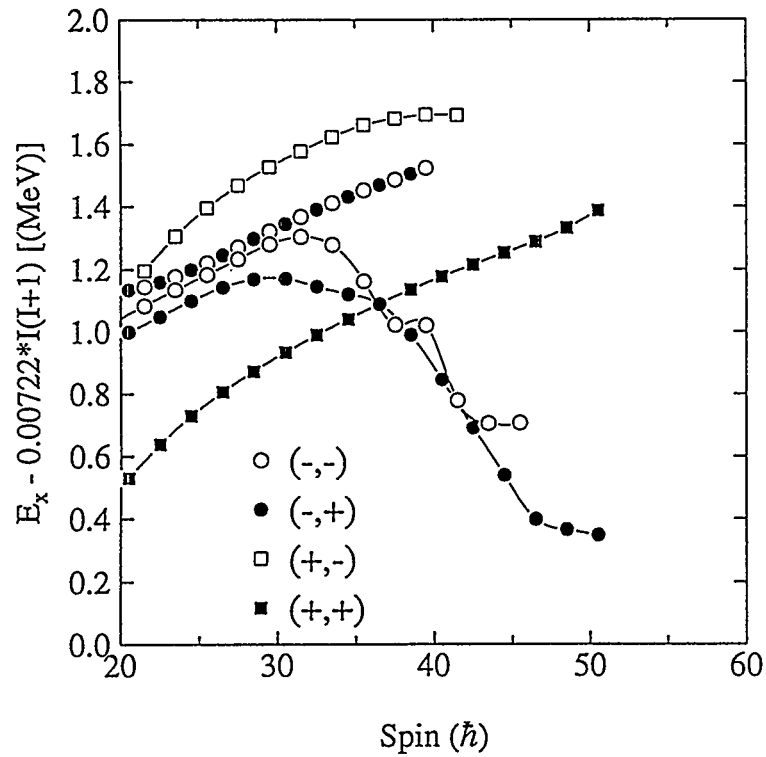
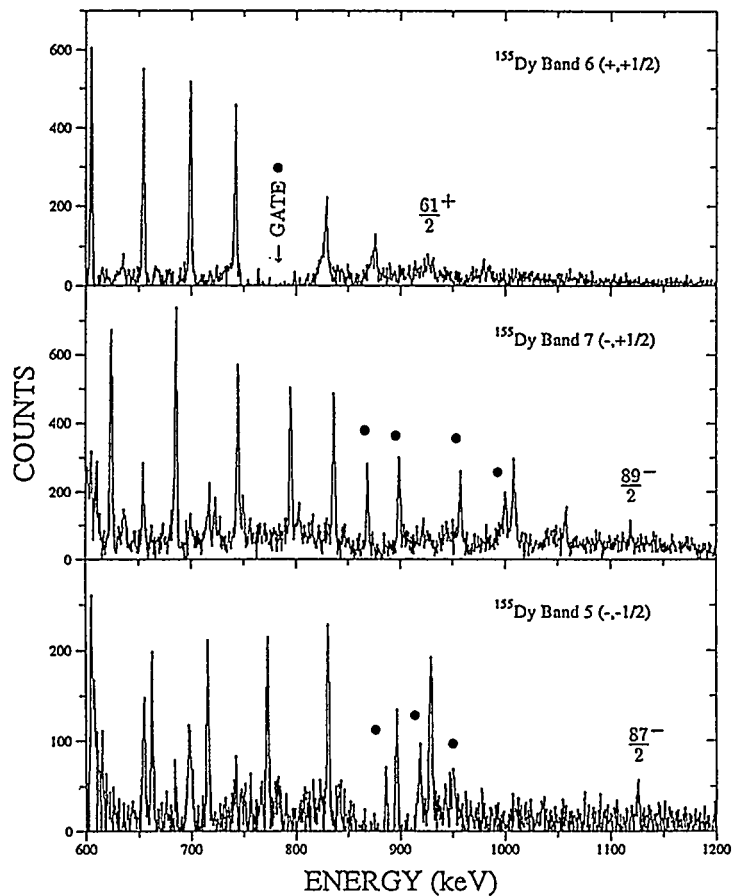


Fig. 4. Excitation energy minus a rigid rotor reference for selected bands in  $^{155}\text{Dy}$ .  
 Fig. 5. Coincidence spectra from the thick target data for selected bands in  $^{155}\text{Dy}$ .



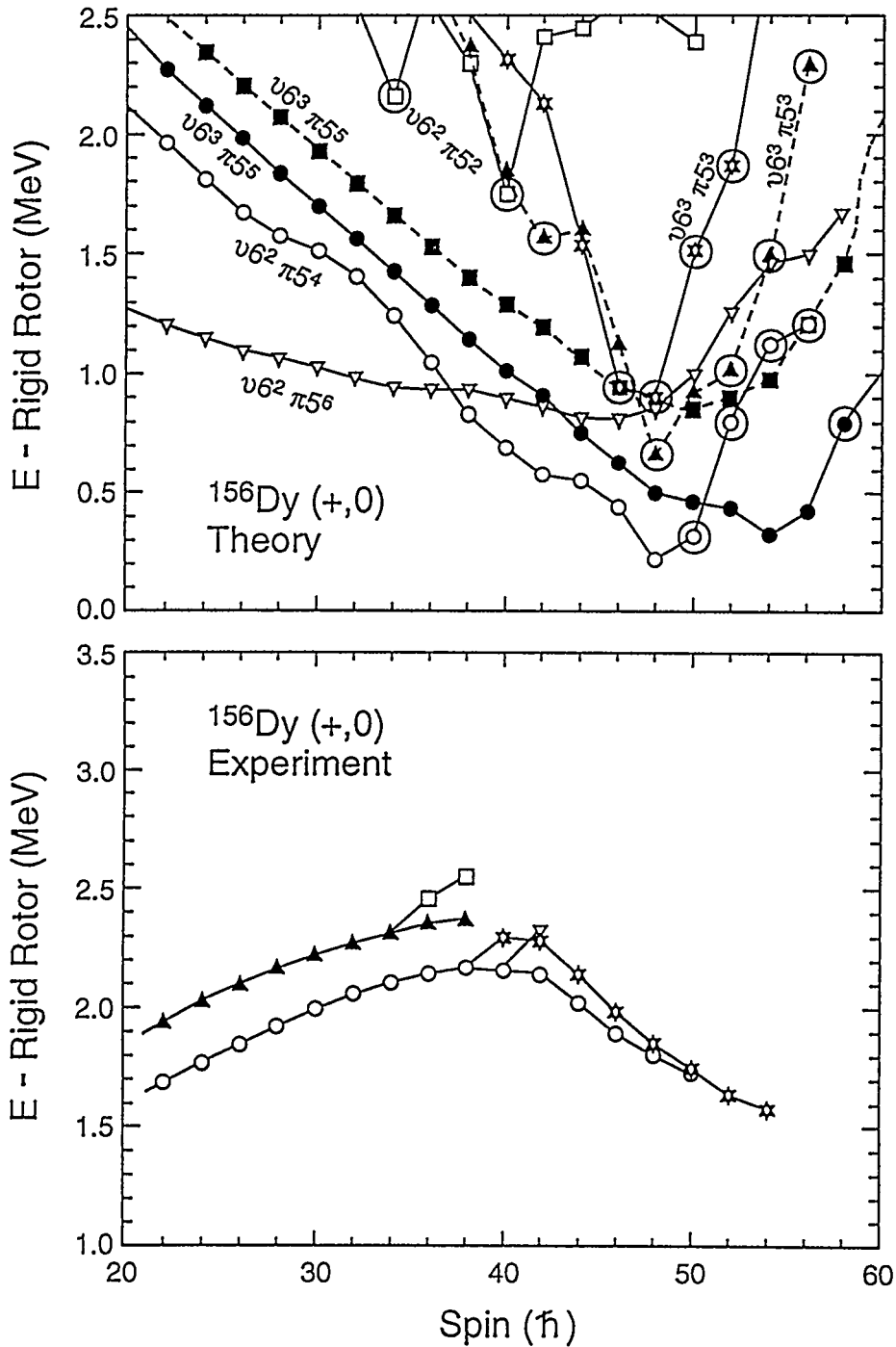


Fig. 6. Excitation energy minus a rigid rotor reference plots for experiment (bottom) and unpaired cranking calculations by T. Bengtsson and I. Ragnarsson (top). Encircled theoretical data points indicate oblate ( $\gamma = 60$ ) states.

# Warm Rotating Nuclei

T. Døssing\*

*Physics Division, Argonne National Laboratory,  
Argonne, IL 60439, USA*

**Abstract:** The damped rotational motion of a well deformed nucleus is discussed in qualitative terms. Fluctuations of two-dimensional  $\gamma$ -ray spectra are shown to provide an overall support of the damping picture. Finally, some current problems in the understanding of fluctuations are discussed.

## 1 Introduction

The improving quality of multi- $\gamma$ -ray detector systems will make it possible during the next few years to push the frontier of detection of discrete  $\gamma$ -transitions up in rotational frequency and heat energy (heat energy = the energy above yrast). In level schemes of rotating nuclei, the quest for higher rotational frequency is manifested as new lines added on top of already known lines, and the quest for higher heat energy shows up as new, weakly populated bands to the left or right of the already known bands. Of the order of 10 to 20 resolved rotational bands in a nucleus has become the typical number for normal deformed nuclei in the spectra we have witnessed at this conference, and these have been obtained with the present generation of high resolution systems. The 10 to 20 resolved bands typically cover the heat energy interval up to around 500 keV for rare earth nuclei.

The subject of the present paper is the rotational motion above this heat energy. We know from studies of  $E_{\gamma_1} \times E_{\gamma_2}$  spectra that with increasing heat energy the manifestation of rotational motion in the nucleus changes from well behaved rotational bands into damped rotation. Here, the emphasis will be on illustrative discussions of the basic physics of damped rotation, continuing on to describe also in qualitative terms the current status and unsolved problems, with special emphasis on the information contained in fluctuations of  $E_{\gamma_1} \times E_{\gamma_2}$  spectra. Shapes of damped spectra in two- and three dimensions are discussed by Silvia Leoni at this conference.

Since the discrete spectroscopy is about to be able to address the region of heat energy for the onset of damping, it may be appropriate to outline properties of discrete bands, which will be relevant also for discussion of damped rotation.

\* permanent address: The Niels Bohr Institute, University of Copenhagen, Copenhagen, Denmark.

The multitude of rotational bands in neighbouring nuclei allows for a systematic search for the elementary excitations, described by their parity, excitation energy and alignment. Both at normal and superdeformed shapes, such an analysis provides an overall success for the rotating mean field in describing the excitations [1]. However, certain band properties require a consideration of how specific orbits pull on the overall shape of the nucleus, while other bands, such as the bands containing  $\Delta I = 4$  staggering, and identical bands point to couplings between the rotational motion and the elementary excitations which lie outside the standard rotating mean field treatment, and which are not yet fully understood.

For the quantities we are concerned with here, an important property of mean field states is the additivity of the elementary excitations. Without specifically referring to mean field states, the question of the independence of excitations can be addressed experimentally by investigating the statistics of level distances. For angular momenta above 20 units, typically two to four level spacings for each parity-signature may be achieved, and their level distances generally confirm the independence of excitations [2].

With increasing heat energy, the energy spacings between the rotational bands will decrease exponentially, and one expects that interactions between them leads to a more complex picture with many cross-over transitions, and manifestations of level repulsion where two bands cross. In the presently known 10 to 20 rotational bands of typical rare earth nuclei, such properties are seen here and there, but not yet in any systematic way. By implementing fully the new generation of detector systems, the next 20 bands will be added on, going up to heat energy around 900 keV, where we expect a persistent and systematic occurrence of band mixing.

## 2 Damped Rotation

To learn about the region of rotational damping experimentally, we must at present analyse unresolved  $\gamma$ -spectra, the so-called quasi-continuum spectroscopy. Most of the damped decay will probably continue to be hidden from discrete spectroscopy. Indeed, in a rare earth nucleus around the modest heat energy  $U = 2$  MeV, we are already at level number 200 of each of the four parities and signatures, the distance between levels being about 2 keV. The rotational decay out of each state branches out to about 25 different transitions. The construction of a level scheme with such properties is well beyond the capability of the present- and near future detection systems.

Based upon the success of the rotating mean field description of the low heat energies, the description of rotational damping takes cranked mean field states as basis rotational bands, providing the rotational E2 transitions. In this basis, the damping comes about through mixing. Eventually, at high heat energy, compound nucleus states arise, with GOE properties.

The situation in warm rotating nuclei differs from that of non rotating nuclei in one important respect. The rotational decay probes the difference in mixing between two neighbouring angular momenta  $I$  and  $I - 2$  (and, if one looks at  $E_{\gamma_1} \times E_{\gamma_2}$  spectra, three neighbouring angular momenta [3]). Since this corresponds to a rather modest change



in the rotational frequency, the rotational decay in a way probes the differential of the mixing coefficients with respect to rotational frequency. Furthermore, the rotational decay competes favorably with the statistical transitions which attempt to cool down the nucleus. This allows for studying the differential mixing over several steps, keeping the heat energy, something which is completely excluded for strength function phenomena in non-rotating nuclei.

## 2.1 Illustration of Damped Rotational Motion

At finite temperature, the rotating mean field states acquire a spreading width, due to the coupling to the other mean field states, and finally into the energy eigenstates (compound states) of the rotating nucleus. The quantal strength function describing the rotational strength has been evaluated by Bent Lauritzen *et. al.* [4] The relation between the rotational damping width and the compound spreading width, derived in ref. [4], and later related to dephasing phenomena of collective excitations in condensed matter physics [5], can be illustrated by a simple picture of the damped rotation, figure 1. The compound spreading width of mean field states  $\Gamma_\mu$  measures the inverse of the time during which the nucleus can stay in one mean field state, before hopping to the next. This hopping motion results in a time-variation of the quadrupole field as illustrated in fig. 1, consisting of small segments of harmonic vibration, with frequencies  $2\omega_\mu$ ,  $2\omega_{\mu'}$ ,  $2\omega_{\mu''}$  etc. The frequency distribution of this field is obtained by a Fourier decomposition, the width being the rotational damping width  $\Gamma_{rot}$ .

If the time between hops is very long, the test Fourier frequency will only in very rare cases match two neighbouring segments. Therefore, it should be chosen such as to trace only one of the segments, and it will then go out of phase with the next. The condition for this loss of phase from segment to segment is that  $2\Delta\omega_0\tau_\mu > 1$ , with  $\Delta\omega_0$  being the dispersion of the distribution of rotational frequencies of the basis bands, and  $\tau_\mu = \Gamma_\mu^{-1}$  is the average time spent within a basis band. Under this condition, the Fourier decomposition just gives back the frequency distribution of the basis bands:

$$\Gamma_{rot} \approx 2.35 \times 2\Delta\omega_0 \quad (\text{for } 2\Delta\omega_0 > \Gamma_\mu) \quad (1)$$

where the factor 2.35 for a Gaussian distribution translates from dispersion to FWHM. If, conversely, the time between segments is very short, the harmonic test function for the Fourier analysis can stay in phase with the quadrupole field over many hops. After the time  $t$ , and on the average  $n = \frac{t}{\tau_\mu}$  segments, a dispersion in the phase of the quadrupole field relative to the average is accumulated as a random walk. For a Fourier test frequency, which differs by the frequency  $\delta\omega$  relative to the average, the accumulated phase variance after the time  $t$  is given by

$$\Delta\phi^2 = (2\Delta\omega_0\tau_\mu)^2 \frac{t}{\tau_\mu} + \delta\omega^2 t^2 \quad (2)$$

The condition on the frequency deviation  $\delta\omega$  is that the second term remains small as long as the first term is smaller than one. Taking now  $\delta\omega$  as the width of the Fourier

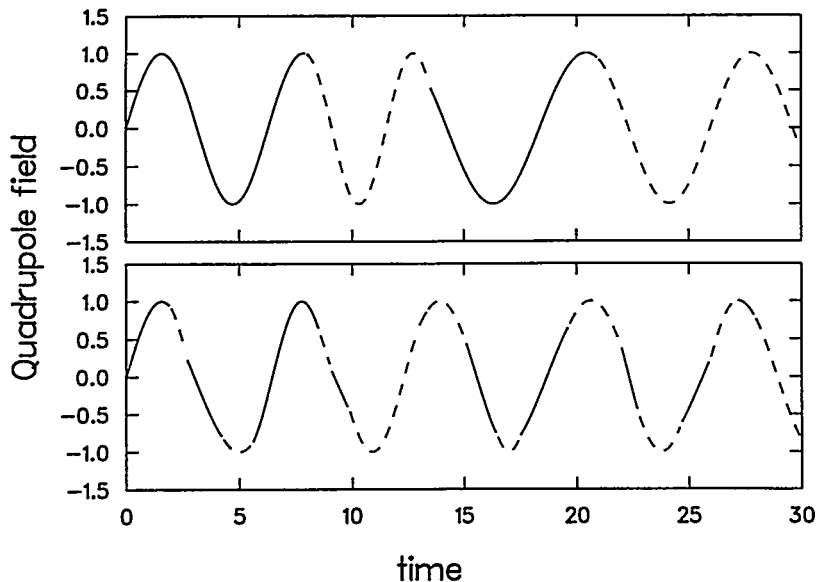


Figure 1: Schematic illustration of the time variation of the quadrupole field outside a nucleus undergoing damped rotation. In the top part of the figure, the hops between basis bands are infrequent,  $2\Delta\omega_0\tau_\mu \approx 1.8$ , and the width of the frequency distribution of the field will be the same as that of the ingoing basis bands. In the bottom part of the figure, the hops between basis bands are frequent,  $2\Delta\omega_0\tau_\mu \approx 0.3$ , leading to a motional narrowing of the frequency distribution of the field.

analysis frequency distribution, one arrives at the following condition:

$$\delta\omega^2 t^2 \approx (2\Delta\omega_0\tau_\mu)^2 \frac{t}{\tau_\mu} \approx 1 \quad (3)$$

from which one obtains

$$\Gamma_{rot} \approx 2\delta\omega \approx 2\frac{1}{t} = 2(2\Delta\omega_0)^2\tau_\mu = 4\Delta\omega_0 \frac{2\Delta\omega_0}{\Gamma_\mu} \quad (\text{for } 2\Delta\omega_0 < \Gamma_\mu) \quad (4)$$

One sees that the frequency distribution in this case becomes more narrow because of the hopping between bands, and one speaks of *motional narrowing*. The above results (1) and (4) are in agreement with the strength function treatment of reference [4], so the simple picture of figure 1 explains in a natural way the more complete and consistent results.

The figure also gives a qualitatively correct picture of the behavior of the quadrupole field.

When one speaks of the damping of a nuclear vibration, the vibrational motion is actually damped into the underlying compound nucleus states, the field outside the nucleus is rapidly damped out. Most often, the nucleus decays by other modes, that is it stops vibrating before one full quantum of energy  $\hbar\omega_{vib}$  has been sent out into the radiation field. This is of course well known from the photo absorption on nuclei, which excites the giant dipole vibration, with a very large damping width.

When one speaks of the damping of the rotational motion, the nucleus keeps rotating together with the hopping motion, eventually emitting many quanta of rotational energy before slowing down considerably. In the rotational case, each basis mean field band is equipped with a rotational decay matrix element, and the coupling of such states preserves these matrix elements. The term "damping" in this case refers to the fuzzy distribution of harmonic frequencies of the quadrupole field.

### 3 Flow line

As just stated, the damped rotational motion can be studied over many transition steps. However, in experiments, we cannot freely select a frequency and temperature distribution. Rather, we have to accept the rotational states as they are populated in the course of the  $\gamma$ -cascades following a (HI,xn) reaction. Decay cascade codes describing how the states at different heat energy and angular momentum are populated in the decay cascades have been operating for many years. However, by a simplified description, we may be able to gain insight into the essential properties of the  $\gamma$  decay cascades [6]. Consider the total decay widths for rotational E2 and statistical E1 decay, and the average heat energy removed in one step of each of these decay modes. Realistic approximations are:

$$\begin{aligned} \Gamma_{E2} &= c_{E2} I^5 & \Gamma_{E1} &= c_{E1} T^5 \\ U &= aT^2 & \Delta U_{E1} &\approx \langle E_\gamma \rangle_{>E1} = 5T & \Delta U_{E2} &\approx 0 \end{aligned} \quad (5)$$

From these basic relations one can derive a transport equation for the average temperature during a decay cascade

$$\frac{dT}{T^5} = \frac{15c_{E1}}{4ac_{E2}} \frac{dI}{I^5} \quad (6)$$

This equation has the solution

$$T = \left( \frac{4ac_{E2}}{15c_{E1}} \right)^{1/4} \frac{I}{(1 + CI^4)^{1/4}} \quad (7)$$

so that the average heat energy during a decay cascade is given by

$$U = \left( \frac{4c_{E2}}{15c_{E1}} \right)^{1/2} a^{3/2} \frac{I^2}{(1 + CI^4)^{1/2}} = c_1 \frac{I^2}{(1 + CI^4)^{1/2}} \quad (8)$$

where  $C$  is an integration constant.

Figure 2 shows solutions to this equation for some illustrative initial conditions, and for parameters relevant for a typical rare-earth nucleus. Going down the decay cascades, one sees that all solutions tend to converge towards the solution with integration constant  $C = 0$ , which defines an *asymptotic flow line*. For initial conditions above the asymptotic flow line, the solution is seen to converge rapidly within roughly the first  $\frac{1}{4}$  of the cascade. The solutions to the average energy displayed in figure 2 can pictorially be describes by stating that the rotational decay width is able to keep the rotating nucleus warm.

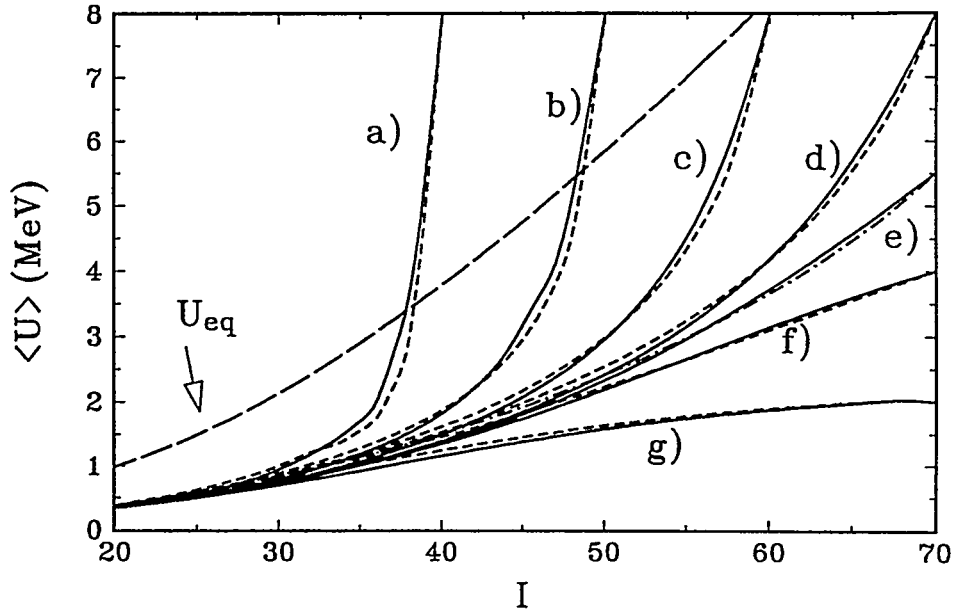


Figure 2: The average heat energy of the flow function obtained by numerical solutions of transport equations (solid lines) are shown together with the analytical approximation described here (dashed lines). The initial angular momenta and average heat energies are  $(I_0, U_0) = (40, 8)$  a),  $(50, 8)$  b),  $(60, 8)$  c),  $(70, 8)$  d),  $(70, 5.5)$  e),  $(70, 4)$  f),  $(70, 2)$  g). The curve labelled  $U_{eq}$  shows the heat energy as function of angular momentum where the E1 and E2 decay widths are equal.

Within the same scheme, also the variance of the heat energy can be treated, with the result

$$\sigma_{U_a}^2 \rightarrow c_2 I^3 \quad \text{for } I \rightarrow 0 \quad (9)$$

and the convergence with decreasing heat energy is found to be even more rapid than for the mean value. Also the yrast feeding be treated

$$-\frac{dP_{yrast}}{d(c_y I)} \approx \frac{1}{5\sqrt{\pi}} (c_y I)^{11/2} \exp(-2c_y I) \quad (10)$$

where the constants  $c_2$  and  $c_y$  of the last two equations are functions of the basic constants  $c_{E1}, c_{E2}, a$ . For a typical rotational rare earth nucleus, the values of the constants are  $c_1 = (\frac{1}{32})^2$ ,  $c_2 = (\frac{1}{46})^3$ , and  $c_y = 0.13$ , in units of MeV and  $\hbar$ .

## 4 Fluctuations of two-dimensional $\gamma$ -spectra

Figure 3 shows a two dimensional  $E_{\gamma_1} \times E_{\gamma_2}$  spectrum, as a landscape plot. The transitions from regular rotational bands can be recognized as ridges, running parallel to the diagonal of the plot at  $E_{\gamma_1} = E_{\gamma_2}$ . Such ridges are clearly visible on both sides of the flat region around the diagonal. Actually, the diagonal lies in the middle of a shallow valley, which goes down about 10 per cent relative to the surrounding smooth landscape. The ridges are superimposed on this smooth landscape. The occurrence of such landscapes

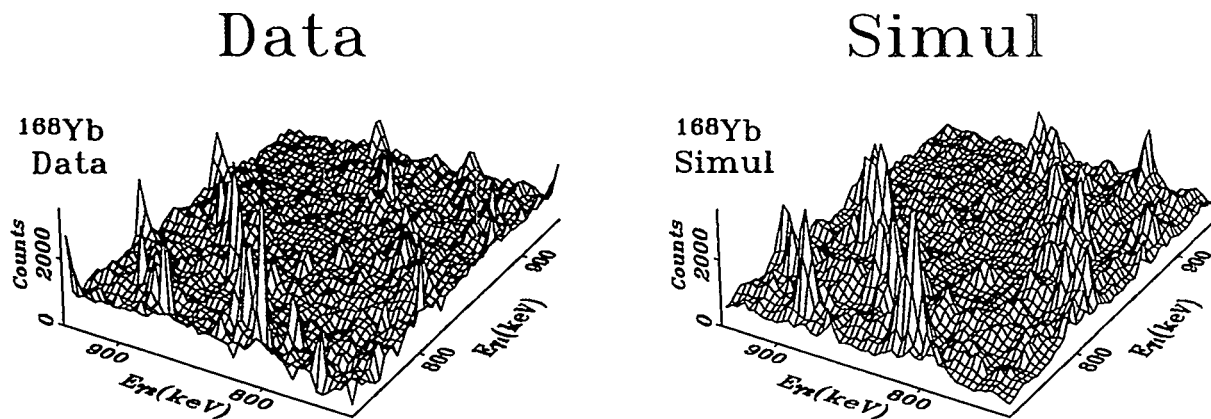


Figure 3: Perspective plot of a part of the two-dimensional  $E_{\gamma_1} \times E_{\gamma_2}$  spectrum for ESSA30 data on  $^{168}\text{Yb}$  (left hand side) and as calculated in simulations with mixed bands (right hand side). The part of the spectrum corresponds to on the average  $3 \times 3$  rotational transitions. On the right hand side of the diagonal, the known resolved discrete band transitions have been taken out.

and their interpretations in the damping picture is discussed by Silvia Leoni at this conference. It is important to realize that one has to go to two-dimensional spectra in order to be able to separate transitions from rotation along regular bands, which fall on the ridges, from damped transitions, which form a smooth spectrum, which can most cleanly be studied at the center of the valley at  $E_{\gamma_1} = E_{\gamma_2}$ .

Here, we shall focus on the roughness of the spectrum, as expressed mathematically through its fluctuations. As first pointed out by Frank Stephens [7], these fluctuations tell about the number of bands which pass through the relevant angular momentum region. By separately studying fluctuations on the ridge and in the valley, one can determine the effective number of transitions emitted along regular rotational bands, and from damped transitions, respectively. The analysis of fluctuations of nuclear spectra from non-overlapping states has been pioneered by Gregers Hansen and coworkers [8], and we take over the principles of their work for our fluctuation analysis.

#### 4.1 Method for Analysis of Fluctuations

It is important that the transition energies and strengths for the nucleus under investigation behave in a sufficiently random way. It should be such as if the nucleus has been picked from a random ensemble of nuclei, characterized by some average properties. These properties are in our case:

- (i) For discrete bands, the transition energy within an interval of width  $\frac{4}{T}$  is a ran-

dom independent variable, whereas the transition strength varies smoothly from band to band.

(ii) For damped transitions, the transition energies and strengths display GOE behavior, that is spectral rigidity for the energies, and Porter-Thomas fluctuations for the transition strengths. The ensuing fluctuations are due to the transitions strength fluctuations.

The fluctuations are normalized to the average spectrum, and the following expression can be derived [9]

$$\frac{\mu_2}{\mu_1} = \frac{N_{eve}}{N_{path}} \frac{P^{(2)}}{P^{(1)}} + 1 \quad (11)$$

Here,  $\mu_2$  is the second moment (or variance) of the two dimensional spectrum, and  $\mu_1$  is the first moment (the average).  $N_{eve}$  is the number of recorded events within a  $\frac{4}{T} \times \frac{4}{T}$  interval of the two dimensional spectrum.  $\frac{P^{(2)}}{P^{(1)}}$  is a dilution factor which arises because of the photopeak width of the detectors.

When the response of the detectors are known, and the quantities  $N_{eve}$ ,  $\mu_1$ ,  $\mu_2$  are determined in an experiment, the *effective number of decay paths*  $N_{path}$  can be determined, both for discrete bands (on the ridges), and damped rotation (in the middle of the valley).

For meaningful numbers to be extracted, one further step has to be taken to separate damped from undamped transitions. In the raw spectrum, the valley is crossed by strong stripes containing coincidences between one transition from a low-lying band and Compton scattered events. These stripes can be strongly reduced by subtraction of a suitable product spectrum, that is performing a so-called COR-subtraction, or by unfolding the spectrum. By unfolding, one runs the risk of introducing spurious fluctuations, but for good detectors these will be relatively weak. Further, for the fluctuations in the valley, the fraction of events containing one or two Compton scattered  $\gamma$ -rays has to be evaluated. A spectrum of Compton scattered transitions is truly continuous, but the actual counts contribute to pure count fluctuations, that is the second term of equation (11). The fluctuations on the ridge are in principle more straightforward, since the ridges only contain photopeak events, and they can be recognized as floating on top of the rest of the spectrum. Due to the additivity of superposed uncorrelated spectra, the ridge intensity and fluctuations can be separated from the background of damped transitions and Compton events, and analyzed separately.

The reader may now have the impression that the original experimental two-dimensional spectra have been distorted and twisted beyond recognition by arbitrary procedures, before one is finally able to determine the variance  $\mu_2$ . This is, however, not the case. Each procedure constitutes a specific step on the way to separate coincidences between the four types of single  $\gamma$ -events, discrete band transitions, damped transitions, statistical decay transitions, and Compton scattered events.

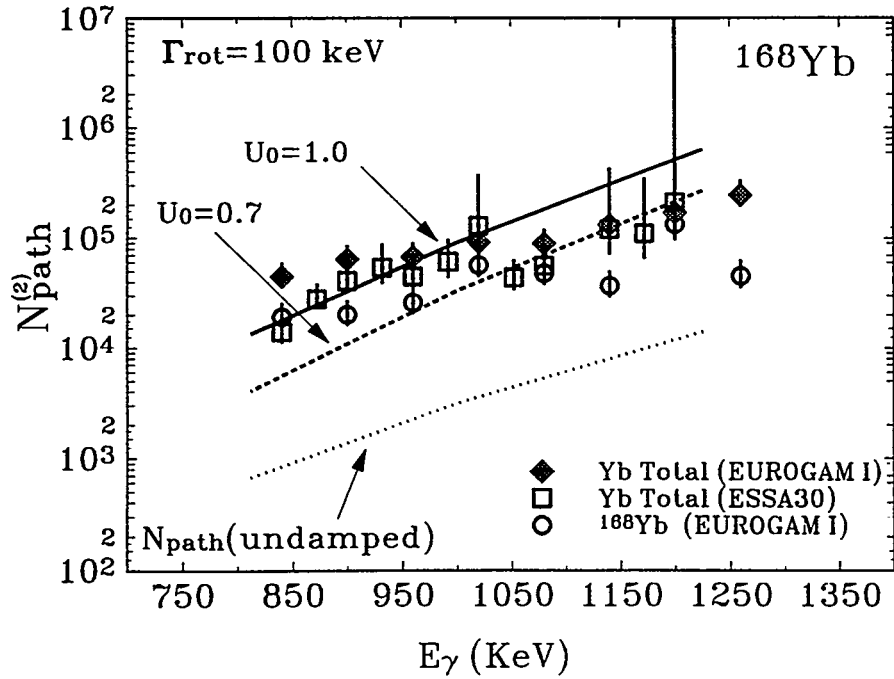


Figure 4: The experimental number of decay paths for valley coincidences in  $^{168}\text{Yb}$  is shown as function of the  $\gamma$ -ray energy (in keV). The solid, dashes and dotted curves show calculations of the number of decay paths, as explained in the text.

## 4.2 Valley fluctuations

Figure 4 shows the effective number of decay paths for damped transitions derived from valley fluctuations in two experiments. The error bars only show the principal uncertainty due to the randomness assumption of selecting the nucleus from an ensemble. This principal uncertainty is very well defined mathematically. In addition, systematic errors can arise through the definition of the smooth spectrum relative to which the fluctuations are measured, or introduced by the procedures just described, and they can roughly be estimated to be a factor 2 up or down. For the EUROGAM I data, the counting statistics is good enough to allow for a third coincidence, used to obtain a clean selection of the  $\gamma$ -rays, which eventually lead into the AB band in  $^{168}\text{Yb}$ . From the ESSA30 experiment to the EUROGAM I, the intensity and the number of events  $N_{eve}$  has increased by about a factor of 10, but still the older and the newer data agree on the number of decay paths within the systematic and principal errors.

From a model of the damped decay, the number of decay paths can be calculated. The simplest case of a one-dimensional spectrum is here used for illustration

$$(n_{path})^{-1} = 2 \sum_i \langle w_i \rangle^2 \quad (12)$$

where  $\langle w_i \rangle$  gives the average probability for each transition, described by the initial state and the final state, within an interval of width  $\frac{4}{2}$ . This interval width provides the natural energy scale for rotational decay, covering two units of angular momentum. Each decay cascade emits on the average one transition within each  $\frac{4}{2}$  interval (and one set of coincidences within each  $\frac{4}{2} \times \frac{4}{2}$  interval).

The curves on figure 4 are calculated with a somewhat more complicated expression than equation (12), taking into account damped coincidences. Also, they are calculated with standard expressions for the level density, and assuming an abrupt onset of damping at the heat energy  $U_0$ . The results display a strong dependence on  $U_0$ . One sees that by comparing the curves for onset energy 700 keV and 1 MeV, that the fluctuations put strong emphasis on the lowest heat energies which display damping. Whereas the region of 700 keV to 1 MeV only carries about 2 to 10 per cent of the flow intensity in the cascades, it carries more than half of the fluctuations. So, the valley fluctuations are primarily sensitive to the region of onset of damping. The dotted curve shows the result of a calculation, in which each state only decays to one final state, but then with wildly fluctuating second moments of inertia, to be able to place counts in the valley. The calculation for the dotted curve is not sensitive to the onset energy of moment of inertia fluctuations.

For both the damped and undamped calculation, the increase in the number of decay paths with increasing  $\gamma$ -ray energy is caused by the increase in the average flow energy of the cascades with increasing angular momentum. The data on figure 4 clearly favour the explanation in terms of damped rotation. However, they also display a much weaker increase in the number of decay paths with energy. The larger number of decay paths at the low energies may be due to the presence of a fifty-fifty per cent admixture of  $^{167}\text{Yb}$  and  $^{168}\text{Yb}$  for these energies. By gating on the AB band in  $^{168}\text{Yb}$ , one is able to select only this nucleus, and this is also seen to be effective at the lower energies. Higher up in  $\gamma$  ray energy, one can see whether some selection of the decay paths which eventually feed into this band is effective. This seems not to be the case, except for at the highest energy around 1250 keV, which looks somewhat strange, and we do not have any explanation.

### 4.3 K selection rules in feeding

A much more dramatic manifestation of selection rules is furnished by the data on figure 5 for  $^{163}\text{Er}$ , where gates have been placed on either the yrast band or one of the high-K bands.

The total number of decay paths as well as the gate on the yrast band show the same behavior as for  $^{168}\text{Yb}$ , but the gating on the high-K bands shows that pronounced K-selection rules must be operative in the feeding of the high-K bands. There are much less states available for feeding the high-K bands than the normal low-lying bands.

### 4.4 Ridge fluctuations

Figure 6 displays the number of decay paths on the ridge for  $^{168}\text{Yb}$ , as function of the ridge number. Roughly speaking, the number of decay paths on the  $n$ 'th ridge gives the number of rotational bands with proper rotational energy correlations surviving over  $n + 1$  decay steps. The data for  $n = 2, 3, 4$  give a consistent picture: it is very hard for bands to keep pure, unmixed and free from drastic changes in alignment or moment of inertia over 6, 8 and 10 units of angular momenta. The drop from  $n = 1$  to  $n = 2$  is



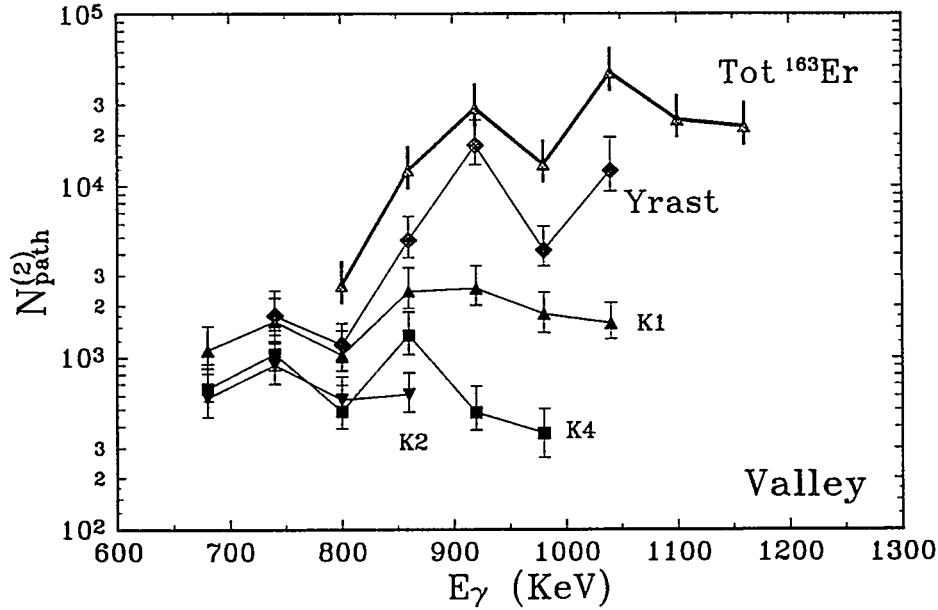


Figure 5: The experimental number of decay paths for valley coincidences of two dimensional spectra in  $^{163}\text{Er}$ . For the curves labelled "Yrast", "K1", "K2" and "K4", an extra coincidence is placed on a specific low lying band.

more problematic, as we shall discuss in the next section. Taking a reasonable average between  $n = 1$  and  $n = 2$ , we reach the conclusion, that there exists in each angular momentum region about 20 to 25 undamped rotational bands. Both ridge and valley fluctuations agree on the heat energy for onset of damping,  $U_0 \approx 700$  keV.

## 5 Discussion

The present fluctuation analysis has been checked in many ways, with respect to the statistical properties. For example, the independence of the transition energies of resolved bands with respect to those of the yet unresolved discrete bands has been checked by comparing fluctuations with or without removal of these bands. As the valley fluctuations are concerned, the constancy of the number of decay paths with respect to division of the data sets into subgroups has been checked. On the basis of these and other tests, it is fair to state that the experimental evaluation of fluctuations is a well defined procedure.

The calculation of the number of decay paths on the basis of an abrupt onset of damping is much more questionable, and also the lack of precise knowledge of the flow properties of the decay cascades adds an uncertainty. Let us mention three significant problems: (i) The lowest lying bands of each parity-signature seem to gain a stronger part of the population relative to the other discrete bands than we estimate from the flow function for the lower heat energies. (ii) The presence of a correlated component of damped transitions underlying the ridge makes the clean separation of undamped and damped transitions in the ridge region questionable. This problem may underly

## Rotational Planes N=1,2,3

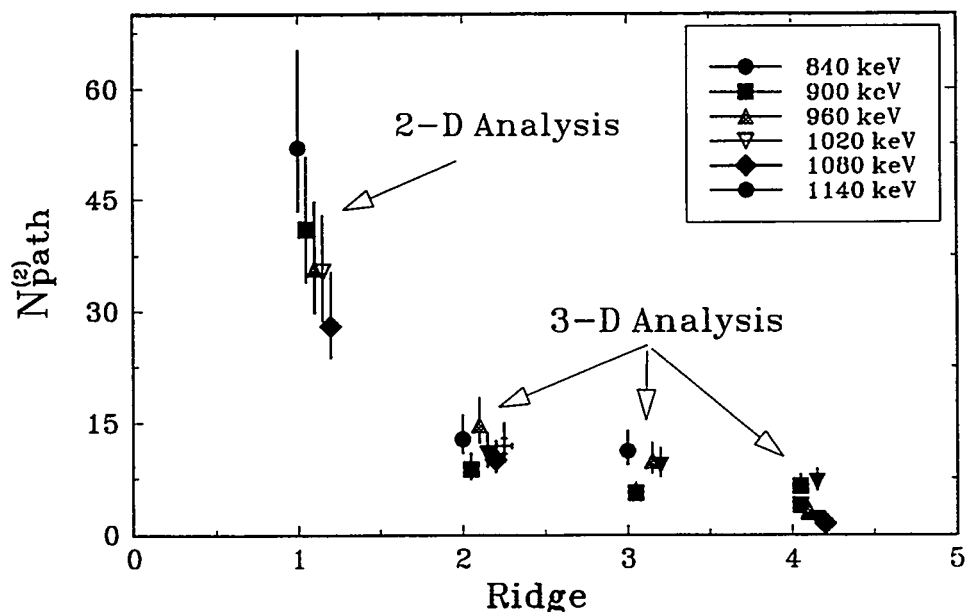


Figure 6: The experimental number of decay paths for ridge coincidences in  $^{168}\text{Yb}$  is shown as function of the ridge number. The results for the first ridge have been obtained on the basis of a two dimensional spectrum, whereas the higher ridge results are obtained from rotational planes [10] in three dimensional spectra.

the jump in number of decay paths from the first to the second ridge on figure 6. (iii) The analysis of valley fluctuations assume a very abrupt onset of damping, with fully developed Porter-Thomas fluctuations of the transition strengths. Still, calculations tell us, that such fluctuations are only fully developed at heat energy 2 MeV [11], that is well above the heat energies, which are mainly responsible for the valley fluctuations.

To address these problems within the band mixing model, a decay cascade code based on mixed bands is presently being developed. The right hand side of figure 3 displays the results of an early version of the cascade code. Results from such simulations can guide us in the understanding of the damped rotation in more details. Especially, they can provide a more direct connection between calculated and experimental spectra. For example, a visual comparison between data and simulations on figure 3 shows first of all an impressive qualitative agreement, and a closer look reveals that the discrete bands receive a too strong feeding in the simulations.

A more quantitative comparison between data and simulations will still be concerned with average properties for groups of states and transitions, such as the rotational damping width and the number of decay paths.

**Acknowledgements:** This work was funded by the U.S. Department of Energy, Nuclear Physics Division, under Contract No. W-31-109-ENG-38. Illuminating discussions with Bent Herskind, Silvia Leoni and Enrico Vigezzi are gratefully acknowledged. Paola Bosetti is gratefully acknowledged providing the data on high-K bands on  $^{163}\text{Er}$ .

## References

- [1] I. Ragnarsson, Nucl. Phys. **A557**(1992)167c
- [2] J.D. Garrett, J.R. German, L. Courtney and J.M. Espino, Proc. Symp. on future directions in Nuclear Physics with  $4\pi$  gamma detections systems of the new generation, Strasbourg, 1991, ed. J. Dudek and B. Haas (American Institute of Physics, 1992)
- [3] S. Leoni, this conference
- [4] B. Lauritzen, T. Døssing and R.A. Broglia, Nucl. Phys. **A457** (1986) 61
- [5] R.A. Broglia, T. Døssing, B. Lauritzen and B.R. Mottelson, Phys. Rev. Lett. **58**(1987)326
- [6] T. Døssing and E. Vigezzi, submitted to Nucl. Phys. **A**(1994)
- [7] F.S. Stephens, in proc. of the Conference on High-Spin Nuclear Structure and Novel Nuclear Shapes, Argonne, Illinois, ANL-PHY-88-2
- [8] P.G. Hansen, B. Jonson and A. Richter, Nucl. Phys. **A518**(1990)13, and references therein.
- [9] B. Herskind, A. Bracco, R. A. Broglia, T. Døssing, A. Ikeda, S. Leoni, J. Lisle, M. Matsuo and E. Vigezzi, Phys. Rev. Lett. **68** (1992) 3008 T. Døssing, B. Herskind, S. Leoni, M. Matsuo, A. Bracco, R.A. Broglia and E. Vigezzi, to be published in Phys. Rep.
- [10] B. Herskind, T. Døssing, D. Jerrestam, K. Schiffer, S. Leoni, J. Lisle, R. Chapman, F. Kahazie and J. N. Mo, Phys. Lett **B276**(1992)4
- [11] M. Matsuo, T. Døssing, E. Vigezzi and R.A. Broglia, Phys. Rev. Lett **70**(1993)2694, M. Matsuo, T. Døssing, B. Herskind and S. Frauendorf, Nucl. Phys. **A564**(1993)345

# Study of the rotational transition strength in the warm nuclei $^{163}\text{Tm}$ and $^{168}\text{Yb}$ .

S. Leoni<sup>1,2</sup>

<sup>1</sup> *The Niels Bohr Institute, University of Copenhagen, Denmark.*

<sup>2</sup> *Department of Physics, University of Milano and INFN Milano, Italy.*

## ABSTRACT

The *Rotational Plane Mapping* method (RPM) is used to analyze the shape of the "central valley" of the 2- and 3-dimensional  $\gamma$ -ray spectra. The method is applied to triple data sets on  $^{163}\text{Tm}$  and  $^{168}\text{Yb}$  nuclei obtained with the NORDBALL and EUROGAM I arrays. If one adopts the simple assumption of *uncorrelated damping*, a simple relation between the measured width and depth of the valley can be given. This relation is not observed in the experimental results. Furthermore, recent realistic band mixing calculations including 2-body residual interactions show the presence of rotational correlations extending into the region of damped motion, pointing to a more complex picture of the damping mechanism.

## 1. Introduction

It has been known for several years [1],[2] that the transition strength in the rotational decay of deformed nuclei is distributed over many final states at high excitation energy above the yrast line. This is called *damping* of the rotational motion. A model describing this phenomenon [3] showed how the rotational strength through each  $E2$  decay step is spread over all the states of the same parity and signature within an interval defined as the rotational damping width  $\Gamma_{rot}$ . In the interpretation of  $\gamma$ - $\gamma$  coincidence spectra it was also assumed that the transition energies at a given angular momentum were selected from the  $B(E2)$  strength function independently of the preceding transitions in the same cascade (*uncorrelated damping*).

In this contribution we will present experimental evidence which shows that this picture may be too simple, and that rotational correlations among successive transitions extend higher up into the damping region (*correlated damping*). This conjecture opens new perspectives in the study of the damping of the rotational motion, and it may shade some light on the gradual transition from regular to damped rotational motion, before a quantal chaotic motion can be assumed at excited energies  $> 2.2$  MeV [4],[5].

## 2. The Rotational Plane Mapping Method on $^{163}\text{Tm}$ and $^{168}\text{Yb}$ nuclei.

A method, based on the simple picture of *uncorrelated damping*, was recently formulated [6],[7],[8],[9], aiming at separating the contributions from regular and damped rotational motion and to a determination of the damping width  $\Gamma_{rot}$  by a study of the shapes of the 2-D and 3-D spectra. It is called *Rotational Plane Mapping* method (RPM).

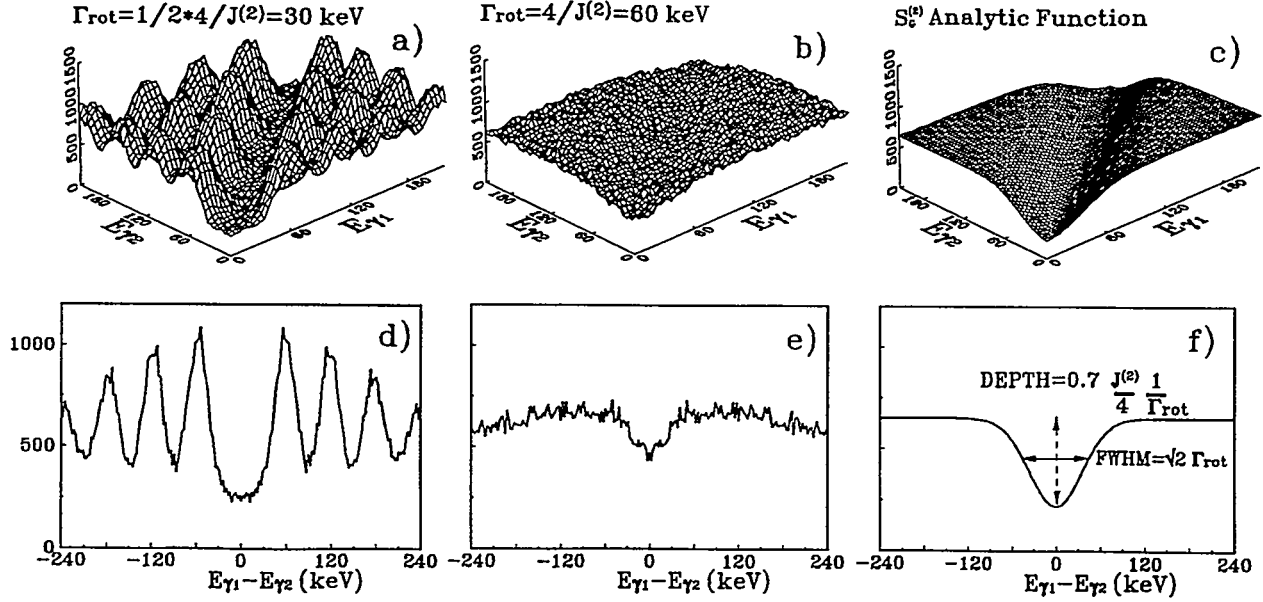


Figure 1: Double coincidence spectra produced by simple simulation calculations of 100000 damped nuclear  $\gamma$ -ray cascades are shown in part a) and b). The damping width values  $\Gamma_{rot} = 30, 60$  keV and constant moment of inertia  $\mathfrak{S}^{(2)} = 70 \text{ MeV}^{-1}$  have been used. Perpendicular cuts across the  $E_{\gamma_1} = E_{\gamma_2}$  diagonal and 60 keV wide are given in part d) and e). The round hills obtained using  $\Gamma_{rot} = 30$  keV are completely smeared out for  $\Gamma_{rot} = 60$  keV, and only a very shallow valley survives. This suggests that, in the limit of  $\Gamma_{rot} \geq 4/\mathfrak{S}^{(2)}$ , the spectrum can be reproduced by the analytical function shown in part c) and e).

The 2-D coincidence spectra are characterized by a valley along the  $E_{\gamma_1} = E_{\gamma_2}$  diagonal. If one assumes that the  $\gamma$ -ray transitions of the damped rotational cascades are *uncorrelated*, the width and the depth of the valley can be simply related to the rotational damping width  $\Gamma_{rot}$ , as illustrated by the simulation calculations of Figure 1 a), b), d) and e).

A set of analytical expressions,  $S^{(2)}$  and  $S^{(3)}$ , have been worked out to describe the distributions of damped events in 2-D as well as 3-D coincidence spectra, if  $B(E2)$  strength functions of either Gaussian or Breit-Wigner forms are assumed. These are the two different shapes expected theoretically for the  $B(E2)$  distribution in the limit of low and high level density [3].

For a  $B(E2)$  distribution of Gaussian shape, the following function  $S_G^{(2)}$  is found:

$$S_G^{(2)}(E_{\gamma_1}, E_{\gamma_2}) = \left(\frac{\mathfrak{S}^{(2)}}{4}\right)^2 - \frac{1}{\sqrt{2}} \frac{\mathfrak{S}^{(2)}}{4} \frac{1}{\sqrt{2\pi}\sigma_{rot}} \exp\left(-\frac{(E_{\gamma_1} - E_{\gamma_2})^2}{4\sigma_{rot}^2}\right) \quad (1)$$

where  $\Gamma_{rot} = \sigma_{rot}\sqrt{8\ln 2}$ . In the  $(E_{\gamma_1} - E_{\gamma_2})$  coordinate system the  $FWHM_G$  and the depth  $DEPTH_G$  of the Gaussian valley become:

$$FWHM_G = \sqrt{2} \Gamma_{rot}, \quad DEPTH_G \approx 0.7 \frac{\mathfrak{S}^{(2)}}{4} \frac{1}{\Gamma_{rot}} \quad (2)$$

The two last equations tell us that, if the simple picture of *uncorrelated damping* is fulfilled, both the FWHM and the DEPTH of the valley can be used as a measure of the rotational damping width  $\Gamma_{rot}$ , as shown in Figure 1 c) and f).

The analogous expression for the 3-D coincidence spectrum is:

$$\begin{aligned}
S_G^{(3)}(E_{\gamma_1}, E_{\gamma_2}, E_{\gamma_3}) &= \left(\frac{\mathfrak{S}^{(2)}}{4}\right)^3 \\
&- \frac{1}{\sqrt{2}} \left(\frac{\mathfrak{S}^{(2)}}{4}\right)^2 \frac{1}{\sqrt{2\pi}\sigma_{rot}} \left[ \exp\left(-\frac{(E_{\gamma_1} - E_{\gamma_2})^2}{4\sigma_{rot}^2}\right) + \exp\left(-\frac{(E_{\gamma_1} - E_{\gamma_3})^2}{4\sigma_{rot}^2}\right) + \exp\left(-\frac{(E_{\gamma_2} - E_{\gamma_3})^2}{4\sigma_{rot}^2}\right) \right] \\
&+ \frac{2}{\sqrt{3}} \left(\frac{\mathfrak{S}^{(2)}}{4}\right) \left(\frac{1}{\sqrt{2\pi}\sigma_{rot}}\right)^2 \exp\left(-\frac{(E_{\gamma_1} - E_{\gamma_m})^2 + (E_{\gamma_2} - E_{\gamma_m})^2 + (E_{\gamma_3} - E_{\gamma_m})^2}{2\sigma_{rot}^2}\right)
\end{aligned} \quad (3)$$

where  $E_{\gamma_m} = (E_{\gamma_1} + E_{\gamma_2} + E_{\gamma_3})/3$  is the average transition energy. Expressions similar to equations (1) and (3) can be obtained starting from a  $B(E2)$  distribution of Breit-Wigner shape [6],[8].

Instead of using directly the 2-D and 3-D experimental spectra, it becomes particularly useful to perform the analysis on the 3-D/2-D *tilted rotational planes*. The planes can be obtained dividing the rotational planes

$$E_{\gamma_1} - E_{\gamma_3} = N \times (E_{\gamma_3} - E_{\gamma_2}) \pm \delta/2 \quad (4)$$

with  $N=1,2,3$  and  $4$ , by the usual 2-D coincidence matrix. In this way one enhances the sensitivity of the method to the distribution of purely damped events [7],[9]. The thickness  $\delta$  of the planes corresponds to the dispersion in the second moment of inertia ( $\approx 20$  keV), and it assures that all the rotational correlations satisfying equation (4) are included in one of the planes. After removal of the known ridge structures, both the width and the depth of the 3-D/2-D valley can be fitted by the  $S^{(3)}/S^{(2)}$  function, averaging over the 4 planes  $N = 1, 2, 3$  and  $4$ . As a consequence of these equations the combined valley has  $\text{FWHM} \approx 2 \times \sqrt{2}\Gamma_{rot}$  for Gaussian functions, and  $\text{FWHM} \approx 2 \times 2\Gamma_{rot}$  for Breit-Wigner functions.

The method was used to analyze the two different nuclei  $^{163}\text{Tm}$  [9] and  $^{168}\text{Yb}$  [10]. The data sets have been obtained with the NORDBALL and EURO GAM I arrays, with the reactions  $^{130}\text{Te}(^{37}\text{Cl}, 5 - 4n)^{162,163}\text{Tm}$ ,  $E=166$  MeV, and  $^{124}\text{Sn}(^{48}\text{Ca}, 5 - 4n)^{167,168}\text{Yb}$ ,  $E=210$  MeV, with the final statistics of  $2.5 \times 10^8$  and  $8 \times 10^8$  triple and higher fold events, respectively. The results obtained from the RPM analysis of the 3-D/2-D valleys of the two nuclei are shown in Figure 2. In both cases the FWHM of the valley is rather constant and corresponds to a rotational damping width  $\Gamma_{rot}=80,100$  keV for  $^{163}\text{Tm}$  and  $^{168}\text{Yb}$  respectively, if a Gaussian shaped function is used in the fitting procedure. These values are about a factor of 2 smaller than theoretically predicted [3]. The basic problem in this analysis is that the depth of the valley decreases as a function of transition energy. Especially for  $E_{\gamma} \geq 900$  keV it does not agree with the measured damping widths. This means that the relations given by the analytical functions (1), (3), shown by the curves of Figure 2, are not satisfied.

The latter results indicate that the simple picture of *uncorrelated damping*, at the basis of the RPM method, can not be used to properly describe the distribution of damped events in 2-D and 3-D spectra.

### 3. Realistic Band-Mixing Calculations.

The assumptions underlying the damping model are presently being investigated

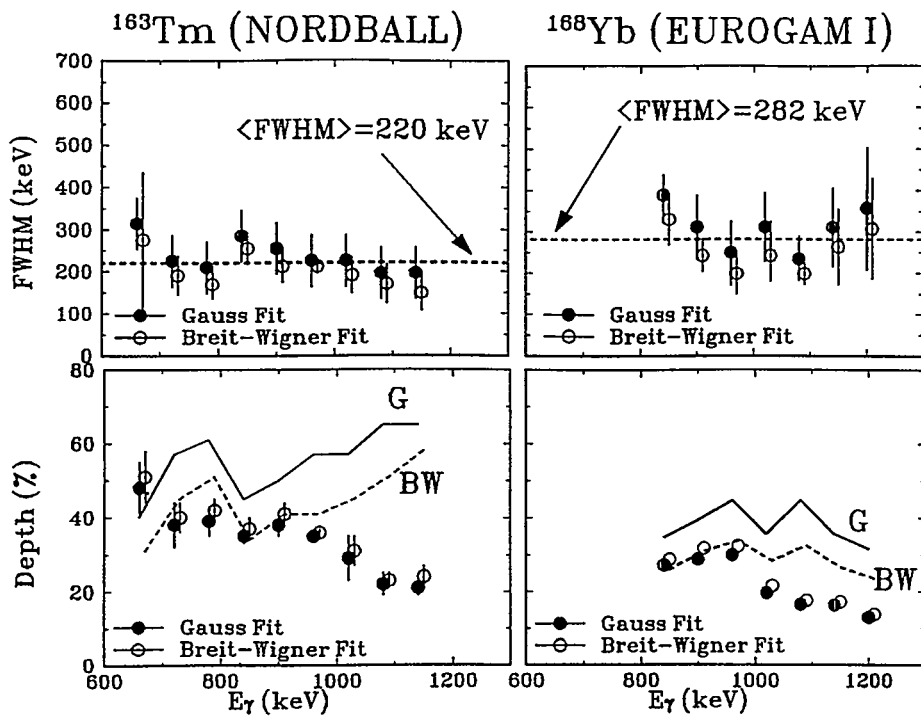


Figure 2: The top part of the figure shows the experimental values obtained for the FWHM of the 3-D/2-D valleys as a function of the  $\gamma$ -ray transition energy for  $^{163}\text{Tm}$  (left) and  $^{168}\text{Yb}$  (right). In the bottom the experimental values obtained for the corresponding depths of the valleys are shown. Both Gaussian (closed circles) and Breit-Wigner (open circles) functions were used to fit the data. The full drawn and dashed lines indicate the expected depth according to the Gaussian function (1) and (3) (solid lines), and to the similar Breit-Wigner expression (dashed lines).

by realistic cranking and band-mixing calculations for rare-earth nuclei [5],[8]. For each even spin value between  $I = 30\hbar$  and  $I = 60\hbar$  the first 1000 levels above yrast have been created by cranked shell model calculations. The residual interaction of the Surface Delta type has been introduced [10]. The lowest 500 mixed bands, up to  $\approx 2.2 - 2.5 \text{ MeV}$  excitation energy above the yrast line, are calculated independently for the 4 configurations, and the distributions of rotational transition strengths between spin  $I$  and  $(I-2)$  have been extracted.

At least for the lowest 200 bands of each parity and signature, the band mixing calculations predict significant rotational correlations in the subsequent steps of the cascade. This is in conflict with the simple picture of *uncorrelated damping*, which is assumed by the RPM technique. This is illustrated in the example of Figure 3. The 2-D plot shows the coincidence pattern obtained selecting only 2 steps rotational decay of the angular momenta sequence  $42 \rightarrow 40 \rightarrow 38$  among the levels 11-40, counted from yrast and summing up the 4 parity-signature configurations of  $^{168}\text{Yb}$ . The diagonal cut of the 2-D pattern shows (Figure 3 b)), in accordance with the damping picture, how the average energy of the two transitions is spread over a large energy interval. The fit through a Gaussian function (full drawn line) gives  $\text{FWHM} = 181 \text{ keV}$  and  $E_{\text{mean}} = 954 \text{ keV}$ . However, the perpendicular projection on the  $(E_{\gamma_1} - E_{\gamma_2})$  axis (Figure 3 c)) shows two components of near Gaussian shapes centered around the energy expected for the ridge  $(E_{\gamma_1} - E_{\gamma_2}) = 4/\mathcal{S}^{(2)}$ . The wide component has a  $\text{FWHM} = 235 \text{ keV}$ , while the narrow component has only a  $\text{FWHM} = 49 \text{ keV}$ .

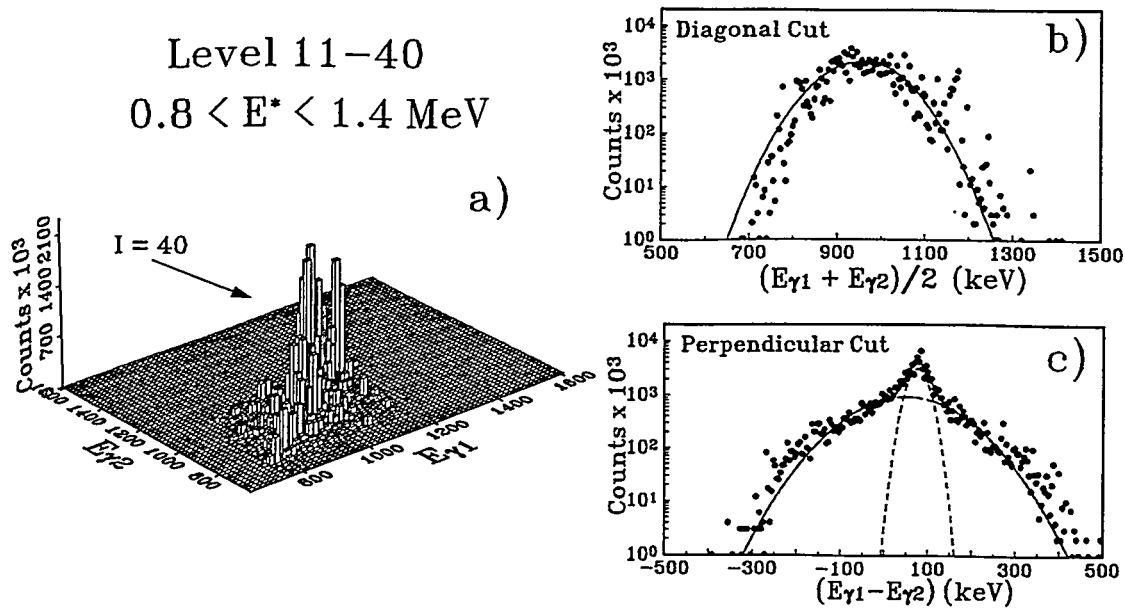


Figure 3: The rotational correlations predicted by the band mixing calculations [5] are shown in the 2-D plot for the angular momenta sequence  $42 \rightarrow 40 \rightarrow 38$  for the group of levels 11-40 of  $^{168}\text{Yb}$ , corresponding to the excitation energy region  $0.8 \leq E^* \leq 1.4 \text{ MeV}$ , summing up the 4 spin and parity configurations. Figure b) and c) show the projections on the  $(E_{\gamma 1} + E_{\gamma 2})/2$  and  $(E_{\gamma 1} - E_{\gamma 2})$  axis, respectively. As one can see, a strong correlation between the two transition energies can be observed in the difference as a narrow component, but not in the sum.

A further investigation has shown that the narrow component mostly originate from contributions of the strongest components of the 2 steps decay  $(I+2) \rightarrow I \rightarrow (I-2)$ , while the weak components especially contribute to the wide distribution, as illustrated in the left part of Figure 4.

The intensity and the width of the wide and narrow components have been fitted using two independent Gaussian functions, as function of the excitation energy above yrast and for different values of spin. In general one observes that the wide component behaves as expected for damped transitions, having a  $\text{FWHM} \approx 200 - 400 \text{ keV} \approx \sqrt{2}\Gamma_{rot}$ , while the FWHM of the narrow part is  $\approx 50 - 80 \text{ keV}$ . With increasing heat energy, the intensity of the narrow component decreases, and correspondingly the wide component grows. This is shown in the right part of Figure 4 for  $I = 40\hbar$ .

This latter observation, together with the fact that the narrow component seems to be mostly originated from strong correlations along subsequent steps of the damped cascade, may suggest that a remnant of rotational correlations extends higher up well into the damping region, before the rotational motion becomes fully damped.

## 5. Conclusions

The study of the 2-D and 3-D spectrum shapes along the central valley by the *Rotational Plane Mapping Method* has shown that our present understanding of the complex mechanisms of the damping of the rotational motion is rather limited. Band mixing calculations clearly indicate that the simple picture of *uncorrelated damping*



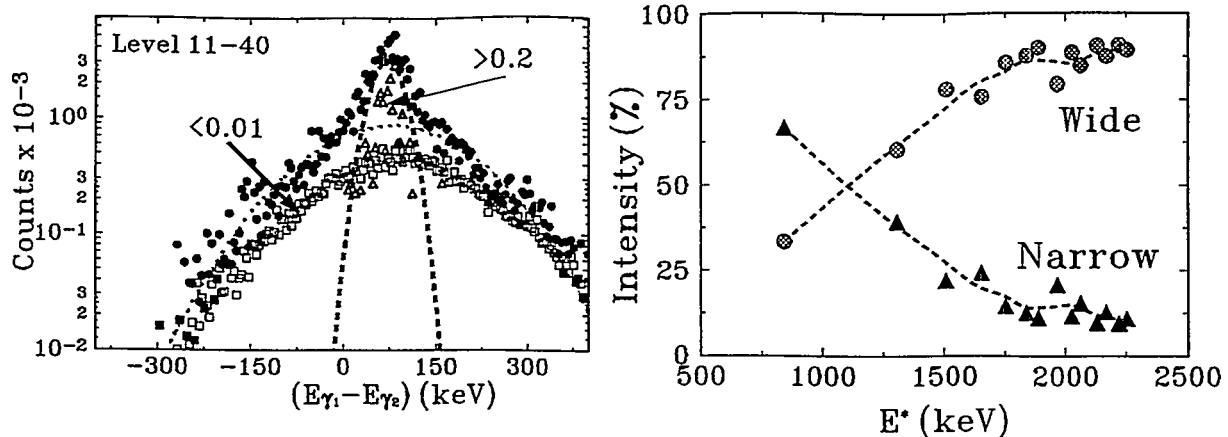


Figure 4: The left side of the figure shows, for the group of level 11-40 at spin  $I = 40\hbar$ , the total ridge coming from  $\gamma$ - $\gamma$  correlations (full circles), compared to the contribution from components with a probability larger than 0.2 (open triangles). Also shown is a sum of all the weak contributions smaller than 0.01. As one can see, the strongest correlations contribute mostly to the narrow part of the ridge. The intensity of the wide and narrow components at  $I = 40\hbar$  are shown as function of excitation energy in the right part of the figure.

can not be fully accounted for, and that rotational correlations are still present in the region of the rotational damping. They manifest themselves as a narrow component in the strength function associated with the quadrupole rotational decay of two consecutive transitions (generating the so-called first ridge in a  $\gamma$ - $\gamma$  coincidence spectrum, and so far related only to  $\Gamma_{rot}$ ).

Attempts are being made to better understand to nature of the narrow component and to include rotational correlations into a more complex picture of the damping of the rotational motion.

The work has been supported by the Danish Natural Science Research Council.

- [1] J. C. Bacelar et al., Phys. Rev. Lett., 55 (1985) 1958-61.
- [2] J. E. Draper et al., Phys. Rev. Lett., 56 (1986) 309-312.
- [3] B. Lauritzen, T. Døssing, R. A. Broglia, Nucl. Phys., A 457 (1986) 61-83.
- [4] B. Herskind et al., Phys. Rev. Lett. 68 (1992).
- [5] M. Matsuo et al., Phys. Rev. Lett. 70, (1993), 2694.
- [6] B. Herskind et al., Phys. Lett. B276 (1992) 4-10.
- [7] S. Leoni, Ph.D. Thesis, University of Milano, 1992.
- [8] P. Rasmussen, Master Thesis, The Niels Bohr Institute, 1993.
- [9] S. Leoni et al., submitted to Nucl. Phys.
- [10] A. Fitzpatrick et al., submitted to Nucl. Phys.
- [11] A. Faessler, Fortschr. Phys. 16, 309 (1968).

# Chaos in Nuclear Physics: Statistical Aspects of Excited Nuclear States

Sven Åberg

Dept of Mathematical Physics, Lund Institute of Technology, PO Box 118, S-221 00 Lund, Sweden

**Abstract:** The hydrogen atom in a strong magnetic field is compared to the excited atomic nucleus. A simple model, based on random matrix theory, is utilized for the general description of level dynamics in mixed regular and chaotic systems. We find that different types of level statistics, such as nearest neighbour distributions (NND),  $\Delta_3$ -statistics, wave function analyses, curvature distributions etc, show different sensitivity to the "chaoticity parameter". The E2-decay of the excited, rapidly rotating nucleus is described as a discrete Markov process, and the fully chaotic situation is found to correspond to a diffusive decay where the variance of the excitation energy varies linearly with the angular momentum. Possible consequences in multi- $\gamma$  correlation measurements are discussed.

## 1 Introduction

The hydrogen atom in a strong magnetic field has become one of the standard examples for studying quantum chaos. The nice features of this problem include the possibility of performing accurate classical as well as quantum mechanical calculations (see for example [1, 2]) which in addition can be tested in experiments. Chaos in the classical problem is controlled by one scaling variable,  $\varepsilon = E\gamma^{-2/3}$ , where  $E$  is the energy and  $\gamma$  is the strength of the magnetic field (in units of  $2.35 \cdot 10^5$  T). In fig.1a the Poincaré surface of section shows the behaviour of the electron moving in some classical orbits in the combined Coulomb and magnetic field corresponding to  $\varepsilon = -0.25$ . It is seen that most parts of the phase space has become chaotic. The remaining non-chaotic orbits can be identified as "rotational" orbits, in which the electron moves approximately perpendicular to the magnetic field, (contrary to the "vibrational" orbits, where the electron moves along the magnetic field, and which already have become chaotic), see ref [2].

In fig.1b the corresponding quantum mechanical calculation shows how the energy levels behave as functions of the magnetic field strength at approximately the same value of  $\varepsilon$ . The irregularity of the energy levels is obvious, and there is a clear tendency for most of the energy levels to avoid level crossings. However, the energy levels which have the largest slope move seemingly unperturbed. These states can be identified with the non-chaotic classical "rotational" orbits seen as regular in fig.1a. We thus notice how classical chaos (related to breaking of constants of motion) is related to avoided crossing (breaking of "almost" good quantum numbers). In this case we can even follow how specific classical orbits become chaotic in the quantal spectrum.

At  $\varepsilon \geq -0.13$  all orbits are chaotic. By performing level statistical analyses of the quantum levels [1] one can identify the transition from order to chaos as a subsequent change of level statistics from Poisson (the eigen energies are randomly distributed following a Poisson process) to GOE (Gaussian Orthogonal Ensemble; the features of the energy levels and eigenfunctions can be described by an ensemble of random matrices with Gaussian distributed matrix elements). This and several other examples led Bohigas et al to conjecture [3] that

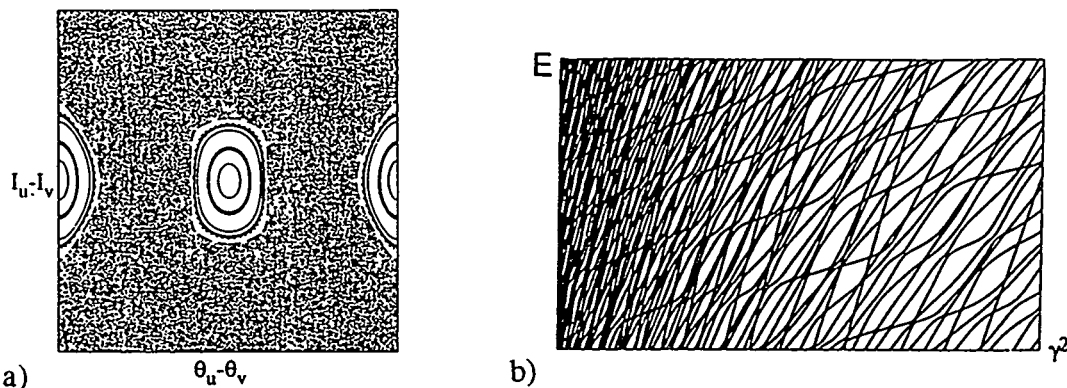


Figure 1: Classical (Poincaré surface of section) and quantum mechanical view (energy levels) of the hydrogen atom in a strong magnetic field. The scaled variable  $\varepsilon$  is approximately the same in both cases, -0.25 and -0.20, respectively, which corresponds to a situation where chaos and order coexists. (From [2].)

“the quantum mechanical version (in the semiclassical limit) of a classically chaotic system follows GOE-statistics”.

But what about the nuclear case? Assuming reflection symmetric shapes the single-particle motion in a deformed and rotating nuclear potential preserves parity and signature as good quantum numbers. Chaotic motion in the nuclear potential corresponds to the mixing of states within these symmetry classes. Like the rotational orbits in the H-atom case we can identify single-particle orbits which are much more persistent to the distortion, i.e. to the rotation and deformation. These are particularly the intruder orbits which originate from other oscillator shells than what is mainly seen around the Fermi surface, and consequently have a quite different structure. This effect is best seen at the superdeformation where orbits from high-N shells appear around the Fermi level. In fig.2 we see the very weak interaction e.g. between the [770]1/2 orbital and the [521]3/2 orbital, while a strong interaction is seen e.g. between [651]1/2 and [642]5/2. This implies that the corresponding classical motion is much more regular for the high-N orbits than for other surrounding orbits.

But, while the excitation spectrum of the H-atom corresponds to the excitation of the electron to different states in the one-body field, the excitation spectrum of the nucleus is

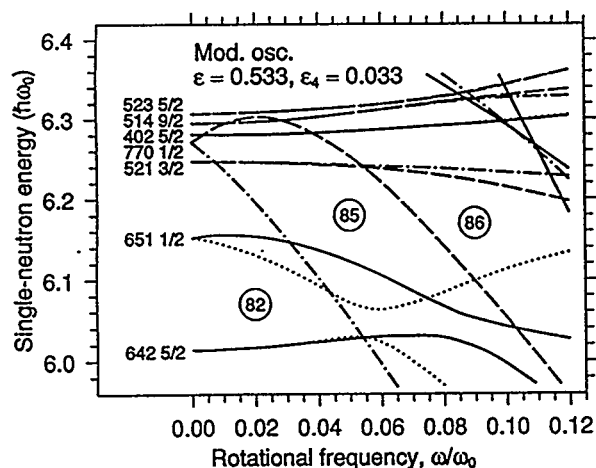


Figure 2: Neutron single-particle levels at superdeformation plotted vs the rotational frequency.

much more complicated. In fact, only a small fraction of states correspond to excitations in the one-body field (the level density,  $\rho_{1p1h} \sim E_{exc}$ ), while most excited states are many-body excitations ( $\rho_{total} \sim \exp(a\sqrt{E_{exc}})$ ). Consequently, chaoticity in the nucleus is not explicitly determined by the shape or rotation of the potential, but rather by the residual interaction between the many-body configurations. The almost good quantum numbers may thus correspond to deformed (and rotating) shell model occupation numbers, and the force that break these “almost good quantum numbers” is (mainly) the residual two-body interaction.

## 2 Level Dynamics

In order to mimic the transition from “order” to “chaos” in the quantum spectrum we set up the following random matrix model [4]:

$$H(I) = H_o + \Delta \cdot H_1 + I \cdot A \quad (1)$$

where

$$(H_o)_{ij} \in \delta_{ij}G(0, \sqrt{\frac{2}{N}}), \quad (2)$$

$$(H_1)_{ij} \in (1 - \delta_{ij})G(0, \sqrt{\frac{1}{N}}), \quad (3)$$

$$(A)_{ij} \in \delta_{ij}G(0, \sigma_A \sqrt{\frac{1}{N}}), \quad (4)$$

i.e.  $H(I)$  constitutes an ensemble of  $N$ -dimensional random matrices where  $H_o$  and  $A$  are diagonal and  $H_1$  is non-diagonal, all with Gaussian distributed matrix elements with mean value  $m$  and standard deviation  $\sigma$ ,  $G(m, \sigma)$ . The two parameters  $\Delta$  and  $\sigma_A$  determine the properties of the system. By choosing  $\Delta$  in the interval  $[0,1]$  we may study the smooth transition from Poisson to GOE. At  $\Delta=0$  we have  $H(0) \equiv H^{Poisson}$  and at  $\Delta=1$   $H(0) \equiv H^{GOE}$ . In this paper the external parameter,  $I$ , describes angular momentum, but it could as well describe other variables such as time, strength of a magnetic field, or the quadrupole moment. It is found [4] that  $\Delta \cdot N$  is an invariant.

The eigenvalue problem

$$H\phi_i = E_i\phi_i \quad (5)$$

is solved by numerical diagonalization of an ensemble of  $N \times N$  matrices (as a standard we shall take  $N=400$ ). When  $\Delta = 0$  the energy spectrum,  $E_i(I)$ , corresponds to a set of unperturbed rotational bands (for simplicity we let the rotational bands have a linear dependence on angular momentum). The subsequently added interaction,  $\Delta \cdot H_1$ , corresponds to a residual (many-body) interaction between the bands. In general, the slope,  $\partial E_i / \partial I$  corresponds to (the negative of) the rotational frequency, but could in general be velocity, the quadrupole moment etc. The parameter,  $\sigma_A$ , controls the dispersion in slope, i.e. in rotational frequency. The curvature,  $\partial^{(2)} E_i / \partial I^{(2)}$ , consequently corresponds to  $-1/J^{(2)}$ , where  $J^{(2)}$  is the dynamical moment of inertia, but could as well be “acceleration”, magnetic susceptibility, etc.

From several calculations (see e.g. [5, 6]) it seems as GOE properties appear when the nondiagonal matrix elements in average are of the size of the mean level spacing of the diagonal matrix elements, i.e. in the model above (at  $I=0$ ) when

$$\Delta \cdot \frac{1}{\sqrt{N}} \sim \sqrt{\frac{2}{N}} \cdot \frac{1}{N} \Rightarrow \Delta \sim \frac{1}{N}, \quad (6)$$

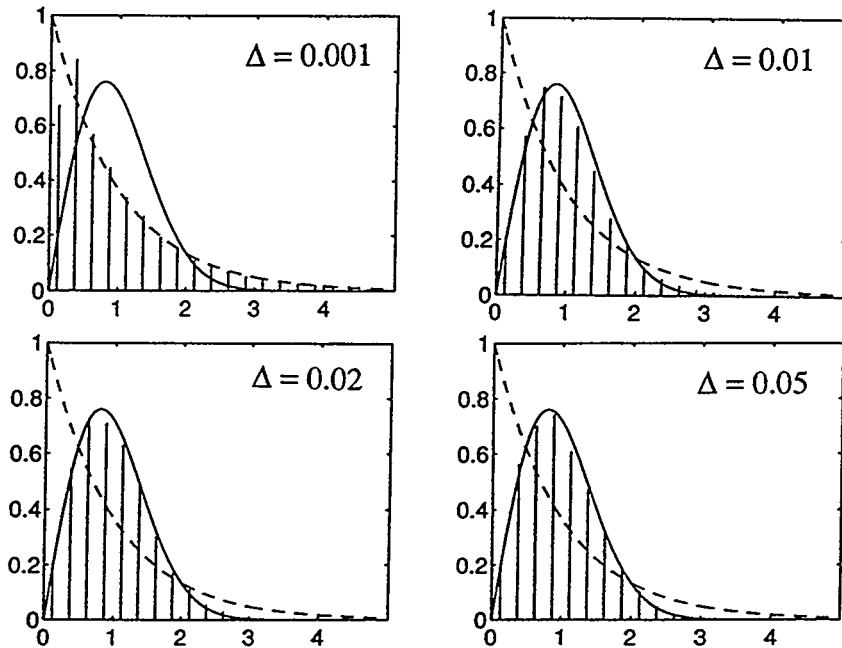


Figure 3: Nearest neighbours distributions for different values of the mixing parameter  $\Delta$ . The GOE and Poisson limits are shown for comparison.

which implies that the GOE properties are expected at much smaller values of  $\Delta$  than corresponds to the full GOE. For  $N=400$  we thus expect the GOE properties already when  $\Delta \approx 0.02$ .

In fig.3 the nearest neighbours distributions are shown for some different values of  $\Delta$ . As expected, the GOE curve is reproduced for  $\Delta \gtrsim 0.02$ . If, on the other hand, we study the  $\Delta_3$ -statistics (or quite similarly the variance of the  $\Delta_3$ -statistics) for  $\Delta = 0.02$  the corresponding GOE curve is followed up to a maximum value,  $L_{max} \approx 20$ , of the correlation distance,  $L$ , in the energy spectrum. For larger  $L$ -values  $\Delta_3(L)$  becomes larger than the corresponding GOE values. When a smaller  $\Delta$ -value is used the deviations appear at a smaller  $L_{max}$  value. The reason for this final range of the GOE correlations is that the wave functions are localized. With a localization length (or spreading width) according to Fermis golden rule,  $\Gamma_\mu \approx 2\pi\rho_o\Delta^2$ , there cannot be any GOE correlations between two wave functions when their mutual energy distance is larger than, say  $2.5\Gamma_\mu$ . This gives  $L_{max} \approx 2.5\rho\Gamma_\mu$ , i.e.  $L_{max} \approx 5\pi\rho_o\rho\Delta^2$ , that excellently reproduces the calculated values of  $L_{max}$  vs  $\Delta$ , see ref [4]. The chaotic features of the wave functions are thus not global for  $\Delta \ll 1$ , but we have rather an energy spectrum where the individual states show a (translational invariant) local chaos. By measuring  $L_{max}$  in a realistic nuclear spectrum we thus indirectly measure the average size of the (residual) nuclear two-body interaction.

It can be mentioned that the wave function components follow the Porter-Thomas distribution when  $\Delta \gtrsim 0.1$ , i.e. for considerably larger  $\Delta$ -values than for which e.g. the NND follows the GOE curve [4].

A dynamic feature that can be obtained from the energy level spectrum,  $E_i$  vs  $I$ , is the curvature. It was conjectured [7] that the curvature distribution shows a generic behaviour for the quantum chaotic spectrum:

$$P(k) = C_\nu(1 + k^2)^{-(\nu/2+1)}, \quad (7)$$

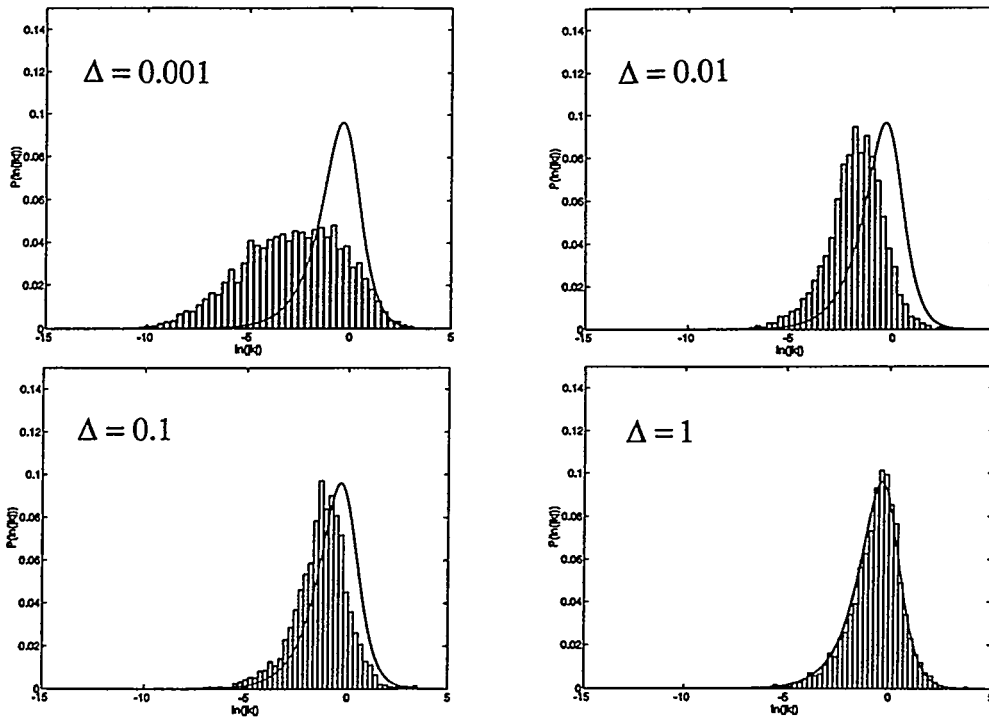


Figure 4: Curvature distributions for four different values of the mixing parameter,  $\Delta=0.001$ ,  $0.01$ ,  $0.1$  and  $1$ . As a comparison the expression for the generic curvature distribution, eq.(7) with  $\nu=1$ , is shown in each figure. The curvatures are scaled and plotted on a logarithmic scale.

where  $C_\nu$  is a constant,  $k$  is the scaled curvature,  $k = K(\pi\sigma_\omega^2\rho)^{-1}$ ,  $K$  being the calculated curvature,  $K = d^{(2)}E/dI^{(2)}$ ,  $\sigma_\omega$  the average dispersion in slope, and  $\rho$  is the level density. The curvature distribution thus only depends on the symmetry class,  $\nu=1, 2$  and  $4$  for GOE, GUE and GSE, respectively.

From our model (eqs.(1-5)) we may calculate the curvature distribution also for mixed systems, and in fig.4 scaled curvature distributions are shown for  $\Delta=0.001, 0.01, 0.1$  and  $1$ . The generic distribution is not obtained until  $\Delta \approx 1$ , i.e. when the model corresponds to full GOE. It is interesting to note that in a realistic model of the excited high-spin states including a schematic two-body interaction, e.g. of the superdeformed spin  $50^+$  states in  $^{152}\text{Dy}$  [6], the energy spectrum shows GOE properties measured in terms of NND and  $\Delta_3$  statistics, while the scaled curvature distribution strongly deviates from eq.(7); there are considerably many more levels with small curvatures than is expected from eq.(7). We shall also note that experimental  $J^{(2)}$ -moments of inertia are obtained at finite differences in angular momenta. This implies a severe principal restriction on the possibility to experimentally reproduce the generic curvature distribution.

### 3 Diffusion in the E2-Cascade

The  $\gamma$ -cascade that follows a HI collision after neutrons and the statistical  $\gamma$  rays have been emitted, mainly consists of stretched E2-transitions. The additional cooling through E1 transitions is omitted in the present study. We thus focus on the excitation energy region a few MeV above the yrast line.

We describe the occupation density of excited states with a given angular momentum and

parity by the column vector,  $\bar{\rho}$ , i.e.  $\rho_i(I)$  is the occupation density of the excited state  $i$  at spin  $I$  (and fixed parity). Obviously  $\sum_{i=1}^N \rho_i(I) = 1$  for all  $I$ -values. The evolution of the occupation density versus spin can be described by a transition operator,  $\mathbf{T}^I$ :

$$\bar{\rho}(I-2) = \mathbf{T}^I \bar{\rho}(I), \quad (8)$$

where  $\mathbf{T}^I$  is represented by an  $N \times N$  matrix with matrix elements

$$(\mathbf{T}^I)_{ij} = | \langle \psi_i^{I-2} | \mathcal{M}(E2) | \psi_j^I \rangle |^2 (E_j(I) - E_i(I-2))^5, \quad (9)$$

where the matrix element simply becomes

$$\mathcal{M} = c(\psi^{I-2})^t (\psi^I), \quad (10)$$

providing the E2 matrix element along an unperturbed rotational band is constant ( $=c$ ) for all bands, and zero between different unperturbed bands.  $(\psi^I)$  is a matrix representation of the eigenvectors at spin  $I$  expressed in a basis of unperturbed bands.

Starting at spin  $I_0$  with the occupation density  $\bar{\rho}(I_0)$  the occupation density at spin  $I_0 - 2n$  becomes

$$\bar{\rho}(I_0 - 2n) = \mathbf{T}^{I_0-2n} \cdot \mathbf{T}^{I_0-2n+2} \dots \cdot \mathbf{T}^{I_0} \bar{\rho}(I_0). \quad (11)$$

Since  $\bar{\rho}(I-2)$  only depends on  $\mathbf{T}^I$  and on  $\bar{\rho}(I)$  (and not on  $\bar{\rho}(I+2)$ , etc) the Markov condition is fulfilled, and since  $\sum_{j=1}^N (\mathbf{T}^I)_{ij} = 1$  for all  $i$ -values,  $\mathbf{T}^I$  is a statistical transition matrix. In general  $\mathbf{T}^I \neq \mathbf{T}^{I+2}$  which means eq.(11) describes a non-homogeneous process. If we neglect the  $E_j^5$ -dependence in  $\mathbf{T}$ , and furthermore assume that  $\mathbf{T}^I \approx \mathbf{T}^{I+2} \equiv \mathbf{T}$ , we have a time-homogeneous Markov process, i.e. the time- or angular momentum-evolution of the occupation density can be written as a mapping

$$\bar{\rho}(I_0 - 2n) = \mathbf{T}^n \bar{\rho}(I_0). \quad (12)$$

The transition matrix,  $\mathbf{T}$ , then completely determines the process.

We can distinguish between three different cases which are illustrated in fig.5: a) A non-chaotic process corresponding to a localized transition matrix, b) A chaotic process with a delocalized  $\mathbf{T}$ , and c) A chaotic process but with a localized  $\mathbf{T}$ . In case a) the "chaoticity" parameter is small,  $\Delta = 0.001$ , implying that the band crossings are more or less ignored. Consequently, the E2-transitions mainly occur along well-defined rotational bands. For a  $\Delta$ -value corresponding to chaotic states, that is used in b) and c), each state at a given  $I$ -value is completely mixed (ergodic states). This implies that the decay is spread out over several daughter states, and the transition matrix is strongly delocalized as is seen in fig.5b. If, however, the wave function has not changed sufficiently much when  $I$  is changed to  $I-2$ , the overlap  $\langle \psi_i(I) | \psi_j(I-2) \rangle \approx \delta_{i,j}$ , and the transitions mainly occur along bands without any level crossings. This means large transition matrix elements along the diagonal of  $\mathbf{T}$ , see fig.5c. The latter situation appears when  $\sigma_A$  is small, and it corresponds to a dynamical process with completely *chaotic states* but with *regular decay*. This can be characterized as a "suppression of chaos" [6]. Case c) can be related to the phenomenon "motional narrowing" [8, 6].

A consequence of the above analysis is that the diffusion of energy (the variance of occupied excited states) shows a basically different variation with angular momentum when the level

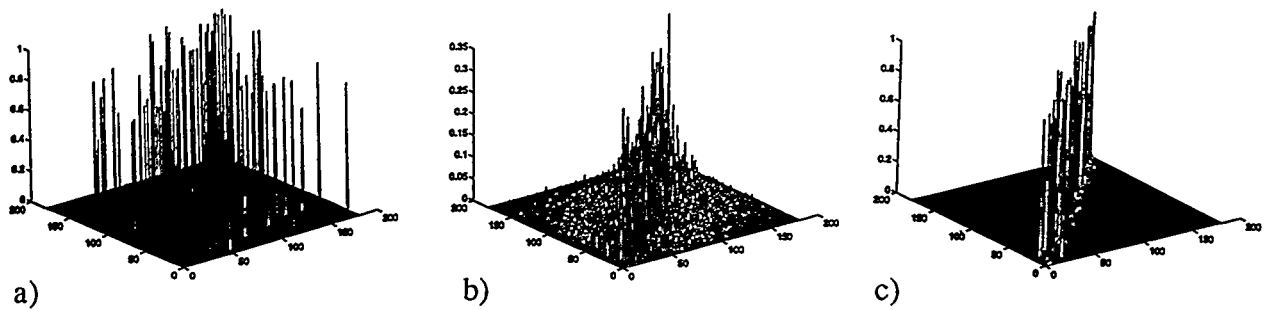


Figure 5: Transition matrices ( $I = 2 \rightarrow I = 1$ ) for the three typical cases discussed in the text: a)  $\Delta = 0.001, \sigma_A = 1$ , b)  $\Delta = 0.1, \sigma_A = 1$  and c)  $\Delta = 0.1, \sigma_A = 0.1$ . In each case the transition probabilities are plotted on the height scale and the initial and final state numbers on the x- and y-axis, respectively. Note the difference in scale.

spectrum is chaotic or regular:

$$Var(E_{exc}) \sim \begin{cases} (I - I_0) & \text{if chaotic spectrum} \\ (I - I_0)^2 & \text{if regular spectrum.} \end{cases} \quad (13)$$

We thus expect an angular momentum (or time) evolution behaviour similar to what is obtained for other disordered systems, as e.g. the kicked rotor or Brownian motion. The behaviour given by eq.(13) is also obtained in numerical simulations of a more realistic model with realistic many-particle configurations obtained from cranking model calculations and with a (schematic) residual two-body interaction [6]. In this case the effect of the  $E_\gamma^5$  factor was tested as well as a release of the condition of spin independent transition matrices. The behaviour of eq.(13) was found to remain. Studying the total energy diffusion (i.e. the spread in  $E_{\gamma_1} + E_{\gamma_2} + \dots$ ) vs angular momentum in multi- $\gamma$  ray measurements could thus be a way to distinguish between a regular and a chaotic energy spectrum.

## References

- [1] A. Hönl and D. Wintgen, Phys. Rev. A39 (1989) 5642.
- [2] D. Delande, in *Chaos and Quantum Physics*, Proc. Les Houches summer school 1989, eds M.-J. Giannoni, A. Voros and J. Zinn-Justin (North-Holland 1991) p.665
- [3] O. Bohigas, M. Giannoni and C. Schmit, Phys. Rev. Lett. 52 (1984) 1.
- [4] P. Persson and S. Åberg, to be publ.
- [5] T. Guhr and H.A. Weidenmüller, Ann. Phys. (N.Y.) 193 (1989) 472.
- [6] S. Åberg, Prog. Part. Nucl. Phys. Vol. 28 (1992) 11.
- [7] J. Zakrzewski and D. Delande, Phys. Rev E47 (1993) 1650.
- [8] B. Lauritzen, T. Døssing and R. Broglia, Nucl Phys. A457 (1986) 61.



**Decay from Superdeformed to Normal States: Measured and Calculated Spectra of the Connecting  $\gamma$  rays\***

T. L. Khoo

on behalf of collaborators from  
Argonne, Berkeley, Bonn, CSNSM-Orsay, Daresbury, Davis,  
IPN-Orsay, Livermore, Liverpool, Lyon, York

The talk given at the conference synthesizes different investigations on the decay from superdeformed (SD) bands. Each work, performed by different collaborations, is described in the following three pages; names of the coauthors are given there. A further discussion of the spectrum from decay out of the SD band in  $^{192}\text{Hg}$  is given by Henry *et al*<sup>1</sup>.

Spectra of the  $\gamma$  rays connecting SD and normal states in  $^{192,194,191}\text{Hg}$  have been extracted from measurements performed at EUROGAM I and GAMMASPHERE (Early Implementation Phase). The spectra are found to have a quasicontinuous component and sharp peaks from the vicinity of the normal yrast line. The spectra define:

- (a) the mechanism for decay out of the SD well;
- (b) the average number of steps in the decay; and
- (c) the excitation energies and spins of the SD states.

Structure in the quasicontinuous component arises from a superposition of statistical  $\gamma$  rays and transitions which are emitted near the yrast region. The spectra have similarities with the  $\gamma$  spectrum emitted after neutron capture. Both cases are examples of statistical decay from a sharp highly excited level.

The structure in the quasicontinuous component is qualitatively reproduced in calculations of statistical decay from SD states, which is due to mixing with a sea of dense normal states. Fluctuations of the level density arise as the number of excited quasiparticles increases in a step-wise manner. These fluctuations and a pairing "gap" (region of depleted levels) give rise to structure in the decay-out spectra, which is more pronounced in an even-even nucleus than in a odd-even nucleus, where the "gap" is filled. These expectations are in accord with the measured spectra, which show more structure in  $^{192,194}\text{Hg}$  than in  $^{191}\text{Hg}$ .

---

<sup>1</sup>R. G. Henry *et al*, Phys. Rev. Let. **73**, 777 (1994).

\*Work supported by U.S. Dept. of Energy under Contract Nos. W-31-109-ENG-38, DE-FG02-87ER40346, W-7405-ENG-48, DE-AC03-76F00098, the National Science Foundation, SERC (UK) and IN2P3 (France).

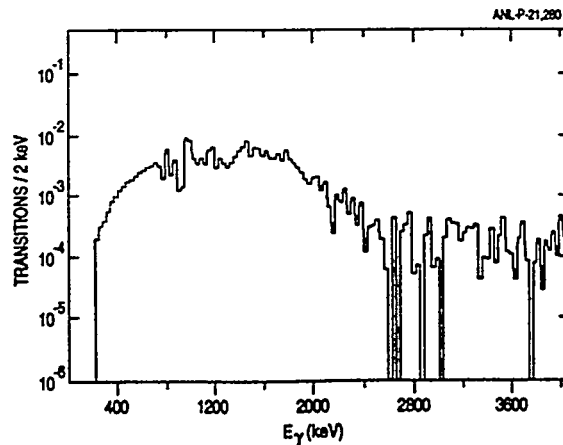
## DECAY FROM SUPERDEFORMED TO NORMAL STATES IN $^{192}\text{Hg}$ : SPECTRUM OF CONNECTING $\gamma$ RAYS

T. Lauritsen<sup>a</sup>, R.G. Henry<sup>a</sup>, T.L. Khoo<sup>a</sup>, I. Ahmad<sup>a</sup>, M.P. Carpenter<sup>a</sup>, B. Crowell<sup>a</sup>,  
T. Dossing<sup>a,j</sup>, R.V.F. Janssens<sup>a</sup>, F. Hannachi<sup>b</sup>, A. Korichi<sup>c</sup>, C. Schuck<sup>b</sup>, F. Azaiez<sup>c</sup>, C.W.  
Beausang<sup>d</sup>, R. Beraud<sup>e</sup>, C. Bourgeois<sup>c</sup>, R.M. Clark<sup>f</sup>, I. Deloncle<sup>b</sup>, J. Duprat<sup>e</sup>, B. Gall<sup>b</sup>,  
H. Hubel<sup>g</sup>, M.J. Joyce<sup>d</sup>, M. Kaci<sup>b</sup>, Y. Lecoq<sup>e</sup>, M. Meyer<sup>e</sup>, E.S. Paul<sup>d</sup>, N. Perrin<sup>c</sup>, N.  
Poffe<sup>ai</sup>, M.G. Porquet<sup>b</sup>, N. Redon<sup>e</sup>, H. Sergolle<sup>c</sup>, J.F. Sharpey-Schafer<sup>d</sup>, J. Simpson<sup>h</sup>,  
A.G. Smith<sup>b</sup>, R. Wadsworth<sup>f</sup>, P. Willsau<sup>g</sup>

We have used a new approach to study the decay out of SD states: instead of trying to decipher the highly fragmented individual decay pathways, we extract the spectrum of all  $\gamma$  rays following the decay. SD states in  $^{192}\text{Hg}$  were populated in the  $^{160}\text{Gd}(^{36}\text{S},4n)$  reaction with a 159 MeV beam from the SERC Daresbury Tandem Accelerator and  $\gamma$  rays were detected with the EUROGAM array. The  $\gamma$  spectrum coincident with pairwise gates on SD lines was measured. A distinction between  $\gamma$  rays which precede and follow the SD band is made on the basis of the Doppler shift, where possible. ( $\gamma$  rays from the decay out of the SD band are emitted after the evaporation residues are stopped in a backing.) However, the spectrum of statistical  $\gamma$  rays feeding the SD band has to be calculated, using a model which is able to reproduce all observables connected with feeding of SD states.

The spectrum (see Fig.) of  $\gamma$  rays connecting SD and normal states has a statistical-like distribution, with a superposed prominent bump between 1.3 and 2.2 MeV, as well as sharp normal yrast transitions (not shown in Fig.). The average number of steps from the SD band to the normal yrast line is  $3.2 \pm 0.6$ ; the SD state from which the decay predominantly occurs has excitation energy above the yrast line of  $4.3 \pm 0.9$  MeV and its spin is  $10.1 \pm 0.7 \hbar$ . The statistical-like decay spectrum shows that a SD state decays by coupling with the dense sea of normal states in which it is embedded. The  $\gamma$  spectra corresponding to the different stages of the  $\gamma$  cascade through a SD band directly reveal an unusual sequence of chaos, order, chaos and order. In particular, the sudden transition from equally-spaced sharp SD lines to a thermal decay spectrum shows a transition from a cold ordered SD system (isolated within a secondary well) to a hot chaotic one (in the primary well).

**Fig. 1:** Spectrum of  $\gamma$  rays connecting the SD and normal states in  $^{192}\text{Hg}$ .



<sup>a</sup>Argonne National Laboratory; <sup>b</sup>CSNSM-Orsay; <sup>c</sup>IPN-Orsay; <sup>d</sup>Liverpool; <sup>e</sup>IPN Lyon; <sup>f</sup>York; <sup>g</sup>Bonn; <sup>h</sup>SERC, Daresbury; <sup>i</sup>Oxford;

## Spectra from Decay out of Superdeformed Bands in $^{194}\text{Hg}$ and $^{191}\text{Hg}$ \*

R. G. Henry,<sup>a</sup> T. L. Khoo,<sup>a</sup> T. Lauritsen,<sup>a</sup> T. Døssing,<sup>a</sup> D. Gassmann,<sup>a</sup> I. Ahmad,<sup>a</sup> D. Blumenthal,<sup>a</sup> M. P. Carpenter,<sup>a</sup> B. Crowell,<sup>a</sup> S. Harfenist,<sup>a</sup> R. V. F. Janssens,<sup>a</sup> D. Nisius,<sup>a,b</sup> J. A. Becker,<sup>c</sup> M. J. Brinkman,<sup>c</sup> B. Cederwall,<sup>d</sup> M. A. Deleplanque,<sup>d</sup> R. M. Diamond,<sup>d</sup> J. E. Draper,<sup>e</sup> C. Duyar,<sup>e</sup> P. Fallon,<sup>d</sup> E. A. Henry,<sup>c</sup> R. W. Hoff,<sup>c</sup> J. R. Hughes,<sup>c</sup> I. Y. Lee,<sup>d</sup> E. Rubel,<sup>e</sup> F. S. Stephens,<sup>d</sup> and M. A. Stoyer<sup>c</sup>

The spectrum connecting superdeformed (SD) and normal states in  $^{192}\text{Hg}$  (Ref. 1) contains a quasicontinuous component on which is superimposed a broad bump. It is proposed (Ref. 2) that this clustering of transition strength is due to pairing, which leads to a region ('gap') of depleted level density up to  $\sim 1.2$  MeV above the yrast line. A prediction of this model is that the bump should be pronounced in an even-even nucleus, where there is a significant reduction of levels in the 'gap' and significantly weaker in an odd-even nucleus, where levels fill the 'gap'.

To test this prediction, we have extracted the spectrum of  $\gamma$  rays coincident with pairwise gates on SD lines in  $^{194}\text{Hg}$  and  $^{191}\text{Hg}$ , with the expectation that the bump should be significant in only the former case. In each case, measurements were performed with GAMMASPHERE. Reactions used were  $^{150}\text{Nd}(^{48}\text{Ca},4n)^{194}\text{Hg}$ ,  $^{174}\text{Yb}(^{22}\text{Ne},5n)^{191}\text{Hg}$ , and  $^{150}\text{Gd}(^{36}\text{S},5n)^{191}\text{Hg}$ , with beams from the LBL 88" Cyclotron. The data analysis on  $^{194}\text{Hg}$  is almost complete, while that on  $^{191}\text{Hg}$  is still in progress. The spectra coincident with the yrast SD bands in  $^{192,194}\text{Hg}$  are nearly identical above 1 MeV, with prominent bumps between 1.4 and 2.2 MeV—see Fig., where the spectra are normalized to be correct for an  $A_2$  of  $-0.12$ , appropriate for only statistical decay. In contrast, preliminary analysis on  $^{191}\text{Hg}$  shows that this bump is significantly attenuated. Hence, the tentative indication is that pairing may indeed lead to observable effects in the spectra following decay out of SD bands. This raises the hope that the decay out of SD bands may now provide a tool for studying the reduction of pairing in excited nuclear states.

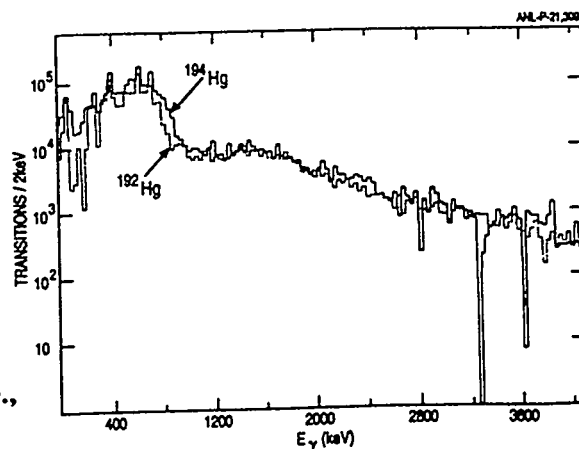
The remarkable similarity between the spectra of  $^{192}\text{Hg}$  and  $^{194}\text{Hg}$  for  $E_\gamma > 1$  MeV supports the suggestion (Ref. 1) that the decay between SD and normal states is a statistical process, which leads to some interesting ramifications, e.g. for inferring the spins of SD band members.

Another observation from the  $^{194}\text{Hg}$  spectrum is that the high-energy edge of a strong broad E2 peak around 700 keV shows approximately full Doppler shift. This means that this structure is from excited SD bands which feed the yrast SD band.

1. T. Lauritsen et al, abstract to this Conf.

2. T. Døssing et al, abstract to this Conf.

\*Work supported by U.S. Dept. of Energy, under Contract Nos. W-31-109-ENG-38, DE-FG02-87ER40346, W-7405-ENG-48, DE-AC03-76SF00098 and by the National Science Foundation. <sup>a</sup>Argonne National Lab., <sup>b</sup>Purdue University; <sup>c</sup>Lawrence Livermore Lab., <sup>d</sup>Lawrence Berkeley Lab., <sup>e</sup>Univ. of California



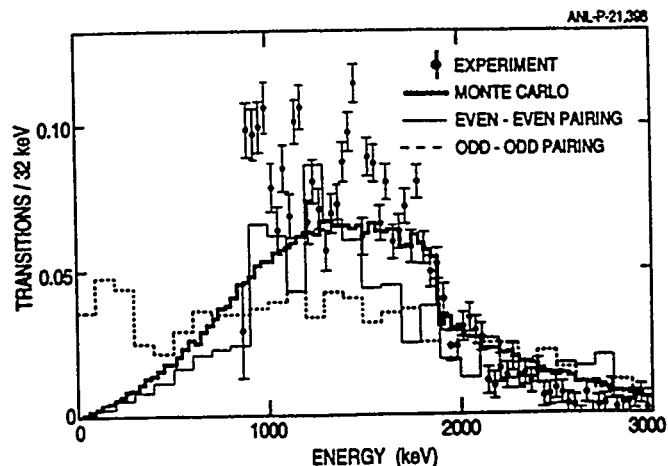
# CALCULATION OF THE SPECTRUM OF STATISTICAL $\gamma$ -RAYS EMITTED IN THE DECAY-OUT OF SUPERDEFORMED BANDS

T. Døssing, T. L. Khoo, T. Lauritsen, I. Ahmad, D. Blumenthal, M. P. Carpenter, B. Crowell, R. G. Henry, R. V. F. Janssens, and D. Nisius  
 Physics Division, Argonne National Laboratory, Argonne, IL 60439, USA

The energy spectra of  $\gamma$  rays depopulating superdeformed bands are calculated in two models, both based on the decay occurring through mixing with a near-lying normal state 4.3 MeV above the yrast line. In one model, we perform a Monte Carlo simulation of the  $\gamma$  cascade, with an additional single last-step transition from around 1.7 MeV above the normal yrast line. The second model is based on a theory which self-consistently treats the weakening of pairing correlations with increasing number of quasiparticle excitations. Many-quasiparticle excitations are generated using a single-particle spectrum with equidistant spacing. Pairing correlations are treated in various schemes: BCS, number projected BCS, and diagonalization of the states after number projection.

Fig. 1 shows the experimental spectrum [1] for  $^{192}\text{Hg}$ , together with spectra calculated with the statistical Monte Carlo simulation and with the BCS approximation for even-even and for odd-odd systems. The strength of the pairing interaction is chosen to produce a BCS gap parameter  $\Delta = 0.8$  MeV in the ground state of the even systems, and the spacings of the neutron and proton single particle spectra are 0.29 and 0.41 MeV, respectively. It is found that the bump around 1.3 MeV seen in the spectrum is more pronounced with increasing pairing strength. Furthermore, it is strong in an even-even nucleus, but becomes rapidly attenuated in the odd-even and odd-odd systems. The bump arises from a combination of piling up of the spectra from the sequential steps of the deexcitation cascade and from clustering in energy of transitions across the pair 'gap' in the even-even system. Preliminary calculations without pairing, but with a gap in the single particle spectrum at the Fermi energy, produce smooth spectra without a bump.

Fig. 1: Statistical spectra from decay-out the SD band in  $^{192}\text{Hg}$  [1]; experimental spectrum [1] and calculated spectra from statistical Monte Carlo model (thick line) and from the pairing model for even-even (thin line) and odd-odd (dashed) systems.



[1] T. Lauritsen *et al.*, abstract to this conference

# Decay of the $^{194}\text{Pb}$ Superdeformed Band

M.J. Brinkman\*

*Lawrence Livermore National Laboratory  
Livermore, California 94550*

Abstract: Three experiments using the  $^{174}\text{Yb}(^{25}\text{Mg},5n)$  reaction at a beam energy of 130 MeV have been performed utilizing the Early Implementation of GAMMASPHERE. The goal of these experiments was to study the decay of the known superdeformed states in  $^{194}\text{Pb}$  to the normal low-lying levels in this nucleus. The statistical decay of this band appears to be suppressed with respect to its  $^{194}\text{Hg}$  isobar. A single discrete transition at 2.746(2) MeV in coincidence with both the superdeformed band and the normal states through which it decays has been identified in these experiments. The evidence for this transition and a discussion of its placement will be presented.

## 1. Introduction

Despite a wealth of experimental information on the superdeformed (SD) nuclei in the  $A \sim 190$  mass region [Fi94], a number of the most fundamental properties of these structures remain unmeasured. Macroscopic quantities such as the excitation energy and the well depth of the second minimum and the width of the barrier separating the SD and the low-lying ground state minima remain unmeasured quantities as do fundamental microscopic parameters such as the spins and the parities of the SD levels. Direct experimental measurement of these quantities requires that the decay pathways linking SD and low-lying normal states be observed.

The SD bands in the  $A \sim 190$  mass region all have a similar intensity curve. The intensity of the SD bands increase with decreasing spin at the top of the bands until an intensity plateau is reached at intermediate spins. The intensity of the bands then stay approximately constant until they abruptly depopulates within one to two transitions. The SD band intensity non-preferentially populates a number of the low-lying normal states. This observation, coupled with the fact that previous experiments which have attempted to identify the SD decay pathways in the  $A \sim 190$  mass region have been unsuccessful, has served as the primary piece of experimental evidence that the SD states decay via a statistical process.

The  $^{194}\text{Pb}$  nucleus was chosen as an optimal candidate for observing discrete decay of a SD band for five reasons. 1)  $^{194}\text{Pb}$  has a well-studied, strongly populated ground state SD band [Br90,Th90,Hü90]. 2) All Pb isotopes are singly magic in the ground state serving to reduce the level density in the continuum through which decay of the SD band will proceed. 3) The  $^{194}\text{Pb}$  SD band exists to low angular momentum which reduces the number of possible decay pathways. 4) The low-lying nuclear structure of  $^{194}\text{Pb}$  is well understood from both HI,xn [Fa91,Br91] and  $\beta$ -decay studies [vD87]. 5) Long-lived isomers isolate the low spin ( $\leq 12 \hbar$ ) normal states from the high spin structures.

## 2. Experimental Details

Three experiments were performed using the Early Implementation of Gammasphere. In each of these three experiments three thin ( $\sim 500 \mu\text{g}/\text{cm}^2$  each), stacked self-supporting foils of isotopically enriched  $^{174}\text{Yb}$  were bombarded by a 130-MeV  $^{25}\text{Mg}$  beam. The predominant channels in this reaction were  $^{193,194,195}\text{Pb}$  and  $^{192}\text{Hg}$  with approximate relative production yields of 10%, 60%, 20%, and 7%, respectively. Of particular importance is the relatively low yield of  $^{192}\text{Hg}$  created in this reaction because the most intense  $^{192}\text{Hg}$  superdeformed band has energies that are identical (within  $\sim 0.5$  keV) to those in the  $^{194}\text{Pb}$  band over a range of angular frequencies from 100 keV to 280 keV.

---

\* Current Address: Oak Ridge National Laboratory  
Oak Ridge, Tennessee 37831

**Table I:**

$E_\gamma$ (keV) <sup>a</sup>	$J^\pi_i \rightarrow J^\pi_f$ <sup>b,c</sup>	$I(\text{SD})^d$	$I(2746)^{e,f}$
170.7	8 → 6	64 (9)	?g
178	(8-) → 7-	9 (4)	—
214.1	10 → 8	85 (6)	82 (15)
257.3	12 → 10	100 (3)	96 (15)
261	(8-) → 7-	6 (3)	—
281	5- → 4+	41 (10)	—
299.2	14 → 12	99 (2)	98 (10)
302	8+ → 6+	~8	—
340.3	16 → 14	98 (2)	103 (14)
380.7	18 → 16	101 (2)	124 (18)
420.2	20 → 18	100 (2)	75 (22)
421	7- → 5-	23 (6)	—
458.4	22 → 20	78 (3)	84 (13)
496.0	24 → 22	82 (3)	47 (12)
532.6	26 → 24	64 (2)	65 (12)
568.8	28 → 26	55 (5)	60 (13)
576	4+ → 2+	77 (6)	105 (13)
595	6+ → 4+	21 (6)	94 (14)
603.7	30 → 28	33 (4)	55 (18)
638.3	32 → 30	34 (4)	45 (19)
672	? → 2+	3 (2)	—
672.6	34 → 32	18 (2)	22 (14)
965	2+ → 0+	78 (9)	95 (14)
1308	2 <sub>2</sub> <sup>+</sup> → 0+	24 (4)	—

- a) Superdeformed bands members given to 0.1 keV
- b) Putative spins of SD band members from spin fit analysis [Be90]
- c) Spins and parities of low-lying normal levels from reference [VD87]
- d) Relative intensity from double-gated triples spectrum normalized to the 257.2-, 299.2- 340.3, and 380.7-keV transitions
- e) Relative intensity in the background subtracted gate on the 2746-keV transition normalized to the 299.2- and 340.3-keV transitions.
- f) — denotes a state for which an upper limit of  $\leq 5\%$  can be placed.
- g) Data does not allow a determination whether this transition is seen.

The presence of the bump has been interpreted to be caused by the redistribution of energy levels due to ground state pairing. If this interpretation is correct, it is not surprising that  $^{194}\text{Pb}$ , being singly magic, would show a marked reduction in this feature compared to  $^{194}\text{Hg}$ . To the extent that this moderate energy bump is characteristic of the overall statistical part of the decay of the SD bands, however, the statistical contribution to the decay of the  $^{194}\text{Pb}$  band appears to be suppressed.

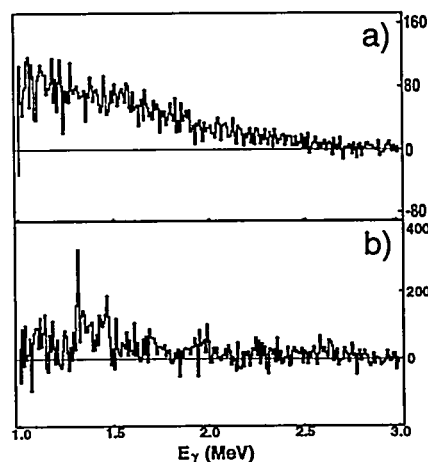


**Figure 2:** Spectra from 1 to 3 MeV created by the method described in Section 4 of the text. a) Spectrum associated with the  $^{194}\text{Hg}$  SD band. b) Spectrum associated with the  $^{194}\text{Pb}$  SD band.

per channel to eliminate statistical fluctuations, normalized to the total number of counts between 3 and 4 MeV, and the background spectrum is subtracted from the peak spectrum.

For  $^{194}\text{Hg}$  this simplified analysis technique provides spectra that are qualitatively similar to those shown in references He94 and Kh94, with the exception of the exponential portion of the spectra at high energies which is over subtracted (by definition) in our method. In figure 2 we provide excerpts of spectra generated using our technique for both  $^{194}\text{Hg}$  and  $^{194}\text{Pb}$  in the region of the “noticeable bump.” As can be seen in comparing these spectra, the bump which appears quite readily in the  $^{194}\text{Hg}$  is absent from the  $^{194}\text{Pb}$  spectrum.

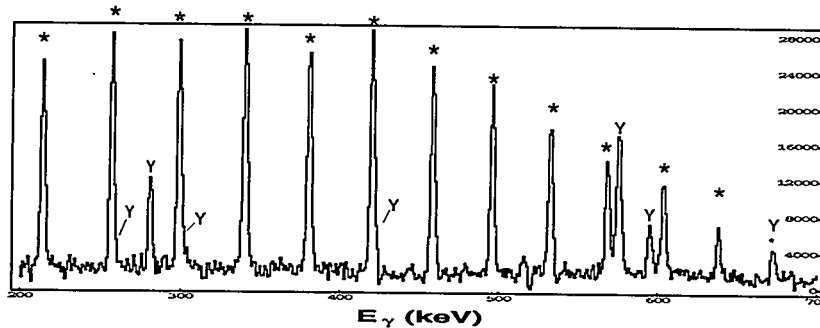


**Figure 1:** The  $^{194}\text{Pb}$  SD band in a double-gated triples spectrum. The SD band members are denoted by \*'s and the known low-lying yrast lines in coincidence with the SD band are denoted by Y's.

The first experiment was used to provide potential candidates for discrete transitions connecting the superdeformed and normal states. The second experiment provided an independent verification of the candidate transitions, while the third was used as a final cross-check. During all times in our analysis we have kept separate the three data sets. The discussion that follows will focus on the results from the largest data set (i.e., the second experiment).

Thirty-two Compton-suppressed detectors were in place for the second experiment with 15 located at backward angles (three rings of five detectors each at  $173^\circ$ ,  $147^\circ$ , and  $143^\circ$  with respect to the beam), 13 detectors at forward angles (two rings of five detectors at  $13^\circ$  and  $33^\circ$ , and three detectors at  $37^\circ$ ), and four detectors at  $90^\circ$ . The second experiment consisted of twenty eight-hour shifts of beam time during which  $1.3 \times 10^8$  unfolded triples events were recorded.

In Figure 1, we present the background subtracted spectrum produced by summing all unique pairwise combinations of gates set on the known members of the  $^{194}\text{Pb}$  SD band from the second experiment. In this spectrum the most intense SD transitions have approximately 40,000 counts. Also seen in coincidence are a number of low-lying normal states through which the SD band depopulates.

### 3. Simple Observables

There are two observables that can be extracted from the data in a relatively straightforward manner. These are the average spin at which the SD band depopulates and the average spin at which the SD intensity reenters the low-lying level scheme. In Table 1, we summarize the relative intensities of all known transitions in coincidence with the  $^{194}\text{Pb}$  SD band. From the results presented in Table 1 the value of the average depopulating spin is found to be  $7.0 \pm 1.1 \hbar$ . The average spin at which the SD band intensity re-enters the normal states is found to be  $5.3 \pm 1.2 \hbar$ . The difference of approximately  $2 \hbar$  angular momentum between the SD depopulation and the re-entrance of its intensity is in good agreement with similar values found in other studies [He94] and is in qualitative agreement with what is expected from both statistical and discrete decay processes from the SD band.

### 4. Statistical Decay

Recently an Argonne led collaboration has undertaken studies of the complete spectrum of  $\gamma$ -rays associated with the decay of the SD bands in the Hg isotopes to study the statistical decay properties of the SD bands [He94,Kh94]. Of particular interest is a "noticeable bump" between 1.3 and 2.2 MeV that has been associated with the final step in the decay of the SD bands.

We have undertaken a grossly simplified version of this type of analysis in order to make qualitative comparisons between the decay of the  $^{194}\text{Pb}$  SD band and its isobaric complement  $^{194}\text{Hg}$ . The method we have used is to construct double-gated triples spectra of the SD band in question and an associated background spectrum. These spectra are then compressed to 16 keV

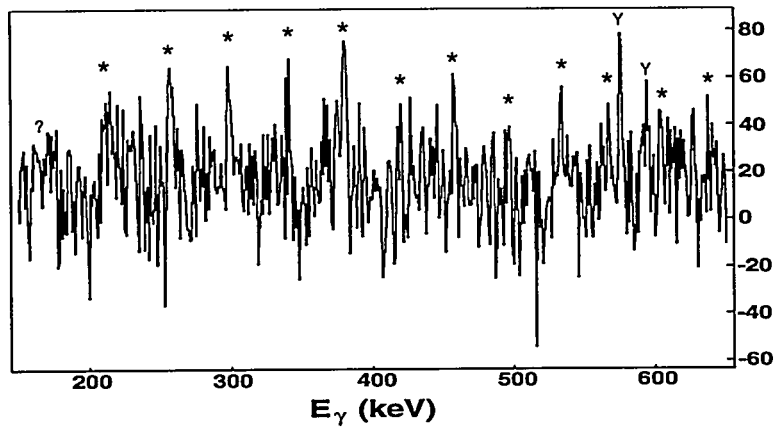


**Figure 3:** The  $^{194}\text{Pb}$  SD band in coincidence with the 2.746(2)-MeV transition. The SD band members are denoted by \*'s and the known low-lying yrast lines in coincidence with the SD band are denoted by Y's.

## 5. Discrete Decay

We have searched for high-energy transitions in coincidence with the known SD band members as candidates for discrete transitions connecting the SD and normal states in  $^{194}\text{Pb}$ . Since this analysis takes place at the limits of existing experimental sensitivity, we have four independent criteria that must be met for a transition to be considered a viable candidate. 1) A proposed candidate must appear in all three data sets and its intensity must be consistent with the intensity of the SD band. 2) The candidate must track the intensity of the SD band members under a number of different gating conditions and background subtraction variations. 3) The full-width at half-maximum of the peak, corrected for the energy of the transition, must be consistent with the measured values of other peaks. 4) The peak was checked to ensure that it was not visible in the total projection to eliminate the possibility of a strong transition “leaking” through the gating and background subtraction requirements.

During the above analysis a *single* transition in the energy range of 2–4 MeV was found that met the above requirements. This transition has an energy of 2.746(2) MeV and a  $4\sigma$  significance. Although not seen in a total projection (see criteria 4, above), we have set a 10 keV wide gate on this transition in a raw  $E_\gamma$ - $E_\gamma$  coincidence matrix. Two 40 keV background gates were set starting at 60 keV below the low energy edge and 20 keV above the high energy edge of the peak gate, respectively. The spectra resulting from these two background gates were summed together and normalized to  $\sim 85\%$  of the total number of counts in the peak spectrum. This summed and normalized spectrum was then subtracted from the peak spectrum, and a portion of the resulting spectrum is provided in Figure 3.

Clearly visible in Figure 3 are all 11 members of the  $^{194}\text{Pb}$  SD band in the range  $214.1 \text{ keV} \leq E_\gamma \leq 638.3 \text{ keV}$ . We are unable to determine whether the  $8 \rightarrow 6$  SD band transition at 170.7-keV is in coincidence with the transition at 2.746-MeV transition due to an unresolvable clump of intensity centered near the appropriate energy.

A similar procedure to the one described above was performed with the peak and background gates shifted down and up by 20 keV. For the spectra gated on 2730 keV (2770 keV) a total of 2 (4) peaks were found with energies corresponding to the SD band members, 6 (3) regions were found that were negatively correlated with the known SD band members, and the remaining 3 (4) regions were near the average background. From this study we find that the peak at 2.746 MeV is in coincidence with the SD band, and that this is not a general feature of this energy region.

In Figure 3 we have also marked the transition energies of the known low-lying normal states through which the SD band depopulates. In clear coincidence with the 2.746-MeV transition are the 595- and 576-keV transitions corresponding to the  $6^+ \rightarrow 4^+$  and  $4^+ \rightarrow 2^+$  low-lying transitions. Although not shown in this spectrum the 965-keV  $2^+ \rightarrow 0^+$  is also in coincidence with



the 2.746-MeV transition. A complete list of normalized intensities in coincidence with this transition is provided in Table 1. Of particular interest is the lack of evidence for both the 280-keV transition which runs parallel to and the 302-keV transition which directly feeds the 595-keV transition. Furthermore, within errors the 595-, 575- and 965-keV transitions each contain the full intensity of the SD band. Thus, it is clear that the 2.746-keV transition preferentially feeds the low-lying  $6^+$  state.

With direct experimental evidence that the 2.746-MeV transition feeds exclusively into the low-lying  $6^+$  state, we can eliminate the possibility that it is the first step in a purely statistical decay of the  $^{194}\text{Pb}$  SD band, which should non-preferentially populate all low-lying normal states in coincidence with the band. While it is possible that this transition is a direct single step transition which connects the SD and normal structures, the available experimental evidence does not rule out the possibility that it is a single member of a multi-transition cascade depopulating the SD structure. If this is the case, however, the 2.746-MeV transition must lie near the final step of the cascade chain since no branching to multiple low-lying states is observed.

Since the low-lying  $6^+$  state has an excitation energy of 2.135(1) MeV, we can assign a minimum excitation energy for the SD level which depopulates through the 2.746-MeV transition (i.e., either the spin 8 or 6 superdeformed level) to be 4.881 (2) MeV. By extrapolating the SD band to a spin of  $0 \hbar$ , the bandhead excitation energy is either 4.471 or 4.641 MeV assuming the depopulation of the SD spin 8 or 6 level, respectively.

We have been unable to measure the transition multipolarity. Assuming that the 2.746-MeV transition is a stretched E2, it carries 6(2)% of the full superdeformed band intensity. Furthermore, if this transition is in direct competition with the SD  $8 \rightarrow 6$  transition, the 2.746 has a  $B(E2) \approx 4 \times 10^{-4}$  Wu. Assuming  $L = 1$ , this transition carries 10(3)% of the band intensity and would have  $B(E1) \approx 1 \times 10^{-4}$  Wu.

### Acknowledgments:

This work was supported by the United States Department of Energy under contract No. W-7405-ENG-48. I wish to acknowledge all of the members of the collaboration who helped in acquisition and analysis of the data presented in this paper: J.A. Becker, L.P. Farris, E.A. Henry, J.R. Hughes, and R. Hoff from Lawrence Livermore National Laboratory, B. Cederwall, M.A. Deleplanque, R.M. Diamond, P. Fallon, I.Y. Lee, A.O. Macchiavelli, and F.S. Stephens from Lawrence Berkeley Laboratory, L.A. Bernstein, J.A. Cizewski, H.Q. Jin, and W. Younes from Rutgers University, C. Duyar, J.E. Draper, and E. Rubel, from the University of California-Davis, and W.H. Kelly and D.T. Vo from Iowa State University.

### References:

- Be90 J.A. Becker et al., *Phys. Rev.* **C46** (1992) 889.
- Br90 M.J. Brinkman et al., *Z. Phys.* **A336** (1990) 115.
- Br91 M.J. Brinkman, *Superdeformation in the A ~ 190 Mass Region and Shape Coexistence in  $^{194}\text{Pb}$* , Rutgers University, unpublished dissertation, October 1991
- Fa91 B. Fant et al., *Jour. Phys.* **G17** (1991) 319.
- Fi94 *Table of Superdeformed Nuclear Bands and Fission Isomers*, R.B. Firestone and B. Singh, eds., LBL-35916.
- He94 R.G. Henry et al., *Phys. Rev. Lett.* **73** (1994) 777.
- Hü90 H. Hübel et al., *Nucl. Phys.* **A520** (1990) 125c.
- Kh94 T.L. Khoo, contribution to this conference.
- Th90 K. Theine et al., *Z. Phys.* **A336** (1990) 113.
- vD87 P. van Duppen et al., *Phys. Rev.* **C35** (1987) 1861.

# Decay of the highly deformed band in the nucleus $^{137}\text{Nd}$

S. Lunardi, R. Venturelli, D. Bazzacco, C. Rossi-Alvarez

Dipartimento di Fisica and INFN, Sezione di Padova, Padova, Italy

C.M. Petrache<sup>1)</sup>, G. de Angelis

INFN, Laboratori Nazionali di Legnaro, Legnaro, Italy

D. Bucurescu, C. Ur

Institute of Physics and Nuclear Engineering, Bucharest, Romania

**Abstract:** *Transitions linking the highly-deformed band to low-deformation states have been established in  $^{137}\text{Nd}$ . Spin and parity have been assigned to the band confirming that it is built on a  $\nu i_{13/2}[660]1/2^+$  configuration. The sudden termination of the highly-deformed band at  $I^\pi = 29/2^+$  is explained through the disappearance of the second minimum in the potential energy surface.*

Several superdeformed (SD) or highly-deformed (HD) rotational bands have been discovered in recent years in the Cerium-Neodymium region. These bands originate from a secondary prolate minimum in the potential energy surface at  $\beta_2=0.35\div 0.40$ , which is associated with the occupation of the  $\nu i_{13/2}[660]1/2^+$  intruder orbital [1]. Many features of the HD rotational bands are analogous to those of the SD bands in the  $A=150$  and  $A=190$  mass regions. One such feature is the sudden depopulation of the bands to levels at normal deformation. The depopulation appears to be fragmented in many pathways and is therefore very difficult to detect. Many attempts have been made in order to identify discrete transitions linking the states in the SD energy minimum to the normal-deformed (ND) structures. In the  $A=130$  mass region the deformation in the second minimum is somewhat smaller than in the heavier mass regions and furthermore, the ND states have also a relatively large prolate deformation  $\beta_2=0.20\div 0.25$ . Therefore, it is likely that the decay-out of the SD structure to the ND one proceeds by means of a small number of discrete transitions which should then be sufficiently strong to be observed experimentally. The advent of the new generation of large detector arrays has greatly improved the sensitivity in detecting weak transitions and by now the decay-out of the HD bands in the nuclei  $^{133}\text{Nd}$  [2] and  $^{135}\text{Nd}$  [3] has been studied in such a detail that the excitation energy and the spin of the bands could be firmly established. These experimental results prove definitely the predicted  $i_{13/2}$  character of the HD bands. In  $^{133}\text{Nd}$  the decay of the HD band has been explained, also in a quantitative way, in terms of an accidental mixing of the HD states with the ND levels [2]. Within this interpretation it is also understood why the band ends at spin  $17/2^+$ . A different interpretation of the decay-out has been given in  $^{135}\text{Nd}$  where the HD band ends at spin  $25/2^+$  and no mixing with ND levels has been observed; the sudden disappearance of the band seems here to be related to the disappearance of the HD potential energy minimum as indicated by Total Routhian Surface (TRS) calculations [3].

With the purpose of understanding in a more systematic way the decay-out mechanism of the HD bands in the mass  $A=130$  region, we have studied the heavier odd

isotope  $^{137}\text{Nd}$  where such a band was identified some time ago [4]. From a lifetime measurement using the Doppler Shift Attenuation Method [5] a deformation of  $\beta_2 = 0.22$  has been extracted which is the smallest among the HD bands in this region. Calculations which consider the occupation of the  $i_{13/2}$  orbital give for  $^{137}\text{Nd}$  a deformation  $\beta_2$  of 0.27-0.29. Since the measured value is much lower, the possibility of the occupation of the  $h_{9/2}$  has been also suggested [5]. The knowledge of the parity of the levels in the HD band is therefore essential if we want to discriminate between the two different possibilities.

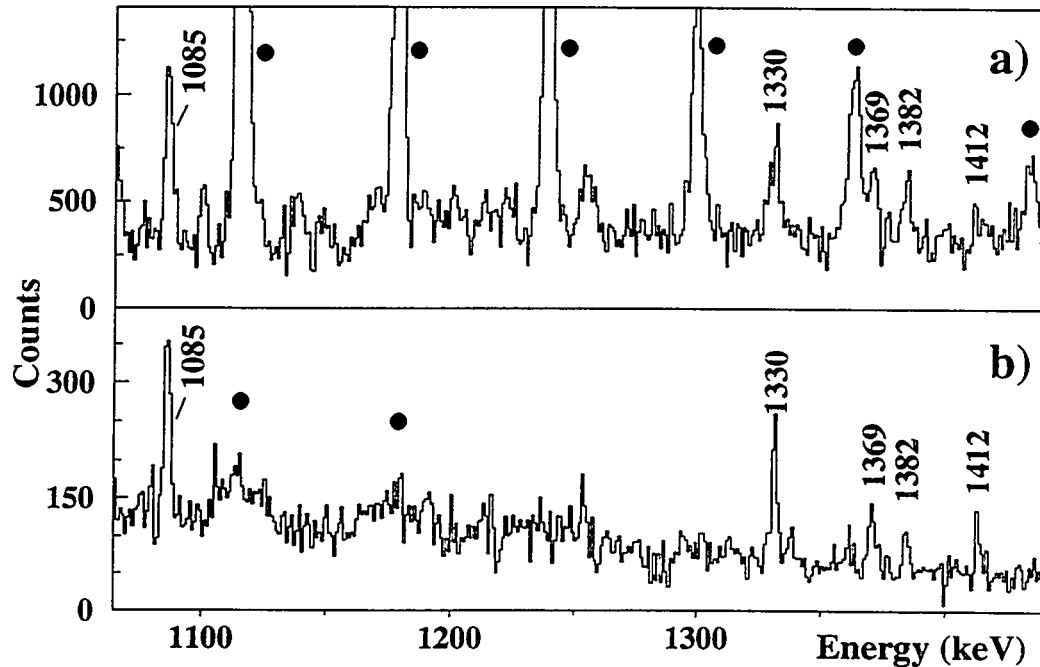


*Fig. 1. a) High energy part of a doubly gated spectrum, with gates set on transitions in the HD band of  $^{137}\text{Nd}$ , obtained in the  $^{110}\text{Pd} + ^{30}\text{Si}$  reaction using thin self-supporting targets. b) Same as a) but for the  $^{123}\text{Sb} + ^{19}\text{F}$  reaction and with a gold-backed target. Transitions belonging to the HD band are labeled with full dots; transitions connecting the HD band to the ND states are labeled with their energies.*

We have studied the  $^{137}\text{Nd}$  nucleus through the  $^{110}\text{Pd}(^{30}\text{Si},3n)$  reaction at a beam energy of 125 MeV. Actually, this beam energy has been chosen for the study of HD bands in the nuclei  $^{136}\text{Nd}$  and  $^{136}\text{Pr}$  but the  $^{137}\text{Nd}$  nucleus is also populated with appreciable cross-section. The GASP array with 40 Compton suppressed Ge detectors and the BGO ball has been used for a standard coincidence measurement, where only triple or higher fold events have been collected. Two different experiments have been performed with the  $^{30}\text{Si}$  beam, one with a gold-backed  $^{110}\text{Pd}$  target and one with a stack of thin  $^{110}\text{Pd}$  foils. The first experiment was mainly aimed to the establishment of the level scheme of  $^{137}\text{Nd}$ , as only few levels were known in the literature [6]. The HD band of  $^{137}\text{Nd}$  is populated in this reaction at the same level as that of the  $^{136}\text{Nd}$  nucleus which is however the dominant reaction channel. This fact confirms earlier results on the odd-even dependence of the population of the HD bands in Nd nuclei. By proper selection of the BGO ball parameters and using the

triples data we could obtain very clean spectra for both bands. In Fig. 1a we show the high energy part of a doubly-gated spectrum, with gates set on all transitions previously assigned to the  $^{137}\text{Nd}$  band. In that spectrum it is evident that the band is in coincidence with a few transitions in the energy range 1-1.5 MeV. These high energy transitions appear as sharp lines in the backed target experiment where, in the same energy range, the transitions of the HD band are completely smeared by

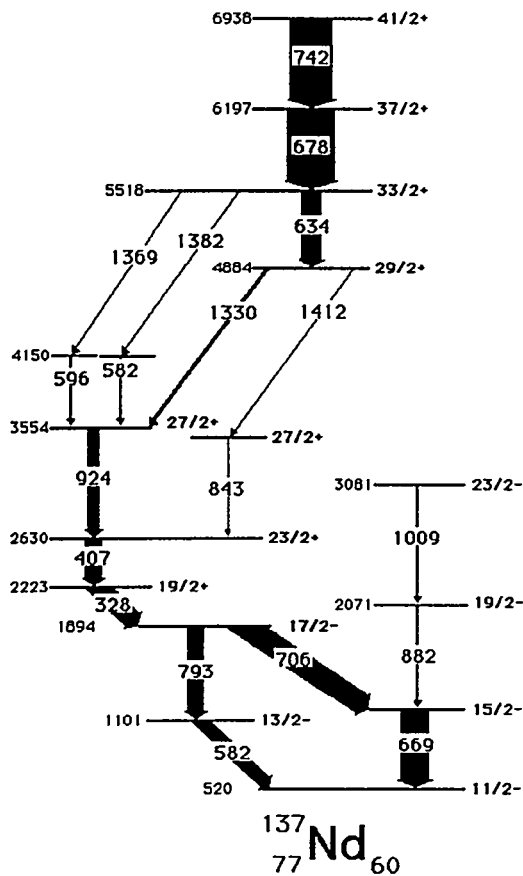


Fig. 2. Partial level scheme of  $^{137}\text{Nd}$  showing the bottom of the HD band and the transitions linking the HD band to the normal deformed states. The width of the arrows is proportional to the coincidence intensity when gating on the HD band.

Doppler broadening. From this evidence we concluded that those transitions lie at the bottom of the band and that they link the HD band to the ND states. In order to better characterize the linking transitions we have performed a new experiment with the reaction  $^{123}\text{Sb} + ^{19}\text{F}$  at 97 MeV. Only a gold-backed target has been used in this case. Fig. 1b shows a portion of a doubly-gated spectrum with gates set on some of the low lying HD band transitions. Now only the linking transitions are apparent in the spectrum, since the HD band E2 transitions are completely broadened during the slowing down process in the gold backing. With the high statistics obtained in the  $^{19}\text{F}$  experiment, we could establish clear coincidence relationships between four of the newly found linking transitions and some other transitions belonging both to the HD band and to the ND part of the scheme. These four transitions (1330, 1369, 1382 and 1412 keV) could be rather easily placed in the level scheme thus fixing unambiguously the excitation energy of the HD band in  $^{137}\text{Nd}$  (see Fig. 2). From the analysis of the angular correlation data (using the detectors at  $36^\circ$  with respect to the beam axis against those at  $90^\circ$ ) a  $\Delta I=1$  character was derived for these four transitions. Furthermore their anisotropy is similar to that of known M1 transitions and is much larger than that of other E1 transitions which are also seen in the reaction. This fact implies that the high energy linking transitions have mixed M1+E2 character. Spin and parity  $29/2^+$  could therefore be fixed for the lowest level of the HD band at 4884 keV, thereby proving the  $i_{13/2}$  character of the HD band of this nucleus.

Several other transitions which are likely to connect the HD band to the ND

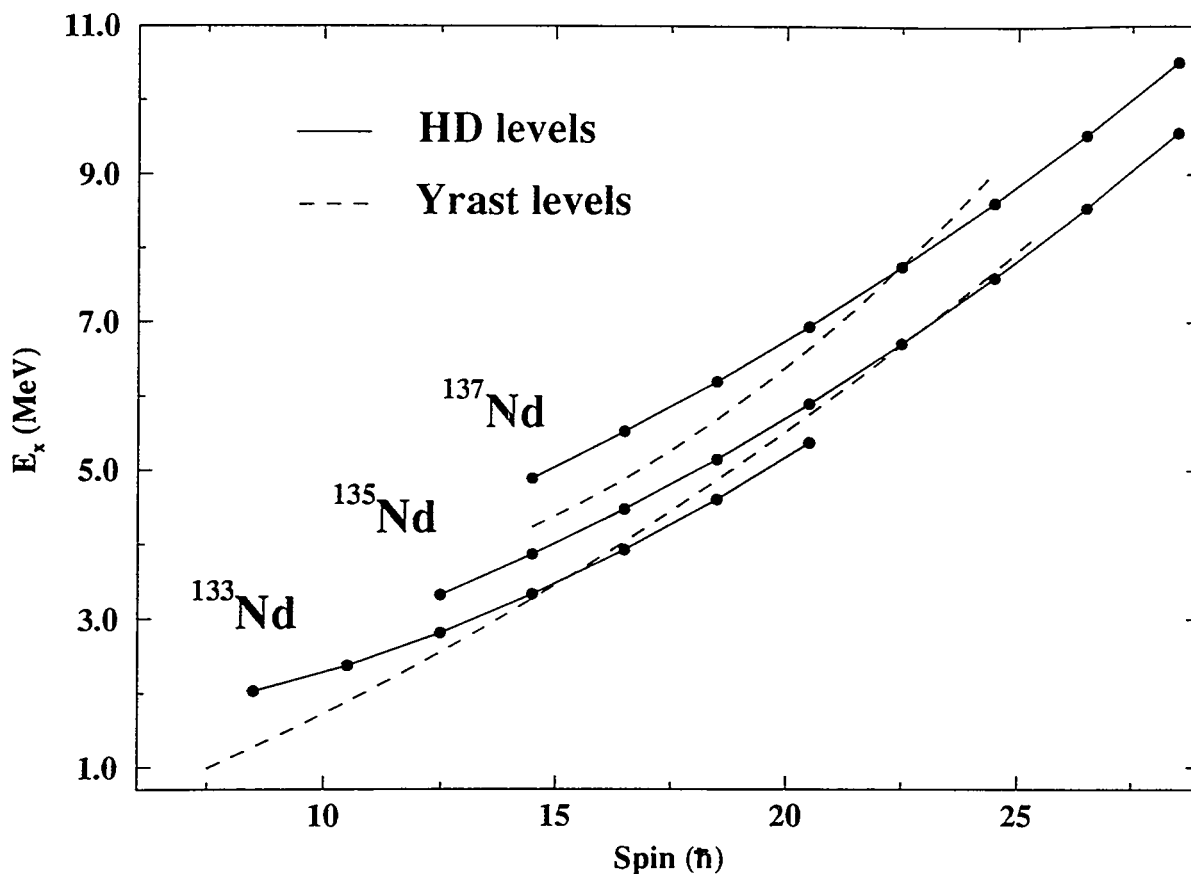


Fig. 3. Excitation energy versus spin for the HD bands of  $^{133}\text{Nd}$ ,  $^{135}\text{Nd}$  and  $^{137}\text{Nd}$ . The yrast lines, which for  $^{133}\text{Nd}$  and  $^{135}\text{Nd}$  are almost coincident, are also drawn.

levels are also seen in the data but we could not place them in the level scheme. As a matter of fact, the four linking transitions of Fig. 2 account for only  $\approx 25\%$  of the band intensity. We note here that in the case of  $^{133}\text{Nd}$ , where the HD band has the lowest excitation energy, the complete decay-out of the HD band has been determined whereas in  $^{135}\text{Nd}$ , where the HD band is at an intermediate excitation energy with respect to  $^{133}\text{Nd}$  and  $^{137}\text{Nd}$ , the known linking transitions account for  $\approx 70\%$  [3] of the HD band intensity. It seems from this result that an almost linear relation exists between the missing intensity and the excitation energies of the HD band with respect to the ground state. This fact simply states that, with increasing excitation energy the number of paths open for the decay out of the band is also increasing, with the consequence that it becomes difficult to detect them all.

In Fig. 3 we report the excitation energy of the HD bands of  $^{133}\text{Nd}$ ,  $^{135}\text{Nd}$  and  $^{137}\text{Nd}$  together with their yrast lines. A fact which is immediately evident from that figure is that the HD bands, which are yrast and therefore strongly populated at higher spins, cross the ND yrast line at different points of the  $E_x$ -I plane and that they continue down to lower spins until they lie  $\approx 600$  keV above yrast where they suddenly disappear. The lowest spins ( $17/2^+$  for  $^{133}\text{Nd}$ ,  $25/2^+$  for  $^{135}\text{Nd}$  and  $29/2^+$  for  $^{137}\text{Nd}$ ) reached by the HD bands seem, from this picture, to be simply

related to their excitation energy above the yrast line. As already mentioned in the introduction, for  $^{133}\text{Nd}$  a convincing explanation of the decay-out process through mixing of levels has been given [2]. This interpretation does not hold for the two heavier Nd nuclei and especially for  $^{137}\text{Nd}$  where the established decay-out proceeds through rather strong M1 transitions. We have performed TRS calculations for  $^{137}\text{Nd}$  and found that at high rotational frequencies it has a triaxial minimum ( $\beta_2=0.27$ ,  $\gamma \approx 15^\circ$ ) associated to the  $i_{13/2}$  configuration. With decreasing frequency the shape changes to a more prolate one ( $\beta_2=0.29$ ,  $\gamma \approx 2^\circ$ ). The prolate minimum disappears

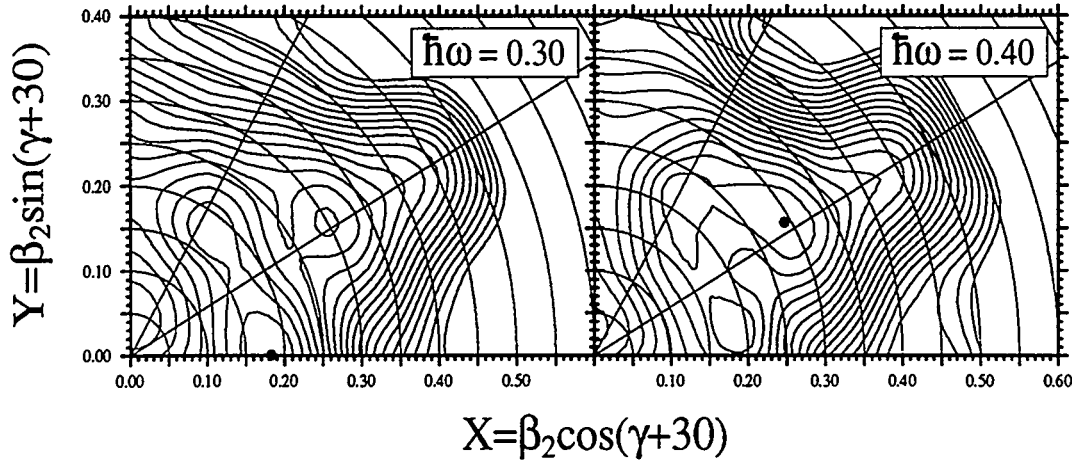


Fig. 4. Total routhian surface calculations for the lowest  $(\pi, \alpha) = (+, +1/2)$  configuration in  $^{137}\text{Nd}$  at two rotational frequencies. The prolate minimum at  $\beta_2 \approx 0.30$  is associated with the  $i_{13/2}$  configuration. At the lower frequency a triaxial minimum ( $\beta_2 = 0.18$ ,  $\gamma \approx -30^\circ$ ), associated with the odd neutron in a  $N=4$  configuration, appears.

at  $\hbar\omega \approx 0.3$  MeV where a triaxial shape ( $\beta_2 = 0.18$ ,  $\gamma \approx -30^\circ$ ), associated with a  $N=4$  configuration, minimizes the total energy of the nucleus (see Fig. 4). This is exactly the point where the HD band in  $^{137}\text{Nd}$  disappears. A similar behaviour is seen also in  $^{135}\text{Nd}$  [3] where, in the same way, at lower frequencies the prolate minimum associated with the HD band changes towards an oblate one.

In conclusion, we established the decay-out of the HD band of  $^{137}\text{Nd}$  and confirmed its predicted  $i_{13/2}$  character. Unlike  $^{133}\text{Nd}$  where the HD bands does not continue at lower spins because of an accidental mixing with ND states, in  $^{137}\text{Nd}$  the band ends at spin  $29/2^+$  and  $\hbar\omega \approx 0.3$  MeV since the second minimum associated with HD band disappears at that point.

<sup>1)</sup> Permanent address: Institute of Physics and Nuclear Engineering, Bucharest, Romania

- [1] R. Wyss et al., Phys. Lett. **B215** (1988) 211.
- [2] D. Bazzacco et al., Phys. Rev. **C49** (1994) R2281.
- [3] R. M. Clark et al., Poster at this conference, Proceedings Vol. 1, p. 9.
- [4] R. Wadsworth et al., J. Phys. **G13** (1987) L207.
- [5] S. M. Mullins et al., Phys. Rev. **C45** (1992) 2683.
- [6] J. Gizon et al., Nucl. Phys. **A222** (1974) 557.

# Collective Motion in Superheavy Elements

J. J. Gaardhøje, Trine Tveter, A. Atac, B. Herskind,  
W. Korten, T. Ramsøy, G. Sletten,  
Niels Bohr Institute, University of Copenhagen, Denmark  
F. Camera, A. Bracco, B. Million, M. Pignanelli,  
University of Milano and INFN, Milano, Italy  
H. Nifenecker, A. Menthe, J. A. Pinston, F. Schussler,  
Institut des Science Nucleaires, Grenoble, France  
W. Krolas, A. Maj,  
Nievodniczanski Inst. for Nucl. Sci., Krakow, Poland  
J. Bacelar, A. Buda, H. v. d. Ploeg  
KVI, Groningen, Netherlands

*Abstract: We have studied the high energy gamma ray from the decay of highly excited  $^{272}\text{Hs}$  nuclei and their daughters. A difference technique was used to isolate decays occurring in the conglomerate system prior to fission. Strong dipole-collectivity is observed. From the yield of pre-fission gamma rays a lifetime for the Hs compound nuclei can be derived.*

## 1 Introduction

Important efforts have, in the past two decades been devoted to synthesizing elements with charge number in excess of 100, the so-called superheavy elements. The experimental approach has been based on the fusion of heavy targets with projectiles with  $A=40-50$  at energies near the barrier and the subsequent identification of the meta-stable residues. The used reactions have been designed to populate cold compound nuclei with the objective of reducing the probability of fission and the evaporation of particles. The usage of low energy reactions and heavy projectiles has however the consequence of severely limiting the production cross section. The current record in the identification of heavy elements presently rests with the identification of a handful of residues of element 109.

Although the meager production cross section makes it virtually impossible to study in any detail the properties of these elements it may nevertheless be possible to obtain some nuclear structure information on such heavy nuclei by producing them in fusion reactions using energetic heavy ions. In such a case one must pay the price that the nuclei are produced at high excitation energy and evaporate numerous particles. On the other hand it turns out that the fusion cross sections between the reaction partners is very strongly enhanced when using beams with energies in excess of 7-8 MeV/nucleon. Furthermore, as has emerged from the last 10 years of fission research, fission is a slow process that predominantly occurs rather late in the cooling of the heavy system. Thus the system is expected to hold together for a significant amount of time so that it can be studied before it

fissions, for example by measuring the gamma ray emission associated with the decay of the Giant Dipole Resonance (GDR) built on the excited states of the system. This radiation is known to contain information on various aspects of excited nuclei such as their collectivity, sizes, shapes, fluctuations and timescales. [1,2]

## 2 Experiments

Figure 1 shows the basic idea of the experiments that we have carried out in order to study the emission of GDR gamma rays from  ${}_{108}^{272}\text{Hs}$  nuclei and its daughters. The upper panel shows the experimental arrangement at the SARA accelerator in Grenoble. The high energy gamma rays from the GDR decay were recorded in the 8 large  $\text{BaF}_2$  detectors of the HECTOR collaboration [3] that were placed at 40 cm from the target in a plane perpendicular to the beam. An array of 7 small of  $\text{BaF}_2$  was located upstream close to the target, inside the scattering chamber, and served as a time trigger. In order to define the reaction mechanism and hence also the initial excitation energy of the formed nuclei, we have concentrated on events leading to symmetric fission. The fission fragments were detected in 4 position sensitive parallel plate avalanche counters (PPAC) located slightly forward of the target. In the experiment we determine the flight time and direction of the fragments. This allows us, based on the knowledge of the CM velocity and assuming that the mass of the fragments adds up to the total mass, to calculate the mass split, the kinetic energy of the fragments and their angle of turning in the CM frame.

A main problem in the analysis of measured GDR gamma ray spectra from reactions involving fissioning nuclei is that the GDR gamma rays can be emitted not only from the compound system *prior* to fission but also by the excited fragments *after* fission. Since the resonance energy scales as roughly  $E_{\text{GDR}} = 79A^{-1/3}$ , the GDR centroids in the system with mass A and in the fragments with mass A/2 will be separated by about 3-4 MeV. As typical GDR width in hot nuclei are of the order of 6-10 MeV this energy separation is not sufficient to disentangle the two contributions. It is possible to analyse the entire spectrum with the aid of statistical model calculations that incorporate the decay of the primary system and of the fragments (see talk of Peter Paul at this meeting).

We have chosen a different approach, as illustrated in the bottom part of fig. 1. The main idea[4] is based on the expectation that, since fission is a slow process, it only occurs after the conglomerate system has cooled significantly by (the faster) particle evaporation. This makes it possible, in principle, possible to cancel out the post fission GDR emission by comparing gamma ray spectra from two reactions at different energies. Indeed, if the initial excitation energy of both compound nuclei is sufficiently high, emission from the fragments produced in both reactions will be similar. Thus a subtraction of the two total spectra should



# GDR IN SUPERHEAVY ELEMENTS

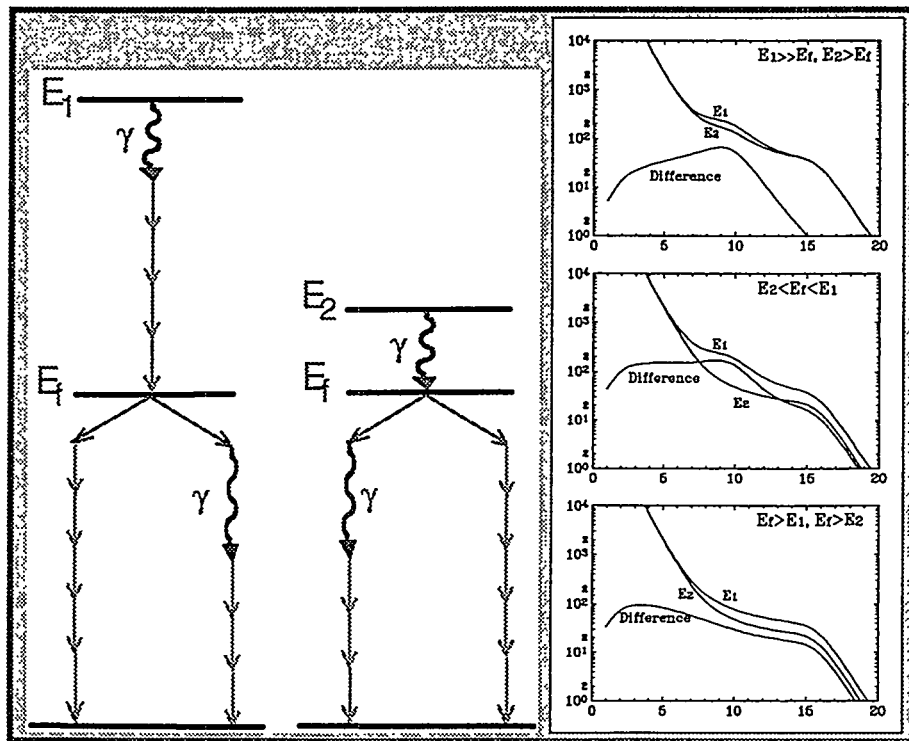
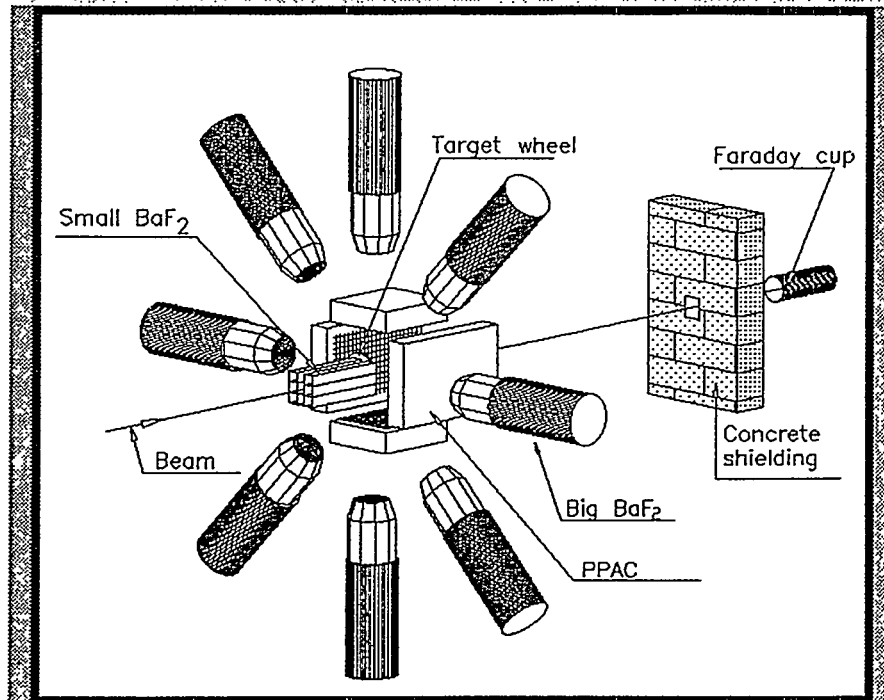


Figure 1: Top: the HECTOR array at the SARA accelerator in Grenoble. Bottom: Schematic illustration of the concept of the experiment (see the text).

## 272 MeV $^{37}\text{Cl} + ^{232}\text{Th}$

Stony Brook exp.

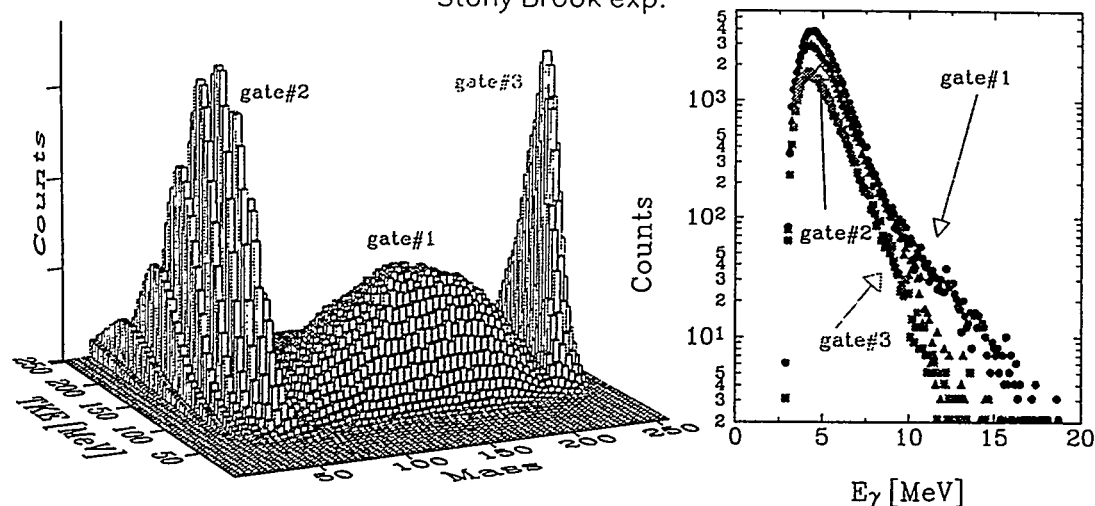


Figure 2: Left: distribution of total kinetic energy vs. fragment mass for two particles detected in a pair of PPAC. Right: Gamma ray spectra in coincidence with various gates on the TKE-mass distribution.

result only in the part not common to the two reactions, i.e. *the additional gamma rays emitted before fission* by the hotter system. This argument assumes that the typical excitation energy at which fission starts to play a role does not depend significantly on the initial excitation energy. This seems indeed to be the case, as may be seen from analyses of pre- and post-fission neutron multiplicities [2]. In the less than ideal situation where fission is a competing channel at high excitation energy for one or both reactions, the situation will be less clear and the post-fission contribution will not cancel out entirely (lower two panels in the right side of figure 1).

That indeed the selection of symmetric fission events leads to the highest excitation energies (fusion-fission) can be seen from the gamma ray spectra, shown in fig. 2 that have been gated by different regions of the total kinetic energy and fragment mass.

In order to test these conjectures we have studied the reaction  $^{40}\text{Ar} + ^{232}\text{Th} \rightarrow ^{272}\text{Hs}$  at bombarding energies 6.8, 10.5 and 15.5 MeV/nucleon using the SARA accelerator at the ISN in Grenoble. These reactions form Hassium compound nuclei with excitation energies around 105, 230 and 380 MeV, respectively.

### 3 Results

#### 3.1 The pre-fission spectrum

The comparison of the total gamma decay spectra at the three bombarding energies is displayed in fig. 3. All spectra are in coincidence with the detection of symmetric fission in the PPAC's. Spectra have been normalised based on the measured absolute gamma ray multiplicities per reaction.

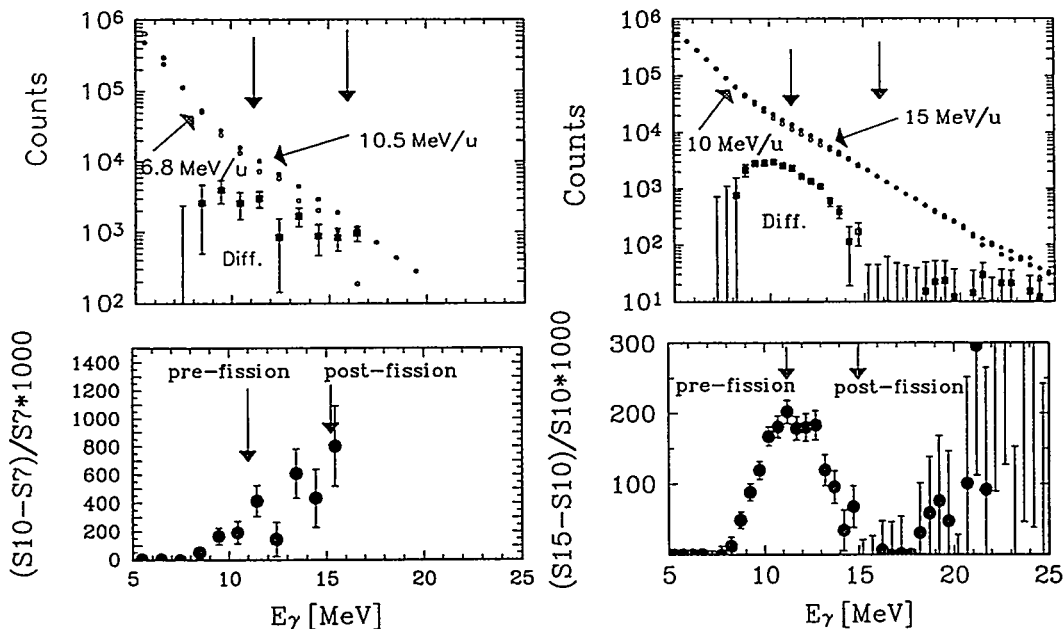


Figure 3: Measured gamma ray spectra in coincidence with binary symmetric fission. Left:  $E(^{40}\text{Ar})= 6.8\text{MeV/u}$  and  $10.5\text{ MeV/u}$ ,; right:  $E(^{40}\text{Ar})= 10.5\text{MeV/u}$  and  $15.5\text{ MeV/u}$ . Difference spectra are also shown.

The left hand side show the comparison of the spectra at the two lower bombarding energies (6.8 and 10.5 MeV/nucleon). The difference between the two gamma ray spectra is shown on a logarithmic scale in the upper panel and in a linear representation in the lower panel. The latter has been obtained by dividing the difference spectrum by the spectrum of lower energy. Although the counting statistics in the reaction of lower energy are poor above 15 MeV it is nevertheless clear that some pre-fission emission is present. It also appears that fission still competes at these energies as may be recognized by the rise in difference yield around 15 MeV (the expected energy of the GDR in the fission fragments).

The situation is much clearer in the comparison of the two higher energies (10.5 and 15.5 MeV/nucleon) shown in the right hand side of fig.3. In this case it appears that the post fission yield indeed cancels out in the subtraction, disclosing clearly the presence of the pre-fission GDR component.

This idea is strongly supported by the comparison of the same spectra with statistical model calculations show in fig. 4. The overlaid curves show the ex-

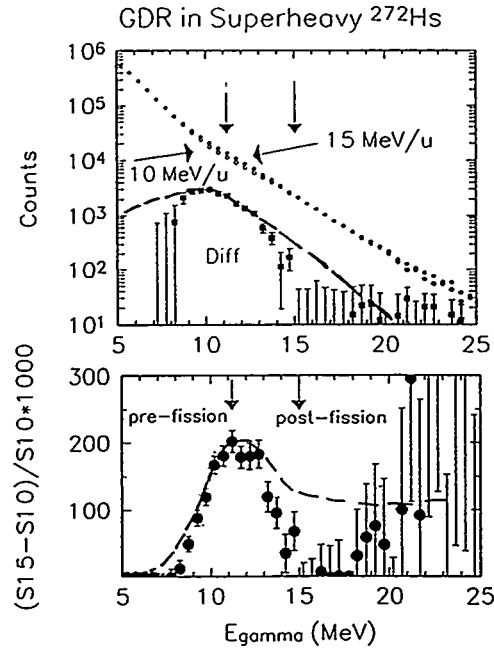


Figure 4: Same figure as in the right hand side of figure 3, but now with superimposed statistical model calculations of the gamma decay in a nucleus with  $A=272$ .

pected gamma ray spectra for the pre-fission contribution, calculated at excitation energies between 230 and 380 MeV. The GDR centroid is 12.2 MeV in perfect agreement with the extrapolation of the ground state systematics. The width is 7 MeV. We will not quote a number for the absolute pre-fission multiplicity at this stage of the analysis, although it appears that it may be somewhat reduced as compared to the full statistical model expectation. A possible reason for this could be a quenching of the collective strength above  $E^* \approx 300\text{MeV}$  as is observed in the  $A=100$  region [1]. If such a quenching occurs at about the same excitation energy in this mass region (thus at much smaller excitation energy per nucleon than in the mass 100 region) it would have the interesting consequence of supporting the notion of a characteristic time for the building of a collective vibration determined by the balance between the neutron width and the intrinsic GDR width [1].

### 3.2 The pre-fission angular distribution

As a further check that we are indeed dealing with dipole radiation we have measured the angular distribution of the emitted gamma rays with respect to the direction of the total angular momentum [1]. This is equivalent to measuring the angular distribution with respect to the fission axis, exploiting the fact that the same gamma ray detector measures two angles, depending on which pair of PPAC's have fired (see fig. 5). The lower part of the figure shows the expected anisotropies for different nuclear shapes and orientations. The likely ones are PC

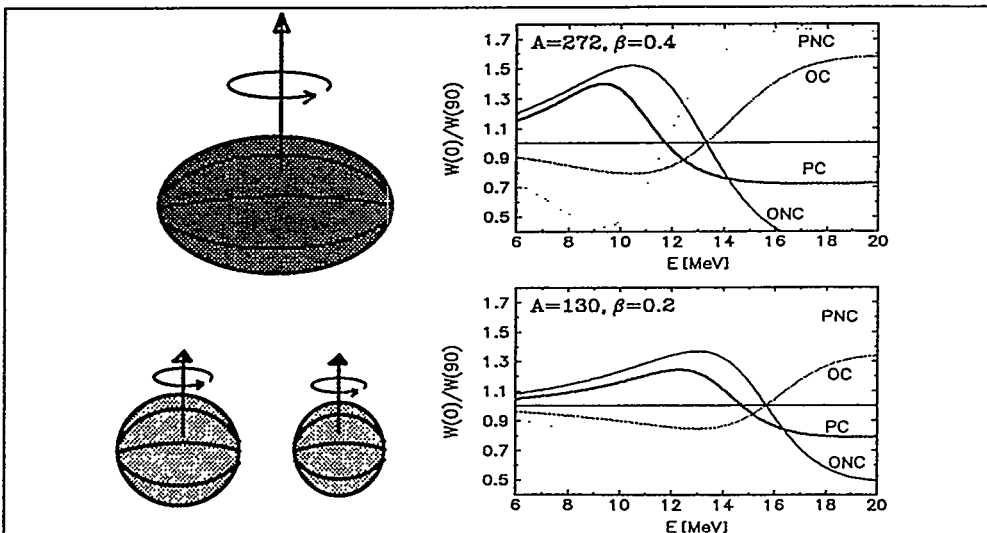
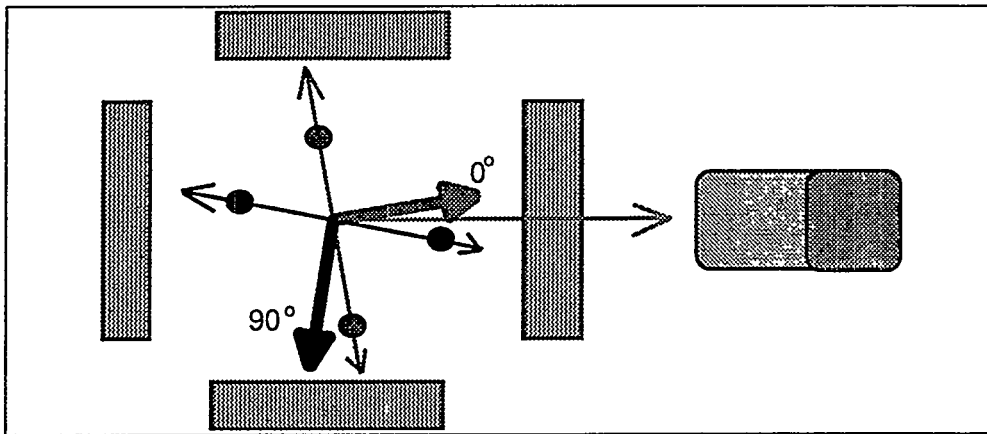
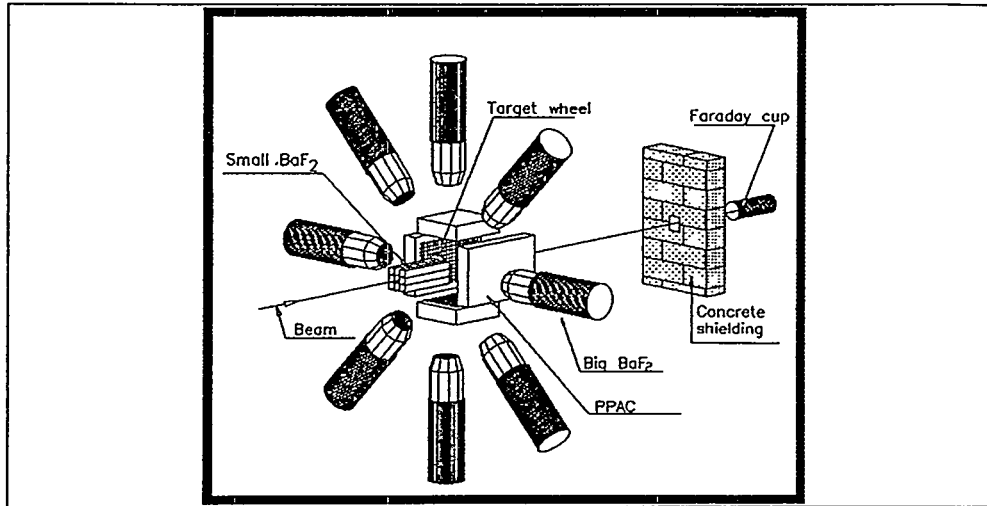


Figure 5: Conceptual plot of the idea underlying the angular distribution measurement with respect to the direction of the total angular momentum of the fissioning nucleus. The lower panel shows the expected anisotropies for various nuclear shapes and orientations.

## Neutron pile-up

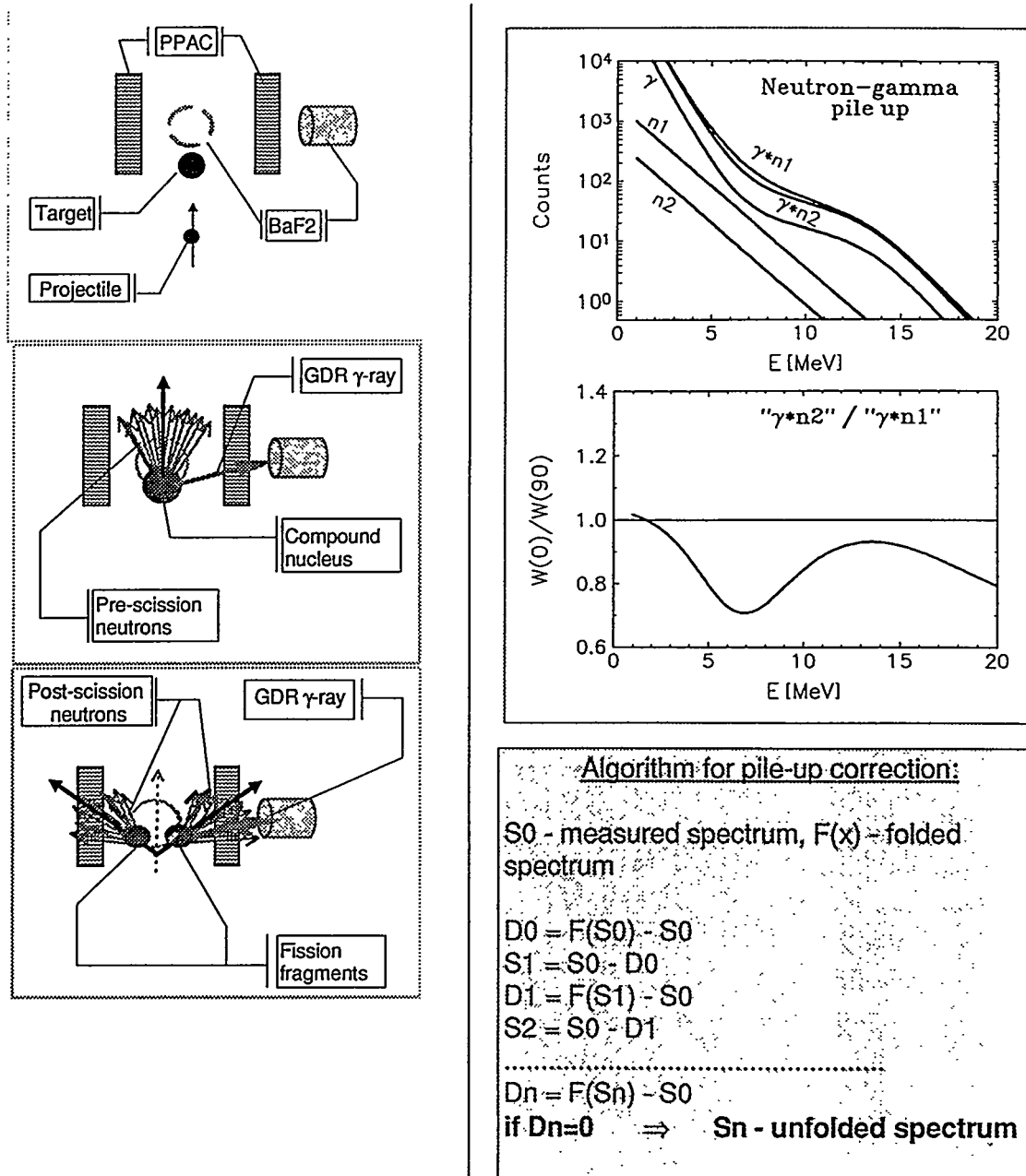


Figure 6: Illustration of the neutron-gamma pile-up problems discussed in the text. With the listed algorithm the gamma ray spectra can be efficiently and accurately unfolded.

### GDR gamma ray Anisotropy: 272Hs

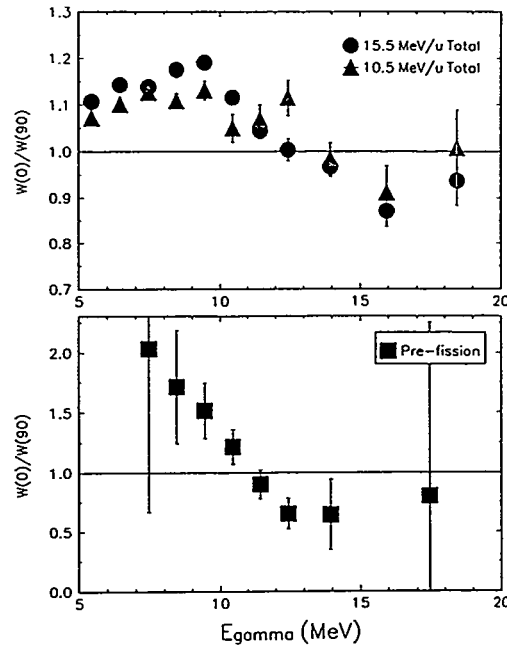


Figure 7: Measured gamma ray anisotropies with respect to the direction of the total angular momentum for the total spectra at 10.5 and 15.5 MeV/u (top panel), and for the difference (bottom panel).

(prolate collective) and ONC (oblate non-collective).

It turns out that before this is possible it is necessary to correct the measured spectra for neutron-gamma pile up arising from the very special geometry of the experimental arrangement. Indeed, post-fission neutron emission is strongly focused along the direction of fission leading to a distortion of the spectrum at one angle. Fig. 6 illustrates the situation and lists a simple algorithm that can be used to unfold the spectra based on the knowledge of the shape and multiplicity of the measured neutron spectra. This rapidly converging routine has been satisfactorily checked against an efficient hardware pile-up rejection in a subsequent experiment [6].

The resulting anisotropies with respect to the angular momentum direction for the total spectra at 10.5 and 15.5 MeV/nucleon and for the corresponding difference spectrum are shown in fig. 8. A pattern of the measured anisotropies consistent with dipole emission from the expected liquid drop shapes for a high mass system is observed. The magnitude of the anisotropy, for the difference spectrum, is close to the expected asymptotic limit of 2 around  $E_\gamma \approx 8$  MeV. This suggests that the role of thermal and orientation fluctuations is small as might be expected as the difference spectrum most likely correspond the very high angular momenta of the compound nucleus ( $\approx 100\hbar$ ).

## 4 Outlook

We conclude that we can isolate the pre-fission GDR in hot Hs nuclei and their daughters using the described difference technique. A key to the success of this procedure is the usage of reactions with high projectile energies that ensures high fusion-fission cross section and populates nuclei at excitation energies at which fission does not yet compete.

We find that the excited Hassium nuclei exhibit a significant dipole collectivity with GDR parameters consistent with those extrapolated from the ground state systematics.

From these measurements we can also infer directly a lower limit for the lifetime of the excited superheavy nuclei. This is illustrated in figure 8 which shows the expected lifetime of the system (given by the neutron evaporation lifetime) as a function of the excitation energy (temperature) of the system. We observe no fission competition down to about 200 MeV. Thus the lifetime must be quite a bit longer than  $10^{-21}$  seconds. We observe some pre-fission yield down to at least 100 MeV. Thus the lifetime must be around  $5 \cdot 10^{-21}$  to  $10^{-20}$  seconds.

As a closing remark we speculate as to the possibility of exploiting the strongly enhanced fusion cross sections and the rather long fission lifetimes to populate the predicted island of stable superdeformed nuclei around  $Z=114$ . In this case a hot system should be formed with an excess of particles that will evaporate during the cooling of the system. We consider the possibility that the GDR gamma ray emission in the last stages of the cooling might further increase the fission survival possibility.

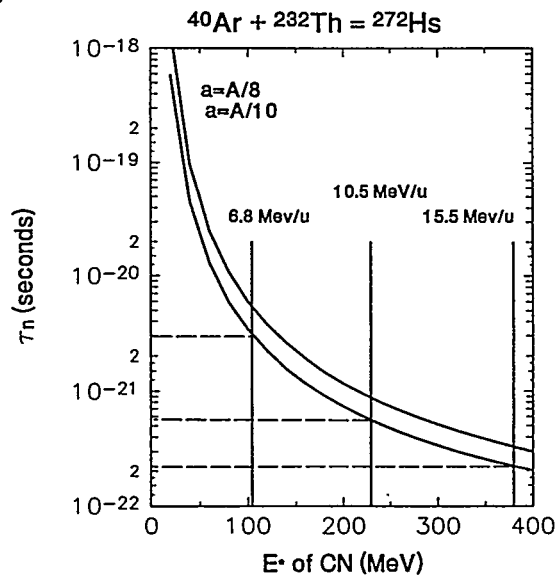


Figure 8: Lifetime for neutron emission as a function of the  $E^*$  of the compound nucleus calculated for 2 values of the level density parameter  $a$ . Excitation energies of the nuclei produced in the reactions are indicated.



## 5 Acknowledgements

We acknowledge the support of the Carlsberg Foundation, the Danish Natural Science Research Council, The Norwegian Research Foundation, the Istituto Nazionale di Fisica Nucleare and the Polish State Committee for Scientific Research (KBN. grant. no. 204519101/p.01).

## 6 References

1. J.J.Gaardhøje. *Ann. Rev. Nuc. Part. Sci.* vol.42 (1992) 483
2. P.Paul + M.Thoenessen. *Ann. Rev. Nuc. Part. Sci.* vol. vol. 44 (1994) to appear.
3. A. Maj, J. J. Gaardhøje, A. Atac, S. Mitarai, J. Nyberg, A. Virtanen, A. Bracco, F. Camera, B. Million, M. Pignanelli. *Nucl. Phys.* A571 (1994) 185
4. J.J.Gaardhøje and A. Maj, *Nucl. Phys.* A520 (1990) 575.
5. T. Tveter, J. J. Gaardhøje, A. Atac, B. Herskind, W. Korten, T. Ramsøy, G. Sletten, F. Camera, A. Bracco, B. Million, M. Pignanelli, H. Nifenecker, A. Menthe, J. A. Pinston, F. Schussler, W. Krolas, A. Maj, J. Bacelar, A. Buda, H. v. d. Ploeg. To be subm. to *Phys. Rev. Lett.*
6. A. Maj, J. J. Gaardhøje, T. Tveter, A. Bracco, F. Camera, M. Matiuzzi, D. Hofmann, P. Paul, S. Schadman, I. Diozegi, J. Bacelar. To be published.

# Fission and Internal Pair Studies of Hot Giant Resonances

P. Paul, D. J. Hofman, S. Schadmand, R. Varma and S. R. Banerjee

*Department of Physics, State University of New York at Stony Brook, NY*

The Giant Dipole Resonance is a fundamental collective mode whose basic properties are now well understood in hot nuclei up to temperatures of a few MeV. Its vibrational energy and intrinsic strength are essentially unaffected by temperature. Thus the rate of GDR  $\gamma$ -ray emission in a hot compound nucleus can serve as a clock for competing nuclear decay processes. One of the most interesting application is the study of the time scale of nuclear mass flow in the fission process, as a function of nuclear temperature. This subject has been pursued in very heavy nuclei with a series of experiments using  $\gamma$ -ray-fission coincidence studies to explore the slowing down of the fission process due to nuclear viscosity [1]. In these studies the time scale of the fission flux build-up inside the barrier, the flow across the fission barrier and the flow from saddle to the scission point can all be expressed by the linear friction coefficient  $\gamma$  which may differ inside and outside of the saddle. Fig. 1 shows the reliability of the method for the case [2] of hot  $^{224}\text{Th}$ . The  $\gamma$ -ray spectrum in coincidence with fission fragments must be decomposed into the contribution emitted from the CN inside and outside the saddle, and the spectrum emitted from the hot fission fragments. Fig. 1 indicates how well the residue left after subtraction of the fission fragment spectrum is fitted by the GDR spectrum from the hot CN, with the friction coefficient  $\gamma$  as major fit parameter. One obtains  $\gamma = 10$  indicating a strongly overdamped mass flow ( $\gamma = 1 =$  critical damping). In addition  $\gamma$ -ray-fission coincidence measurements allow determination of the shape and deformation of the emitting system from the  $\gamma$ -fission angular correlation. The bottom panel of Fig. 1 shows the correlation produced by a collective prolate (or non-collective oblate) deformed compound system.

Such large damping puts our theoretical understanding of nuclear dissipation to the test. It is clear from a comparison of the hot time scales with those in cold nuclei that, somehow, this strong dissipation must involve a temperature dependence of  $\gamma$ . One-body dissipation which is the widely accepted damping process can just barely account for the dissipative strength, but it has a very weak temperature dependence. Two-body viscosity has a strong temperature dependence but is so far believed to be much too weak to account for the large damping. As large damping at high excitation energies is now widely accepted we report on recent experiments that demonstrate rather directly the strong  $T$  dependence of  $\gamma$ . Fig. 2 shows the example of  $^{240}\text{Cf}$  formed in the reaction  $^{32}\text{S} + ^{208}\text{Pb}$  at 200 and 230 MeV [3]. At the lower energy the  $\gamma$ -ray spectrum is fitted perfectly with a statistical calculation *without* any dissipation, and the correlation shows no clear evidence for the presence of the CN system. This means that no GDR  $\gamma$ -rays are seen from the hot CN before it fissions. However, only 30 MeV higher, the  $\gamma$  spectrum shows a clear excess indicating the presence of dissipation and a strong correlation indicates the presence of  $\gamma$ -rays from the deformed long-lived CN.

A more complete analysis is possible [4] for the system  $^{16}\text{O} + ^{208}\text{Pb}$  which forms  $^{224}\text{Th}$ . In this case, in addition to the  $\gamma$ -multiplicity, the fusion evaporation cross

section [5] as well as the pre- and post-fission neutron multiplicity have been measured and all of these are affected by nuclear viscosity. Fig. 3 shows a statistical model fit first again without dissipation (dashed lines). Below 100 MeV bombarding energy the non-dissipative model explains the fusion-evaporation cross section as well as the  $\gamma$ -ray spectrum. However, above  $\sim 100$  MeV these fits underpredict the  $\gamma$ -ray yield and the fusion evaporation cross section. Introducing the dissipation coefficient as a free parameter one obtains excellent fits (full lines) with a parameter  $\gamma$  that increases rapidly above 100 MeV. The resultant temperature dependence is indicated in the bottom panels of Fig. 3 and can be fitted with either a linear or quadratic dependence. This strong dependence is a challenge to the theory.

Several recent theoretical attempts have been successful in explaining this rise, as well as the size of dissipation, e.g. by introducing large rotation into the two-body dissipation models (and indeed, all these experiments produce the CN at high angular momenta). In a more general (albeit speculative) attempt to understand this T dependence we draw attention to the analogy with the dissipation in liquid  ${}^3\text{He}$ . There the attenuation of a sound wave (this is an semi-infinite system) increases at first like  $T^2$  until dissipation becomes so strong in the interior that the wave changes from zero-sound to regular sound. From that point on dissipation decreases as  $T^{-2}$ . Although the analogy is flawed because the nucleus (even Th) is not a very large system and the nuclear medium is a very dilute Fermi liquid, nevertheless the experimental similarity is intriguing and may perhaps guide further experiments.

For example, as the sound wave changes from zero-sound to first sound, the wave velocity changes from the Fermi velocity to the sound velocity in nuclear matter  $v_s = 1/\sqrt{3} \cdot v_F$ . This affects strongly the energy of another fundamental mode of nuclear matter, the isoscalar Giant Monopole Resonance (GMR). In both infinite nuclear matter and in finite nuclei, its energy is proportional to the wave velocity and would therefore strongly decrease as dissipation increases. This decrease is much more than what is predicted by finite-temperature regular particle-hole calculation.

Experimentally the GMR in hot nuclei might be detectable through a measurement of internal  $e^+ - e^-$  pair conversion. Observing the pairs in good angle resolution allows the separation of the  $L=0$  mode from higher L modes. Two detectors have been developed over the last few years which are designed to measure internal pairs from giant resonances with high efficiency. These are the PEPSI detector [7] from KVI (an adaptation of an orange spectrometer) and the open-geometry plastic phosphor pair detector from Stony Brook [8]. Both detectors are taking data and have demonstrated quite successfully that internal pair conversion from giant resonances can be quantitatively detected. Unfortunately, as Fig. 4 shows [6], about a factor of 1000 has to be overcome to see the GMR against the internal pair conversion of the GDR. However, experimental progress has reduced the goal to about a factor of 4 (in light nuclei where isospin can help) to  $\leq 100$  in heavy nuclei. We present here some results from the reaction  ${}^{19}\text{F} + {}^{181}\text{Ta} \rightarrow {}^{200}\text{Pb}$  at a low beam energy of 95 MeV chosen to eliminate fission [9]. Fig. 5 gives the transition energy spectrum of pairs. This spectrum is in quantitative agreement with the experimental GDR  $\gamma$ -ray spectrum multiplied by the energy dependent E1 internal pair conversion coefficient (indicated by dots). The excess peak at 6 MeV is the remainder of the strong  $0^+ \rightarrow 0^+$  transition. Fig. 6 demonstrates that the detailed kinematic variables of the pair decay

are well understood. These include the  $e^+ - e^-$ -correlation (a) which shows the E1 character of the pair transition, the energy sharing between the pair partners (b), the net momentum orientation relative to the beam (c) and the di-hedral angle between the pair plane and the reaction plane (d). All of these depend in detail on the  $\Delta L$  of the transition. The GEANT simulations which include the detector geometry describe these histograms well. These first results hold out the hope that, with better statistics, one may apply additional cuts to reduce the E1 "background" in favor of E0 transitions. Such experiments are now in progress.

In summary, GDR experiments demonstrate conclusively an energy threshold for strong dissipation in the range between  $E^* = 50$  to  $80$  MeV (temperatures between  $1.2$  and  $1.4$  MeV) with a temperature dependence proportional to  $T$  or  $T^2$ . If this behavior signals the transition from zero-sound to first sound in the nuclear interior, it could have implications for nuclear compressibility. Attempts to study dissipation in the properties of the nuclear compression mode at finite temperatures through internal pair decay have made experimental progress and have reached a level of technical maturity. However, actual observation of the GMR is still one to two orders of magnitudes away from reality.

## References

- [1] P. Paul, Nucl. Phys. **A569**, 73c (1994)
- [2] I. Dioszegi, D.J. Hofman, C. P. Montoya, S. Schadmand, P. Paul, Phys. Rev. **C46**, 627 (1992)
- [3] D. J. Hofman, B. B. Back, I. Dioszegi, C. P. Montoya, S. Schadmand, R. Varma, P. Paul, Phys. Rev. Letters **72**, 470 (1994)
- [4] D. J. Hofman, B. Back and P. Paul, to be published
- [5] K. Brinkman, A. L. Caraley B. J. Fineman, N. Gan, J. Velkovska, R. L. McGrath, Phys. Rev. **C50**, 309 (1994)
- [6] C. P. Montoya, S. Schadmand, I. Dioszegi, D. J. Hofman, P. H. Zhang, P. Paul, Zeitsch. Phys **A340**, 371 (1991)
- [7] A. Buda, J. Bacelar et al., Nucl. Instr. Meth. **A335**, 479 (1993)
- [8] C. P. Montoya, S. Schadmand R. Varma, P. H. Zhang, R. Butsch, I. Dioszegi, D. J. Hofman, P. Paul, Nucl. Instr. Meth. **A334**, 437 (1993)
- [9] S. Schadmand, Ph.D. thesis, State University of NY at Stony Brook (1994)
- [10] M. Thoennessen, Ph.D. thesis, State University of NY at Stony Brook (1988)

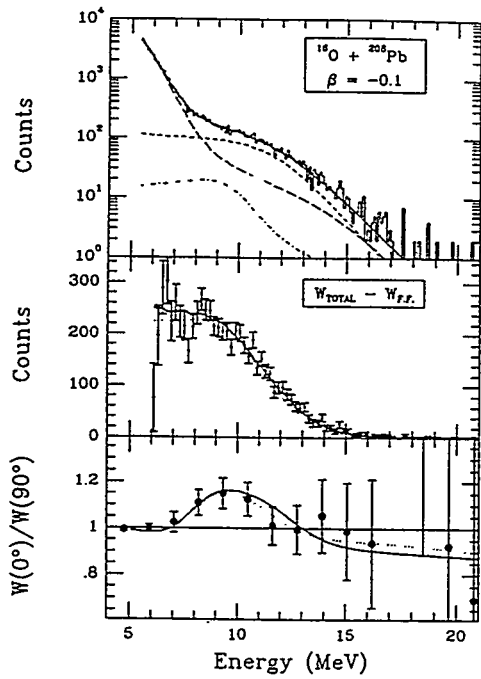


Figure 1: Decomposition of the GDR  $\gamma$ -ray spectrum in  $^{224}\text{Th}$  into pre- and post-fission  $\gamma$ -rays (top). The center panel shows the CN contribution and a fit with a dissipative statistical model.

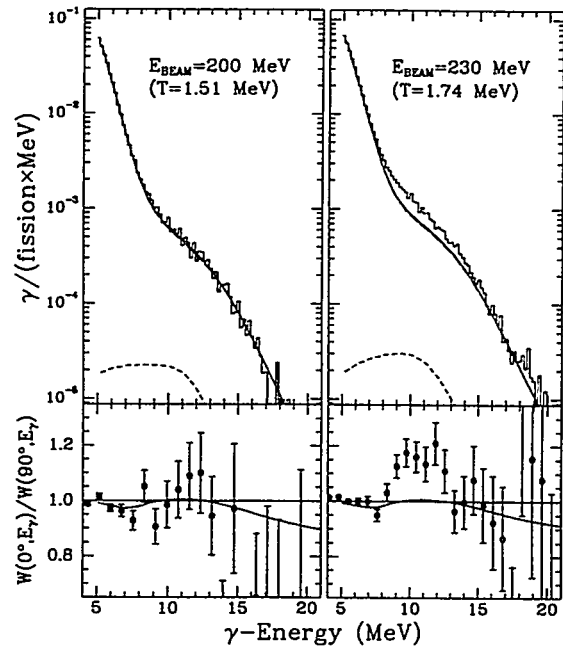


Figure 2: GDR energy spectrum and  $\gamma$ -fission angular correlation in the  $^{32}\text{S} + ^{208}\text{Pb} \rightarrow ^{240}\text{Cf}$  reaction, at two closely spaced bombarding energies.

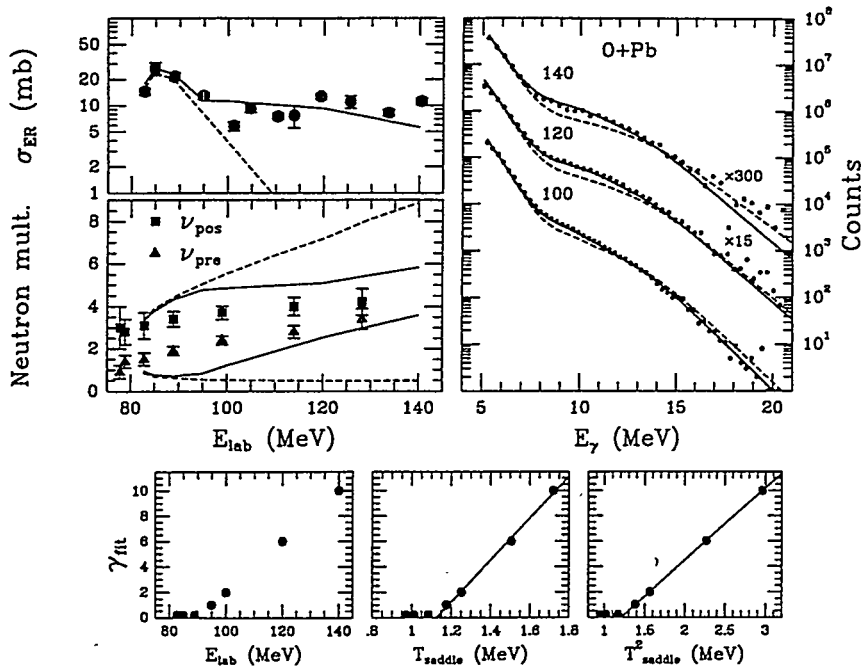


Figure 3: Analysis of fusion-evaporation, pre- and post-fission neutron multiplicities (top left) and  $\gamma$ -ray spectrum (top right) with a statistical model without (dashed lines) and with (full lines) dissipation. The extracted dissipation coefficient  $\gamma_{FIT}$  and its temperature dependence is shown in the bottom panels.

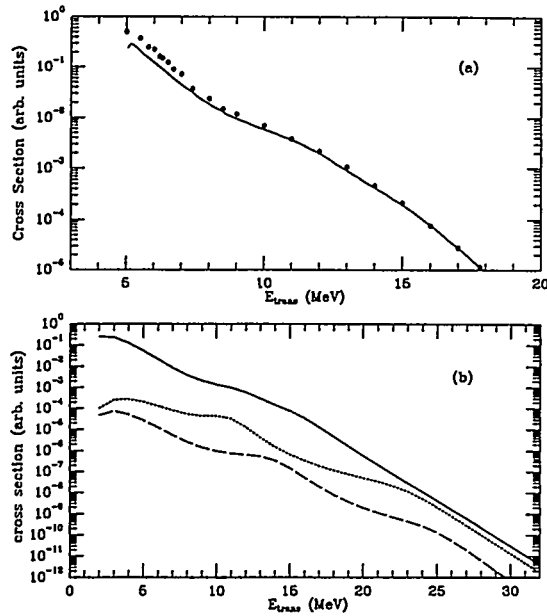


Figure 4: Top panel:  $\gamma$  spectrum from the GDR observed in the  $^{19}\text{F} + ^{181}\text{Ta}$  reaction [10] and fit with a statistical code. Bottom panel: Internal pair transition spectrum calculated for  $L=1$  (top),  $L=2$  (center) and  $L=0$  (bottom) giant resonances in the same reaction.

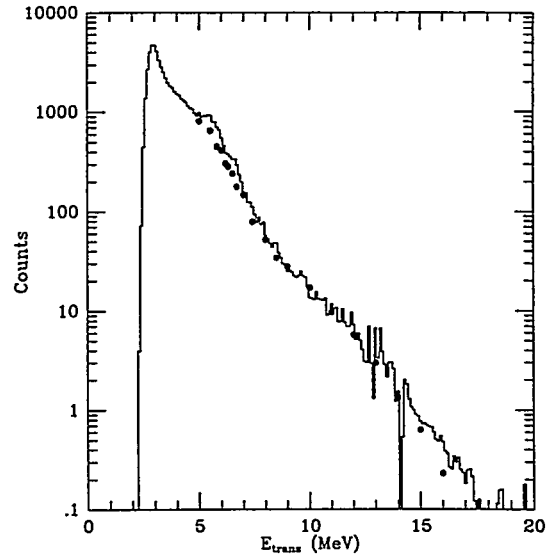


Figure 5: Experimental internal pair transition spectrum observed in the  $^{19}\text{F} + ^{181}\text{Ta} \rightarrow ^{200}\text{Pb}$  reaction (histogram) and the spectrum predicted from the pair-converted experimental  $\gamma$ -spectrum (points).

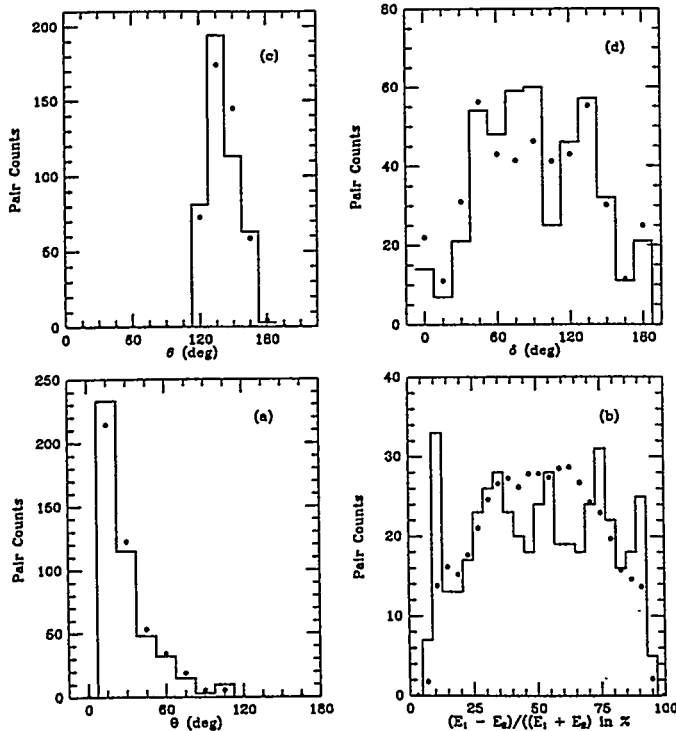


Figure 6: Comparison between various experimentally observed (histograms)  $e^+ - e^-$  correlations and energy sharing and GEANT simulations (points). The various panels are explained in the text.

# Periodic Orbits and New Shell Structure Generated by a Combination of Quadrupole and Octupole Deformations

K. Arita and K. Matsuyanagi

*Department of Physics, Kyoto University, Kyoto 606, Japan*

## 1. Introduction

In this talk, we would like to present a simple model in which a prominent shell structure emerges for a combination of quadrupole and octupole deformations. We shall then discuss the origin of such a new shell structure in terms of the periodic orbits and their bifurcations.

Importance of shell effects for the occurrence of reflection-asymmetric deformed shapes have been lively discussed in various region of nuclei [1,2] and also in micro-clusters [3,4].

According to the semi-classical theory, the shell structure, i.e., the oscillating structure in the single-particle level density is generated by classical closed orbits with short periods. Thus, our task is to identify important periodic orbits and study how they are born and how their properties change as function of deformation parameters.

This subject is deeply related with the general subjects of quantum chaos; in particular, quantum manifestation of bifurcation phenomena in classical Hamiltonian dynamics. We would like to emphasize that, although “quantum chaos” in the chaotic limit has been much discussed, bifurcation of periodic orbits is characteristic for mixed systems where regular and chaotic motion coexist and remains largely unexplored. Finite quantum systems possessing both quadrupole and octupole deformations are situated in an intermediate region between regular and chaotic systems [5,6], and therefore provide us with a very good opportunity to study, from both theory and experiment, this important subject.

## 2. Model

Let us consider the reflection-asymmetric deformed oscillator Hamiltonian

$$h = \frac{\mathbf{p}^2}{2M} + \frac{1}{2}M\omega_{\perp}^2(x^2 + y^2) + \frac{1}{2}M\omega_z z^2 - \lambda_{30}M\omega_0^2 [r^2 Y_{30}]'', \quad (1)$$

where the double primes denote that the variables in square bracket are defined in terms of the doubly-stretched coordinates  $x_i'' = (\omega_i/\omega_0)x_i$ . We calculate classical periodic orbits and quantum energy spectra for this Hamiltonian as functions of the deformation parameters  $\delta_{\text{osc}} = (\omega_{\perp} - \omega_z)/\bar{\omega}$  and  $\lambda_{30}$ .

### 3. An Example

In the previous work [7], we discussed the superdeformed case with the frequency ratio  $\omega_{\perp}/\omega_z = 2$ . Today, we first show the result [8] for an irrational ratio  $\omega_{\perp}/\omega_z = \sqrt{3}$ .

#### A new shell structure

Figure 1 shows the single-particle spectrum calculated as a function of  $\lambda_{30}$ . There is no prominent shell structure at  $\lambda_{30} = 0$  because of irrationality of the frequency ratio. However, a significant shell structure appears at  $\lambda_{30} \simeq 0.3$ . The oscillating level density smoothed by means of the Strutinsky method is shown in Fig. 2. A prominent shell structure is clearly seen. Evidently, this new shell structure is generated by an octupole deformation superposed on the quadrupole deformation. You can also notice a supershell pattern associated with the interference between classical periodic orbits with the periods  $T \simeq 2\pi/\omega_{\perp}$  and  $2\pi/\omega_z$ , which we discussed in the previous work [7].

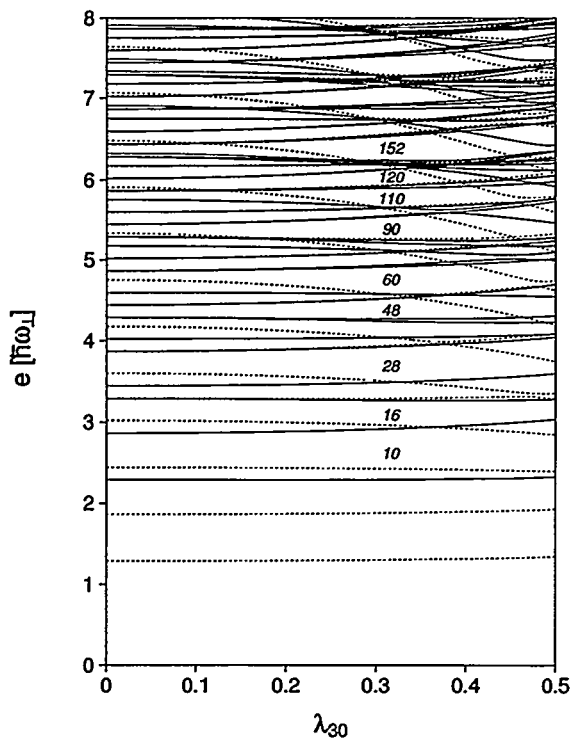


Figure 1

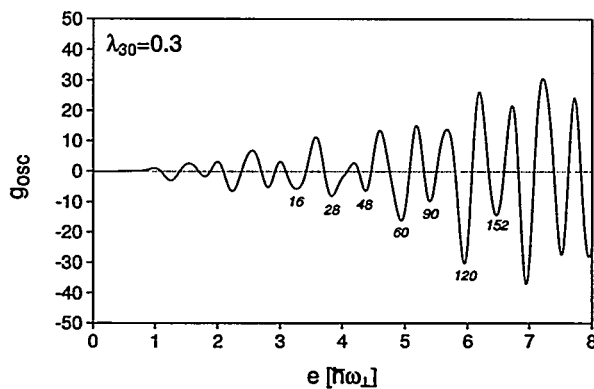


Figure 2



Classical periodic orbits and bifurcations

Figure 3 shows some periodic orbits for  $\lambda_{30} = 0.3$ . We have found that the orbit named PB (planar B-type) is born at  $\lambda_{30} \simeq 0.29$  due to the bifurcation of orbit IL (isolated linear orbit along the  $z$ -axis). Likewise, orbits PC and PD are born by the bifurcation at  $\lambda_{30} \simeq 0.28$ .

To see how these bifurcations occur, let us examine the Poincaré surface of section. Due to the axial symmetry, our system is two dimensional with cylindrical coordinates  $(\rho, z)$  having a fixed angular momentum  $p_\phi$ . Figure 4 are the Poincaré sections  $(\rho, p_\rho)$  with  $z = 0, p_z < 0$ , and  $p_\phi = 0$ . The origin corresponds to the orbit IL, which is stable at  $\lambda_{30} = 0.28$  and accompanies tori about it. These tori are significantly distorted until the bifurcation occurs at  $\lambda_{30} = 0.283$ . Thus, at  $\lambda_{30} = 0.29$  we find a pair of islands (associated with the stable orbit PD) and a pair of saddles (unstable orbit PC). At  $\lambda_{30} = 0.292$ , another bifurcation occurs generating a new pair of islands (seen for  $\lambda_{30} = 0.3$ ) associated with the stable orbit PB. Then, the central torus becomes unstable.

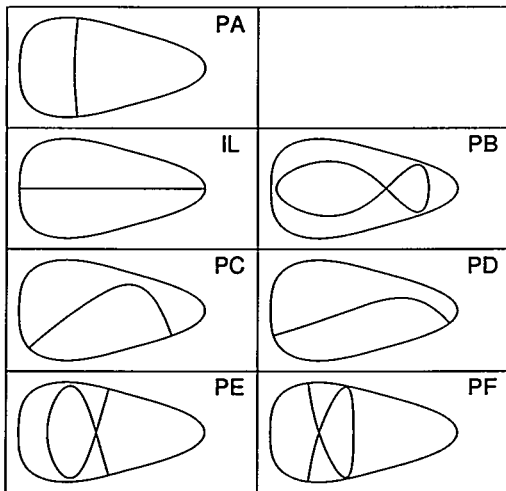


Figure 3

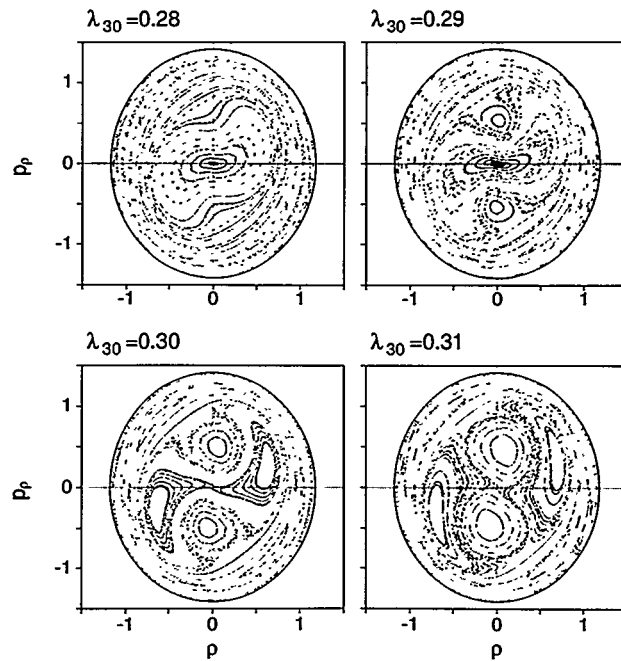


Figure 4

### Classical-quantum correspondence

To find the link between the quantum shell structure seen in Figs. 1, 2 and the properties of the classical periodic orbits, let us consider the Fourier transform of the single-particle level density  $g(E; \lambda_{30}) = \sum_n \delta(E - E_n)$ ,

$$F(s) = \int_0^\infty dE \frac{1}{\sqrt{E}} g(E) e^{isE}. \quad (2)$$

According to the Gutzwiller trace formula, the oscillating part of the level density is represented as a sum of contributions from periodic orbits. Combining this with the scaling property of our Hamiltonian  $H(\alpha\mathbf{p}, \alpha\mathbf{q}) = \alpha^2 H(\mathbf{p}, \mathbf{q})$ , we expect that the Fourier transform will exhibit peaks at the periods of the classical periodic orbits, the height of each peak representing the intensity of the contributing orbit.

Figure 5 shows absolute values of the Fourier transform as a function of both  $s$  and  $\lambda_{30}$ . Let us notice that the peak at  $s \simeq \sqrt{3}$  (in unit of  $T_\perp = 2\pi/\omega_\perp$ ) significantly grows up with increasing octupole deformation, and reaches the maxima at  $\lambda_{30} = 0.3 \sim 0.4$ . This value of  $s$  just corresponds to the periods of the newly born orbits PB, PC and PD. In this way, we find a nice classical-quantum correspondence. In particular, the prominent shell structure at  $\lambda_{30} \simeq 0.3$  may be regarded as a quantum manifestation of the bifurcations of classical periodic orbits.

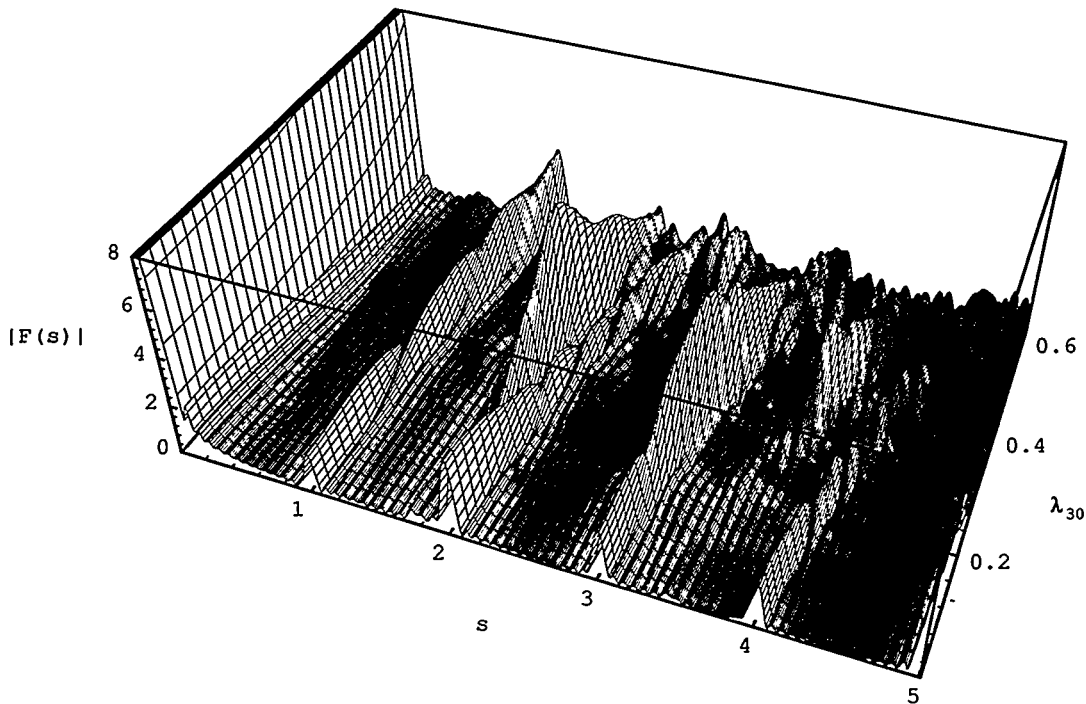


Figure 5

#### 4. Contour Map of the Shell-Structure Energy

Next, let us investigate how the shell structure changes when both the quadrupole and octupole deformation parameters are varied. As a measure of the intensity of shell effect, we define

$$I_{\text{sh}} \equiv \sqrt{\frac{1}{N_{\text{max}}} \sum_{N < N_{\text{max}}} \left( \frac{E_{\text{sh}}(N)}{N^{1/3}} \right)^2}, \quad (3)$$

where  $E_{\text{sh}}(N)$  is the shell structure energy for particle number  $N$ .

Figure 6 shows a contour map of  $I_{\text{sh}}$ . The significant maxima on the horizontal axis at  $\delta_{\text{osc}} = -0.75, 0.0, 0.6$  and  $0.86$  correspond to oblate-superdeformed, spherical, prolate-superdeformed and hyperdeformed shapes, respectively. The thick lines represent the points where various kinds of bifurcation occur. We see that some thick lines run along the ridges of the  $I_{\text{sh}}$ -contour, indicating the significance of their contributions to the shell effect [9].

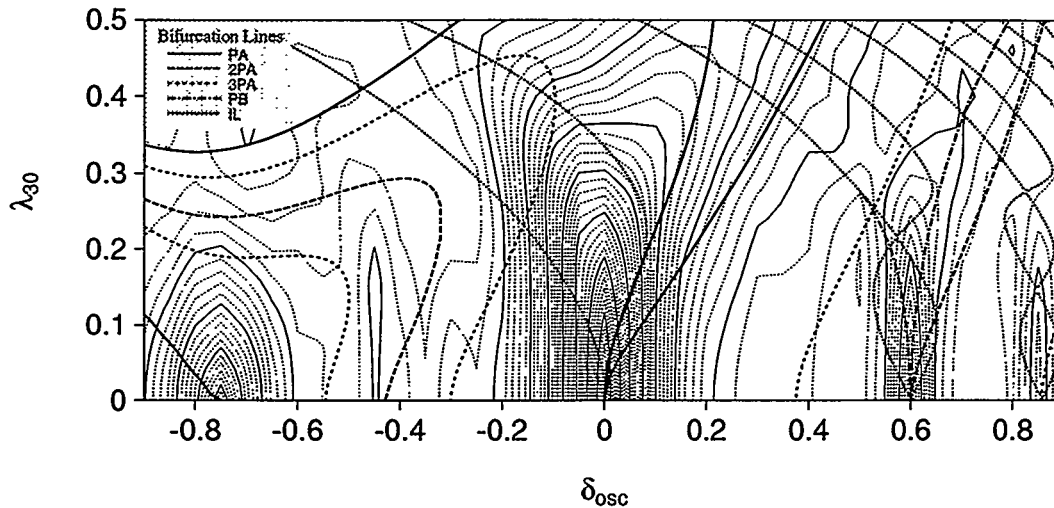


Figure 6

## 5. Concluding Remarks

We have discussed the origin of the shell structure appearing in a reflection-asymmetric deformed oscillator potential in terms of classical periodic orbits and their bifurcations. It would be an interesting future subject to study how the nice classical-quantum correspondence found for the Hamiltonian (1) persists in more realistic Hamiltonian like Woods-Saxon potential including the spin-orbit term.

## References

- [1] S. Åberg, H. Flocard and W. Nazarewicz, *Ann. Rev. Nucl. Part. Sci.* 40 (1990), 439.
- [2] W. Nazarewicz et al., *Nucl. Phys.* A429 (1984), 269.
- [3] I. Hamamoto, B. R. Mottelson, H. Xie and X. Z. Zhang, *Z. Phys.* D21 (1991), 163.
- [4] S. Frauendorf and V. V. Pashkevich, preprint FZR-37 (1994).
- [5] W. D. Heiss, R. G. Nazmitdinov and S. Radu, *Phys. Rev. Lett.* 72 (1994), 2351.
- [6] W. Bauer, D. McGrew and V. Zelevinsky, *Phys. Rev. Lett.* 72 (1994), 3771.
- [7] K. Arita and K. Matsuyanagi, *Prog. Theor. Phys.* 91 (1994), 723.
- [8] K. Arita, to be published in *Phys. Lett. B*.
- [9] K. Arita and K. Matsuyanagi, in preparation.

**A Superdeformed Band with a Unique Pattern of Decay:  
Possible Evidence for Octupole Vibration in  $^{190}\text{Hg}$**

B. Crowell,<sup>1</sup> R.V.F. Janssens,<sup>1</sup> M.P. Carpenter,<sup>1</sup> I. Ahmad,<sup>1</sup> R.G. Henry,<sup>1</sup>  
S. Harfenist,<sup>1,4</sup> T.L. Khoo,<sup>1</sup> T. Lauritsen,<sup>1</sup> D. Nisius,<sup>1,5</sup> A.N. Wilson,<sup>2</sup> J.F.  
Sharpey-Schafer<sup>2</sup> and J. Skalski<sup>3</sup>

(1) Argonne National Laboratory, Argonne, Illinois 60439; (2) Oliver Lodge  
Laboratory, University of Liverpool, P O Box 147, Liverpool L69 3BX, United  
Kingdom; (3) Soltan Institute for Nuclear Studies, Hoza 69, 00-681 Warsaw; (4)  
Student research participant, Georgia Tech, Atlanta, GA 30332; (5) graduate  
student from Purdue Univ., West Lafayette, IN 47907

**Abstract:** An excited superdeformed (SD) band has been observed in  $^{190}\text{Hg}$  which decays to the lowest-energy (yrast) SD band rather than to the less deformed states as observed in most known SD bands in the A~150 and A~190 regions. The most plausible interpretation of this very unusual decay pattern associates this band with a collective structure built on an octupole-vibrational phonon in the SD well.

A major focus of current research with large arrays of gamma-ray detectors is to map out the spectrum of single-particle excitations in superdeformed nuclei in the A~150 and A~190 regions. Surprisingly, however, no excitations have been identified consisting of vibrations about a superdeformed equilibrium shape, despite predictions of marked octupole softness in both regions. This softness is calculated [1] to extend to the non-axially symmetric modes with K=1,2 and 3, which are less often energetically favored at normal deformations. For the K=0 and 1 modes, it has been suggested [2] that the bands containing an octupole-vibrational phonon could be experimentally distinguished by an unusual decay path, through extremely strong ( $\sim 10^{-2}$  W.u.) E1 transitions leading to the lowest-lying band. Among the A~190 nuclei,  $^{190}\text{Hg}$  is predicted [1] to be one of the softest with respect to the K=0 and K=1 octupole deformations.

In the present experiment, superdeformed gamma-ray cascades resulting from the reaction  $^{160}\text{Gd}(^{34}\text{S},4n)^{190}\text{Hg}$  were observed with the Early

Implementation phase of GAMMASPHERE, using beams provided by the LBL 88-inch cyclotron striking a stack of three self-supporting  $0.5 \text{ mg/cm}^2$  Gd foils. An event was recorded whenever three or more Compton-suppressed Ge detectors fired within 50 ns of one another. The resulting 660 million events were sorted into a three-dimensional histogram,[3] and doubly gated one-dimensional spectra were created using the method of background-subtraction described in ref. [4].

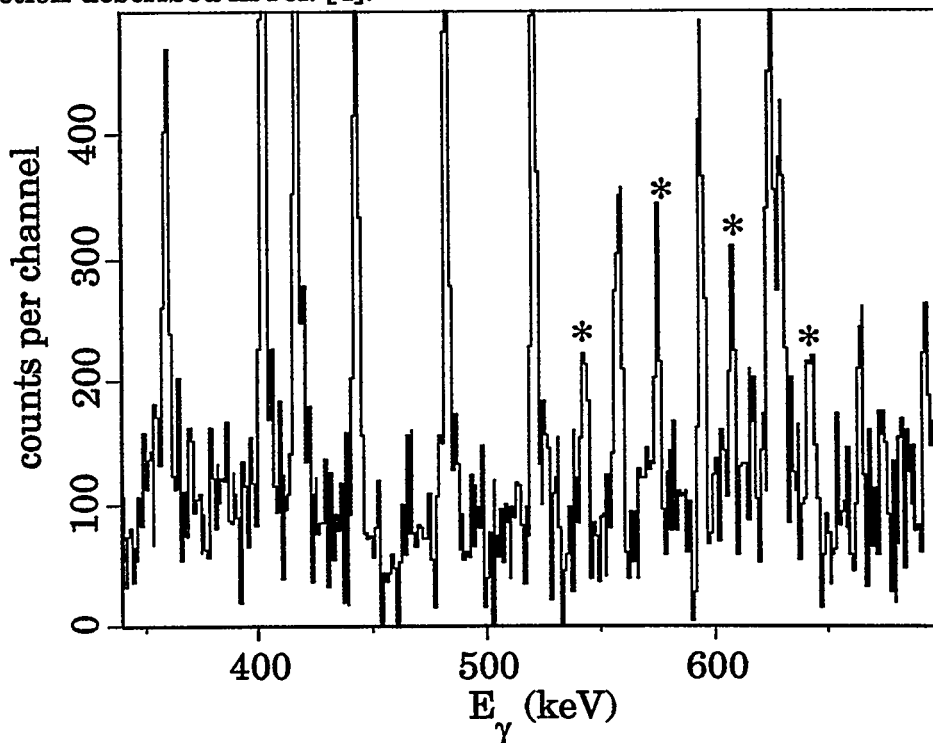


**Fig. 1** . Background-subtracted spectrum created by summing combinations of gates on the vacuum and excited superdeformed bands in  $^{190}\text{Hg}$ . Asterisks mark transitions in the excited band.

Unexpectedly, the spectrum in coincidence with the previously observed [6] lowest-lying superdeformed band in  $^{190}\text{Hg}$  revealed a new superdeformed band (fig. 1), populated approximately ten times more weakly, which proved to decay to the first band with high probability. The branching ratios of the 576, 543 and 512 keV transitions in the excited band (fig. 2) relative to the corresponding probabilities of depopulation to the vacuum band were measured to be 3(1), 1.2(3) and 0.8(2), respectively, in dramatic contrast to the usual pattern of decay of superdeformed states, in which each band remains aloof from the others until its flux spills out into the normally deformed states. Gating on pairs of transitions in the new band, without any

requirement of a coincidence with lines in the vacuum band, allowed the determination of a probability of only  $4 \pm 31\%$  for the usual type of decay, directly to the normally deformed well.

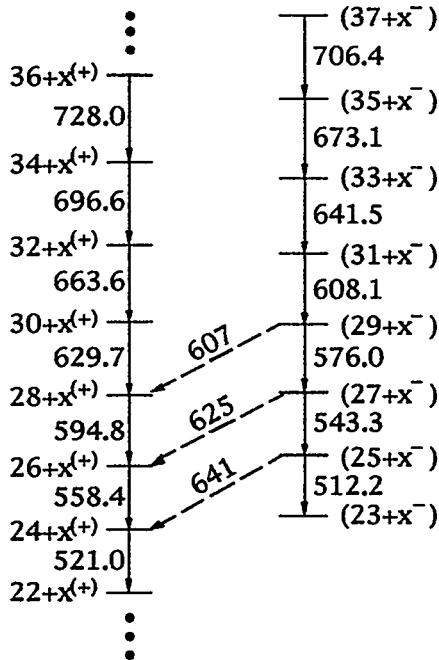


Fig. 2. Partial level-scheme of states in the SD well of  $^{190}\text{Hg}$ .

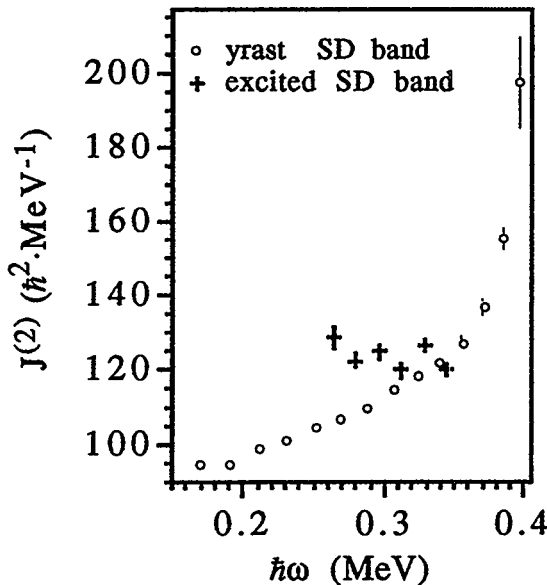


Fig. 3. Moments of inertia of SD bands in  $^{190}\text{Hg}$ .

Assuming that the transition quadrupole moment of the new band is equal to the  $18(3)$  e-b moment of the vacuum band,[6] the extracted partial half-lives of the out-of-band branches are  $110(30)$ ,  $120(30)$  and  $180(80)$  fs. These transitions have themselves tentatively been identified in the spectra. Although the proposed lines (fig. 2) are unfortunately all doublets with other transitions associated with superdeformation in  $^{190}\text{Hg}$ , they have been picked out through an examination of centroid shifts and patterns of coincident intensities, as described in ref. [5]. With these energies in hand, the strengths of the transitions are found to be about  $10^{-2}$ ,  $1$ , or  $10^3$  W.u., respectively, if they are of E1, M1, or E2 character. M1 or E2 strengths such as these would be orders of magnitude larger than those expected for configuration-changing transitions in a deformed nucleus [7]. (The mechanism suggested in ref. [8] for the occurrence of very strong M1 transitions between signature partners cannot apply here, assuming that the lowest-lying band

corresponds to the BCS vacuum, with  $K=0$ , in the superdeformed well.) The extracted E1 strengths, in contrast, are very close to those predicted in ref. [2]

for transitions from the superdeformed K=0 one-octupole-phonon state to the 0<sup>+</sup> superdeformed state of <sup>192</sup>Hg.

The  $\mathcal{J}^{(2)}$  moment of inertia of the new band is also unusual (fig. 3). In all other superdeformed bands in even-even nuclei in the A~190 region,  $\mathcal{J}^{(2)}$  shows a uniform behavior of rising gradually as a function of rotational frequency, and the magnitude of  $\mathcal{J}^{(2)}$  varies slowly from nucleus to nucleus [9]. The larger  $\mathcal{J}^{(2)}$  of the new band is consistent with the enhanced deformation calculated in ref. [2] for the K=0 octupole-vibrational state in <sup>192</sup>Hg at zero rotational frequency. The near constancy of  $\mathcal{J}^{(2)}$  may be due to blocking of the rotational alignment of neutrons, since the neutron j<sub>15/2</sub> state nearest the Fermi level is occupied in many of the two-quasiparticle states which are available to form the microscopic structure of an octupole-vibrational state in this nucleus.

The octupole-vibrational picture, then, appears to be a consistent one for the description of the many unusual properties of this superdeformed band, but it should be stressed that this is only one possible scenario. It is also hoped that a more definitive measurement of the gamma-ray energies of the inter-band transitions will be achieved in experiments in the near future.

#### ACKNOWLEDGMENTS

The authors wish to thank J. Kuehner and G. Hackman for making available their software for sorting data into three-dimensional histograms, and P.-H. Heenen, W. Nazarewicz and M. Riley for valuable discussions. This work was supported by the Department of Energy, Nuclear Physics Division, under contract no. W-31-109-ENG-38.

#### REFERENCES

- [1] S. Mizutori, et al., Nucl. Phys. **A557**, 125c (1993).
- [2] J. Skalski, et al., Nucl. Phys. **A551**, 109 (1993); P. Bonche, et al., to be published.
- [3] J.A. Kuehner, J.C. Waddington and D. Prévost, Proc. of the International Conference on Nuclear Structure at High Angular Momentum, Ottawa, May 1992, AECL-10613, p. 413.
- [4] B. Crowell et al., submitted to NIM.
- [5] B. Crowell et al., to appear in Phys. Lett. B.



- [6] M.W. Drigert et al., Nucl. Phys. **A530**, 452 (1991); I.G. Bearden et al., in Proc. Int. Conf. on Nuclear Structure at High Angular Momentum, Ottawa, May 1992, AECL-10613, p. 10.
- [7] K.E.G. Löbner, Phys. Lett **26B**, 369 (1968).
- [8] P.B. Semmes, I. Ragnarsson and S. Åberg, Phys. Rev. Lett. **68**, 460 (1992).
- [9] R.V.F. Janssens and T.L. Khoo, Ann. Rev. Nucl. Part. Sci. **41**, 321 (1991).

# Multi-Phonon States in $^{232}\text{Th}$

W. Korten, P. Bröcking, H. Hübel, W. Pohler, U.J. van Severen, P. Willsau (Institut für Strahlen und Kernphysik, Univ. Bonn), Th. Kröll, Th.W. Elze, M. Kaspar, I. Peter, K. Vetter (Institut für Kernphysik, Univ. Frankfurt), T. Haertlein, Ch. Ender, P. Reiter, D. Schwalm (MPI für Kernphysik, Heidelberg), J. Gerl, Th. Happ, H. Schaffner, R. Schubert, H.J. Wollersheim (GSI Darmstadt), D. Bazzacco, D. Napoli, C. Rossi Alvarez (INFN Padova and Legnaro)

## Introduction

The nucleus  $^{232}\text{Th}$  is particularly well suited for an investigation of multi-phonon excitations since it shows well developed rotational bands built on low-lying one-phonon vibrational excitations and two-phonon states are predicted below the pairing-gap energy ( $E_{pg} \approx 1.6\text{MeV}$ ). In a recent publication [1] a rotational band built on a  $4^+$  state at 1414 keV was reported in  $^{232}\text{Th}$ . This state shows all the characteristics of a nearly-harmonic two-phonon  $\gamma$ -vibrational state: (i) the excitation energy of the band-head is about twice the excitation energy of the  $2^+$   $\gamma$ -vibrational state; (ii) the band decays exclusively into the  $\gamma$ -band and (iii) the reduced transition probabilities  $B(E2)$  – deduced from the Coulomb-excitation strength – and decay branching ratios are in agreement with the values expected for a harmonic surface-vibration. Since the excitation energy is close to the pairing-gap it is expected that contributions of individual quasi-particle excitations are small.

In reference [1] the collectivity of the 1414 keV state in  $^{232}\text{Th}$  was determined from Coulomb-excitation calculations which reproduce the intensities of the observed  $\gamma$ -decays. This method is sensitive to all matrix elements which contribute significantly to the population of the state of interest. In particular, the  $B(E2)$  value will be affected by an additional  $E4$ -strength which cannot be ruled out by measuring the  $\gamma$ -ray intensity only. Furthermore, the existence of unidentified higher-lying levels, e.g. multi-phonon states, will affect the observed strength of the two-phonon state. In this contribution we report on a direct lifetime measurement using the recoil-distance method (RDM) and a new search for two- and multi-phonon states in  $^{232}\text{Th}$  with the Ga.Sp. spectrometer. The latter experiment became possible because of the high efficiency of the new  $4\pi$  Anti-Compton Ge spectrometers which is now large enough to measure coincidences between the few  $\gamma$ -rays depopulating the multi-phonon excitations.

## The Recoil-Distance Experiment

Coulomb-excitation of  $^{232}\text{Th}$  was performed with a 410 MeV  $^{90}\text{Zr}$  beam provided by the heavy-ion accelerator facility at the MPI für Kernphysik, Heidelberg. A natural thorium target of  $2\text{ mg/cm}^2$  thickness and a gold retardation foil of  $4\text{ mg/cm}^2$  thickness were stretched and mounted in the Bonn plunger device [2]. We modified the standard RDM by replacing the stopper foil with a thin 'retardation' foil in which the recoiling nuclei are slowed down. This produces two components in the  $\gamma$ -ray spectrum, corresponding to the different velocities. By a proper choice of the thickness of the retardation foil the partially-shifted component can be placed at an uncontaminated position in the spectrum.

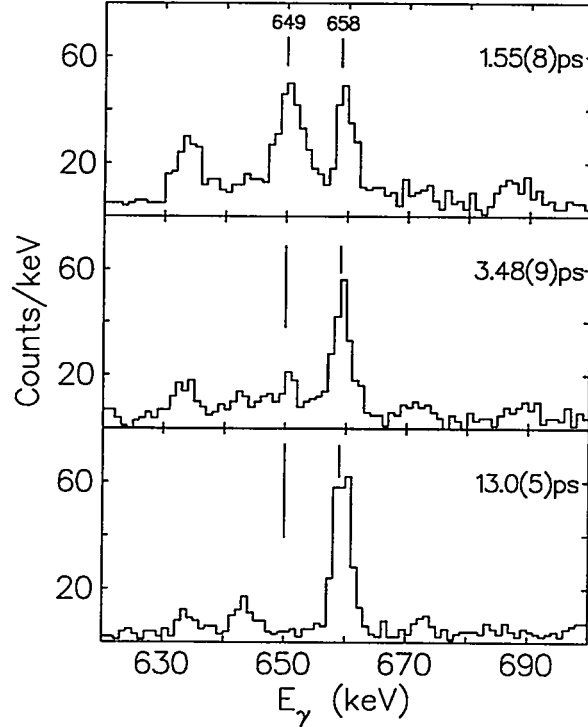


Figure 1: Gamma-ray spectra of the  $4_{\gamma\gamma}^+ \rightarrow 2_{\gamma}^+$  transition for the three foil distances of 21, 47 and 180  $\mu\text{m}$  (from the top) corresponding to the time-of-flight values given in the figure.

Since the excitation probability of the two-phonon state is only a few percent, its decay  $\gamma$ -rays were selected from a severe background of stronger transitions by the Heidelberg-Darmstadt Crystal Ball (CB) spectrometer [3] with 153 NaI(Tl) detectors. To identify the Doppler-shifted components in the  $\gamma$ -ray spectrum a Ge detector was mounted at  $0^\circ$ . The back-scattered projectiles were detected in a segmented annular Si detector covering an angular range from  $122^\circ$  to  $150^\circ$  with respect to the beam direction to enhance collisions with small impact parameters.

Measurements were performed at three different distances between target and retardation foil of approximately 20, 50 and 180  $\mu\text{m}$ . To determine the time-of-flight between the two foils from the experimental data we used the known lifetimes [4] and  $B(E2)$  values [5] within the ground-state band of  $^{232}\text{Th}$ . From a comparison of the measured intensity splitting in the ground-state band transitions with a simulated decay-path time-of-flight values of  $T_f = 1.55(8)$ ,  $3.48(9)$  and  $13.0(5)$  ps could be deduced. In the data acquisition particle- $\gamma$ -ray coincidences between the Si and the Ge detector were recorded together with the data from the CB. At a beam intensity of 0.2 pA 3.3, 2.4 and  $2.0 \cdot 10^6$  events could be recorded at the three distances.

The previous Coulomb-excitation measurement [1] has shown that the 1414 keV state decays exclusively into the  $\gamma$ -band. To enhance this decay in the Ge spectrum the  $\gamma$ -ray of the subsequent decay of the  $2_{\gamma}^+$  state was demanded in the CB together with the additional requirement that no other  $\gamma$ -rays were recorded in any CB detector. With this gating rather clean Ge spectra dominated by the decay of the  $4_{\gamma\gamma}^+$  state could be extracted as is shown in fig. 1. In the spectrum taken at the largest distance

(lower part of fig. 1) only the fully-shifted ('fast') component of the decay is seen at 658 keV. Thus contaminations can be excluded in the region around 649 keV where the partially-shifted ('slow') component is expected. This distance was also used to select the optimal gating conditions described above. For the smaller distances the partially-shifted component of the decay clearly develops. The intensities deduced from these spectra are compiled in table 1.

To determine the lifetime from these  $\gamma$ -ray intensities the integrated decay intensities were calculated for a given time-of-flight as a function of the lifetime assuming a prompt feeding of the two-phonon state. This assumption is justified since higher-lying states which subsequently feed into the two-phonon state are weakly excited [1] and further suppressed by the gating conditions. The only deviation from an exponential decay which has to be taken into account is the time dependence of the angular correlation. For the decay of the two-phonon state the unperturbed angular correlation has been measured in a thick-target experiment. The time-dependence of the angular correlation caused by the vacuum deorientation effect was described within the parametrisation of Abragam and Pound [6] which has been used successfully to describe the deorientation of the ground-state band in  $^{232}\text{Th}$  [7]. With these assumptions lifetime values as given in table 1 were extracted.

$T_f$ [ps]	$Y_{fast}$	$Y_{slow}$	$\frac{Y_{fast}}{Y_{slow}}$	$\tau$ [ps]
1.55(8)	155 (21)	227 (24)	0.68(12)	3.24(54)
3.48(9)	170 (17)	73 (20)	2.33(70)	3.13(65)
13.0(5)	224 (16)	0 (10)	—	—

Table 1: Intensities of the fast and slow component in the decay of the two-phonon state, as measured at the three distances, and the deduced lifetime values.

From their weighted average we obtain for the lifetime of the  $4_{\gamma\gamma}^+$  state in  $^{232}\text{Th}$

$$\tau(4_{\gamma\gamma}^+) = 3.2 \pm 0.4 \pm 0.5 \text{ ps}$$

The first error is the statistical uncertainty while the second one includes the uncertainty in the parameters of the angular correlation [7] as well as the estimated influence of small time-dependent variations in the distance between the two foils. From the measured lifetime we deduce the reduced transition probability using the known branching ratios [1] of the decay of the 1414 keV state

$$B(E2; 4_{\gamma\gamma}^+ \rightarrow 2_{\gamma}^+) = 0.15 \pm 0.04 e^2 b^2$$

This value is typical for vibrational excitations in actinide nuclei and supports the interpretation as a two-phonon excitation. Within the experimental uncertainty it is also consistent with the result deduced from the Coulomb-excitation yields [1]. Hence, any additional E4-strength which would result in a smaller  $B(E2)$  value from

the Coulomb-excitation measurement, is inconsistent with the lifetime measurement, because the E4 matrix element does not contribute to the decay probability. Therefore a large E4 contribution to the excitation of this K=4 state can be ruled out and its interpretation as a hexadecupole vibration becomes unlikely.

For the one-phonon  $2_{\gamma}^{+}$  state a B(E2) value has been deduced from Coulomb-excitation with  $\alpha$ -particles [8]

$$B(E2; 2_{\gamma}^{+} \rightarrow 0^{+}) = 0.0294 \pm 0.0014 e^2 b^2$$

which leads to the following ratio of B(E2) values

$$R(E2) = \frac{B(E2; 4_{\gamma\gamma}^{+} \rightarrow 2_{\gamma}^{+})}{B(E2; 2_{\gamma}^{+} \rightarrow 0^{+})} = 5.1 \pm 1.4$$

While for harmonic surface vibrations in a deformed nucleus a ratio of  $R(E2) = 25/9 \approx 2.8$  is expected, e.g. from the rotation vibration model (RVM) [9], the measured collectivity is somewhat larger.

Although this simple model neither takes into account any unharmonicities of the vibrations, it should be pointed out, however, that unharmonicities usually decrease the collectivity. It would be very interesting to see whether more refined approaches can reproduce not only the measured excitation energy and decay pattern, but also the slight enhancement in collectivity of the two-phonon state.

## The Ga.Sp. experiment

The second experiment was performed at the LNL Legnaro using the  $4\pi$  array Ga.Sp. with 40 HPGe detectors and 80 BGO crystals and the PYRAMID array [10] of parallel-plate counters covering the backward hemisphere ( $80^{\circ} \leq \theta_{lab} \leq 160^{\circ}$ ) for the detection of scattered projectiles. Here, a  $1.7 \text{ mg/cm}^2$   $^{232}\text{Th}$  target was bombarded with a 265 MeV  $^{58}\text{Ni}$  beam with an intensity of up to 9 pA. In the data acquisition particle- $\gamma\gamma$  coincidences between the PYRAMID array and the Ge detectors were recorded. After a careful Doppler-shift correction with respect to the direction of the recoiling nucleus and subtracting random coincidences a  $\gamma\gamma$  coincidence matrix with  $9 \cdot 10^6$  events could be sorted.

While the analysis of this run is still in progress we present the first results concerning multi-phonon states [11]:

The known two-phonon  $K^{\pi}=4^{+}\gamma\gamma$ -band can be extended, possibly to a  $10_{\gamma\gamma}^{+}$  state at 2039 keV. Higher lying states which decay into the  $\gamma\gamma$ -band are only very weakly excited. A new state at 1054 keV is observed which decays exclusively into the one-phonon  $\beta$ -band. Its excitation energy is larger by a factor of  $\approx 1.4$  compared to the one-phonon state, while for a harmonic two-phonon vibration approximately twice the excitation energy is expected.

Most promising are coincidences with decays of the  $K^{\pi}=0^{-}$  octupole band as is shown in fig. 2. In addition to known decays out of the  $K^{\pi}=1^{-}$  octupole band some new states were found which fit perfectly into Coriolis-mixing calculations for these bands. The search for the missing  $K=3^{-}$  member of the octupole quadruplet is still in progress. The group of lines marked in fig. 2 lead to three new states at 1353 keV, 1387 keV and 1467 keV which are excellent candidates for the  $0^{+}$ ,  $2^{+}$  and  $4^{+}$ -members of a  $K^{\pi}=0^{+}$  two-phonon octupole band. These spin assignments still have

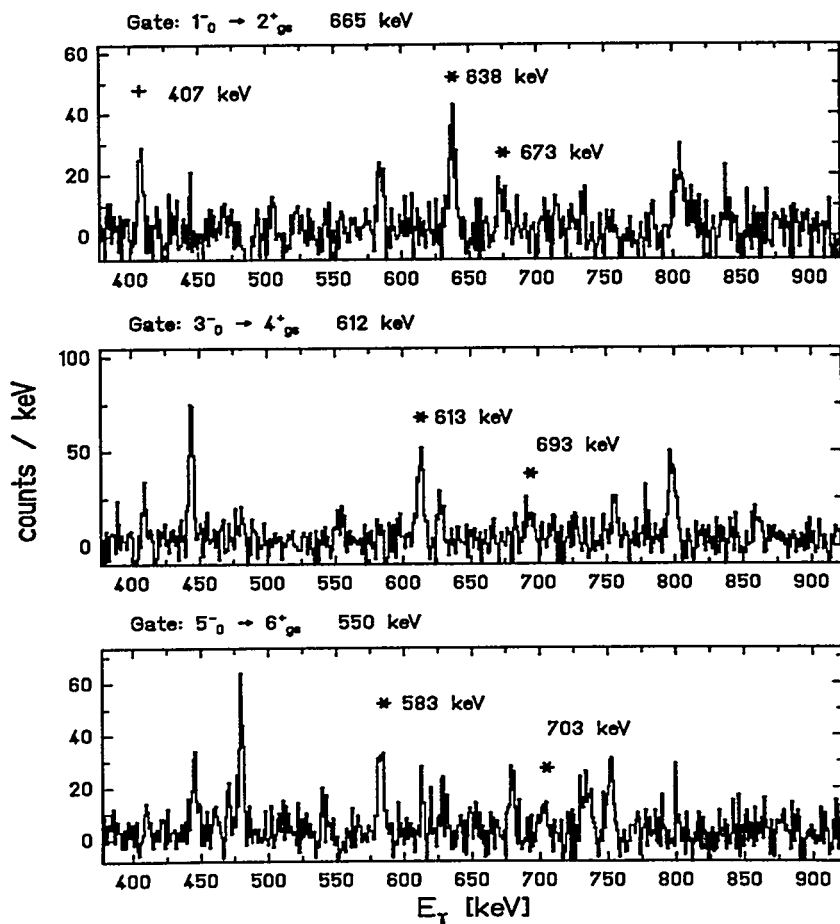


Figure 2: Gamma-ray spectra gated on transitions depopulating the  $K^\pi=0^-$  octupole band. Lines indicated with an (\*) are decays from a new band, possibly the  $K^\pi=0^+$  two-phonon octupole band.

to be proven by the angular correlations, but are very likely from the decay pattern. The band would have nearly the same moment of inertia as the  $K^\pi=0^-$  one-phonon octupole band. The excitation energy of the band head is nearly twice the energy of the  $K=0^-$  one-phonon band ( $E_0=702.1$  keV).

## References

- [1] W. Korten, T. Haertlein, J. Gerl, D. Habs, D. Schwalm, Phys. Lett. B317, 19 (1993)
- [2] P. Bröcking, Diploma Thesis, Univ. Bonn, (1994)
- [3] V. Metag, D. Habs, D. Schwalm, Comm. Nucl. Part. Phys. Vol. 16, 213 (1986)
- [4] M.W. Guidry et al., Nucl. Phys. A266, 228 (1976)
- [5] H. Ower et al., Nucl. Phys. A388, 421 (1982)
- [6] A. Abragam and R.V. Pound, Phys. Rev. 92, 943 (1953)
- [7] W. Korten et al., to be published
- [8] F.K. McGowan and W.T. Milner submitted to Nucl. Phys. A
- [9] V. Oberacker, W.T. Pinkston, H.G.W. Kruse, Rep. Prog. Phys. 48, 327 (1985)
- [10] K. Vetter et al., Nucl. Instr. Meth. A344, 607 (1994)
- [11] Th. Kröll et al., Universität Frankfurt, Annual Report 1993

# Physics with Radioactive Beams

W. Nazarewicz\*, J. Dobaczewski†, and T.R. Werner‡

Joint Institute for Heavy Ion Research and Physics Division

Oak Ridge National Laboratory

P.O. Box 2008, Oak Ridge, Tennessee 37831, USA

Department of Physics and Astronomy, University of Tennessee  
Knoxville, Tennessee 37996, USA

Institute of Theoretical Physics, Warsaw University  
ul. Hoża 69, PL-00-681 Warsaw, Poland

PACS numbers: 21.10.-k, 21.60-n

The nature of drip-line nuclei, i.e., weakly bound nuclei with extreme isospin values, is one of the most exciting challenges today, both experimentally and theoretically. The coupling between bound states and the particle continuum invites strong interplay between various aspects of nuclear structure and reaction theory. Perspectives for new physics far from stability are discussed.

## 1. Introduction

There are many examples of *nuclear exotica* that attract our attention, e.g., nuclear states at extreme angular momenta, extreme deformations, and extreme excitation energies. In this presentation, we shall concentrate on yet another limit of nuclear structure at extreme conditions. Namely, we shall discuss some aspects of physics of drip-line nuclei. Thanks to exotic (radioactive) ion beam (RIB) facilities, we are on the verge of invading this new territory in an unprecedented way.

From the theoretical point of view, spectroscopy of exotic nuclei offers a unique test of those components of effective interactions that depend on isospin degrees of freedom; because of dramatic extrapolations involved, it invites a variety of theoretical approaches. Since the parameters of interactions used in the usual shell-model or mean-field calculations are determined so as to reproduce the properties of known nuclei, the parameters may not always be proper in the calculation of drip-line nuclei. One hopes, however, that spectroscopy of exotic nuclei, by means of radioactive ion beam techniques, will lead to a better determination of forces, at least those interaction components that depend on isospin degrees of freedom.

---

\*email address: witek@utkvx.utk.edu

†email address: dobaczew@fuw.edu.pl

‡email address: tomek@orph28.phy.ornl.gov

## 2. Unique features of drip-line nuclei

Experiments with radioactive beams will make it possible to look closely into many exciting aspects of the nuclear many-body problem. Although an experimental excursion into new territories of the chart of the nuclides will offer many excellent opportunities for traditional nuclear structure (new regions of quadrupole and octupole deformation, new regions of shape isomers, including superdeformations, i.e., “old” physics in the “new” regime), there are also many unique features of exotic nuclei (weak binding, large diffuseness, large spatial dimensions) that define “new” physics in the “new” regime.

Some of the topics related to RIB physics are schematically presented in Fig. 1. On the neutron-rich side, there appears a region of neutron halos, loosely bound few-body systems (see Ref. [1] for a review). A classic example is  $^{11}\text{Li}$ , which was investigated at Berkeley by Tanihata *et al.* in 1985 [2], and explained theoretically by Hansen and Jonson [3] in terms of a spatially extended three-body Borromean system consisting of

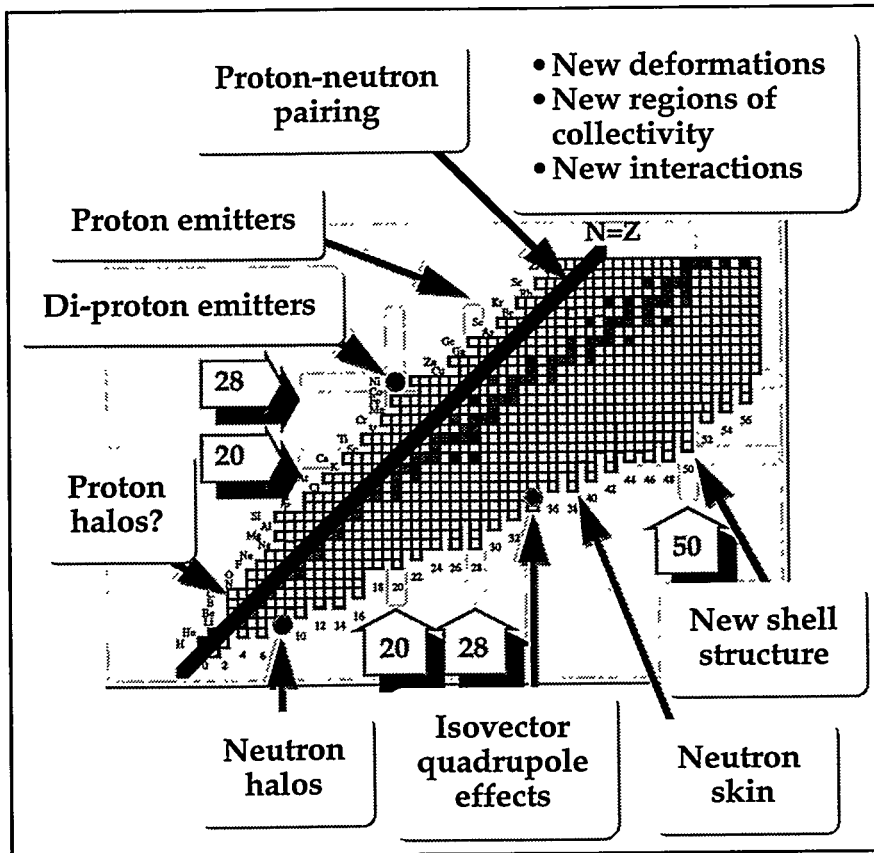


Figure 1. Schematic representation of new phenomena to be explored with the help of exotic beams.

the  $^9\text{Li}$  core and two valence neutrons. In the heavier neutron-rich nuclei, where the mean field is better applicable, the separation into a “core” plus “valence-space” nucleons is not too meaningful. However, also in those nuclei the weak neutron binding implies



large spatial dimensions and the existence of the neutron skin (i.e., a dramatic excess of neutrons at large distances). The relation between the weak binding and the neutron skin is illustrated in Fig. 2, which shows the neutron and proton densities for  $^{132,150,172}\text{Sn}$  calculated [4] within the Hartree-Fock-Bogolyubov (HFB) approach with the SkP effective interaction.

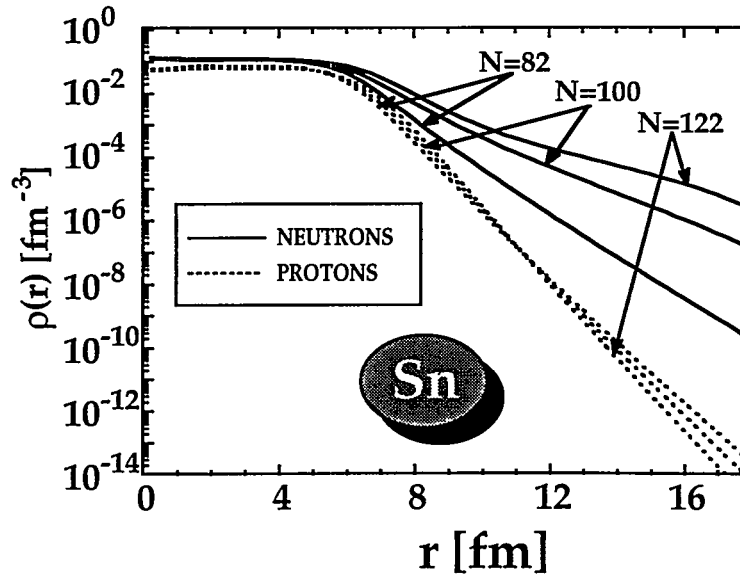


Figure 2. Neutron and proton densities for neutron-rich Sn isotopes calculated with the HFB-SkP approach. From Ref. [4].

As a consequence of the very diffuse neutron density, the self-consistent mean field of neutron drip-line nuclei is expected to be markedly different compared to nuclei close to the beta-stability line. The presence of the neutron skin implies a strong isovector dependence of the average potential and the appearance of a completely new shell structure (see discussion in Sec. 4).

On the proton-rich side, physics is different but equally interesting. Because of the Coulomb barrier which tends to localize the proton density in the nuclear interior, the existence of proton halos is rather unlikely (maybe except for the very light nuclei). On the other hand, just because of the Coulomb barrier, nuclei beyond the proton drip line are quasibound with respect to proton decay. The associated lifetimes, ranging from  $10^{-6}$ s to a few seconds, are sufficiently long to obtain a wealth of spectroscopic information. Unlike the alpha decay process, which is difficult to interpret because of the formation process, proton radioactivity is an excellent example of quantum-mechanical tunneling. Lifetimes of spherical proton emitters directly provide an indication of the angular momentum of the quasibound proton [5]. Experimental and theoretical investigations of proton emitters (or di-proton emitters such as doubly-magic  $^{48}\text{Ni}$ ) will open up the wealth of new physics associated with the residual-interaction-coupling between bound states and extremely narrow resonances in the region of very low density of single-particle levels [6]. In this

context, studies of deformed proton emitters (Nilsson scheme built on bound states and resonances!) are of particular interest.

The closeness of the Fermi level to the particle continuum makes the theoretical description of drip-line nuclei a very challenging task. To put things in some perspective, Fig. 3 displays the average potential wells, characteristic of a typical beta-stable system ( $^{120}\text{Sn}$ ), a neutron drip-line system ( $^{150}\text{Sn}$ ), and a proton drip-line system ( $^{100}\text{Sn}$ ). While the low-energy structure of  $^{120}\text{Sn}$  is almost exclusively determined by the particle-hole

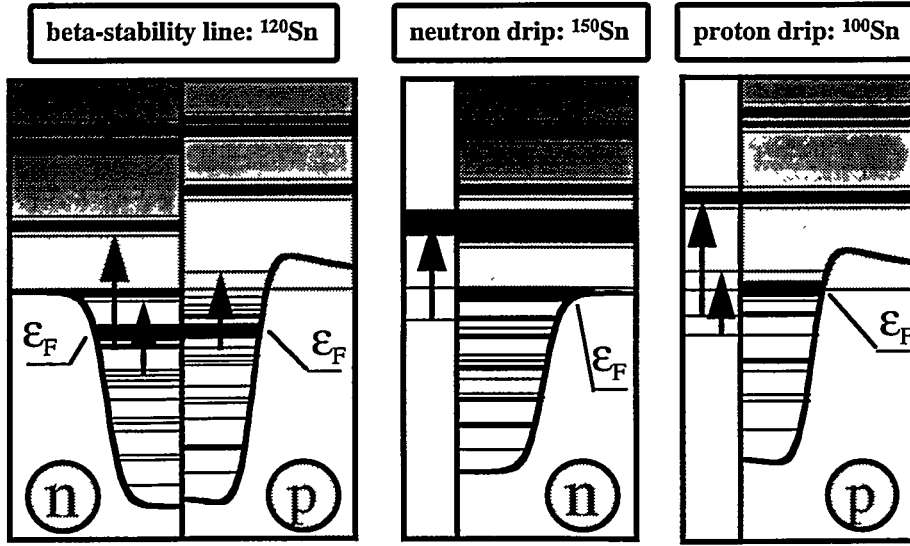


Figure 3. Schematic illustration [7] of coupling between bound states and particle continuum in drip-line nuclei. The potential wells are represented by the average Woods-Saxon field (plus Coulomb potential for protons).

or pair excitations across the Fermi level from bound states to bound states, the lowest particle-hole or pair modes in drip-line nuclei are embedded in the particle continuum.

Pairing correlations play a very special role in drip-line nuclei. This is seen from approximate HFB relations between the Fermi level,  $\lambda$ , pairing gap,  $\Delta$ , and the particle separation energies. For instance, the neutron separation energies  $S_n$  and  $S_{2n}$  are given by [8, 9]

$$S_n \approx -\lambda_n - \Delta, \quad (1)$$

$$S_{2n} \approx -2\lambda_n, \quad (2)$$

which leads to the following conditions for the one-neutron and two-neutron drip-lines:

$$S_n = 0 \implies \lambda_n + \Delta = 0, \quad (3)$$

$$S_{2n} = 0 \implies \lambda_n = 0. \quad (4)$$

In particular, condition (3) nicely illustrates the crucial role of the pairing interaction for determining the one-neutron drip line; it shows the equal importance of the single-particle

field characterized by  $\lambda$  (determined by the particle-hole component of the effective interaction) and the pairing field,  $\Delta$  (determined by the particle-particle part of the effective interaction).

Needless to say, the physics of exotic nuclei has strong astrophysical implications, especially in the context of the r-process [10, 11] and rp-process [12] mechanisms. Nuclear masses, decay rates, and cross sections are the basic quantities determining the results of nuclear reaction network calculations.

### 3. Old models in new regime

Because of the closeness of the particle continuum, the traditional models of nuclear structure used to calculate masses, deformations, and pairing properties (such as shell correction method, BCS approximation) become very inaccurate or simply wrong when approaching the drip line. Consequently, any tool of nuclear structure theory that aims at describing many-body correlations starting from the mean-field-based single-particle basis (such as shell-model, BCS, RPA, etc.) has to be modified in the new regime.

As discussed above, due to the scattering of nucleons from bound shell-model orbitals to unbound states, the standard shell-model treatment (based on the splitting of a Hamiltonian into a one-body single-particle term and a two-body “residual interaction” term) seems inappropriate when applied to drip-line nuclei. For weakly bound nuclei, continuum states have to be taken into account explicitly. The resulting continuum shell model (CSM) [6, 13, 14] properly takes into account decay channels; in the CSM there are no effective one-body potentials, the interaction has a two-body character and the single-particle energies are calculated self-consistently.

In the mean-field calculations, the most important residual interaction is the pairing force. This interaction plays a unique role in loosely bound nuclei due to the scattering of nucleonic pairs from bound states to the positive-energy particle continuum. In the BCS or BCS-like methods based on quasibound states, this leads to the presence of a “particle gas” surrounding the nucleus [15]. Indeed, the BCS wave function can be explicitly decomposed into contributions from bound states and quasibound states:

$$\Psi_{BCS} = \prod_{i, \epsilon_i < 0} (U_i + V_i a_i^\dagger a_i^\dagger) \prod_{j, \epsilon_j > 0} (U_j + V_j a_j^\dagger a_j^\dagger) |0\rangle. \quad (5)$$

While the bound-state-part in (5) represents the localized wave function, i.e., it decays asymptotically, the second part represents the contribution from quasibound states and leads to non-localized densities with incorrect asymptotic behavior. Indeed, although the nuclear densities eventually vanish at large distances by construction (finite size of the basis, finite size of the box in which calculations are performed), the wave functions of positive-energy states are not properly localized inside the nuclear volume. This problem is overcome in the HFB method with a realistic pairing interaction in which the coupling of bound states to the particle continuum is correctly taken into account [15].

Figure 4 displays theoretical two-proton separation energies,  $S_{2p}$ , for the even-even  $N=18, 20$ , and  $22$  isotones obtained in the HFB and HF+BCS calculations with the SkP effective interaction of Ref. [15]. In the HF+BCS variant, the self-consistent pairing gaps obtained from the HFB calculations were used within the fixed-gap approximation. The position of the proton drip line is consistent with the experimental measurements by Borrel

*et al.* [16] and the analysis by Brown [17] based on the isobaric mass multiplet equation. In particular, the nucleus  $^{46}\text{Fe}$  has been found to be bound to two-proton decay while  $^{42}\text{Cr}$  and  $^{48}\text{Ni}$  – not. The values of  $S_{2p}$  obtained in the HFB and HF+BCS calculations are very

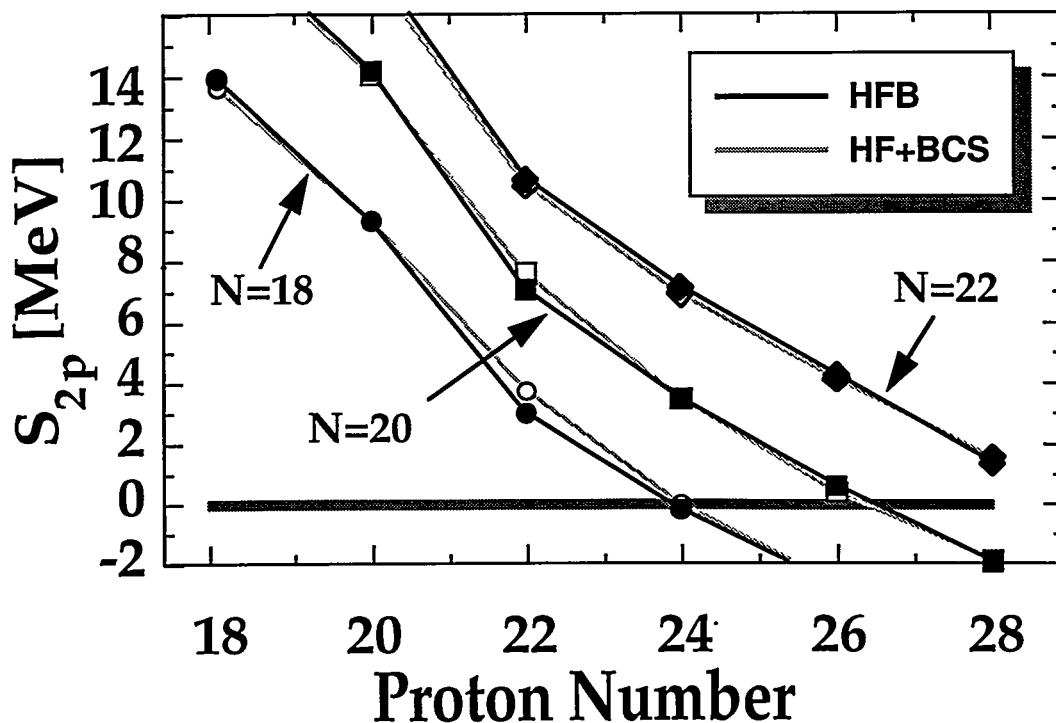


Figure 4. Two-proton separation energies for the even-even  $N=18$ ,  $20$ , and  $22$  isotones predicted in the HFB and HF+BCS calculations with the SkP interaction.

similar. However, the agreement does not extend to other quantities such as radii [15]. The effect of the unphysical proton gas is clearly seen in the behavior of the charge radii,  $r_c$ . As seen in Fig. 5, in the HFB calculations the charge radii behave very smoothly as a function of  $Z$ . On the other hand, in the HF+BCS model there is a dramatic increase in  $r_c$  for the proton-rich nuclei resulting from the unphysical occupation of positive-energy quasibound states (see also the discussion in Ref. [18]). It is worth noting, that the oscillatory behavior of  $r_c$  (resulting in kinks at the proton subshell closures at  $Z=14$ ,  $20$ , and  $28$ ) in the HF+BCS variant reflects the variation of the proton pairing gap with particle number.

The microscopic-macroscopic method (shell correction approach) is a very useful tool for calculating nuclear masses, deformations, and barriers. In the recent Ref. [7], a shell-correction method was applied to nuclei far from the beta stability line and its suitability to describe effects of the particle continuum was discussed. Although there had been some suggestions in the past on how to generalize the Strutinsky averaging procedure for finite potentials [19], no entirely satisfactory answer seems to exist.

The shell correction can be calculated by taking the difference between the sum of

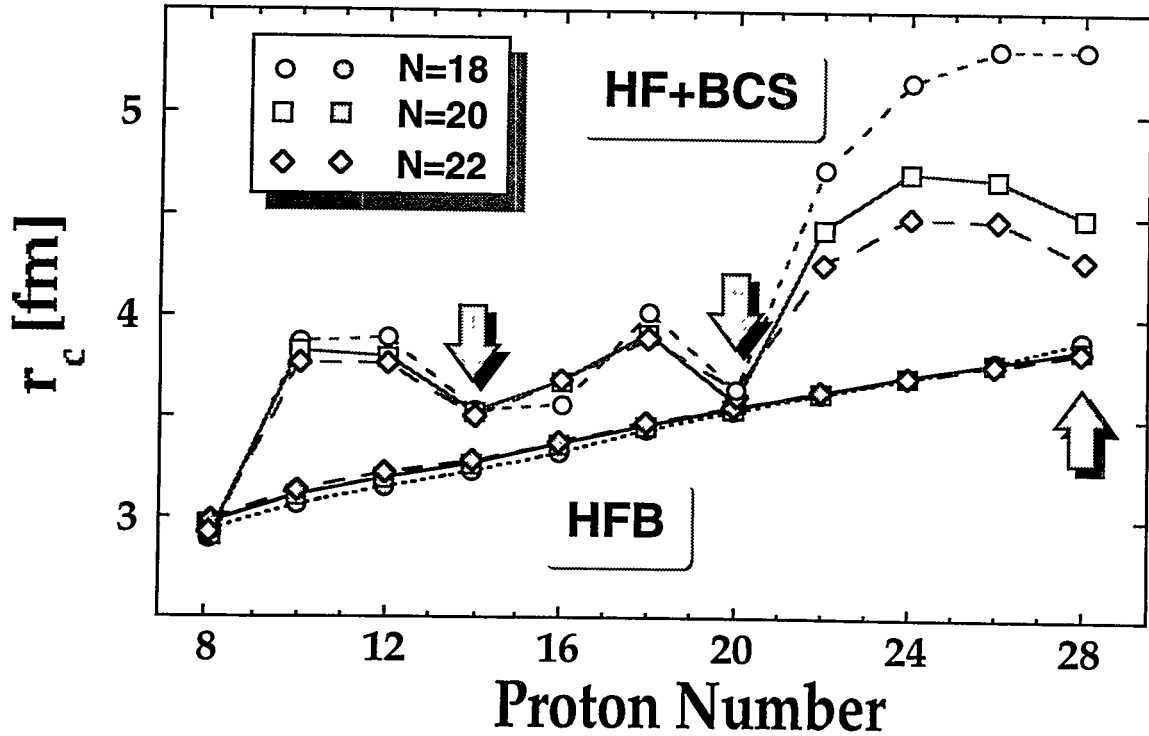


Figure 5. Same as in Fig. 4 but for the charge radii. In the HFB calculations, the values of  $r_c$  vary very smoothly with  $Z$  and they do not seem to be influenced by the weak binding, i.e., there is no indication for the proton halo. The arrows indicate the proton subshell closures at  $Z=14$ ,  $20$ , and  $28$ .

occupied levels and the average value, i.e.

$$E_{\text{shell}} = E_{\text{s.p.}} - \tilde{E}_{\text{s.p.}} = \sum_{i-\text{occ}} \epsilon_i - \int_{-\infty}^{\tilde{\lambda}} \epsilon \tilde{g}(\epsilon) d\epsilon, \quad (6)$$

where  $\tilde{\lambda}$  is the smoothed Fermi level and  $\tilde{g}$  is the mean single-particle level density. For finite-depth potentials, the integral in Eq. (6) should be replaced by a sum over bound single-particle states and an integral over positive-energy single-particle continuum. In many cases, however, the effect of the continuum is simulated by using the positive-energy quasibound states [20]. In the following, the Strutinsky averaging procedure including quasibound states will be referred to as the standard averaging method (SAM).

A proper treatment of resonances is not an easy task, especially for deformed systems. A viable approach is the semiclassical averaging based on the partition function method (Wigner-Kirkwood expansion, WK), proved [21] to be equivalent with the Strutinsky approach. In the semiclassical approximation, the Fermi energy,  $\lambda_{\text{sc}}$ , is determined by

$$N = \mathcal{L}_{\lambda_{\text{sc}}}^{-1} \left( \frac{Z(\beta)}{\beta} \right), \quad (7)$$

and the smoothed energy of the system is

$$\tilde{E}_{sc} = N\lambda_{sc} - \mathcal{L}_{\lambda_{sc}}^{-1} \left( \frac{Z(\beta)}{\beta^2} \right), \quad (8)$$

where  $\mathcal{L}$  denotes the Laplace transform and  $Z$  is the semiclassical partition function

$$Z(\beta) = \frac{2}{h^3} \int e^{-\beta H_c} (1 + \hbar w_1 + \hbar^2 w_2 + \dots) d^3 p d^3 r, \quad (9)$$

where  $H_c$  is the classical one-body Hamiltonian of the system and the  $w$ 's are defined in terms of the one-body potential. The partition function method was shown to be an excellent tool for computing the average single-particle energy [22–24].

The predicted two-neutron separation energies for the neutron-rich tin and lead isotopes are shown in Figs. 6 and 7, respectively. The two-neutron separation energies (top)

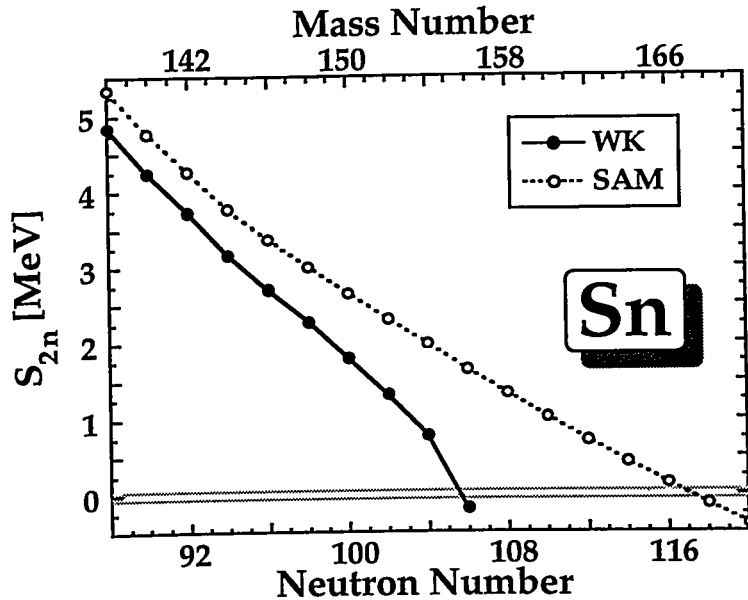


Figure 6. Two-neutron separation energies for the even neutron-rich tin isotopes predicted in the shell-correction method with the WS average potential and the Yukawa-plus-exponential macroscopic model. The results based on the semiclassical Wigner-Kirkwood method (solid line, WK) are compared with those obtained using the standard averaging (dotted line, SAM) including quasibound states. From Ref. [7].

were computed directly from calculated binding energies of even-even nuclei. As seen in Figs. 6 and 7, the influence of the continuum on the calculated positions of driplines is quite significant. The two-neutron separation energies calculated in the WK method are systematically lower than those obtained in the SAM and the difference approaches  $\sim 1.6$  MeV at  $N=106$ . This difference results in a shift in the position of the two-neutron dripline. According to the semiclassical approach, the nucleus  $^{156}\text{Sn}_{106}$  appears at the

two-neutron drip line, while in the SAM calculations there are several ( $\sim 5$ ) more stable even-even tin isotopes expected.

For the lead isotopes the Fermi level in the WK method becomes positive at  $N \sim 175$ , and consequently no solution to the particle number equation (7) can be found. At the

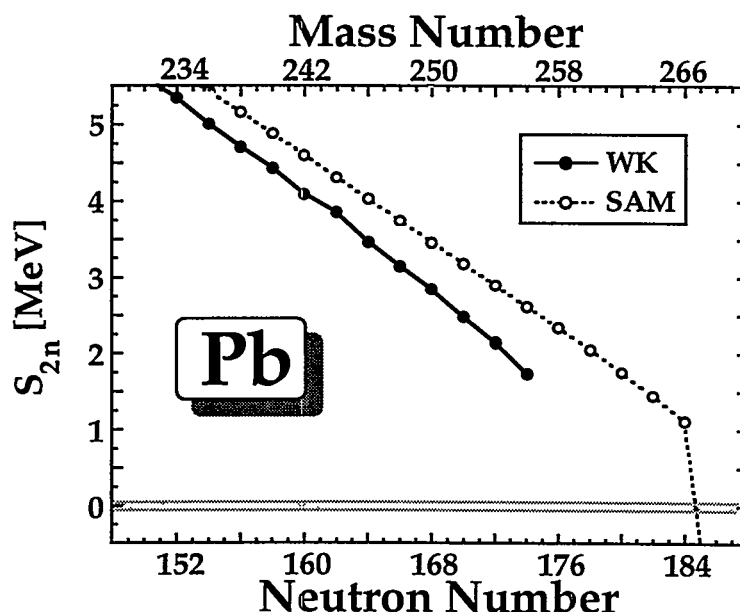


Figure 7. Same as in Fig. 6 except for the neutron-rich lead isotopes.

same time, the value of  $S_{2n}$  for  $N \sim 174$  is still positive (Fig. 7) and equal to about 1.7 MeV. This constitutes a contradiction because, according to Eq. (2), the values of  $S_{2n}$  and  $\lambda_n$  should vanish simultaneously at the two-neutron drip line. In the self-consistent theory (e.g., HF+BCS or HFB), the Fermi energy is equal to the derivative of the total energy (ground state energy of the even-even system) with respect to the particle number. However, in the shell-correction method this relation is violated due to the particle-number inconsistency inherent to the macroscopic-microscopic model. Indeed, in the microscopic-macroscopic method, one can introduce five different Fermi energies, namely,

$$\lambda_{\text{tot}} = \lambda_{\text{macr}} - \tilde{\lambda} + \lambda_{\text{s.p.}} + \delta\lambda, \quad (10)$$

where  $\lambda_{\text{tot}}$  is related to the neutron separation energy,  $\lambda_{\text{macr}}$  represents the macroscopic Fermi energy,  $\tilde{\lambda}$  (or  $\lambda_{\text{sc}}$  in the WK method) is the smoothed neutron Fermi energy,  $\lambda_{\text{s.p.}}$  is the neutron Fermi energy of the single-particle model (e.g., obtained from the BCS equations), and  $\delta\lambda$  contains contributions from the smoothed pairing energy and the proton shell correction. In self-consistent approaches based on the two-body Hamiltonian, the requirement  $\lambda_{\text{tot}} = \lambda_{\text{s.p.}}$  is fulfilled automatically. In the shell-correction method this requirement can be referred to as the *Fermi-level self-consistency condition*:

$$\lambda_{\text{macr}}(Z, N) = \tilde{\lambda}(Z, N) \quad \text{or} \quad \lambda_{\text{macr}}(Z, N) = \lambda_{\text{sc}}(Z, N) \quad (11)$$

for the SAM or WK methods, respectively. The parameters of the microscopic model are usually adjusted to selected single-particle properties of nuclei close to the beta-stability line, and the parameters of the macroscopic model are found by a global fit to masses and fission barriers. Therefore, it is not surprising that when extrapolating far from stability, the particle-number dependences of  $\lambda_{\text{macr}}$  and  $\tilde{\lambda}$  are different and, consequently, the relation between the Fermi energy and the separation energy is lost.

#### 4. Shell structure of exotic nuclei

A significant progress has been achieved in theoretical description of shell structure near the particle drip lines. Recent analysis based on the HFB approach [25] indicates that there is a significant isospin dependence of spherical shell effects in medium-mass and heavy nuclei. Figure 8 shows the expectation values of the single-particle Hamiltonian in the canonical basis for the  $A=120$  isobars. For the isobaric chain of  $A=120$ , the neutron Fermi energy approaches zero near  $N=82$ . As seen in Fig. 8, the  $N=82$  shell gap dramatically decreases near the neutron-drip line. This effect is primarily caused by a lowering of single-particle (canonical) energies of low- $j$  orbitals relative to those of high- $j$  orbitals. Such an effect results from a strong interaction between bound orbitals and the low- $j$  continuum, whereas the interaction with high- $j$  resonance states is much

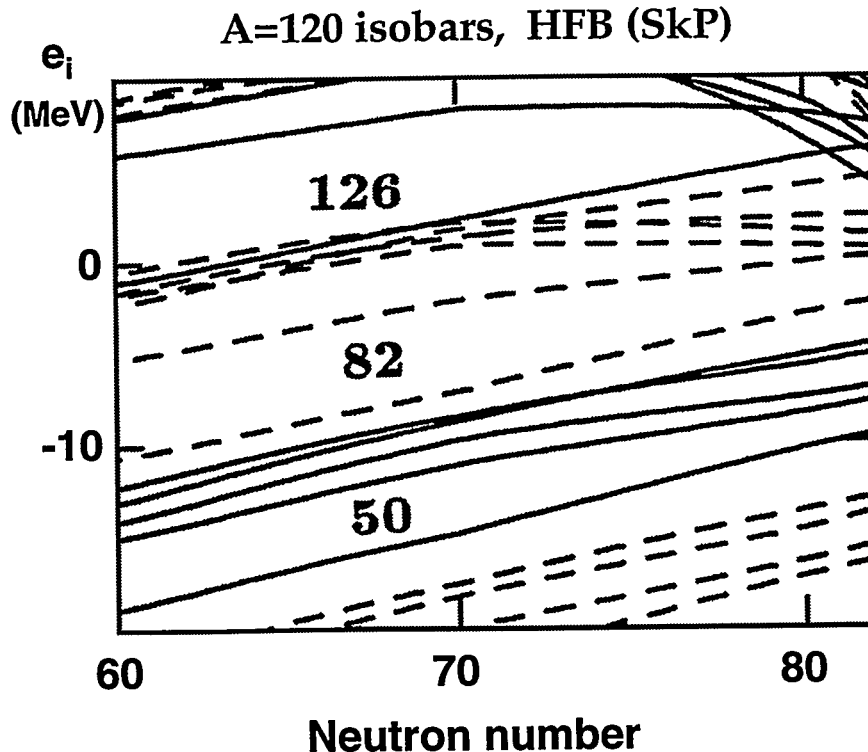


Figure 8. Spherical single-particle levels for the  $A=120$  isobars calculated in the SkP HFB model as a function of neutron number. Solid (dashed) lines represent the orbitals with positive (negative) parity. From Ref. [25].



less effective in modifying bound orbitals. For heavier systems with  $N > 82$  there are more high- $j$  orbitals in major shells and the lowering of low- $j$  subshells (which, in addition, are located at the top of shells) is not sufficient to close the gaps completely. According to calculations, the disappearance of shell effects at the neutron-drip line is only expected in the systems with  $N \leq 82$ . At the proton-drip line, the quenching occurs only for light systems with  $Z \leq 28$ , because the Coulomb barrier prevents the low- $j$  continuum from approaching bound states.

An interesting result of Ref. [25] was the observation that, due to the large diffuseness of the neutron density and central potential, the single-particle spectrum of neutron-drip-line nuclei resembles that of a harmonic oscillator with a spin-orbit term. In the following work [4], it has been suggested that the weakening of shell effects in drip-line nuclei results from a correct treatment of pairing and the continuum. In particular, the density dependence of pairing interactions seems to play a crucial role.

## 5. Exotic modes

The presence of the spatially-extended neutron skin implies the existence of low-energy isovector modes in neutron-rich nuclei. Two such modes are illustrated schematically in Fig. 9. The middle diagram shows the low-energy electric isovector dipole mode associated with vibrations of the neutron skin with respect to the rest of the system (“pygmy” resonance). The r.h.s. diagram shows the system with very different static quadrupole deformations for protons and neutrons. Such a nucleus, if it exists, is expected to have very interesting rotational behavior and unusual magnetic properties.

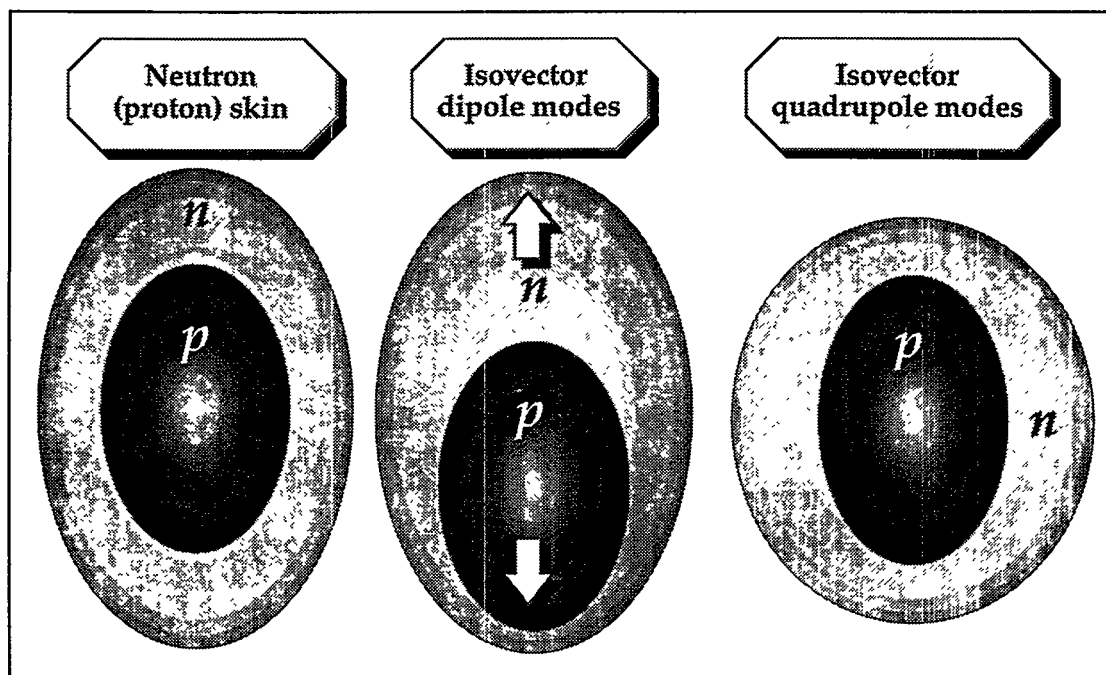


Figure 9. Schematic illustration of collective modes associated with the neutron skin.

Recently, systematic self-consistent calculations for neutron-rich nuclei around magic  $^{44}\text{S}_{28}$  were performed using Skyrme Hartree-Fock and relativistic mean field (RMF) methods [26]. The calculations suggest strong deformation effects in this region due to the  $f_{7/2} \rightarrow fp$  core breaking. In particular, the magic nucleus  $^{44}\text{S}_{28}$  is predicted to be deformed in both models. Strong quadrupole isovector effects were obtained in deformed sulfur nuclei far from stability. This is illustrated in Fig. 10 which shows the difference between predicted neutron and proton deformations,  $\Delta\beta_2 \equiv \beta_2^n - \beta_2^p$ . The deformations were defined by means of the standard relation between the quadrupole moment,  $Q_0$ , and the rms radius,  $\langle r_p^2 \rangle$ . For instance, the proton quadrupole deformation is given by

$$Q_0^p = \sqrt{\frac{5}{\pi}} Z \langle r_p^2 \rangle \beta_2^p. \quad (12)$$

Similarly, one can extract quadrupole deformations of neutron ( $\beta_2^n$ ) and mass ( $\beta_2^A$ ) distributions. It is seen that when approaching the neutron drip-line, the values of  $\beta_2^n$  are systematically smaller than those of the proton distribution. An opposite effect is seen around the proton drip-line. The largest difference,  $|\Delta\beta_2| \sim 0.10$ , is obtained in the RMF model for  $^{54}\text{S}$ . The behavior of  $\Delta\beta_2$  can be partly attributed to the isotonic behavior of rms radii. Indeed, the value of  $Q_0$  depends both on the angular anisotropy *and* the radial dependence of the nucleonic density. In the drip line nuclei, due to spatially extended wave functions, the “radial” contribution to  $Q_0$  might be as important as the “angular” part. The insert in Fig. 10 illustrates the dependence of the  $Q_0^n/Q_0^p$  ratio on the  $N/Z$  ratio. The lack of shell fluctuations in  $Q_0^n/Q_0^p$  in the RMF model at  $N > 26$  is consistent with the calculated large prolate deformations. Interestingly, above  $N=28$ ,  $\Delta\beta_2(\text{RMF})$  decreases steadily with neutron number, while the  $Q_0^n/Q_0^p(\text{RMF})$  ratio intersects the  $N/Z$  line (rigid geometric limit) only at  $N > 34$ .

New pairing modes are expected to show up in medium-mass  $N=Z$  nuclei. In fact, the role played by the  $T=0$  pairing depends strongly on the neutron excess. For  $N=Z$  systems the  $T=0$  pairing mode is more important than a  $T=1$  mode (see Ref. [27] for review). For nuclei with small neutron excess,  $N-Z=2$ , a  $T=0$  pairing is comparable to a  $T=1$  pairing [28] and for heavier  $N > Z$  nuclei, where protons and neutrons at the Fermi surface are in different spatial states, a  $T=1$  pair field dominates.

## 6. Summary

The study of matter with radioactive beams of nuclei is one of the most exciting challenges of low-energy nuclear physics today. The present review has been focused on the microscopic structure of exotic nuclei far from stability. Although we mainly concentrated on the ground-state properties, the physics of excited states in loosely bound systems is extremely interesting and difficult. Theoretically, it will demand new approaches, approximations, and techniques. Experimentally, the combination of radioactive ion beams and the new-generation multidetector arrays should open up many new avenues of exploration.

## Acknowledgements

Oak Ridge National Laboratory is managed for the U.S. Department of Energy by Martin Marietta Energy Systems, Inc. under Contract No. DE-AC05-84OR21400. The Joint

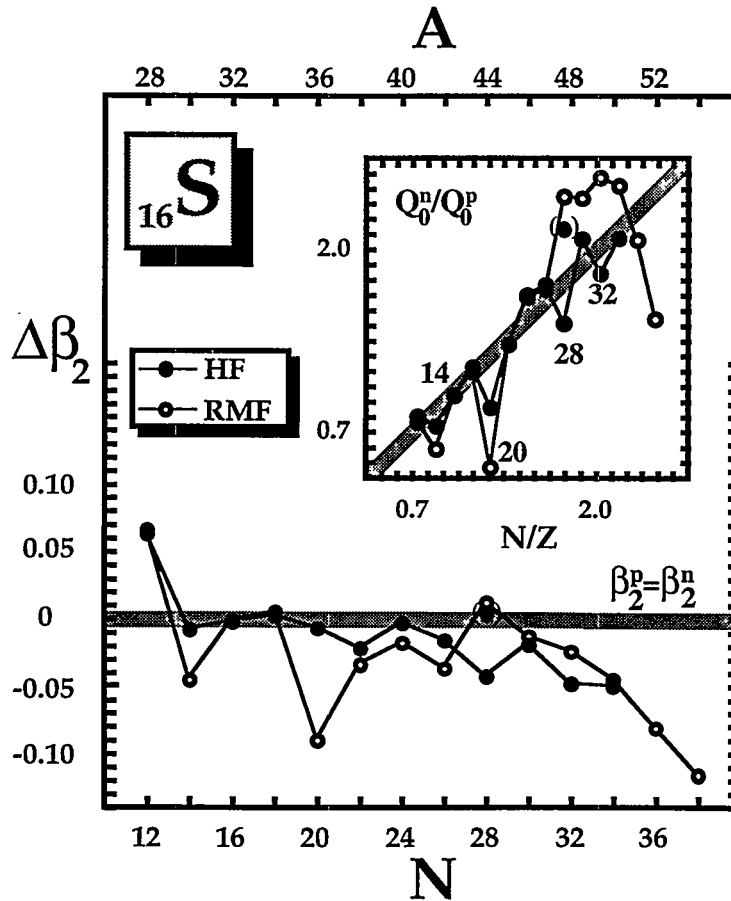


Figure 10. Difference  $\Delta\beta_2 \equiv \beta_2^n - \beta_2^p$  for the even-even sulfur isotopes calculated with the HF and RMF models as a function of neutron number. The insert shows the ratio of neutron and proton quadrupole moments versus  $N/Z$ . From Ref. [26].

Institute for Heavy Ion Research has as member institutions the University of Tennessee, Vanderbilt University, and the Oak Ridge National Laboratory; it is supported by the members and by the Department of Energy through Contract No. DE-FG05-87ER40361 with the University of Tennessee. Theoretical nuclear physics research at the University of Tennessee is supported by the U.S. Department of Energy through Contract No. DE-FG05-93ER40770. This work was partly supported by the Polish Committee for Scientific Research under Contract No. 20450 91 01.

## REFERENCES

1. A. Mueller and B. Sherril, *Annu. Rev. Nucl. Part. Sci.* **43**, 529 (1993).
2. I. Tanihata *et al.*, *Phys. Lett.* **B160** (1985) 380; *Phys. Rev. Lett.* **55**, 2676 (1985).
3. P.G. Hansen and B. Jonson, *Europhys. Lett.* **4**, 409 (1987).
4. J. Dobaczewski, W. Nazarewicz, and T. Werner, to be published.
5. S. Hofmann, in: *Particle Emission from Nuclei*, ed. by M. Ivascu and D.N. Poenaru

(CRC, Boca Raton, 1989), Vol. 2, Chap. 2; in: *Handbook on Nuclear Decay Modes*, to be published.

6. U. Fano, Phys. Rev. **124**, 1866 (1961).
7. W. Nazarewicz, T.R. Werner, and J. Dobaczewski, Phys. Rev. **C**, in press.
8. R. Smolańczuk and J. Dobaczewski, Phys. Rev. **C48**, R2166 (1993).
9. M. Beiner, R.J. Lombard, and D. Mas, Nucl. Phys. **A249**, 1 (1975).
10. K.-L. Kratz, J.-P. Bitouzet, F.-K. Thielemann, P. Möller, and B. Pfeiffer, Astrophys. J. **403**, 216 (1993).
11. W.M. Howard, S. Goriely, M. Rayet, and M. Arnould, Astrophys. J. **417**, 713 (1993).
12. M.F. Mohar *et al.*, Phys. Rev. Lett. **66**, 1571 (1991).
13. R.J. Philpott, Nucl. Phys. **A289**, 109 (1977).
14. D. Halderson and R.J. Philpott, Nucl. Phys. **A345**, 141 (1980).
15. J. Dobaczewski, H. Flocard and J. Treiner, Nucl. Phys. **A422**, 103 (1984).
16. V. Borrel *et al.*, Z. Phys. **A344**, 135 (1992).
17. A. Brown, Phys. Rev. **C43**, R1513 (1991).
18. J. Dobaczewski and W. Nazarewicz, Phys. Rev. Lett. **73**, 1869 (1994).
19. F.A. Ivanyuk and V.M. Strutinsky, Z. Phys. **A290**, 107 (1979).
20. M. Bolsterli, E.O. Fiset, J.R. Nix, and J.L. Norton, Phys. Rev. **C5**, 1050 (1972).
21. B.K. Jennings, Nucl. Phys. **A207**, 401 (1973).
22. B.K. Jennings, R.K. Bhaduri and M. Brack, Phys. Rev. Lett. **34**, 228 (1975).
23. B.K. Jennings and R.K. Bhaduri, Nucl. Phys. **A237**, 149 (1975).
24. J. Caro, E. Ruiz Arriola and L.L. Salcedo, Preprint Universidad de Granada UG-DFM-32/94.
25. J. Dobaczewski, I. Hamamoto, W. Nazarewicz, and J.A. Sheikh, Phys. Rev. Lett. **72**, 981 (1994).
26. T.R. Werner, J.A. Sheikh, W. Nazarewicz, M.R. Strayer, A.S. Umar, and M. Misu, Phys. Lett. **B333**, 303 (1994).
27. S. Åberg, H. Flocard and W. Nazarewicz, Ann. Rev. Nucl. Part. Sci. **40**, 439 (1990).
28. H. Wolter, A. Faessler and P. Sauer, Nucl. Phys. **A167**, 108 (1971).

# Near-yrast Structures in Neutron-rich Nuclei

W R Phillips

Department of Physics and Astronomy  
University of Manchester  
Manchester, M13 9PL, UK

## 1. INTRODUCTION

The observation with large  $\gamma$ -detector arrays of triple and higher fold coincidences between  $\gamma$ -rays which occur in the decay of prompt fission fragments is a powerful tool for probing the mechanism of fission and the structure of neutron-rich fission fragments. Low-energy fission, such as spontaneous fission or fission induced by slow neutrons, produces the most neutron-rich fragments and this paper is only concerned with low-energy fission. Measurements on the prompt  $\gamma$ -rays gives details of the fragments' mass, charge and spin distributions as well as determining yrast and near-yrast decay schemes, and the former, global, information can be related to model predictions of mass splits and mechanisms of spin generation. There is thus much to be learned from prompt fission  $\gamma$ -rays but since the conference is chiefly concerned with nuclear structure and spectroscopy this paper will concentrate solely on those topics. Before proceeding to specific items a few remarks on low-energy fission will put the array experiments in perspective: (i) The average spin in the prompt  $\gamma$ -emitting fragments is  $\sim 7-8\hbar$ . The spin distribution is skew and the highest spin state from which transitions can be placed in a particular decay scheme depends upon the yield of the species studied and the sensitivity of the  $\gamma$  array. With EUROGAM 1 [1] transitions from states with spin  $\sim 16\hbar$  have been observed in strongly produced fragments; (ii) Over 200 separate fragments are produced in spontaneous fission with yields greater than 0.1%. The very large number of  $\gamma$ -rays produced makes use of a high-sensitivity array essential for disentangling effects in identified nuclei or fragment pairs; (iii) The average number of neutrons emitted per fission in the decay of  $^{248}\text{Cm}$ , for example, is 3.2. The average  $N/Z$  ratio for a  $\gamma$ -emitting fragment is thus  $\sim 1.55$ . With EUROGAM 1 data the most neutron-rich isotopes studied so far have been  $^{104}\text{Zr}$  ( $N/Z = 1.60$ ) and  $^{150}\text{Ba}$  ( $N/Z = 1.68$ ).

In the following sections of this paper we discuss three aspects of the nuclear structure of neutron-rich nuclei, studied using EUROGAM 1 to detect prompt  $\gamma$ -rays from the fission of  $^{248}\text{Cm}$ . A source of strength  $\sim 2\mu\text{Ci}$  was made by embedding curium oxide in a potassium chloride pellet. This was placed in the centre of the EUROGAM 1 array, which consisted of 45 suppressed Ge detectors augmented by 5 LEPS detectors. Construction of three-dimensional histograms containing triple- $\gamma$  coincident events enabled the fast creation of one-dimensional spectra of  $\gamma$ -rays in coincidence with any two supplied gating energies, thus maximising the selectivity needed to separate the decays in fragments being studied from decays in the many other products of the fission process.

## 2. LIFETIMES IN Nd ISOTOPES

Lifetime measurements of medium to high-spin nuclear states (with spin quantum number  $I \geq 10$ ) have in the past been confined to neutron-deficient nuclei produced in fusion-evaporation reactions, and the stable species excited by Coulomb excitation; states with lifetimes less than  $\sim 2\text{ps}$  have been measured using the DSAM, modified to measure the lifetimes of states with  $12 \geq I \geq 16$  in the fragments from spontaneous fission.

The technique previously described [2][3] for identifying new neutron-rich isotopes from  $\gamma$ -ray coincidence data was used to identify transitions in  $^{156}\text{Nd}$ . These transitions were then used as gates to generate the partial level scheme shown in Fig.1. Previously the ground state band of  $^{152}\text{Nd}$  was known up to spin  $I = 8$ [4][5], and that of  $^{154}\text{Nd}$  also to spin  $I = 8$ [6]. The previous level schemes for both these nuclei have been confirmed and extended and these are also shown in Fig.1. The average quadrupole moment of the low-spin  $2_1^+$ ,  $4_1^+$  and  $6_1^+$  levels in  $^{152}\text{Nd}$  (populated in the  $\beta^-$  decay of  $^{152}\text{Pm}$ ) has been inferred from electronic-timing measurements of state lifetimes [7] to be  $6.09(11)$  eb.

At spins above  $I = 10$  symmetrically broadened lineshapes were observed for  $\gamma$  rays emitted

from states with lifetimes in the range 1-2 ps, ie comparable to the stopping time of the fission fragments in the pellet.

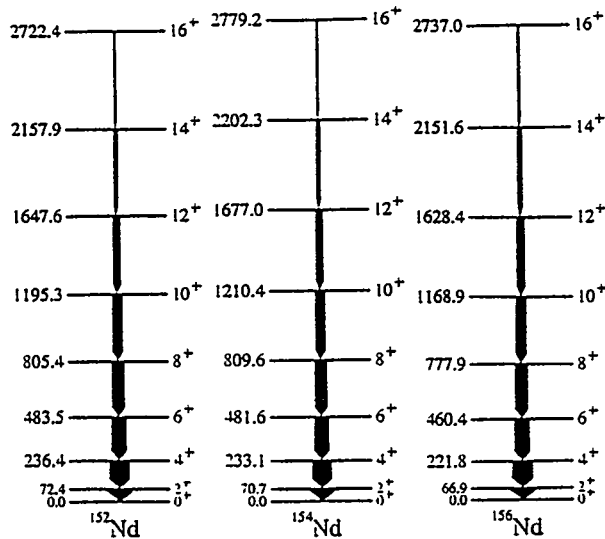
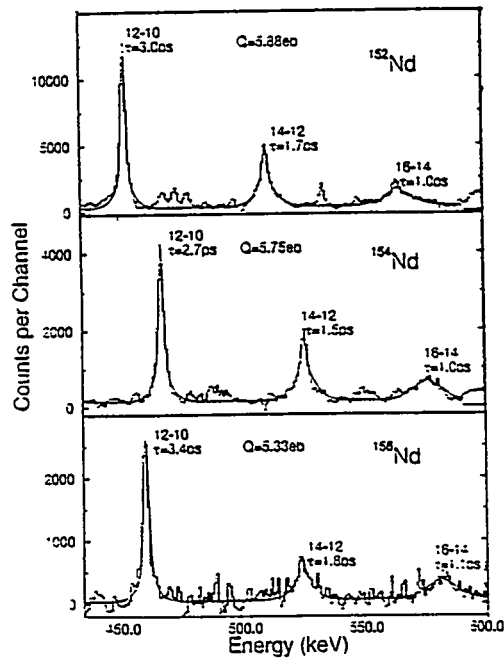


Fig. 1 Partial decay schemes for  $^{152}\text{Nd}$ ,  $^{154}\text{Nd}$ ,  $^{156}\text{Nd}$ .  
 Fig. 2 Lineshapes in the  $\gamma$ -ray energy spectra of  $^{152}\text{Nd}$ ,  $^{154}\text{Nd}$ ,  $^{156}\text{Nd}$ .



To determine the state lifetimes from the Doppler broadened lineshapes the velocity history of the Nd fragments as they stop in the source pellet was simulated using electronic and nuclear stopping powers given by the computer code ZBL [8]. The initial fragment kinetic energy distribution was assumed to be Gaussian with its centroid and width taken from Ref. [9]. The simulation produced a two-dimensional data matrix which was used in conjunction with a simulation of the decay process to generate lineshapes that were compared with the experimental data.

The lineshapes in each of the nuclei  $^{152}\text{Nd}$ ,  $^{154}\text{Nd}$ ,  $^{156}\text{Nd}$  between spin  $I = 12$  and 16 were fitted separately with a simple decay model that assumed a rotational band with a constant intrinsic quadrupole moment ( $Q$ ) which was varied to obtain the best fit to the data. To account for feeding of the  $I = 16$  states, each band has had its rotational energy sequence extended with three fictitious transitions which were assigned the same quadrupole moment as the observed band. Sidefeeding of the  $I = 12$  and 14 states was determined to be about 30 percent of the appropriate decay intensities from the integrated photopeak areas in the  $\gamma$ -ray spectra. In spontaneous fission, where the fragments are formed at rather low spin and excitation energy, the sidefeeding of the yrast states is thought to be direct and fast compared to the lifetimes of the medium spin yrast states. In the model the sidefeeding intensity was assumed to be a result of prompt, direct feeding (feeding time = 0 ps). The fictitious continuation of the band was also assumed to have 30 percent prompt sidefeeding to each level. Fig. 2 shows the lineshapes in  $^{152}\text{Nd}$ ,  $^{154}\text{Nd}$ ,  $^{156}\text{Nd}$  with resulting fits superimposed upon the data. In the fitting procedure the data and simulated spectra were compared over regions that included the lineshapes but excluded the large regions of background between them. The quadrupole moments along with their statistical uncertainties are  $5.88 \pm 0.08 \text{ eb}$  ( $^{152}\text{Nd}$ ),  $5.75 \pm 0.10 \text{ eb}$  ( $^{154}\text{Nd}$ ) and  $5.33 \pm 0.16 \text{ eb}$  ( $^{156}\text{Nd}$ ). These results are subject to systematic errors due to uncertainties in the stopping powers (contributing an uncertainty of about 10 percent to the transition quadrupole moments) and in the way that the feeding is modeled (the introduction of a long, 200 fs delay in the sidefeeding increases the solution quadrupole moments by about 3 percent). Due to these systematic errors it can only be noted that, for  $^{152}\text{Nd}$ ,  $Q(I = 12 - 16)$  is consistent with  $Q(I = 2 - 6)$ . However, as the same model and stopping powers are used for each of the three isotopes it is expected that these results are a reliable measurement of



The excitation energies of these identified  $2q\nu$  excitations, together with the positions of the  $3/2^+$  and  $5/2^-$  levels in  $^{101}\text{Zr}$ , were used to determine the strength  $G$  of the pairing interaction, giving the first direct measurement in such neutron-rich nuclei. There is a question about the proper size of the strength  $G$ . Strutinsky-type calculations[12] of the potential energy surfaces (PES) require a value smaller than given by usual prescriptions in order to reproduce the large deformations observed in the ground states of the Sr and Zr isotopes with neutron number  $N \geq 60$ . Microscopic calculations[13] also effectively use a small pairing strength when reproducing ground-state properties in this region.

Fig. 5 shows the value of  $G$  which reproduces the excitation energy of the  $4^-$   $2q\nu$  level in  $^{102}\text{Zr}$ , plotted as a function of the parameter  $\epsilon$  which gives the extent of the axially symmetric quadrupole deformation. Values of  $\epsilon$  between 0.25 and 0.35 ( $0.27 < \beta < 0.38$ ) give agreement with the positions of the  $3/2^+[411]$  and  $5/2^-[532]$  levels observed [3] in  $^{101}\text{Zr}$ . The calculations also predict that, of the many bands based on two quasi-particle excitations, levels in the band based on the  $4^-$   $2q\nu$  state are yrast, and are thus those expected to be observed in the present experiments. The upper line on Fig. 5 gives  $G$  values calculated without any spin-spin interaction influencing the  $2q\nu$  excitation energy; the lower line assumes a 200 keV upward shift of the excitation energy due to this effect. The value of the pairing energy  $\delta_\nu$  determined from calculated neutron separation energies in  $^{101-103}\text{Zr}$  using  $\beta = 0.35$  and the lower value of  $G$  on Fig. 5 is equal to 1.1 MeV, in reasonable agreement with the value of  $\sim 0.8$  MeV obtained from the masses [14] of  $^{100-103}\text{Zr}$ .

A closely similar value of  $G$  is found for  $^{100}\text{Zr}$ , and agreement also obtained between calculated  $\delta_n$  of 1.3 MeV with the value of  $\sim 1.1$  MeV obtained from masses. The preliminary conclusion of the analysis is thus that the neutron pairing strength  $G$  is close to  $20/A$  MeV, as found in other regions of the nuclear chart, but larger than the value used in recent calculations of potential energy surfaces.

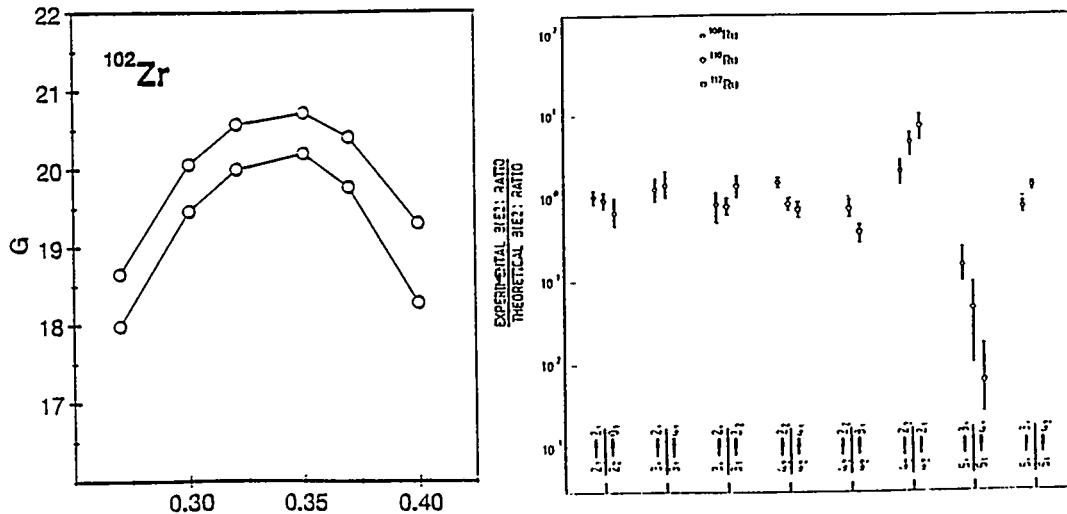


Fig. 5 Values of the pairing strength  $G$  which fit the observed position of the  $4^-$  band-head in  $^{102}\text{Zr}$ . Units of  $G$  are  $\text{MeV} \times A$ .

Fig. 7 Experimentally determined  $B(E2)$  ratios divided by predicted ratios for the transitions indicated along the  $x$ -axis

#### 4. THE ROLE OF TRIAXIALITY IN RU ISOTOPES

To date there is little good evidence in known even-even nuclei of levels with properties which



follow closely those expected for rotations of ground states with stable triaxial deformations. The excitation energy  $E(2_2^+)$  is an indication of the strength of triaxial-driving nucleon correlations; if  $E(2_2^+)$  is much less than the pairing gap (typically  $\sim 2$  MeV in the region of neutron-rich nuclei near  $A = 100$ ) the tendency towards triaxiality is strong. The even-even  $^{108-114}\text{Ru}$  isotopes have some of the lowest known  $E(2_2^+)$  values and are among the best candidates for close examination of the degree to which nuclear ground states can adopt rigid, axially-asymmetric shapes.

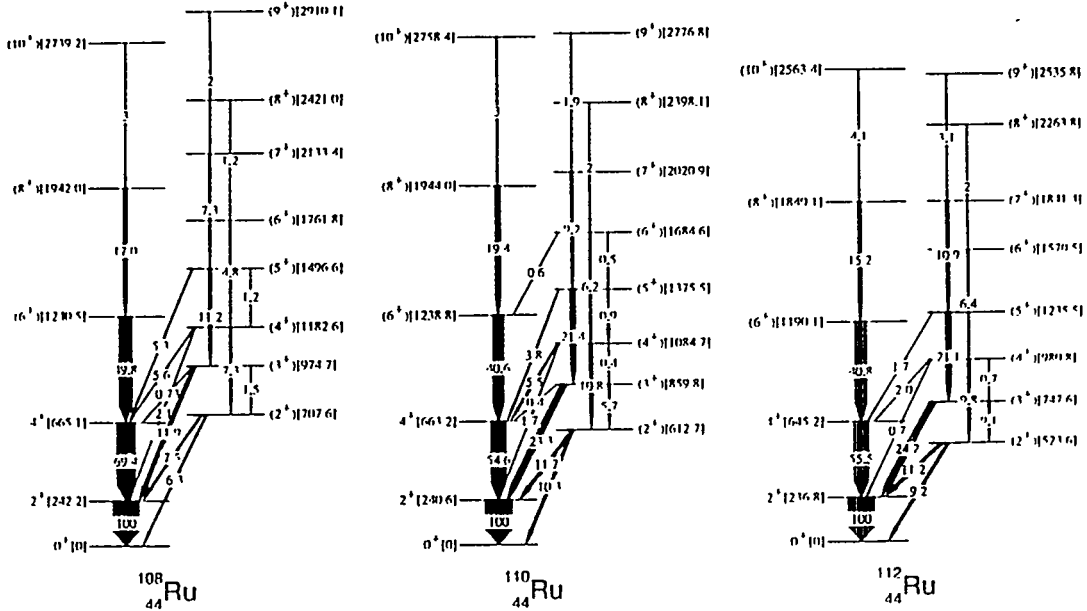


Fig. 6 Partial decay schemes for  $^{108,110}\text{Ru}$  and  $^{112}\text{Ru}$ .

Previous work [15] on stable Ru isotopes suggested a phase transition from near-spherical nuclei to soft triaxial-rotors as the neutron number increased. Later data [16] on  $^{106}\text{Ru}$  and  $^{108}\text{Ru}$  suggested triaxial deformations with increasing rigidity. Recent experiments [17] on low-spin levels in  $^{108,110}\text{Ru}$  and  $^{112}\text{Ru}$  confirmed this trend. As in Ref. [16], level spacings and  $\gamma$ -ray branching ratios of the  $2_2^+$  and  $3_1^+$  levels were in reasonable agreement with the RTR model.

Fig. 6 shows partial decay schemes for even-even  $^{108-112}\text{Ru}$ ; less extensive data were determined for the new isotope  $^{114}\text{Ru}$ . The spin and parity assignments on Fig. 6 are based on previous work [16,17] and on the observed decay paths of the levels. In addition, the angular correlations measured for pairs of  $\gamma$  rays which start from levels with spins  $I \leq 7\hbar$ , and which connect  $\Delta I = 2$  states, are consistent with stretched electric quadrupole (E2) transitions. The decay schemes of Fig. 6 have many features in common with schemes for rotations of triaxial ground states. The values of the parameter  $\gamma$  deduced from the excitation energies  $E(2_1^+)$  and  $E(2_2^+)$  are consistent with those deduced from the  $\gamma$ -ray branching ratios of the  $2_2^+$  levels for  $^{108}\text{Ru}$  and  $^{110}\text{Ru}$ , and in reasonable agreement for  $^{112}\text{Ru}$ . The former set of  $\gamma$  values are  $22.5^0$ ,  $24.2^0$ ,  $26.4^0$  and  $27.2^0$  for  $A = 108, 110, 112$  and  $114$  respectively; the latter set are  $22.7(2)^0$ ,  $23.9(3)^0$  and  $25.4(2)^0$  for  $A = 108, 110$  and  $112$  respectively. Branching ratios could not be determined for  $^{114}\text{Ru}$  because of the near-equality of the energies of the  $2_1^+$  to  $0_1^+$  and  $3_1^+$  to  $2_2^+$  transitions. The excitation energies  $E(3_1^+)$  and  $E(4_1^+)$  are in good agreement with the RTR predictions. The spacings of the remaining levels are not in good agreement overall with the pure RTR model, which predicts over the above range of  $\gamma$  values a level staggering which is not observed.

The main area of agreement between the present data and the simple RTR lies in the observed ratios of reduced E2 transition probabilities  $B(E2)$ . These were deduced from measured  $\gamma$ -ray branching ratios on the assumption that all decays were pure E2, as would be the case for rotational levels and as observed [16] to a good approximation in  $^{106}\text{Ru}$  and  $^{108}\text{Ru}$ . Fig. 7 shows these ratios

plotted in units of the ratios predicted [18] by the RTR. The predictions for each isotope used the  $\gamma$  value obtained from the appropriate  $2_1^+$  and  $2_2^+$  excitation energies, with an error of  $\pm 0.5^0$  assigned in each case. There is good overall agreement. Where branching ratios were too weak to be observed, experimental limits were also in agreement with predictions. The predicted  $B(E2; 5_1^+ \rightarrow 4_1^+)$  is very small compared to others. Because of this any discrepancy between theory and experiment for ratios involving  $B(E2; 5_1^+ \rightarrow 4_1^+)$  can be removed without significantly affecting other comparisons by postulating a small magnetic dipole contribution to the  $\Delta I = 1$   $\gamma$ -ray transitions.

Confidence in the reality of axially *symmetric* shapes arises both because of level properties and because of the agreement between experiment and PES predictions of deep minima at the expected places. Similar agreement is anticipated for nuclei which may have axial *asymmetry*, but the results of Ref. [17] which predict only shallow minima at non-zero  $\gamma$  values do not suggest rigid axial asymmetry in the Ru isotopes studied. Macroscopic-microscopic PES calculations [12] predict  $\gamma$  values near  $20^0$ , but in order to reproduce the large deformations observed in the neutron-rich Sr and Zr isotopes, require an unexpectedly small pairing interaction to be used. The data presented here encourage further theoretical work on the neutron-rich nuclei near  $A = 100$ .

The results presented in this paper are the work of several collaborators; J L Durell, C J Pearson, W R Phillips, J A Shannon, A G Smith, W Urban and B J Varley from the University of Manchester; I Ahmad, C J Lister, L R Morss, K L Nash and C W Williams from Argonne National Laboratory; N Schulz, E Lubkiewicz and M Bentaleb from CNRS, Strasbourg; and N Rowley and K Jain from the Universities of Manchester and Surrey.

### References

- [1] F Beck, Prog. Part. Nucl. Phys. **28**, 443 (1992)
- [2] M A C Hotchkis *et al*, Phys. Rev. Lett. **64**, 3123 (1990)
- [3] M A C Hotchkis *et al*, Nucl. Phys. **A530**, 111 (1991)
- [4] J B Wilhelmy, S G Thompson, R C Jared and E Cheifetz, Phys. Rev. Lett. **25**, 1122 (1970)
- [5] R Chapman, W McLatchie and J E Kitching, Nucl. Phys. **A186**, 603 (1972)
- [6] E Cheifetz, J B Wilhelmy, R C Jared and S G Thompson, Phys. Rev. **C4**, 1913 (1971)
- [7] M Hellstrom, H Mach, B Fogelberg, D Jerrestam and L Spanier, Phys. Rev. **C47**, 545 (1993)
- [8] J F Ziegler, J P Biersack and U Littmark, The Stopping and Range of Heavy Ions in Solids (1985) Pergamon Press
- [9] V E Viola, K Kwiatkowski and M Walker, Phys. Rev. **C31**, 1550 (1985)
- [10] G Lhersonneau *et al*, Z. Phys. **A332**, 243 (1989)
- [11] H Mach *et al*, Phys. Lett. **B230**, 21 (1989)
- [12] R R Chasman, Z. Phys. **A339**, 111 (1991)
- [13] P Bonche *et al*, Nucl. Phys. **A443**, 39 (1985)
- [14] G Audi and A H Wapstra, Nucl. Phys. **A565**, 1 (1993)
- [15] J Stachel *et al*, Nucl. Phys. **A383**, 429 (1982)
- [16] J Stachel *et al*, Z. Phys. **A316**, 105 (1984)
- [17] J Äystö *et al*, Nucl. Phys. **A515**, 365 (1990)
- [18] P P Day and C A Mallman, ANL Report, ANL-6184 (1960)

# Separation and Identification of $^{100}\text{Sn}$ at the GSI Projectile Fragment Separator FRS

R. Schneider, J. Friese, J. Reinhold, K. Zeitelhack, T. Faestermann, R. Gernhäuser,  
H. Gilg, F. Heine, J. Homolka, P. Kienle, H. J. Körner

Physik-Department E12, Technische Universität München, D-85747 Garching, Germany

H. Geissel, G. Münzenberg, K. Sümmerer

Gesellschaft für Schwerionenforschung, P.O. Box 110552, D-64220 Darmstadt, Germany

The region of nuclei around the doubly-magic shell closure at  $N=Z=50$  has been studied for a long time involving large experimental efforts, mainly undertaken at on-line mass separators (see Ref.[1] and references therein). Nevertheless, the isotope  $^{100}\text{Sn}$  has yet remained undiscovered. The lightest Sn isotopes studied so far were  $^{103}\text{Sn}$  [2] and  $^{101}\text{Sn}$  [3]. In both cases the observation was facilitated by the  $\beta$ p-decay of these isotopes, whereas for  $^{100}\text{Sn}$   $\beta$ -decay is expected [4]. For the neighbouring nuclei, these hindrance factors can be studied only for more complicated multiparticle-multihole configurations.

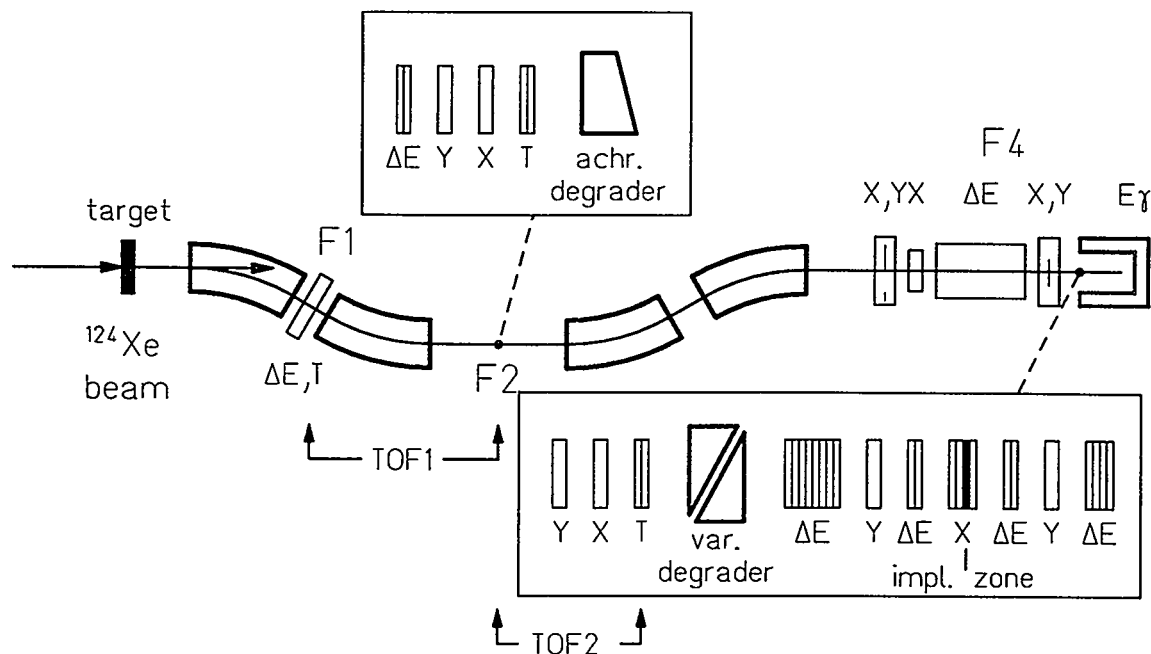


Figure 1: Experimental setup for the separation and identification of  $^{100}\text{Sn}$  and neighbouring isotopes at the fragment separator FRS.

The systematic studies of high-energy Xe projectile fragmentation performed previously in our collaboration [5] have encouraged us to attempt the identification of  $^{100}\text{Sn}$  with this novel technique. In particular, we hoped to benefit from an enhancement of measured cross sections for  $^{129}\text{Xe}$  fragments [5] compared to the EPAX formula [6]. In our experiment, we used a  $^{124}\text{Xe}$  beam of 1095 A·GeV from the GSI

heavy-ion synchrotron SIS impinging onto a  $6 \text{ g/cm}^2$  beryllium target. The  $^{100}\text{Sn}$  fragments were separated and identified in-flight with the GSI fragment separator FRS [7]. We achieved both, a clean spatial separation essentially free from background, and an in-flight identification with respect to nuclear charge and mass without ambiguities due to different ionic charge states which pose problems at lower bombarding energies. First results from this experiment have been published [8]. Almost simultaneously with our discovery,  $^{100}\text{Sn}$  has been observed at the LISE separator at GANIL, using intermediate-energy projectile-fragmentation of  $58 \text{ A}\cdot\text{MeV}$   $^{112}\text{Sn}$  [9].

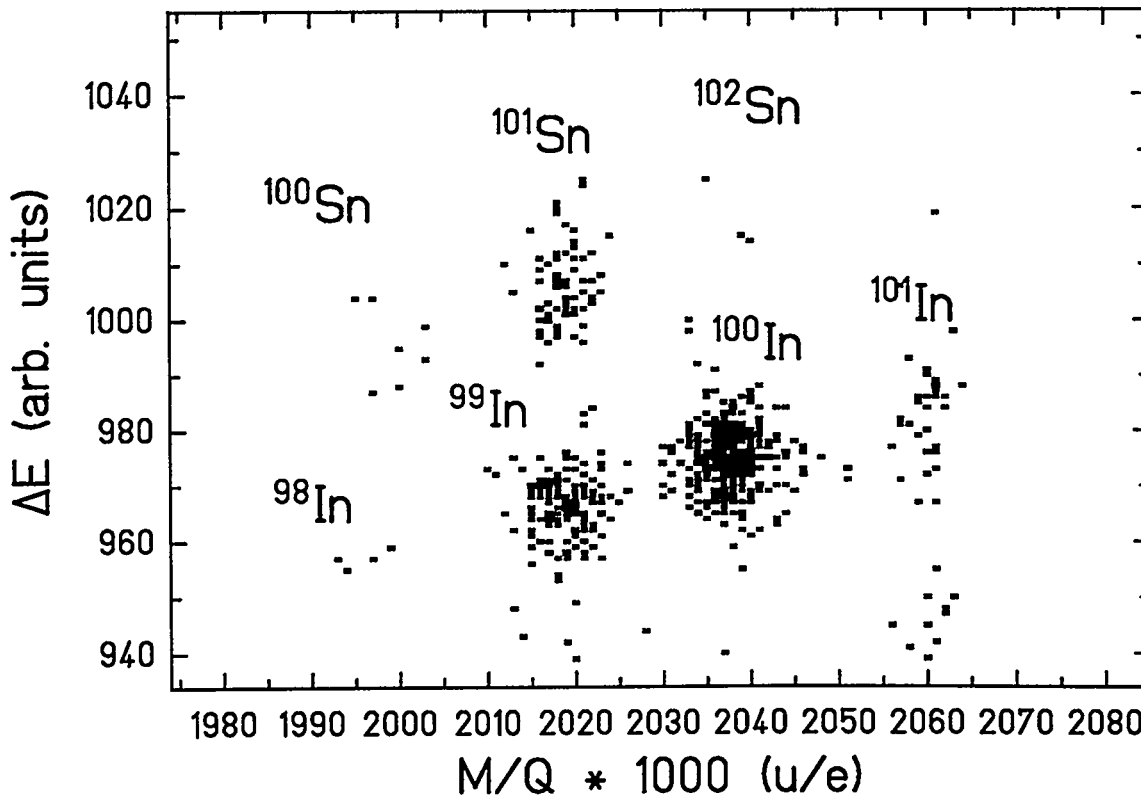


Figure 2: Energy-deposition *vs.*  $M/Q$  measured in the final focal plane F4 of the FRS for a setting corresponding to  $^{100}\text{Sn}$ . Note the strong suppression of  $^{102}\text{Sn}$  and  $^{101}\text{In}$  despite there larger cross sections.

A schematic lay-out of the FRS and the detectors used to identify the fragments in our experiment is shown in Fig. 1. A thick wedge-shaped aluminum degrader of  $6.3 \text{ g/cm}^2$  in the midplane of the FRS ("F2") was used to achieve isotopic separation of the fragments and to focus them achromatically at the final focal plane ("F4"). For decay studies one selected isotope was implanted into a stack of silicon detectors mounted at F4. The isotopic identification in-flight was achieved by combining the magnetic rigidity analysis with multiple time-of-flight and energy-deposition measurements. The energy deposition of the ions (marked " $\Delta E$ " in Fig. 1) was measured with the help of a four-anode ionization chamber placed at F4 in front of the implantation detector. The resolution obtained with the ionization chamber amounted to  $Z/\Delta Z \simeq 150$ . Velocities were measured in the second quarter of the FRS ("TOF1" in

Fig.1) and behind the achromatic degrader (“TOF2”). Nuclear-mass-to-charge ratios  $M/Q$  were determined from the measured flight times and positions at F2 and F4. A resolution of  $\frac{\Delta(M/Q)}{M/Q} \simeq 6 \cdot 10^{-3}$  (FWHM) was obtained.

The absolute  $M/Q$  calibration was verified by separating well-known, abundant fragments and implanting them into the silicon detector stack. As an example, about 70 nuclei of the  $\alpha$  emitter  $^{108}\text{Te}$  were implanted into the desired silicon slice and identified by observing correlated  $\alpha$  decays with  $E_\alpha = 3.32$  MeV.

Fig. 2 shows a scatter plot of  $\Delta E$  vs.  $M/Q$  obtained with the FRS setting for  $^{100}\text{Sn}$ . The individual isotopes are clearly resolved. We attribute 7 events to the isotope  $^{100}\text{Sn}$ . The majority of the events are assigned to  $^{101}\text{Sn}$  [3], the new isotope  $^{99}\text{In}$ , and  $^{100}\text{In}$  [10]. The four events at  $M/Q \simeq 2.0$  and  $\Delta E \simeq 960$  a.u. in Fig. 2 are preliminarily attributed to  $^{98}\text{In}$ .

The data shown in Fig. 2 have been accumulated in 277 hours of beam time during which a total of  $1.7 \cdot 10^{13}$  projectiles hit the target. The preliminary effective production cross section for  $^{100}\text{Sn}$  of 5 pb is based on *calculated* effective transmission values which include the ion-optical transmission and the absorption in all layers of matter downstream from the target [11]. Secondary production in the target has not been taken into account. The *experimental* transmission values will be extracted from a more detailed analysis of the data. The preliminary cross sections for  $^{100}\text{Sn}$  and neighbouring isotopes agree surprisingly well with the prediction from the EPAX systematics [6], which means that the enhancement observed for  $^{129}\text{Xe}$  fragments is absent for  $^{124}\text{Xe}$  fragments (see Fig. 3). This could be related to the smaller number of bound levels in nuclei above  $^{100}\text{Sn}$  through which the evaporation cascade towards  $^{100}\text{Sn}$  passes.

event #	$\beta$ -energy of $^{100}\text{Sn}$ [MeV]	measured decay times [s]		
		$^{100}\text{Sn}$	$^{100}\text{In}$ $\tau = 9s$	$^{100}\text{Cd}$ $\tau = 90s$
1	0.7	0.716	6.6	
2	1.6	1.208		36
3	1.4	1.219	13.3	35
4	2.7	0.655		69
5				26
6	1.5	0.98		
7	1.6	3.02	9.1	

Table 1: Decay events following the implantation of  $^{100}\text{Sn}$  nuclei in the Si-strip implantation detector

A first analysis of decay events following the implantation of seven  $^{100}\text{Sn}$  nuclei into the stack of Si detectors at F4 reveals that four of them are particularly safe candidates because they (i) have been observed with extremely low random-

background rates, and (ii) show two or more signals from the sequence of mother-daughter-granddaughter decays (see Table 1), including one (event number 3) where all three generations are present with the right delay times. From these decay events (which corroborate independently their assignment to  $^{100}\text{Sn}$ ) we deduce a half-life of  $^{100}\text{Sn}$  of  $0.66^{+0.66}_{-0.22}$  s. This half-life is in excellent agreement with the one predicted by Rykaczewski et al. [12] of 0.6 s. It agrees also with the more recent calculation of Brown and Rykaczewski [4] of 0.53 sec, thus corroborating in some sense their GT hindrance factor of about 4. In agreement with the latter theoretical study, all our decay events involve  $\beta$ -decay, excluding a significant contribution of  $\beta$ -delayed proton-emission.

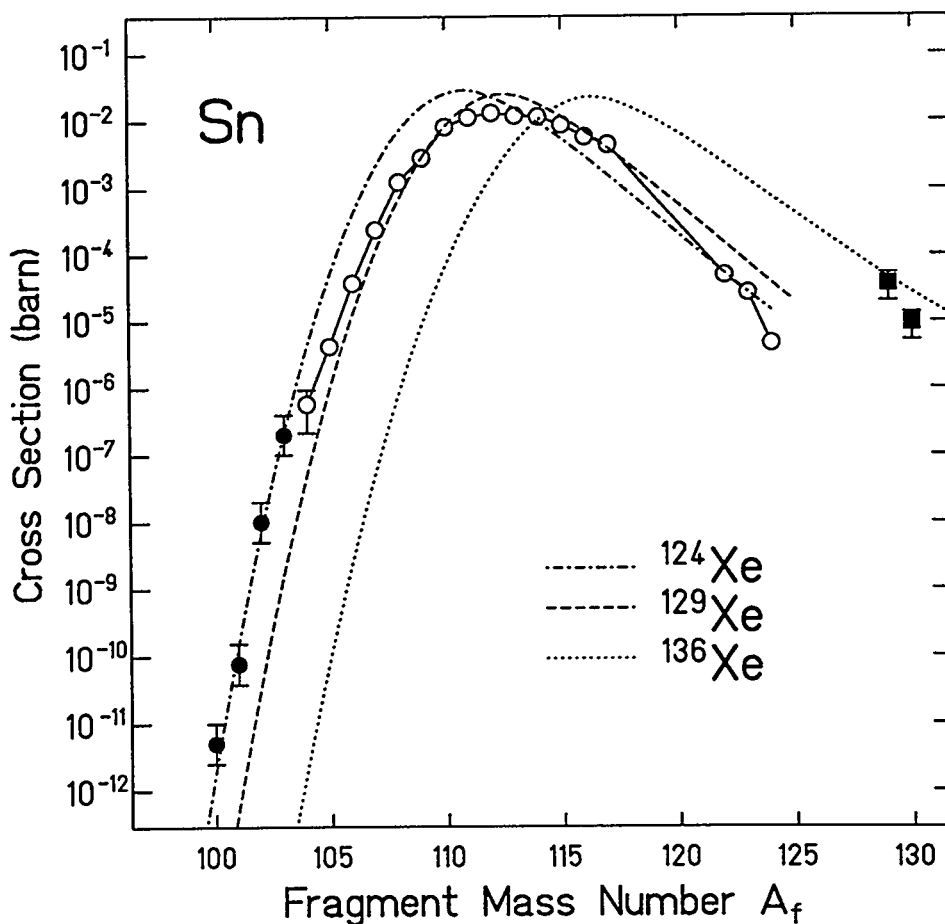


Figure 3: Cross sections for the formation of Sn isotopes in high-energy projectile-fragmentation reactions with  $^A\text{Xe}$  projectiles of different neutron excess (Ref.[5] and this work). The results for  $^{124}\text{Xe}$  are from the on-line analysis and therefore very preliminary. The curves are the predictions of the EPAX parametrization [6].

We conclude that despite the small number of events observed in our study, the low background rates together with the high granularity of our implantation detector

allowed to measure the half-life and the principal decay mode of  $^{100}\text{Sn}$  with considerable accuracy. Similar results will be obtained for the new isotope  $^{104}\text{Sb}$  and the decay of  $^{105}\text{Sb}$  where a small ground-state proton-emission branching has been observed [13].

## References

- [1] K. Rykaczewski, Proc. 6<sup>th</sup> Int. Conf. on Nuclei far from Stability, Bernkastel-Kues, Germany, 1992, IOP Conference Series 132 (IOP Publishing, Bristol, 1993) p. 517.
- [2] P. Tidemand-Petersson et al., Z. Physik A **302**, 343 (1981).
- [3] Z. Janas et al., GSI-Preprint 94-47, to be published in Physica Scripta.
- [4] B.A. Brown and K. Rykaczewski, to be published in Phys. Rev. Lett.
- [5] J. Friese et al., Nucl. Phys. **A553**, 753c (1993); Proc. 9<sup>th</sup> High-Energy Heavy-Ion Study, Berkeley, California (1993).
- [6] K.Sümmerer et al., Phys. Rev. C **42**, 2546 (1990).
- [7] H. Geissel et al., Nucl. Instr. Meth. in Phys. Res. **B70**, 286 (1992).
- [8] R. Schneider et al., Z. Phys. A **348**, 241 (1994).
- [9] M. Lewitowicz et al.: Phys. Lett. **B332**, 20 (1994).
- [10] Kurcewicz, W. et al.: Z. Physik A **308**, 21 (1982).
- [11] Schwab, T.:Ph.D. thesis, GSI-Report GSI-91-10 (1991).
- [12] K. Rykaczewski et al., Proc. Int. Conf. on Nuclei far from Stability, NFFS-5, Rousseau Lake, Canada (1987).
- [13] R.J. Tighe et al., Phys. Rev. C **49**, R2871 (1994).

## The $N = 40$ neutron subshell closure in the $^{68}\text{Ni}$ nucleus

R. Broda<sup>1</sup>, B. Fornal<sup>1</sup>, W. Królas<sup>1</sup>, T. Pawlat<sup>1</sup>, D. Bazzacco<sup>2</sup>, S. Lunardi<sup>2</sup>,  
C. Rossi-Alvarez<sup>2</sup>, R. Menegazzo<sup>2</sup>, G. de Angelis<sup>3</sup>, P. Bednarczyk<sup>3</sup>,  
J. Rico<sup>3</sup>, D. De Acuña<sup>3</sup>, P. J. Daly<sup>4</sup>, R. H. Mayer<sup>4</sup>, M. Sferrazza<sup>4</sup>,  
H. Grawe<sup>5</sup>, K. H. Maier<sup>5</sup>, R. Schubart<sup>6</sup>

The well known level structure of  $^{90}\text{Zr}$  [1] clearly demonstrates the subshell closure at  $Z = 40$  proton number. The lowest excited state is the 1.76 MeV  $0^+$  level, the first  $2^+$  excitation appears at 2.19 MeV and the particle-hole ( $p_{1/2}^{-1}g_{9/2}$ )  $5^-$  excitation comes down in energy below the  $4^+$  state and shows up as a long-lived isomer. In all nuclide chart there are only two nuclei, which give a realistic chance to look for similar features at the neutron number  $N = 40$ . Both of these nuclei lie very far from the stability line and are not easily available for spectroscopic investigation. The first one, the extremely neutron deficient  $Z = N = 40$   $^{80}\text{Zr}$ , was produced recently using the heavy-ion fusion reaction and a highly selective experimental setup [2]. It was found to be strongly deformed and did not show any trace of shell closure signature. The other candidate with the  $N = 40$  neutron number and closed proton shell is the  $^{68}\text{Ni}$  nucleus. It lies relatively close to the stability line, but it is located on the neutron-rich side, and it cannot therefore be produced by fusion-evaporation reactions. In fact, the only known excitation in  $^{68}\text{Ni}$ , a  $0^+$  state at 1.77 MeV was assigned using the  $^{70}\text{Zn}(^{14}\text{C}, ^{16}\text{O})$  two-proton transfer reaction [3]. Whereas any experimental information on higher spin states was absent, the discussion of subshell closure and possible similarity to the  $^{90}\text{Zr}$  case was rather limited. In our effort to identify higher spin excitations in  $^{68}\text{Ni}$ , we used deep-inelastic reactions induced by  $^{64}\text{Ni}$  projectiles on heavy target nuclei.

Recently we exploited such processes to study the neutron-rich Ni isotopes produced in  $^{208}\text{Pb} + 350$  MeV  $^{64}\text{Ni}$  collisions [4]. The experiment performed at the HMI Berlin, using the thick  $^{208}\text{Pb}$  target and the OSIRIS 12 gamma detector array had much broader scope. It also involved spectroscopic investigation of nuclei in the  $^{208}\text{Pb}$  region and included more complete study of the  $^{208}\text{Pb} + ^{64}\text{Ni}$  colliding system. Specifically, the in-beam and off-beam (pulsed beam) coincidence data as well as subsequent radioactivity measurements allowed us to determine nearly full distribution of the production yields of almost 300 nuclei produced in quasielastic and deep-inelastic processes. At the 350 MeV  $^{64}\text{Ni}$  beam energy, which is approx. 40 MeV above the Coulomb barrier, but significantly below the extra-push energy needed to fuse the system, these processes exhaust nearly all of the total reaction cross-section. A schematic distribution of the production yields obtained for this system in the light fragment region is shown in Fig. 1. As expected from the trends governing the mass and charge transfer in deep-inelastic collisions, the observed distribution covers a broad region of nuclei and involves many neutron-rich products. In particular the population of neutron-rich nickel isotopes extends to the  $^{69}\text{Ni}$  isotope; this opened a way to perform spectroscopic study for isotopes populated with higher yields. The measured  $\gamma$ - $\gamma$  coincidences allowed us to extend significantly the level schemes of  $A = 64$  to 67 nickel isotopes as presented in Ref. [4].

- 
- 1 H.Niewodniczański Institute of Nuclear Physics, Kraków, Poland
  - 2 Dipartimento di Fisica dell'Università and INFN, Padova, Italy
  - 3 INFN Laboratori Nazionali di Legnaro, Italy
  - 4 Purdue University, West Lafayette, Indiana, USA
  - 5 Hahn-Meitner-Institut Berlin, Germany
  - 6 Universität Göttingen, Germany



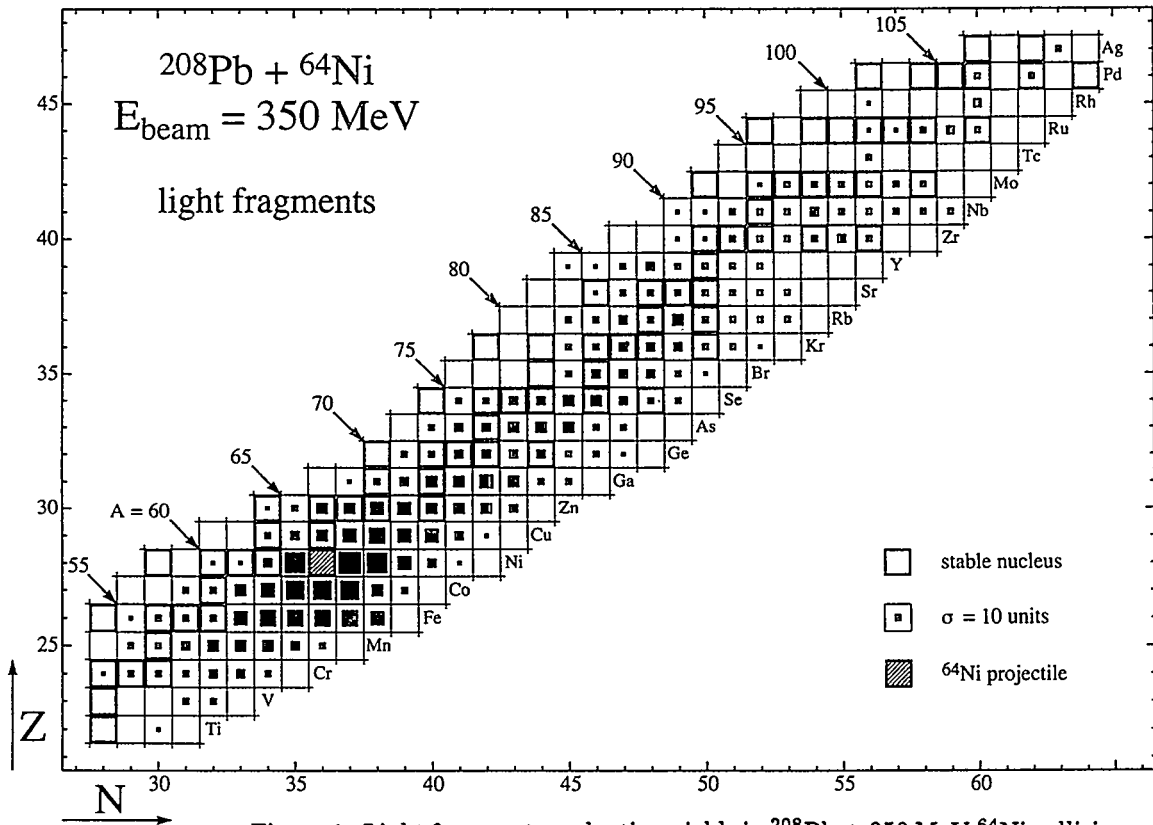


Figure 1. Light fragment production yields in  $^{208}\text{Pb} + 350 \text{ MeV } ^{64}\text{Ni}$  collisions.

In that experiment the production of  $^{68}\text{Ni}$  was clearly indicated, but no  $\gamma$ -ray could be positively identified with this isotope due to insufficient statistics. To improve the experimental conditions we performed at the INFN Legnaro a similar measurement for the  $^{130}\text{Te} + ^{64}\text{Ni}$  system, using the much more powerful GASP multidetector array. The 275 MeV  $^{64}\text{Ni}$  beam bombarded a  $1.2 \text{ mg/cm}^2$   $^{130}\text{Te}$  target located in the array center and placed on a  $14 \text{ mg/cm}^2$   $^{208}\text{Pb}$  backing to stop all reaction products. The  $\gamma$ - $\gamma$  coincidences were stored without any restriction on the multiplicity and the beam was pulsed with 200 ns repetition time in order to separate the prompt and delayed events.

In our search we were guided by simple shell model expectations that the  $^{68}\text{Ni}$  level spectrum, like that of  $^{90}\text{Zr}$ , should feature a long-lived  $5^-$  isomer as well as a significant increase of the  $2^+$  excitation energy as compared to the lighter Ni isotopes. Inspection of the appropriate energy region of the  $\gamma$ - $\gamma$  coincidence data revealed a cascade of two coincident transitions of 814 keV and 2033 keV energy, which matched expectations perfectly for the  $5^- \rightarrow 2^+ \rightarrow 0^+$  yrast cascade in  $^{68}\text{Ni}$ . Both transitions follow the decay of the long-lived isomer and they appeared in both, the  $^{208}\text{Pb}$  and  $^{130}\text{Te}$  target experiments with intensities consistent with the expected production yields of the  $^{68}\text{Ni}$  isotope. In order to clarify the isotopic identification, we performed a  $\gamma$ - $\gamma$  cross-coincidence analysis of the superior statistics GASP data for the  $^{130}\text{Te} + ^{64}\text{Ni}$  reaction system, and the key results are presented in Fig. 2. When a gate was set on a known strong transition of a specific Ni product, the coincidence spectrum showed not only other  $\gamma$ -rays of that Ni nucleus but also known  $\gamma$ -rays belonging to various Te partner products occurring simultaneously in the exit channel. Approximate yields of the Te products could be estimated from the  $\gamma$ -ray intensities (Fig.2).

For example, at the top of Fig. 2 the tellurium isotope yields in coincidence with the  $^{64}\text{Ni}$  1346 keV  $\gamma$ -ray demonstrates, apart from the predominant inelastic scattering process, that  $^{64}\text{Ni}$  appears frequently in the exit channel accompanied by Te partners lighter than  $^{130}\text{Te}$ ; apparently, processes involving up to four neutron evaporation contribute substantially. Moving down in Fig. 2, for each heavier Ni isotope, the pattern of tellurium reaction partners shifts towards lighter mass with a characteristic sharp cut-off at the high mass end in line with the  $A = 194$  total mass of the system. For  $^{68}\text{Ni}$ , shown at the bottom, the long-lived isomer restricts the cross-coincidences observed to events in which the direct, prompt population of the presumed 2033 keV  $2^+$  state takes place. Nevertheless, the high statistics of the GASP data for the  $^{130}\text{Te} + ^{64}\text{Ni}$  system allowed us to establish prompt coincidences between the 2033 keV line and several transitions of Te isotopes with mass numbers  $A = 126$  to 122.

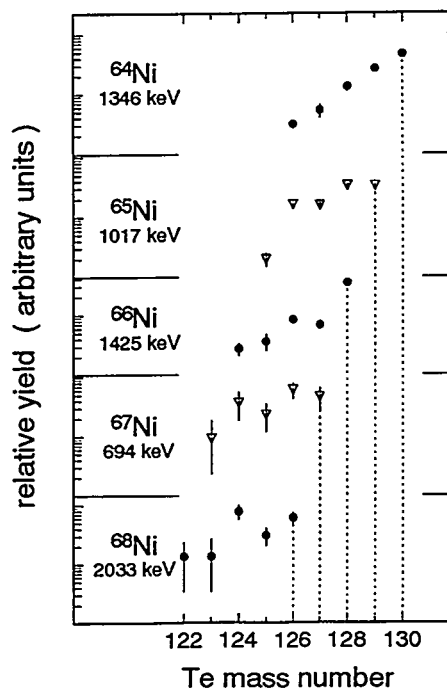


Figure 2. Distributions of Te isotopes established from  $\gamma$  cross-coincidences with the indicated gamma lines from  $^{64}\text{Ni}$  to  $^{68}\text{Ni}$ .

This pattern of Te partner products settles the assignment of the 2033 keV transition to the  $^{68}\text{Ni}$  nucleus, which is formed by a transfer of at least four neutrons to the  $^{64}\text{Ni}$  projectile and subsequent evaporation of zero to four neutrons from the primary products. The above result established also the ordering in the 814–2033 keV isomeric decay cascade, the 814 keV must be the expected  $5^- \rightarrow 2^+$  E3 isomeric transition. In order to strengthen this assignment we performed a separate experiment to measure the half-life of the isomer. This experiment was also performed with the GASP array at the INFN Legnaro, using the same  $^{130}\text{Te} + ^{64}\text{Ni}$  system and the beam pulsing in the range from micro- to milliseconds. Along with the  $\gamma$ - $\gamma$  coincidence data, single counts from all detectors were stored in the off-beam periods as a function of time. This singles data were clean enough to observe the isomeric decay and to select the beam pulsing condition (3 ms – on, 10 ms – off) for the main run used in the half-life determination. The obtained decay curves are displayed in Fig. 3. The weighted average gave the isomeric half-life of  $T_{1/2} = 0.86(5)$  ms, which indicates the 0.022 W.u. retarded 814 keV E3 transition and practically excludes the M2, M3 or higher multipolarity assignments. In all energy range there was no other line which could be attributed to the same isomer decay; specifically the upper limit of 3 % was set for the intensity of the presumed E5 cross-over transition. We concluded that the present results with high probability establish the expected  $5^-$  isomer in  $^{68}\text{Ni}$  decaying by a two transition E3–E2 cascade to the  $0^+$  ground state.

The high energy section of the prompt coincidence spectrum taken with the 2033 keV gate revealed the 1114 keV line; it is much weaker than the strong 814 keV isomeric transition, but clearly belongs to the nucleus and was also observed in the  $^{208}\text{Pb}$  target experiment. It established yet another state in  $^{68}\text{Ni}$ , lying 300 keV above the  $5^-$  isomer.

From the systematics we assigned tentatively this state as the  $4^+$  excitation, although the  $3^-$  assignment cannot be excluded.

In Fig. 4 the systematics of the lowest excited states in even nickel isotopes is displayed. The present results for the  $^{68}\text{Ni}$  isotope are outlined and compared with the shell model calculations shown to the right. The observed increase of the  $^{68}\text{Ni}$   $2^+$  state energy, by more than 600 keV compared to the  $^{66}\text{Ni}$ , indicates a significant subshell closure at neutron number  $N = 40$ . The  $5^-$  excitation, attributed predominantly to the  $p_{1/2}g_{9/2}$  configuration, moves down in energy when the subsequent neutron pairs shift the Fermi level towards the  $g_{9/2}$  orbital. As expected it attains the minimum energy at  $N = 40$  and becomes isomeric, which is very well reproduced by the calculations.

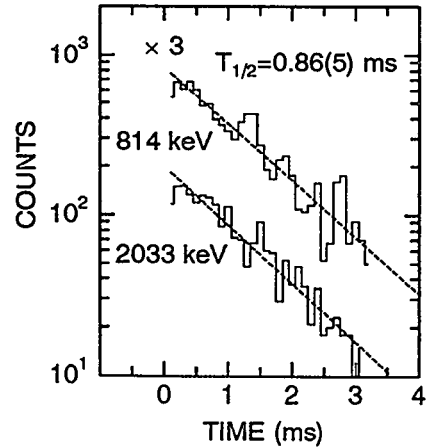


Figure 3. Decay curves for the  $5^-$   $^{68}\text{Ni}$  isomer.

The shell model calculations shown in Fig. 4 have been discussed in detail in Ref. [4]. Taking an inert  $^{56}\text{Ni}$  core and a  $p_{3/2}, f_{5/2}, p_{1/2}, g_{9/2}$  truncated model space, two approaches were used; one with a schematic modified surface delta interaction (MSDI) and the other (S3V) with realistic two-body matrix elements derived by Sinatkas et al. [5]. The results of the S3V approach generally better agree with experimental levels and for  $^{68}\text{Ni}$  they are presented in Fig. 4. The observed excellent agreement of the four known experimental levels with calculated ones nicely supports our spin-parity assignments.

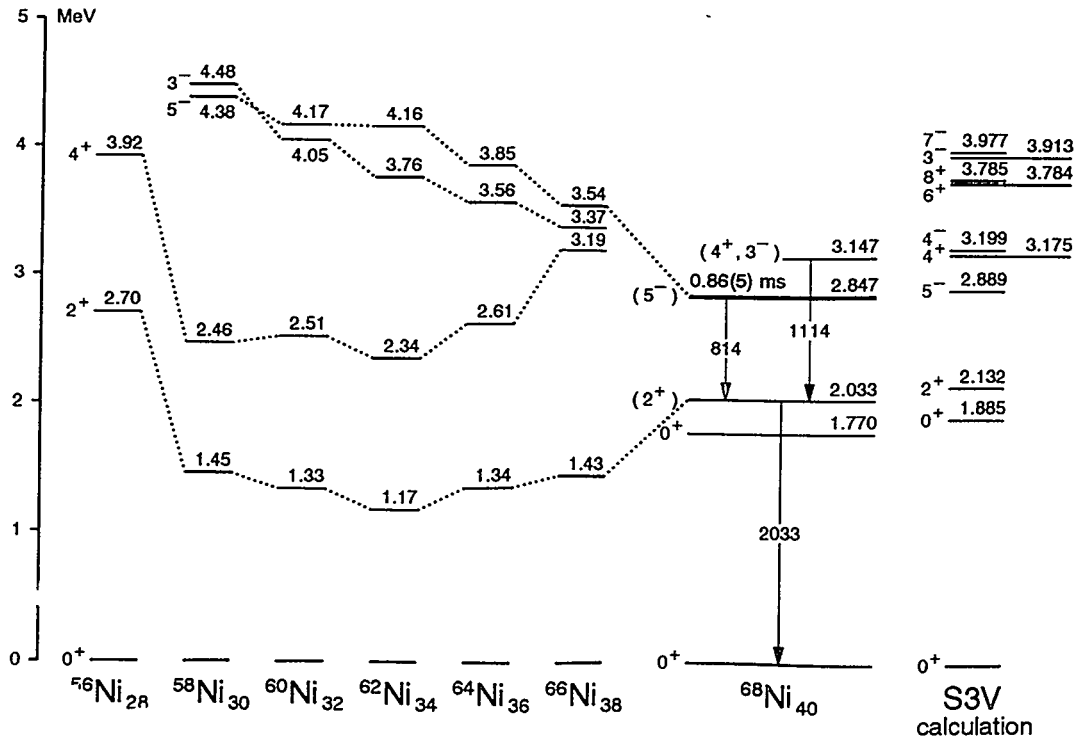


Figure 4. Systematics of selected states in even Ni isotopes. The  $^{68}\text{Ni}$  results are outlined and compared with the S3V shell model calculations (see text).

In the same time it is worthwhile to note that the calculated high spin  $6^+$ ,  $8^+$  and  $7^-$  states give a clear warning for future experimental attempts to locate these states. The  $g_{9/2}^2$   $8^+$  state might well be a long-lived isomer, which would significantly obscure the identification procedure.

Important result of the present work is the measured half-life of the  $5^-$  isomer, which gives the  $B(E3, 5^- \rightarrow 2^+) = 6.0(3) e^2(\text{fm})^6 = 0.022 \text{ W.u.}$  The calculated  $B(E3)$  value within the S3V approach for the E3 neutron effective charge  $1e$  gave the value of  $0.023 \text{ W.u.}$ , which is in surprisingly close, and probably accidental agreement with experiment. A corresponding E3 transition known in the  $^{90}\text{Zr}$  is 10 times faster with  $B(E3) = 0.22 \text{ W.u.}$  [1]. The shell model calculations performed in an identical way for  $^{90}\text{Zr}$  indicate that the structure of the involved  $5^-$  and  $2^+$  states is very similar to the  $^{68}\text{Ni}$  case and cannot account for the observed difference in the transition speed. The most probable explanation must be attributed to the much larger E3 effective charge for protons and to the different amplitudes of the  $2^+ \times 3^-$  component in the Zr and Ni  $5^-$  state structure. This collective component is not included in the shell model calculations, but the lower energy of the  $3^-$  excitation in Zr isotopes as compared to Ni nuclei may cause its more significant role in the  $^{90}\text{Zr}$  case and enhancement of E3 transition.

In conclusion, we have shown that the structure of neutron-rich nuclei can be successfully studied using the deep-inelastic processes in heavy-ion collisions. We have identified three new states in the  $^{68}\text{Ni}$ , which establish this isotope as the spherical shell model nucleus and indicates a significant subshell closure at the  $N = 40$  neutron number.

Further analysis in progress and future experiments are now directed towards a search for higher lying states in  $^{68}\text{Ni}$  and attempt to locate the  $8^+ g_{9/2}^2$  excitation. The perspectives to extend the search to even more neutron-rich Ni isotopes look also promising.

This work has been supported in part through the agreement on scientific cooperation between Poland and Italy and between Poland and Germany and by the Polish Scientific Committee under grant no. 224319203.

## References

- [1] L.P.Ekstrom and J.Lyttkens-Linden, *Nucl. Data Sheets* **67** (1992) 579.
- [2] C.J.Lister, M.Campbell, A.A.Chishti, W.Gelletly, L.Goettig, R.Moscrop, B.J.Varley, A.N.James, T.Morrison, H.G.Price, J.Simpson, K.Connell, O.Skeppstedt, *Phys. Rev. Lett.* **59** (1987) 1270.
- [3] M.Bernas, Ph.Dessagne, M.Langevin, G.Parrot, F.Pougheon, E.Quiniou, P.Roussel, *J. Physique Lett.* **45** (1984) 851.
- [4] T.Pawlat, R.Broda, W.Królas, A.Maj, M.Ziębliński, H.Grawe, R.Schubart, K.H.Maier, J.Heese, H.Kluge, M.Schramm, *Nucl. Phys.* **A574** (1994) 623.
- [5] J.Sinatkas, L.D.Skouras, D.Strottman, J.D.Vergados, *J. Phys. G: Nucl. Part. Phys.* **18**, 1377 and 1401 (1992).

# Gamma-ray Spectroscopy using Deep-inelastic Reactions

I. Y. Lee, B. Cederwall, M.-A. Deleplanque, R.M. Diamond, P. Fallon, A.O. Macchiavelli, L.Phair,  
F.S. Stephens, G.J. Wozniak

Lawrence Berkeley Laboratory, Berkeley, CA 94720

J.A. Becker, E.A. Henry

Lawrence Livermore National Laboratory, Livermore, CA 94550

P.F. Hua, D.G. Sarantites

Washington University, St. Louis, MO 63130

J.X. Saladin

University of Pittsburgh, Pittsburgh, PA 15260

C.H. Yu

University of Rochester, Rochester, NY 14627

Neutron rich nuclei are of particular interest since they might reveal new aspects of nuclear structure associated with an excess of neutrons, such as neutron skin and new shell structure and modes of excitation [1]. However, these nuclei have been very difficult to study until now, due to the lack of sensitivity of the available gamma-ray detector arrays. Currently, nuclear high spin states are produced almost exclusively by heavy ion induced fusion reactions and in a few cases by Coulomb excitation. Fusion reaction forms compound nuclei with angular momentum as high as  $70\hbar$ . However, with a stable beam and target, only neutron deficient nuclei can be produced by fusion reactions. Coulomb excitation can be used to study stable nuclei, and in deformed nuclei states with spin up to 30 can be populated. So far, high spin states in neutron rich nuclei and most of the odd-even and odd-odd nuclei near the stability line have not been studied due to the lack of suitable nuclear reactions. Deep-inelastic reactions have been shown to produce a high multiplicity of gamma-rays [2]. In reactions of rare-earth beams with rare-earth targets, a multiplicity of 40 has been observed [3,4]. In addition, neutron-rich nuclei such as  $^{177}\text{Tm}$ ,  $^{180}\text{Yb}$ , and  $^{184}\text{Lu}$  have been identified from  $\beta$ - $\gamma$  spectroscopy following Xe on W reactions [5]. Attempts have been made to use deep inelastic reactions to produce and study high spin states. Recent experiments have shown that states with spin up to 20 have been observed in an in beam study [6], and isomers with spin 10 have been identified in off-beam studies [7]. Since these reactions produce many final nuclei, a high efficiency gamma-ray detector array, such as Gammasphere, is needed to resolve the cascades through high fold coincidence measurement.

To test the feasibility of using deep-inelastic reactions to populate high spin states in neutron-rich products, we have carried out the reaction  $^{48}\text{Ca} + ^{176}\text{Yb}$  at beam energies of 250 and 275 MeV. A self-supporting metallic target with a thickness of about  $1\text{ mg/cm}^2$  was bombarded with a beam of  $2\text{ pnA}$  from the 88" cyclotron at LBL. A thin target was used to allow both the projectile- and target-like fragments to decay outside the target so that gamma rays from short lived high-spin states can be observed as sharp lines after Doppler shift correction. An annular Silicon strip detector with an inner diameter of 2 inches and an outer diameter of 4 inches was used to detect the scattered fragments. This detector covered polar angles from  $55^\circ$  to  $67^\circ$  with 16 concentric strips on the front surface and the full range of azimuthal angles with 16 sectors on the back surface. The early implementation of Gammasphere with 36 detectors was used to detect the gamma-rays. Coincidence events with at least one

fragment and two clean gamma rays detected were taken at a rate of 1000/sec.

The velocity vector of the target-like product was calculated from the measured energy and angle of the projectile-like product assuming a 2-body reaction and the Doppler-shift correction of the gamma rays was based on this vector and the direction of the gamma ray. Two- and three-fold gamma-ray-coincidence data were analyzed to determine level schemes. So far, gamma rays from Er, Tm Yb and Hf nuclei have been identified from this data set. Figure 1 shows the spectra of even-even nuclei from the two-fold data, and figure 2 compares the spectra of  $^{178}\text{Yb}$  from single gated two-fold and double-gated triple data. It is obvious that in order to study the weakly populated nuclei such as  $^{178}\text{Yb}$  the three-fold data are essential. The production cross sections of these nuclei, determined from the gamma ray yields of the low spin states are shown in Figure 3. About 10 nuclei around the target  $^{176}\text{Yb}$  have been identified. As expected, the distribution drifts from the target in the direction of smaller neutron and proton number. Nuclei with more neutrons or protons than the target have smaller yield than nuclei with fewer neutrons. This is partly due to the equilibration of the neutron-to-proton ratio of the projectile and target and partly due to the evaporation of neutrons from the excited fragments. With this setup, we were able to study nuclei produced with a cross section as low as 0.1 mb/sr. It is estimated that about 20 projectile-like nuclei and a comparable number of target-like nuclei are produced with cross section greater than 0.1 mb/sr. So far, some even-odd and odd-odd nuclei, such as  $^{173}\text{Yb}$  and  $^{174}\text{Tm}$  (which are expected to be produced from the systematics of the yield distribution), were not identified because very little is known about their level schemes.

The gamma-ray yield of even-even Yb nuclei as a function of spin is shown in figure 4. It can be seen that states with spin as high as 20 can be populated in this reaction. The yields decrease when the spin increases at about the same rate for all nuclei except for  $^{176}\text{Yb}$  which has a higher yield at low spin most likely due to additional contributions from quasi-elastic reactions (e.g. Coulomb excitation). Before this study, only a few transitions in the yrast band were known in  $^{175,177}\text{Yb}$  and  $^{178}\text{Yb}$ . This work extended the yrast band of  $^{178}\text{Yb}$  to spin 12 and both signatures of yrast bands in  $^{175,177}\text{Yb}$  to spin about 20.

Figure 5 shows the moment of inertia of the Yb nuclei as a function of rotational frequency. The new results of  $^{178}\text{Yb}$  give a rather flat moment of inertia curve which indicates a small value for the interaction strength of the  $i_{13/2}$  neutron AB crossing. The expected sharp backbend is likely occur just above spin 12. It would be interesting to observe higher spin states with more statistics or using a reaction which makes products with higher angular momentum.

In conclusion, we have established that with a high efficiency gamma-ray array, it is possible to study neutron rich nuclei produced in deep inelastic reactions. These reactions extended the range of nuclei for high spin structure study in the neutron rich direction by about 10 neutron numbers. With more powerful gamma ray detector arrays being constructed, it will soon be possible to increase the sensitivity by a factor of 10. We are also planning to use a heavier projectile to bring more angular momentum into the products.

- [1] W. Nazarewicz, This proceedings.
- [2] P. Glassel et. al., Phys Rev. Lett. 38(1977)331.
- [3] R. J. McDonald et. al., Nucl. Phys. A373(82)54.

- [4] A. J. Pacheco et. al., Nucl. Phys. A397(1983)313.
- [5] K. Rykaczewski et. al., Nucl. Phys. A499(1989)529.
- [6] H. Tokai et. al., Phys. Rev. C38(1988)1247.
- [7] R. Broda et. al., Phys.. Rev. Lett. 68(1992)1671.

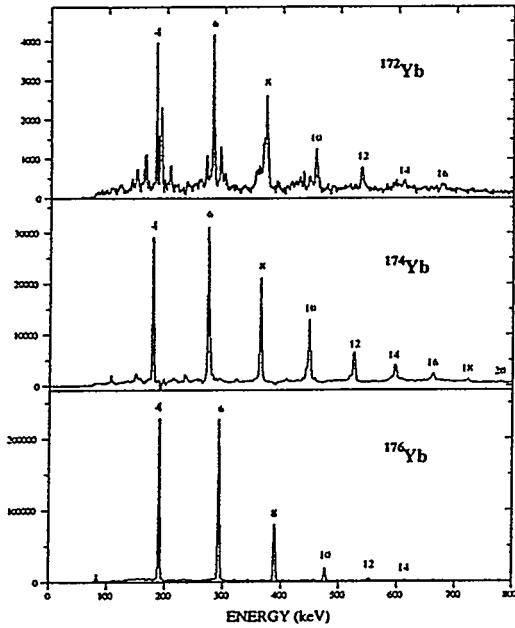


Figure 1. Spectra of  $^{172,174,176}\text{Yb}$  from double- $\gamma$ -coincidence data.

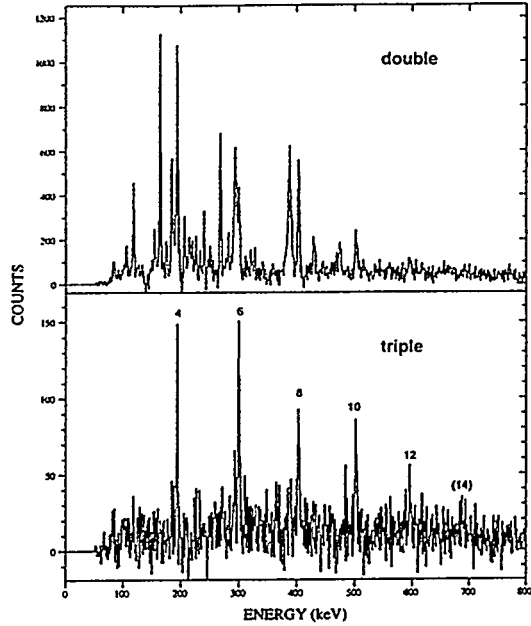


Figure 2. Spectra of  $^{178}\text{Yb}$  from double and triple coincidence data.

**48Ca + 176Yb 250 MeV, 55 - 67 degree**

**production cross section (mb/sr)**

						<b>178Hf</b>	
						<b>0.1</b>	
		<b>172Yb</b>	<b>174Yb</b>	<b>175Yb</b>	<b>176Yb</b>	<b>177Yb</b>	<b>178Yb</b>
		<b>0.53</b>	<b>3.1</b>	<b>2.4</b>	<b>38.1</b>	<b>0.8</b>	<b>0.1</b>
<b>169Tm</b>			<b>173Tm</b>				
			<b>0.3</b>				
		<b>170Er</b>					
		<b>0.25</b>					

Figure 3. Production cross sections of target-like nuclei deduced from gamma-ray yields.

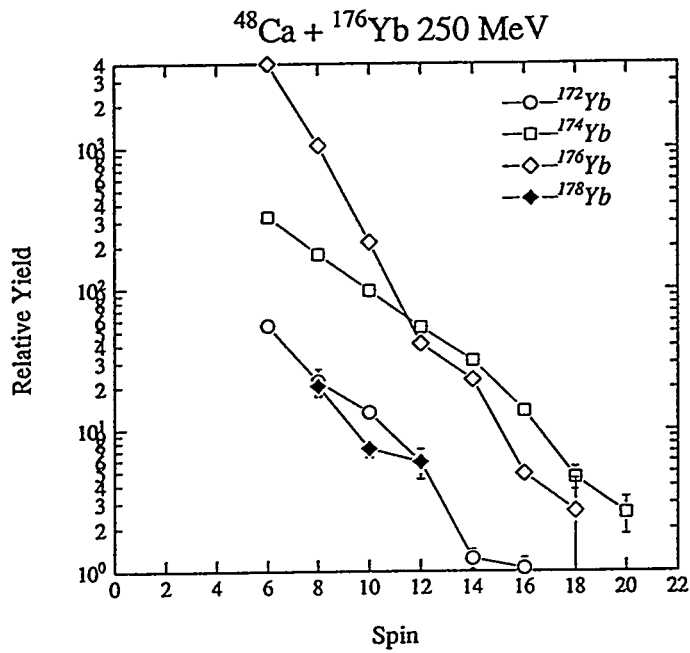


Figure 4. Gamma-ray yield of Yb nuclei as a function of spin.

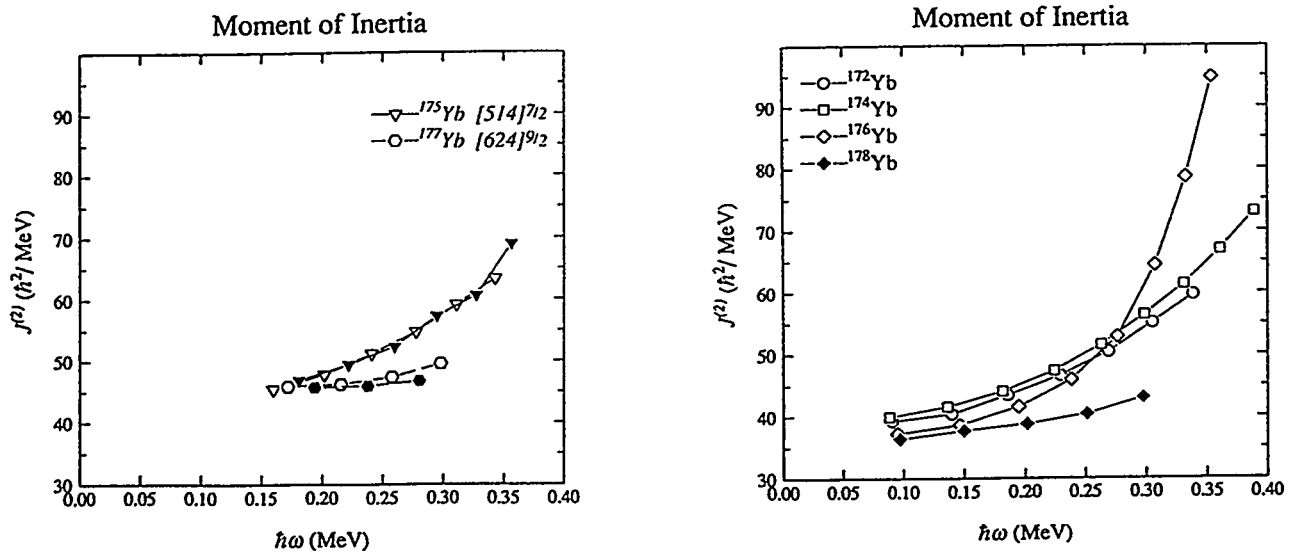


Figure 5. Moment of inertia of Yb nuclei determined from this work.



## IMPRESSIONS I

J F Sharpey-Schafer

*Oliver Lodge Laboratory, The University, Liverpool, L69 3BX, UK*

My first impression of this conference is that it has been a VERY GOOD MEETING! This has been partly due to the great enthusiasm of the participants and the excellence of the physics they have been presenting, but also due to the very pleasant surroundings and the perceptive skills of our hosts, the Conference Organisers.

I was delighted by the many new things I learnt at this conference. Not only new physics but even new ploys of conferencepersonship (TLK please note!). There were many such ploys but I will mention only a few, which I formulate as:

### Sharpey's Rules:

1. (first day) "If you are not sure you have understood the question, ask for it to be translated into Russian". In these circumstances I at least will then be utterly sure that I have indeed not understood the question.
- n. (yesterday) "Don't read what is in Teng Lek Khoo's mind". This is a quote from Robert Janssens and was triggered by Teng Lek's enthusiasm running away with him causing him to receive a delegation of three irate persons.
- p. (reminder) "Buy David Radford a pint". The  $\gamma$ -ray spectroscopy community owes a large debt to David Radford of Chalk River Laboratories, who has unselfishly supplied his \*\*\*\* 8R data analysis software [1] to all and sundry. He has even overcome the difficulties caused by different versions of the utterly standard UNIX!

There were many excellent talks at this conference and I have only time to mention a sub-set which made a particular impact with me personally.

The conference started with Ben Mottelson who seems to have taken a new lease of life since his involvement with ECT\* in Trento. No doubt he has been inspired by the ambience, flair and culture of Italy. Not only nuclear physics, but physics in general, owes a great deal to Ben for his many contributions to our subject. But most impressively he has, over many years, inspired so many of us with his enthusiasm and love of a really intriguing problem to solve. We all witnessed this in his talk, the first of this conference, on the staggering of energy levels in some superdeformed bands [2].

Thomas Dossing has also been inspired [3]. In his case by the ambience, flair and culture of Chicago. At last we had a clear insight into the effects of rotational damping in

the  $\gamma$ -ray continuum. The nub of his message was that: "Rotation keeps the nucleus warm". Sylvia Leoni went on to discuss experiments testing Thomas' theories. She makes an excellent job of putting over very complex analysis succinctly and very quickly. She is helped in this by the fact that she can speak at least twice as fast as her mentor, Bent Herskind. I understand that Sylvia was trained by her mother who can still speak twice as fast again as Sylvia! More importantly, a new phenomenon had been observed [4]: that there are strongly correlated decays in the continuum.

The  $\Delta I = 4$  staggering of superdeformed energy levels discussed by Mottelson and Pavlichenkov is very complex to establish experimentally. A clear and accurate picture of the difficulties and results was given by Bo Cederwall. But, in masterly form and maintaining a very long standing reputation, Joe Hamilton pointed out that almost similar effects could be seen in data on normally deformed nuclei taken by himself and his colleagues some 10 to 15 years ago.

The discovery [5] of discrete superdeformed states in  $^{152}\text{Dy}$  had an enervating effect on nuclear spectroscopy. Firstly, it turns out that different regions of superdeformation in the nuclear chart have very different properties and physics. Secondly, it caused us all to look at nuclei of ANY shape in a new and more critical light. This has inspired us to look for new phenomena, other than superdeformation, and to return to look at some of the old results from a new angle.

A new area of superdeformation near  $A = 80$  has been found by the Oak Ridge/Washington University groups [6,7] and was discussed by Dave Cullen and Demetrios Sarantites. The systematics of the bridging superdeformation between  $A = 130$  and  $A = 150$  has been investigated by the McMaster/Chalk River groups using the  $8\pi$  spectrometer. These data for  $N = 80$  were discussed [8] by Simon Mullins. The glimpse of hyperdeformation seen by the Chalk River groups [9] in the  $^{120}\text{Sn}(^{37}\text{Cl},\text{pxn})$  reaction was confirmed in an experiment at GA.SP discussed [10] by Giuseppe Viesti. Clearly the new very efficient  $\gamma$ -ray spectrometer arrays will have to devote a special effort to determine if this sighting is real or a mirage.

Paul Nolan reminded us that actually the FIRST discrete superdeformed band was seen [11] almost 10 years ago in  $^{132}\text{Ce}$ . Recently excited and identical superdeformed bands have been seen [12] in the  $A = 130$  region. The observation and understanding of the decay out of the superdeformed bands in the  $A = 130$  region has been a triumph for the Legnaro/Padua groups using GA.SP. Santo Lunardi showed the most beautiful systematics of level mixing in the decays out of superdeformed bands in  $^{133,135,137}\text{Nd}$ .

A wealth of data has been taken in the last few years on excited bands in the superdeformed wells of  $A \sim 150$  nuclei. This was illustrated [12] by Con Beausang who showed several weakly excited SD bands in  $^{152}\text{Dy}$ . These data establish  $^{152}\text{Dy}$  as having a doubly magic superdeformed configuration and give clues to the lowest particle-hole excitations across the closed shells. Con even found crop circles and goats in his colourful 2-D plots using "quantum chromatic enhancement". Later, certain disrespectful ex-research

students of mine, even found old goats in their data! Both Beausang, and later Ben Crowell in  $^{190}\text{Hg}$ , showed [12,13,14] bands which had evidence for their decays to the yrast superdeformed bands. Both of them speculated that these decays could be caused by the excited bands having octupole vibrational components in their structures.

A new development has been the ability to observe the M1 cross-transitions between signature partner superdeformed bands. Jean Duprat described [15] how these had first been used to determine the single particle neutron g-factors in  $^{193}\text{Hg}$  and then these measurements had been extended to the odd proton nucleus  $^{195}\text{Tl}$  and to neutron-proton configurations in  $^{194}\text{Tl}$ . M1 transitions between superdeformed bands have also been seen [12] in  $^{133}\text{Pr}$  by the Liverpool/Grenoble groups.

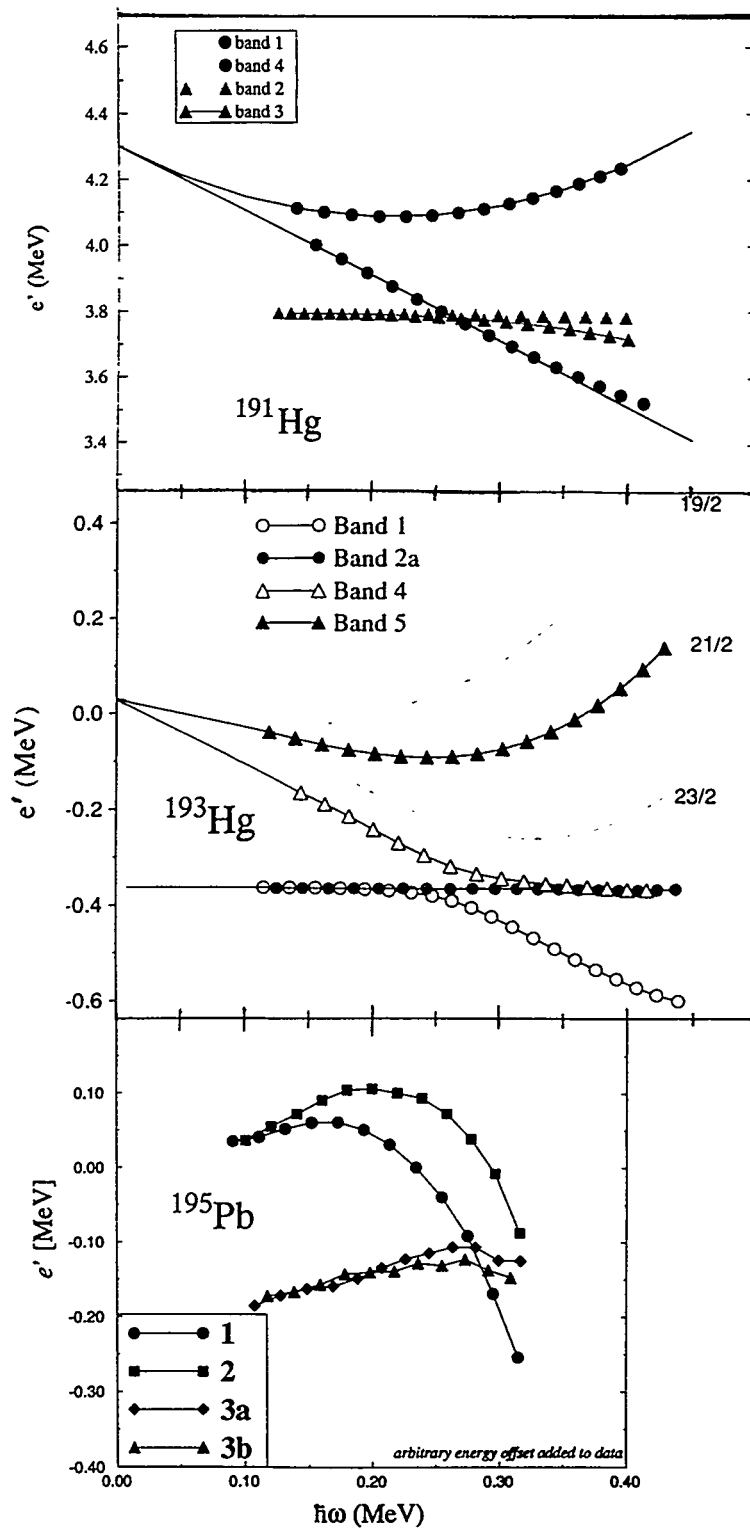
There have been many searches for superdeformed bands in odd mass Pb nuclei, but without success until now. The prize goes to the Livermore group, using the early implementation of Gammasphere, who have found SD bands in both  $^{195}\text{Pb}$  [16] and  $^{193}\text{Pb}$  [17]. These data add to the beautiful data, shown in a poster [18] by the Argonne group, on signature splitting in the  $j_{15/2}$   $N = 7$  neutron superdeformed band. The progressive decrease in the observed [18,19,16] signature splitting from  $^{191}\text{Hg} \rightarrow ^{193}\text{Hg} \rightarrow ^{195}\text{Pb}$  is shown in fig. 1. As Flocard pointed out in his talk [20], it is data like these that are making the severest test of calculations and the *a priori* effective interactions used.

There were many talks graphically illustrating that the big  $\gamma$ -ray spectrometer arrays are not just about the physics of superdeformation. Among the most interesting talks were those on the physics of high-K structures and on different types of terminating bands. Very impressive systematic data has been obtained on traditional high-K isomers and the bands built upon them by the Canberra groups lead by George Dracoulis. In his talk [21] Dracoulis discussed the way pairing was killed by the progressive increase in the number of excited quasi-particles. This was illustrated by measurements [22] in  $^{177}\text{Ta}$ , where the neutron and proton pairing strengths were calculated as a function of spin. He also showed that the properties of the bands built on the high-K isomers changed as the pairing strength declined.

Different types of terminating bands were discussed at this conference. The great expansion in our knowledge of discrete states at spins between 40 and 50  $\hbar$  at normal deformations was revealed in the talks of Simpson [23] and Riley [24]. The  $^{157,158}\text{Er}$  nuclei can form a stable oblate mean field at spin 40  $\hbar$  and above. The structure and configurations of the bands that terminate are now well established [25,26] for both positive and negative parity bands in both nuclei. The terminating bands in Er and Dy nuclei were referred [27] to by Ragnarsson as "abrupt" terminations. He contrasted these with what he called "smooth" terminations, evidence for which had been observed by Fossan and his group [28] in nuclei near  $^{109}\text{Sb}$ .

A subject not mentioned so much at this conference were very recent and interesting results on fission. It is clear that the data on superdeformed bands in Hg, Tl and Pb nuclei contain information on how much angular momentum a nucleus can hold before it fissions.

Fig. 1 Routhian plots of superdeformed bands showing the signature splitting of the  $N = 7$   $j_{15/2}$  orbitals in  $^{191}\text{Hg}$  [18],  $^{193}\text{Hg}$  [19] and  $^{195}\text{Pb}$  [16].



The recent data [29] on the observation of superdeformation in an  $\alpha 4n$  channel leading to  $^{192}\text{Hg}$  shows that the variation of intensity of the superdeformed band with angular momentum is independent of whether the original compound nucleus was Hg or Pb. This shows that the  $\alpha$  particle, at least, is emitted by the compound nucleus before it decides to fission or not to fission. Additionally, recent analysis at Orsay [30] of fission fragment spectra from fission that has taken place in competition with reactions leading, after neutron evaporation, to the nucleus  $^{194}\text{Pb}$  show that the fission is symmetric and is centred on  $^{194}\text{Pb}$  itself. This suggests that most fission, at low fusion energies, takes place *after* charged particle and neutron emission so that this kind of fission is a *slow* process taking place  $10^{-16}$  to  $10^{-15}$  s after fusion and competing directly with  $\gamma$ -decay. I am convinced that the new big arrays will open up new fields of nuclear physics that we can study using  $\gamma$ -ray spectroscopy and that the fission process after fusion will be one of these new fields.

To conclude: I have the distinct impression that our subject of nuclear spectroscopy near the Coulomb Barrier is in the best possible shape that a research area could hope to be. Mother Nature continues to shower us with her bounties! I am continually amazed what complex, elegant entities nuclei are and I cannot understand why we have such good fortune in our collective ability to find new physics in these delectable little laboratories. Indeed those of us who have had the guts to stick with  $\gamma$ -ray spectroscopy, in the face of dire prognostications of the usual uncreative Jonahs and in spite of siren calls to burn ourselves in intermediate energy collisions and mythical quark-gluon plasmas, will continue to give our funding agencies very good value for money. Personally I am very glad that I have not been searching for an inapplicable "equation-of-state" in collisions dominated by multifragmentation. (I have always failed to understand why they are not looking for a "fundamental equation" for nuclear matter. Perhaps they had not got round to reading Callen's nice book on Thermodynamics [31]?) After much work it appears that multifragmentation etc at energies near 1 GeV/amu are entirely dominated by the normal statistics of the available phase space. It does not seem much of a fun result to me! I am slightly more charmed by the search for the quark-gluon plasma. However, as a well known East Coast physicist once said: "The trouble with the quark-gluon plasma is that it is too dense to get the signal out". There are a very few nice experiments in this field, for instance those which show that the strange quark is thermalized [32]. But, I will bet that we observe  $\gamma$ -rays in a hyperdeformed nuclear mean field before a clear signal of the existence of the quark-gluon plasma is measured!

In nuclear spectroscopy we are enjoying ourselves and being very creative. We are in good shape. Our techniques and data are elegant and beautiful. We are continually finding new phenomena and the theories we use have intellectual bite. The protagonists in this research are fascinated by it and are full of enthusiasm. We are confident that the future of our subject is very bright.

## References

1. D.C. Radford, Proc. Int. Seminar on the Frontier of Nucl. Spectr., ed. Y. Yoshizawa, H. Kusakari and T. Otsuka, World Sci. (1993) p229.
2. B.R. Mottelson; these proceedings.
3. T. Dossing; these proceedings.
4. S. Leoni; these proceedings.
5. P.J. Twin, B.M. Nyakó, A.H. Nelson, J. Simpson, M.A. Bentley, H.W. Cranmer-Gordon, P.D. Forsyth, D. Howe, A.R. Mokhtar, J.D. Morrison, J.F. Sharpey-Schafer and G. Sletten; Phys. Rev. Lett. 57 (1986) 811.
6. D.M. Cullen; these proceedings.
7. D.G. Sarantites; these proceedings.
8. S.M. Mullins; these proceedings.
9. A. Galindo-Uribarri, H.R. Andrews, G.C. Ball, T.E. Drake, V.P. Janzen, J.A. Kuehner, S.M. Mullins, L. Persson, D. Prévost, D.C. Radford, J.C. Waddington, D. Ward and R. Wyss; Phys. Rev. Lett. 71 (1993) 231.
10. G. Viesti; these proceedings.
11. P.J. Nolan, A.J. Kirwan, D.J.G. Love, A.H. Nelson, D.J. Unwin and P.J. Twin; J. Phys. G11 (1985) L17.
12. P.J. Nolan; these proceedings.
13. B.F. Crowell; these proceedings.
14. B.F. Crowell, R.V.F. Janssens, M.P. Carpenter, I. Ahmad, S. Harfenist, R.G. Henry, T.L. Khoo, T. Lauritsen, D. Nisius, A.N. Wilson, J.F. Sharpey-Schafer and J. Skalski; Phys. Lett. B333 (1994) 320.
15. J. Duprat; these proceedings.
16. L.P. Farris; these proceedings.
17. R. Hughes et al; to be published.
18. M.P. Carpenter et al; contributions to this conference, p31.
19. M.J. Joyce et al; Phys. Lett. B (in press).
20. H. Flocard; these proceedings.
21. G.D. Dracoulis; these proceedings.
22. M. Dasgupta, P.M. Walker, G.D. Dracoulis, A.P. Byrne, P.H. Regan, T. Kibédi, G.J. Lane and K.C. Young; Phys. Lett. B328 (1994) 16.
23. J. Simpson; these proceedings.
24. M.A. Riley; these proceedings.
25. J. Simpson, M.A. Riley, S.J. Gale et al; Phys. Lett. B327 (1994) 187.
26. S.J. Gale, J. Simpson et al; J. Phys. G (in press).
27. I. Ragnarsson; these proceedings.
28. D.B. Fossan; these proceedings.
29. J. Duprat et al; Z. Phys. A349 (1994) 5.
30. M.G. Porquet et al; to be published.
31. H.B. Callen; "Thermodynamics" 2 ed. Pub. Wiley (New York).
32. E. Andersen et al (NA36 collaboration); Phys. Lett. B294 (1992) 127; B316 (1993) 603 and B327 (1994) 433.  
J. Rafelski, H. Rafelski and M. Danos; Phys. Lett. B294 (1992) 131.

## IMPRESSIONS, PERSPECTIVES.

B. Herskind,

The Niels Bohr Institute, University of Copenhagen, Denmark

The nuclear structure field and in particular the branch of high spin physics, the topic of this conference held in one of its "homelands", Berkeley, is a very rich one indeed, as we all have witnessed during the present week. As expressed in the previous talk so brilliantly, there are a wealth of new "Physics from Large  $\gamma$ -ray Detector Arrays", explored in great detail from both the experimental and the theoretical side. It is almost trivial to note, that the two-sided viewpoints and inspirations, is one of the basic reasons for the tremendous progress obtained every year, perhaps most typical demonstrated this time by Ben Mottelson's stimulating discussion of C4 symmetries, and Francis Beck's report of the latest news from EUROGAM II, showing an even more accurate and convincing determination of the energy differences in the observed staggering of a superdeformed band in  $^{149}\text{Gd}$ .

I myself, has been strongly stimulated and strengthened in my beliefs, that it is not a too ambitious goal for us to talk about "Complete Spectroscopy", in the sense that it may be possible soon with the rapid advances in  $\gamma$ -spectroscopy, both on the experimental and theoretical side, to obtain a completely satisfactory description of the nuclear spectra produced in compound-, transfer-, or Coulex reactions, self-consistently, with respect to both discrete and quasi-continuum structures. In general, we would like to learn much more about the influence of rotation on the nuclear structure, the breaking of the time reversal symmetries in the intrinsic frame, the deviation from the mean field description, quenching of the static pair correlations and the role of pairing at the highest spin, the role of higher multipoles, exotic shapes and shape fluctuations and much more. Most of this must be learned from the quantal structure of the lowest lying states at high spin. As shown by Thomas Døssing in his talk the regular rotational bands and configurations accessible to discrete spectroscopy is limited to  $\approx 10$  bands on the average for each parity and signature, before the branching between the bands become dominating at higher excitation energies  $E^* - E_{yrast} \leq 800$  keV. Above this region, with the exception of high-K- and strongly deformed (SD) bands, we may have to be satisfied with analysis methods and theoretical comparisons of the statistical type such as analyzing fluctuations [1], covariances, auto-correlations, [2] nearest-neighbor distributions, strength distributions,  $\Delta_3$ -statistics and distributions of curvatures as discussed so enthusiastically by Sven Åberg.

However, we still have a lot to learn before this goal is reached. So far it seems that the most important information comes from one of the two parameters of the  $\gamma$ -ray spectra, the *transition energy*  $E_\gamma$ . When occurring in rotational cascades, it can be conveniently transformed into rotational frequency  $\hbar\omega$ , static and dynamical moment of inertia,  $\mathfrak{S}^{(1)}$  and  $\mathfrak{S}^{(2)}$ , relative alignments  $i$  and excitation energy of the configurations, and thereby almost directly compared to calculated configurations.

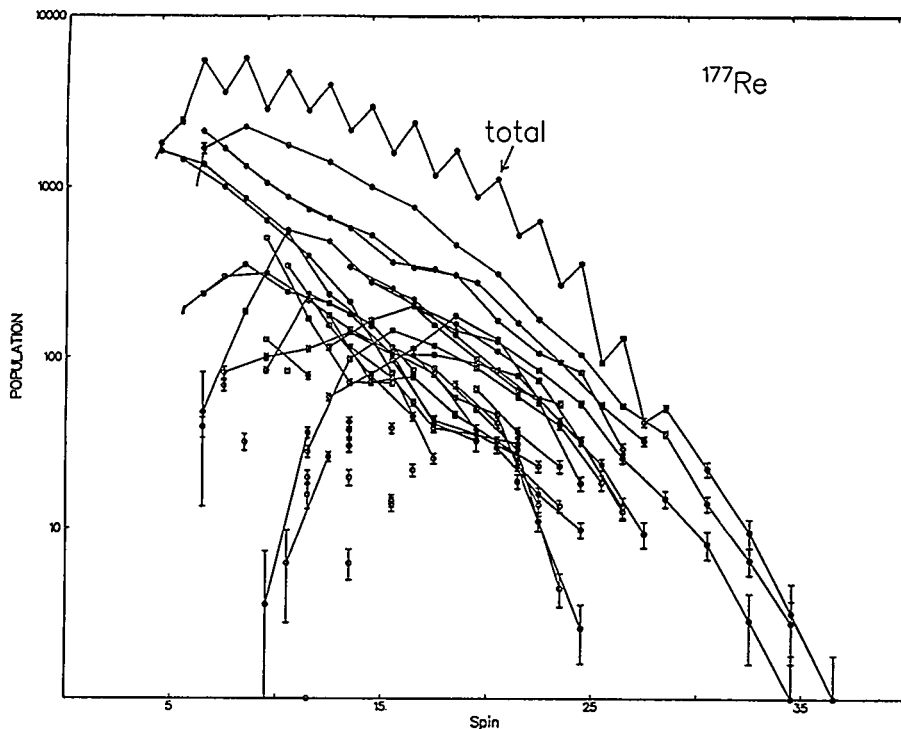


Figure 1: *Population intensity observed for the rotational bands in  $^{177}\text{Re}$ . The curve marked "total" correspond to the sum of all observed transitions for a given  $I \rightarrow I-2$ . The second highest curve correspond to the intensity of the yrast transitions, showing a weak staggering effect. The data is taken from [9].*

The second parameter in the spectra the *intensity*,  $N_\gamma$  is much more difficult to make useful, and hitherto not so popular. Nevertheless, it may be noted that the accuracy obtained by modern analysis methods, most exquisitely represented by the RADWARE package, developed by David Radford, and now used extensively in discrete line spectroscopy, for the determination of the transition energy and intensity of the discrete lines in spectra are very good. Because self-consistency with respect to the intensity balances required by the proposed level scheme is taken into account, the values reach a very high confidence level. In fact, in studies of the quasi-continuum, the intensity relations are the most important element in the analysis.

I therefore would like to take this opportunity to advocate for a more complete analysis scheme to be developed, in which also the *intensity* of the spectral distributions plays an equally important role.

Let me first show a couple of very interesting examples of discrete line intensities, which have not been discussed at this meeting, the first from an analysis of Robert Bark et. al. [3] for a study of  $^{177}\text{Re}$  on NORDBALL. Components of more than 30 rotational bands have been identified in this work, for which the intensity of many of the bands have been extracted and plotted in fig. 1. The total, equal to the sum of all the observed intensities shows a very strong even-odd spin staggering, whereas the yrast line shows a "C4" type staggering. If the sidefeeding intensity



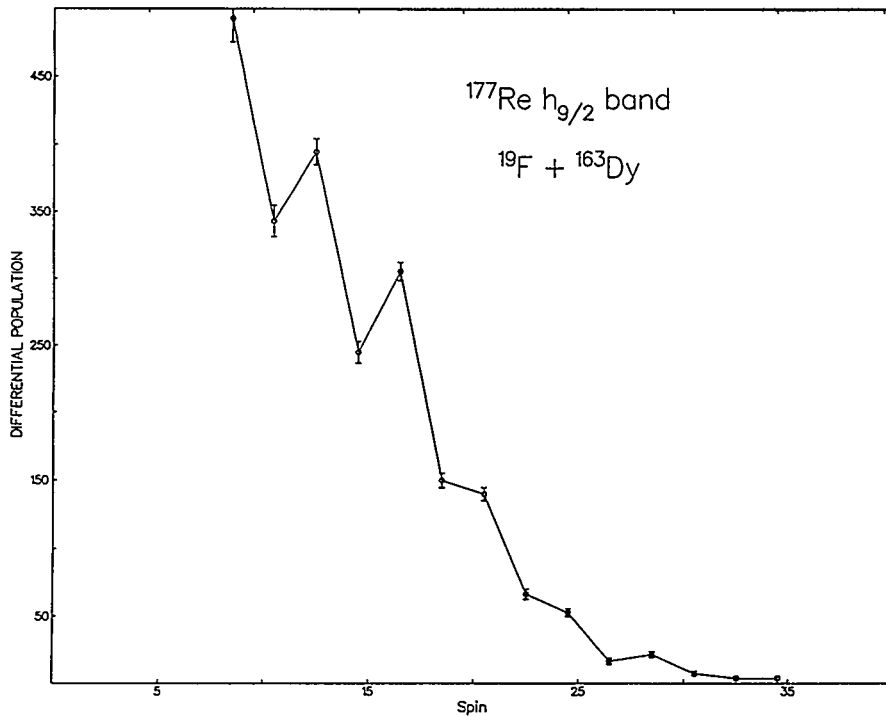


Figure 2: The sidefeeding intensity of the yrast band in  $^{177}\text{Re}$  corresponding to the "differential population" of the yrast line shown in fig. 1.

for the yrast band is plotted as shown in fig. 2, the "C4" effect is rather clear.

In the second example I would like to refer to the talk given by P. Twin in the "Perspective in Nuclear Structure 1993" Symposium last summer [4], where the population intensity of the superdeformed yrast band in  $^{152}\text{Dy}$  is shown to be almost 50 % larger with "symmetric reactions",  $^{74}\text{Ge}(^{82}\text{Se},4n)$ , compared to the most frequently used  $^{108}\text{Pd}(^{48}\text{Ca},4n)$  asymmetric reactions when formed at the same excitation energy, high enough to reach the highest angular momentum in the fusion reaction. The data is shown in fig. 3. We would indeed like to understand these, as well as many other effects identified by the intensity.

Secondly, I am concerned about some of the many beautiful comparisons we have seen presented at this meeting, often with extremely good agreement between parameter values deduced from the experimentally determined transition energies and similar values calculated in very simplified models sometimes without pairing correlations and most often without considering the effects of residual interactions. By adjusting f.ex. the deformation parameters for each configuration independently, it seems possible to describe the observed structures quite well. *On the other hand, we know now that it is necessary to include the two body residual interaction in the Hamiltonian before diagonalization*, to be able to describe the features in the quasi-continuum, e.g. the damped rotational motion. It may be interesting in this connection to see how large effect the Surface Delta Interaction (SDI) [5] also will have on the lowest lying discrete bands. Referring to the cranking calculations of Matsuo et.al. [6], and Vigezzi et.al. [7], discussed by Thomas Døssing and Silvia

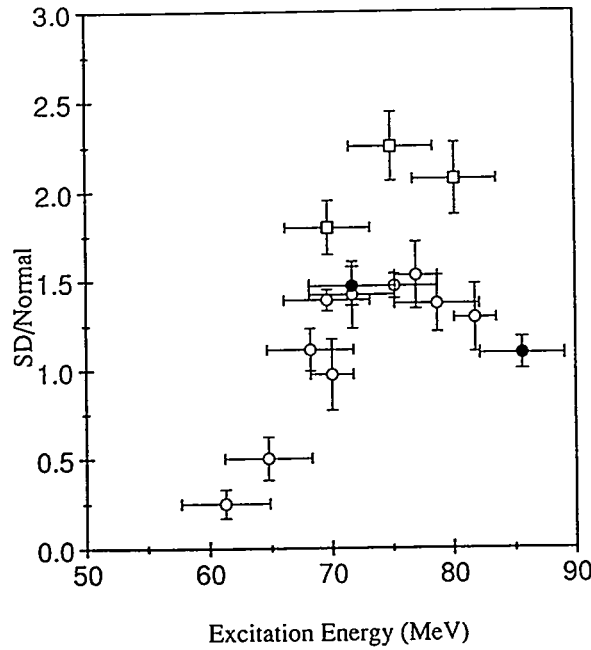


Figure 3: The fraction of SD cascades relative to the total population of the  $^{152}\text{Dy}$  channel (as measured from the 68 ns  $17^-$  isomer) as function of the excitation energy in the  $^{156}\text{Dy}$  compound nucleus. The data points are: open circles and closed circles from the  $^{108}\text{Pd}$  ( $^{48}\text{Ca}, 4n$ ) reaction using TESSA3 or EURO GAM I in Daresbury, respectively, whereas the squares are from the  $^{74}\text{Ge}$  ( $^{82}\text{Se}, 4n$ ) reaction. The figure is from ref. [4].

Leoni, I would like to show in fig. 4 the energy differences obtained with or without the SDI included in the diagonalization, calculated as function of spin for the lowest 3 configurations of each parity and signature. Only values for  $I \geq 30$  are considered here, since pairing correlations are not included in these calculations. Although the interaction strength on average is in the order of  $V=10$  keV, large differences of typically 200 keV are observed for the individual configurations, though in some cases as shown for the lowest lying parity, signature  $(\pi, \alpha) = (-, 1)$  states in fig. 4, the deviation can be as large as 600 keV. However, parts of these shifts, are associated with the low multipoles of the interaction, and may be accounted for by quasi-particle BCS transformation, and minimization of the energies of the mean field with respect to deformation.

The effect from residual interactions are large on the energies, as demonstrated in fig. 4, but even larger indeed on the intensities as shown in fig. 5, where the lowest 9 states of  $(\pi, \alpha) = (-, 1)$  in  $^{168}\text{Yb}$  also have been discussed in [6]. The predictions show here a very large branching  $n_{branch} \equiv (\sum 1/w_{ij}^2)^{-1} = 2.17$  of the decay strength already for the 5-th state at an excitation energy of 720 keV. Here  $w_{ij}$  is defined as the fraction of rotational strength from a level  $i$  at spin  $I$ , going to level  $j$  at spin  $I-2$ . It is conceivable that the sensitivity of the new  $\gamma$ -ray arrays will be high enough to accurately investigate these branchings in the higher excited states, at least until the branching  $n_{branch}$  become significantly larger than 2. The branching out of the decay is found to depend crucially on the higher multipoles of the residual interaction.

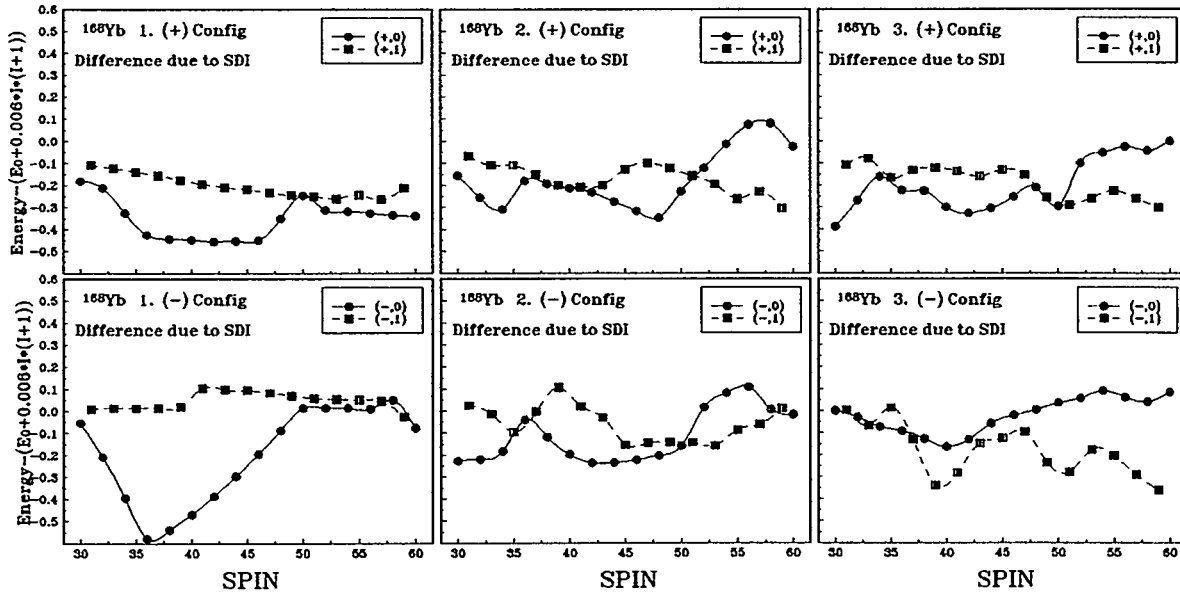


Figure 4: Energy differences as function of spin for the lowest 3 configurations of each parity and signature in  $^{168}\text{Yb}$  calculated in the cranking model of [6] with or without SDI included in the diagonalization of the Hamiltonian.

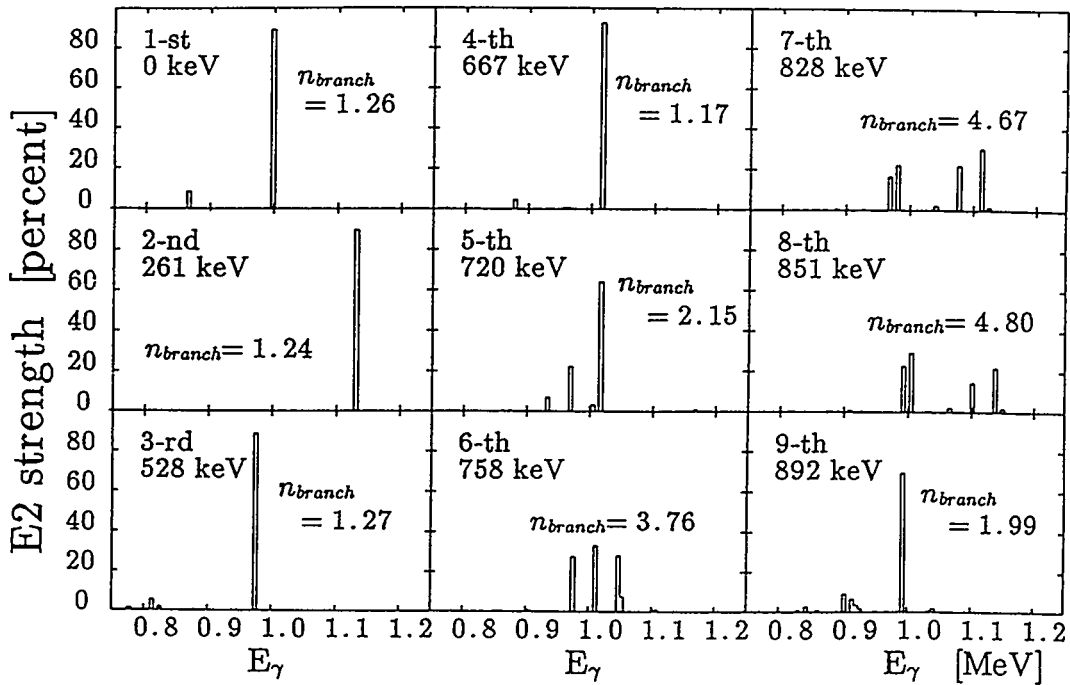


Figure 5: The calculated rotational  $E2$  strength distributions as function of the  $\gamma$ -ray energy for the lowest 9 levels with  $(\pi, \alpha) = (-, 1)$  in  $^{168}\text{Yb}$  at  $\omega = 0.5$  MeV. The branching number as well as the energy counted from the yrast line are also shown for each level.

To be able to make an overall comparison between the accurately determined experimental observables,  $E_\gamma$ ,  $N_\gamma$ ,  $I$ ,  $\tau$  and corresponding quantities calculated within the different models discussed at this conference we need a good, flexible and interactive *decay model*. Let me illustrate what I mean by referring to the model of Coulomb excitation [9] and the original "de Boer-Winther" code as well as the more extended versions, which have been extremely useful during the last 3 decades for the study of states which are accessible to Coulomb excitation. For the study of very high spin states we need similar models to "completely" describe the well understood decay process of competing E1, E2 and M1 transitions of  $\Delta I = 0,1,2$  types, from the entry states formed in the reactions to the final states at the yrast line, via a flow through microscopically calculated levels. The distribution of transition strength, for each decay step may be deduced from band mixing calculations and adapted as in the well known COULEX case. It is anticipated that one may start with calculated levels and transition strengths based on a given model, like the examples shown from the cranking model of Matsuo et. al. with SDI interactions included, [6] and then allow for adjustments of the matrix elements most sensitive to the observables by an interactive iterative procedure. In this way one may study the important differences between the model under investigation and the experimental data in a more global way.

A more complete decay model may also consider the decay between discrete structures within different potential barriers, and at higher excitation energies competition with evaporated particles and spontaneous fission. The latter type of calculations may be needed to explain the population intensity puzzle, shown in fig. 3.

The principles of the procedures discussed above are sketched in fig. 6. The first and most simple comparisons in this scheme would be the experimental and theoretical level schemes, which with the proper input by the help of RADWARE can be produced in very flexible forms for comparisons. More sensitive comparisons may be made by the standard analysis techniques, but as the level statistics improve in the coming years, I am convinced that the statistical analysis techniques almost exclusively used to day for the study of the quasi-continuum, will be very useful in discrete line spectroscopy as well.

I am happy to say that this is not only a dream, since the first steps towards reality has been taken, although at the moment mostly aiming at quasi-continuum studies, by the development of the simulation model for discrete decay of A. Bracco et. al. [8,7], and briefly discussed by Thomas Døssing and Silvia Leoni at this conference. In this model the first 400 levels for each parity and signature, including strength functions and full branchings between all possible states are inserted, with extrapolations to higher excitation energies according to expectations from the damping model. So far only E2( $\Delta I=2$ ) and E1( $\Delta I=0$ ) are considered. Let me within this framework show you in fig. 7 and 8 how theoretical level schemes including the expected feeding and intensity patterns looks like for the lowest lying 10 bands of  $(\pi, \alpha) = (+, 0)$  for  $I \geq 20 \hbar$ , for different intensity limits. It is clearly seen in these

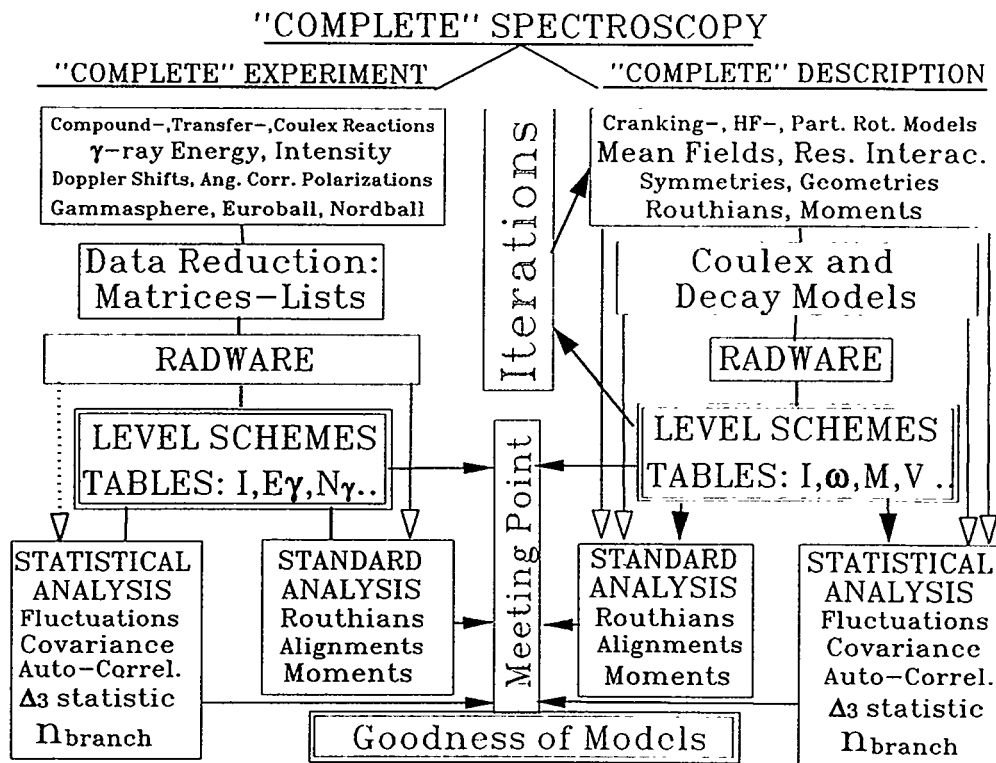


Figure 6: The principles of the "complete" analysis scheme discussed in the text is shown.

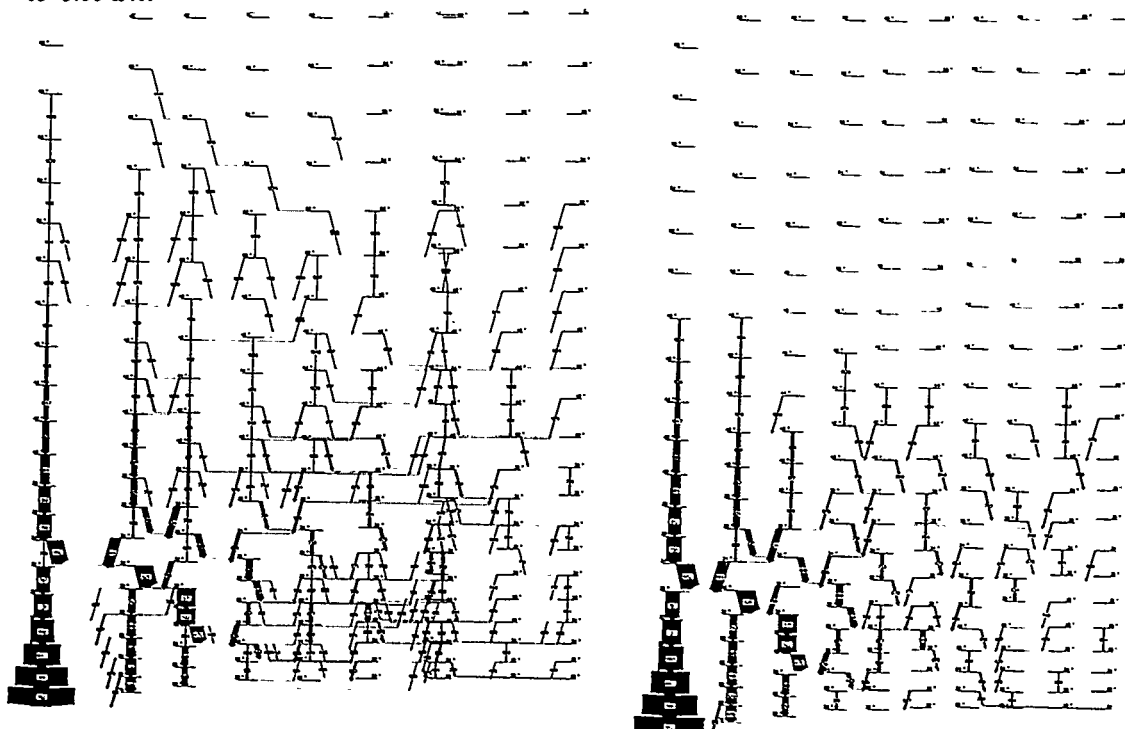


Figure 7: The calculated level scheme for  $^{168}\text{Yb}$  for the lowest 10 levels of  $(\pi, \alpha) = (+, 0)$  from spin 20-60  $\hbar$ . The 112 E2 transitions found to be above 0.5 % of the total intensity going into  $^{168}\text{Yb}$  are shown in the right part of the figure. In the left part 247 E2 transitions are shown with an intensity limit of 0.05 %. The figure is based on simulation calculations of S. Frattini, as discussed in [8,7].

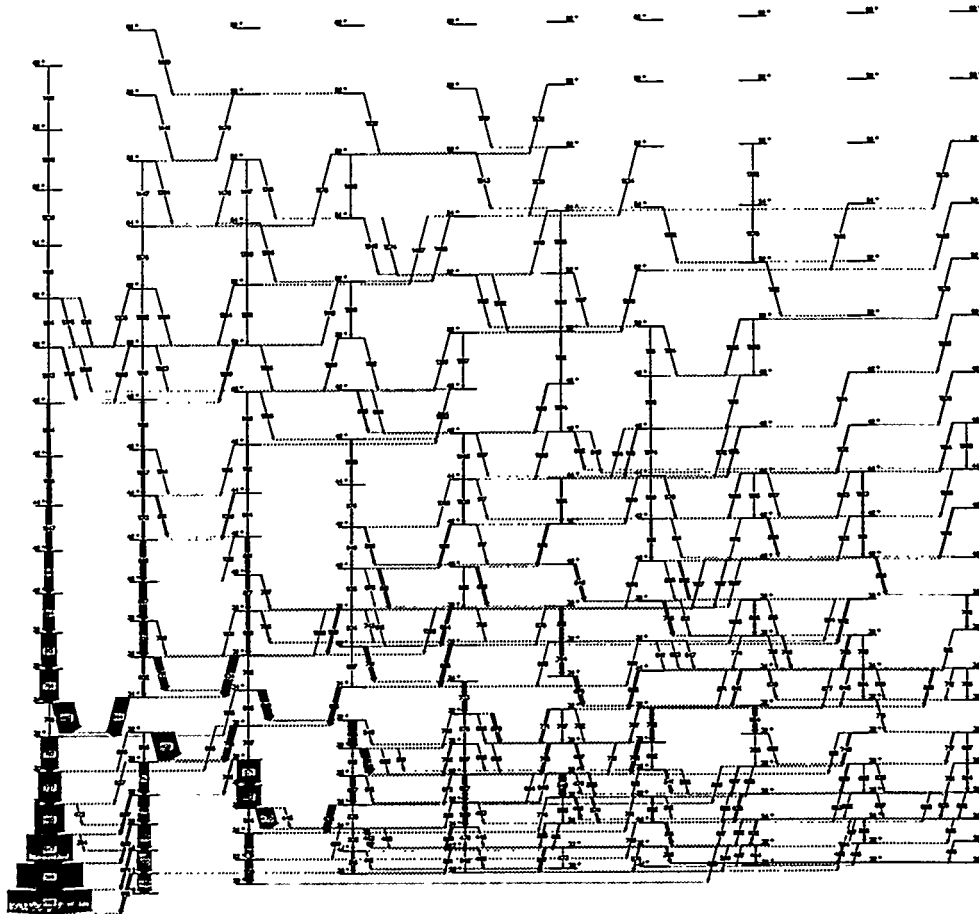


Figure 8: *The calculated level scheme for  $^{168}\text{Yb}$  for the lowest 10 levels of  $(\pi, \alpha) = (+, 0)$ . 361 rotational E2 transitions with an intensity larger than  $4 * 10^{-5}$  are shown. The figure is based on calculations of S. Frattini, as discussed in [8,7].*

two figures how the spectrum become much more complex, depending on the sensitivity of the experiment. The spectrum shown in fig 8 would roughly correspond to the "discrete" structures one may expect to see in  $^{168}\text{Yb}$  with  $(\pi, \alpha) = (+, 0)$ , below the on-set of rotational damping at higher excitation energies, using a powerful array as EUROGAM II. Please note the significant branching between the many close lying states even in this cold region, a type of branching only very rarely observed to day. With NORDBALL or GASP one may rather expect to see the spectra shown in fig 7 in the right and left part respectively, with much less branching because the sensitivity limit is too poor to observe the branching. It is also noted that in the right part of fig 7, only 3 regular rotational cascades are observed, (shown with vertical arrows) together with bits and pieces of the other bands. After the full GAMMASPHERE and EUROBALL III come into operation, within a few years the tools would be available indeed to find the most of the branchings which are there, although I must say that it will still be quite a challenge to study a level scheme, where only one quarter above  $I = 20 \hbar$  is shown in fig. 8, in full detail. If we wish to see the branchings in the full angular momentum range, for normally deformed nuclei, with "standard feeding" a selectivity for intensities of  $10^{-6}$  may be required.

The work has been supported by the Danish Natural Science Foundation. Stimulating discussions with T. Døssing, R. Bark, S. Frauendorf, G. Hagemann, M. Matsuo, and E. Vigezzi are gratefully acknowledged.

## References

- [1] B. Herskind, A. Bracco, R.A. Broglia, T. Døssing, A. Ikeda, S. Leoni, J. Lisle, M. Matsuo and E. Vigezzi, *Phys. Rev. Lett.* **68**, (1992), 3008
- [2] T. Døssing, B. Herskind, S. Leoni, M. Matsuo, A. Bracco, R. A. Broglia, and Vigezzi, To be published in *Physics Report* (1994).
- [3] R. Bark, G.B. Hagemann, B. Herskind, H.J. Jensen, W. Korten, M. Bergström, A. Brockstedt, H. Carlsson, A. Norlund, H. Ryde, P. Bosetti, S. Leoni, P. Tjøm and F. Ingebretsen, (to be published).
- [4] P. Twin, *Nucl. Phys.* **A574** (1974) 51c.
- [5] I. M. Green and S.A. Mozkowski, *Phys. Rev.* **139**, B790 (1965).
- [6] M. Matsuo, T. Døssing, B. Herskind, S. Frauendorf, *Nucl. Phys.* **A564** (1993) 345-365.
- [7] E. Vigezzi, S. Frattini, P. Bosetti, A. Bracco, R.A. Broglia, T. Døssing, B. Herskind, S. Leoni and M. Matsuo, in *Proc. of the Workshop on Heavy-Ion Fusion: Exploring the Variety of Nuclear Properties, Padova 1994*, to be published.

- [8] A. Bracco, S. Frattini, P. Bosetti, T. Døssing, B. Herskind, S. Leoni, M. Matsuo and E. Vigezzi. Proc. of VII Int. Conf. on Nuclear Reaction Mechanisms, Varenna 1994, E Gadioli ed., to be published.
- [9] K. Alder and Aa. Winther *Electromagnetic Excitations, Theory of Coulomb Excitation with Heavy Ions*, North-Holland, Amsterdam, (1975.), see also same authors, Academic Press, New York, (1966).



# IMPRESSIONS

Ikuko HAMAMOTO

Department of Mathematical Physics, University of Lund, Lund, Sweden.

Since I am the last one of those three speakers who talk about the impressions of this conference, I thought that the previous two speakers would already cover all interesting subjects, before I got a chance to say something. The topics, which were not particularly mentioned by the previous two speakers and which were of my personal interests, were, among others, recent developments in the field of multiple phonon states (especially talked by D.Schwalm and W.Korten) and identical bands (by several speakers). However, instead of expressing my impressions about those topics, I would like to use this opportunity to talk about " $\Delta I = 4$  structure" (or alternatively, we call it " $\Delta I = 2$  staggering") in superdeformed rotational bands, supplementing B.Mottelson's talk [1] given at the very beginning of this conference. Since Mottelson talked about all basic points of our model [2], I myself would rather concentrate on showing some numerical examples so as to discuss the result of the model in comparison with available experimental data.

Taking the Hamiltonian which satisfies the required geometry [1, 2]

$$H = AI_3^2 + B_1(I_1^2 - I_2^2)^2 + B_2(I_1^2 + I_2^2)^2 \quad (1)$$

where  $A$  is a large positive value and  $B_1 = 1$ , the regular  $\Delta I = 4$  structure for the rotational bands,  $A1$  and  $B1$ , in even- $A$  nuclei and for all rotational bands in odd- $A$  nuclei may be obtained if we choose vanishing or very small values of  $|B_2|$ .

First, we present the case of  $B_2 = 0$ . In fig.1 (fig.2) we show calculated splittings of the yrast quartet for three values of  $A$  around 100 (500). The figure is obtained by a direct diagonalization of the Hamiltonian and plots the eigenvalues of the lowest  $A1$  state from which a smooth averaged  $I$ -dependent term has been subtracted. The definition of the smooth part,  $\Delta E_\gamma^{ref}(I)$ , is exactly the same as the one used in ref. [3]. Corresponding to the semi-classical treatment in which the tunneling amplitude involves a factor,  $\cos[\frac{\pi}{2}(I - \sqrt{\frac{A}{4B_1}})]$ , in the quantal problem the calculated  $\Delta I = 2$  staggering vanishes when the equation

$$I - \sqrt{\frac{1}{4}(\frac{A}{B_1} - \frac{3}{2}\hbar^2)} = \text{odd integer} \quad (2)$$

is satisfied irrespective of the value of  $I$  being integer or half-integer. For even-integer  $I$ -values and  $B_1 = 1$  eq.(2) is satisfied for  $A = 5.5, 37.5, 101.5, 197.5, 325.5, 485.5, \dots$ . Accordingly, the phase of the staggering for  $A < 101.5$  (485.5) is opposite to that for  $A > 101.5$  (485.5) in fig.1 (fig.2). From figs.1 and 2 we see that the  $A$  value cannot be taken much larger than 100 (for an already fixed value

of  $B_1 = 1$ ) if we should approximately obtain the amount of  $\Delta I = 2$  staggering which is reported presently for superdeformed bands [3, 4, 5]. For larger values of  $A$  the calculated amplitude of  $\Delta I = 2$  staggering becomes very small quickly as  $I$  increases. For this reason, we employ a value of  $A$  to be around 100 in all numerical examples presented in the following.

From figs.1 and 2 it is seen that for an  $I$ -independent  $A$  value the  $\Delta I = 2$  staggering amplitudes decreases monotonically as  $I$  increases. More precisely speaking, this monotonical decrease occurs for values of  $A > 26.5$ . For  $I$ -independent values of  $A < 26.5$  the calculated amplitudes of  $\Delta I = 2$  staggering in fact increases as  $I$  increases. However, we find that for such small values as  $A < 26.5$  the rotational axis does not stay localized in the equatorial plane for the angular momentum values of our present interests. Observed  $\Delta I = 2$  staggering amplitudes do not seem to show a simple monotonic decrease as  $I$  increases. However, from figs.1 and 2 it is seen that if we take, for example, a mild  $I$ -dependence of parameter  $A$ , which may easily be expected in superdeformed bands, we can make the calculated amplitudes of the  $\Delta I = 2$  staggering  $I$ -independent or even an increasing function of  $I$ . In all three superdeformed bands in  $^{194}\text{Hg}$  a phase inversion of the  $\Delta I = 2$  staggering seems to be observed experimentally [4]. The phase inversion cannot be obtained for  $I$ -independent parameters,  $A$  or  $B_1$ , with the condition  $B_2 = 0$ . However, the inversion can be obtained at a value of  $I$ , if parameters  $A$  and/or  $B_1$  vary so that eq.(2) is satisfied while  $I$  (= integer or half-integer) increases by two units.

Secondly, we present the result with the parameter  $B_2 \neq 0$ . Taking the values of  $B_1 = 1$  and  $A \approx 100$ , the value of  $B_2$  must be appreciably smaller than, say 0.02, in order to ensure that the rotation is about an axis lying approximately in the equator, if we are interested in the region of angular momentum up till  $60\hbar$ . In fig.3 calculated amplitudes of the  $\Delta I = 2$  staggering obtained from the quantum-mechanical diagonalization are plotted for three values of  $B_2$ , choosing  $A = 101.5$  for which the staggering vanishes for  $B_2 = 0$ . Calculated increasingly larger amplitudes of the staggering for  $B_2 = +0.01$  in the region of  $I > 50$  in fig.3 is a sign of the fact that the system is going to rotate about the  $C_{4v}$  axis (= 3-axis). For  $B_2 = -0.01$  the staggering phase is opposite and the staggering amplitude decreases for larger values of  $I$ . The decrease of the  $\Delta I = 2$  staggering amplitudes for larger  $I$ -values is generally obtained for  $B_2 < 0$ , since in the classical treatment (see, ref.[1, 2]) the energy of the minima (=  $B_2 I^4$ ) is then rapidly decreasing while the energy of the saddle points increases as  $I$  increases.

In the semi-classical treatment with  $B_2 \neq 0$  (but  $|B_2| \ll 1$ ) we can obtain the expression for the real part of the action

$$\Re S_{12} = \frac{\pi}{2} \left( I - \sqrt{\frac{A}{4B_1}} \right) + B_2 \frac{\pi}{2} \left( \frac{1}{4\sqrt{AB_1}} I^2 + \frac{\sqrt{A}}{8B_1\sqrt{B_1}} \right) \quad \text{for } I > \sqrt{\frac{A}{4B_1}} \quad (3)$$

The appearance of the  $I^2$  inside the parentheses in the second term on the r.h.s. already indicates that the presence of an appreciable amount of the  $B_2$  term in the

Hamiltonian in (1) destroys the regular  $\Delta I=4$  structure. However, since here we have assumed  $|B_2| \ll 1$  the contribution of the  $B_2$  term to the real part of the action is anyway small. Nevertheless, the expression of this contribution indicates the possibility of inverting the phase of  $\Delta I=2$  staggering at some  $I$  values, even when we keep the parameters in the Hamiltonian to be  $I$ -independent. The phase inversion is expected to occur for an  $I$  value which is larger or smaller than the  $I$  value that satisfies the condition (2) (with a given integer value on r.h.s.) depending on the sign of  $B_2$ , since the second term on the r.h.s. of (3) depends linearly on  $B_2$ . In fig.4 calculated amplitudes of the  $\Delta I=2$  staggering obtained from the quantum-mechanical diagonalization are shown for  $A=120$ . We note that the phase inversion is observed for  $B_2 = +0.01$  around  $I = 44$ , namely for a positive value of  $B_2$  since  $A = 120 > 101.5$ .

Up till now all numerical examples of the  $\Delta I=4$  structure have been taken from rotational bands with even- $I$  values in even- $A$  nuclei. As the third example, I demonstrate that the behaviour of the  $\Delta I=2$  staggering can be quite different between even-even and odd- $A$  nuclei or between signature partners in odd- $A$  nuclei, even if the parameters,  $(A, B_1, B_2)$ , are exactly the same. Since the parameters which satisfy eq.(2) are different, depending on whether the angular momentum  $I$  is even-integer or odd-integer or  $\frac{1}{2} \pmod{2}$  or  $-\frac{1}{2} \pmod{2}$ , the staggering amplitude for a given set of parameters is, in general, different depending on those four cases of  $I$  values. Thus, within our present model we may state, for example, that so-called identical superdeformed bands may show, in general, different  $\Delta I=2$  staggering behaviour. Taking  $A=100$ ,  $B_1=1$  and  $B_2=0$ , in fig.5 the calculated  $\Delta I=2$  staggering for the yrast  $A1$  band with even-integer  $I$  values is compared with that for the yrast  $E1'$  band with  $I = \frac{1}{2} \pmod{2}$ . Since in the case of even-integer  $I$  values the parameters are very close to those which satisfy eq.(2), the staggering amplitude is pretty small for the  $A1$  band. In fig.6 we compare the calculated  $\Delta I=2$  staggerings of two signature-partner bands in odd- $A$  nuclei, choosing  $A=90$ . Namely, the yrast  $E1'$  band with  $I = -\frac{1}{2} \pmod{2}$  and the one with  $I = \frac{1}{2} \pmod{2}$ . For  $A=90$  we observe a clear difference between the staggering amplitudes of the signature-partner bands. Within the present model the difference of the  $\Delta I=2$  staggering behaviour in signature-partner bands is a sensitive function of the  $A$ -value.

## References

1. B. Mottelson, talk given in this Conference.
2. I. Hamamoto and B. Mottelson, Phys. Lett. **B333** (1994) 294.
3. S. Flibotte et al, Phys. Rev. Lett. **71** (1993) 4299.
4. B. Cederwall et al, Phys. Rev. Lett. **72** (1994) 3150.
5. B. Cederwall et al, talk given in this Conference.

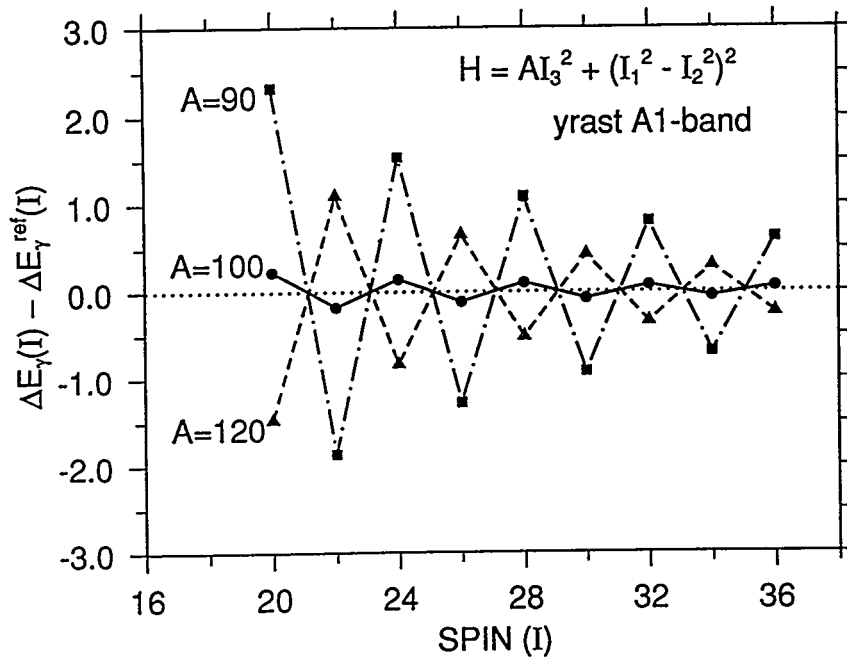


Figure 1 : Splittings of yrast quartet. The figure is obtained by direct diagonalization of the rotational Hamiltonian and plots only the eigenvalue of the lowest  $A_1$  state from which a smooth averaged  $I$ -dependent term has been subtracted [3]. The effect of the  $I$ -independent phase shift in eq.(2) is clearly visible ; for the value  $A=101.5$  the  $\Delta I=4$  term completely vanishes.

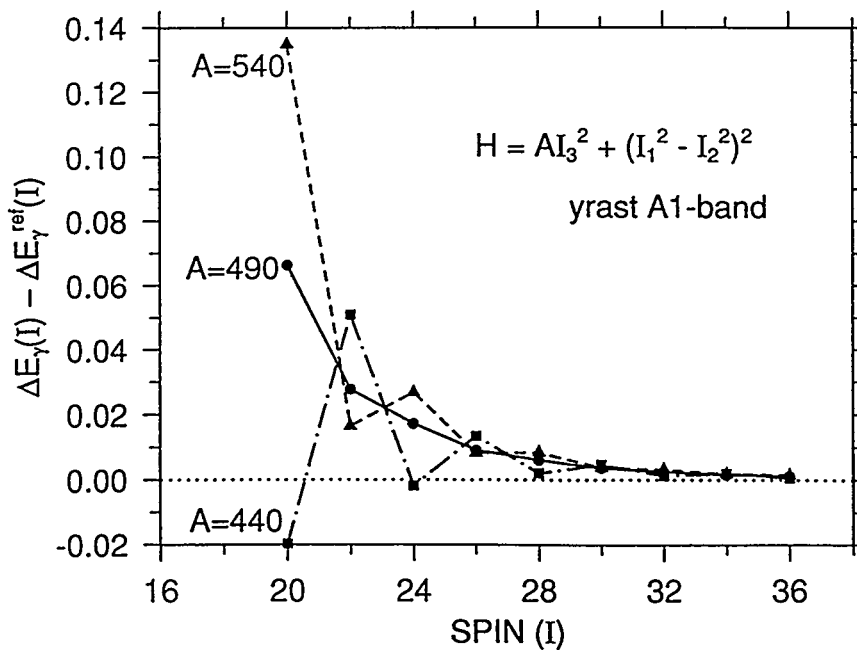


Figure 2 : The same as in fig.1, but for  $A$  values around 500 . For the value  $A=485.5$  the  $\Delta I=4$  term completely vanishes.

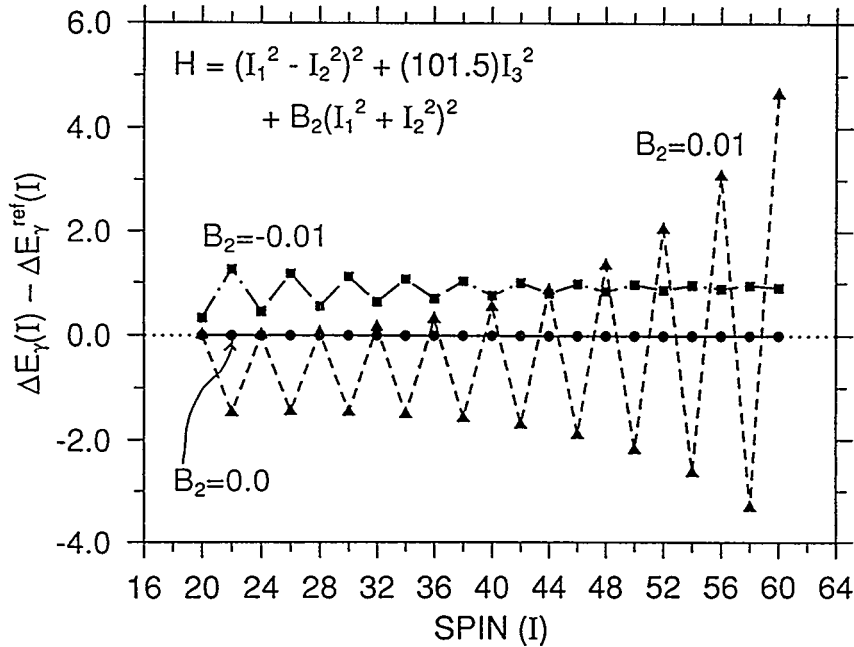


Figure 3 : Effect of introducing small nonzero values of  $B_2$  parameter on calculated  $\Delta I=2$  staggering structure of the yrast  $A_1$  band. The figure is obtained from the quantum-mechanical diagonalization. The value of  $A=101.5$  is chosen so that the calculated staggering vanishes exactly for  $B_2 = 0$ . The values for  $B_2 = -0.01$ ,  $0.0$ , and  $+0.01$  are denoted by filled squares, filled circles, and filled triangles, respectively.

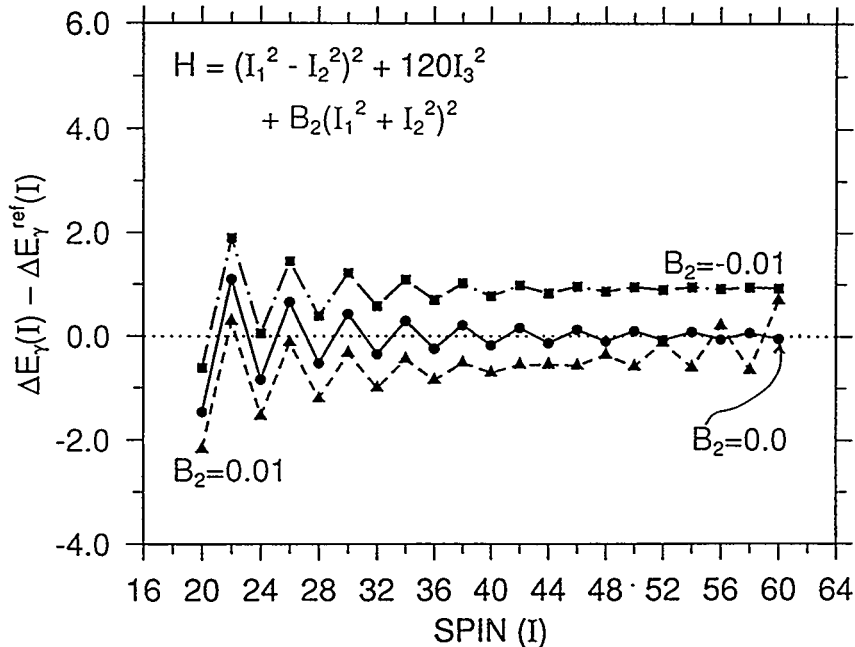


Figure 4 : The same as in fig.3 except used values of  $A$ . For  $A = 120$  the staggering appears also for  $B_2 = 0$ . The values for  $B_2 = -0.01$ ,  $0.0$ , and  $+0.01$  are denoted by filled squares, filled circles, and filled triangles, respectively. For  $B_2 = +0.01$  the phase inversion of the staggering occurs around  $I = 44$ .

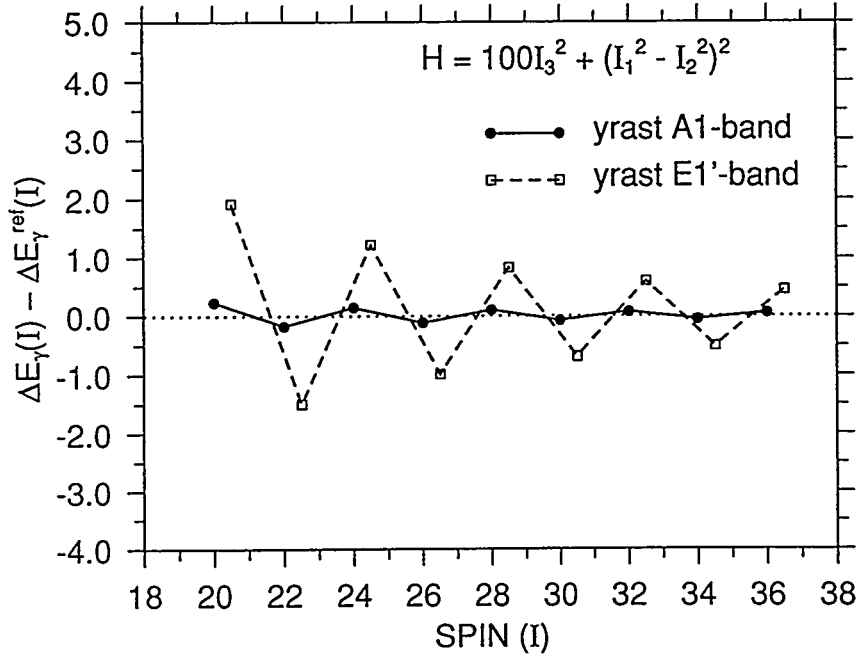


Figure 5 : Comparison between the  $\Delta I=2$  staggering for the yrast A1 band with even  $I$  values with that for the yrast  $E1'$  band with  $I = \frac{1}{2} \pmod{2}$  values.

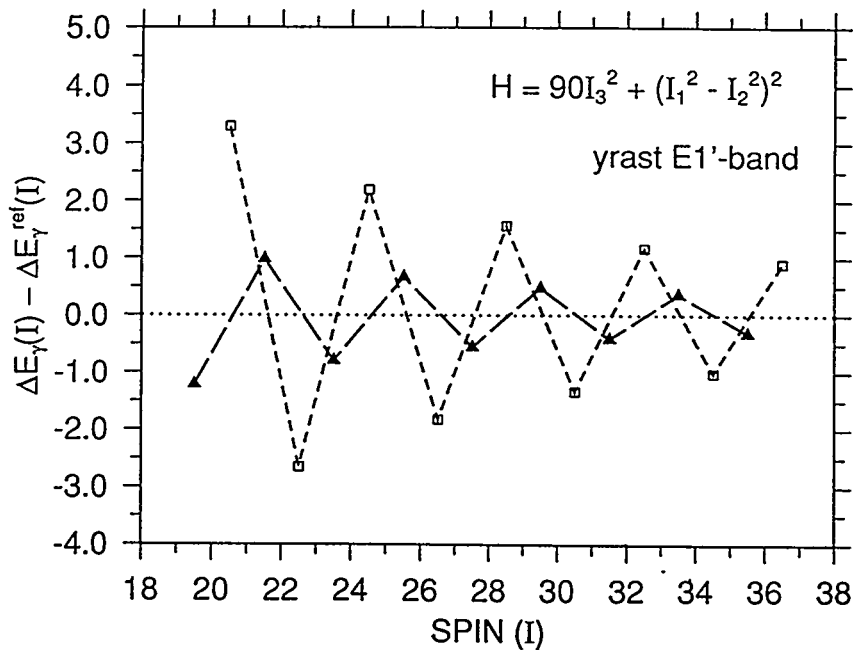


Figure 6 : Comparison between the  $\Delta I=2$  staggering for the two signature-partner bands. Namely, the yrast  $E1'$  band with  $I = \frac{1}{2} \pmod{2}$  values and that with  $I = -\frac{1}{2} \pmod{2}$  values.



# Physics from Large $\gamma$ -Ray Detector Arrays

<i>Morning</i>		Tuesday	Wednesday	Thursday	Friday	Saturday
<u>Topic</u>		<u>C4 Symmetry</u>	<u>Identical Bands</u>	<u>HF Results, Pairing</u>	<u>Continuum, Chaos</u>	<u>Far from Stability</u>
<u>Speakers</u>	8:30	Welcome Mottelson Pavlichenkov Cederwall Break	8:30 Ring Fallon Baktash Zhang Nolan Break	8:30 Flocard Wyss Dracoulis Farris Break	8:30 Dossing Leoni Aberg Break	8:30 Nazarewicz Phillips Suemmerer Broda Lee
<u>Topic</u>		<u>New Regions</u>	<u>Symmetries, SD</u>	<u>Band Termination</u>	<u>SD Decay</u>	<u>Break</u>
<u>Speakers</u>	11:20	Cullen Mullins Viesti End	10:50 Kreiner Nisius Beausang Duprat	10:40 Ragnarsson Fossan Simpson Riley End	11:00 Khoo Brinkman Lunardi End	11:00 Impressions 11:30 Sharpey-Schafer Herskind Hamamoto 12:30 End
	12:30	End	12:10 End	12:10 End	End	End
<i>Afternoon</i>		Tuesday	Wednesday	Thursday	Friday	
<u>Topic</u>		<u>New Effects in Rot</u>	<u>Other Detector Systems</u>	<u>EXCURSION</u>	<u>Coupled GR</u>	
<u>Speakers</u>	2:00	Quentin Shimizu Hagemann Break	2:00 Lister Saranites Bednarczyk Maier Gerl		2:00 Schwalm Gaardhoje Paul Break	
<u>Topic</u>		<u>Tilted Axis Cranking</u>	<u>Detector Developments</u>		<u>Octupoles</u>	
<u>Speakers</u>	3:30	Frauendorf Walker Hubel Clark Hamilton End	3:50 Break 4:20 Macchiavelli Beck Eberth End		4:30 Matsuyanagi Crowell Korten End	
	5:50	End				
<i>Evening</i>		Tuesday	Wednesday	Friday		
<u>Monday</u>						
<u>Reception</u>	6:00-8:00	GammaSphere Tour 7:30	Banquet 7:00			GammaSphere Users Mtg 7:30





# Conference on Physics From Large $\gamma$ -Ray Detector Arrays

August 2-6, 1994

Svon G. Åberg  
Dept. of Mathematical Physics  
Lund University  
P. O. Box 118  
Lund,  
S-22100 Sweden  
46-46-109633  
46-46-104416

Stephen J. Asztalos  
Nuclear Science Division  
Lawrence Berkeley Laboratory  
1 Cyclotron Road, Bldg. 88  
Berkeley, CA 94720  
(510) 486-5708  
(510) 486-7983

Coral Baglin  
MS 50A/6102  
Lawrence Berkeley Laboratory  
1 Cyclotron Rd.  
Berkeley CA 94720

Cyrus Baktash  
Oak Ridge National Laboratory  
Bldg. 6000, MS 6371  
Oak Ridge, TN 37831-6371  
(615) 576-7949  
(615) 574-1268

David P. Balamuth  
University of Pennsylvania  
209 S. 33rd Street  
Philadelphia, PA 19104-6396  
(215) 898-8144  
(215) 573-3897

Robert Bark  
Niels Bohr Institute  
Tandem Accelerator Laboratory  
Roskilde,  
DK-4000 Denmark  
(45) 46-775600  
(45) 42-373516

John F. Beausang  
University of Liverpool  
Oliver Lodge Laboratory  
Oxford Street  
Liverpool,  
L69 3BX England  
44-51-794-3382  
44-51-794-3348

Francis A. Beck  
Centre de Recherches Nucleaires  
23, rue du Loess  
Strasbourg,  
F-67037 France  
33-88-10-62-87  
33-88-10-62-92

John A. Becker  
Lawrence Livermore National Lab.  
P. O. Box 808, L-280  
Livermore, CA 94550  
(510) 422-9676  
(510) 423-8086

Piotr Bednarczyk  
INFN  
Laboratori Nazionali di Legnaro  
Via Romea, 4  
Legnaro,  
35020 Italy  
39-49-8292311  
39-49-641925

Michael A. Bentley  
Staffordshire University  
School of Sciences  
College Road  
Stoke-on-Trent  
ST4 20E UK  
(44) 782 573 419  
(44) 782 745 506

Lee A. Bernstein  
Dept. of Physics & Astronomy  
Rutgers University  
P. O. Box 849  
Piscataway, NJ 08855  
(908) 445-2405  
(908) 445-4343

Ignacio Birriel  
Department of Physics & Astronomy  
University of Pittsburgh  
Pittsburgh, PA 15260  
(412) 624-9238  
(412) 624-9163

Daniel J. Blumenthal  
Argonne National Laboratory  
9700 South Cass Ave. Bldg. 203  
Argonne, IL 60439  
(708) 252-4048  
(708) 252-2864

Paul Bonche  
Service de Physique Theorique  
C.E. Saclay  
Orme des Meristers  
Gif-sur-Yvette,  
F-91191 France  
69-08-7572  
69-08-81-20

Paola Bosetti  
University of Milano  
Via Celoria 16  
Milano,  
I-20133 Italy  
39-2-2392248  
39-2-2392487

Matthew J. Brinkman  
Oak Ridge National Laboratory  
P. O. Box 2008  
Bldg. 6000, MS 6371  
Oak Ridge, TN 37831-6371  
(615) 241-5332  
(615) 574-1268

Rafael Jan Broda  
Niewodniczanski Inst. of Nuclear Pys.  
Radzikowskiego 152  
Krakow,  
31-342 Poland  
48-12-370222  
48-12-371881

Jacob Burde  
The Racah Institute of Physics  
Hebrew Univ. of Jerusalem  
Jerusalem,  
91904 Israel  
972-2-584433  
972-2-584437

Håkan Carlsson  
Department of Physics  
University of Lund  
Sölvegatan 14  
Lund,  
S-22362 Sweden  
46-46-107706  
46-46-104015

Michael P. Carpenter  
Argonne National Laboratory  
9700 South Cass Avenue  
Argonne, IL 60439  
(708) 252-5365  
(708) 252-2864

Bo W. Cederwall  
Nuclear Science Division  
Lawrence Berkeley Laboratory  
1 Cyclotron Road  
Berkeley, CA 94720  
(510) 486-4243  
(510) 486-7983

Yong Shou Chen  
JIHIR/CIAE  
China Institute of Atomic Energy  
P.O. Box 275 (18)  
Beijing  
102413 China  
(615) 576-5780

S.Y. Frank Chu  
Lawrence Berkeley Laboratory  
1 Cyclotron Road, 50A-6102  
Berkeley, CA 94720  
(510) 486-7648  
(510) 486-5757

Marco Cinausero  
Laboratori Nazionali di Legnaro  
Via Romea 4  
Legnaro (PD),  
35020 Italy  
39-49-8292311  
39-49-641925

Jolie A. Cizewski  
Department of Physics  
Rutgers University  
P. O. Box 849  
Piscataway, NJ 08855  
(908) 932-3884  
(908) 932-4343

Roderick M. Clark  
Nuclear Science Division  
Lawrence Berkeley Laboratory  
1 Cyclotron Road  
Berkeley, CA 94720  
(510) 486-5702  
(510) 486-6707

Douglas Cline  
University of Rochester  
N.S.R.L.  
Rochester, NY 14627  
(716) 275-4934  
(716) 473-5384

Fernando Cristancho  
Dept. of Physics and Astronomy  
University of Pittsburgh  
Pittsburgh, PA 15260  
(412) 624-9238  
(412) 624-9163

Mario L. Cromaz  
University of Toronto  
60 St. George Street  
Toronto,  
M5S 1A7 Canada  
(416) 978-7114  
(416) 978-2537

Benjamin F. Crowell  
Physics Division  
Argonne National Laboratory  
9700 South Cass Avenue  
Argonne, IL 60439  
(708) 252-6210

David M. Cullen  
University of Rochester  
N.S.R.L.  
271 E. River Road  
Rochester, NY 14620  
(716) 275-2703

Dominique P. Curien  
CRN/CNRS  
23 Rue du Loess  
Strasbourg,  
F-67037 France  
33-88-10-6611  
33-88-10-6479

Giacomo de Angelis  
Laboratori Nazionali de Legnaro  
Via Romea 4  
Legnaro,  
35020 Italy  
39-49-8292404  
39-49-641925

Gilles M. de France  
CRN/CNRS  
23 Rue du Loess  
Strasbourg,  
F-67037 France  
33-88-10-6593  
33-88-10-6479

Jim H. De Graaf  
University of Toronto  
60 St. George Street  
Toronto,  
M5S 1A7 Canada  
(416) 978-7114  
(416) 978-2537

Jorrit deBoer  
University of Munich  
Munich,  
Germany

Richard M. Diamond  
Nuclear Science Division  
Lawrence Berkeley Laboratory  
1 Cyclotron Road, Bldg. 88  
Berkeley, CA 94720  
(510) 486-5720  
(510) 486-7983

Joachim Hans Döring  
Department of Physics  
Florida State University  
Tallahassee, FL 32306  
(904) 644-2436  
(904) 644-8630

Thomas Dossing  
Physics Division  
Argonne National Laboratory  
9700 South Cass Avenue  
Argonne, IL 60439  
(708) 252-4036  
(708) 252-3903

George D. Dracoulis  
Department of Nuclear Physics  
Australian National University  
R.S. Phys. kS.E.  
Canberra,  
0200 Australia  
61-6-2492090  
61-6-2490748

Tom Drake  
University of Toronto  
60 St. George Street  
Toronto,  
M5S 1A7 Canada  
(416) 978-7267  
(416) 978-2537

James E. Draper  
Physics Division  
University of California, Davis  
Davis, CA 95616  
(916) 752-1500  
(916) 752-4717

Jean Duprat  
IPN  
Orsay,  
91406 France  
33-1-69416558  
33-1-69417196

John L. Durell  
Department of Physics  
University of Manchester  
Manchester,  
M13 9PL UK  
061-275-4152  
061-275-4149

Cemal Duyar  
Department of Physics  
University of California, Davis  
Davis, CA 95616  
(916) 752-1500

H. Jürgen Eberth  
University of Köln  
Zùlpicher Strasse 77  
Köln,  
D-50937 Germany  
49-221-4702796  
49-221-4705168

Claes Fahlander  
The Svedberg Laboratory  
Uppsala University  
Box 535  
Uppsala,  
S-75121 Sweden  
46-18-183051  
46-18-183833

Paul Fallon  
Lawrence Berkeley Laboratory  
1 Cyclotron Road, Bldg. 88  
Berkeley, CA 94720  
(510) 486-7018

Bjorn Fant  
Department of Physics  
University of Helsinki  
P. O. Box 9  
Helsinki,  
00014 Finland  
358-0-1918387  
358-0-1918378

Lorenzo P. Farris  
Lawrence Livermore National Lab.  
P. O. Box 808  
Livermore, CA 94551  
(510) 423-0749  
(510) 422-0883

Stéphane Flibotte  
Department of Physics  
McMaster University  
1280 Main Street West  
Hamilton, Ont.  
L8S 4M1 Canada  
(905) 525-9140, x23632  
(905) 546-1252

Hubert Flocard

Salley Forbes  
Department of Physics  
University of Liverpool  
Oliver Lodge  
Oxford Street  
Liverpool,  
L69 3BX England  
44-51-794-3379  
44-51-794-3348

David B. Fossan  
Department of Physics  
SUNY @ Stony Brook  
Stonybrook, NY 11794  
(516) 632-8113  
(516) 632-8573

Stefan G. Frauendorf  
Research Center Rossendorf  
PF 510119  
Dresden,  
01314 Germany  
49-351-5913261  
49-351-5913700

Jens-Jorgen Gaardhoje  
Niels Bohr Institute  
Tandem Accelerator Laboratoriet  
Roskilde,  
DK-4000 Denmark  
(45) 4677-5645  
(45) 4237-3516

Umesh Garg  
Physics Department  
University of Notre Dame  
Notre Dame, IN 46556  
(219) 631-7352  
(219) 631-5952

Jerry D. Garrett  
Oak Ridge National Laboratory  
P. O. Box 2008  
Bldg. 6000, MS 6368  
Oak Ridge, TN 37831  
(615) 576-5489  
(615) 574-1268

David F. Gassmann  
Argonne National Laboratory  
9700 South Cass Avenue  
Argonne, IL 60439  
(708) 252-3894  
(708) 252-6210

Jürgen Gerl  
GSI  
Planckstr. 7  
Darmstadt,  
D-64291 Germany  
49-6151-359-643  
49-6151-359-809

Andrée Gizon  
Institute Des Sciences Nucléaires  
53 Avenue Des Martyrs  
Grenoble,  
F-38026 France  
33-76-284000  
33-76-284004

Jean Rene Gizon  
Institute Des Sciences Nucléaires  
53 Avenue Des Martyrs  
Grenoble,  
F-38026 France  
33-76-284023  
33-76-284004

Alan L. Goodman  
Physics Department  
Tulane University  
New Orleans, LA 70118  
(504) 865-5520  
(504) 862-8702

Greg S. Hackman  
Department of Physics  
McMaster University  
1280 Main Street W.  
Hamilton, Ont.  
L8S 4M1 Canada  
(905) 525-9140, x27457  
(905) 546-1252

Gudrun B. Hagemann  
Niels Bohr Institute  
Tandem Accelerator Laboratory  
Roskilde,  
DK-4000 Denmark

Ikuko Hamamoto  
Dept. of Mathematical Physics  
University of Lund, LTH  
P. O. Box 118  
Lund,  
S-22100 Sweden  
46-46-109085  
46-46-104416

Joseph H. Hamilton  
Dept. of Physics & Astronomy  
Vanderbilt University  
Box 1807, Station B  
Nashville, TN 37235  
(615) 322-2828  
(615) 343-7263

Fazia Hannachi  
Institut Natl. de Physique Nucleaire  
Batiments 104-108  
Orsay, Campus,  
91405 France  
33-1-6941-5081  
33-1-6941-5008

Michael Hass  
Weizmann Institute of Science  
Rehovot,  
76100 Israel  
972-8-342231  
972-8-344106

Karl Hauschild  
Department of Physics  
University of York  
York,  
Y01 5DD UK  
44-904-432242  
44-904-432214

Paul-Henri Heenen  
Université Libre de Bruxelles  
PNTPM-Campus Plaine-C.P. 229  
Brussels,  
B-1050 Belgium  
32-2-650-5558  
32-2-650-5045

Eugene A. Henry  
Lawrence Livermore National Lab.  
P. O. Box 808, L-231  
Livermore, CA 94550  
(510) 422-5532  
(510) 422-3160

Bent Herskind  
Niels Bohr Institutet  
Tandem Accelerator Laboratoriet  
Roskilde,  
DK-4000 Denmark

Richard W. Hoff  
Lawrence Livermore National Lab.  
P. O. Box 808, M/S L-231  
Livermore, CA 94526  
(510) 422-6664  
(510) 422-3160

Herbert C. Hübel  
Inst. für Strahlen-und Kernphysik  
University of Bonn  
Nussallee 14-16  
Bonn,  
D-53115 Germany  
49-228-73-3277  
49-228-73-3728

John R. Hughes  
Lawrence Livermore National Lab.  
P. O. Box 808, L-280  
Livermore, CA 94550  
(510) 423-5848  
(510) 422-0883

Finn Ingebretsen  
Institute of Physics  
University of Oslo  
Box 1048  
Blindern 0316  
Oslo,  
3 Norway

Robert V. Janssens  
Physics Division  
Argonne National Laboratory  
9700 South Cass Avenue  
Argonne, IL 60439  
(708) 252-8426  
(708) 252-6210

Victor P. Janzen  
AECL Chalk River Laboratories  
Chalk River,  
K0J 1J0 Canada  
(613) 584-3311  
(613) 584-1800

Haoqiang Jin  
Oak Ridge National Laboratory  
P. O. Box 2008  
MS 6371  
Oak Ridge, TN 37831-6371  
(615) 574-1268

Noah R. Johnson  
Oak Ridge National Laboratory  
P. O. Box 2008  
Oak Ridge, TN 37831-6371  
(615) 574-4739  
(615) 574-1268

Barna Mátyás Juhász  
Bem tér 18/c.  
Debrecen,  
H-4026 Hungary  
(36)-52-417-266  
(36)-52-416-181

William H. Kelly  
Div. of Undergraduate Education  
National Science Foundation  
4201 Wilson Blvd. Rm 835  
Arlington, VA 22230  
(703) 306-1667  
(703) 306-0445

Teng L. Khoo  
Argonne National Laboratory  
Phy. 203  
9700 South Cass Avenue  
Argonne, IL 60439  
(708) 252-4034  
(708) 252-6210

Noémie Koller  
Department of Physics  
Rutgers University  
New NJ 08903  
(908) 445-2525  
(908) 445-4343

Tetsuro Komatsubara  
Tandem Accelerator Center  
University of Tsukuba  
Ibaraki,  
305 Japan

Amel Korichi  
Institut Natl. de Physique Nucleaire  
Batiments 104-108  
Orsay, Campus,  
91405 France  
  
33-1-6941-7471

Wolfram Korten  
ISUP, University of Bonn  
Nussallee 14-16  
Bonn,  
D-53115 Germany  
49-228-732633  
49-288-733728

Dennis G. Kovar  
U. S. Department of Energy  
ER-23/GTN  
Washington, D.C. 20585  
(301) 903-3613  
(301) 903-3833

Andrés J. Kreiner  
Tandar/Dept. de Fisica  
C.N.E.A.  
Av. del Libertador 8250  
Buenos Aires,  
1429 Argentina  
(541) 755-8660  
(541) 755-8710

Reiner Krücken  
Institute for Nuclear Physics  
University of Cologne  
Zùlpicher Str. 77  
Köln,  
D-50937 Germany  
49-221-4703644  
49-221-4705168

Gerfried J. Kumbartzki  
Department of Physics  
Rutgers University  
Piscataway, NJ 08854  
(908) 932-2407  
(908) 932-4343

Eduardo Landulfo  
Department of Physics & Astronomy  
University of Pittsburgh  
Pittsburgh, PA 15260  
(412) 624-9238  
(412) 624-9163

Greg J. Lane  
Department of Nuclear Physics  
Australian National University  
Canberra, ACT,  
0200 Australia  
(616) 249-2083  
(616) 249-0748

Torben Lauritsen  
Argonne National Laboratory  
9700 South Cass Ave.,B203  
Argonne, IL 60439  
(708) 252-4026  
(708) 252-6210

I'Yang Lee  
Lawrence Berkeley Laboratory  
1 Cyclotron Road  
Berkeley, CA 94720  
(510) 486-5727  
(510) 486-7983

Silvia Leoni  
Niels Bohr Institute  
Tanderu Accelerator Laboratory  
Roskilde,  
DK 4000 Denmark  
45-4677-5600  
45-42-373516

Rainer M. Lieder  
Institute für Kernphysik  
KFA Juelich  
Juelich,  
D-52425 Germany  
49-2461-614114  
49-2461-613930

Christopher J. Lister  
Argonne National Laboratory  
9700 South Cass Avenue  
Argonne, IL 60439-4843  
(708) 252-4040  
(708) 252-2864

Giovanni Lo Bianco  
Dipartimento di Fisica  
University di Milano  
Via Celoria 16  
Milano,  
20133 Italy  
39-2-2392217  
39-2-2392487

Renee L. Lucas  
Centre d'Etudes de Saclay  
DAPNIA/SPHN  
Gif Sur Yvette,  
F-91191 France  
33 (1) 6908-3663  
33 (1) 6908-7584



Santo Lunardi  
Department of Physics  
University of Padova  
Via Marzolo, 8  
Padova,  
35131 Italy  
39-49-831792  
39-49-844245

Yixiao Luo  
Institute of Modern Physics  
No. 253 Nachang Road  
Lanzhou,  
73000 China  
86-931-8828951-215  
86-931-23600

Wenchao Ma  
Vanderbilt University  
P. O. Box 1807, Station B  
Nashville, TN 37235  
(615) 322-2646  
(615) 343-7263

Augusto O. Macchiavelli  
Nuclear Science Division  
Lawrence Berkeley Laboratory  
1 Cyclotron Road  
Berkeley, CA 94720  
(510) 486-4428  
(510) 486-7983

K. Hugo Maier  
HMI, Berlin  
Postfach 390128  
Berlin,  
14091 Germany  
49-30-8062-2737  
49-30-8062-2293

Michael R. Maier  
Lawrence Berkeley Laboratory  
1 Cyclotron Road  
Berkeley CA 94720  
USA  
(510) 486-5599  
(510) 486-4122

Masayuki Matsuo  
Kyoto University  
Yukawa Inst. for Theo. Physics  
Sakyo-ku Kitashirakawa  
Kyoto,  
606-01 Japan  
81-75-753-7008  
81-75-753-7010

Kenichi Matsuyanagi  
Department of Physics  
Kyoto University  
Faculty of Science  
Kitashirakawa  
Kyoto,  
606 Japan  
(81) 75-753-3841  
(81) 75-753-3886

Nicole A. Matt  
Rutgers University  
P. O. Box 849  
Piscataway, NJ 08855  
(908) 932-2405  
(908) 932-4400

Joe McGrory  
U.S. Department of Energy  
ER-23, G312/GTN  
Washington, D.C. 20585  
(301) 903-3613

William C. McHarris  
Michigan State University, NSCL  
Cyclotron Lab.  
East Lansing, MI 48823  
(517) 353-5961  
(517) 353-5967

Dennis P. McNabb  
Dept. of Physics & Astronomy  
Rutgers University  
Busch Campus  
Piscataway, NJ 08855-0849  
(908) 445-2405  
(908) 445-4343

Rami A.K. Mehrem  
Lawrence Livermore National Lab.  
P. O. Box 808, L-412  
Livermore, CA 94550  
(510) 423-8087

Aram Mekjian  
Physics Dept.  
Rutgers University  
PO Box 849  
Piscataway NJ 08854  
908-932-4343

Eugene F. Moore  
North Carolina State University  
Box 8202  
Raleigh, NC 27695-8202  
(919) 515-6138  
(919) 515-6538

Steven A. Moszkowski  
Department of Physics  
University of California, Los Angeles  
Los Angeles, CA 90024  
(310) 825-4186  
(310) 206-5668

Ben R. Mottelson  
Niels Bohr Institute  
Blegdamsvej 17  
Copenhagen,  
2100 Denmark  
(45) 35-32-5231  
(45) 31-38-9157

Simon M. Mullins  
Dept. of Physics & Astronomy  
McMaster University  
1280 Main Street West  
Hamilton, Ont.  
L8S 4M1 Canada  
(905) 525-9140, x23345  
(905) 546-1252

Sanjeevan Naguleswaran  
Department of Physics  
University of Notre Dame  
Notre Dame, IN 46556  
(219) 631-7716  
(219) 631-5952

Takashi Nakatsukasa  
Res. Ctr. for Nuclear Physics  
Osaka University  
10-1, Mihagaoka  
Ibaraki, Osaka,  
567 Japan  
(81) 6-879-8940  
(81) 6-879-8899

Witold Nazarewicz  
Physics Division  
Oak Ridge National Lab./JHIR  
Bldg. 6003, MS 6373  
Oak Ridge, TN 37831  
(615) 574-4580  
(615) 574-4745

David T. Nisius  
Argonne National Laboratory  
9700 South Cass Avenue  
Argonne, IL 60439  
(708) 252-3894  
(708) 252-6210

Michael J. Nitschke  
Lawrence Berkeley Laboratory  
1 Cyclotron Road, 71-259  
Berkeley, CA 94720  
(510) 486-7770  
(510) 486-7981

Paul J. Nolan  
University of Liverpool  
Oliver Lodge Laboratory  
Oxford Street  
Liverpool,  
L69 3BX England  
44-51-794-3377  
44-51-794-3348

Naoki Onishi  
Institute of Physics  
3-8 Komaba, Meguro-ku  
Tokyo,  
153 Japan  
81-3-5454-6512  
81-3-3489-2904

Ashwani Kumar Pande  
Nuclear Science Centre  
P. O. Box 10502  
New Delhi,  
110067 India  
091-11-6893955  
091-11-6892601

Vitaly V. Pashkevich  
Bogolubov Lab. of Theoretical Phys.  
Joint Institute for Nuclear Research  
Dubna,  
141980 Russia  
(7095) 926-2295  
(7096) 216-5084

Edward S. Paul  
University of Liverpool  
P. O. Box 147  
Oxford Street  
Liverpool,  
L69 3BX England  
44-51-794-3381  
44-51-794-3348

Peter Paul  
Department of Physics  
SUNY @ Stony Brook  
Stonybrook, NY 11794  
(516) 632-8115  
(516) 632-8573

Igor M. Pavlichenkov  
Kurchatov Inst./Russian Natl. Ctr.  
Moscow,  
123182 Russia  
7-095-196-9586  
7-095-882-5804

William R. Phillips  
Department of Physics  
University of Manchester  
Oxford Road  
Manchester,  
M13 9PL UK  
61-275-4105  
61-275-4149

Alan R. Poletti  
Department of Physics  
University of Auckland  
Private Bag 92019  
Auckland,  
New Zealand  
64-9-3737-599,x8853  
64-9-3737-445

David C. Radford  
Chalk River,  
K0J 1J0 Canada  
(613) 584-3311  
(613) 584-1800

Nadine Redon  
Institut Natl. de Physique Nucleaire  
43 Bd du 11 Nov. 1918  
Lyon-Villeurban  
69622 France  
33-7243-1064  
33-7244-8004

Mark A. Riley  
Department of Physics  
Florida State University  
Tallahassee, FL 32306  
(904) 644-1429  
(904) 644-8630

Matti J. Piiparinen  
Department of Physics  
University of Jyväskylä  
Seminaarink 15  
Box 35  
Jyväskylä,  
Fin-40351 Finland  
358-41-602373  
358-41-602351

Avril Quarrie  
Nuclear Science Division  
Lawrence Berkeley Laboratory  
1 Cyclotron Road, Bldg. 88  
Berkeley, CA 94720  
(510) 486-5384  
(510) 486-7983

Ingemar Ragnarsson  
Dept. of Mathematical Physics  
Lunds University  
Lund Institute of Technology  
P. O. Box 118  
Lund,  
S-221 Sweden  
46-46-109083  
46-46-104416

Walter Reviol  
Department of Physics  
University of Tennessee  
IMP Lanzhou  
Knoxville, TN 37996-1200  
(615) 974-7802  
(615) 974-7843

Peter Ring  
Technical University, Munich  
James Franck Str. 1  
Garching,  
D-85748 Germany  
49-89-3209-2353  
49-89-3209-2296

Stephane Pilotte  
University of Ottawa  
150 Louis Pasteur  
Ottawa,  
K1N 6NS Canada  
(613) 564-2277  
(613) 564-6712

Philippe G. Quentin  
C.E.N. de Bordeaux Gradignan  
B.P. 120  
Gradignan,  
F-33170 France  
33-56-75-19-58  
33-56-75-11-80

John O. Rasmussen  
Lawrence Berkeley Laboratory  
1 Cyclotron Road  
Berkeley, CA 94720  
(510) 486-6318  
(510) 486-6707

Lee L. Riedinger  
Department of Physics  
University of Tennessee  
Knoxville, TN 37996-1200  
(615) 974-3466  
(615) 974-2805

Hans B. Ryde  
Department of Physics  
University of Lund  
Lund,  
S-22362 Sweden  
46-46-107705  
46-46-104015

Juerg Saladin  
Department of Physics & Astronomy  
University of Pittsburgh  
Pittsburgh, PA 15260  
(412) 624-9233  
(412) 624-9163

Demetrios G. Sarantites  
Washington University  
St. Louis, MO 63130  
(314) 935-6504  
(314) 935-6184

Michael R. Satteson  
Department of Physics  
Rutgers University  
P. O. Box 849  
Piscataway, NJ 08855  
(908) 932-2405  
(908) 932-4343

Nancy C. Schmeing  
McMaster University  
c/o AECL Research  
Chalk River,  
K0J1J0 Canada  
(613) 584-8811, x1735  
(613) 584-1800

Claire A. Schuck  
C.S.N.S.M., France  
Batiment 104  
Orsay,  
91405 France  
33-1-6941-5239  
33-1-6941-5008

Dirk Schwalm  
MPI für Kernphysik  
Postfach 103980  
Heidelberg,  
D-69029 Germany  
49-6221-516360  
49-6221-516540

Paul B. Semmes  
Physics Department  
Tennessee Technological University  
Box 5051  
Cookeville, TN 38505  
(615) 372-3145  
(615) 372-6172

Henri Sergolle  
Institut Natl. de Physique Nucleaire  
Batiments 104-108  
Orsay, Campus,  
91405 France  
33-1-6941-7325  
33-1-6941-7471

Darek Seweryniak  
The Svedberg Laboratory  
Uppsala University  
Box 535  
Uppsala,  
S-75121 Sweden  
46-18-183051  
46-18-183833

John F. Sharpey-Schafer  
Physics Department  
University of Liverpool  
Oxford Street  
Liverpool,  
L69 3BX England  
44-51-794-3380  
44-51-794-3348

Yoshifumi R. Shimizu  
Department of Physics  
Kyusku University  
6-10-1 Hakozaki  
Fukuoka,  
812 Japan  
81-92-641-1101, x4144  
81-92-633-4525

John Simpson  
Daresbury Laboratory  
Keckwick Lane  
Warrington,  
Cheshire  
WA4 4AD UK  
7-0925-603171

Geirr Sletten  
Niels Bohr Institutet  
Tandem Accelerator Laboratory  
Roskilde,  
DK-4000 Denmark  
(45) 46-775609  
(45) 42-373516

Frank S. Stephens  
Nuclear Science Division  
Lawrence Berkeley Laboratory  
1 Cyclotron Road, Bldg. 88  
Berkeley, CA 94720  
(510) 486-5724  
(510) 486-7983

Marie-Agnes Stephens  
Nuclear Science Division  
Lawrence Berkeley Laboratory  
1 Cyclotron Road, Bldg. 88  
Berkeley, CA 94720  
(510) 486-5384  
(510) 486-7983

Mark A. Stoyer  
Lawrence Berkeley Laboratory  
1 Cyclotron Road, 71-259  
Berkeley, CA 94720  
(510) 486-7774  
(510) 486-7981

Andrew E. Stuchbery  
Department of Nuclear Physics  
Australian National University  
Canberra Act,  
0200 Australia  
(616) 249-2097  
(616) 249-0748

Klaus Sümmerer  
GSI Darmstadt  
Postfach 110552  
Darmstadt,  
D-6100 Germany  
49-6151-359-0

Xiangfu Sun  
Institute of Modern Physics  
No. 253 Nachang Road  
Lanzhou,  
73000 China  
86-931-8828951-215  
86-931-23600

James Symons  
Lawrence Berkeley Laboratory  
1 Cyclotron Road, 70A-3307  
Berkeley, CA 94720

Samuel L. Tabor  
Department of Physics  
Florida State University  
Tallahassee, FL 32306  
(904) 644-5528  
(904) 644-8630

Naoki Tajima  
Institute of Physics  
University of Tokyo  
Komaba 3-8-1, Meguroku  
Tokyo,  
153 Japan  
3-5454-6544  
3-3467-1281

Gurgen M. Ter-Akopian  
Flerov Lab. of Nuclear Reactions  
Joint Institute for Nuclear Research  
Dubna,  
141980 Russia  
(7095) 924-3914  
(7096) 216-5083

Per Olav Tjøm  
Department of Physics  
P. 131048  
Oslo,  
0316 Norway  
47-22-856462  
47-22-856422

Livius M. Trache  
Texas A&M University  
Cyclotron Institute  
College Station, TX 77801-3366  
(409) 845-1411  
(409) 845-1899

Peter J. Twin  
University of Liverpool  
Oliver Lodge Laboratory  
Oxford Street  
Liverpool,  
L69 3BX England  
44-51-794-3378  
44-51-794-3348

Peter van Brentano  
Institute für Kernphysik  
Zülpicher Str. 77  
Köln,  
50937 Germany  
49-221-470-3456  
49-221-470-5168

Giuseppe Viesti  
Department of Physics  
University of Padova  
Via Marzolo 8  
Padova,  
I-35131 Italy  
39-49-831771  
39-49-844245

Enrico Vigezzi  
I.N.F.N. Sezione di Milano  
Via G. Celoria 16  
Milano,  
I-20133 Italy  
39-2-23-92-251  
39-2-23-92-487

C. Martin Vincent  
Department of Physics & Astronomy  
University of Pittsburgh  
Pittsburgh, PA 15260  
(412) 624-9039  
(412) 624-9163

Andrea Vitturi  
Dipartimento di Fisica  
Universita Padova  
Via Marzolo 8  
Padova,  
35131 Italy  
39-49-831770  
39-49-844245

Luo Vixiao  
Institute of Modern Physics  
No. 253 Nachang Road  
Lanzhou,  
China  
86-0931-8881100

Duc Vo  
Ames Iowa 50011  
  
(613) 584-3311  
(613) 584-1800

Duc Vo  
Iowa State University  
523 Denver  
Waterloo IA 50702

Peter von Brentano  
Institut für Kernphysik  
Zülpicher Str. 77  
Köln,  
50937 Germany  
49-221-470-3456  
49-221-470-5168

Victor V. Voronov  
Bogolubov Lab. of Theoretical Phys.  
Joint Institute for Nuclear Research  
Box 79  
Dubna,  
141980 Russia  
(7-095) 926-2295  
(7-096) 216-5084

Robert Wadsworth  
Department of Physics  
University of York  
York,  
YO1 5DD UK  
904-432242  
904-432214

Philip M. Walker  
Department of Physics  
University of Surrey  
Guildford,  
GU25XH UK  
483-300800, x2728  
483-259501

John C. Walpe  
Department of Physics  
University of Notre Dame  
Notre Dame, IN 46556  
(219) 631-7716  
(219) 631-5952

David Ward  
AECL Chalk River Laboratories  
Chalk River,  
K0J 1J0 Canada  
(613) 584-3311  
(613) 584-1800

Yasuo Watanabe  
Fuji Electric Co., Ltd.  
c/o Lawrence Berkeley Lab.  
1 Cyclotron Road, 70A-3307  
Berkeley, CA 94720  
(510) 486-7590  
(510) 486-6707

Morton S. Weiss  
Lawrence Livermore National Lab.  
P. O. Box 808, L-297  
Livermore, CA 94550  
(510) 422-4094  
(510) 422-9523

Tomasz R. Werner  
ORNL/Univ. of Tennessee  
P. O. Box 2008, Bldg. 6003  
Oak Ridge, TN 37831  
(615) 574-4576  
(615) 574-4745

David F. Winchell  
Department of Physics  
University of Pennsylvania  
209 S. 33rd Street  
Philadelphia, PA 19104  
(215) 898-8832  
(215) 898-2010

Ramon A. Wyss  
Physics Department  
Royal Institute of Tech./KTH  
Frescativagen 24  
Stockholm,  
S-10405 Sweden  
46-8-161107  
46-8-158674

Sun Xiangfu  
Institute of Modern Physics  
No. 253 Nachang Road  
Lanzhou,  
China  
86-0931-8881100

Walid Younes  
Dept. of Physics & Astronomy  
Rutgers University  
Piscataway, NJ 08855-0849  
(908) 445-2405  
(908) 445-4343

Chang-Hong Yu  
University of Rochester  
271 East River Road  
Rochester, NY 14627  
(716) 275-4941

Larry Zamick  
Department of Physics  
Rutgers University  
P. O. Box 849  
Piscataway, NJ 08855  
(908) 932-3874  
(908) 932-4343

Jing Ye Zhang  
Department of Physics  
University of Tennessee  
IMP Lanzhou  
Knoxville, TN 37996-1200  
(615) 974-7814  
(615) 974-7843